frontiers | Research Topics

Advances and trends in nutraceutical and functional plant-based food

Edited by
Gengjun Chen and Marina Carcea

Published in
Frontiers in Nutrition

ISSN 1664-8714
ISBN 978-2-83252-018-5
DOI 10.3389/978-2-83252-018-5

About Frontiers

Frontiers is more than just an open access publisher of scholarly articles: it is a pioneering approach to the world of academia, radically improving the way scholarly research is managed. The grand vision of Frontiers is a world where all people have an equal opportunity to seek, share and generate knowledge. Frontiers provides immediate and permanent online open access to all its publications, but this alone is not enough to realize our grand goals.

Frontiers journal series

The Frontiers journal series is a multi-tier and interdisciplinary set of open-access, online journals, promising a paradigm shift from the current review, selection and dissemination processes in academic publishing. All Frontiers journals are driven by researchers for researchers; therefore, they constitute a service to the scholarly community. At the same time, the *Frontiers journal series* operates on a revolutionary invention, the tiered publishing system, initially addressing specific communities of scholars, and gradually climbing up to broader public understanding, thus serving the interests of the lay society, too.

Dedication to quality

Each Frontiers article is a landmark of the highest quality, thanks to genuinely collaborative interactions between authors and review editors, who include some of the world's best academicians. Research must be certified by peers before entering a stream of knowledge that may eventually reach the public - and shape society; therefore, Frontiers only applies the most rigorous and unbiased reviews. Frontiers revolutionizes research publishing by freely delivering the most outstanding research, evaluated with no bias from both the academic and social point of view. By applying the most advanced information technologies, Frontiers is catapulting scholarly publishing into a new generation.

What are Frontiers Research Topics?

Frontiers Research Topics are very popular trademarks of the *Frontiers journals series*: they are collections of at least ten articles, all centered on a particular subject. With their unique mix of varied contributions from Original Research to Review Articles, Frontiers Research Topics unify the most influential researchers, the latest key findings and historical advances in a hot research area.

Find out more on how to host your own Frontiers Research Topic or contribute to one as an author by contacting the Frontiers editorial office: frontiersin.org/about/contact

Advances and trends in nutraceutical and functional plant-based food

Topic editors

Gengjun Chen — Kansas State University, United States

Marina Carcea — Council for Agricultural and Economics Research (CREA), Italy

Citation

Chen, G., Carcea, M., eds. (2023). *Advances and trends in nutraceutical and functional plant-based food*. Lausanne: Frontiers Media SA.

doi: 10.3389/978-2-83252-018-5

Table of contents

frontiers | Frontiers in Nutrition

TYPE Editorial
PUBLISHED 13 March 2023
DOI 10.3389/fnut.2023.1168826

OPEN ACCESS

EDITED AND REVIEWED BY
Alejandro Cifuentes,
CIAL (CSIC), Spain

*CORRESPONDENCE
Gengjun Chen
✉ bgkphld@gmail.com

SPECIALTY SECTION
This article was submitted to Nutrition and Food Science Technology, a section of the journal Frontiers in Nutrition

RECEIVED 18 February 2023
ACCEPTED 28 February 2023
PUBLISHED 13 March 2023

CITATION
Chen G and Carcea M (2023) Editorial: Advances and trends in nutraceutical and functional plant-based food. *Front. Nutr.* 10:1168826. doi: 10.3389/fnut.2023.1168826

Editorial: Advances and trends in nutraceutical and functional plant-based food

Gengjun Chen[1]* and Marina Carcea[2]

[1]Department of Grain Science & Industry, Kansas State University, Manhattan, KS, United States, [2]Council for Agricultural Research and Economics, Rome, Italy

KEYWORDS

plant-based food, bioactive nutrients, delivery system, functional properties, bioavailability, novel food processing, nutraceuticals

Editorial on the Research Topic
Advances and trends in nutraceutical and functional plant-based food

The production of large amounts of animal-based foods (such as meat, fish, eggs, and milk) has been suggested as one of the negative impacts on global environmental sustainability. Traditional livestock production for food typically causes more pollution and water use, which cause higher greenhouse gas emissions and lead to greater losses in biodiversity. As a result of environmental, ethical, and health concerns, the market for plant-based food is expanding rapidly, and the food industry is creating a new generation of plant-based products to meet this demand. Plant-based foods are commonly classified into vegetables, cereals, legumes, fruits, and nuts, and their derived processed counterparts such as baked goods, pasta, breakfast cereals, vegetable preserves, fermented fruits and vegetables, meat analogs, plant-based emulsions, gels, oils, and other delivery systems. Algae and mushrooms are also being explored as sources of novel foods.

Compared to animal-based food, there has been increasing scientific research on plant-based foods because of their potential sustainability and health-related benefits as foods rich in starch, proteins, lipids, dietary fiber, and phytonutrients. From microalgae to legumes, the potential health benefits of these vegetable ingredients are being explored and tested (1, 2). Cutting-edge techniques such as nanotechnology and encapsulation are being used to enhance the efficacy and bioavailability of components, making them even more attractive to consumers (3). The main challenge is to achieve nutrition and functionality in these plant-based foods using healthy and sustainable plant-derived ingredients with desirable appearance, flavor, sensory, and other physicochemical attributes (2, 3). It is also argued that large quantities of nutraceuticals and functional foods have to be consumed to achieve the alleged health benefits, despite the fact that the safety and health implications of plant bioactive compounds are not fully clear.

Eleven quality papers, eight research articles, and three review articles are published on this Research Topic. The following topics were investigated: "*Citrus peel flavonoid extracts—potential beneficial bioactivities and regulation of intestinal microecology in vitro*" (Li et al.); the role of macelignan in inhibiting Tau phosphorylation and Aβ aggregation in the cell model (Gu et al.); the potential benefits of using soybean press cake as an effective

substrate for the commercial production of conjugated linoleic acid and eicosapentaenoic acid by *Bifidobacterium lactis* (Azari et al.); chrysanthemum flavonoids' main components, luteolin and luteoloside, and their potential hypolipidemic mechanism (Sun et al.); the potential antidepressant effects of chlorella and lion's mane mushroom complex as a dietary supplement (Chou et al.); the improvement of maize grain filling through novel high planting density and varying nitrogen application rate (Ren et al.); the assessment of golden-flowered tea (*Camellia nitidissima* Chi) fractions and their anti-non-small cell lung cancer (NSCLC) effects *in vitro* and *in vivo* (Wang et al.); "*The nutritional value of the extrusion-processed, micronutrient-fortified corn snacks enriched with protein and dietary fiber*" (Shah et al.). The reviews include a summary of the phytochemistry, pharmacology, and promising traditional uses of *Lagenaria siceraria* Molina (Standl.) fruit (Saeed et al.); ethnobotanical and pharmacological aspects of *Allium sativum* L. (garlic), with notes on its phytochemistry, ethnopharmacology, toxicological aspects, and clinical studies (Tudu et al.); and the advances in the study of *Syzygium aromaticum* (L) Merr. Perry, an aromatic plant in tropical regions worldwide, including information on its composition, phytochemistry, bioactive substances, and potential applications (Xue et al.).

In conclusion, the present Research Topic provides several examples of nutraceutical and functional plant-based foods and their applications. We hope it can provide new insights into innovative scientific understanding in this area and promote interest in further work and studies required for the development of nutraceuticals and functional plant-based foods.

Author contributions

GC drafted the manuscript. GC and MC provided critical review and insight and revised the final version of the editorial. All authors contributed to the article and approved the submitted version.

Acknowledgments

The editors of this topic would like to thank all authors and reviewers for their contributions to the present collection.

Conflict of interest

The authors declare that the research was conducted in the absence of any commercial or financial relationships that could be construed as a potential conflict of interest.

Publisher's note

References

1. Katiyar R, Arora A. Health promoting functional lipids from microalgae pool: a review. *Algal Res*. (2020) 46:101800. doi: 10.1016/j.algal.2020.101800

2. Nadeeshani H, Senevirathne N, Somaratne G, Bandara N. Recent trends in the utilization of pulse protein in food and industrial applications. *ACS Food Sci Technol*. (2022) 2:722–37. doi: 10.1021/acsfoodscitech.1c00448

3. Tan YB, McClements DJ. Plant-based colloidal delivery systems for bioactives. *Molecules*. (2021) 26:6895. doi: 10.3390/molecules26226895

frontiers | Frontiers in Nutrition

ORIGINAL RESEARCH
published: 18 May 2022
doi: 10.3389/fnut.2022.892558

Inhibitory Effects of Macelignan on Tau Phosphorylation and Aβ Aggregation in the Cell Model of Alzheimer's Disease

Liang Gu[1,2†], Nan Cai[1,2†], Meiting Li[1], Decheng Bi[1,3], Lijun Yao[1], Weishan Fang[1], Yan Wu[4], Zhangli Hu[1], Qiong Liu[1], Zhijian Lin[5], Jun Lu[1,3,6,7] and Xu Xu[1*]*

[1] Shenzhen Key Laboratory of Marine Bioresources and Ecology and Guangdong Provincial Key Laboratory for Plant Epigenetics, College of Life Sciences and Oceanography, Shenzhen University, Shenzhen, China, [2] Digestive Diseases Center, The Seventh Affiliated Hospital, Sun Yat-sen University, Shenzhen, China, [3] School of Science and School of Interprofessional Health Studies, Faculty of Health and Environmental Sciences, Auckland University of Technology, Auckland, New Zealand, [4] Instrumental Analysis Center, Shenzhen University, Shenzhen, China, [5] Department of Neurology, Peking University Shenzhen Hospital, Shenzhen, China, [6] School of Public Health and Interdisciplinary Studies, Faculty of Health and Environmental Sciences, Auckland University of Technology, Auckland, New Zealand, [7] Maurice Wilkins Centre for Molecular Discovery, Auckland, New Zealand

OPEN ACCESS

Edited by:
Gengjun Chen,
Kansas State University, United States

Reviewed by:
Sook Yee Gan,
International Medical University, Malaysia
Cheng-Shi Jiang,
University of Jinan, China

***Correspondence:**
Jun Lu
jun.lu@aut.ac.nz
Xu Xu
xuxu@szu.edu.cn

[†] These authors have contributed equally to this work

Specialty section:
This article was submitted to Nutrition and Food Science Technology, a section of the journal Frontiers in Nutrition

Received: 09 March 2022
Accepted: 25 April 2022
Published: 18 May 2022

Citation:
Gu L, Cai N, Li M, Bi D, Yao L, Fang W, Wu Y, Hu Z, Liu Q, Lin Z, Lu J and Xu X (2022) Inhibitory Effects of Macelignan on Tau Phosphorylation and Aβ Aggregation in the Cell Model of Alzheimer's Disease. Front. Nutr. 9:892558. doi: 10.3389/fnut.2022.892558

Alzheimer's disease (AD) is a neurodegenerative disorder mainly affecting old population. In this study, two Tau overexpressing cell lines (SH-SY5Y/Tau and HEK293/Tau), N2a/SweAPP cell line, and 3×Transgene (APPswe/PS1M146V/TauP301L) mouse primary nerve cell lines were used as AD models to study the activity and molecular mechanism of macelignan, a natural compound extracted from *Myristica fragrans*, against AD. Our study showed that macelignan could reduce the phosphorylation of Tau at Thr 231 site, Ser 396 site, and Ser 404 site in two overexpressing Tau cell lines. It also could decrease the phosphorylation of Tau at Ser 404 site in mouse primary neural cells. Further investigation of its mechanism found that macelignan could reduce the phosphorylation of Tau by increasing the level of autophagy and enhancing PP2A activity in Tau overexpressing cells. Additionally, macelignan could activate the PERK/eIF2α signaling pathway to reduce BACE1 translation, which further inhibits the cleavage of APP and ultimately suppresses Aβ deposition in N2a/SweAPP cells. Taken together, our results indicate that macelignan has the potential to be developed as a treatment for AD.

Keywords: Alzheimer's disease, macelignan, AMPK pathway, autophagy, PERK/eIF2α pathway

INTRODUCTION

Alzheimer's disease (AD) is a neurodegenerative disorder with a global public fitness priority identified by the World Health Organization (1). In the past few decades, four United States Food and Drug Administration (FDA)-approved medications have been used for managing cognitive impairment and dysfunction symptoms of AD (2). However, these clinical medicines can only alleviate the symptom of AD rather than remedy it (3). There are presently >100 compounds in AD clinical trials (4). Although a lot have been known about the pathogenesis since the first report of AD in 1907 (5), there is no effective treatment to date. Searching for new treatment is still an on-going task for scientists and physicians.

The pathological features of AD encompass amyloid plaques, neurofibrillary tangles (NFTs), and neuroinflammation (6). Amyloid plaques and NFTs are typical pathological facets. NFTs mainly consist of intracellular paired helical filaments (PHFs) of the abnormal hyperphosphorylated form of tau protein (7). Under normal circumstances, Tau promotes the assembly and steadiness of microtubules and the transport of vesicles in neuro cells (8). When Tau encounters the released kinase, it is hyperphosphorylated. The hyperphosphorylated Tau further leads to Tau oligomerization. These hyperphosphorylated Tau are converted to a range of filaments, such as PHFs, which aggregate into NFTs (2). The existence of NFTs in the cytoplasm of neurons leads to the loss of communication and signal processing between neurons, causing neuronal apoptosis (9). Based on this, methylene blue has been used in an AD clinical trial with promising outcomes (10). The mechanism study in a tauopathy mouse model suggests that methylene blue could reduce Tau fibrillization and aggregation, and induce autophagy to alleviate neuron dying (11).

Amyloid plaques are formed through the precipitation of amyloid β-protein (Aβ) outside nerve cells. Aβ peptide is produced when β-amyloid precursor protein (APP) is sequentially cleaved by β-secretase and γ-secretase. The aberrancy cleavage of APP and the mutations of γ- and β-secretase all account for the abnormal manufacturing of Aβ peptide, which may increase the neuron loss and synaptic damage, and amyloid plaques (12). Many pharmaceutical companies have committed resources to develop Aβ-targeted drugs. However, many compounds, such as Verubecestat and Avagacestat, have failed in phase 3 clinical trials. Owing to the elusive pathogenesis of AD, the single-target anti-AD drugs appear to be unsuccessful based on failed clinical trials (13, 14). Hence, multi-target drugs are now proposed to fight against AD (15).

Natural compounds are gaining attention due to their bioactivities. *Myristica fragrans* (*M. fragrans*) is a tropical evergreen tree native to Indonesia and cultivated in India, Iran, the West Indies, and South America. Mace is the seed of nutmeg plant, *M. fragrans*, containing components such as flavonoids, neolignans, and lignans. Among these components, lignan has shown great therapeutic potential in various diseases (16). Macelignan (MLN, CAS 107534-93-0) is a sort of lignan derived from *M. fragrans* mace. Pharmacological studies have shown that MLN possesses a broad range of properties, such as anti-inflammatory (17), anti-cancer (18), anti-bacterial (19), and hepatoprotective activity (20). Studies have found that MLN could effectively reduce the hippocampal microglial activation induced by lipopolysaccharide in rat's brain, and suppress the spatial memory impairments caused by lipopolysaccharide in mice (21). Nevertheless, MLN's effect on the pathophysiology of AD is still unknown.

In this study, the anti-AD activity of MLN and its possible mechanism of action were investigated through Tau hyperphosphorylation and Aβ production in a number of AD cell models.

Abbreviations: AD, Alzheimer's disease; Aβ, amyloid β-protein; APP, β-amyloid precursor protein; AMPK, AMP-activated protein kinase; BSA, bovine serum albumin; CCK, cell counting kit; DAPI, 4′,6-Diamidino-2-Phenylindole, Dihydrochloride; DMEM, Dulbeco's modified Eagle's medium; FBS, fetal bovines serum; FDA, United States Food and Drug Administration; HEK293, human embryonic kidney 293; HRP, orseradish peroxidase; LC3, microtubule-associated protein II light chain3; LKB1, liver kinase B1; MLN, macelignan; mTOR1, mammalian target of rapamycin; NC, nitrocellulose filter; NFTs, neurofibrillary tangles; PBS, phosphate-buffered saline; PFA, paraformaldehyde; p-AMPK, phospho-AMPK; p-LKB1, phospho-LKB1; RIPA, radioimmunoprecipitation assay; SIRT1, silent information regulator of transcription 1; SPF, specific pathogen-free; ThT, thioflavin T.

MATERIALS AND METHODS

Materials

MLN was bought from Selleck Chem (Houston, TX, United States). Thioflavin T (ThT), Dimethyl Sulfoxide, Paraformaldehyde (PFA) and 4',6-Diamidino-2-Phenylindole (DAPI) were purchased from Sigma-Aldrich (St. Louis, MO, USA). Fetal bovine serum (FBS) was procured from Gibco (Grand Island, NY, USA). Gluta MAX, L-glutamine, B27 supplement, Dulbecco's Modified Eagle's medium (DMEM), trypsin, opti-MEM, penicillin, neurobasal medium, MEM Non-Essential Amino Acids Solution (MEM NEAA), and streptomycin were purchased from Biological Industries (Kibbutz Beit Haemek, Israel). Bicinchoninic acid (BCA), cell counting kit (CCK)-8 and cell lysis buffer were obtained from KeyGen Biotech (Nanjing, Jiangsu Province, China). Phosphate-buffered saline (PBS) and Hank's balanced salt solution (HBSS) were purchased from Hyclone (Logan, UT, USA). Antibodies of AMP-activated protein kinase [AMPK (2532)], p-AMPK (2535), liver kinase B1 [LKB1 (3047)], p-LKB1 (3482), silent information regulator of transcription 1 [SIRT1 (9475)], p62 (5114), Beclin-1 (3495), mechanistic target of rapamycin [mTOR 2983)], p-mTOR (2971), p70 S6K (2708), p-p70 S6K (9205), microtubule-associated protein II light chain3 [(LC3, 12741)], eIF2α (9722), p-eIF2α (9721), PERK(3192), p-PERK(3179) and β-actin (3700) were procured from Cell Signaling Technology (Beverly, MA, USA). Antibodies of Tau-5 (ab80579), pS396-Tau (ab109390), pS404-Tau (ab92676), pT231-Tau (ab151559), MAP2 (ab5392), PP2Aα (ab137825), PP2Aα + β (ab32104), APP (ab32136), BACE1 (ab2077) and horseradish peroxidase (HRP)-conjugated secondary antibodies were bought from Abcam (Cambridge, UK). Antibodies of Aβ (803002) was procured from Biologend (Signet, USA). Bovine serum albumin (BSA) and other chemical reagents used in this study were purchased from Shanghai Macklin Biochemical (Shanghai, China).

Cell Culture

SH-SY5Y/Tau cells were durably transfected with the longest human Tau 441 cDNA from human neuroblastoma SH-SY5Y cells (Shanghai Cell Bank of the Chinese Academy of Sciences, Shanghai, China). DMEM/F-12 medium blended with 10% FBS, 1% GlutaMAX, 1% MEM NEAA and 1mM sodium pyruvate were used to culture SH-SY5Y/Tau cells. Human embryonic kidney 293 (HEK293) cells with stable expression of the longest human Tau 441 cDNA were created and named as HEK293/Tau, a gift from Professor Jianzhi Wang of Tongji Medical College, Huazhong University of Science and Technology. HEK293/Tau

cells were cultured in the medium containing 90% DMEM, 10% FBS, and G-418 antibiotics (0.2 mg/mL). Swedish mutant APP overexpressed in mouse neuroblastoma N2a cells. The cells have been named N2a/SweAPP cells. The cell line was a gift and provided by Professor Yunwu Zhang from Xiamen University. N2a/SweAPP cells were cultured in 50% DMEM medium blended with 40% opti-MEM medium and 10% FBS. All cell culture media were added with 100 unit/mL penicillin and 100 μg/mL streptomycin. All cells were maintained under a humidified environment of 95% air and 5% CO_2 at 37 °C.

Primary Neuron Acquisition and Culture

Mice were stably transfected with mutant human APPswe,TauP301L genes and mutant mice gene PS1M146V (called 3 × Transgene-AD mouse) were bought from the Jackson Laboratory (JAX order number 3591206, Bar Harbor, ME, USA). The 3 × Transgene-AD mice were bred at 12 h mild 12 h darkish stipulations of specific pathogen-free (SPF) circumstances. All animal experiments were conducted with the approval of the Laboratory Animal Ethics Committee of Shenzhen University (Permit Number:SYXK 2014-0140) and in accordance with the guidelines and regulations for animal experiments. The hippocampus of the new-born (within 24 h) 3 × Transgene-AD mice was used to obtain the primary neuron cells. The pre-cold HBSS was used to wash the dissected hippocampal tissues, then hippocampal tissues were cut into small portions using a surgical blade. These fragments were transferred to a new plate containing papain (2 mg/mL) and digested for 30 min at 37°C. The digested cells were filtrated and then centrifuged at 1,000 *g* for 5 min. After discarding the supernatant, the cell pellets were resuspended in medium and plated on poly-L-lysine (0.1 mg/mL)-coated plates. A neurobasal medium containing 2% B27 supplement, 1% L-glutamine, 100 unit/mL penicillin, and 100 μg/mL streptomycin was used to culture the primary neuron cells in a humidified 5% CO_2 environment at 37°C.

Cell Viability Assay

Cells (5×10^3 cells/well) were incubated in a 96-well plate with different concentrations (0, 10, 15, and 20 μM) of MLN for 24 h. After the treatment, supernatant was removed, and 100 μL solution containing 10% CCK-8 solution and 90% DMEM medium was added to each well. The absorbance of each well was measured at 450 nm using a Spectra Max microplate reader (Thermo Scientific, Hudson, NH, USA) after 2 h incubation at 37°C.

Immunofluorescence Assay

Cells were uniformly seeded in confocal dishes, incubated overnight, and then stimulated with 20 μM MLN for 24 h. Cold PBS was used to rinse the cells for three times and then 4% PFA was added to cells at room temperature for 15 min. Cells were blocked by PBS solution containing 10% (w/v) goat serum and 0.1% Triton X-100 at room temperature for 1 h. After that, primary antibodies were added to the cells and incubated for 24 h at 4°C. Cells were then washed thrice with PBS and incubated for 1 h with Alexa Fluor-conjugated secondary antibody at the room temperature. Cell nuclei were stained with DAPI. Confocal microscope (Carl Zeiss, Thornwood, NY, USA) was used to examine the stained samples. Images were acquired and processed by using the ImageJ software (https://imagej.nih.gov/ij/).

Transmission Electron Microscopy Analysis

Samples containing R3-Tau (20 μM), and heparin (16 μM) were incubated for 24 h at 37 °C with or without MLN (20 μM). After the incubation, each sample was blanketed on a 230-mesh copper grid (Beijing Zhongjingkeyi Technology Co.) and incubated at room temperature for 2 min. Then, after washed twice with distilled water, 5 μL of 1% uranyl acetate (w/v, H_2O) was dropped on the copper mesh and stained for 1 min. Filter paper was used to remove unbond uranyl acetate. Samples were dried at room temperature. A JEM-1230 transmission electron microscope (JEOL, Tokyo, Japan) was used to obtain images of the samples at a magnification of 50,000x.

Thioflavin-T Fluorescence Assay

Freshly prepared R3-Tau, heparin, and ThT were dissolved in 50 mM PBS and blended with 5, 10, 15, 20 μM MLN, or Dimethyl Sulfoxide (Ctrl group). And Blank group was added with heparin, Dimethyl Sulfoxide and ThT. Each well of the cell seeding 96-well plate was added with 200 μL of the above mixture and incubated at 37°C. A microplate reader (Fluoroskan Ascent FL, Thermo Scientific) was used to excite the samples at 440 nm and record absorbance at 485 nm filter. The intensity of the fluorescence of each sample at one-of-a-kind time points was recorded.

Western Blot Analysis

After being treated with MLN, cells were gathered and washed with cold PBS three times. Cell lysis buffer containing 1% PMSF (100 mM), 1% protease, and phosphatase inhibitor was added to the cells on ice for 30 min. Protein concentrations of lysates were measured using the BCA kit. Proteins were then separated through SDS-PAGE. After strolling of SDS-PAGE, the proteins were transferred onto a nitrocellulose filter (NC) membrane (Merch/Millipore, Schwalbach, Germany). The NC membranes were blocked with 5% BSA solution for 1 h and incubated with primary antibodies for 24 h at 4°C. TBST (Tris-buffered saline, 0.1% Tween 20) solution was used to wash the membranes for three times. HRP-conjugated secondary antibody was added and incubated at the room temperature for 1 h. After washing membranes three times with TBST, the specific binding proteins were shown by LAS3000 luminescent image analyzer (Fujifilm Life Science, Tokyo, Japan) after adding an enhanced chemiluminescence solution.

Statistics

Results were presented as mean ± standard deviation (SD) of at least triplicate independent experiments in every group. Statistical analyses were carried out by using the GraphPad Prism 5.0 software (GraphPad Software, San Diego, CA, USA). Unpaired Student's-test was used for the comparison of two groups. The values of $^{*}\ p < 0.05$, $^{**}\ p < 0.01$, and $^{***}\ p < 0.001$, stand for statistically significant differences.

RESULTS

MLN Suppressed the Aggregation of Tau *in vitro*

Tau can be induced to form Tau fibers by heparin sodium *in vitro*, thus imitating the nerve fiber tangles formed by abnormal aggregation of Tau *in vivo*. Thioflavin T could bind to the beta structure of nerve fibers to emit fluorescence. In order to investigate the effects of MLN on Tau aggregation intuitively, we used the fluorescence assay of ThT and TEM. As shown in **Figure 1A**, the intensity of fluorescence of R3-Tau increased as time progress. In contrast, the intensity of fluorescence in the MLN treatment group was significantly suppressed in a concentration-dependent manner. The inhibition of R3-Tau aggregation by MLN could be more directly observed with TEM analysis. The TEM images confirmed that the nerve fiber tangles in the MLN were much less than that in the control (**Figure 1B**). Results of TEM and ThT experiments indicated that MLN had a suppression effect on Tau aggregation.

MLN Reduced Tau Phosphorylation in Tau Overexpressing Cells and 3 × Tg-AD Mouse Primary Neuron Cells

SH-SY5Y/Tau and HEK293/Tau cells are two nerve cell lines that could overexpress Tau. 3 × Tg-AD mouse primary neurons are able to fully simulate the pathological features of AD, hence are considered to be the ideal cell model for studying AD. In this study, the effects and the mechanism of MLN on Tau phosphorylation were investigated by using these cells. After being incubated with different concentrations (0, 5, 10, 15, 20 μM) of MLN for 24 h, the cell viability assay showed that MLN were not cytotoxic to both SH-SY5Y/Tau and HEK293/Tau cells (**Figure 2A**). Total Tau and phosphorylated Tau in SH-SY5Y/Tau, HEK293/Tau, and 3×Transgene-AD mouse primary neuron cells were measured. As shown in **Figures 2B,C**, the protein levels of pS396-Tau/Tau, pS404-Tau/Tau, and pT231-Tau/Tau were substantially diminished at a dose-dependent manner in Tau over-expressing cells. The immunofluorescence staining results were consistent with that of western blot (**Figure 2D**), which confirmed that MLN had an inhibitory effect on pS404-Tau expression in HEK293/Tau cells. Results in the 3×Transgene-AD mouse primary neurons were similar to that of Tau over-expressing cells. After treatment with 20 μM MLN, the intensity of green fluorescence, which represented the levels of pS404-Tau, in primary neuron cells was decreased significantly, and the total Tau showed no significant change, which suggests that MLN treatment can reduce phosphorylated Tau levels (**Figure 2E**).

MLN Promoted PP2A Activity in Tau Overexpressing Cells

PP2A is a kind of phosphatase that regulates the phosphorylation of Tau, which is closely related to the Alzheimer's disease (22). Studies have shown that sodium selenate could enhance PP2A activity and improve cognitive impairment in a PP2A-dependent manner in AD models with the aid of dysregulating Tau phosphorylation (23). The effects of MLN on PP2A activity was investigated in this study. Results were shown in **Figures 3A,B**. PP2A α and PP2A α + β activities were significantly enhanced at a concentration-dependent manner. In general, MLN treatment promotes PP2A activity in Tau over-expressing cells.

MLN Enhanced Autophagy in Tau Overexpressing Cells

Autophagy is an essential degradation pathway in mammalian cells to eliminate abnormal protein aggregation and accountable for protein homeostasis and neuronal health. Autophagy is associated with many neurodegenerative diseases (24). Beclin-1, LC3 and p62 are usually regarded as specific markers of autophagy, and the adjustments in their expression are often associated with the changes in autophagy. In this study, the effects of MLN on autophagy was investigated. As shown in **Figures 4A,B**, the expressions of Beclin-1 and LC3 II/LC3 I increased significantly by MLN treatment, while the expression of p62 decreased. These autophagy-related protein expression adjustments demonstrated that MLN could activate autophagy.

MLN Activated the AMPK/MTOR Signal Pathway to Enhance Autophagy

To understand the mechanism by which MLN activates autophagy, the related signal pathways were investigated. Cell extracts from SH-SY5Y/Tau and HEK293/Tau were analyzed using Western blot for the expression and phosphorylation level of AMPK, mTOR, and p70 S6K. As shown in **Figure 4C**, the protein levels of p-AMPK increased in a dose-dependent manner with MLN treatment. The phosphorylation of mTOR and p70 S6K were dose-dependently reduced. However, the expressions of AMPK, mTOR, and p70 S6K showed no significant changes. These changes indicated that MLN could upregulate the AMPK/mTOR signal pathway to promote autophagy. AMPK is a vital nutrient sensor. The changes in AMPK phosphorylation are always linked to energy metabolism. Thus, the variations in the AMPK upstream regulation proteins SIRT1 and LKB1 were examined. As shown in **Figures 4C,D**, the protein levels of SIRT1 and p-LKB1 increased when treated with MLN. In summary, after MLN treatment, the AMPK/mTOR signal pathway in SH-SY5Y and HEK293/Tau cells were upregulated, which activated the cellular level of autophagy.

MLN Enhanced PERK/eIF2α Signal Pathway to Decline Aβ Aggregation in N2a/SweAPP Cells

Since Aβ deposition is one of pathogenesis in AD, the effects of MLN on Aβ in N2a/SweAPP cells were investigated. After incubating with one of the concentrations (0, 5, 10, 15, 20 μM) of MLN for 24 h, N2a/SweAPP cell viability was measured, which indicated that MLN was not cytotoxic (**Figure 5A**). Then, the expressions of Aβ and APP in N2a/SweAPP were examined using Western blot assay. Results showed that MLN decreased APP and Aβ expression in a dose-dependent manner (**Figures 5B,C**). Immunofluorescence staining results were consistent with that of Western blot, which confirmed that MLN had a downregulation effect on Aβ (**Figure 5D**). Next, the mechanism of Aβ inhibition

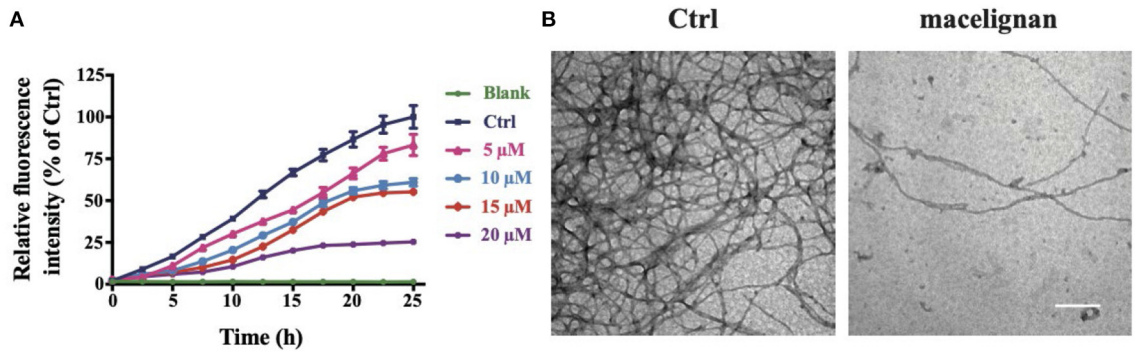

FIGURE 1 | Macelignan (MLN) inhibits Tau aggregation *in vitro*. **(A)** The effects of MLN on real-time ThT fluorescence intensity detection of R3-Tau. **(B)** The effects of MLN (20 μM) on R3-Tau aggregation by TEM images. Scale bar = 500 nm.

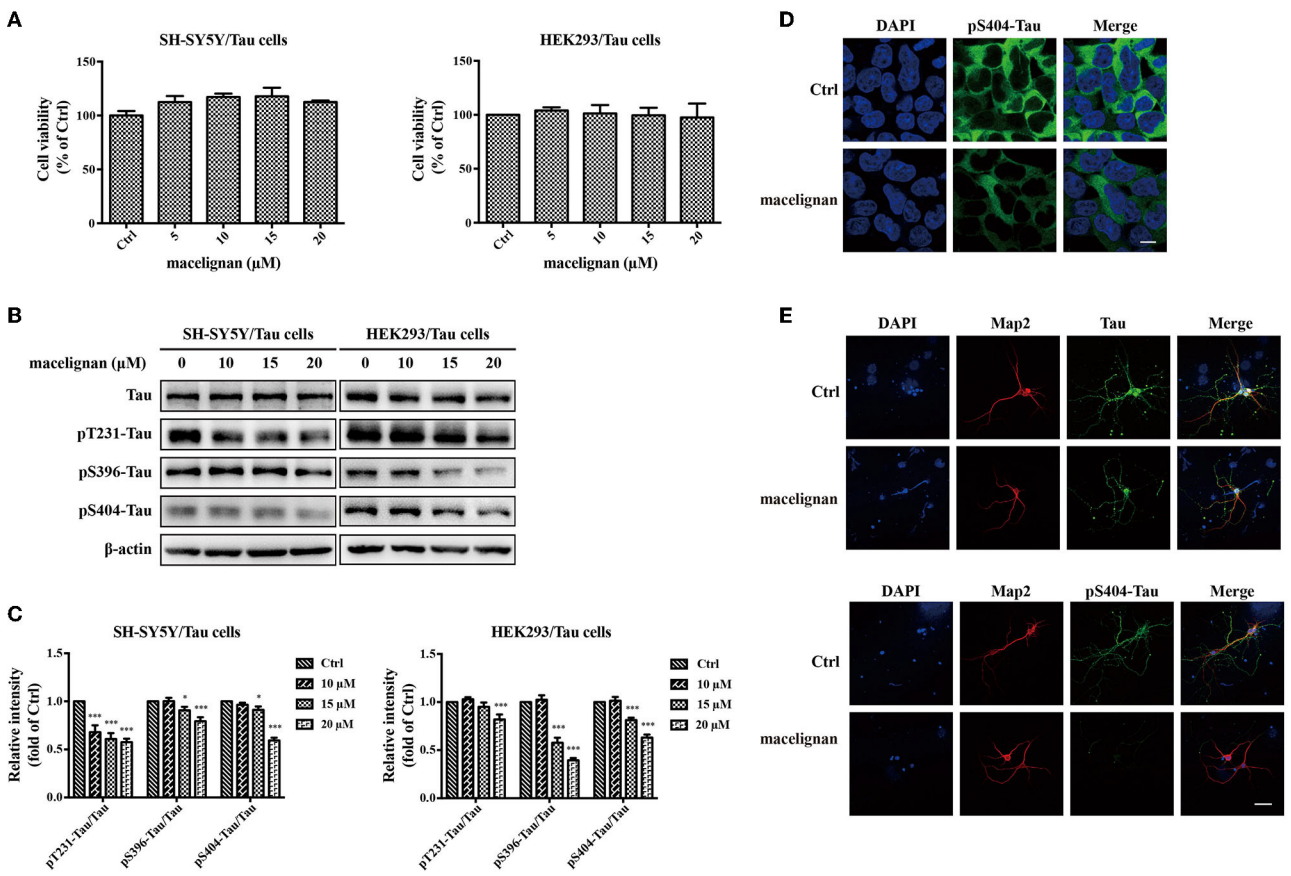

FIGURE 2 | Macelignan (MLN) inhibits Tau phosphorylation in Tau overexpressing cells and 3×Transgene-AD mouse primary neuron cells. **(A)** SH-SY5Y/Tau and HEK 293/Tau cells were incubated in serial concentrations of MLN (0, 5, 10, 15, and 20 μM) for 24 h and then the effect of MLN on cell viability was measured by the CCK-8 assay. **(B)** The effect of MLN on the protein levels of Tau, pS396-Tau, pS404-Tau and pT231-Tau in Tau over-expressing cells were determined by Western blot analysis. **(C)** The protein relative intensity of Tau, pS396-Tau, pS404-Tau, pT231-Tau in Tau over-expressing cells was shown. β-actin was used as a loading control in the Western blot analysis. All results were from independent triplicate experiments, $^{*}p < 0.05$, $^{**}p < 0.01$, and $^{***}p < 0.001$ vs. control. Immunofluorescence staining was used to show the effect of MLN on Tau and its phosphorylation. DAPI (in blue) was used to stain the nuclei. Map2 (in red) and Tau or pS404-Tau (in green) were stained using their antibodies. **(D)** The staining results in HEK/293 cells (scale bar=10 μm) were shown. **(E)** The staining results in primary neuron cells (Scale bar=50 μm) were shown.

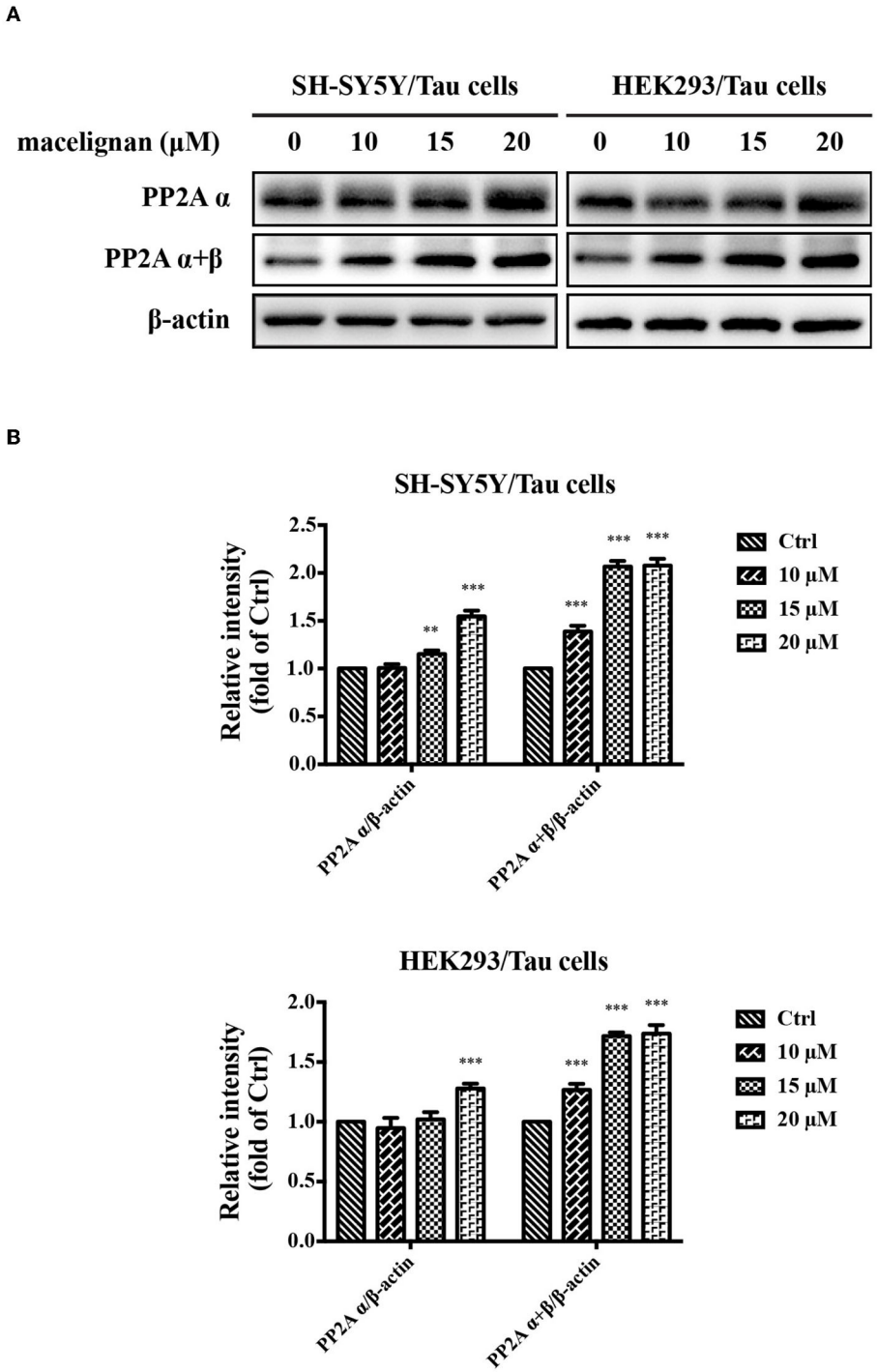

FIGURE 3 | Macelignan (MLN) promotes PP2A activity in Tau overexpressing cells. **(A)** SH-SY5Y/Tau and HEK293/Tau cells were added with series concentrations of MLN (0, 10, 15 and 20 μM) for 24 h, and then the effects of MLN on the levels of PP2A α and PP2A α + β were determined using Western blot analysis. **(B)** The protein relative intensity of PP2A α and PP2A α + β in Tau over-expressing cells were shown. β-actin was used as a loading control in the Western blot analysis. All results were from three independent experiments, $^{*}p < 0.05$, $^{**}p < 0.01$, and $^{***}p < 0.001$ vs. control.

was explored. Considering that BACE1 is the key rate-limiting enzyme (25) accountable for Aβ deposition and the PERK/eIF2α signal pathway is highly drawn into BACE1 translation (26), whether MLN regulates PERK/eIF2α signal pathway to reduce Aβ deposition was investigated. As shown in **Figures 5E,F**, the phosphorylation of PERK and eIF2α in N2a/SweAPP

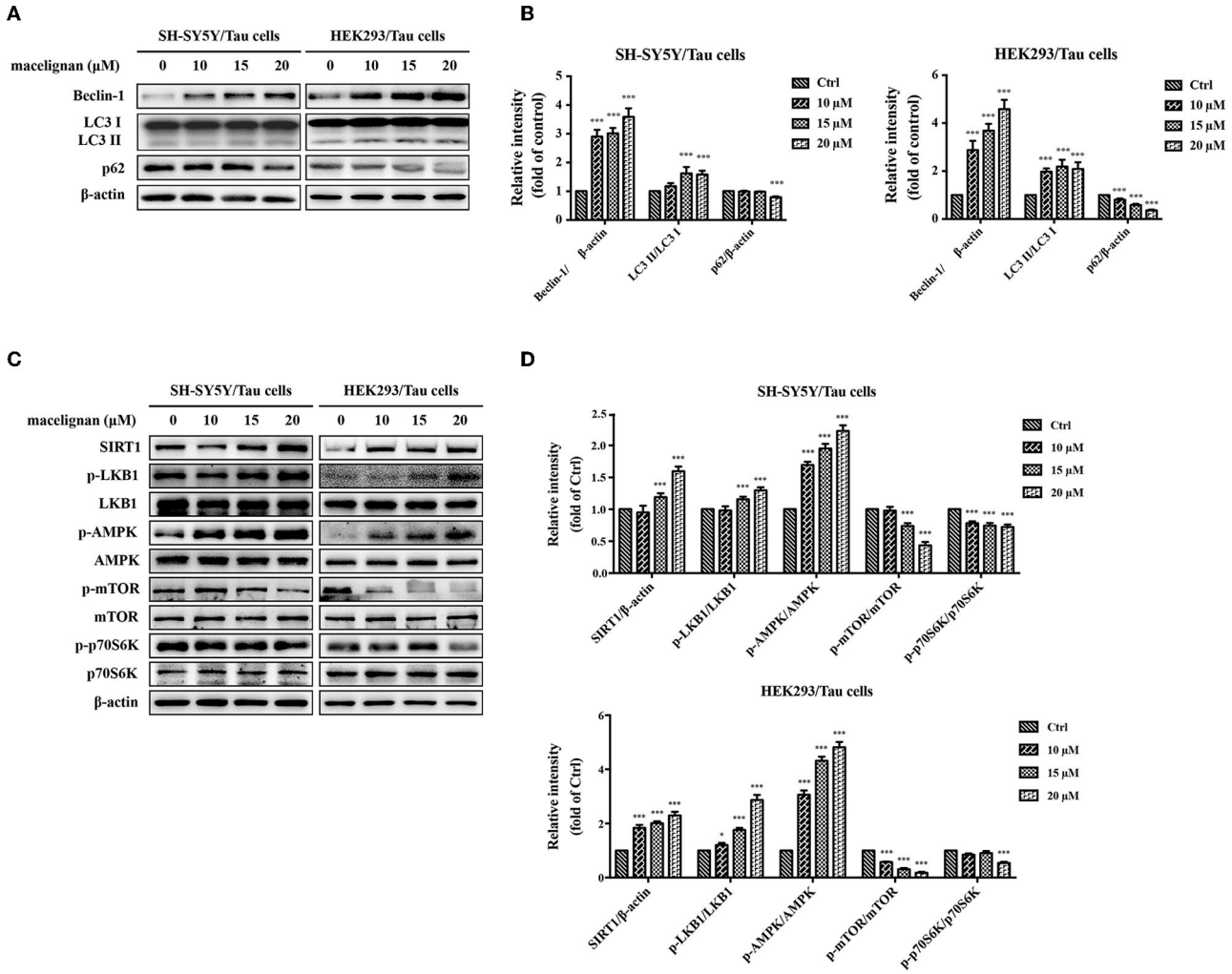

FIGURE 4 | Macelignan (MLN) enhances autophagy in Tau overexpressing cells. SH-SY5Y/Tau and HEK293/Tau cells were incubated with series concentrations of MLN (0, 10, 15 and 20 μM) for 24 h and then their effects on the levels of autophagy-related proteins (Beclin-1, LC3, p62) were measured by Western blot analysis and presented in **(A)**. The differences of relative intensity of those proteins were shown in **(B)**. Effects of MLN on the AMPK/mTOR pathway-related protein (SIRT1, LKB1, AMPK, mTOR, p70S6K) were measured by Western blot and shown in **(C)**. The differences of relative intensity of those proteins were shown in **(D)**. β-actin was used as a loading control in the Western blot analysis. All results were from three independent experiments, $^{*}p < 0.05$, $^{**}p < 0.01$, and $^{***}p < 0.001$ *vs.* control.

cells decreased after MLN treatment. Taken together, the Aβ deposition, expression of APP, and phosphorylation of PERK and eIF2α were all decreased in a dose-dependent manner in N2a/SweAPP cells with the treatment of MLN.

DISCUSSION

Recent statistics show that 6.2 million Americans have AD and will increase to 13.8 million by 2060 (27). Although some clinical drugs can alleviate the symptoms of AD, there is no cure. In the present research, it is found that MLN had a good anti-AD potential through reducing Tau phosphorylation and decreasing Aβ aggregation.

Here, it was observed that MLN could decrease the R3-Tau's ThT fluorescence intensity at a dose-dependent manner and inhibit the aggregation of Tau *in vitro*, which were comparable to the results of a previous study (28), suggesting MLN has neuroprotective effects. It was additionally noticed that the phosphorylation of Tau was significantly reduced at Ser 404 site in primary cortical neurons and a significant decrease in phosphorylated Tau at Ser 396, Ser 404, and Thr 231 site in SH-SY5Y/Tau and HEK293/Tau cells in response to MLN treatment. Nerve fiber tangles caused by abnormally excessive ranges of phosphorylation of Tau are one of the typical pathological aspects of AD (2). It is known that under normal circumstances, Tau exists in neurons, induces the microtubule bunching, maintains microtubule stability, and normalize axonal transport of nerves

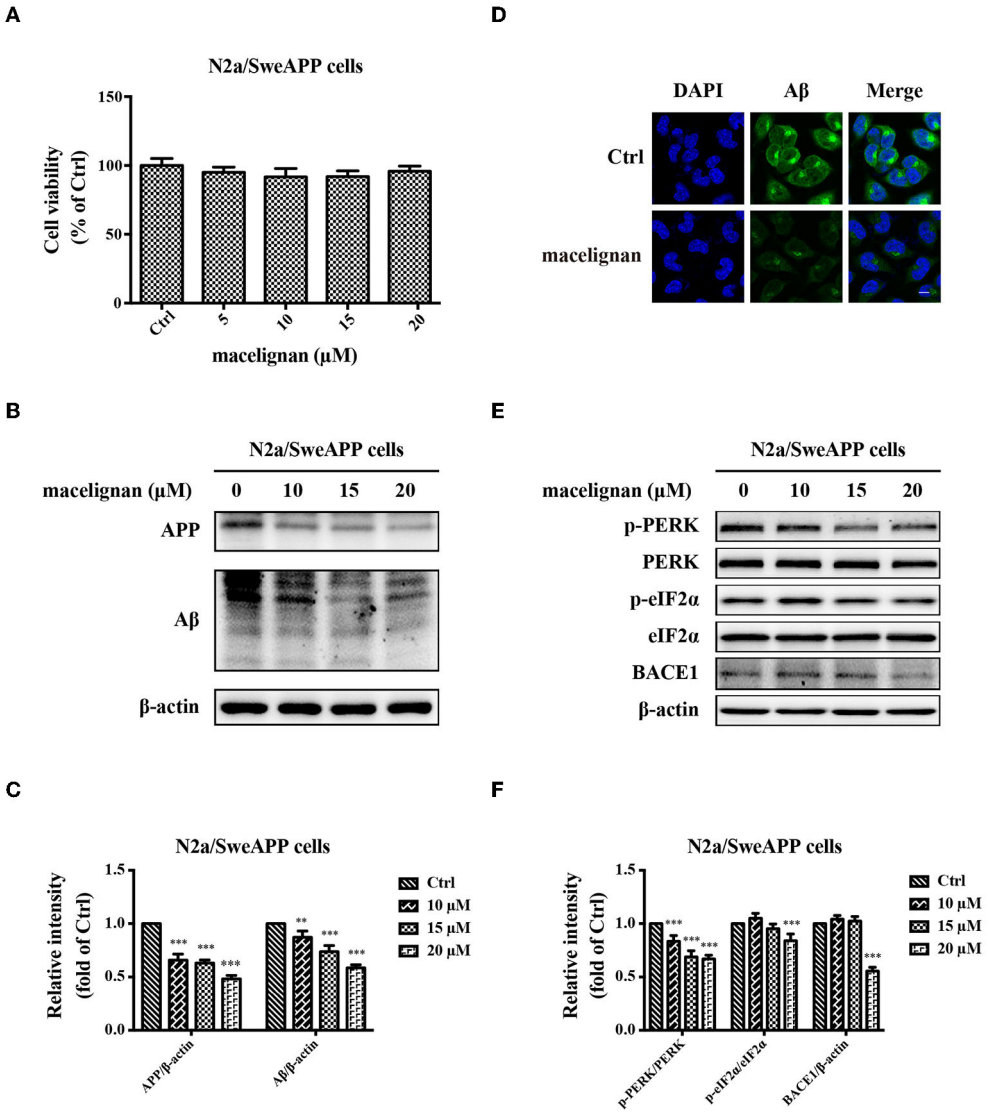

FIGURE 5 | Maceglinan (MLN) decreases Aβ production in N2a/SweAPP cells. **(A)** The effects of macelignan on N2a/SweAPP cell viability were measured by CCK-8 assay. **(B)** N2a/SweAPP cells were added with series concentrations of MLN (0, 5, 10, 15 and 20 μM) for 24 h and then the effects of MLN on the expression of APP and Aβ were determined by Western blot analysis, and the differences in protein relative intensity were shown in **(C)**. **(D)** Immunofluorescence staining was used to show the effects of MLN on Aβ. DAPI (in blue) was used to stain the nuclei, and Aβ (in green) was stained by using Aβ antibody. Scale bar=10 μm. **(E)** eIF2α and PERK were analyzed by using Western blot assay. And **(F)** The differences of relative intensity of p-PERK/PERK, p-eIF2α/eIF2α, and BACE1 bands were shown. β-actin was used as a loading control in the Western blot analysis. All results were from independent triplicate experiments, $^{*}p < 0.05$, $^{**}p < 0.01$, and $^{***}p < 0.001$ vs. control.

(29). When hyperphosphorylation happens to Tau, its bound affinity to microtubules and depolymerization decrease (30). It has been reported that decreasing Tau hyperphosphorylation has been considered as an approach to improve cognition (31). Our present study found that MLN could reduce the expression of Tau phosphorylation, which may further inhibit Tau aggregation and the formation of nerve fiber tangles.

It has been suggested that a number of post-translational changes of Tau play an important function in the aggregation of Tau linked to AD, and Tau phosphorylation is the primary one amongst those post-translational modifications (32). The disruption of the balance between Tau kinase and phosphatase activities is considered the cause of the unusual Tau phosphorylation (33). Decrease in phosphatase activity is related to ordinary phosphorylation and aggregation of Tau in AD (34). PP2A is a kinase related to Tau phosphorylation, consisting of a structural A subunit (α and β subtypes), a highly variable regulatory subunit B, and a catalytic C subunit (α and β subtypes) (35, 36). Previous studies have proven that the inhibition of PP2A activity results in Tau hyperphosphorylation and spatial memory deficiency (37), which indicates that PP2A might be a therapeutic target for AD. In the present study, we

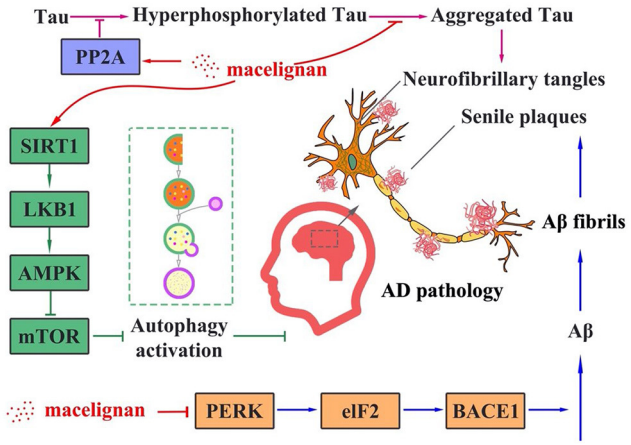

FIGURE 6 | The proposed molecular mechanism of macelignan on anti-Alzheimer's Disease activity.

demonstrated that the treatment of MLN could enhance the activity of PP2A, which may contribute to the downregulation of Tau phosphorylation.

Previous studies have proven autophagy can manage the renewal of soluble cytoplasmic proteins, as a result decreasing the accumulation of atypical proteins, which prevents neurodegenerative diseases (11, 38, 39). Further studies have found that the expression of Beclin-1 is significantly reduced in Beclin-1-deficient transgenic mice, which leads to a decrease of autophagy in neurons which is the reason for neurodegenerative diseases (40). LC3 is one of the biomarkers of autophagy, which is crucial for forming autophagosomes during autophagy (41). Another biomarker of autophagy, p62, can interact with LC3 to remove protein aggregation (42). Our research found that levels of LC3 and Beclin-1 were increased, and p62 was decreased in SH-SY5Y/Tau and HEK293/Tau cells after the treatment of MLN. AMPK is a vital energy sensor in cells. Some studies found that the downregulation of AMPK may relate to neurodegenerative diseases such as AD (43). Our results showed that MLN could upregulate AMPK phosphorylation, further downregulating the expression of p-mTOR and p-p70S6K to activate autophagy in Tau overexpressing cells. Previous studies found that the activation of SIRT1 in the brain could modulate amyloid neuropathology in the AD brain (44), and other studies also indicated that SIRT1 could regulate the AMPK/mTOR pathway (45). LKB1 is an upstream enzyme of AMPK, which regulates the activation of AMPK through phosphorylation (46). Our results showed that MLN could stimulate SIRT1 to activate LKB1 phosphorylation, which further promotes phosphorylated AMPK expression. This suggests that MLN could stimulate SIRT1 and LKB1, the upstream enzymes of AMPK. In turn, this results in AMPK activation to improve cellular energy metabolism, which promotes autophagy to decrease the hyperphosphorylation of Tau. All those ultimately prevent phosphorylated Tau to form NFTs.

Recently, multi-target strategy against AD has become a research focus. We thereby hypothesize that apart from Tau phosphorylation inhibition, MLN may have an effect on amyloid plaques as well. To explore this effect, we used N2a/SweAPP cells, which overexpress APP as well as BACE1 and Aβ. We showed that MLN could decrease Aβ and APP expression in N2a/SweAPP cells. Endoplasmic reticulum performs many critical cellular functions in the body, including protein homeostasis and lipid formation. When proteins in the endoplasmic reticulum are misfolded, they trigger endoplasmic reticulum stress, which in response makes phosphorylated eIF2α to induce the timely closure of protein synthesis to protect cells (47). However, hyperphosphorylation of eIF2α can persistently inhibit the translation of protein synthesis, which may lead to synaptic failure, accompanied by abnormal expression of synaptic proteins, and ultimately cause neurodegenerative changes and memory deficits (48). A previous study verified that *Thamnolia vermicularis* extracts could diminish the phosphorylation of PERK and eIF2α in CHO-APP/BACE1 cells and astrocytes, which indicates that the response to the misfolded protein is involved in the amyloid plaque formation (49). Our results are consistent with the previous findings, showing that MLN can decrease the phosphorylation of PERK and eIF2α to reduce BACE1 expression. Therefore, we conclude that MLN can activate the misfolded protein response-related signal pathway to reduce BACE1 translation, which further inhibits the cleavage of APP and ultimately suppresses Aβ deposition.

A previous study has demonstrated that MLN has a neuroprotective property by assuaging neuroinflammation (50). Different from this result, our results illustrate that MLN could improve AD via reduction of both Tau hyperphosphorylation and Aβ aggregation. Taken all results together, the proposed molecular mechanism for MLN in AD treatment is that MLN could activate PP2A and SIRT1/AMPK/mTOR signaling-mediated autophagy to reduce Tau phosphorylation. In the meantime, it also activates the PERK/eIF2α signal pathways to suppress Aβ deposition. The summarized molecular mechanism is shown in **Figure 6**.

CONCLUSION

In summary, our results show that MLN can inhibit both Tau hyperphosphorylation and Aβ production, which indicates that MLN has the potential to be developed as a treatment for AD.

DATA AVAILABILITY STATEMENT

The original contributions presented in the study are included in the article/supplementary material, further inquiries can be directed to the corresponding authors.

AUTHOR CONTRIBUTIONS

XX and JL: conceptualization and supervision. LG, NC, ML, and DB: data curation. LG, NC, LY, WF, and YW: formal

analysis. ZH, XX, and JL: funding acquisition. LG, NC, QL, and ZL: investigation. LG, NC, and XX: methodology and writing–original draft. ZH, QL, XX, and JL: resources. JL: writing–review and editing. All authors gave final approval and agreed to be accountable for all aspects of the work.

FUNDING

This work was supported by the National Natural Science Foundation of China (32172193, 31970366, and 41876188), National Key R&D Program of China (2018YFD0901106 and 2018YFA0902500), the Science and Technology Innovation Commission of Shenzhen (JCYJ20190808141415052), Medical Scientific Research Foundation of Guangdong Province of China (A2021219), and Grant Plan for Demonstration City Project for Marine Economic Development in Shenzhen (No. 86). Royal Society of New Zealand Catalyst Seeding Fund (21-AUT-005-CSG).

ACKNOWLEDGMENTS

The authors would like to thank the Instrumental Analysis Center of Shenzhen University for their assistance in our experiments.

REFERENCES

1. Lane CA, Hardy J, Schott JM. Alzheimer's disease. *Eur J Neurol.* (2018) 25:59–70. doi: 10.1111/ene.13439
2. Long JM, Holtzman DM. Alzheimer disease: an update on pathobiology and treatment strategies. *Cell.* (2019) 179:312-39. doi: 10.1016/j.cell.2019.09.001
3. Salloway S, Sperling R, Fox NC, Blennow K, Klunk W, Raskind M, et al. Two phase 3 trials of bapineuzumab in mild-to-moderate Alzheimer's disease. *N Eng J Med.* (2014) 370:322–33. doi: 10.1056/NEJMoa1304839
4. Hara Y, McKeehan N, Fillit HM. Translating the biology of aging into novel therapeutics for Alzheimer disease. *Neurology.* (2019) 92:84–93. doi: 10.1212/WNL.0000000000006745
5. Trejo-Lopez JA, Yachnis AT, Prokop S. Neuropathology of Alzheimer's disease. *Neurotherapeutics.* (2021). doi: 10.1007/s13311-021-01146-y
6. Briggs R, Kennelly SP, O'Neill D. Drug treatments in Alzheimer's disease. *Clin Med.* (2016) 16:247–53. doi: 10.7861/clinmedicine.16-3-247
7. Eftekharzadeh B, Daigle JG, Kapinos LE, Coyne A, Schiantarelli J, Carlomagno Y, et al. Tau protein disrupts nucleocytoplasmic transport in Alzheimer's disease. *Neuron.* (2018) 99:925–40. doi: 10.1016/j.neuron.2018.07.039
8. Querfurth HW, LaFerla FM. Alzheimer's disease. *N Engl J Med 362.* (2010) 329–44. doi: 10.1056/NEJMra0909142
9. Uddin MS, Tewari D, Mamun AA, Kabir MT, Niaz K, Wahed MII, et al. Circadian and sleep dysfunction in Alzheimer's disease. *Ageing Res Rev.* (2020) 60:101046. doi: 10.1016/j.arr.2020.101046
10. Gauthier S, Feldman HH, Schneider LS, Wilcock GK, Frisoni GB, Hardlund JH, et al. Efficacy and safety of tau-aggregation inhibitor therapy in patients with mild or moderate Alzheimer's disease: a randomised, controlled, double-blind, parallel-arm, phase 3 trial. *Lancet.* (2016) 388:2873–84. doi: 10.1016/S0140-6736(16)31275-2
11. Congdon EE, Wu JW, Myeku N, Figueroa YH, Herman M, Marinec PS, et al. Methylthioninium chloride (methylene blue) induces autophagy and attenuates tauopathy in vitro and in vivo. *Autophagy.* (2012) 8:609–22. doi: 10.4161/auto.19048
12. Bergmans BA, De Strooper B. γ-secretases: from cell biology to therapeutic strategies. *Lancet Neurol.* (2010) 9:215–26. doi: 10.1016/S1474-4422(09)70332-1
13. Doody RS, Thomas RG, Farlow M, Iwatsubo T, Vellas B, Joffe S, et al. Phase 3 trials of solanezumab for mild-to-moderate Alzheimer's disease. *N Eng J Med.* (2014) 370:311–21. doi: 10.1056/NEJMoa1312889
14. Fan L-Y, Chiu M-J. Combotherapy and current concepts as well as future strategies for the treatment of Alzheimer's disease. *Neuropsychiatr Dis Treat.* (2014) 10:439. doi: 10.2147/NDT.S45143
15. Benek O, Korabecny J, Soukup O. A perspective on multi-target drugs for alzheimer's disease. *Trends Pharmacol Sci.* (2020) 41:434–45. doi: 10.1016/j.tips.2020.04.008
16. Paul S, Hwang JK, Kim HY, Jeon WK, Chung C, Han J-S. Multiple biological properties of macelignan and its pharmacological implications. *Arch Pharm Res.* (2013) 36:264–72. doi: 10.1007/s12272-013-0048-z
17. Jung YW, Lee BM, Ha MT, Tran MH, Kim JA, Lee S, et al. Lignans from Saururus chinensis exhibit anti-inflammatory activity by influencing the Nrf2/HO-1 activation pathway. *Arch Pharm Res.* (2019) 42:332–43. doi: 10.1007/s12272-018-1093-4
18. Thuong PT, Hung TM, Khoi NM, Nhung HT, Chinh NT, Quy NT, et al. Cytotoxic and anti-tumor activities of lignans from the seeds of Vietnamese nutmeg Myristica fragrans. *Arch Pharm Res.* (2014) 37:399–403. doi: 10.1007/s12272-013-0185-4
19. Yogiara H, wang SJ, Park S, Hwang JK, Pan JG. Food-grade antimicrobials potentiate the antibacterial activity of 1,2-hexanediol. *Lett Appl Microbiol.* (2015) 60:431–9. doi: 10.1111/lam.12398
20. Sohn JH, Han KL, Kim J-H, Rukayadi Y, Hwang J-K. Protective effects of macelignan on cisplatin-induced hepatotoxicity is associated with JNK activation. *Biol Pharm Bull.* (2008) 31:273–7. doi: 10.1248/bpb.31.273
21. Cui C-A, Jin D-Q, Hwang YK, Lee I-S, Hwang JK, Ha I, et al. Macelignan attenuates LPS-induced inflammation and reduces LPS-induced spatial learning impairments in rats. *Neurosci Lett.* (2008) 448:110–4. doi: 10.1016/j.neulet.2008.10.035
22. Voronkov M, Braithwaite SP, Stock JB. Phosphoprotein phosphatase 2a: a novel druggable target for Alzheimer's disease. *Future Med Chemist.* (2011) 3:821–33. doi: 10.4155/fmc.11.47
23. Clark AR, Ohlmeyer M. Protein phosphatase 2A as a therapeutic target in inflammation and neurodegeneration. *Pharmacol Ther.* (2019) 201:181–201. doi: 10.1016/j.pharmthera.2019.05.016
24. Menzies FM, Fleming A, Rubinsztein DC. Compromised autophagy and neurodegenerative diseases. *Nat Rev Neurosci.* (2015) 16:345–57. doi: 10.1038/nrn3961
25. Ghosh AK, Osswald HL. BACE1 (β-secretase) inhibitors for the treatment of Alzheimer's disease. *Chemical Soc Rev.* (2014) 43:6765–813. doi: 10.1039/C3CS60460H
26. O'Connor T, Sadleir KR, Maus E, Velliquette RA, Zhao J, Cole SL, et al. Phosphorylation of the translation initiation factor eIF2α increases BACE1 levels and promotes amyloidogenesis. *Neuron.* (2008) 60:988–1009. doi: 10.1016/j.neuron.2008.10.047
27. Alzheimer's disease facts and figures. *Alzheimers Dement.* (2021) 17:327–406. doi: 10.1002/alz.12328
28. Cai N, Chen J, Bi D, Gu L, Yao L, Li X, et al. Specific degradation of endogenous tau protein and inhibition of tau fibrillation by tanshinone IIA through the Ubiquitin-proteasome pathway. *J Agric Food Chem.* (2020) 68:2054–62. doi: 10.1021/acs.jafc.9b07022
29. Duan AR, Jonasson EM, Alberico EO, Li C, Scripture JP, Miller RA, et al. Interactions between tau and different conformations of tubulin: implications for tau function and mechanism. *J Mol Biol.* (2017) 429:1424–38. doi: 10.1016/j.jmb.2017.03.018
30. Alonso AD, Cohen LS, Corbo C, Morozova V, ElIdrissi A, Phillips G, et al. Hyperphosphorylation of tau associates with changes in its

function beyond microtubule stability. *Front Cell Neurosci.* (2018) 12:338. doi: 10.3389/fncel.2018.00338
31. Congdon EE, Sigurdsson EM. Tau-targeting therapies for Alzheimer disease. *Nat Rev Neurol.* (2018) 14:399–415. doi: 10.1038/s41582-018-0013-z
32. Martin L, Latypova X, Terro F. Post-translational modifications of tau protein: implications for Alzheimer's disease. *Neurochemist Int.* (2011) 58:458–71. doi: 10.1016/j.neuint.2010.12.023
33. Martin L, Latypova X, Wilson CM, Magnaudeix A, Perrin M-L, Terro F. Tau protein phosphatases in Alzheimer's disease: the leading role of PP2A. *Ageing Res Rev.* (2013) 12:39–49. doi: 10.1016/j.arr.2012.06.008
34. Gong C-X, Iqbal K. Hyperphosphorylation of microtubule-associated protein tau: a promising therapeutic target for Alzheimer disease. *Current medicinal chemistry.* (2008) 15:2321–8. doi: 10.2174/092986708785909111
35. Cho US, Xu W. Crystal structure of a protein phosphatase 2A heterotrimeric holoenzyme. *Nature.* (2007) 445:53–7. doi: 10.1038/nature05351
36. O'Connor CM, Perl A, Leonard D, Sangodkar J, Narla G. Therapeutic targeting of PP2A. *Int J Biochem Cell Biol.* (2018) 96:182–93. doi: 10.1016/j.biocel.2017.10.008
37. Shentu YP, Huo Y, Feng XL, Gilbert J, Zhang Q, Liuyang ZY, et al. CIP2A Causes Tau/APP phosphorylation, synaptopathy, and memory deficits in Alzheimer's Disease. *Cell Rep.* (2018) 24:713–23. doi: 10.1016/j.celrep.2018.06.009
38. Nixon RA. The role of autophagy in neurodegenerative disease. *Nat Med.* (2013) 19:983–97. doi: 10.1038/nm.3232
39. Sarkar S, Davies JE, Huang Z, Tunnacliffe A, Rubinsztein DC. Trehalose, a novel mTOR-independent autophagy enhancer, accelerates the clearance of mutant huntingtin and alpha-synuclein. *J Biol Chem.* (2007) 282:5641–52. doi: 10.1074/jbc.M609532200
40. Pickford F, Masliah E, Britschgi M, Lucin K, Narasimhan R, Jaeger PA, et al. The autophagy-related protein beclin 1 shows reduced expression in early Alzheimer disease and regulates amyloid β accumulation in mice. *J Clin Invest.* (2008) 118:2190–9. doi: 10.1172/JCI33585
41. Bernard A, Klionsky DJ. Defining the membrane precursor supporting the nucleation of the phagophore. *Autophagy.* (2014) 10:1–2. doi: 10.4161/auto.27242
42. Perez SE, He B, Nadeem M, Wuu J, Ginsberg SD, Ikonomovic MD, et al. Hippocampal endosomal, lysosomal, and autophagic dysregulation in mild cognitive impairment: correlation with Aβ and tau pathology. *J Neuropathol Experiment Neurol.* (2015) 74:345–58. doi: 10.1097/NEN.0000000000000179
43. Vingtdeux V, Chandakkar P, Zhao H, d'Abramo C, Davies P, Marambaud P. Novel synthetic small-molecule activators of AMPK as enhancers of autophagy and amyloid-β peptide degradation. *FASEB J.* (2011) 25:219–31. doi: 10.1096/fj.10-167361
44. Zhang Z, Shen Q, Wu X, Zhang D, Xing D. Activation of PKA/SIRT1 signaling pathway by photobiomodulation therapy reduces Aβ levels in Alzheimer's disease models. *Aging Cell.* (2020) 19:e13054. doi: 10.1111/acel.13054
45. Jung TY, Ryu JE, Jang MM, Lee SY, Jin GR, Kim CW, et al. Naa20, the catalytic subunit of NatB complex, contributes to hepatocellular carcinoma by regulating the LKB1-AMPK-mTOR axis. *Exp Mol Med.* (2020) 52:1831–44. doi: 10.1038/s12276-020-00525-3
46. Hardie DG, Ross FA, Hawley SA. AMPK: a nutrient and energy sensor that maintains energy homeostasis. *Nat Rev Mol Cell Biol.* (2012) 13:251–62. doi: 10.1038/nrm3311
47. Naidoo N, Brown M. The endoplasmic reticulum stress response in aging and age-related diseases. *Front physiol.* (2012) 3:263. doi: 10.3389/fphys.2012.00263
48. Erguler K, Pieri M, Deltas C. A mathematical model of the unfolded protein stress response reveals the decision mechanism for recovery, adaptation and apoptosis. *BMC Syst Biol.* (2013) 7:16. doi: 10.1186/1752-0509-7-16
49. Li C, Guo X-d, Lei M, Wu J-y, Jin J-z, Shi X-f, et al. Thamnolia vermicularis extract improves learning ability in APP/PS1 transgenic mice by ameliorating both Aβ and Tau pathologies. *Acta Pharmacol Sinica.* (2017) 38:9–28. doi: 10.1038/aps.2016.94
50. Jin D-Q, Lim CS, Hwang JK, Ha I, Han J-S. Anti-oxidant and anti-inflammatory activities of macelignan in murine hippocampal cell line and primary culture of rat microglial cells. *Biochem biophys res commun.* (2005) 331:1264–9. doi: 10.1016/j.bbrc.2005.04.036

Conflict of Interest: The authors declare that the research was conducted in the absence of any commercial or financial relationships that could be construed as a potential conflict of interest.

Publisher's Note: All claims expressed in this article are solely those of the authors and do not necessarily represent those of their affiliated organizations, or those of the publisher, the editors and the reviewers. Any product that may be evaluated in this article, or claim that may be made by its manufacturer, is not guaranteed or endorsed by the publisher.

frontiers | Frontiers in Nutrition

ORIGINAL RESEARCH
published: 24 May 2022
doi: 10.3389/fnut.2022.888745

Citrus Peel Flavonoid Extracts: Health-Beneficial Bioactivities and Regulation of Intestinal Microecology *in vitro*

*Ping Li, Xu Yao, Qingqing Zhou, Xia Meng, Tao Zhou and Qing Gu**

Key Laboratory for Food Microbial Technology of Zhejiang Province, College of Food Science and Biotechnology, Zhejiang Gongshang University, Hangzhou, China

Citrus peel and its extracts are rich in flavonoids, which are beneficial to human health. In this study, the extraction, component analysis, biological activity and intestinal microbiota regulation of citrus peel flavonoid extracts (CPFEs) were investigated. CPFEs from 14 Chinese cultivars were purified by ultrasound-assisted extraction and XAD-16 macroporous resin. The total flavonoid content of lemon was greatest at 103.48 ± 0.68 mg/g dry weight (DW) by $NaNO_2$-$Al(NO_3)_3$-NaOH spectrophotometry. Using high-performance liquid chromatography–diode array detection, the highest concentrations of naringin, hesperidin and eriocitrin were found in grapefruit (52.03 ± 0.51 mg/g DW), chachiensis (43.02 ± 0.37 mg/g DW) and lemon (27.72 ± 0.47 mg/g DW), respectively. Nobiletin was the most polymethoxylflavone in chachiensis at 16.91 ± 0.14 mg/g DW. CPFEs from chachiensis and grapefruit had better antioxidant activity, α-glucosidase inhibitory and sodium glycocholate binding ability. In addition, chachiensis and grapefruit CPFEs had positive effects on intestinal microecology, as evidenced by a significant increase in the relative abundance of *Bifidobacterium* spp., and production of short-chain fatty acids, especially acetic acid, by a simulated human intestinal model. Collectively, our results highlight the biological function of CPFEs as prebiotic agents, indicating their potential use in food and biomedical applications.

Keywords: citrus peel, flavonoid, bioactivity, intestinal microbiota, short-chain fatty acids

OPEN ACCESS

Edited by:
Gengjun Chen,
Kansas State University, United States

Reviewed by:
Biao Yuan,
China Pharmaceutical University, China
Antonella Smeriglio,
University of Messina, Italy

****Correspondence:***
Qing Gu
guqing2002@hotmail.com

Specialty section:
This article was submitted to Nutrition and Food Science Technology, a section of the journal Frontiers in Nutrition

Received: *03 March 2022*
Accepted: *28 April 2022*
Published: *24 May 2022*

Citation:
Li P, Yao X, Zhou Q, Meng X, Zhou T and Gu Q (2022) Citrus Peel Flavonoid Extracts: Health-Beneficial Bioactivities and Regulation of Intestinal Microecology in vitro. Front. Nutr. 9:888745. doi: 10.3389/fnut.2022.888745

INTRODUCTION

Citrus fruits of the family Rutaceae are popular with consumers around the world, and large numbers are processed industrially. However, a high proportion of waste is generated by industrial citrus processing because of the thick, inedible peel and large inedible seeds. In recent years, citrus by-products have been used in animal feed production or in the extraction of biofunctional components such as pectin, essential oils and flavonoids (1, 2). The development of citrus by-products into high value-added dietary supplements can not only produce functional foods with health benefits but also help to solve the environmental pollution caused by citrus peel landfills and processing wastewater (3).

Citrus peel forms around 40%−50% of the total fruit mass, and is a substantial source of biologically-active substances that enhance health, especially flavonoids (4). The total flavonoid content (TFC) is mainly composed of flavanones and polymethoxylflavones (PMFs),

including naringin, hesperidin, narirutin, nobiletin and neohesperidin (5). The most abundant flavonoids vary between different citrus fruits; for example, mandarins and hybrids contain more hesperidin, pummelos contain more naringin, and lemon has the most eriocitrin (6, 7). The major flavonoid from *Citrus unshiu* peel is quercetagetin (8) and anthocyanin is only found in blood oranges (9). Flavonoids in citrus peel are recognized as a good source of dietary antioxidants, and protect cells by hydrogen transfer, free radical scavenging, and divalent metal ion chelation (10). They also help to regulate metabolic syndrome and type 2 diabetes, as manifested by α-glucosidase inhibition, insulin sensitization and decreased blood lipid levels (11). The compositions of flavonoids are closely related to the biological properties. The content of hesperidin in *C. unshiu* peel extracts was positively correlated with the antioxidant activity; hesperetin and naringenin were related to the inhibition of xanthine oxidase and α-glucosidase activities (12).

There is accumulating evidence that dietary flavonoids influence the microbial population of human colon (13). Most dietary flavonoids are poorly absorbed from the small intestine and up to 90% of these compounds are metabolized by the intestinal microflora in the colon (14). Flavonoid and its metabolites interact with the intestinal microflora by inhibiting the growth of pathogenic bacteria and promoting that of beneficial bacteria, and regulate the production of short-chain fatty acids (SCFAs), secondary bile acids and tryptophan metabolites, thereby contributing to maintenance of intestinal homeostasis (15). SCFAs, mainly acetic, propionic and butyric acids, are generated by fermentation of soluble dietary fiber by the gut microbiota, which facilitates nutrient absorption, energy metabolism, maintenance of the intestinal mucosal barrier and strong immunity (15–17). However, limited data suggest that different CPFEs differentially affect gut microbiota composition and abundance, and subsequently alter SCFAs production. Such differences may be related to the main flavonoid components in different CPFEs.

Animal models have been used to study the effects of dietary flavonoids on the intestinal microflora. Supplemental feeding with naringenin (the aglycone of naringin) attenuated colon damage and inflammation symptoms in a dextran sulfate sodium-induced murine model of colitis, suggesting that naringin helps maintain the integrity of the intestinal wall, by protecting the intestinal tight junction barrier (18). Human studies of gut microorganisms *in vivo* are not usually ethically and economically feasible, so *in vitro* simulated human intestinal models have been proposed as an alternative method to study the relationships between the intestinal microbial composition and food components.

In this study, we selected 14 representative citrus cultivars in China and purified CPFEs with ultrasound-assisted extraction and macroporous resin. Quantitatively analysis of 11 components in different CPFEs was performed by high-performance liquid chromatography-diode array detection (HPLC-DAD). We further analyzed the antioxidant, α-glucosidase inhibition and bile salt binding capacity of CPFEs, and their potential effects on microbial composition and SCFAs production were characterized using an *in vitro* simulated human intestinal model.

MATERIALS AND METHODS

Experimental Reagents

Rutin, eriocitrin, naringin, hesperidin, didymin, poncirin, naringenin, hesperitin, sinensetin, nobiletin, tangeretin, α-glucosidase (from *Saccharomyces cerevisiae*), acarbose and 5-O-demethylnobiletin were from Yuanye Bio-Technology Co., Ltd. (Shanghai, China). Tryptone and yeast extract were from Oxoid Co., Ltd. (Basingstoke, UK). Acetic acid, propionic acid, butyric acid, isobutyric acid, valeric acid, and isovaleric acid were from Dr. Ehrenstorfer (Augsburg, Germany). Sodium glycocholate was from Sigma-Aldrich Co., Ltd. (St. Louis, MO, USA). Other reagents and solvents were analytical grade, from Sinopharm Chemical Reagents Co., Ltd. (Shanghai, China).

Extraction of Flavonoids From Citrus Peel

Fresh citrus fruits were purchased from local suppliers in China (**Supplementary Table 1**). Flavonoid extracts were prepared by ultrasound-assisted extraction and clean-up on hydrophobic macroporous resin XAD-16, as described previously, with some modifications (19). Citrus peel powder was dried at 40°C for 48 h and then dispersed in 52% ethanol (material-to-liquid ratio of 1 g/42 ml). Ethanol was added to the extract at a final concentration of 80% (v/v) after 17 min of ultrasonic extraction at 325 w. The crude flavonoids were obtained by centrifuging at 8,000 *g* for 15 min after standing at 4°C for 12 h, retaining the supernatant and removing the ethanol by rotary evaporation under 60°C (Buchi R-300, Switzerland). The crude flavonoid extract at a concentration of 107 μg/ml (2 column volumes) was loaded onto the column of macroporous resin XAD-16 at a flow rate of 1.5 ml/min, then eluted with 50% (v/v) ethanol solution (5 column volumes). CPFEs were concentrated by rotary evaporation and then freeze dried (Alpha 1–4 LSC, Martin Christ, Osterode, Germany) for further analysis.

Citrus Flavonoid Compositions of CPFEs

TFC Determination

The TFC of CPFEs were measured using the $NaNO_2/Al(NO_3)_3/NaOH$ spectrophotometric method (20). In brief, 1.00 ml of CPFEs, 0.30 ml of 5% $NaNO_2$ (m/v) and 1.00 ml of 60% ethanol (v/v) were added into a volumetric flask and stored at room temperature for 6 min. 0.30 ml of 10% $Al(NO_3)_3$ (m/v) was added and incubated for another 6 min, then 2.00 ml of 1 M NaOH was added. After incubating for 10 min at room temperature, the absorbance was measured at 510 nm by SpectraMax 190 Microplate Reader (Molecular Devices, San Jose, CA). TFC values were expressed as rutin equivalents (mg) per gram DW.

Flavonoid Compositions Analysis

Eleven flavonoids were identified in CPFEs by an Agilent 1260 Infinity HPLC system (Agilent Technologies, Santa Clara, CA, USA) coupled with DAD and a Sun FireTM C18 column (4.6 × 150 mm I. D. × 5 μm, Phenomenex, Torrance, CA) at room

temperature. The mobile phases consisted of 0.1% acetic acid (A) and acetonitrile (B). The initial phase composition was 15% B, then ramped linearly to 25% B at 5 min, 30% B at 15 min, 40% B at 25 min, 55% B at 35 min, 60% B at 40 min and back to 15% B at 45 min, at a flow rate of 0.7 ml/min. The main flavanones (eriocitrin, naringin, hesperidin, didymin, poncirin, naringenin, and hesperitin) and PMFs (sinensetin, nobiletin, tangeretin, and 5-O-demethylnobiletin) were quantified by comparison with authentic standard solutions at detection wavelengths of 283 and 330 nm, respectively.

Antioxidant Capacity of CPFEs

Antioxidant capacity was determined by the 2,2-diphenyl-1-picrylhydrazyl (DPPH) free radical scavenging activity, 2,2′-azino-bis (3-ethylbenzthiazoline-6-sulfonic acid; ABTS) free radical scavenging activity, ferric reducing antioxidant power (FRAP), and cupric reducing antioxidant capacity (CUPRAC) methods, and expressed as mg Trolox equivalent (TE) per gram DW (21). The total antioxidant potency composite (APC) index was the average of antioxidant index of above four methods, and calculated as described previously: APC index = (measure score/maximum score) × 100% (20).

DPPH Determination

The DPPH free radical scavenging activity was determined as described previously with minor modifications (22). A mixture of DPPH (0.20 mM, 1 ml) and CPFE (5.00 mg/ml, 80 μl) was incubated at 25°C in the dark for 30 min, then the absorbance recorded at 517 nm (SpectraMax 190 Microplate Reader, USA).

ABTS Determination

ABTS index was tested by an ABTS method kit (Nanjing Jiancheng Bioengineering Co. Ltd., China). ABTS working solution was prepared with detection buffer, ABTS stock solution and peroxide solution (diluted 40 times with PBS, pH 7) at a ratio of 76:5:4 (v/v/v). Ten microliter of the sample solution (5 mg/ml) was mixed with 170 μl of ABTS working solution and 20 μl of peroxidase (diluted 10 times with detection buffer) thoroughly for 6 min, and the absorbance was recorded at 405 nm.

FRAP Determination

Ferric reducing antioxidant power was determined by a total antioxidant capacity assay kit (Nanjing Jiancheng Bioengineering Co. Ltd., China), following the manufacturer's instructions. CPFE (5 mg/ml, 5 μl) was mixed with FRAP radical solution (180 μl) and incubated in the dark for 5 min at 37°C then the absorbance was recorded at 593 nm.

CUPRAC Determination

The CUPRAC assay was performed as described previously (23). The assay mixture, of $CuCl_2$ (0.01 M, 500 μl), neocuproine (0.075 M, 500 μl), ammonium acetate buffer (1 M, pH 7.0, 500 μl) and CPFE (5 mg/ml, 60 μl) was incubated at 25°C for 1 h, transferred to a 96-well microplate, then the absorbance recorded at 450 nm.

α-Glucosidase Inhibition Assay

α-Glucosidase inhibition was determined as described previously with some modifications (15). A mixture of CPFE (10 mg/ml, 50 μl) and of α-glucosidase (2 U, pH 6.8, 250 μl) was incubated at 37°C for 10 min. *p*-nitrophenyl glucoside (*p*NPG, 5 mM, 250 μl) was added and incubated for 10 min. Na_2CO_3 (0.20 mM, 450 μl) was added to stop the reaction. The reaction mixture was transferred to a 96-well plate (200 μl per well) and the absorbance measured at 405 nm. Acarbose (α-glucosidase inhibitor/diabetes treatment, 12.5 μM) was used as the positive control. The percentage inhibition of α-glucosidase was calculated according to the following formula:

$$\alpha - \text{glucosidase inhibition } (\%) = \left[1 - \frac{(OD_s - OD_b) - OD_a}{OD_s - OD_b}\right] \times 100\%, \quad (1)$$

where:

$$OD_s : \text{sample} + \alpha - \text{glucosidase} + p\text{NPG} + OD_{\text{after reaction}},$$
$$OD_b : \text{sample} + \alpha - \text{glucosidase} + \text{buffer} + OD_{\text{after reaction}},$$
$$OD_a : \text{acarbose} + \alpha - \text{glucosidase} + p\text{NPG} + OD_{\text{after reaction}}.$$

Bile Salt Binding Capacity Determination Assay

Salt binding capacity was calculated by a standard curve with sodium glycocholate as bile acid (24). A mixture of CPFEs (10 mg/ml, 1 ml) and pepsin (10 mg/ml, 1 ml) was incubated in an orbital shaker at 120 rpm and 37°C for 1 h, and then the pH was adjusted to 6.3 with NaOH (0.10 M). Trypsin (10 mg/ml, 4 ml) and salt solutions (1 mM, 4 ml) were added and incubated for 1 h. Precipitated material was removed by centrifugation (4,000 g, 20 min), supernatant (2.5 ml) and H_2SO_4 (60% v/v, 7.5 ml) were mixed and heated at 70°C for 25 min, then cooled in an ice bath for 5 min. The reaction mixture was transferred to a 96-well plate and the absorbance was recorded at 387 nm.

Fecal Sample Collection and Processing

Fecal samples were collected from seven healthy volunteers (three males and four females, numbered 1–7) according to the following criteria: (1) aged from 20 to 35, (2) a body mass index of 18.5–23.9 kg/m^2, (3) normal diet and not vegetarian, (4) no history of bowel disorders, (5) no antibiotics or probiotics used in the previous 6 months. All donors were provided written informed consent, and the study was approved by the Ethics Committee of the Zhejiang Gongshang University and Zhejiang Academy of Agricultural Sciences (Zhejiang Province, China). Fresh fecal samples were immediately collected, weighed and diluted in anaerobic, sterile phosphate-buffered saline (PBS, pH 7, 0.10 M) to prepare 10% fecal homogenate suspensions (w/v).

Simulated Intestinal Fermentation *in vitro*

Each culture consisted of sterilized VIS medium (5 ml) (25), fecal suspension (500 μl), and CPFE sample (0.10 g/ml, 500 μl). PBS (500 μl) instead of CPFE solution was used as the blank control. Anaerobic fermentation (10% H_2, 10% CO_2 and 80% N_2) was

performed at 37°C in an anaerobic workstation (DG250, Don Whitley Scientific, Bingley, UK). After 24 h, fecal fermentation suspension (1 ml) was collected in an Eppendorf tube for DNA sequencing and SCFA concentration determination.

DNA Extraction and Sequencing

Genomic DNA was extracted from the fecal fermentation suspension with a QIAamp PowerFecal DNA extraction kit, according to the manufacturer's instructions. 16S rDNA gene high-throughput sequencing of the V3–V4 region was performed by Biomarker Bio-Tech Co., Ltd. (Beijing, China), with an Illumina MiSeq platform. Sequencing primers were 338F (forward primer, ACTCCTACGGGAGGCAGCAG) and 806R (reverse primer, GGACTACHVGGGTWTCTAAT). Analysis was performed using the SILVA database, to assign operational taxonomic units (OTUs) with 97% similarity. Based on the OTU analysis, intestinal microbial richness and diversity were evaluated by Alpha diversity (Ace, Chao, Simpson and Shannon) using the Uparse and Mothur software systems. The bacterial community composition among groups was analyzed at the levels of phylum, class, order, family and genus. Differentially abundant taxa were identified by the linear discriminant analysis (LDA) effect size (LEfSe) with LDA score of 4.0.

Determination of SCFAs

The contents of acetic, propionic, butyric, isobutyric, valeric and isovaleric acid in fermentation samples were measured by gas chromatography-mass spectrometry (GC–MS) (26). The identification and quantification of chromatographic peaks was achieved by comparison with authentic standards, with crotonic acid (20 mM) as the internal standard. Fermentation medium (500 μl) were mixed with crotonic acid metaphosphate solution (100 μl), and frozen at −30°C for 24 h. The solution was thawed and centrifuged at 8,000 g and 4°C for 3 min, then filtered using a 0.22-μm membrane (Millipore, Burlington, MA). Sample (1 μl) was injected into a GC system fitted with a DB-FFAP GC column (30 m × 0.25 mm I. D. × 0.25 μm, Agilent, China) and H_2 flame ionization detector. The initial column temperature was 75°C, then increased to 180°C, at 20°C /min and maintained for 1 min, then increased to 220°C at 50°C/min, maintained for 1 min. Both injector and detector temperatures were 250°C. The flow rates of carrier gas N_2, make-up gas H_2, and air were 20, 30, and 300 ml/min, respectively.

Statistical Analysis

All data were expressed as mean ± standard deviation. The significant differences among samples were analyzed using *T*-test, one-way ANOVA and Tukey's test. The value of $P < 0.05$ was considered as statistically significant. Statistical analysis and figuring drawing were carried out using SPSS 22.0 (IBM, Armonk, NY) and GraphPad Prism 8.0 (GraphPad Software Inc., San Diego, CA, USA).

RESULTS

TFC and Flavonoid Compositions of CPFEs

The TFC values of 14 CPFEs from different Chinese citrus fruits such as mandarins, oranges, pummelos, kumquats, hybrids and citrons were determined (**Table 1**). Lemon had the highest TFC (103.48 ± 0.68 mg/g DW), followed by satsuma orange (96.22 ± 0.51 mg/g DW), chachiensis (86.54 ± 0.63 mg/g DW), grapefruit (72.82 ± 1.56 mg/g DW) and fertile orange (67.98 ± 0.86 mg/g DW). Bergamot had the lowest concentration at 27.62 ± 1.25 mg/g DW.

The contents of seven major flavanones (eriocitrin, naringin, hesperidin, didymin, poncirin, naringenin, and hesperitin) and four PMFs (sinensetin, nobiletin, tangeretin, and 5-O-demethylnobiletin) presented significant variation among 14 citrus cultivars (**Table 1**), calculated by standard curves using HPLC-DAD (**Supplementary Table 2**). HPLC chromatograms of the standards are shown in **Figure 1**. Naringin, hesperidin and eriocitrin were the major flavanones, as previously reported (27–29). Abundant naringin was in the CPFEs from grapefruit (52.03 ± 0.51 mg/g DW), majia pomelo (44.57 ± 0.74 mg/g DW), and apple pomelo (40.62 ± 0.14 mg/g DW). However, there was little naringin in the CPFEs from satsuma mandarin, chachiensis, lemon and bergamot. Hesperidin was abundant in the CPFEs from mandarins (satsuma mandarin, chachiensis and ponkan), sweet oranges (lane late navel oranges and blood orange) and hybrids (dekopon and fertile orange), all exceeding 35.00 mg/g DW. In CPFEs from apple pomelo, grapefruit, sichuan kumquat, longyan kumquat and bergamot, the contents of hesperidin were <3.50 mg/g DW. The greatest content of eriocitrin was detected in lemon (27.72 ± 0.47 mg/g DW), and lowest in ponkan (0.47 ± 0.01 mg/g DW). Poncirin was highest in CPFEs (11.67 ± 0.06 mg/g DW), and naringenin was not found in detected mandarin, pummelo and kumquat species.

Compared with flavanones, most CPFEs had lower PMF levels. The contents of sinensetin, nobiletin and tangeretin in chachiensis were the highest at 2.31 ± 0.00 mg/g DW, 16.91 ± 0.14 mg/g DW, and 1.59 ± 0.01 mg/g DW, respectively, followed by satsuma orange (1.61 ± 0.00 mg/g DW, 5.90 ± 0.01 mg/g DW, and 3.87 ± 0.01 mg/g DW) and lane late navel orange (1.84 ± 0.02 mg/g DW, 5.67 ± 0.01 mg/g DW, and 0.73 ± 0.00 mg/g DW). Nobiletin was proved to be the most dominant PMF in mandarins and sweet oranges. The principal PMFs found in grapefruit were tangeretin and nobiletin (27), but our results show that these two PMFs were almost nonexistent. 5-O-Demethylnobiletin was only detected in satsuma mandarin at 0.34 ± 0.00 mg/g DW, but not in most citrus varieties.

Beneficial Biological Activities of CPFEs

The antioxidant capacity of CPFEs was measured by four separate assays, namely, DPPH, ABTS, FRAP and CUPRAC (**Table 2**). The DPPH values varied from 17.51 ± 0.34 mg TE/g DW (bergamot) to 55.12 ± 0.08 mg TE/g DW (satsuma orange). There was no significant change in ABTS assay with the other three methods. The highest ABTS radical ability was found in majia pomelo. The CPFEs of mandarins and hybrids presented significantly higher FRAP and CUPRAC

TABLE 1 | Contents of total flavonoids, flavanones and PMFs in CPFEs (mg/g DW).

Cultivar	TFC	Flavanones							PMFs			
		Eri	Nar	Hed	Did	Pon	Nag	Het	Sin	Nob	Tan	DN
Satsuma mandarin	96.22 ± 0.51^{b}	2.76 ± 0.09^{f}	0.19 ± 0.01^{i}	41.33 ± 0.21^{b}	4.97 ± 0.02^{b}	0.42 ± 0.00^{c}	ND	0.13 ± 0.00^{g}	1.61 ± 0.00^{d}	5.90 ± 0.01^{b}	3.87 ± 0.01^{a}	0.34 ± 0.00^{a}
Chachiensis	86.54 ± 0.63^{c}	1.93 ± 0.04^{g}	0.17 ± 0.03^{i}	43.02 ± 0.37^{a}	2.55 ± 0.01^{d}	0.09 ± 0.00^{f}	ND	0.05 ± 0.00^{h}	2.31 ± 0.00^{b}	16.91 ± 0.14^{a}	1.59 ± 0.01^{b}	ND
Ponkan	67.17 ± 0.67^{e}	0.47 ± 0.01^{i}	22.86 ± 0.15^{e}	42.05 ± 0.11^{b}	0.70 ± 0.01^{f}	11.67 ± 0.06^{a}	ND	0.29 ± 0.00^{c}	0.06 ± 0.00^{h}	1.33 ± 0.01^{d}	0.28 ± 0.00^{e}	0.04 ± 0.00^{b}
Lane late navel orange	53.45 ± 0.59^{h}	5.71 ± 0.03^{d}	4.57 ± 0.03^{g}	40.16 ± 0.23^{c}	1.24 ± 0.16^{e}	0.43 ± 0.01^{c}	0.26 ± 0.01^{a}	1.37 ± 0.03^{a}	1.84 ± 0.02^{c}	5.67 ± 0.01^{b}	0.73 ± 0.00^{c}	0.08 ± 0.00^{b}
Blood orange	60.71 ± 0.63^{g}	0.96 ± 0.02^{h}	2.24 ± 0.16^{h}	35.07 ± 0.12^{e}	2.55 ± 0.06^{d}	0.23 ± 0.07^{d}	0.09 ± 0.00^{d}	0.07 ± 0.00^{h}	0.16 ± 0.00^{g}	0.59 ± 0.00^{e}	0.17 ± 0.00^{f}	0.03 ± 0.00^{b}
Apple pomelo	50.60 ± 0.80^{i}	1.74 ± 0.53^{g}	40.62 ± 0.14^{c}	1.77 ± 0.13^{h}	0.08 ± 0.01^{i}	0.15 ± 0.01^{e}	ND	0.20 ± 0.00^{e}	ND	0.11 ± 0.00^{g}	ND	ND
Majia pomelo	52.27 ± 0.39^{h}	2.80 ± 0.03^{f}	44.57 ± 0.74^{b}	1.84 ± 0.37^{h}	0.33 ± 0.01^{g}	0.09 ± 0.01^{f}	ND	0.05 ± 0.00^{h}	0.18 ± 0.00^{g}	0.30 ± 0.00^{f}	0.02 ± 0.00^{g}	ND
Grapefruit	72.82 ± 1.56^{d}	4.91 ± 0.11^{e}	52.03 ± 0.51^{a}	ND	0.07 ± 0.00^{i}	0.16 ± 0.01^{e}	ND	0.05 ± 0.00^{h}	ND	0.04 ± 0.00^{h}	ND	ND
Dekopon	62.33 ± 1.07^{f}	0.95 ± 0.01^{h}	29.56 ± 0.51^{d}	39.25 ± 0.91^{c}	4.49 ± 0.16^{c}	1.23 ± 0.06^{c}	0.15 ± 0.00^{c}	0.23 ± 0.04^{d}	2.66 ± 0.05^{a}	1.77 ± 0.01^{c}	0.04 ± 0.00^{g}	ND
Fertile orange	67.98 ± 0.86^{e}	4.78 ± 0.10^{e}	10.97 ± 0.45^{f}	37.35 ± 0.38^{d}	10.50 ± 0.04^{a}	0.38 ± 0.09^{c}	0.18 ± 0.01^{b}	0.07 ± 0.00^{h}	0.13 ± 0.01^{g}	0.34 ± 0.00^{f}	0.04 ± 0.00^{g}	ND
Lemon	103.48 ± 0.68^{a}	27.72 ± 0.47^{a}	0.02 ± 0.00^{j}	24.51 ± 0.18^{f}	0.19 ± 0.01^{h}	0.07 ± 0.00^{f}	0.03 ± 0.00^{f}	0.08 ± 0.01	0.69 ± 0.00^{f}	0.32 ± 0.00^{f}	ND	ND
Sichuan kumquat	30.85 ± 0.56^{k}	9.29 ± 0.20^{b}	1.96 ± 0.08^{h}	0.49 ± 0.00^{j}	1.52 ± 0.01^{e}	ND	0.10 ± 0.00^{d}	0.74 ± 0.00^{b}	0.87 ± 0.00^{e}	0.12 ± 0.00^{g}	0.04 ± 0.00^{g}	ND
Longyan kumquat	32.47 ± 0.96^{j}	5.70 ± 0.92^{d}	11.40 ± 0.27^{f}	3.11 ± 0.12^{g}	0.62 ± 0.02^{f}	1.69 ± 0.02^{b}	ND	0.18 ± 0.00^{f}	0.93 ± 0.00^{e}	1.93 ± 0.00^{c}	0.38 ± 0.00^{d}	0.03 ± 0.00^{b}
Bergamot	27.62 ± 1.25^{l}	8.55 ± 0.02^{c}	0.16 ± 0.00^{i}	3.18 ± 0.01^{g}	0.17 ± 0.00^{h}	0.24 ± 0.00^{d}	0.07 ± 0.01^{e}	0.08 ± 0.01^{h}	ND	0.46 ± 0.00^{e}	ND	ND

TFC, total flavonoid content; Eri, eriocitrin; Nar, naringin; Hed, hesperidin; Did, didymin; Pon, poncirin; Nag, naringenin; Het, hesperitin; Sin, sinensetin; Nob, nobiletin; Tan, tangeretin; DN, 5-O-demethyl-nobiletin.
Results were the mean ± SD (n = 3) on a dried weight (g) of citrus peel flavonoid extracts. Flavonoid contents were calculated as mg rutin equivalents (RE)/g DW. ND, not detected. Different letters above the error bars in the same column indicate significant differences among varieties based on Tukey's test ($P < 0.05$).

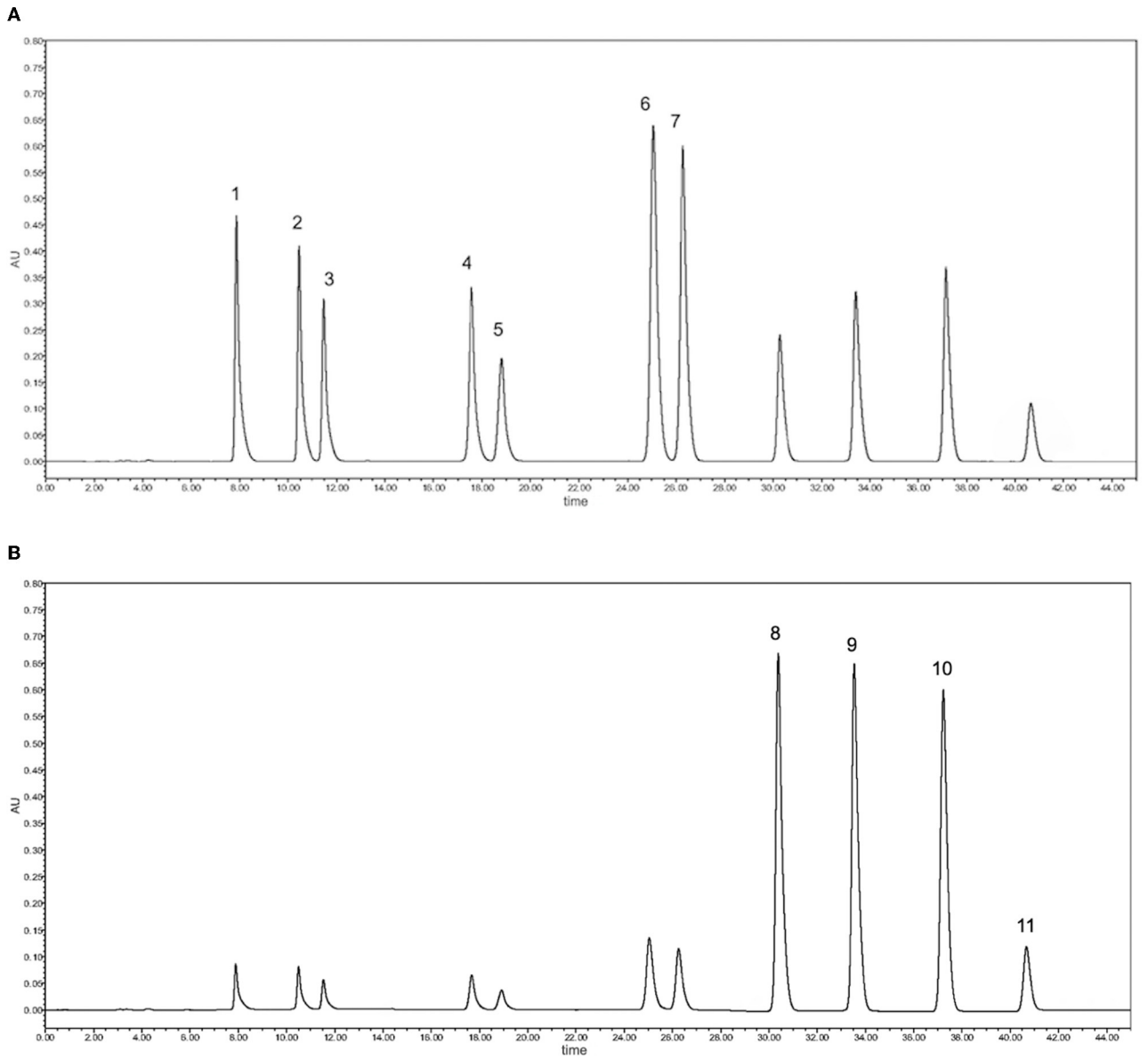

FIGURE 1 | Main flavanones and PMFs were quantified by HPLC-DAD. **(A)** Chromatogram of flavanone standards at 283 nm: 1, eriocitrin; 2, naringin; 3, hesperidin; 4, didymin; 5, poncirin; 6, naringenin; 7, hesperitin. **(B)** Chromatogram of PMF standards at 330 nm: 8, sinensetin; 9, nobiletin; 10, tangeretin; 11, 5-O-demethylnobiletin.

values than other cultivars. The overall antioxidant capacity was expressed in APC index, which varied from 39.69 to 92.19%. The top five APC index were classified as grapefruit (92.19%), chachiensis (89.13%), satsuma orange (87.68%), lemon (86.86%) and fertile orange (80.26%), indicating that these CPFEs have better antioxidant properties.

Citrus peel flavonoid extracts from mandarins and hybrids had higher inhibitory activity on α-glucosidase than these of sweet oranges, pummelos, kumquats and citrons (**Figure 2A**). CPFEs with the highest inhibitory effect on α-glucosidase was chachiensis (59.87 ± 1.09%), followed by dekopon (53.38 ± 2.53%), fertile orange (46.21 ± 1.50%), lemon (43.23 ± 0.90%) and satsuma orange (42.21 ± 0.90%). Bergamot, sichuan kumquat and longyan kumquat possessed lower inhibitory activity with values of 27.79 ± 0.57, 15.05 ± 1.06, and 14.69 ± 0.42%, respectively.

The binding capacity of CPFEs to sodium glycocholate ranged from 0.36 ± 0.01 to 0.44 ± 0.00 μmol/mg (**Figure 2B**). The difference between various CPFEs was not as significant as antioxidant activity and α-glucosidase inhibition. CPFEs from ponkan (0.44 ± 0.00 μmol/mg), dekopon (0.44 ± 0.01 μmol/mg), grapefruit (0.44 ± 0.01 μmol/mg) and majia pomelo (0.43 ± 0.01 μmol/mg) had higher sodium glycocholate binding capacity, suggesting that they have a cholesterol-lowering

TABLE 2 | Antioxidant potency composite index of 14 CPFEs (mg TE/g DW).

Cultivars	DPPH	ABTS	FRAP	CUPRAC	APC (%)	Rank
Satsuma orange	55.12 ± 0.08^{a}	17.15 ± 0.22^{h}	76.25 ± 0.75^{c}	25.87 ± 0.27^{d}	87.68	3
Chachiensis	43.19 ± 0.11^{c}	20.12 ± 0.12^{e}	88.84 ± 1.13^{a}	25.87 ± 0.17^{d}	89.13	2
Ponkan	27.44 ± 0.24^{i}	21.37 ± 0.15^{b}	79.30 ± 1.11^{b}	25.03 ± 0.06^{e}	79.99	6
Lane late navel orange	32.67 ± 0.16^{g}	21.04 ± 0.16^{bc}	53.59 ± 0.43^{g}	18.87 ± 0.12^{h}	69.51	9
Blood orange	36.03 ± 0.13^{e}	20.36 ± 0.06^{de}	66.99 ± 1.20^{e}	21.02 ± 0.10^{g}	75.87	7
Apple pomelo	17.95 ± 0.24^{l}	21.42 ± 0.08^{b}	25.18 ± 0.60^{lk}	8.39 ± 0.05^{k}	46.33	12
Majia pomelo	20.18 ± 0.38^{k}	22.35 ± 0.11^{a}	28.51 ± 0.60^{i}	10.76 ± 0.11^{i}	51.34	11
Grapefruit	53.73 ± 0.10^{b}	21.25 ± 0.06^{b}	74.68 ± 0.86^{c}	27.04 ± 0.35^{c}	92.19	1
Dekopon	34.71 ± 0.11^{f}	20.07 ± 0.08^{e}	63.75 ± 1.32^{f}	34.71 ± 0.11^{a}	73.59	8
Fertile orange	37.48 ± 0.18^{d}	20.84 ± 0.07^{c}	71.15 ± 1.61^{d}	23.39 ± 0.05^{f}	80.26	5
Lemon	43.16 ± 0.18^{c}	18.95 ± 0.24^{f}	74.95 ± 0.26^{c}	29.35 ± 0.13^{b}	86.86	4
Sichuan kumquat	23.96 ± 0.56^{j}	17.72 ± 0.11^{g}	27.82 ± 0.37^{ij}	9.51 ± 0.03^{j}	46.62	13
Longyan kumquat	28.94 ± 0.13^{h}	20.73 ± 0.12^{cd}	35.80 ± 0.80^{h}	11.01 ± 0.08^{i}	55.77	10
Bergamot	17.51 ± 0.34^{l}	15.85 ± 0.09^{j}	23.78 ± 0.56^{k}	8.60 ± 0.06^{k}	39.69	14

DPPH, free radical scavenging properties by diphenyl-1-picrylhydrazyl radical; ABTS, 2,2′-azino-bis (3-ethylbenzthiazoline-6-sulfonic acid); FRAP, ferric reducing antioxidant capacity; CUPRAC, cupric reducing antioxidant capacity.

Data are shown as the mean ± SD (n = 3). The APC index is the average of the antioxidant potency composite index in all tested CPFEs, and APC index = (measured score / maximum score) × 100%. Different letters above the error bars in the same column indicate significant differences among varieties based on Tukey's test ($P < 0.05$).

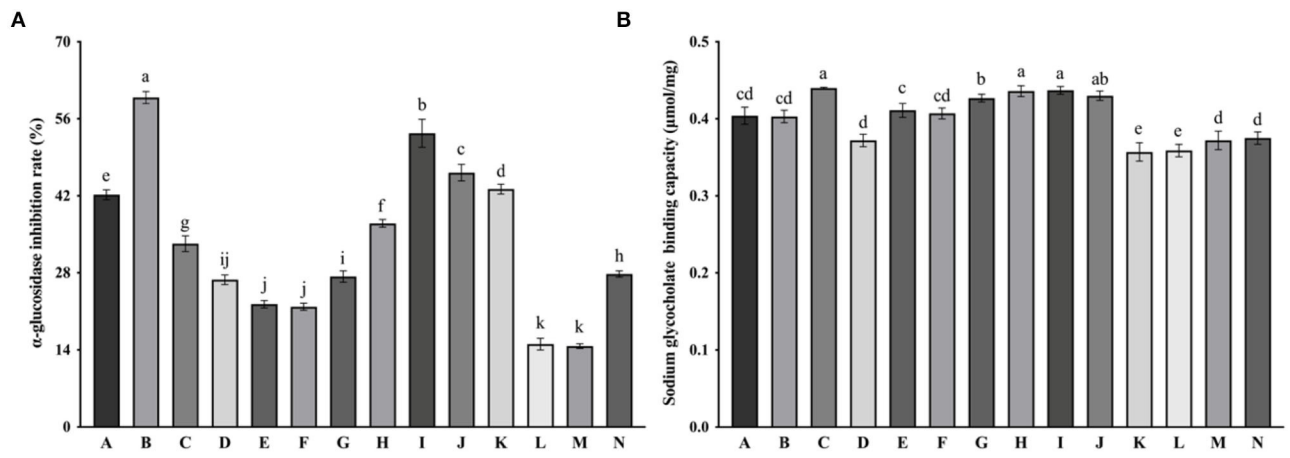

FIGURE 2 | α-Glucosidase inhibition **(A)** and sodium glycocholate binding capacity **(B)** of CPFEs. Data are shown as the mean ± SD ($n = 3$). Different letters the error bars indicate significant differences among varieties based on Tukey's test ($P < 0.05$). A, satsuma orange; B, chachiensis; C, ponkan; D, lane late navel orange; E, blood orange; F, apple pomelo; G, majia pomelo; H, grapefruit; I, dekopon; J, fertile orange; K, lemon; L, sichuan kumquat; M, longyan kumquat; N, bergamot; P, blank control.

effect by inhibiting reabsorption of bile acids. However, some eriocitrin-rich citrus such as lemon (0.36 ± 0.01 μmol/mg) and bergamot (0.38 ± 0.01 μmol/mg) were less binding in our test.

Effects of CPFEs on the Intestinal Microbiota

Microbial composition and abundance in fecal samples fermentated with different CPFEs were compared using 16S rDNA gene amplicons sequencing. Sequences were classified and assigned to OTUs with more than 97% similarity. Alpha diversity was determined using the Ace, Chao, Shannon and Simpson indices (**Supplementary Figure 1**). However, there was no significant change in microbial richness and diversity. Microbial composition analysis showed compositional changes at the phylum level (**Figure 3A**). Bacteroidetes and Firmicutes predominated in the original fecal samples, accounting for more than 90% of the total, but decreased to 70–80% after fermentation with CPFEs. Conversely, the relative abundance of Actinobacter was increased, and the treatment of CPFEs from grapefruit and fertile orange significantly increased Actinobacter abundance to 17.84 and 17.71%, respectively, which only accounted for 10.53% of the blank sample.

At the genus level, the enterotypes of seven volunteers were divided into Enterotype 1 (ET B) and Enterotype 2 (ET P). Subject 1, 2 and 5 belonged to the *Bacteroides*-predominant ET B, and subject 3, 4, 6, and 7 belonged to the

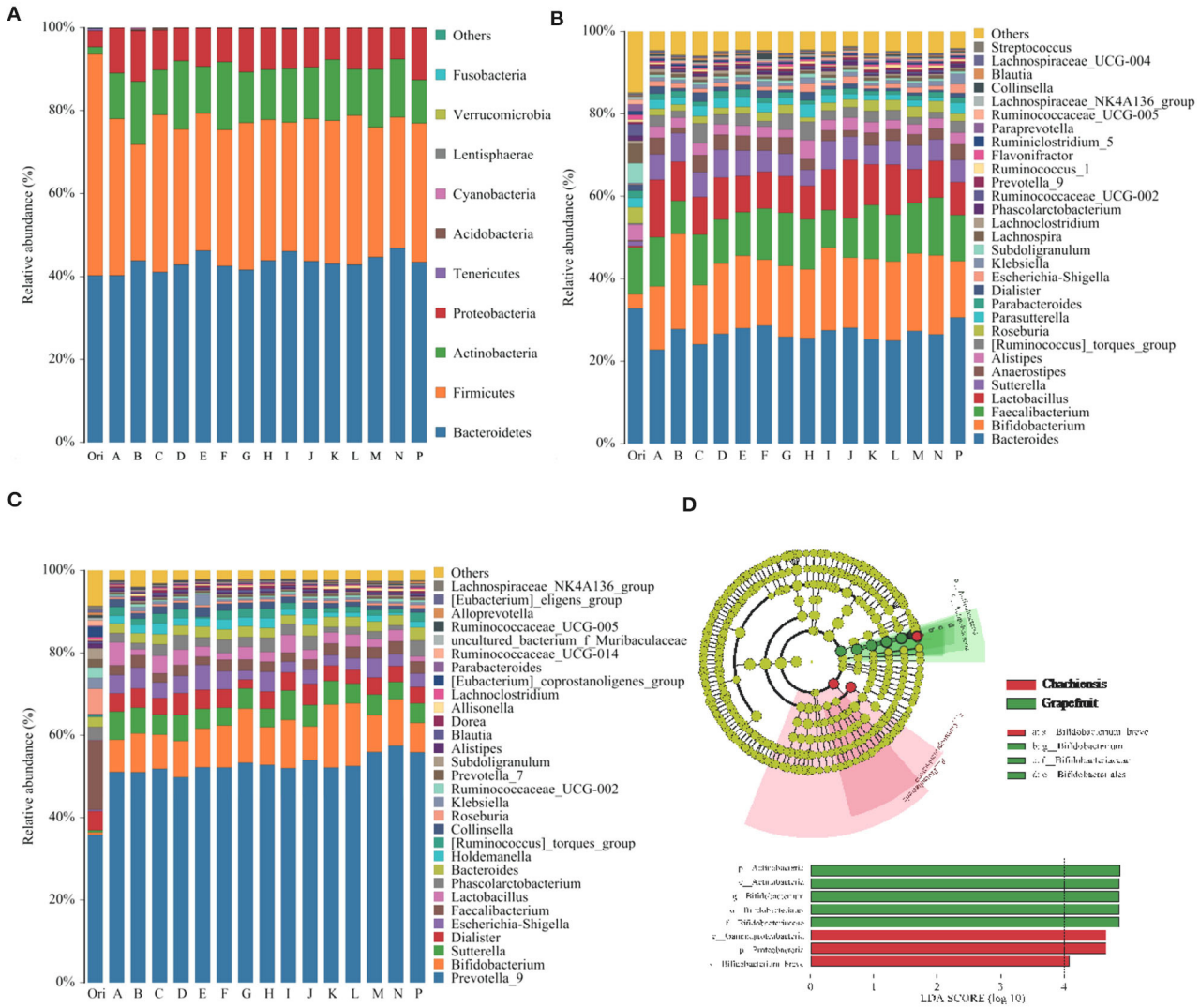

FIGURE 3 | Differences in the distribution and abundance of intestinal microflora in human fecal samples before and after *in vitro* fermentation with CPFEs. **(A)** The compositional changes of intestinal microflora at the phylum level ($n = 3$); **(B)** Test subjects with ET B fecal enterotype at the genus level (subject 1, 2 and 5, $n = 3$); **(C)** Test subjects with ET P fecal enterotype at the genus level (subject 3, 4, 6 and 7, $n = 4$); **(D)** Significant features in microflora of chachiensis and grapefruit CPFEs by LEFSe analysis (LDA > 4.0, $P < 0.05$). A, satsuma orange; B, chachiensis; C, ponkan; D, lane late navel orange; E, blood orange; F, apple pomelo; G, majia pomelo; H, grapefruit; I, dekopon; J, fertile orange; K, lemon; L, sichuan kumquat; M, longyan kumquat; N, bergamot; P, blank control.

Prevotella-predominant ET P. The five genera with the highest relative abundance of ET B were *Bacteroides*, *Bifidobacterium*, *Faecalibacterium*, *Lactobacillus* and *Sutterella* (**Figure 3B**); in ET P, the top five abundances were *Prevotella_9*, *Bifidobacterium*, *Sutterella*, *Dialister* and *Escherichia-Shigella* (**Figure 3C**). After *in vitro* fermentation with CPFEs, *Bacteroides* became slightly less dominant in the ET B enterotype, decreasing from 30.58 to 26% (average of treatment group), and *Prevotella_9* became considerably more dominant in ET P. The average relative abundance of beneficial microbial communities *Lactobacillus* and *Bifidobacterium* markedly increased in both enterotypes. Especially in the chachiensis CPFE group, the proportion of *Bifidobacterium* in the ET B group was the highest at 23.09%; and CPFEs of grapefruit and fertile orange increased *Bifidobacterium* to 14.86 and 14.78%, respectively, in the ET P group.

The LefSe analysis highlighted the differences in relative microbial abundance from phylum to species. In all citrus tested, chachiensis and grapefruit were the two cultivars with significant differences in intestinal microbial composition and abundance (**Figure 3D**). Samples fermented with chachiensis CPFEs had higher levels of the phylum Proteobacteria, class Grammproteobacteria and species *Bifidobacterium breve*. In grapefruit CPFEs, phylum Actinobacteria and genus *Bifidobacterium* were significantly increased. The regulatory effect on intestinal microbiota may be related to the TFC and flavonoid profiles of different CPFEs. Abundant *Bifidobacterium*

spp. in the chachiensis group may be associated with high levels of PMFs. Chen et al. found that oral administration of *Citrus reticulata* cv. Suavissima, rich in nobiletin, tangeretin and 5-demethylnobiletin, significantly increased the abundance of the probiotics such as *Bifidobacterium* spp. and *Lactobacillus* spp. (30).

SCFAs Production and Their Relationship With Microbial Composition

Short-chain fatty acids are the main end-products of indigestible carbohydrate fermentation, and can be used as nutrients by intestinal epithelial cells and the colonic microflora (31). The average levels of total SCFAs generated by fecal microbial fermentations with CPFEs, were all higher than that of the blank control (**Figure 4A**). Acetic acid was the major SCFA produced, accounting for about 80% of the total (**Figure 4B**). The concentrations of acetic acid were significantly higher with chachiensis ($P < 0.05$) and grapefruit ($P < 0.05$) compared with the blank control. However, we did not find significant differences in concentrations of butyric, isobutyric, valeric and isovaleric acids ($P > 0.05$, data not shown).

Spearman's correlation analysis was performed to investigate the differences between microbial compositions at the genus level and SCFA productions (**Figure 5**). Acetic acid was positively correlated with *Bacteroides*, *Parabacteroides*, *Roseburia*, *Lachnospira*, *Klebsiella*, *Alistipes* and *Lachnoclostridium*, and negatively correlated with *Parasutterella*, *Dialister*, *Subdoligranulum* and *Ruminiclostridium*. We can also find that propionic acid was negatively correlated with *Parasutterella*, and positively correlated with the relative abundance of *Roseburia*, *Lanospiraceaece_NK4A136*, *Ruminococcaceae_UCG*, *Alistipes* and *Bifidobacterium*, but not significantly. The positive relationship between butyric, isobutyric and *Bacteroides*, *Parabacteroides* and *Lachnospira* was more obvious. However, valeric and isovaleric acids were not significantly associated with gut microbiota.

DISCUSSION

To the best of our knowledge, this is the first report on the extraction and compositional analysis of flavonoids from the peel of fourteen local Chinese citrus cultivars and their role in regulating the gut microbiota. TFC values of CPFEs in our test were considerably higher than those reported from the same fruits, using ultrasound-assisted extraction alone (4, 23). This appears to be due to the much higher extraction efficiency of macroporous resin XAD-16. Column chromatography with XAD-16 increased the extractable flavonoid content of *Glycyrrhiza glabra* L. leaf from 16.80 to 55.60%, compared with the crude solvent extracts (23). Naringin, hesperidin and eriocitrin are the top three flavanones detected by HPLC-DAD. As previously reported, naringin is rich in hybrids (grapefruit) and pummelos (apple pomelo, majia pomelo); hesperidin is rich in mandarins (satsuma mandarin, chachiensis, ponkan), sweet oranges (lane late navel orange, blood orange), and hybrids (dekopon, fertile orange); and eriocitrin is only enriched in lemon (27–29).

Citrus-derived flavonoids have various human health-promoting functions, such as antioxidant activity, α-glucosidase inhibition and sodium glycocholate binding capacity, which are associated with antihyperglycemic and hyperlipidemic effects (32). Long et al. found that CPFEs with higher content of TFC had stronger antioxidant activities (28). Various *in vitro* and *in vivo* studies have identified that eriocitrin, naringin and hesperidin all have good antioxidant activities, which are beneficial for free radical scavenging, reducing hepatic gluconeogenesis and increasing insulin sensitivity (28, 29, 31, 33). We found that CPFEs with higher APC indices such as grapefruit and chachiensis tend to have higher TFCs.

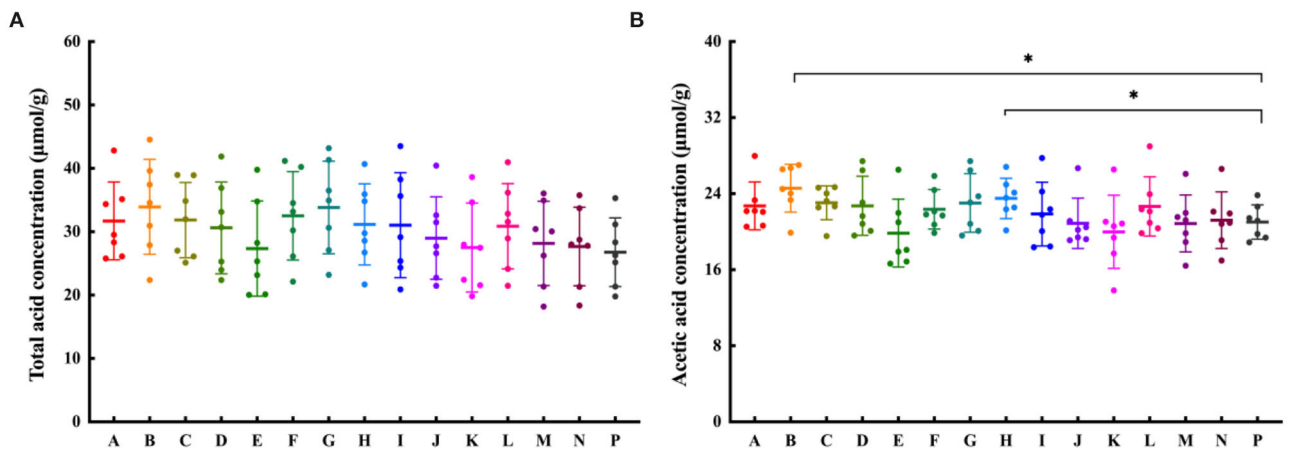

FIGURE 4 | The effect of CPFEs on SCFA production after 24-h *in vitro* fermentation. **(A)** Total SCFA concentration; **(B)** The acetic acid concentration; Data are shown as the mean ± SD ($n = 7$). Significant differences among groups based on *T*-test, * $P < 0.05$. A, satsuma orange; B, chachiensis; C, ponkan; D, lane late navel orange; E, blood orange; F, apple pomelo; G, majia pomelo; H, grapefruit; I, dekopon; J, fertile orange; K, lemon; L, sichuan kumquat; M, longyan kumquat; N, bergamot; P, blank control.

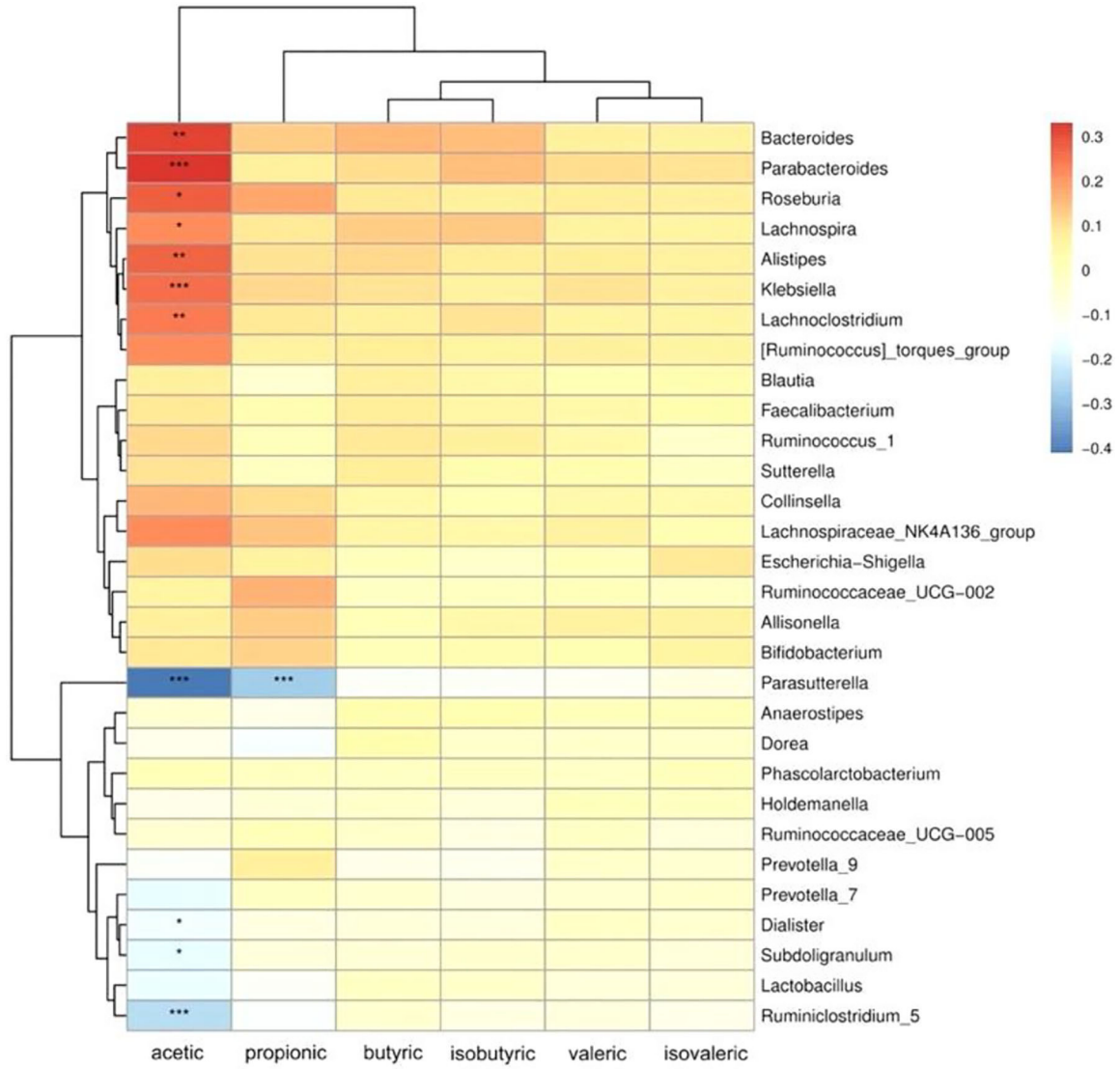

FIGURE 5 | Heatmap of Spearman's rank correlation coefficients between SCFAs production and microbial relative abundance at the genus level. The colors indicate positive (red) or negative (blue) correlations between SCFA production and microbial relative abundance. The *X*-axis shows the different SCFAs, from left to right: acetic acid, propionic acid, butyric acid, isovaleric acid, isobutyric acid, and valeric acid. The *Y*-axis shows different genera. * $P < 0.05$, ** $P < 0.01$, *** $P < 0.001$.

CPFEs from sichuan kumquat, Longyan kumquat and bergamot had lower levels of TFCs and main flavonoids (eriocitrin, naringin, and hesperidin), with poor antioxidant capacity. The richness of naringin and hesperidin in CPFEs can regulate hepatic cholesterol synthesis by inhibiting the activity of 3-hydroxy-3-methylglutaryl-CoA reductase (34, 35). Kwon et al. also found that eriocitrin has cholesterol-lowering properties and inhibits obesity by increasing cellular fatty acid oxidation and energy expenditure, and reducing lipogenesis-related gene expression (36). While CPFEs of apple pomelo and majia pomelo had high content of naringin in our test, their antioxidant activity and α-glucosidase activity were relatively poor. And Zeng et al. showed that hesperidin hydrolysates intensively inhibited α-glucosidase activity whereas hesperidin showed little activity (37). There is limited understanding of the differences in biological activities of various flavonoids. Further analysis on the correlation between the biological activities and main flavonoid components such as hesperidin, naringin and eriocitrin will help the high-value utilization of different varieties of citrus peels and processing wastewater.

Flavonoids derived from citrus peel represent the alterations of gut microbiota. Researchers at the European Molecular Biology Laboratory have proposed the classification of human colonic microbiomes into three "Enterotypes" at the genus level (38). ET B, dominated by genus *Bacteroides*, is associated with high consumption of protein and animal fat. ET P, dominated by genus *Prevotella*, is associated with high carbohydrate consumption. Different enterotypes may be associated with

health status and incidence of diseases. Prebiotics and probiotics affect specific bacterial populations in the intestine, which are associated with an individual's enterotype (39). Only Rodríguez-Daza et al. (40) found that supplementation with polyphenol-rich blueberry fruit powders changed the enterotype of obese mice from the Firmicute/*Ruminococcus* enterotype into the healthier *Prevotella*/Akkermansiaceae enterotype. *Bifidobacterium* have been reported to play important roles in regulating intestinal microbiota and mucosal inflammation, contributing to inhibit obesity, diabetes and inflammatory bowel disease (41, 42). *Bifidobacterium* was significantly increased after cofermentation of chachiensis and grapefruit CPFEs with fecal samples (**Figure 5**), which were associated with the enrichment of naringin and hesperidin, respectively. The effects of naringin and hesperidin on the growth of *Bifidobacterium* strains were dose-dependent (43). In the animal model of high-fat diet, naringin intervention altered the community composition of the gut bacteria, characterized by increased benefits (*Butyricicoccus* etc.) and fewer harmful bacteria (*Campylobacter* etc.) (44).

It is well established that SCFAs are the major components in regulating gut health (45). Dietary citrus flavonoids can alter the abundance of SCFAs in the gut. CPFEs from chachiensis and grapefruit stimulated intestinal acetic acid (**Figure 4B**). Acetic acid is the main SCFA produced by most fecal bacteria and an important pH regulator in the colon, helping to maintain colonic homeostasis (45). Zhang et al. (46) found that dietary supplements with citrus peel extracts have anti-obesity activity, by increasing the amount of fecal acetic acid by 43% and propionic acid by 86%. After 2 months of drinking pasteurized orange juice containing flavanones, the proportions of total SCFA and acetate were increased in the feces of healthy subjects, and the ammonium concentration was reduced (15, 47). We found that acetate is positively associated with *Roseburia* in the gut (**Figure 5**). *Roseburia* is a symbiotic beneficial flora that produces SCFAs, affecting colonic motility, immune responses and anti-inflammatory properties (48). Conversely, *Parasutterella* is inversely proportional to acetic and propionic acids. The feces of IBS patients were rich in *Parasutterella*, which was significantly positively correlated with the ratio of inflammatory cells to epithelial cells (49). These suggest that the probiotic effects of citrus flavonoid, if replicated in humans, may confer health benefits.

CONCLUSIONS

In conclusion, CPFEs from 14 Chinese cultivars were extracted and purified, and seven flavanones and four PMFs were quantitatively analyzed by HPLC-DAD. The results of biological function test showed that CPFEs, especially from chachiensis and grapefruit, had good antioxidant activity, α-glucosidase inhibition and bile acid binding capacity. Furthermore, chachiensis and grapefruit CPFEs were found to promote the growth of intestinal *Bifidobacterium* spp. and increase acetic acid content by *in vitro* simulated human gut models. Our results provided valuable insights into understanding the biofunctional activity and gut microbiota regulation of citrus peel flavonoids. Further studies will be performed to investigate the effects of specific flavonoid components such as naringin, hesperidin and eriocitrin on intestinal disease models.

DATA AVAILABILITY STATEMENT

The datasets presented in this study can be found in online repositories. The names of the repository/repositories and accession number(s) can be found in the article/**Supplementary Material**.

AUTHOR CONTRIBUTIONS

PL and QG: conceptualization and supervision. XY, XM, and QZ: methodology, investigation, and data curation. XY: writing-original draft preparation. QZ and TZ: writing-review and editing. QG: funding acquisition. All authors have read and agreed to the published version of the manuscript.

FUNDING

The work was supported by National Key Research and Development Program of China (2017YFE0122300).

SUPPLEMENTARY MATERIAL

The Supplementary Material for this article can be found online at: https://www.frontiersin.org/articles/10.3389/fnut.2022.888745/full#supplementary-material

REFERENCES

1. Spinelli S, Lecce L, Likyova D, Del Nobile MA, Conte A. Bioactive compounds from orange epicarp to enrich fish burgers. *J Sci Food Agr.* (2018) 98:2582–6. doi: 10.1002/jsfa.8750
2. Putnik P, Bursać Kovačević D, ReŽek Jambrak A, Barba FJ, Cravotto G, Binello A, et al. Innovative "green" and novel strategies for the extraction of bioactive added value compounds from citrus wastes—a review. *Molecules.* (2017) 22:680. doi: 10.3390/molecules22050680
3. Gomez-Mejia E, Rosales-Conrado N, Leon-Gonzalez ME, Madrid Y. Citrus peels waste as a source of value-added compounds: extraction and quantification of bioactive polyphenols. *Food Chem.* (2019) 295:289–99. doi: 10.1016/j.foodchem.2019.05.136
4. Chen QY, Wang D, Tan C, Hu Y, Sundararajan B, Zhou Z. Profiling of flavonoid and antioxidant activity of fruit tissues from 27 Chinese local citrus cultivars. *Plants.* (2020) 9:196. doi: 10.3390/plants9020196
5. Ma YQ, Ye XQ, Fang ZX, Chen JC, Xu GH. Liu DH. Phenolic compounds and antioxidant activity of extracts from ultrasonic treatment of Satsuma Mandarin (*Citrus unshiu* Marc.) peels. *J Agric Food Chem.* (2008) 56:5682–90. doi: 10.1021/jf072474o
6. Khan MK, Abert-Vian M, Fabiano-Tixier AS, Dangles O. Chemat F. Ultrasound-assisted extraction of polyphenols (flavanone glycosides) from orange (*Citrus sinensis* L) peel. *Food Chem.* (2010) 119:851–8. doi: 10.1016/j.foodchem.2009.08.046
7. Minato K, Miyake Y, Fukumoto S, Yamamoto K, Kato Y, Shimomura Y, et al. Lemon flavonoid, eriocitrin, suppresses exercise-induced oxidative damage

in rat liver. *Life Sci.* (2003) 72:1609–16. doi: 10.1016/S0024-3205(02)02443-8
8. Yang X, Kang SM, Jeon BT, Kim YD, Ha JH, Kim YT, et al. Isolation and identification of an antioxidant flavonoid compound from citrus-processing by-product. *J Sci Food Agric.* (2011) 91:1925–7. doi: 10.1002/jsfa.4402
9. Ahmed OM, AbouZid SF, Ahmed NA, Zaky MY, Liu H. An up-to-date review on citrus flavonoids: chemistry and benefits in health and diseases. *Curr Pharm Des.* (2021) 27:513–30. doi: 10.2174/1381612826666201127122313
10. Sarian MN, Ahmed QU. Mat So'ad SZ, Alhassan AM, Murugesu S, Perumal V, et al. Antioxidant and antidiabetic effects of flavonoids: a structure-activity relationship based study. *BioMed Res Int.* (2017) 2017:8386065. doi: 10.1155/2017/8386065
11. Jia Y, Ma Y, Cheng G, Zhang Y, Cai S. Comparative study of dietary flavonoids with different structures as α-glucosidase inhibitors and insulin sensitizers. *J Agric Food Chem.* (2019) 67:10521–33. doi: 10.1021/acs.jafc.9b04943
12. Kim DS, Lim SB. Semi-continuous subcritical water extraction of flavonoids from *Citrus unshiu* peel: their antioxidant and enzyme inhibitory activities. *Antioxidants.* (2020) 9:360. doi: 10.3390/antiox9050360
13. Kaakoush NO, Morris MJ. More flavor for flavonoid-based interventions? *Trends Mol Med.* (2017) 23:293–5. doi: 10.1016/j.molmed.2017.02.008
14. Zhou L, Wang W, Huang J, Ding Y, Pan Z, Zhao Y, et al. *In vitro* extraction and fermentation of polyphenols from grape seeds (*Vitis vinifera*) by human intestinal microbiota. *Food Funct.* (2016) 7:1959–67. doi: 10.1039/C6FO00032K
15. Stevens Y, Rymenant EV, Grootaert C, Camp JV, Possemiers S, Masclee A, et al. The intestinal fate of citrus flavanones and their effects on gastrointestinal health. *Nutrients.* (2019) 11:1464. doi: 10.3390/nu11071464
16. Koh A, De Vadder F, Kovatcheva-Datchary P, Bäckhed F. From dietary fiber to host physiology: short-chain fatty acids as key bacterial metabolites. *Cell.* (2016) 165:1332–45. doi: 10.1016/j.cell.2016.05.041
17. Tan J, McKenzie C, Potamitis M, Thorburn AN, Mackay CR, Macia L. The role of short-chain fatty acids in health and disease. *Adv Immunol.* (2014) 121:91–119. doi: 10.1016/B978-0-12-800100-4.00003-9
18. Perez-Vizcaino F, Fraga CG. Research trends in flavonoids and health. *Arch Biochem Biophys.* (2018) 646:107–12. doi: 10.1016/j.abb.2018.03.022
19. Bas-Bellver C, Andrés C, Seguí L, Barrera C, Jiménez-Hernández N, Artacho A, et al. Valorization of persimmon and blueberry byproducts to obtain functional powders: *in vitro* digestion and fermentation by gut microbiota. *J Agric Food Chem.* (2020) 68:8080–90. doi: 10.1021/acs.jafc.0c02088
20. Seeram NP, Aviram M, Zhang Y, Henning SM, Feng L, Dreher M, et al. Comparison of antioxidant potency of commonly consumed polyphenol-rich beverages in the United States. *J Agric Food Chem.* (2008) 56:1415–22. doi: 10.1021/jf073035s
21. Liew SS, Ho WY, Yeap SK, Sharifudin S AB. Phytochemical composition and *in vitro* antioxidant activities of *Citrus sinensis* peel extracts. *PeerJ.* (2018) 6:e5331. doi: 10.7717/peerj.5331
22. Hamdan D, El-Readi MZ, Tahrani A, Herrmann F, Kaufmann D, Farrag N, et al. Chemical composition and biological activity of *Citrus jambhiri* Lush. *Food Chem.* (2011) 127:394–403. doi: 10.1016/j.foodchem.2010.12.129
23. Dong Y, Zhao M, Sun-Waterhouse D, Zhuang M, Chen H, Feng M, et al. Absorption and desorption behaviour of the flavonoids from *Glycyrrhiza glabra* L. *leaf on macroporous adsorption resins*. *Food Chem.* (2015) 168:538–45. doi: 10.1016/j.foodchem.2014.07.109
24. Chen L, Guo Y, Li X, Gong K, Liu K. Phenolics and related *in vitro* functional activities of different varieties of fresh waxy corn: a whole grain. *BMC Chem.* (2021) 15:14. doi: 10.1186/s13065-021-00740-7
25. Liu G, Chen H, Chen J, Wang X, Gu Q, Yin Y. Effects of *bifidobacteria*-produced exopolysaccharides on human gut microbiota *in vitro*. *Appl Microbiol Biotechnol.* (2019) 103:1693–702. doi: 10.1007/s00253-018-9572-6
26. Zhou WT, Yan YM Mi J, Zhang HC, Lu L, Luo Q, et al. Simulated digestion and fermentation *in vitro* by human gut microbiota of polysaccharides from bee collected pollen of Chinese wolfberry. *J Agric Food Chem.* (2018) 66:898–907. doi: 10.1021/acs.jafc.7b05546
27. Xing TT, Zhao XJ, Zhang YD Li YF. Fast separation and sensitive quantitation of polymethoxylated flavonoids in the peels of citrus using UPLC-Q-TOF-MS. *J Agric Food Chem.* (2017) 65:2615–27. doi: 10.1021/acs.jafc.6b05821
28. Long XY, Zeng XG, Yan HT, Xu MJ, Zeng QT, Xu C, et al. Flavonoids composition and antioxidant potential assessment of extracts from Gannanzao Navel Orange (*Citrus sinensis* Osbeck Cv. Gannanzao) peel. *Nat Prod Res.* (2021) 35:702–6. doi: 10.1080/14786419.2019.1593162
29. Huang R, Zhang Y, Shen SY, Zhi ZJ, Cheng H, Chen SG, et al. Antioxidant and pancreatic lipase inhibitory effects of flavonoids from different citrus peel extracts: an *in vitro* study. *Food Chem.* (2020) 326:126785. doi: 10.1016/j.foodchem.2020.126785
30. Chen J, Wang Y, Zhu T, Yang S, Cao J, Li X, et al. Beneficial regulatory effects of polymethoxyflavone-rich fraction from Ougan (*Citrus reticulata* cv. Suavissima) fruit on gut microbiota and identification of its intestinal metabolites in mice. *Antioxidants.* (2020) 9:831. doi: 10.3390/antiox9090831
31. Shen W, Xu Y, Lu YH. Inhibitory effects of citrus flavonoids on starch digestion and antihyperglycemic effects in HepG2 cells. *J Agric Food Chem.* (2012) 60:9609–19. doi: 10.1021/jf3032556
32. Zhao CY, Wang F, Lian YH, Xiao H, Zheng JK. Biosynthesis of citrus flavonoids and their health effects. *Crit Rev Food Sci Nutr.* (2020) 60:566–83. doi: 10.1080/10408398.2018.1544885
33. Jung UJ, Lee MK, Park YB, Kang MA, Choi MS. Effect of citrus flavonoids on lipid metabolism and glucose-regulating enzyme mRNA levels in type-2 diabetic mice. *Int J Biochem Cell Biol.* (2006) 38:1134–45. doi: 10.1016/j.biocel.2005.12.002
34. Kim HJ, Oh GT, Park YB, Lee MK, Seo HJ, Choi MS. Naringin alters the cholesterol biosynthesis and antioxidant enzyme activities in LDL receptor-knockout mice under cholesterol fed condition. *Life Sci.* (2004) 74:1621–34. doi: 10.1016/j.lfs.2003.08.026
35. Bok SH, Lee SH, Park YB, Bae KH, Son KH, Jeong TS, et al. Plasma and hepatic cholesterol and hepatic activities of 3-hydroxy-3-methyl-glutaryl-CoA reductase and acyl CoA: cholesterol transferase are lower in rats fed citrus peel extract or a mixture of citrus bioflavonoids. *J Nutr.* (1999) 129:1182–5. doi: 10.1093/jn/129.6.1182
36. Kwon EY, Choi MS. Eriocitrin improves adiposity and related metabolic disorders in high-fat diet-induced obese mice. *J Med Food.* (2020) 23:233–41. doi: 10.1089/jmf.2019.4638
37. Zheng MY, Lu S, Xing J. Enhanced antioxidant, anti-inflammatory and α-glucosidase inhibitory activities of citrus hesperidin by acid-catalyzed hydrolysis. *Food Chem.* (2021) 336:127539. doi: 10.1016/j.foodchem.2020.127539
38. Costea PI, Hildebrand F, Arumugam M, Bäckhed F, Blaser MJ, Bushman FD, et al. Enterotypes in the landscape of gut microbial community composition. *Nat Microbiol.* (2018) 3:8–16. doi: 10.1038/s41564-017-0072-8
39. Asto E, Mendez I, Rodriguez-Prado M, Cune J, Espadaler J, Farran-Codina A. Effect of the degree of polymerization of fructans on *ex vivo* fermented human gut microbiome. *Nutrients.* (2019) 11:1293. doi: 10.3390/nu11061293
40. Rodriguez-Daza MC, Roquim M, Dudonne S, Pilon G, Levy E, Marette A, et al. Berry polyphenols and fibers modulate distinct microbial metabolic functions and gut microbiota enterotype-like clustering in obese mice. *Front Microbiol.* (2020) 11:2032. doi: 10.3389/fmicb.2020.02032
41. Guo X, Cao XD, Fang XG, Guo AL Li EH. Inhibitory effects of fermented Ougan (*Citrus reticulata* cv. Suavissima) juice on high-fat diet-induced obesity associated with white adipose tissue browning and gut microbiota modulation in mice. *Food Funct.* (2021) 12:9300–4. doi: 10.1039/D0FO03423A
42. Sost MM, Ahles S, Verhoeven J, Verbruggen S, Stevens Y, Venema K, et al. citrus fruit extract high in polyphenols beneficially modulates the gut microbiota of healthy human volunteers in a validated *in vitro* model of the colon. *Nutrients.* (2021) 13:3915. doi: 10.3390/nu13113915
43. Gwiazdowska D, Juś K, Jasnowska-Małecka J, Kluczyńska K. The impact of polyphenols on Bifidobacterium growth. *Acta Biochim Pol.* (2015) 62:895–901. doi: 10.18388/abp.2015_1154
44. Mu H, Zhou Q, Yang R, Zeng J, Li X, Zhang R, et al. Naringin attenuates high fat diet induced non-alcoholic fatty liver disease and gut bacterial dysbiosis in mice. *Front Microbiol.* (2020) 11:585066. doi: 10.3389/fmicb.2020.585066
45. Morrison DJ, Preston T. Formation of short chain fatty acids by the gut microbiota and their impact on human metabolism. *Gut Microbes.* (2016) 7:189–200. doi: 10.1080/19490976.2015.1134082

46. Zhang M, Zhu J, Zhang X, Zhao DG, Ma YY Li D, et al. Aged citrus peel (chenpi) extract causes dynamic alteration of colonic microbiota in high-fat diet induced obese mice. *Food Funct.* (2020) 11:2667–78. doi: 10.1039/C9FO02907A
47. Lima ACD, Cecatti C, Fidelix MP, Adorno MAT, Sakamoto IK, Cesar TB, et al. Effect of daily consumption of orange juice on the levels of blood glucose, lipids, and gut microbiota metabolites: controlled clinical trials. *J Med Food.* (2019) 22:202–10. doi: 10.1089/jmf.2018.0080
48. Lordan C, Thapa D, Ross RP, Cotter PD. Potential for enriching next-generation health-promoting gut bacteria through prebiotics and other dietary components. *Gut Microbes.* (2020) 11:1–20. doi: 10.1080/19490976.2019.1613124
49. Chen YJ, Wu H, Wu SD, Lu N, Wang YT, Liu HN, et al. Parasutterella, in association with irritable bowel syndrome and intestinal chronic inflammation. *J Gastroenterol Hepatol.* (2018) 33:1844–52. doi: 10.1111/jgh.14281

Conflict of Interest: The authors declare that the research was conducted in the absence of any commercial or financial relationships that could be construed as a potential conflict of interest.

frontiers | Frontiers in Nutrition

ORIGINAL RESEARCH
published: 27 July 2022
doi: 10.3389/fnut.2022.916728

Production and Optimization of Conjugated Linoleic and Eicosapentaenoic Acids by *Bifidobacterium lactis* in Cold-Pressed Soybean Cake

Samin Rafi Azari[1], Mohammad Hojjatoleslamy[1†], Zeinab E. Mousavi[1,2], Hossein Kiani[1,2] and Sayed Mohammad Ali Jalali[3,4†]*

[1] Department of Food Science and Technology, Shahrekord Branch, Islamic Azad University, Shahrekord, Iran, [2] Bioprocessing and Biodetection Laboratory, Department of Food Science and Engineering, Campus of Agriculture and Natural Resources, University of Tehran, Karaj, Iran, [3] Department of Animal Sciences, Faculty of Agriculture and Veterinary Medicine, Shahrekord Branch, Islamic Azad University, Shahrekord, Iran, [4] Research Center of Nutrition and Organic Products, Shahrekord Branch, Islamic Azad University, Shahrekord, Iran

OPEN ACCESS

Edited by:
Gengjun Chen,
Kansas State University, United States

Reviewed by:
Mohamed Fawzy Ramadan Hassanien,
Umm al-Qura University, Saudi Arabia
Maghsoud Besharati,
University of Tabriz, Iran

***Correspondence:**
Mohammad Hojjatoleslamy
mohojjat@gmail.com

†ORCID:
Mohammad Hojjatoleslamy
orcid.org/0000-0003-2015-1458
Sayed Mohammad Ali Jalali
orcid.org/0000-0002-9261-4776

Specialty section:
This article was submitted to Nutrition and Food Science Technology, a section of the journal Frontiers in Nutrition

Received: *09 April 2022*
Accepted: *01 June 2022*
Published: *27 July 2022*

Citation:
Azari SR, Hojjatoleslamy M, Mousavi ZE, Kiani H and Jalali SMA (2022) Production and Optimization of Conjugated Linoleic and Eicosapentaenoic Acids by Bifidobacterium lactis in Cold-Pressed Soybean Cake. Front. Nutr. 9:916728. doi: 10.3389/fnut.2022.916728

Background and Purpose: In regard to the biosynthesis of conjugated linoleic acid (CLA) and eicosapentaenoic acid (EPA) by some bacteria, the objective of this study was to evaluate the efficiency of solid-state fermentation based on soybean pressed cake (SPC) to produce CLA and EPA by *Bifidobacterium lactis*. The objective of this study was to evaluate the efficiency of solid-state fermentation based on SPC to produce CLA and EPA by *B. lactis*.

Methods: Process conditions including humidity, inoculation level, and temperature parameters were optimized by adopting the response surface methodology (RSM) method (response surface method) and the design expert software. Accordingly, a homogeneous SPC paste substrate at 60, 70, and 80% humidity was prepared with different inoculation levels at 30, 37, and 44°C to assess the strain behavior. The introduced SPC consisted of 60% humidity, 2% inoculation level at 37°C, and 60% humidity, and 4% inoculation level at 30 and 44°C; it also included 6% inoculation level at 37°C, 70% humidity at 2% inoculation level, at 30 and 44°C, and 4% inoculation level at 37°C. Also, SPC with 80% humidity at 2% and 4% inoculation levels, and at 30 and 44°C was obtained. To confirm the accuracy of the conditions, an experiment was conducted according to the defined requirements.

Results: The results were compared with the predicted data, which showed a significant difference. Under optimized conditions, with an inoculation level of 4% on the SPC medium with 70% humidity and at 37°C, *B. lactis* strains could yield 9*cis*-, 11 *trans*-linoleic and eicosapentaenoic at 0.18 and 0.39% of the total fatty acids.

Conclusion: So, the potential benefits of using SPC as an inexpensive substrate for the commercial production of CLA and EPA should be noted.

Keywords: conjugated linoleic acid (CLA), EPA, *Bifidobacterium lactis*, soybean pressed cake, RSM

INTRODUCTION

Conjugated linoleic acid (CLA) consists of a set of positional and geometric isomers of octadecadienoic acid (LA) with a conjugated double bond bonding system (–C=C–C=C–) initiated from 9, 10, or 11 carbons. All settings of *cis*-trans, *trans*-cis, *cis-cis* and *trans-trans* are possible in each of the three positional systems (1–3). There exist at least 28 known CLA isomers (4), among which *cis* 9 and *Trans* 11 (mostly in meat and dairy) have anti-cancer properties. *Trans* 10 isomer, *cis* 12 (mostly in vegetable oil) (5), is active in the body's fat reduction and weight loss, as well as the increase of energy consumption (6, 7). It is the most abundant and important in terms of naturalness, with about 85 and 10%, respectively (1, 8).

On the other hand, CLA is a natural unsaturated *trans* fatty acid (1) available in the meat and milk fat of sheep, goats and deer (1, 9–10). Despite being a specific *trans* fatty acid, it is categorized as non-trans, according to FDA; it is also known as a safe GRAS (7, 11–13). In addition, eicosapentaenoic acid (EPA) is one of the most unsaturated fatty acids of omega-3 type with a potentially beneficial effect on the cardiovascular system (14) in different volumes, within the range of 0.1 to 2.6 g in some fish types, especially cold-water fish. It is found in a group of seaweed. A group of bacteria like *gamaproteobacteria* and *schwannellas* can biosynthesize this fatty acid (15). Although EPA is a nutrient and is produced as a supplement, it is also called a drug because of its specific function and result. Studies show that taking EPA supplements in people with high blood triglyceride levels can reduce the level of this fat by up to 33% (16).

In the recent years, more attention has been paid to the production of healthy and safe food products because consumers are looking for more natural foods (17) to improve their health through its active ingredients (13). Fats are one of the main components of foods; due to their association with cardiovascular diseases, diabetes and obesity, there are many concerns about the type and amount of their consumption, because the quality of fat in the diet (9) is of great importance.

Despite the anti-nutritional nature of some lipids (6), such as *trans* and saturated fatty acids, another group of lipids has shown beneficial physiological effects. In this regard, fatty acids have received much attention due to their positive effect on the prevention of a number of diseases (7, 9). For this reason, the necessity of using biotechnological ways to produce healthy fats has attracted much attention, with a good potential in terms of producing safe and healthy fat products, as shown in the studies focused on producing and incorporating them into foods (4, 18, 19).

In this context, one of these health-promoting or pragmatic lipids is conjugated linoleic acid (CLA), the isomer of CLA 9-cis, 11trans, which has a potentiating effect on the transmission of PPARγ (fatty acids) nucleus, the main regulator of fat cell differentiation. It acts as a stimulant of adiponectin secretion, and this mechanism can partially counteract the anti-hypertensive, anti-hyperlipidemic, anti-angiogenic effects (effective in preventing cancer metastasis), as well as offering atherosclerotic, anti-cancer and anti-diabetic properties helpful for improving the human's health (1, 7, 10).

In contrast, the CLA isomer, trans10, could increase cis12 lipolysis, reducing the function of fatty acid synthesis (20), as well as being associated with proatrogenic effects, insulin resistance, and inflammation (5, 17). In addition, CLA has other beneficial physiological effects, such as increasing body muscle, improving the immune system, providing antioxidants (free radical scavengers), serving as an anti-allergy agent and reducing platelet coagulation (2, 7, 18, 21).

The development of economic technologies to increase the nutritional value and bioactive compounds of natural resources (such as cereals and grains) has attracted considerable attention in the recent years (22). Every year, large quantities of residues are produced in the agricultural and food industries; if the recycling of this waste is well managed, it could have many economic and environmental benefits (23). In addition, the use of metabolites can generate new sources (24, 25). The waste of food oil factories is a problem in developed countries; it is of particular importance to researchers due to environmental issues (26) as the seeds of oil products are a significant share the production. So, it is considered as a source. Moreover, for proper evaluation, waste recycling can be important in terms of economic, environmental, social and ecological aspects. Therefore, conversion of biomass into high value-added compounds can be very beneficial (23). As the use of agricultural waste in industry also reduces production costs, it usually accounts for 25 to 50 percent of total production costs (7). Its consumption improves various biological parameters related to the human's health.

Soybean is the most commonly produced oil crop in the world. Soybean oil is primarily used in the production of shortening, margarines, cooking/frying oils, salad dressings, and mayonnaise (27). Soybeans are currently one of the most important foods (28); they are the second largest source of vegetable oil worldwide (after palm oil), with a high economic value (29). They also have a strategic potential in food safety and bioactive compounds for human needs (30). In addition, they could be regarded as one of the most popular plant foods used in food and medicine. Soybeans are mechanically pressed to extract oil by cold pressing or chemically processed with organic solvents such as hexane. The cold press method leads to products free of organic solvents (31). After the production of oil from oil seeds, valuable by-products (cakes / meal) rich in proteins, few lipids, carbohydrates, and bioactive compounds may be obtained (30, 32, 33). In addition, they could be considered as a rich source of protein, as they contain amino acids, oligosaccharides, vitamins B and E, and minerals (34). Also, they contain isoflavones that can promote the growth of microorganisms. Moreover, soybean mills can use them as a substrate in biological fermentation processes to produce fatty acids (35). Soybean cake is an important source for bioactive compounds such as phenolic compounds and lecithin which are proved that have health benefits (27). In addition using this waste can help the environmental condition and providing huge economic benefits (36).

One of the oldest processes applied by humans is the solid state fermentation used for food (11). Solid fermentation is a biological process with a high potential for bio-enhancing the conversion of plant wastes into many valuable compounds (22). Solid state fermentation has many advantages, including cost-effectiveness,

low water consumption, less volume of equipment, high efficiency production per unit volume and easier aerobic process. In addition, there is an increase of the oxygen diffusion rate in wet solids (37, 38). The selection of bacteria capable of synthesizing CLA or CLNA under *in vitro* condition is the first step required to evaluate the possible effect of their production during food fermentation or their impact on the surface of the intestine. Conversion and isomer patterns depend on various factors (37). In this regard, bifidobacteria have attracted much attention; they are considered as the most interesting genus for the in-situ production of CFA (6). There is also some evidence showing that the ability to convert linoleic acid (LA) to CLA is strain specific, (5) and that the conversion rates vary, depending on growth conditions and matrix (39). Few studies have been, however, performed on the production of fatty acids with the help of a group of bacteria such as *Bifidobacterium* and *Lactobacillus* species, which are mainly used as probiotics (18). Most strains of *Bifidobacterium* are more efficient at synthesizing CLA and conjugated linolenic acid (CLNA), despite producing lower levels of conjugated fatty acids (37, 40).

Not only do they have the potential to accelerate the production or recovery of conjugated linoleic acid and CLNA from LA and α-linolenic acid (ALA) (6, 20, 21, 34, 37, 39, 40), but also have the ability to grow in soybean litter and use its carbohydrates (sucrose, raffinose and stachyose) by modifying the substrate to increase its nutritional and functional properties (13, 34, 41). By producing the enzyme α-galactosidase or β-glucosidase and also, hydrolyzing the proteins in it, lactic acid can be produced with a decrease in pH. The capability of some species of LAB, including propionibacteria and bifidobacteria, to in-vitro conjugate LA or LNA has been considered for many years. Producing functional foods enriched in conjugated fatty acids by using them as starter or adjunct culture can be considered a promising topic for further development and study (39). Innovation has always been the key to success. We should make the optimal use to ensure future progress and success. Given to the rate of obesity and mortality due to cardiovascular diseases, diabetes and cancer (silent death), especially in the young generation (2), soybean meal can be considered as an excellent, natural, low-cost and cost-effective substitute serving as a substrate for use in solid state fermentation (SSF) for the production of fatty acids (7, 13, 20). The aim of this study was, therefore, to produce beneficial fatty acids (CLA) and (EPA) by *Bifidobacterium lactis* on a soybean meal-based substrate as a natural, rich, suitable, inexpensive and available environment to return part of the waste of food oil factories in the production cycle.

MATERIALS AND METHODS

Materials

Bifidobacterium lactis (BBo4, Persian TypeCulture Collection) was provided from the Microbial Collection of the Microbiology Laboratory, Department of Food Science and Engineering, University of Tehran, Iran. The SPC and chemical solutions were provided from Ghiam Kesht and Sanat Company (Iran) and Merck (Germany), respectively.

Preparation of the Bacteria

In this process, the bacterium was linearly cultured twice, each for 24 h, in an MRS agar medium containing 0.5 gram per liter L-cysteine and placed in an anaerobic incubator (Model D-91126, Memmert Co., Germany) at 37°C. To enrich bacteria, they were first put in an MRS broth medium and incubated three times, each for 24 h, at 37°C. The cells were collected at the end of the growth phase in the MRS broth through the centrifuge and rinsed twice to obtain $1.5^* 10^7$ in 0.5 Mcfarland standard; then the tirbidity of the batcerial suspension was adjusted to the 0.5 Mcfarland standard ($1.5^* 10^8$). The inoculation size was optimized to support solid bed fermentation; thus, dilutions of 2, 4, 6% were made. To draw the growth kinetics, curve was made by the first degree equation ($rx = dCx / dt = \mu Cx\text{-}KdCx$) (41, 42). After bacteria transfer to the broth media, the agar rate absorption at 0, 1, 2, 3, 4, 6, and 18 h was measured to draw the curve (**Figure 1**).

Substrate Preparation

The SPC was taken out of the refrigerator and rinsed twice with water; then it was soaked in distilled water for 12 h. In the last stage, the surface water was wholly discarded, and SPC was rinsed again and poured in a mixer to be homogenized. About 150 g of this homogenized soybean paste was weighed by a digital scale of (0.0001 g) high accuracy that was put into a flask and sterilized by autoclave (Iran Tolid Medical Industries Co.) at 121°C for 15 min. After cooling, humidity was measured in the oven at 105°C; the humidity content of the meal was calculated as the base humidity.

Inoculation of Bacteria Into the Culture Medium

When the sterilized homogenized SPC reached the room temperature, the conjugated mixture without inoculation was considered as the control. Without adding any additives like vitamin k, hemein and sucrose, the microbial suspension was inoculated at 2, 4, and 6%. After that, it was homogenized (13) at three humidity levels (60, 70, and 80%) and poured on the plates; then they were incubated at 30, 37, and 44°C for 48 h as the response surface methodology (RSM) response levels (**Table 1**). The cells volume after inoculation was about 3, 6, and 9^*10^7 CFU/g, with 2, 4, and 6% inoculation, respectively. After 48 h, to ensure the purity of the inoculated bacteria, the slide was prepared and colored through the gram method; this was observed through the Olympus optical microscope, thus confirming the purity of bifidobacteria.

Microbial Count

Cell viability was determined through the dilution surface method in the MRS agar. After the inoculation of the solution, ten tubes were prepared. Each tube was placed on the MRS agar plate in the incubator for 24 h at 37°C; the results were expressed as CFU/g (13).

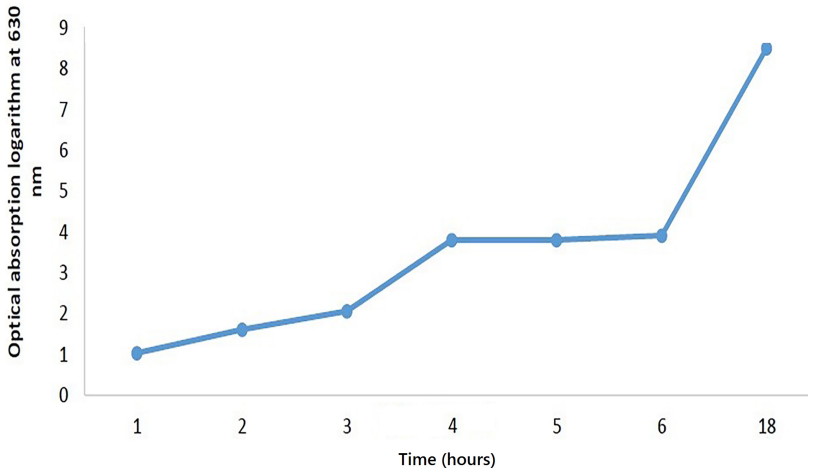

FIGURE 1 | *Bifidobacterium lactis* growth curve.

Measuring pH Changes

The pH changes of the samples after inoculation time (0, 24, and 48 h) were recorded by a pH meter (Model 826 Metrohem Co., Swiss) and reported as Response 1 (7, 13), as can be seen in **Table 1**.

Measurement of Conjugated Linoleic Acid by Spectrophotometer

After 48 h incubation, rapid spectrophotometry based on UV absorption was used for bifidobacteria screening and determination of their growth ability, producing CLA according to (5). The culture sample was centrifuged through the refrigerated centrifuge (Model 3-30K, Sigma Co., Germany) at 13,000 rpm; then 1 ml of the supernatant was mixed with 2 ml of isopropanol and vortexed after adding 1.5 ml hexane. Subsequently, the sample was held for 5 min at room temperature and the hexane layer was collected. Then the absorption rate was determined by a spectrophotometer (Biochrome WPA, United Kingdom) at 233 nm. The data were recorded as response 2 in the RSM model (**Table 1**).

TABLE 1 | Independent variables and response data in the response surface method (RSM) method.

Run	Real values (coded)			Response 1 = pH at 48 h	Response 2 = Absorbance
	X1	X2	X3		
1	37 (0)	60 (−1)	2 (−1)	5.5	0.2
2	44 (1)	70 (0)	2 (−1)	5.3	0.5
3	44 (1)	60 (−1)	4 (0)	5.4	0.45
4	37 (0)	80 (1)	2 (−1)	5.45	0.43
5	37 (0)	60 (−1)	6 (1)	5.35	0.55
6	30 (−1)	60 (−1)	4 (0)	5.41	0.51
7	44 (1)	80 (1)	4 (0)	5.48	0.5
8	37 (0)	80 (1)	6 (1)	5.1	0.7
9	30 (−1)	70 (0)	2 (−1)	5.2	0.72
10	44 (1)	70 (0)	6 (1)	5.3	0.67
11	30 (−1)	80 (1)	4 (0)	4.68	0.9
12	30 (−1)	70 (0)	6 (1)	4.64	1.2
13	37 (0)	70 (0)	4 (0)	4.3	2.2
14	37 (0)	70 (0)	4 (0)	4.2	2.15
15	37 (0)	70 (0)	4 (0)	4.15	2.21
16	37 (0)	70 (0)	4 (0)	4.1	2.25
17	37 (0)	70 (0)	4 (0)	4	2.24

X1: Temperature, X2: Humidity, X3: Inoculation.

Fatty Acids Analysis

The modified Folch method was used for the lipid extraction of the SPC (20). Accordingly, 5 g of the sample was mixed and vortexed with a 100 ml 2:1 chloroform/methanol mixture; then it was centrifuged at 5,000 rpm and passed through Whatman paper No. 0.22. After that, 5 ml of distilled water was added to the filtered liquid, which was vortexed and centrifuged again for 10 min under the same conditions. At this stage, the upper phase was discarded and the lower phase was evaporated at 40°C and 80rpm by the rotary evaporator (IKA RV 10 model). The fatty acids composition of the sample was determined by the gas chromatography (GC) method (10); the National Standard of Iran No. 13126-2 was applied for the separation and methylation of fatty acids to produce fatty acid methyl ester (FAME). FAMEs were then separated and quantified in a gas chromatograph (Nexis 2030 Shimadzu model, Japan) equipped with a flame ionization detector (FID) and capillary column (Dikmacap-2330; 60 m × 0.25 mm × 0.20 μm), with the injector and detector temperature of 250°C and 260°C, respectively. The injection volume was 1 μl and hydrogen was used as the carrier gas with a flow rate of 2 ml/min. The column temperature, which began at 60°C, was held for 2 min. The temperature was raised to 200°C at a rate of 10°C min^{-1}; then it was raised to a final of 240°C. This temperature was held for 7 min. The method of identifying the fatty acids was determined by comparison with the known mix fatty acids methyl standards. The data were presented as the percent of total fatty acids (TFA).

Experimental Design and Statistical Analysis

The RSM method and the Box Behnken Design (BBD) were applied to predict and optimize the efficiency of a particular process and to maximize production through the response level method. Numerical optimization was also applied to obtain the appropriate answers. This design was actuated with three factors, each at three levels and with five repetitions in the center point, including 17 experimental tests. The homogeneous soybean meal pastes with 60, 70, and 80% humidity (X2) as the substrate and different inoculation values of 2, 4, and 6% (X3), at 30, 37, and 44°C (X1), were selected as the variables to assess the maximization of the bacterial strain response. In the RSM method, for each dependent variable, a model is defined, where the main and interacting factors on each variable are expressed (43, 44). The multivariate model was expressed through the Eq. 1.

$$Yn = b0 + \sum_{i=1}^{3} bixi + \sum_{i=1}^{3} biixij + \sum_{i \neq j=1}^{3} bijxixj \quad (1)$$

where, Yn is the predicted answer, b0 is the constant coefficient, bi refers to the linear effects, bii is the quadratic effect, bij is the interaction, and xi and xj are the independent variables. Then the maximum and minimum limits of each variable were coded. The codes assigned to the independent variables are presented in **Table 1**. The optimal conditions were determined according to the response level method. The first and second factors (Temperature and Humidity: X1 and X2), without applying the third factor (Inoculation:X3), were involved in comparing the results. At this stage, the experiment was designed to allow the optimal conditions. The data were analyzed using the ANOVA Design Expert (Ver. 11) and SPSS (Ver. 16) software.

RESULTS AND DISCUSSION

The Behavior of *Bifidobacterium* on the Substrate

The growth of *B. lactis* on the SPC is represented in **Figure 1**. To assess the growth pattern of microbes on this medium, the microbial population was compared with a specific culture of the MRS agar and the best growth pattern of microorganisms, in regard to the four variables during fermentation. So, pH, temperature and microbial growth stages are the most critical factors in the biological production and viscosity of inoculated linoleic acid (45). The growth of bifidobacteria on the SPC was evaluated in different conditions including pH, temperature, humidity and inoculum percentage.

The results showed that microorganisms could well grow in the substrate at different humidity, temperature and inoculum levels. At the beginning of the fermentation process, the bacterial population did not increase considerably. Due to the adaptation of the microorganisms to the new growth environment, there was no significant change in cell population and pH. However, after 18 h of fermentation, there was a sharp decrease in pH from 6.6 to 5.8. In addition, the cell population augmented the initial value. After 24 h, the bacterium entered the logarithmic phase, reaching its maximum population; the tarnished state due to this increase was evident on the medium. In the last h of fermentation (48 h), the decrease in the bacteria count was apparent by a lower drop of pH, at all humidity levels and 30 and 37°C, except 44°C. In contrast, the pH of the control sample remained unchanged. In general, the fermentation process of bifidobacteria lactis was within 8–48 h (7, 11, 40); however, in this experiment, the highest bacterial growth occurred within 24–48 h after inoculation. After the complete fermentation of the substrate, the bacteria growth rate in the SPC culture medium followed a descending trend. After approximately 48 to 72 h, it stopped, leading to the death of some bacteria. After 24 h of fermentation, no more change in pH was observed and a decrease in the decline of the cell population occurred. It was also found that with the increase of the fermentation time, the oligosaccharides and crude protein content of the soybean meal was consumed by bacteria, and solid-state fermentation could considerably increase the solubility of the protein in substrate amino acids (34). The hydrolysis of proteins in the fermented SPC depends on the type of bacterial strain and the substrate humidity content (42, 46). It was found that an increase in the produced lactic acid volume in the culture medium decreased the pH rate. Another influential factor is the inoculated bacteria level in their growth kinetics. Optimal bacterial growth depends on the internal and external humidity of the culture medium surface. Primary substrate humidity is a vital factor in bacterial growth, and a humidity level above 50% in SSF promotes the development of microorganisms (40, 45). After fermentation, the loss of high humidity content could lead to the increased

TABLE 2 | Analysis of variance related to pH and absorbance data obtained from the Box Behnken Design.

		Measurement	
Source	**Degree of freedom**	**pH**	**Absorbance**
Model	9	0.5633***	1.081633***
X_1	1	0.3003***	0.183013***
X_2	1	0.1128*	0.08405***
X_3	1	0.1405**	0.201613***
X_1X_2	1	0.164**	0.0289*
X_1X_3	1	0.0784*	0.024025*
X_2X_3	1	0.01	0.0016
X_1^2	1	0.765***	1.827164***
X_2^2	1	1.87***	3.890533***
X_3^2	1	1.2***	2.55348***
Residual	7	0.0094	0.00247
Lack of Fit	3	0.0053	0.00369
Pure Error	4	0.0125	0.00155
Cor Total	16		
R^2		98.72%	98.82%
R^2 adj		97.07%	99.60%

****, **, *: Significant at $p \leq 0.001$., $p \leq 0.01$, $p \leq 0.05$.*
X_1 : Temperature, X_2 : Humidity, X_3 : Inoculation; MS: Mean Square.

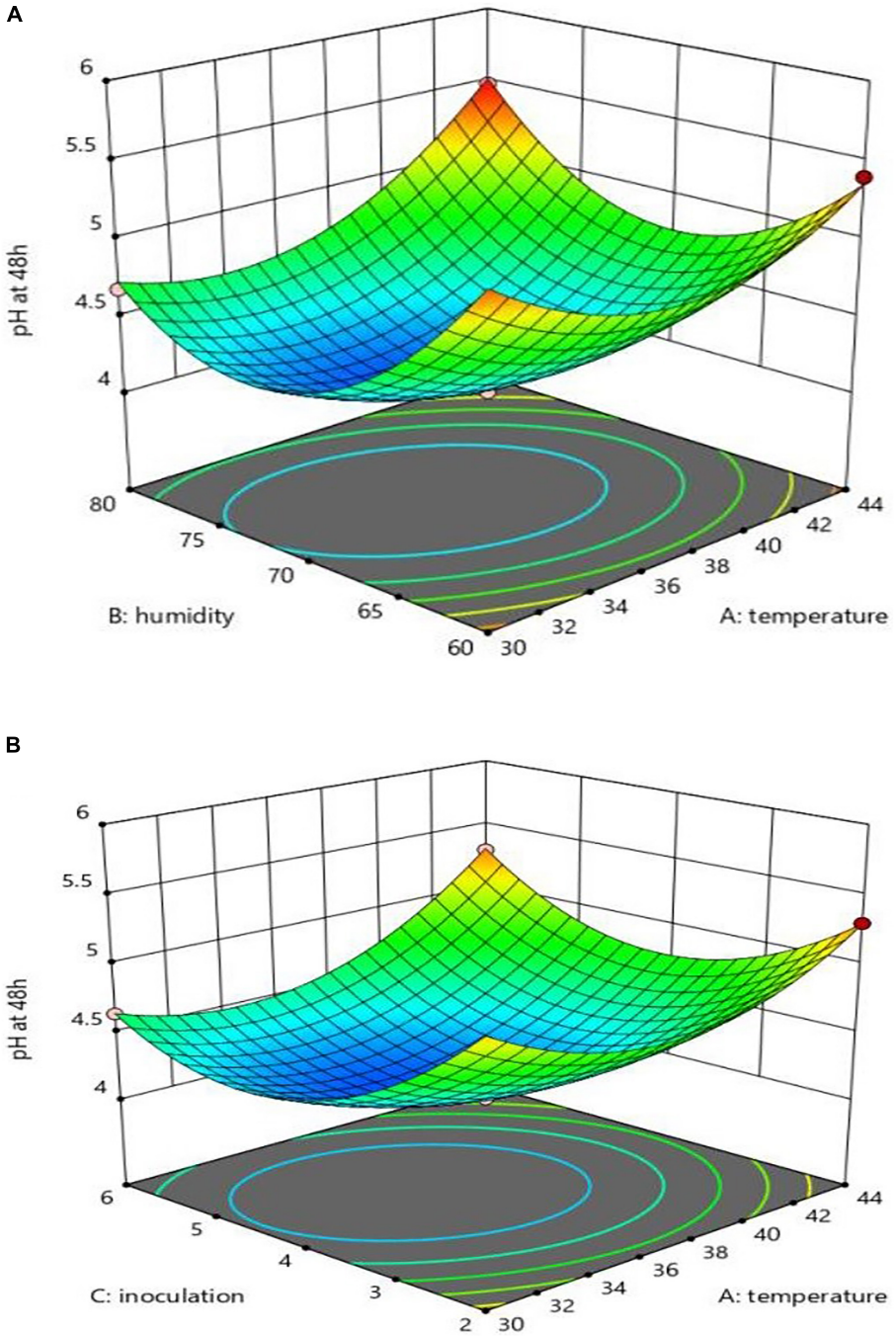

FIGURE 2 | Interaction effect of temperature and humidity **(A)**, and temperature and inoculation **(B)** on pH.

material concentration at the culture medium, thus indicating the end of the growth phase (11). Bifidobacteria lactis in the SPC exhibited high compatibility at 70% humidity and 4% inoculation level, with the lowest pH of (4.0) at 37°C, (**Table 1**). After 48 h fermentation, no more change in pH was observed and a decline in cell population occurred. The bacteria count reduction rate after 48 h was due to the decrease in the pH and volume of the nutrients. No provision of the nutritional demand for microorganisms and low humidity could prevent their growth (11, 13, 40).

Optimal Conditions Based on the Response Level

The results of the variance analysis of pH and absorption indices are tabulated in **Table 2**. The parameters R^2-sq, R^2 sq - (adj),

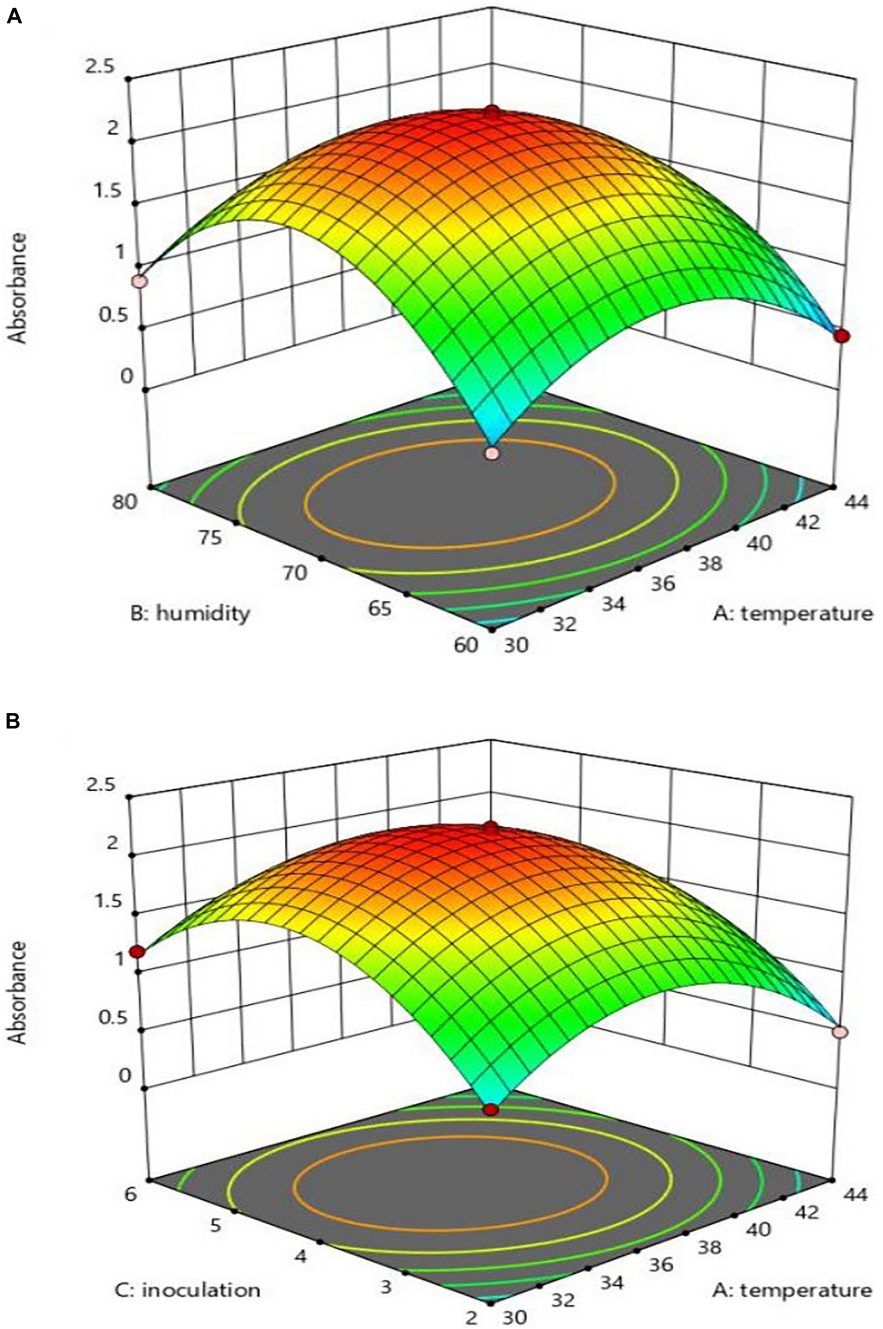

FIGURE 3 | Interaction effect of temperature and inoculation **(A)**, and temperature and humidity **(B)** on absorption.

and *p*-value indicated a high correlation between the observed and predicted values (47). Data analysis based on the linear model was, however, insignificant for all factors, and the most significant and high correlation model was the quadratic one. The high volumes of R^2-sq and R^2- adj for the models (98.72 and 97.07%) with pH and (98.82 and 99.6%) absorption response levels indicated that the predicted models for CLA and EPA production were suitable and of high regression coefficients. Lack of fit did not, however, show a significant effect. The first ($P < 0.05$) and second ($P < 0.001$) degree effects of the three parameters, namely, X1 (temperature), X2 (humidity) and X3 (inoculation), had a significant interaction with X1, X2 and X1 and X3 in terms of pH response absorption. Their interactions were significant at ($P < 0.05$) (**Table 2**).

pH Changes

Assessments run on the pH changes in each of the variables (48 h at the substrate) revealed that 44 degrees had a preventive effect

on CLA production. The substrate pH was not reduced, as shown in **Figure 2**; meanwhile, the inoculation level had a positive impact, as compared to humidity, on increasing production (reduced pH), as can be seen in **Figure 2**. The interactions of X1 and X2 and X1 and X3 on production were, however, negative. Meanwhile, inoculation had no significant impact on humidity, as can be seen in **Figures 2A,B**. A separate analysis of the practical factors on the production yield showed an increase of temperature from 30 to 37°C, humidity from 60 to 70%, and inoculation from 2 to 4%. With the rise of temperature from 37 to 44°C (only after 24 h), humidity from 70 to 80%, and inoculation from 4 to 6%, the pH level followed a descending trend; after 48 h injection, the substrate pH remained unchanged at 44°C. The equation of pH changes based on these three parameters and their interactions, according to the significance of the coefficients of the equation, is expressed as follows:

$$\begin{aligned} \mathrm{pH} \;=\; & 4.15 + 0.194X_1 \;- 0.119X_2 - 0.132X_3 + 0.426X_1^2 \\ & +0.666X_2^2 + 0.534X_3^2 + 0.203X_1X_2 + 0.14X_1X_3 \end{aligned} \quad (2)$$

Note that because the interaction effect of X2 and X3 was insignificant, as shown in **Table 2**, they are not expressed in this equation.

The interaction diagram of X1_ X3 and X1 _X2 at 70% and the inoculation of 4% indicated that the highest pH was at 44°C and the inoculation of 6 and 2%, as shown **Figure 2A**; also, the temperature of 44°C and humidity of 80% should be mentioned, as can be seen in **Figure 2B**. For pH less than 4.2, the approximate inoculation range was estimated to be 3.5–5.0, and temperature was 31.9–38.9°C.

Absorption

Assessing the variables' absorption rate revealed that X2 had a more significant effect on the absorption rate than X1 and X3, while significant interactions could harm production. The 3D figures are based on the X1 and X3 interaction absorption rate, as shown in **Figures 3A,B**. The interaction effect of X1*X2 and X1*X3 on pH 48 h after inoculation revealed the highest absorption level results when pH was at its lowest, that is, X1 at 37°C, X3 at 4% and X2 at 70%, as can be seen in **Figures 3A,B**. Simultaneous optimization through the utility volume of 0.991% in the soybean meal was significant for all three responses. The correlations between the independent variables of the experiment and the absorption level concerning the insignificant nature of X2 and X3 interactions, according to **Table 2**, are expressed in Eq. 3:

$$\begin{aligned} \mathrm{Abs.} \;=\; & 2.21 - 0.151X_1 + 0.103X_2 + 0.159X_3 - 0.659X_1^2 \\ & -0.961X_2^2 + 0.779X_3^2 - 0.085X_1X_2 - 0.078X_1X_3 \end{aligned} \quad (3)$$

Bacterial Screening at the Production Rate

Bifidobacterium lactis was screened to produce EPA and CLA by measuring the absorbance at 233 nm. *B. lactis* in the SPC at different X1, X2, and X3 levels (except 44°C) 48 h after inoculation, at a decreased pH index, revealed the production ability of other volumes (42). The highest absorption rate (more than 2) in the culture medium was observed at 70% humidity, 37°C and 4% inoculation level, with a 4.15 pH level. At the temperature of 44°C, humidity of 80% and inoculation level of 6%, there was a negative effect on production, as also shown by (25). According to the optimal surface model, the highest production occurred in the central region, with the temperature of 36–37°C, inoculation level of 3.5–5%, and humidity of 68–72%. The highest optimum point of the predicted volume from the operations consisted of 36.040°C, 70.532% humidity, 4.222% inoculation and absorption point >2.231, as can be seen in

TABLE 3 | The optimal value of different independent variables (temperature, humidity, and inoculation) and responses based on the highest absorption rate at the lowest pH.

		Optimum value
Variable	Temperature	36.040
	Humidity	70.532
	Inoculation	4.222
Response	pH at 48 h	4.114
	Absorbance	2.231
	Appropriateness	0.991

TABLE 4 | Fatty acids composition (% total fatty acids) of the SPC with (B) and without *Bifidobacter lactis* (A).

Fatty acids	A	B	Inoculation change (Δ*)
C12:0	1.55	1.27	−0.28
C14:0	1.26	1.73	+0.47
C14:1	0.41	0.3	−0.11
C15:0	0.26	1	+0.74
C15:1	0.29	0.18	−0.11
C16:0	18.57	29.3	+10.37
C16:1	0.21	0.23	+0.2
C17:0	0.22	0.3	+0.8
C17:1	ND	0.11	+0.11
C18:0	13.35	24.81	+11.35
C18:1t	0.34	0.22	−0.12
C18:1c	27.45	14.82	−12.63
C18:2t	0.29	0.31	+0.2
C18:2c	30.41	19.89	−10.52
C18:3t	ND	0.4	+0.4
C18:3c	1.92	1.86	−0.6
C20:0	0.68	0.56	−0.12
CLA c9t11	ND	0.18	+0.18
CLA t10c12	ND	ND	ND
C20:1	0.13	ND	−0.13
C20:2	ND	0.1	+0.1
C20:4n-6	ND	ND	ND
C22:0	0.51	0.44	−0.7
C22:1	ND	0.35	+0.35
C20:5 n-3(EPA)	ND	0.39	+0.39
C24:0	0.56	0.2	−0.54
C24:1	0.07	ND	−0.07
C22:6 n-3 (DHA)	ND	ND	ND

*Δ = *B*−*A, ND: not detectable.*

Table 3. The experimental results, thus, confirmed the optimal rates. The substrate concentration strongly affected LA/LNA to CLA containing the produced oil conversion rate through the *B. lactis* strain (48). The CLA production was variable due to the response of bifidobacteria lactis to the substrate fatty acids level and composition (37). pH and temperature could be, therefore, regarded as important environmental parameters that change the structure and affect the diversity of distribution (49, 50).

Fatty Acids Composition

The fatty acids (FA) profile of the SPC inoculated with (48 h) and without *B. lactis* and their changes are presented in **Table 4**. The most positive changes of FAs were seen in the two main strains of saturated FA (palmitic (C16:0) and stearic (C18:0) acids, with the inoculation of Bifidobacteria on the SPC. On the other hand, the mono and polyunsaturated FA (oleic (C18: 1n-9) and linoleic (C18: 2n-6) acids, which had the highest proportion of FAs in the SPC, showed the most negative change by bacterial inoculation (**Table 4**). *B. lactis* is a bacterial strain that can easily adapt itself to using substrate nutrients (37), such as FAs, for its growth. This bacterium can convert linoleic acid to CLA with the linoleate isomerase enzyme (5). Furthermore, it breaks down the proteins of the soybean meal, producing free amino acids and other compounds, with the substrate having more buffering capacity. On the other hand, fermentation of various carbohydrates in the substrate causes the production of lactic acid, reducing the pH value of the culture medium of *Bifidobacterium* (7). The 4% inoculation rate of *Bifidobacterium* in the SPC containing 70% humidity and incubated at 37 ° C showed the highest pH reduction, producing 9*cis* and 11*trans* CLA (c9-t11 CLA) and EPA at 0.18 and 0.39% of the total FA, respectively (**Table 4**). Meanwhile, the other isomers of CLA such as t10-c12 CLA were not detected (47). Moreover, *B. lactisis*, as other lactic acid bacteria such as *Lactobacillus plantarum* (42)), can grow on the SSF SPC. The soybean meal pressed cake has sufficient nutrient levels (13) to support the growth of these bacteria without the need to add carbohydrate and protein supplements (7, 9). Another researcher has also mentioned that the FAs proportion and their isomer types are dependent on pH, temperature, microbial inoculation level, substrate concentration and activation method used for bacterial strain (48).

CONCLUSION

Using microbial cultures in producing and increasing CLA and EPA concentrations in fermented foods is not an easy task and usually of meager yield. Despite the lower potency of *B. lactis* (BBo4, Persian Type, Culture Collection, Iran), as compared to other bifidobacteria strains, due to the value of pure isomer produced, this study was performed to evaluate the potency of the SPC as an almost oil-free substrate, considering SPC as one of the most source for bioactive compounds (26) extracted oil may contain these healthy materials although the huge waste of soybean oil production can supply the cheap and safe substrate for CLA and EPA production (37). The use of soybean meal increased lactic acid during solid-state fermentation. Due to the intrinsic properties of soybean meal, it increased the substrate fatty acids, thus producing conjugated linoleic and eicosapentaenoic acids. Given the experimental design conditions and methods adopted in the production of cheap isomers at a low cost, by considering the health features and probiotic aspects of the *B. lactis* strain, the soybean meal could be considered as a natural (plant) substrate available for producing this substance. While the findings here are valuable, more in-depth studies should be run in regard to the type of sub-bedding produced by the microbial strain through considering dietary supplements for the higher concentrations of CLA. It was revealed that the oil produced from plant waste could be adopted and the microbial isomerization method could be used to produce bioactive compounds and to make valuable substances; in addition to reducing the food production costs, it could decrease such outlets' expenses. This, in turn, would improve the added value therein. At this age of recycling waste, in regard to healthy foods, resorting to natural waste products is of importance, in addition to protecting the environment.

In this context, the previous research has mostly focused on identifying CLA / CLNA-producing bacteria, evaluating production under general growth conditions, and using substrate concentration by chromatography / spectrophotometry through Bifidobacteria on soybean. The capability of some species of LAB including propionibacteria and bifidobacteria to in-vitro conjugate the LA or LNA has been shown over the years. Producing functional foods enriched in conjugated fatty acids by using it as a starter or adjunct culture can be considered a promising topic to for further development and study (38).

DATA AVAILABILITY STATEMENT

The original contributions presented in this study are included in the article/supplementary material, further inquiries can be directed to the corresponding author.

AUTHOR CONTRIBUTIONS

SA was mainly responsible for all phases of this research. MH developed the idea and guided the whole project and conducted analyses. ZM helped in the microbial analysis. HK and SJ also helped to improve the research and the manuscript. All authors contributed to the article and approved the submitted version.

FUNDING

This study was supported by the Islamic Azad University, Grant Number: 76576.

ACKNOWLEDGMENTS

We appreciate the Laboratory of Faculty of Agriculture, Tehran University, for providing the microbial strain. We also thank Ghiam Company for providing the press cake used in this study.

REFERENCES

1. Dhiman TR, Satter LD, Pariza MW, Galli MP, Albright K, Tolosa MX. Conjugated linoleic acid (CLA) content of milk from cows offered diets rich in linoleic and linolenic acid. *J Dairy Sci.* (2000) 83:1016–27. doi: 10.3168/jds.S0022-0302(00)74966-6
2. Erinc H, Isler IH. Optimization of conjugated linoleic acid production from safflower oil and purification by low temperature crystallization. *Acta Aliment.* (2019) 48:37–46. doi: 10.1556/066.2018.0008
3. Shaikh AE, Pawar A, Parmar H, Vadgama RN, Lali AM, Odaneth AA. Conjugated linoleic acid production by lactic acid bacteria: a bio-transformation study in media with oil hydrolysates. *J Appl Biotechnol Bioeng.* (2018) 5:321–7. doi: 10.15406/jabb.2018.05.00158
4. Shayanmehr MR, Elhamirad AH, Armin M. Optimization of conjugated linoleic acid (Cla) synthesis conditions applying it in milk enrichment. *J Res Innov Food Sci Technol.* (2021) 9:375–88. doi: 10.22101/jrifst.2020.216650.1145
5. Raimondi S, Amaretti A, Leonardi A, Quartieri A, Gozzoli C, Rossi M. Conjugated linoleic acid production by bifidobacteria: screening, kinetic, and composition. *Biomed Res Int.* (2016) 2016:8654317. doi: 10.1155/2016/8654317
6. Salsinha AS, Pimentel LL, Fontes AL, Gomes AM, Rodríguez-Alcalá LM. Microbial production of conjugated linoleic acid and conjugated linolenic acid relies on a multienzymatic system. *Microbiol Mol Biol Rev.* (2018) 82:e00019-18. doi: 10.1128/mmbr.00019-18
7. Correa Deza MA, Rodríguez de Olmos A, Garro MS. Solid state fermentation to obtain vegetable products bio-enriched with isoflavone aglycones using lactic cultures. *Rev Argent Microbiol.* (2019) 51:201–7. doi: 10.1016/j.ram.2018.04.006
8. den Hartigh LJ. Conjugated linoleic acid effects on cancer, obesity, and atherosclerosis: a review of pre-clinical and human trials with current perspectives. *Nutrients.* (2018) 11:370. doi: 10.3390/nu11020370
9. Afarin M, Alemzadeh I, Yazdi ZK. Conjugated linoleic acid production and optimization via catalytic reaction method using safflower oil. *Int J Eng Trans B Appl.* (2018) 31:1166–71. doi: 10.5829/ije.2018.31.08b.02
10. Martha R, Toharmat T, Rofiah N, Anggraeni D. Comparison of extraction methods for fatty acid and conjugated linoleic acid quantification in milk. In: *Proceedings of the IOP Conference Series: Materials Science and Engineering*. Bristol: IOP Publishing (2019). p. 42022.
11. Van Nieuwenhove CP, Teran V, Nelina S. Conjugated linoleic and linolenic acid production by bacteria: development of functional foods. In: Rigobelo EC editor. *Probiotics*. London: InTech (2012). doi: 10.5772/50321
12. Kuhl GC, Lindner JDD. Biohydrogenation of linoleic acid by lactic acid bacteria for the production of functional cultured dairy products: a review. *Foods.* (2016) 5:13. doi: 10.3390/foods5010013
13. Rodríguez de Olmos A, Correa Deza MA, Garro MS. Selected lactobacilli and bifidobacteria development in solid state fermentation using soybean paste. *Rev Argent Microbiol.* (2017) 49:62–9. doi: 10.1016/j.ram.2016.08.007
14. Adkins Y, Kelley DS. Mechanisms underlying the cardioprotective effects of omega-3 polyunsaturated fatty acids. *J Nutr Biochem.* (2010) 21:781–92. doi: 10.1016/j.jnutbio.2009.12.004
15. Zhang J, Burgess JG. Enhanced eicosapentaenoic acid production by a new deep-sea marine bacterium *Shewanella electrodiphila* MAR441T. *PLoS One.* (2017) 12:e0188081. doi: 10.1371/journal.pone.0188081
16. Wang Y, Lin Q, Zheng P, Li L, Bao Z, Huang F. Effects of eicosapentaenoic acid and docosahexaenoic acid on chylomicron and VLDL synthesis and secretion in Caco-2 cells. *Biomed Res Int.* (2014) 2014:684325.
17. Lehnen TE, da Silva MR, Camacho A, Marcadenti A, Lehnen AM. A review on effects of conjugated linoleic fatty acid (CLA) upon body composition and energetic metabolism. *J Int Soc Sports Nutr.* (2015) 12:36. doi: 10.1186/s12970-015-0097-4
18. Linares DM, Gómez C, Renes E, Fresno JM, Tornadijo ME, Ross RP, et al. Lactic acid bacteria and bifidobacteria with potential to design natural biofunctional health-promoting dairy foods. *Front Microbiol.* (2017) 8:846. doi: 10.3389/fmicb.2017.00846
19. Martins SV, Madeira A, Lopes PA, Pires VMR, Alfaia CM, Prates JAM, et al. Adipocyte membrane glycerol permeability is involved in the anti-adipogenic effect of conjugated linoleic acid. *Biochem Biophys Res Commun.* (2015) 458:356–61. doi: 10.1016/j.bbrc.2015.01.116
20. Villar-Tajadura MA, Rodríguez-Alcalá LM, Martín V, Gómez De Segura A, Rodríguez JM, Requena T, et al. Production of conjugated linoleic and conjugated α-linolenic acid in a reconstituted skim milk-based medium by bifidobacterial strains isolated from human breast milk. *Biomed Res Int.* (2014) 2014:725406. doi: 10.1155/2014/725406
21. Terán V, Pizarro PL, Zacarías MF, Vinderola G, Medina R, Van Nieuwenhove C. Production of conjugated dienoic and trienoic fatty acids by lactic acid bacteria and bifidobacteria. *J Funct Foods.* (2015) 19:417–25. doi: 10.1016/j.jff.2015.09.046
22. Chen Y, Wang Y, Chen J, Tang H, Wang C, Li Z, et al. Bioprocessing of soybeans (*Glycine max* L.) by solid-state fermentation with *Eurotium cristatum* YL-1 improves total phenolic content, isoflavone aglycones, and antioxidant activity. *RSC Adv.* (2020) 10:16928–41. doi: 10.1039/c9ra10344a
23. Şahin S, Elhussein EAA. Valorization of a biomass: phytochemicals in oilseed by-products. *Phytochem Rev.* (2018) 17:657–68. doi: 10.1007/s11101-018-9552-6
24. Laufenberg G, Kunz B, Nystroem M. Transformation of vegetable waste into value added products: (A) the upgrading concept; (B) practical implementations. *Bioresour Technol.* (2003) 87:167–98. doi: 10.1016/S0960-8524(02)00167-0
25. Cravotto G, Mariatti F, Gunjevic V, Secondo M, Villa M, Parolin J, et al. Pilot scale cavitational reactors and other enabling technologies to design the industrial recovery of polyphenols from agro-food by-products, a technical and economical overview. *Foods.* (2018) 7:130. doi: 10.3390/foods7090130
26. Food and Agriculture Organization of the United Nations [FAO]. *Food Wastage Footprint Impacts on natural resources. Technical Report*. Rome: FAO (2013). p. 249.
27. Ketenoglu O, Kiralan SS, Kiralan M, Ozkan G, Ramadan MF. Cold pressed black cumin (*Nigella sativa* L.) seed oil. In: Ramadan MF editor. *Cold Pressed Oils: Green Technology, Bioactive Compounds, Functionality, and Applications*. Amsterdam: Elsevier (2020). p. 53–64. doi: 10.1016/b978-0-12-818188-1.00006-2
28. Karuga J. *10 Countries With Largest Soybean Production- WorldAtlas.com*. (2018). Available online at: worldatlas.com/articles/world-leaders-in-soya-soybean-production-by-country.html (accessed March 18, 2020).
29. Wang D, Thakker C, Liu P, Bennett GN, San KY. Efficient production of free fatty acids from soybean meal carbohydrates. *Biotechnol Bioeng.* (2015) 112:2324–33. doi: 10.1002/bit.25633
30. Freitas CS, Da Silva GA, Perrone D, Vericimo MA, Dos S, Baião D, et al. Recovery of antimicrobials and bioaccessible isoflavones and phenolics from soybean (*Glycine max*) meal by aqueous extraction. *Molecules.* (2019) 24:74. doi: 10.3390/molecules24010074
31. Durazzo A, Fawzy Ramadan M, Lucarini M. Editorial: cold pressed oils: a green source of specialty oils. *Front Nutr.* (2022) 8:836651. doi: 10.3389/fnut.2021.836651
32. del Carmen Villalobos M, Serradilla MJ, Martín A, Ordiales E, Ruiz-Moyano S, De Guía Córdoba M. Antioxidant and antimicrobial activity of natural phenolic extract from defatted soybean flour by-product for stone fruit postharvest application. *J Sci Food Agric.* (2016) 96:2116–24. doi: 10.1002/jsfa.7327
33. Tangkhawanit E, Siriamornpun S. Bioactive compounds, biological activity, and starch digestibility of dried soy residues from the soybean oil industry and the effects of hot-air drying. *J Sci Food Agric.* (2022) 102:1719–28. doi: 10.1002/jsfa.11514
34. Popoviæ S, Hromiš N, Šuput D, Bulut S, Romaniæ R, Laziæ V. Valorization of by-products from the production of pressed edible oils to produce biopolymer films. In: Ramadan MF editor. *Cold Pressed Oils*. Amsterdam: Elsevier (2020). p. 15–30. doi: 10.1016/b978-0-12-818188-1.00003-7
35. Zhang ST, Shi Y, Zhang SL, Shang W, Gao XQ, Wang HK. Whole soybean as probiotic lactic acid bacteria carrier food in solid-state fermentation. *Food Control.* (2014) 41:1–6. doi: 10.1016/j.foodcont.2013.12.026
36. Gutiérrez LF. Conjugated linoleic acid in milk and fermented milks: variation and effects of the technological processes. *Vitae.* (2016) 23:134–45. doi: 10.17533/udea.vitae.v23n2a06
37. Ramadan-Hassanien MF. Total antioxidant potential of juices, beverages and hot drinks consumed in Egypt screened by DPPH in vitro assay. *Grasas Aceites.* (2008) 59:254–9. doi: 10.3989/gya.2008.v59.i3.516
38. Fontes AL, Pimentel L, Rodríguez-Alcalá LM, Gomes A. Publisher correction: effect of PUFA substrates on fatty fcid Profile of *Bifidobacterium breve* Ncimb 702258 and CLA/CLNA production in commercial semi-skimmed milk. *Sci Rep.* (2019) 9:4671. doi: 10.1038/s41598-019-40320-3

39. Aziz T, Sarwar A, Daudzai Z, Naseeb J, Din JU, Aftab U, et al. Conjugated fatty acids (CFAS) production via various bacterial strains and their applications. A Review. *J Chil Chem Soc.* (2022) 67:5445–52. doi: 10.4067/S0717-97072022000105445
40. Senizza A, Callegari ML, Senizza B, Minuti A, Rocchetti G, Morelli L, et al. Effects of linoleic acid on gut-derived *Bifidobacterium breve* DSM 20213: a transcriptomic approach. *Microorganisms.* (2019) 7:710. doi: 10.3390/microorganisms7120710
41. Su LW, Cheng YH, Hsiao FSH, Han JC, Yu YH. Optimization of mixed solid-state fermentation of soybean meal by lactobacillus species and *Clostridium butyricum*. *Polish J Microbiol.* (2018) 67:297–305. doi: 10.21307/pjm-2018-035
42. Farazandehnia N. The evaluation of antimicrobial effect of fermented Probiotic milk produced *Lactobacillus casei*, *Lactobacillus plantarum*, *Bifidobacterium* and *Bifidobacterium angultum*. *Iran J Med Microbiol.* (2016) 10:31–8.
43. Park MJ, General T, Lee SP. Physicochemical properties of roasted soybean flour bioconverted by solid-state fermentation using *Bacillus subtilis* and *Lactobacillus plantarum*. *Prev Nutr Food Sci.* (2012) 17:36–45. doi: 10.3746/pnf.2012.17.1.036
44. Aksoylu Özbek Z, Günç Ergönül P. Optimisation of wall material composition of freeze–dried pumpkin seed oil microcapsules: interaction effects of whey protein, maltodextrin, and gum Arabic by D–optimal mixture design approach. *Food Hydrocoll.* (2020) 107:105909. doi: 10.1016/j.foodhyd.2020.105909
45. Ghamari M, Tabatabaei YF, Alemzade I, Vosooghi M, Varidi M, Safari H. Optimization of culture medium containing date waste for lipase production by *Aspergillus niger* using RSM method. *J Food Sci Technol.* (2017) 14:85–96.
46. Zhang P, Li H, Zhao W, Xiong K, Wen H, Yang H, et al. Dynamic analysis of physicochemical characteristics and microbial communities of *Aspergillus*-type douchi during fermentation. *Food Res Int.* (2022) 153:110932. doi: 10.1016/j.foodres.2021.110932
47. Zhao S, Hu N, Huang J, Liang Y, Zhao B. High-yield spore production from *Bacillus licheniformis* by solid state fermentation. *Biotechnol Lett.* (2008) 30:295–7. doi: 10.1007/s10529-007-9540-1
48. Salimi F, Fattahi M, Hamzei J. Optimization of celery seed essential oil extraction and its antioxidant activity using response surface methodology and ultrasound-assisted. *J Hortic Sci.* (2018) 32:171–83.
49. Gorissen L, Raes K, De Smet S, De Vuyst L, Leroy F. Microbial production of conjugated linoleic and linolenic acids in fermented foods: technological bottlenecks. *Eur J Lipid Sci Technol.* (2012) 114:486–91. doi: 10.1002/ejlt.201100239
50. Alhajabdalla M, Mahmoud H, Nasser MS, Hussein IA, Ahmed R, Karami H. Application of response surface methodology and Box-Behnken design for the optimization of the stability of fibrous dispersion used in drilling and completion operations. *ACS Omega.* (2021) 6:2513–25. doi: 10.1021/acsomega.0c04272
51. Zhang Y, Ishikawa M, Koshio S, Yokoyama S, Dossou S, Wang W, et al. Optimization of soybean meal fermentation for aqua-feed with *Bacillus subtilis* natto using the response surface methodology. *Fermentation.* (2021) 7:306. doi: 10.3390/fermentation7040306

Conflict of Interest: The authors declare that the research was conducted in the absence of any commercial or financial relationships that could be construed as a potential conflict of interest.

Publisher's Note: All claims expressed in this article are solely those of the authors and do not necessarily represent those of their affiliated organizations, or those of the publisher, the editors and the reviewers. Any product that may be evaluated in this article, or claim that may be made by its manufacturer, is not guaranteed or endorsed by the publisher.

frontiers | Frontiers in Nutrition

TYPE Original Research
PUBLISHED 24 August 2022
DOI 10.3389/fnut.2022.998946

OPEN ACCESS

EDITED BY
Gengjun Chen,
Kansas State University, United States

REVIEWED BY
Guanghao Li,
Yangzhou University, China
Jiban Shrestha,
Nepal Agricultural Research Council, Nepal

*CORRESPONDENCE
Congfeng Li
licongfeng@caas.cn
Ying Jiang
jiangying@syau.edu.cn

SPECIALTY SECTION
This article was submitted to Nutrition and Food Science Technology, a section of the journal Frontiers in Nutrition

RECEIVED 20 July 2022
ACCEPTED 02 August 2022
PUBLISHED 24 August 2022

CITATION
Ren H, Zhao M, Zhou B, Zhou W, Li K, Qi H, Jiang Y and Li C (2022) Understanding physiological mechanisms of variation in grain filling of maize under high planting density and varying nitrogen applicate rate. *Front. Nutr.* 9:998946. doi: 10.3389/fnut.2022.998946

Understanding physiological mechanisms of variation in grain filling of maize under high planting density and varying nitrogen applicate rate

Hong Ren[1,2], Ming Zhao[1], Baoyuan Zhou[1], Wenbin Zhou[1], Kemin Li[1], Hua Qi[2], Ying Jiang[2]* and Congfeng Li[1]*

[1]Institute of Crop Science, Chinese Academy of Agricultural Sciences/Key Laboratory of Crop Physiology and Ecology, Ministry of Agriculture and Rural Affairs, Beijing, China, [2]College of Agronomy, Shenyang Agricultural University, Shenyang, China

Grain filling is a critical process for achieving a high grain yield in maize (*Zea mays* L.), which can be improved by optimal combination with genotype and nitrogen (N) fertilization. However, the physiological processes of variation in grain filling in hybrids and the underlying mechanisms of carbon (C) and N translocation, particularly under various N fertilizations, remain poorly understood. The field experiment was conducted at Gongzhuling Farm in Jilin, China. In this study, two maize hybrids, i.e., Xianyu 335 (XY335) and Zhengdan958 (ZD958) were grown with N inputs of 0, 150, and 300 kg N ha^{-1} (N0, N150, and N300) in 2015 and 2016. Results showed that the N application significantly optimized grain-filling parameters for both maize hybrids. In particular, there was an increase in the maximum filling rate (G_{max}) and the mean grain-filling rate (G_{mean}) in XY335 by 8.1 and 7.1% compared to ZD958 under the N300 kg ha^{-1} (N300) condition, respectively. Simultaneously, N300 increased the small and big vascular bundles area of phloem, and the number of small vascular bundles in peduncle and cob at the milking stage for XY335. XY335 had higher root bleeding sap (10.4%) and matter transport efficiency (8.4%) of maize under N300 conditions, which greatly enhanced the ^{13}C assimilates and higher C and N in grains to facilitate grain filling compared to ZD958. As a result, the grain yield and the sink capacity for XY335 significantly increased by 6.9 and 6.4% compared to ZD958 under N300 conditions. These findings might provide physiological information on appropriate agronomy practices in enhancing the grain-filling rate and grain yield for maize under different N applications, namely the optimization variety and N condition

noticeably increased grain filling rate after silking by improving ear vascular structure, matter transport efficiency, and enhancing C and N assimilation translocation to grain, eventually a distinct improvement in the grain sink and the grain yield.

KEYWORDS

maize, grain filling, ^{13}C-photosynthates, vascular bundle structure, matter transport efficiency

Introduction

A critical process for achieving high grain yield in maize is grain filling, which is closely associated with kernel number and weight and determined by grain-filling rate (GFR) and period (GFP) (1, 2). The grain filling was affected by nitrogen (N) application and crop genotype, which has been well documented (3, 4). Although increasing plant density improves the grain yield of maize, leaf mutual shading would reduce the pollination rate and photosynthesis, which adversely affect GFR (5) and GFP (6), not only affects grain weight but also kernel number (7, 8). A growing number of studies on N effect on grain filling tend to favor that GFR is more influential than GFP in achieving high grain yield (4, 9). However, the physiological mechanism of N influencing the GFR between two maize hybrids is still unclear, especially under high plant density. Therefore, further research is needed to resolve this question and thus we might gain better insights into the mechanisms of increasing maize grain yield by investigating the grain-filling characteristics between various levels of N inputs.

Three essential factors, assimilate supply, matter transport, and sink capacity, influence grain filling (10–12). Grain filling depends on the grain carbon (C) assimilates obtained from both the C remobilized from reserves of C pools in vegetative organs either pre- or post-anthesis and assimilates currently produced in photosynthetic tissues. Nitrogen has a major role in the initiation of sink size establishment and C (i.e., sucrose) and N assimilates supporting kernel development and growth in interdependent ways during the grain-filling period (13, 14). However, the majority of relevant studies had focused on how N supply alters the final kernel number or N allocation in various parts of plants, while played little attention to how N supply influences C assimilates allocation to kernels during the grain-filling to maturity stages (10, 12, 15). Thus, the determination of C assimilates allocation before and after anthesis would be beneficial to understand the response mechanisms of GFR and GFP between maize hybrids grown with different amounts of N fertilizer.

A robust matter-transport system within a plant is an essential prerequisite for C assimilates allocation from sources to meet the high assimilates requirements of sink establishment, namely kernel development, and growth (16–19). Root bleeding sap is one of the key factors to boost the matter transport system, because its quantity and components reveal the shoot growth potential and root activity (20, 21). Higher matter transport efficiency (MTE) is greatly dependent on the vascular bundle system because this system is the main channel for transporting C and N compounds (14). Both the amount and area of vascular bundles play a crucial role in transporting photosynthates and nutrients (22, 23). Our previous study clearly shows that N fertilizer management increased the number of the small vascular bundle to strongly affect matter transport and crop grain production (9), but played little attention to how crop variety selection and N interaction influence matter transport to grain. Thus, revealing how crop genotype and N application influence the traits of vascular bundles in crops would deepen our understanding of the variability in matter transport and nutrient allocation in crops.

Kernel's ability to utilize and absorb assimilates was highly dependent on N fertilization and crop genotype. Appropriate high N fertilizer input has been shown to increase dry matter accumulation and distribution to reproductive organs and is associated with better efficiency in the use of C assimilates by kernels (15, 24, 25). However, little information was available about the physiological processes and carbon (C) and N translocation of different maize hybrids in grain filling, particularly under various N fertilizations. Here, we investigated some of the complex relationships involved in maize grain development and yield production as affected by genotype and N supply. Our specific aims were to (1) compare grain-filling attributes and grain yields between two maize hybrids in response to various levels of N supply, (2) reveal underlying mechanisms of C assimilates allocation in the grain-filling process of maize hybrid with high sink capacity and grain yield, (3) and explore how matter transport and vascular bundle characteristics relate to crop grain-filling and differ in response to various N supplies between two maize hybrids.

Materials and methods

Experimental site descriptions

A field experiment was conducted at Gongzhuling, Jilin Province (43°31'N, 124°48'E), China during the maize growing season of April–October in 2015 and 2016. The experimental

soil was black earth (Hapli-Udic Cambisol) with the following soil properties: pH 6.3, organic matter 26.6 g kg^{-1}, total N 1.6 g kg^{-1}, available P 62.3 mg kg^{-1}, and available K 148.40 mg kg^{-1}. These values were obtained from soil sampled from the 0 to 20 cm soil profile before this study. During maize growing seasons, air temperatures above 10°C were summed to calculate the effective cumulative temperature, which was 1631.3°C in 2015 and 1616.0°C in 2016. Cumulative rainfalls were 409.6 mm in 2015 and 643.7 mm in 2016.

Experimental design and crop management

In a split-plot design, two maize hybrids were established as the main plots and three N levels were established as subplots, totaling 18 plots with three replications. Each plot was 45 m^2 in area (7.5 m length × 6 m width). Two widely grown high-yielding spring maize varieties, Xianyu 335 (XY335; It was bred by the American Pioneer Company. The parental inbred lines are PH4CV and PH6WC. PH6WC and PH4CV come from the SS and NSS heterotic groups of M America, respectively.) and Zhengdan 958 (ZD958; It was bred by the Henan Academy of Agricultural Sciences. The parental inbred lines are Zheng58 and Chang7-2, which came from the PA and SPT heterotic groups in China, respectively.), were planted in the main plots. Three N fertilizer (urea) levels, 0 kg ha^{-1} (N0), 150 kg ha^{-1} (N150), and 300 kg ha^{-1} (N300), were individually applied in the subplots. The N was applied before the sowing, jointing, and silking stages of maize at a ratio of 5:3:2 for the three applications. Both phosphorus [$Ca_3(PO_4)_2$] and potassium (KCl) fertilizers were applied at 100 kg ha^{-1} before sowing in 2015 and 2016. Maize was planted in rows with a 60 cm row spacing and 90,000 pl ha^{-1} density on April 29th and April 30th and manually harvested on October 1st and September 30th in 2015 and 2016, respectively. Pests, weeds, and diseases were well-controlled and no irrigation was applied throughout the two growing seasons.

Data collection

Sampling and grain-filling parameters

From the beginning of maize pollination, 50 plants that visually appeared uniform in growth were marked in each plot to record the date of ear pollination. Three ears among the marked pollinated plants were collected every 7–15 days for a total of five time points in 2015 and six time points in 2016 (19). We then collected 100 kernels from the middle part of each ear and initially dried them in an oven at 105°C for 40 min before drying to a constant weight at 80°C. Then we determined the 100-kernel weight as a measure of the grain-filling process by fitting a logistic equation (Eq. 1) according to Wei et al. (4).

$$W = A/(1 + BEXP^{-Ct}) \quad (1)$$

In the above equation, W is the 100-kernel weight (g) and t is the number of days after pollination. The estimated parameters A, B, and C represent final mass, the coefficient at the initial stage, and growth rate, respectively. A second equation (Eq. 2), derived by taking the first derivative of Eq. 1 (4), was used to estimate effective grain-filling duration and kernel growth rate:

$$Dw/dt = A \times B \times C \times EXP^{-Ct}/(1 + B \times EXP^{-Ct})^2 \quad (2)$$

The following equations describe the determination of additional grain-filling parameters of maize. Kernel weight at the maximum grain-filling rate was determined by $(W\ max) = A/2$. The maximum grain filling rate equation is $(G\,\max) = (C \times W\ max) \times [1 - (W\ max/A)]$. The mean grain filling rate equation is $(G\ mean) = (A/2) \times (C/6)$. The active grain-filling period was determined by $(P) = 6/C$.

Root activity (TTC reducing capacity) and malondialdehyde content

At the milking stage, 0–60 cm of soil root was selected, then it was divided into 0–15,15–30, and 30–60 cm of three layers to measure the root activity and malondialdehyde (MDA) content in 2015 and 2016. Root activity (TTC reducing capacity) was measured according to the method of Duncan and Widholm (26).

Malondialdehyde (MDA) content was measured as follows: 0.3 g root was selected in each sample, 2 ml 10% TCA solution was added, and then it was finely ground. Then, it was poured into a centrifugal tube, 6 mL TCA was added to wash, put the homogenate into a centrifuge tube (4,000 r/min for 10 min), and the supernatant was collected. Take 2 mL supernatant, add into 2 mL 0.6% TBA solution, mix and plug in the tube, put into a seal with plastic wrap, kept the mixture at 100°C for another 30 min. Taking supernatant to obtain OD values at 532 and 450 nm. The CK is a TCA solution. Finally, calculate the MDA content (μmol/g) by $C\left(\mu mol\ L^{-1}\right) = 6.45 \times A532 - 0.56 \times A450$.

^{13}C-photosynthate distribution and C/N ratio between plant organs

We used the ^{13}C isotope as a tracer in a labeling experiment to evaluate the effect of maize hybrids and N fertilizer levels on the ^{13}C-photosynthate distribution among plant organs in 2016. Six plants of robust and uniform growth were selected in each plot for ^{13}C-labeling at the third day after silking. Mylar plastic bags (length 1 m, width 15 cm, and thickness 0.1 mm) were used to encase the ear leaf. Then, 50 ml of $^{13}CO_2$ was injected into the bags. After the enclosed leaves were allowed to continue photosynthesizing for 60 min, the bags were removed from the ear leaf in each plot.

TABLE 1 Effect of nitrogen fertilization level on grain yield component and sink capacity between two maize hybrids in 2015 and 2016.

Year	Genotype	N level	KNP (ear^{-1})	TKW (g)	GY ($kg\ ha^{-1}$)	SC ($g\ m^{-2}$)	NPF (No.)	TNF (No.)
2015	XY335	N0	335 ± 13.5d	233 ± 3.3e	5445 ± 31.8f	626 ± 33.1f	478 ± 1.1e	396 ± 11.7d
		N150	410 ± 4.4c	271 ± 4.5c	8992 ± 48.0d	940 ± 6.0d	698 ± 4.7c	500 ± 10.8c
		N300	505 ± 13.0a	286 ± 3.6b	12313 ± 28.8a	1258 ± 14.4a	760 ± 7.2a	601 ± 3.5a
	ZD958	N0	336 ± 4.8d	253 ± 1.3d	6073 ± 33.3e	681 ± 7.7e	472 ± 4.4e	389 ± 7.7d
		N150	415 ± 12.6bc	283 ± 1.3b	9568 ± 82.9c	999 ± 10.3c	662 ± 8.8d	499 ± 12.2c
		N300	432 ± 16.0b	315 ± 4.5a	11387 ± 19.0b	1184 ± 20.3b	717 ± 8.3b	565 ± 11.0b
2016	XY335	N0	321 ± 16.0d	229 ± 0.5f	4778 ± 52.5f	588 ± 28.1f	538 ± 4.0d	384 ± 4.6d
		N150	460 ± 12.0bc	280 ± 1.9d	8984 ± 23.4d	1068 ± 20.1d	727 ± 9.0b	539 ± 4.2c
		N300	535 ± 10.1a	328 ± 2.3b	12627 ± 35.6a	1438 ± 12.2a	771 ± 5.9a	633 ± 17.0a
	ZD958	N0	312 ± 2.0d	273 ± 1.6e	5485 ± 50.4e	681 ± 6.8e	524 ± 5.3d	360 ± 20.0d
		N150	449 ± 1.2c	317 ± 2.3c	9602 ± 69.4c	1128 ± 16.7c	675 ± 14.5c	518 ± 28.0c
		N300	480 ± 16.0b	340 ± 3.7a	11836 ± 39.3b	1339 ± 25.3b	702 ± 19.0bc	590 ± 19.7b
ANOVA	Year (Y)		***	***	NS	***	***	*
	Nitrogen (N)		***	***	***	***	***	***
	Genotype (G)		***	***	*	*	***	***
	N × G		***	NS	***	***	***	NS
	Y × N × G		***	NS	***	NS	***	**

KNP, Kernel number per ear^{-1}; TKW, 1,000-kernel weight; GY, Grain yield; SC, Sink capacity; NPF, Number of pollinated florets; TNF, Total number of florets. N0, N150, and N300 indicate 0, 150, and 300 kg ha^{-1} N applied, respectively.
Different letters indicate significant differences between treatments at a 5% level.
*, **, and *** indicate different significance at 5, 1, and 0.1% level, respectively.
NS, no significance.

Labeled plants from each plot were harvested at two time points. The first set of three plants was sampled 24 h after the ^{13}C-labeling of leaves. The remaining three $^{13}CO_2$-labeled plants were harvested when they reached the physiological maturity stage (R6). All plant samples were divided into ear leaves, other leaves, stem, sheath, cob, ear bracts, and grain. All plant materials were heated at 105°C for 1.5 h and then dried to constant weights at 80°C before milling into fine powders. Using 5 mg of each powdered sample, we determined isotopic abundance using an Isoprime 100 instrument (Isoprime100, Cheadle, United Kingdom). Significance analysis was performed on the same growth stage between treatments at a 5% level. For C and N content determination in 2016, all leaf fractions from each plant were mixed together as a single leaf sample and then analyzed along with the remaining stem and grain samples according to the method mentioned in a previous study (27).

Vascular bundles number and area and matter transport efficiency

At the maize milking stage of the 2016 growing season, the plant fractions of the basal-stem, peduncle internode, and cob internode were obtained from five plants per in each plot according to Piao et al. (28). The plant samples were fixed using the Kano fixative solution ($V_{aceticacid}/V_{alcohol}$ = 1:3) and were stored in 70% ethanol solution before obtaining images of vascular bundle structure. Images were captured using a Zeiss Axio Scope with a 5 × /0.3 numerical aperture and a 10 × /0.3 NA Axio HRc camera (Carl Zeiss Inc., Ontario, CA, United States). Then, we analyzed images using the ZEN analysis system (Axio Lab A1, Zeiss, Germany) to obtain relevant data regarding the area occupied by large and small vascular bundles and xylem and phloem per vascular bundle. The average values from 18 adjacent vascular bundles were recorded for each treatment. Significant analysis was performed on the same positions between treatments at a 5% level.

Root bleeding sap was collected from at the basal internode of the stem. The protocol for the collection of sap was according to the method described in previous studies by Piao et al. (28). Then, the total areas of big/small vascular bundles were calculated according to Eq. 3. The matter transport efficiency (MTE, mg $mm^{-2}\ h^{-1}$) was calculated using Eq. 4 (28).

$$\begin{aligned}&\text{Total area of big / small vascular bundle}\\&= \text{signal area of big /small vascular bundle}\\&\times \text{total number of big /small vascular bundle}\end{aligned} \tag{3}$$

$$MTE = RBS / VAB \tag{4}$$

Here, *RBS* refers to the rate of root bleeding-sap collected from 17:00 to 05:00 of the next day (mg h^{-1}), and *VBA* refers to the vascular bundle area in the basal stem internode (mm^2).

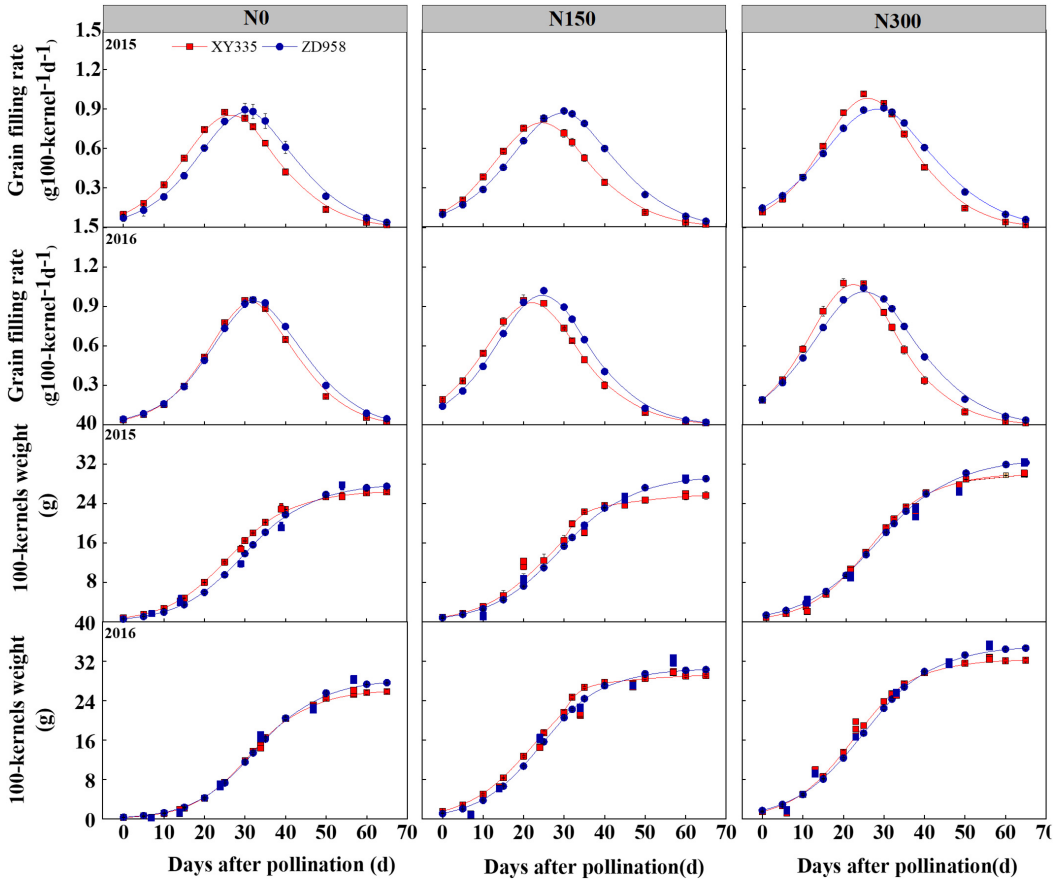

FIGURE 1
Dynamics of 100-kernel weight and grain filling rate of two maize hybrids after pollination under various N levels applied in 2015 and 2016. N0, N150, and N300 indicate 0, 150, and 300 kg N ha^{-1} applied, respectively. The values shown are the mean ± SE (n = 3).

Count of florets, grain yield, kernel number per spike, and 1,000-kernel weight

On the 10th day after maize pollination in 2015 and 2016, the husk leaves were removed from 10 ears selected from each plot after the total number of florets per ear was recorded. The number of pollinated florets included two counts by simply shaking: Both falling and withered silks in ovary silk junction were counted as the number of fertilized florets. The number of fresh silk that was not fell off was recorded as the number of unpollinated florets (29).

At the maturity stage of maize, four rows of maize in each plot were harvested to determine grain yield (grain yields were standardized to 14% moisture), kernel number per plant, and 1,000-kernel weight. Sink capacity was determined by Eq. 5 as described by Yoshinaga et al. (30).

$$\text{Sink capacity} = KNP \times KW \times \textit{plant number per unit area} \quad (5)$$

Here, *KNP* refers to the kernel number per ear^{-1}, *KW* is kernel weight and *the plant numbers per unit area* were obtained from a 1 m^2 area in each plot.

Results

Grain components, grain yield, and sink capacity

There were significant effects from the factors of Year (Y), Nitrogen (N), and Genotype (G) on kernel number per ear^{-1} (KNP), 1,000-kernel weight (TKW), grain yield (Y effect on grain yield not included), sink capacity, number of pollinated florets (NFP), and the total number of florets (TNF) (**Table 1**). For both varieties, increasing the levels of N applied to soils significantly increased KNP by an average of 10.8% and TKW by 9.2% between N150 and N300. Increasing the levels of N applied grain yield increases by an average of 22.7% and sink capacity by an average of 20.6% between N150 and N300. Interestingly, averagely a lower TKW (6.4%) but a higher NPF (7.3%) and KNP (12.4%) were observed for XY335 compared to those for ZD958, which contributed to 7.5% (2015) and 6.3% (2016) increases in KWP of XY335 from that of ZD958 under the N300 treatment. Conversely, under the N0 and N150 treatments,

KWP values for ZD958 compared to those for XY335 appeared greater but without significant difference (Table 1).

Grain filling characteristics

After maize pollination, the changes in 100-kernel weight for both varieties appeared in three stages of increasing change from gradual to rapid to slight increases over time (Figure 1). Initially, there was no obvious difference between varieties, when the weights were gradually increased. Then the 100-kernel weight of XY335 rose higher than that of ZD958 when both weights were rapidly increasing in the N0 and N150 treatments in 2015. Accordingly, for grain-filling rate, XY335 presented higher and lower values at the time periods of 14–32 and 35–60 days after pollination compared to that of ZD958 in 2015, respectively. Similar trends were observed in the 2016 growth season as well but with slightly higher and lower differences between varieties. Generally, XY335 achieved G_{max} sooner than ZD958 achieved it in each study year (Figure 1).

In general, increasing N levels promoted W_{max}, G_{max}, and G_{mean} for both maize varieties, particularly in N300. Higher G_{max} and G_{mean} values were observed for ZD958 in comparison to those of XY335 in N0 and N150 conditions, whereas the G_{max} and G_{mean} values obtained from ZD958 were on average 8.1 and 7.1% lower than the respective values from XY335 in the N300 conditions. Notably, XY335 had shorter GFPs on averages of 5.3, 2.7, and 15.4% than those of ZD958 in the N0, N150, and N300 levels, respectively (Table 2).

C and N contents and C/N ratio in maize organs

In maize stems, N application (N150 and N300) significantly increased C and N contents at both the silking and maturity stages compared to those of N0 (Figure 2). At both growth stages, the C/N ratio in stems decreased gradually with the increase in amounts of applied N. Additionally, significantly greater N contents were measured in ZD958 stems than in XY335 stems grown under N-treated conditions, which resulted in higher C/N ratios in the stems of XY335 than in ZD958. Most notably, significantly lower C contents were recorded from leaves of XY335 than from leaves of ZD958 at the silking stage in the N0 and N150, while in the N300 treatment they showed the opposite observations in the N0 and N150 treatments. The leaf C and N contents were observed significantly lower in XY335 than that of ZD958 at the maturity stage. As a result, the grains of XY335 were, respectively, 19.8–12.3% and 13.7–3.5% lower in C and N contents compared with those in the grains of ZD958 in the N0 and N150, while higher 16.5% for C and 11.8% for N contents than those of ZD958 in N300 treatment. XY335 performed 5.4% higher C/N ratios than ZD958 under N300 conditions (Figure 2), probably suggesting that differences

TABLE 2 Effect of nitrogen fertilization level on grain filling parameters between two maize hybrids in 2015 and 2016.

Year	Genotype	N level	W_{max}(mg kernel^{-1} d^{-1})	T_{max}(d)	G_{max}(mg kernel^{-1} d^{-1})	GFP(d)	G_{mean}(mg kernel^{-1} d^{-1})
2015	XY335	N0	132.2 ± 1.52d	26.3 ± 0.33c	8.8 ± 0.04d	44.9 ± 0.73d	0.29 ± 0.00d
		N150	128.8 ± 4.20d	25.5 ± 2.04c	8.4 ± 0.38d	46.2 ± 0.90c	0.28 ± 0.01d
		N300	149.9 ± 0.41b	25.9 ± 0.30c	10.2 ± 0.12a	44.2 ± 0.63d	0.34 ± 0.00a
	ZD958	N0	138.9 ± 3.27c	30.1 ± 0.61a	9.0 ± 0.26bc	46.5 ± 0.36c	0.30 ± 0.01c
		N150	147.0 ± 0.38b	29.3 ± 0.22ab	8.9 ± 0.06c	49.8 ± 0.44b	0.30 ± 0.01c
		N300	163.8 ± 0.71a	28.1 ± 0.39b	9.2 ± 0.02b	53.6 ± 0.37a	0.31 ± 0.01b
2016	XY335	N0	129.9 ± 2.16f	31.3 ± 0.16b	9.5 ± 0.09c	40.9 ± 0.96c	0.32 ± 0.01c
		N150	145.8 ± 1.24d	22.0 ± 0.39d	9.6 ± 0.37c	45.5 ± 2.10b	0.32 ± 0.01c
		N300	161.4 ± 1.68b	22.4 ± 0.50d	11.1 ± 0.24a	43.7 ± 1.15b	0.37 ± 0.01a
	ZD958	N0	139.7 ± 0.68e	32.7 ± 0.43a	9.5 ± 0.23c	44.1 ± 1.27b	0.32 ± 0.01c
		N150	151.9 ± 1.63c	24.6 ± 0.05c	10.2 ± 0.08b	44.7 ± 0.51b	0.34 ± 0.00b
		N300	174.7 ± 0.70a	25.1 ± 0.12c	10.4 ± 0.01b	50.4 ± 0.27a	0.35 ± 0.00b
ANOVA		Year (Y)	***	***	***	***	***
		Nitrogen (N)	***	***	***	***	***
		Genotype (G)	***	***	NS	***	NS
		N × G	*	NS	***	***	***
		Y × N × G	***	NS	NS	**	NS

W_{max}, kernel weight increment achieving maximum grain-filling rate; T_{max}, the days reaching the maximum grain-filling rate; G_{max}, maximum filling rate; GFP, active filling phase; G_{mean}, mean grain-filling rate. N0, N150, and N300 indicate 0, 150, and 300 kg ha^{-1} N applied, respectively.
Different letters indicate significant differences between treatments at a 5% level.
*, **, and *** indicate different significance at 5, 1, and 0.1% level, respectively.
NS, no significance.

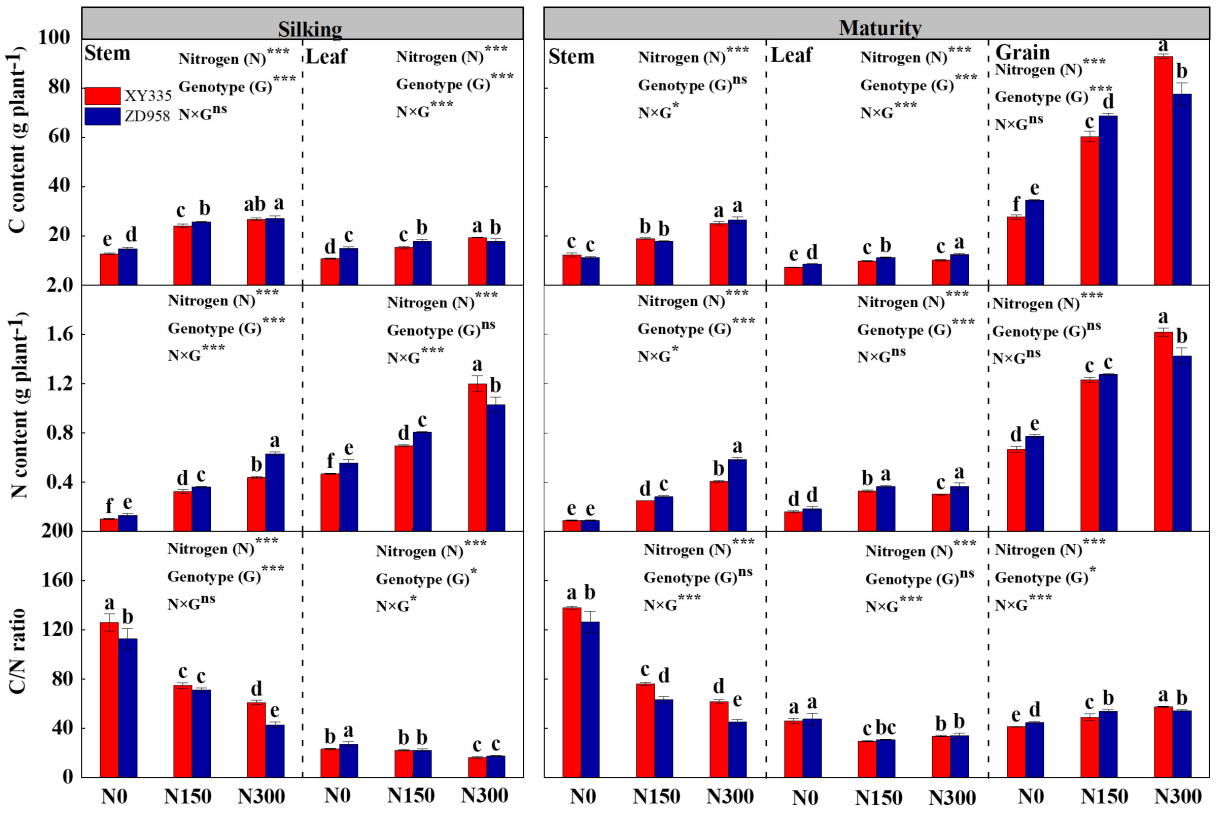

FIGURE 2
N content, C content, and C/N ratio in stem, leaf, and grain of two maize hybrids at silking and maturity stages under various N levels applied in 2016. N0, N150, and N300 indicate 0, 150, and 300 kg N ha^{-1} applied, respectively. Different letters indicate significant differences at a 5% level. The values shown are the mean ± SE (n = 3). The values shown are the mean ± SE (n = 3). *p < 0.05, **p < 0.01, ***p < 0.001, ns, no significance.

between the two cultivars in matter translocation from source to sink occurred from the silking to maturity stages of maize.

Root activity and malondialdehyde contents

Root activity (Year effected on root activity in 30–60 cm not included) and malondialdehyde (MDA) contents were significantly affected by the factors Year (Y), Nitrogen (N), genotype (G), and N × G. Root activity levels gradually raised with the increase of N inputs, while MDA was reduced with increased N rate. As soil depth increased, root activity was reduced, and MDA was observed as an enhanced trend in each N level condition (Figure 3). During 2 years, root activity within the 0-60 cm soil layer samples from XY335 was significantly lower than that of ZD958 in the N0 (17.4%) and N150 (15.4%) treatments. Conversely, greater root activity was observed in XY335 higher than those in ZD958 by averages of 8.9% at the N300 levels. MDA contents in root were higher for XY335 than those for ZD958 by averages of 9.3 and 10.0% in N0 and N150 treatment, while lower 9.7% in XY335 than that of ZD958 at the N300 N level (Figure 3).

Distribution of ^{13}C-photosynthates in tissues at maize silking and maturity stages

The distribution of ^{13}C-photosynthates in each tissue of two maize cultivars was significantly affected by the levels of applied N; however, significant effects on two varieties were only observed from the ^{13}C-photosynthates distributions in the sheath, grain, and cob tissues (Table 3). At the silking stage, similar distribution patterns of ^{13}C-photosynthates in tissues were obtained in the same N-treated plants of both cultivars. Moreover, significantly higher amounts of ^{13}C-photosynthates were distributed in the stems and husk leaves of crops from the N150 and N300 treatments relative to those from the N0 treatment. Accordingly, those labeled-^{13}C captured by other leaves and sheaths were lower in N input treatments than those in treatment without N fertilizer. These results indicated that

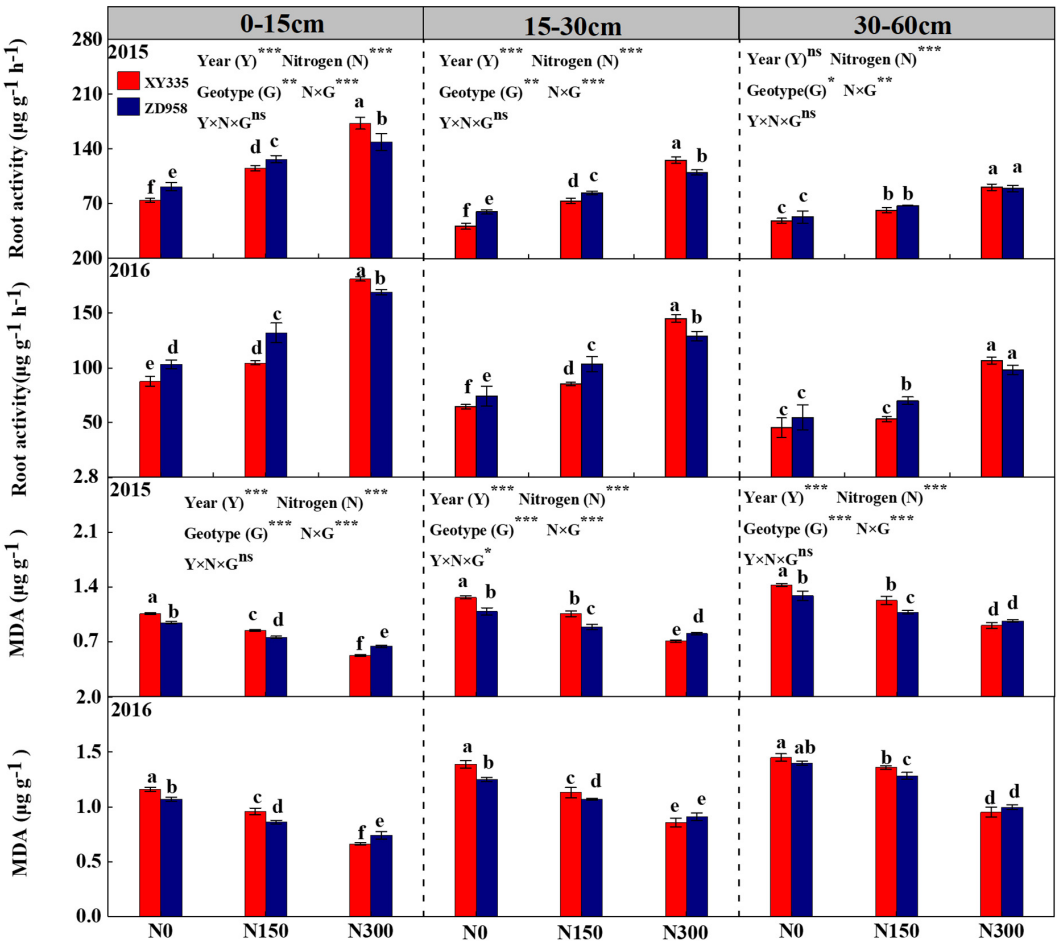

FIGURE 3
Root activity and malondialdehyde (MDA) content of two maize hybrids at the milking stage under various N levels were applied in 2015 and 2016. N0, N150, and N300 indicate 0, 150, and 300 kg N ha^{-1} applied, respectively. The values shown are the mean ± SE (n = 3). *p < 0.05, **p < 0.01, ***p < 0.001, ns, no significance.

N input accelerated ^{13}C-photosynthate allocation to stem and husk leaves at the silking stage.

At maturity, the ^{13}C photosynthetic products in source tissues were transferred to grains in large quantities, and grains as sinks then became the organs containing the most ^{13}C photosynthetic products. XY335 exhibited relatively higher ^{13}C-photosynthate allocation ratios in grain, cob, and husk leaves than ZD958 exhibited in the corresponding tissues. As expected, XY335 exhibited relatively lower ^{13}C-photosynthate allocation in other tissues than ZD958 exhibited in tissues, particularly in leaves. The ratio was lower by 9.8, 18.6, and 25.8% in XY335 than that in ZD958 in the respective N0, N100, and N300 treatments. ^{13}C-photosynthate allocation was significantly reduced in other leaves, sheath, and cob, while it was greater in grains for both maize varieties due to the increased N inputs. Under N300 conditions the ratio of ^{13}C-photosynthate allocation was increased by 14.7% for XY335, and 12.0% for ZD958 from that in N0 and N150 treatment (Table 3).

Traits of vascular bundles in internodes of maize

Overall, the area, number, and density of vascular bundles, regardless of whether the sizes of bundles were categorized as small or large, were significantly affected by N fertilization. Furthermore, the area and number of small vascular bundles and vascular bundle density were significantly influenced by the factor of genotype (Table 4). Increased N fertilization levels vastly raised vascular bundle area, and increasing trends were observed in the xylem and phloem of basal-stem, peduncle, and cob samples for both genotypes at the milking stage. In N0 and N150 treatments, XY335 had a relatively lower total area and total phloem area of small vascular bundles than ZD958. However, in the N300 treatment, XY335 had a relatively higher total area of small vascular bundles than ZD958, particularly in peduncles because of the significantly larger area of phloem. Similar results were also observed for the area of small vascular

TABLE 3 Effect of nitrogen fertilization level on the distribution of ^{13}C-photosynthates among tissues of two maize hybrids at silking and maturity stages in 2015 and 2016.

Year	Growth stages	Genotype	N level	^{13}C-photosynthates distribution in different tissues of maize (%)						
				Stem	Ear leaf	Other leaf	Sheath	Husk leaf	Grain	Cob
2015	Silking	XY335	N0	37.0 ± 1.05c	2.7 ± 0.20c	35.1 ± 1.39ab	20.6 ± 0.54a	4.5 ± 0.40bc	–	–
			N150	40.5 ± 0.42b	2.9 ± 0.16c	33.5 ± 1.01b	17.4 ± 1.22c	5.6 ± 0.20a	–	–
			N300	43.3 ± 0.48a	3.5 ± 0.21ab	31.4 ± 1.10c	16.5 ± 0.46cd	5.3 ± 0.51ab	–	–
		ZD958	N0	36.6 ± 1.33c	3.1 ± 0.27bc	36.4 ± 0.90a	19.3 ± 0.37b	4.6 ± 0.22bc	–	–
			N150	41.5 ± 1.21b	3.6 ± 0.16a	33.7 ± 0.01b	16.9 ± 0.66cd	4.4 ± 0.38c	–	–
			N300	44.4 ± 0.51a	3.3 ± 0.14bc	30.8 ± 0.47c	15.8 ± 0.76d	5.7 ± 0.42a	–	–
	Maturity	XY335	N0	17.9 ± 0.07c	1.3 ± 0.13a	14.0 ± 0.48b	7.1 ± 0.67b	6.4 ± 0.38a	45.5 ± 0.39d	7.5 ± 0.60a
			N150	18.7 ± 0.35b	0.9 ± 0.16ab	10.5 ± 0.28c	6.6 ± 0.47bc	6.5 ± 0.17a	51.9 ± 0.42c	5.1 ± 0.28bc
			N300	18.7 ± 0.59b	0.9 ± 0.02ab	8.6 ± 0.21d	6.0 ± 0.43c	6.6 ± 0.08a	54.9 ± 0.37a	4.6 ± 0.22c
		ZD958	N0	16.3 ± 0.19d	1.2 ± 0.10a	15.3 ± 0.98a	9.7 ± 0.35a	5.5 ± 0.24ab	45.0 ± 0.52d	6.9 ± 0.97a
			N150	18.5 ± 0.34b	0.9 ± 0.12ab	12.4 ± 0.58c	6.1 ± 0.61c	5.5 ± 0.46ab	50.8 ± 0.49c	5.8 ± 0.23b
			N300	19.5 ± 0.47a	0.8 ± 0.02b	10.4 ± 0.52c	6.0 ± 0.53c	4.9 ± 0.25b	53.3 ± 1.18b	5.2 ± 0.14bc
2016	Silking	XY335	N0	36.1 ± 1.47c	3.8 ± 0.20a	33.3 ± 1.85a	23.8 ± 0.53a	3.0 ± 0.16c	–	–
			N150	43.2 ± 0.69b	3.2 ± 0.13c	29.9 ± 0.68bc	18.5 ± 0.69bc	5.2 ± 0.52a	–	–
			N300	46.2 ± 1.96a	3.5 ± 0.16ab	28.0 ± 2.63bc	16.9 ± 1.11c	5.4 ± 0.46a	–	–
		ZD958	N0	35.7 ± 0.97c	3.2 ± 0.17c	34.2 ± 2.27a	22.6 ± 1.15a	4.3 ± 0.69b	–	–
			N150	42.6 ± 0.94b	3.4 ± 0.19bc	29.0 ± 0.73bc	19.8 ± 1.02b	5.2 ± 0.15a	–	–
			N300	47.3 ± 1.58a	3.3 ± 0.11bc	26.2 ± 1.64c	18.1 ± 0.53c	5.1 ± 0.31a	–	–
	Maturity	XY335	N0	18.6 ± 0.78b	1.9 ± 0.11ab	11.9 ± 0.29b	11.2 ± 0.33a	4.5 ± 0.53a	44.2 ± 0.44d	7.7 ± 0.07a
			N150	18.1 ± 0.54bc	1.4 ± 0.02b	9.6 ± 0.19c	7.3 ± 0.24cd	4.6 ± 0.32a	52.4 ± 0.65b	6.6 ± 0.12b
			N300	19.1 ± 0.70b	1.6 ± 0.02b	6.9 ± 0.23d	6.1 ± 0.22e	3.9 ± 0.05b	56.6 ± 0.68a	5.9 ± 0.37bc
		ZD958	N0	17.1 ± 0.80c	2.0 ± 0.57a	13.2 ± 0.18a	11.9 ± 0.63a	3.4 ± 0.44b	46.0 ± 0.99c	6.4 ± 0.77b
			N150	18.2 ± 0.74bc	1.7 ± 0.06ab	11.8 ± 0.43b	7.7 ± 0.85bc	3.7 ± 0.32b	51.0 ± 0.92b	5.9 ± 0.23bc
			N300	20.3 ± 0.18a	1.5 ± 0.11b	9.3 ± 0.28c	6.5 ± 0.52de	2.1 ± 0.08c	55.1 ± 0.54a	5.2 ± 0.22c
ANOVA	Year (Y)			NS	NS	NS	NS	***	***	**
	Nitrogen (N)			*	*	***	***	***	***	*
	Genotype (G)			NS	NS	NS	*	NS	**	***
	N × G			NS	NS	NS	NS	NS	NS	*
	Y × N × G			NS	NS	NS	NS	NS	NS	**

N0, N150, and N300 indicate 0, 150, and 300 kg ha^{-1} N applied, respectively.
Different letters in the same column indicate significant differences between treatments at a 5% level for each growth stage.
*, **, and ** indicate different significance at 5, 1, and 0.1% level, respectively.
NS, no significance; –, no data for use.

bundles due to the larger area of either the xylem or phloem in basal stems and cobs of maize in the N300 treatment.

Similar to the results of the vascular bundle area, the numbers of both large and small vascular bundles were significantly increased by N inputs to both maize varieties. In addition, the number of small vascular bundles was respectively greater on average by 10.6 and 7.8% in the peduncle and cob tissues of XY335 than of ZD958 in the N300 treatment (Table 4). Combining the results of area and number of vascular bundles, XY335 clearly produced a higher vascular bundle density than ZD958 in each tissue of maize no matter what level of N was supplied. The micrographs of vascular bundles of different internodes are presented in Appendix Figures 1, 2.

Root bleeding-sap and matter transport efficiency

Maize crops grown under the N150 and N300 conditions for both varieties produced approximately 1.5–2.8-fold more root bleeding-sap than crops grown under the N0 treatment produced at the silking stage (Table 5). XY335 had a lower cross-sectional area than that of ZD958 both under N150 and N300 conditions, while no significance was observed in the total vascular bundle area in the stem between the two hybrids. Notably, XY335 had a 14.3 and 1.8% lower amount of root bleeding sap than that of ZD958 across the N0 and N150 levels, while 10.4% higher than that of ZD958 in the N300 level. Similar

TABLE 4 Effect of nitrogen fertilization level on vascular bundle traits of two maize hybrids at milking stage in 2016.

Position	Genotype	N level	Area of big vascular bundle (mm^2)			Area of small vascular bundle (mm^2)			Number of vascular bundle		Vascular bundle
			Xylem	Phloem	Total	Xylem	Phloem	Total	Big	Small	density (mm^{-2})
Basal-stem	XY335	N0	3.76 ± 0.16d	0.75 ± 0.07e	8.34 ± 0.36d	2.30 ± 0.31cd	1.55 ± 0.02f	17.42 ± 1.27c	115.4 ± 5.4d	574.8 ± 19.3c	2.85 ± 0.22a
		N150	6.27 ± 0.67b	1.61 ± 0.23c	13.16 ± 1.43b	3.81 ± 0.71b	2.05 ± 0.01d	19.18 ± 0.99b	187.2 ± 10.3b	666.0 ± 23.5bc	3.10 ± 0.19a
		N300	10.19 ± 0.55a	3.65 ± 0.23a	27.99 ± 1.61a	4.70 ± 0.47a	3.39 ± 0.06a	28.55 ± 0.85a	289.7 ± 9.3a	758.9 ± 16.2a	2.87 ± 0.08a
	ZD958	N0	4.95 ± 0.14c	1.09 ± 0.06d	10.56 ± 0.33c	2.03 ± 0.08d	1.66 ± 0.02e	13.86 ± 0.82d	141.5 ± 1.3c	450.4 ± 17.0d	2.46 ± 0.15b
		N150	6.20 ± 0.39b	1.43 ± 0.08c	14.30 ± 0.75b	3.00 ± 0.18c	2.48 ± 0.02c	16.53 ± 0.72c	184.7 ± 10.4b	562.5 ± 10.2c	2.47 ± 0.16b
		N300	10.27 ± 0.46a	3.30 ± 0.16b	27.73 ± 1.37a	4.26 ± 0.37b	2.96 ± 0.17b	27.52 ± 0.82a	280.9 ± 12.9a	756.4 ± 17.1a	2.49 ± 0.08b
Peduncle	XY335	N0	2.24 ± 0.38c	1.16 ± 0.19c	6.18 ± 0.24c	1.31 ± 0.21d	0.30 ± 0.02f	4.48 ± 0.41d	111.9 ± 4.4c	230.1 ± 12.2d	3.86 ± 0.09b
		N150	3.84 ± 0.88b	2.07 ± 0.27bc	12.36 ± 1.05b	2.20 ± 0.25c	0.61 ± 0.02d	9.00 ± 0.12c	144.9 ± 5.6b	350.4 ± 7.1c	4.82 ± 0.26a
		N300	9.23 ± 1.24a	4.91 ± 0.60a	22.92 ± 1.63a	3.71 ± 0.11a	1.45 ± 0.03a	14.54 ± 0.29a	224.6 ± 4.1a	456.7 ± 8.9a	4.72 ± 0.24a
	ZD958	N0	2.30 ± 0.08bc	1.24 ± 0.13c	6.74 ± 0.74c	1.28 ± 0.20d	0.40 ± 0.04e	5.23 ± 0.72d	116.5 ± 2.8c	224.7 ± 10.7d	2.77 ± 0.29d
		N150	3.32 ± 0.26bc	1.77 ± 0.12c	11.57 ± 0.63b	2.15 ± 0.01c	0.73 ± 0.01c	10.05 ± 0.42c	131.1 ± 8.2b	343.1 ± 1.0c	3.23 ± 0.08bc
		N300	8.72 ± 1.26a	4.74 ± 0.55a	22.11 ± 1.43a	3.11 ± 0.05b	1.27 ± 0.04b	12.26 ± 0.37b	219.3 ± 7.3a	408.5 ± 2.5b	3.51 ± 0.14bc
Cob	XY335	N0	0.97 ± 0.22c	0.49 ± 0.08c	5.20 ± 0.82d	0.65 ± 0.06d	0.12 ± 0.01e	1.77 ± 0.20e	57.5 ± 7.7c	91.0 ± 7.4d	0.64 ± 0.01bc
		N150	1.79 ± 0.09b	1.39 ± 0.10b	6.32 ± 0.33bc	1.47 ± 0.13c	0.26 ± 0.01d	3.74 ± 0.09d	63.8 ± 3.8bc	145.6 ± 4.8b	0.71 ± 0.02a
		N300	3.02 ± 0.16a	1.87 ± 0.10a	8.75 ± 0.11a	2.74 ± 0.08a	0.49 ± 0.03a	7.03 ± 0.32a	80.8 ± 1.0a	158.6 ± 7.7a	0.75 ± 0.02a
	ZD958	N0	1.09 ± 0.20c	0.47 ± 0.08c	5.42 ± 0.95cd	0.69 ± 0.04d	0.16 ± 0.01e	2.12 ± 0.08e	58.0 ± 5.0c	93.9 ± 5.9d	0.58 ± 0.03c
		N150	1.99 ± 0.13b	1.46 ± 0.07b	7.10 ± 0.31b	1.37 ± 0.26c	0.32 ± 0.02c	4.33 ± 0.24c	72.2 ± 3.2ab	138.4 ± 3.0bc	0.62 ± 0.01bc
		N300	3.14 ± 0.17a	1.84 ± 0.07a	8.92 ± 0.35a	2.11 ± 0.24b	0.45 ± 0.01b	6.50 ± 0.55b	82.6 ± 1.3a	146.2 ± 7.8b	0.61 ± 0.03bc
ANOVA	Nitrogen (N)		***	***	***	***	***	***	***	***	***
	Genotype (G)		NS	NS	NS	***	***	***	NS	**	***
	N × G		NS	NS	NS	NS	***	*	NS	NS	NS

N0, N150, and N300 indicate 0, 150, and 300 kg ha^{-1} N applied, respectively. AVE indicates the average value from the N treatment.
Different letters in the same column indicate significant differences between treatments at a 5% level for each tissue position.
*, **, and *** indicate different significance at 5, 1, and 0.1% level, respectively.
NS, no significance.

10.3389/fnut.2022.998946

TABLE 5 Effect of nitrogen fertilization level on root bleeding sap and matter transport efficiency of basal-stem internode (MTE) of two maize hybrids at milking stage on N application levels in 2016.

Genotype	N level	Cross sectional area (mm^2)	vascular bundle area (mm^2)	Root bleeding sap ($mg\ h^{-1}$)	MTE ($mg\ mm^{-2}\ h^{-1}$)
XY335	N0	242.7 ± 4.2e	25.8 ± 1.5c	537.5 ± 12.1e	20.0 ± 0.2f
	N150	275.7 ± 7.1d	32.3 ± 0.7b	979.2 ± 5.2c	30.4 ± 0.8d
	N300	365.3 ± 12.8b	56.5 ± 0.8a	2096.9 ± 10.3a	37.1 ± 0.4a
ZD958	N0	241.1 ± 8.0e	24.4 ± 0.5c	626.9 ± 23.5d	25.7 ± 0.9e
	N150	302.5 ± 8.6c	30.8 ± 0.9b	996.9 ± 4.6c	32.3 ± 0.8c
	N300	417.9 ± 14.8a	55.3 ± 2.1a	1878.1 ± 15.8b	34.0 ± 0.7b
ANOVA	Nitrogen (N)	***	***	***	***
	Genotype (G)	**	*	**	***
	N × G	*	NS	***	***

MTE, Matter transport efficiency. N0, N150, and N300 indicate 0, 150, and 300 kg ha^{-1} N applied, respectively.
Different small letters within a column indicate significant differences between treatments at a 5% level for each tissue position.
*, **, and *** indicate different significance at 5, 1, and 0.1% level, respectively; NS, no significance.

to the response of root bleeding-sap, treatments with N input showed dramatically higher MTE relative to those treatments without applied N. Additionally, greater MTE values were found for XY335 by 8.4% compared with those for ZD958 under N300 treatments (Table 5).

Principal component analysis

Principal component analysis was employed to evaluate correlations between indicators tested in this study, and it showed that three principal components contributed to 57.3, 33.7, and 4.5% of the total variation. The 95.5% of the total variation in this study was explained by three principal components (Figure 4). Interestingly, we found that the grain-filling rates (G_{mean} and G_{max}), total number of fertilized florets, matter transport efficiency of the basal-stem internode, grain C, N, and grain C/N ratio at the maturity stage, total phloem area of small vascular bundle in peduncle and cob tissue (TAC), and number of small vascular bundles in peduncle and cob tissues were more related to maize sink capacity than to other indicators included in PC1. Another cluster contained the root activity at the milking stage and the active-filling phase (GFR) was represented by PC2. In addition, root MDA contents at the milking stages contributed to PC3 (Figure 4).

Discussion

Nitrogen × Hybrids: Grain yield and sink capacity

Researchers have demonstrated that higher grain yield occurred through the superior sink capacity (KW × KNP) (31). An appropriate increased N application combined with right maize hybrids could improve dry matter accumulation and distribution to reproductive organs to achieve high sink capacity (15, 24, 25). In this study, the N rate, genotype, and their interaction affected maize sink capacity and grain yield. XY335 performed 9.3 and 9.8% lower sink capacity and grain yield than ZD958 under low N conditions (N0 and N150), whereas N × genotype interaction leads to higher sink capacity and grain yield in XY335 than ZD958 under N300 condition. Although XY335 had a lower 1,000 kernel weight (TKW) than that of ZD958, kernel number per ear (KNP) played a supportive role in compensating for the lower TKW. This compensation observed in XY335 likely contributes to its greater sink capacity and yield (Table 1). Furthermore, the higher KNP of XY335 was attributed to its greater fertilized florets, which was one of the key factors to determine the final kernel number (32, 33), and it is also influenced tremendously by N availability and crop genotype (34).

Grain filling, sink capacity, and grain yield

Grain filling is an important indicator of sink potential and grain yield that significantly and positively correlate with photosynthetic assimilate production and translocation (4, 31, 35). Grain filling is driven by grain filling rate (GFR), grain filling period (GFP), or both, which were greatly affected by N application and genotype (2). Our previous research has shown that an appropriate increase in N application could achieve sufficient and efficient assimilates supply to grain, which contributed to the grain-filling rate for obtaining a higher grain yield of the same hybrid (9). However, our previous studies and other research mainly focused on the effect of grain filling on KW, and less information research on sink capacity in response to GFR or GFP between different genotype hybrids (32, 33, 35). Sink capacity is determined by KNP and potential kernel weight, and the maximum of single kernel weight is likely genetically determined, and thus the further supply of C assimilates could not raise the maximum weight

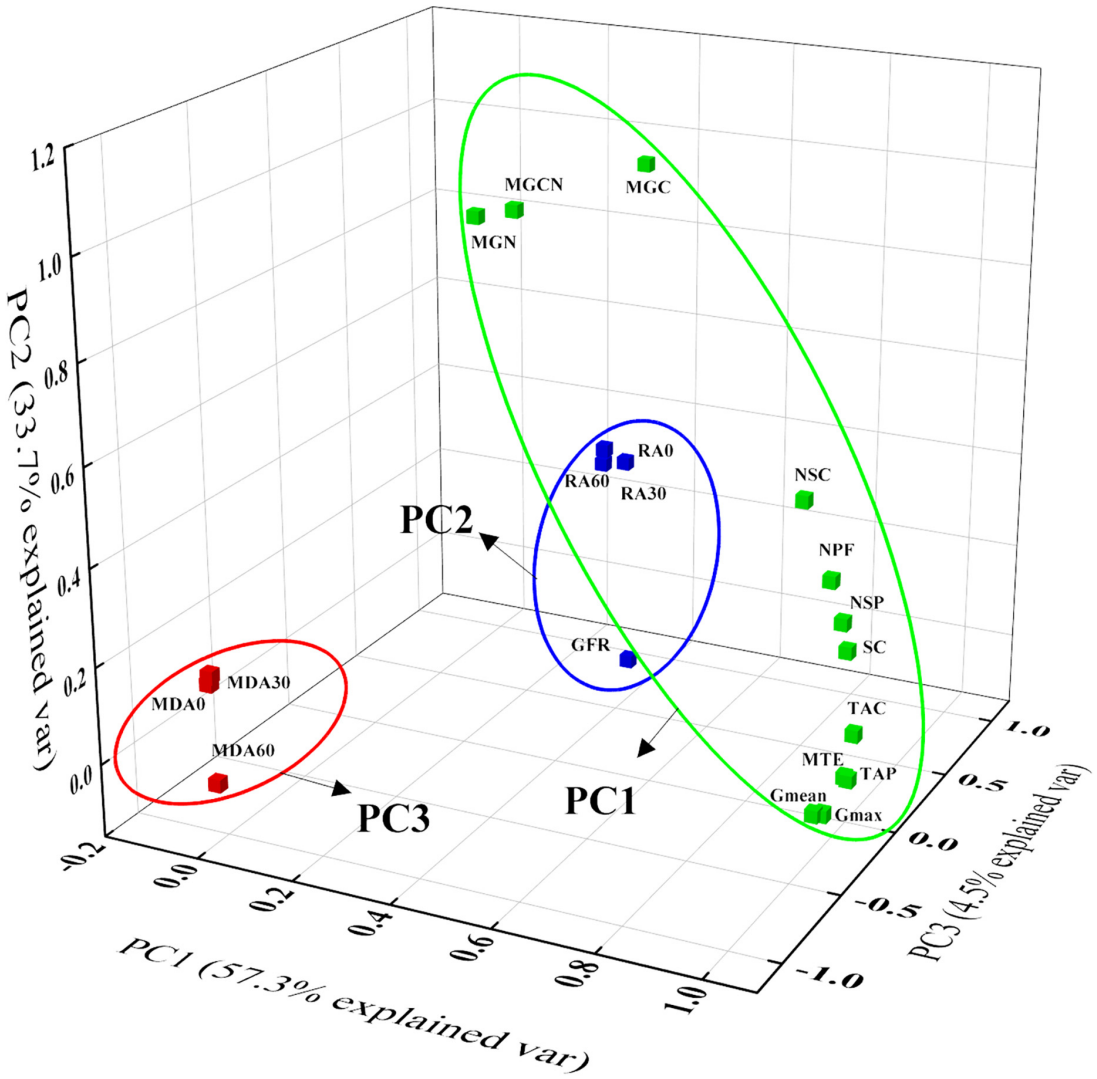

FIGURE 4
Principal component analysis (PCA) of grain filling parameters, vascular bundle structures, grain C, N contents, and leaf enzyme activity. G_{mean} and G_{max}, mean, and maximum grain filling rate; MTE, matter transport efficiency; MGC, MGN, and MGCN, grain C, N contents, and C/N ratio at maturity stage; RA0, RA30, and RA60, root activity in 0–15 cm, 15–30 cm, and 30–60 cm soil layer at milking stage, respectively; MDA0, MDA30, MDA60, and malondialdehyde contents in 0–15 cm, 15–30 cm, and 30–60 cm soil layer at milking stage, respectively; NSP and NSC, number of small vascular bundle in peduncle and cob; TAP and TAC, total phloem area of small vascular bundle in peduncle and cob; GFP, active filling phase; NPF, number of pollinated florets; SC, Sink capacity.

(11, 13). In the determined model of increasing 100-kernel weight over time, we found that the grain weight of XY335 had reached 95.6% of its potential weight at approximately 45 days after pollination, while ZD958 had only reached 86.8% of its potential kernel weight at the same time (Figure 1), which resulted in a shorter GFP and higher G_{mean} and G_{max} for XY335 compared to those of ZD958 (Table 2). These results reveal that lower maximum single-kernel weight in XY335 contributed to relatively shorter GFP and higher KNP, which was likely the main factor influencing the increase in GFR. Results of the PCA analysis confirmed these results showing that the GFR belongs to PC1, while GFP is a part of PC2 (Figure 4). Previous studies also reported that GFR had a slightly and strongly positive correlation with GY than with GFP (4, 9, 35).

Grain filling and C, N translocation and distribution

Simultaneously, the grain filling process of crops not only reflects assimilates supply, but also C and N transport and distribution between organs (36, 37). Increased N supply promotes larger quantities of carbohydrates translocating to

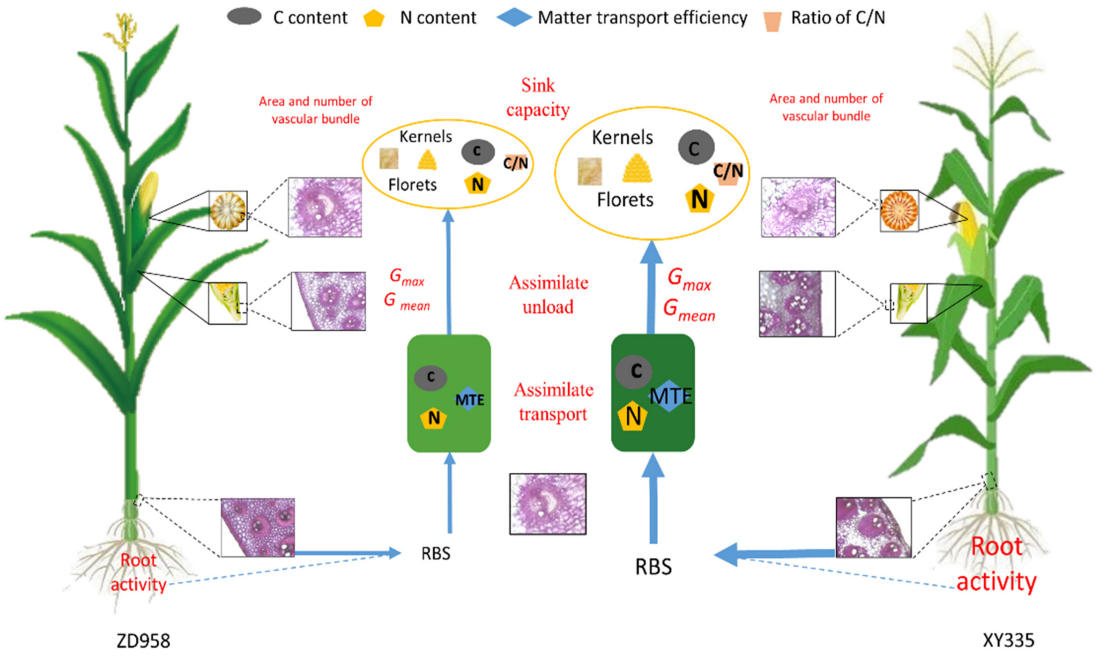

FIGURE 5
Schematic from this study showing the differences in filling parameters and the response of vascular bundle structure, matter transportation, and source–sink relationship on N input levels between maize varieties ZD958 and XY335. RBS, root bleeding sap; MTE, matter transport efficiency; G_{mean} and G_{max}, mean and maximum grain filling rate; GY, grain yield. Different sizes of the same letter represent value differences.

grains, thereby increasing grain yield (38, 39). The present study demonstrated divergent responses in C and N contents in leaf tissues at the silking and maturity stages between two maize hybrids under conditions with various N supplies, which contributed to higher C and N contents in XY335 grains compared to the corresponding contents in ZD958 grains under N300 conditions. In addition, according to the ^{13}C tracer analysis at maturity, generally lower ^{13}C assimilates in XY335 were distributed in the stem, leaf (ear leaf and other leaf), and sheath tissues, but higher values were distributed in husk leaf, grain, and cob tissues compared to those in ZD958, especially in N300 conditions (**Table 3**). These results reflect the higher MTE from source to sink in XY335 relative to that in ZD958, which was likely attributed to the higher GFR in XY335. Furthermore, the C/N ratio plays a greater role in matter translocation between crop tissues rather than C or N contents individually, balance C/N ratio within crops can regulate assimilates translocation from leaves to grains, thereby increasing dry matter accumulation and grain matter (36, 40). In our case, a lower C/N ratio was observed in XY335 grains than that in ZD958 grains at the maturity stage of from N0 and N150 groups, while there were higher ratios of XY335 at the treatment of N300. Also, higher C and N contents were measured in XY335 grains than in ZD958 grains as mentioned above (**Figure 2**). Thus, it could be concluded that not only a stronger C and N translocation from the vegetative organs to grains, but also balanced C/N ratios are required in maize grains applied with appropriate N levels, which is also important in regulating the grain-filling process to achieve high grain yield.

Grain filling is associated with the bleeding sap and vascular bundle structure

Research on bleeding sap primarily aimed to elucidate the mechanism of matter transfer from roots to shoots (41). Bleeding-sap transport nutrient matter between aboveground and underground, which represents the higher amount of N and kernel number, may explain the variations of grain filling between two maize genotypes supplied with contrasting N fertilizer (42, 43). The collected bleeding sap indicated that a lower bleeding sap ratio was observed in XY335 than that in ZD958 at the milking stage in N0 and N150 groups, while there were significantly higher values in XY335 than that from ZD958 at N300 treatment (10.4%). In this study, similar results were also observed for root activity (**Figure 3**). Morita et al. (44) and Noguchi et al. (45) reported that the root-bleeding rate was closely related to root traits in maize, and it could be used to evaluate the physiological activity of root activity. Strong root activity is necessary to increase the accumulation of post-silking dry matter and grain filling (46, 47). Moreover, higher MDA contents will enhance superoxide enzyme activity, which leads to plant senescent (48). XY335 exhibited lower MDA contents

than ZD958 (Figure 3). These findings suggested that the N rate significantly increased root activity and decreased MDA content, thus boosting higher bleeding sap in XY335 than that in ZD958 under sufficiency N application.

The structure of the vascular bundle, as the main channel, determines bleeding sap transport ability (42, 49). They also regulate endosperm C metabolites through translocating sugars and N between tissues (13). For instance, as much as 80% of C assimilated in leaves was transported *via* the phloem to satisfy the metabolic needs of other plant organs (50). Increasing N application can increase the number of small vascular bundles to boost kernel number, and enhanced phloem areas of small vascular bundles are beneficial for assimilation transport to grain (9), determining the total accumulation of assimilation in sink capacity, which affects grain filling characteristic under various conditions (9, 51, 52). However, how the N × genotype interaction changes the number and area of the vascular bundle, and the relationship between the vascular bundle characteristic and the grain filling are still unclear. In this study, there was no significant difference in NSP and NSC under lower N conditions between the two hybrids, while the N300 treatment significantly increased both NSP and NSC more in XY335 than those in ZD958 (Table 4). Moreover, the TAP and TAC values showed similar trends to those of NSP and NSC as N inputs increased (Table 4). Higher NSP and NSC together with larger TAP and TAC contributed to the significantly higher MTE in XY335 relative to that of ZD958 (Table 5). The PCA analysis showed that TAC, NSP, NSC, and MTE correlated well with PC1 (Figure 4), suggesting that these responses related to vascular bundles in XY335 are especially important in promoting bleeding sap and grain filling. The better vascular system benefited MTE, and simultaneously might contribute to the increase in GFR and C and N translocation to florets, which ultimately resulted in the final stronger sink capacity and grain yield (53).

Conclusion

The factors of crop genotype and N fertilizer interacted with optimization of vascular bundle structure of ear tissue in XY335, thus increasing 10.4% bleeding sap and 8.4% MTE than those in ZD958 under N300 condition. Moreover, the regulation of the C/N ratio in XY335 under higher levels of N treatments provided more C assimilates to facilitate floret development and increase the final kernel number. Therefore, these results indicate that the sufficient N input can improve root activity and optimize the vascular bundle system in the ear to boost matter transport efficiency, in turn, increase the transport of C and N into grains and balance the C/N ratio in XY335, which promote a favorable grain filling rate ultimately for enhancing sink capacity and grain yield (Figure 5). These findings, to some extent, could be used to inform maize breeding and cultivation that higher grain-filling rate, sink capacity, and allocation of matter into kernels are significant factors for striving to attain higher grain yields. Moreover, future studies should also focus on optimizing the vascular bundle system in maize peduncle and cob tissues to improve grain yields.

Data availability statement

The original contributions presented in this study are included in the article/supplementary material, further inquiries can be directed to the corresponding authors.

Author contributions

HR: methodology, investigation, data curation, writing—original draft, and funding acquisition. MZ and HQ: formal analysis and resources. BZ: investigation, methodology, and editing. WZ: methodology and data curation. KL: formal analysis. YJ: conceptualization, methodology, writing—review and editing, supervision, and project administration. CL: conceptualization, methodology, resources, writing—review and editing, supervision, project administration, and funding acquisition. All authors read and approved the article.

Funding

This research was supported by the China Agriculture Research System of MOF and MARA (CARS-02-14), the National Natural Science Foundation of China (No. 31971852), and the National Key Research and Development Program of China (No. 2016YFD0300103).

Conflict of interest

The authors declare that the research was conducted in the absence of any commercial or financial relationships that could be construed as a potential conflict of interest.

Publisher's note

References

1. Kato T, Takeda K. Associations among characters related to yield sink capacity in space−planted rice. *Crop Sci.* (1996) 36:1135–9. doi: 10.2135/cropsci1996.0011183X003600050011x

2. Zhou BY, Yue Y, Sun XF, Ding ZS, Ma W, Zhao M. Maize kernel weight responses to sowing date-associated variation in weather conditions. *Crop J.* (2017) 5:43–51. doi: 10.1016/j.cj.2016.07.002

3. Uribelarrea M, Below FE, Moose SP. Grain composition and productivity of maize hybrids derived from the Illinois protein strains in response to variable nitrogen supply. *Crop Sci.* (2004) 44:1593–600. doi: 10.2135/cropsci2004.1593

4. Wei SS, Wang XY, Li GH, Qin YY, Jiang D, Dong ST. Plant density and nitrogen supply affect the grain-filling parameters of maize kernels located in different ear positions. *Front Plant Sci.* (2019) 10:180. doi: 10.3389/fpls.2019.00180

5. Arisnabarreta S, Miralles DJ. Radiation effects on potential number of grains per spike and biomass partitioning in two- and six-rowed near isogenic barley lines. *Field Crops Res.* (2008) 107:203–10. doi: 10.1016/j.fcr.2008.01.005

6. Sandana PA, Harcha CI, Calderini DF. Sensitivity of yield and grain nitrogen concentration of wheat, lupin and pea to source reduction during grain filling. a comparative survey under high yielding conditions. *Field Crops Res.* (2009) 114:233–43. doi: 10.1016/j.fcr.2009.08.003

7. Ishibashi Y, Okamura K, Miyazaki M, Phan T, Yuasa T, Iwaya-Inoue M. Expression of rice sucrose transporter gene OsSUT1 in sink and source organs shaded during grain filling may affect grain yield and quality. *Environ Exp Bot.* (2014) 97:49–54. doi: 10.1016/j.envexpbot.2013.08.005

8. Liu GZ, Yang YS, Guo XX, Liu WM, Xie RZ, Ming B, et al. Coordinating maize source and sink relationship to achieve yield potential of 22.5 Mg ha^{-1}. *Field Crop Res.* (2022) 283:108544. doi: 10.1016/j.fcr.2022.108544

9. Ren H, Jiang Y, Zhao M, Qi H, Li CF. Nitrogen supply regulates vascular bundle structure and matter transport characteristics of spring maize under high plant density. *Front Plant Sci.* (2020) 8:602739. doi: 10.3389/fpls.2020.602739

10. Cárcova J, Uribelarrea M, Borrás L, Otegui ME, Westgate ME. Synchronous pollination within and between ears improves kernel set in maize. *Crop Sci.* (2000) 40:1056–61. doi: 10.2135/cropsci2000.4041056x

11. Borrás L, Slafer GA, Otegui ME. Seed dry weight response to source-sink manipulations in wheat, maize, and soybean: a quantitative reappraisal. *Field Crop Res.* (2004) 86:131–46. doi: 10.1016/j.fcr.2003.08.002

12. Paponov IA, Sambo P, Erley G, Presterl T, Geiger HH, Engels C. Kernel set in maize genotypes differing in nitrogen use efficiency in response to resource availability around flowering. *Plant Soil.* (2005) 272:101–10. doi: 10.1007/s11104-004-4210-8

13. Cázetta JO, Seebauer JR, Below FE. Sucrose and nitrogen supplies regulate growth of maize kernels. *Ann Bot-London.* (1999) 84:747–54. doi: 10.1006/anbo.1999.0976

14. Andersen MN, Asch F, Wu Y, Jensen CR, Naested H, Mogensen VO, et al. Soluble invertase expression is an early target of drought stress during the critical, abortion sensitive phase of young ovary development in maize. *Plant Physiol.* (2002) 130:591–604. doi: 10.1104/pp.005637

15. D'Andrea KE, Otegui ME, Cirilo AG. Kernel number determination differs among maize hybrids in response to nitrogen. *Field Crop Res.* (2008) 105:228–39. doi: 10.1016/j.fcr.2007.10.007

16. Kiniry JR, Tischler CR, Rosenthal WD, Gerik TJ. Nonstructural carbohydrate utilization by sorghum and maize shaded during grain growth. *Crop Sci.* (1992) 32:131–7. doi: 10.2135/cropsci1992.0011183X003200010029x

17. Zhu GH, Ye NH, Yang JC, Peng XX, Zhang J. Regulation of expression of starch synthesis genes by ethylene and ABA in relation to the development of rice inferior and superior spikelets. *J Exp Bot.* (2011) 62:3907–16. doi: 10.1093/jxb/err088

18. D'Andrea KE, Piedra CV, Mandolino CI, Cirilo AG, Otegui ME. Contribution of reserves to kernel weight and grain yield determination in maize: phenotypic and genotypic variation. *Crop Sci.* (2016) 56:697–706. doi: 10.2135/cropsci2015.05.0295

19. Li YB, Tao HB, Zhang BC, Huang SB, Wang P. Timing of water deficit limits maize kernel setting in association with changes in the source-flow-sink relationship. *Front. Plant Sci.* (2018) 9:1326. doi: 10.3389/fpls.2018.01326

20. Bialczyk J, Lechowski Z. Chemical composition of xylem sap of tomato grown on bicarbonate containing medium. *J Plant Nutr.* (1995) 18:2005–21. doi: 10.1080/01904169509365040

21. Peuke AD. The chemical composition of xylem sap in vitis vinifera L.cv, Riesling during vegetative vineyard soils and as influenced by nitrogen fertilizer. *Am J Enol Viticult.* (2000) 51:329–39.

22. Lalonde S, Tegeder M, Throne−Holst M, Frommer WB, Patrick JW. Phloem loading and unloading of sugars and amino acids. *Plant Cell Environ.* (2003) 26:37–56. doi: 10.1046/j.1365-3040.2003.00847.x

23. Feng HJ, Zhang SP, Ma CJ, Liu P, Dong ST, Zhao B, et al. Effect of plant density on microstructure of stalk vascular bundle of summer maize (*Zea mays* L.) and its characteristics of sap flow. *Acta Agron Sin.* (2014) 40:1435–42. doi: 10.3724/SP.J.1006.2014.01435

24. Ciampitti IA, Vyn TJ. Physiological perspectives of changes over time in maize yield dependency on nitrogen uptake and associated nitrogen efficiencies: a review. *Field Crop Res.* (2012) 133:48–67. j.fcr.2012.03.008 doi: 10.1016/j.fcr.2012.03.008

25. Peng Y, Li C, Fritschi FB. Apoplastic infusion of sucrose into stem internodes during female flowering does not increase grain yield in maize plants grown under nitrogen−limiting conditions. *Physiol Plantarum.* (2013) 148:470–80. doi: 10.1111/j.1399-3054.2012.01711.x

26. Duncan DR, Widholm JM. Osmotic induced stimulation of the reduction of the viability dye 2,3,5-triphenyltetrazolium chloride by maize roots and callus cultures. *J Plant Physiol.* (2004) 161:397–403. doi: 10.1078/0176-1617-01237

27. Liu T, Gu L, Dong S, Zhang J, Liu P, Zhao B. Optimum leaf removal increases canopy apparent photosynthesis, 13C-photosynthate distribution and grain yield of maize crops grown at high density. *Field Crop Res.* (2015) 170:32–9. doi: 10.1016/j.fcr.2014.09.015

28. Piao L, Qi H, Li C, Zhao M. Optimized tillage practices and row spacing to improve grain yield and matter transport efficiency in intensive spring maize. *Field Crop Res.* (2016) 198:258–68. doi: 10.1016/j.fcr.2016.08.012

29. Liu X, Wang X, Wang X, Gao J, Luo N, Meng Q, et al. Dissecting the critical stage in the response of maize kernel set to individual and combined drought and heat stress around flowering. *Environ Exp Bot.* (2020) 179:104213. doi: 10.1016/j.envexpbot.2020.104213

30. Yoshinaga S, Takai T, Arai-Sanoh Y, Ishimaru T, Kondo M. Varietal differences in sink production and grain-filling ability in recently developed high yielding rice (Oryza sativa L.) varieties in Japan. *Field Crops Res.* (2013) 150:74–82. doi: 10.1016/j.fcr.2013.06.004

31. Yagioka A, Satoshi H, Kenji KM. Sink production and grain-filling ability of a new high-yielding rice variety, Kitagenki. *Field Crop Res.* (2021) 260:107991. doi: 10.1016/j.fcr.2020.107991

32. Gonzalez VH, Lee EA, Lukens LN, Swanton CJ. The relationship between floret number and plant dry matter accumulation varies with early season stress in maize (*Zea mays* L.). *Field Crop Res.* (2019) 238:129–38. doi: 10.1016/j.fcr.2019.05.003

33. Zhu YG, Chu JP, Dai XL, He MR. Delayed sowing increases grain number by enhancing spike competition capacity for assimilates in winter wheat. *Eur J Agron.* (2019) 104:49–62. doi: 10.1016/j.eja.2019.01.006

34. Parco M, Ciampitti IA, D'Andrea KE, Maddonni G. Prolificacy and nitrogen internal ef–ficiency in maize crops. *Field Crops Res.* (2020) 256:107–12. doi: 10.1016/j.fcr.2020.107912

35. Ren H, Qi H, Zhao M, Zhou WB, Wang XB, Gong XW, et al. Characterization of source–sink traits and carbon translocation in maize hybrids under high plant density. *Agron J.* (2022) 12:961. doi: 10.3390/agronomy12040961

36. Pommel B, Gallais A, Coque M, Quillere I, Hirel B, Prioul JL, et al. Carbon and nitrogen allocation and grain filling in three maize hybrids differing in leaf senescence. *Eur J Agron.* (2006) 24:203–11. doi: 10.1016/j.eja.2005.10.001

37. Liu K, Ma BL, Luan L, Li C. Nitrogen, phosphorus, and potassium nutrient effects on grain filling and yield of high-yielding summer corn. *J Plant Nutr.* (2011) 34:1516–31. doi: 10.1080/01904167.2011.585208

38. Zhang H, Han K, Gu S, Wang D. Effects of supplemental irrigation on the accumulation, distribution and transportation of 13C-photosynthate, yield and water use efficiency of winter wheat. *Agr Water Manage.* (2019) 214:1–8. doi: 10.1016/j.agwat.2018.12.028

39. Paul MJ, Driscoll SP. Sugar repression of photosynthesis: the role of carbohydrates in signalling nitrogen deficiency through Source: sink imbalance. *Plant Cell Environ.* (1997) 20:110–6. doi: 10.1046/j.1365-3040.1997.d01-17.x

40. Dong H, Li W, Eneji A, Zhang D. Nitrogen rate and plant density effects on yield and late–season leaf senescence of cotton raised on a saline field. *Field Crop Res.* (2012) 126:137–44. doi: 10.1016/j.fcr.2011.10.005

41. Engels C, Marschner H. Influence of the form of nitrogen supply on root uptake and translocation of cations in the xylem exudate of maize (*Zea mays* L.). *Environ. Exp. Bot.* (1993) 44:1695–701. doi: 10.1093/jxb/44.11.1695

42. Fukuyama T, Takayama T. Variations of the vascular bundle system in Asian rice cultivars. *Euphytica.* (1995) 86:227–31. doi: 10.1007/BF00016360

43. Zhang ZH, Li P, Wang LX. Identification of quantitative trait loci (QTLs) for the characters of vascular bundles in peduncle related to indica-japonica differentiation in rice (*Oryza sativa* L.). *Euphytica.* (2002) 128:279–84. doi: 10.1023/A:1020802001207

44. Morita S, Okamoto M, Abe J, Yamagishi J. Bleeding rate of field-grown maize with reference to root system development. *Jpn J Crop Sci.* (2000) 69:80–5. doi: 10.1626/jcs.69.80

45. Noguchi A, Kageyama M, Shinmachi F. Potential for using plant xylem sap to evaluate inorganic nutrient availability in soil: i. influence of inorganic nutrients present in the rhizosphere on those in the xylem sap of luffa cylindrica roem.(soil fertility). *Soil Sci Plant Nutr.* (2005) 51:333–41. doi: 10.1111/j.1747-0765.2005.tb00038.x

46. Li H, Liu L, Wang Z, Yang J, Zhang J. Agronomic and physiological performance of high-yielding wheat and rice in the lower reaches of Yangtze River of China. *Field Crop Res.* (2012) 133:119–29. doi: 10.1016/j.fcr.2012.04.005

47. Guan D, Al-Kaisi MM, Zhang Y, Duan L, Tan W, Zhang M, et al. Tillage practices affect biomass and grain yield through regulating root growth, root-bleeding sap and nutrients uptake in summer maize. *Field Crop Res.* (2014) 157:89–97. doi: 10.1016/j.fcr.2013.12.015

48. Miao BH, Han XG, Zhang WH. The ameliorative effect of silicon on soybean seedlings grown in potassium-deficient medium. *Ann Bot-London.* (2010) 105:967–73. doi: 10.1093/aob/mcq063

49. He QP, Dong ST, Gong RQ. Comparison of ear vascular bundles in different maize cultivars. *Acta Agron Sin.* (2010) 33:1187–96.

50. Kalttorres W, Kerr PS, Usuda H, Huber SC. Diurnal changes in maize leaf photosynthesis: i. Carbon exchange rate, assimilate export rate, and enzyme activities. *Plant Physiol.* (1987) 83:283–8. doi: 10.1104/pp.83.2.283

51. Yang JC, Zhang JH, Wang ZQ, Zhu QS, Liu LJ. Water deficit–induced senescence and its relationship to the remobilization of prestored carbon in wheat during grain filling. *Agron J.* (2001) 93:196–206. doi: 10.2134/agronj2001.931196x

52. Monneveux P, Zaidi PH, Sanchez C. Population density and low nitrogen affects yield associated traits in tropical maize. *Crop Sci.* (2005) 45:535–45. doi: 10.2135/cropsci2005.0535

53. Huang X, Qian Q, Liu Z, Sun H, He S, Luo D, et al. Natural variation at the DEP1 locus enhances grain yield in rice. *Nat Genet.* (2009) 41:494–7. doi: 10.1038/ng.352

10.3389/fnut.2022.998946

Appendix

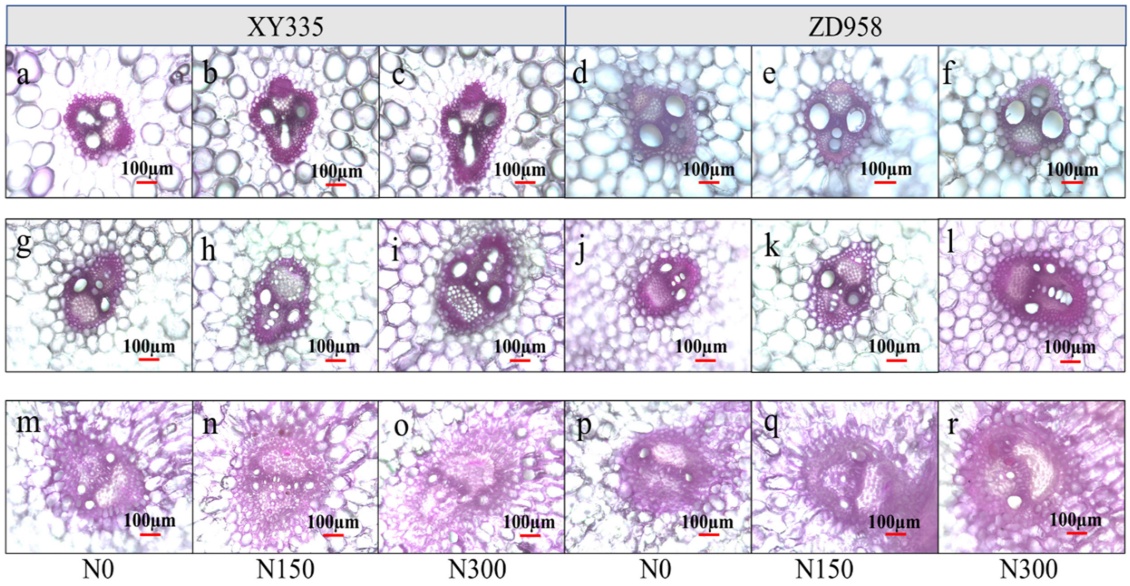

APPENDIX FIGURE 1
The micrograph of big vascular bundles structure at the basal stem internode of XY335 **(a–c)**, ZD958 **(d–f)**, the peduncle internode of XY335 **(g–i)** and ZD958 **(j–l)**, and the cob internode of XY335 **(m–o)** and ZD958 **(p–r)**. N0, N150, and N300 indicate N applied at 0, 150, and 300 kg ha^{-1} levels, respectively.

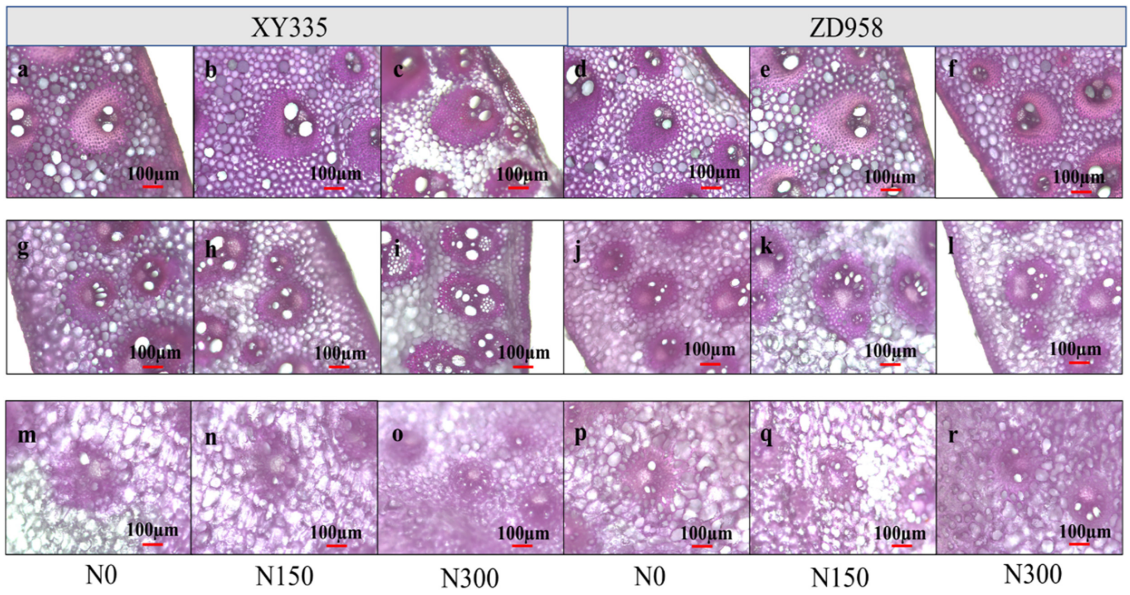

APPENDIX FIGURE 2
The micrograph of small vascular bundles structure at the basal stem internode of XY335 **(a–c)**, ZD958 **(d–f)**, the peduncle internode of XY335 **(g–i)**, and ZD958 **(j–l)**, and the cob internode of XY335 **(m–o)** and ZD958 **(p–r)**. N0, N150, and N300 indicate N applied at 0, 150, and 300 kg ha^{-1} levels, respectively.

frontiers | Frontiers in Nutrition

TYPE Original Research
PUBLISHED 02 September 2022
DOI 10.3389/fnut.2022.977287

OPEN ACCESS

EDITED BY
Gengjun Chen,
Kansas State University, United States

REVIEWED BY
Saeid Abbasi Maleki,
Kermanshah University of Medical Sciences, Iran
Junqing Huang,
Jinan University, China

*CORRESPONDENCE
Po-Hsien Li
pohsien0105@gmail.com
Ming-Fu Wang
mfwang@pu.edu.tw

†These authors have contributed equally to this work

SPECIALTY SECTION
This article was submitted to Nutrition and Food Science Technology, a section of the journal Frontiers in Nutrition

RECEIVED 24 June 2022
ACCEPTED 02 August 2022
PUBLISHED 02 September 2022

CITATION
Chou M-Y, Ho J-H, Huang M-J, Chen Y-J, Yang M-D, Lin L-H, Chi C-H, Yeh C-H, Tsao T-Y, Tzeng J-K, Hsu RJ-c, Huang P-H, Lu W-C, Li P-H and Wang M-F (2022) Potential antidepressant effects of a dietary supplement from the chlorella and lion's mane mushroom complex in aged SAMP8 mice.
Front. Nutr. 9:977287.
doi: 10.3389/fnut.2022.977287

Potential antidepressant effects of a dietary supplement from the chlorella and lion's mane mushroom complex in aged SAMP8 mice

Ming-Yu Chou[1†], Jou-Hsuan Ho[2†], Mao-Jung Huang[3], Ying-Ju Chen[4], Mei-Due Yang[5], Liang-Hung Lin[6], Ching-Hsin Chi[1], Chin-Hsi Yeh[7], Tsui-Ying Tsao[7], Jian-Kai Tzeng[7], Rachel Jui-cheng Hsu[8], Ping-Hsiu Huang[9], Wen-Chien Lu[10], Po-Hsien Li[11]* and Ming-Fu Wang[1,11]*

[1]International Aging Industry Research & Development Center (AIC), Providence University, Taichung, Taiwan, [2]Department of Food Science, Tunghai University, Taichung, Taiwan, [3]School of General Education, Hsiuping University of Science and Technology, Taichung, Taiwan, [4]Ph.D. Program in Health and Social Welfare for Indigenous Peoples, Providence University, Taichung, Taiwan, [5]Department of Surgery, Department of Clinical Nutrition, China Medical University Hospital, Taichung, Taiwan, [6]Division of Allergy, Immunology & Rheumatology, Taichung Tzu Chi Hospital, Buddhist Tzu Chi Medical Foundation, Taichung, Taiwan, [7]Taiwan Chlorella Manufacturing Co., Ltd., Taipei, Taiwan, [8]China Grain Products Research and Development Institute, New Taipei, Taiwan, [9]College of Food, Jiangsu Food and Pharmaceutical Science College, Huai'an City, China, [10]Department of Food and Beverage Management, Chung-Jen Junior College of Nursing, Health Sciences and Management, Chia-Yi City, Taiwan, [11]Department of Food and Nutrition, Providence University, Taichung, Taiwan

Since the 1990s, the prevalence of mental illnesses, such as depression, has been increasing annually and has become a major burden on society. Due to the many side effects of antidepressant drugs, the development of a complementary therapy from natural materials is an urgent need. Therefore, this study used a complex extract of chlorella and lion's mane mushroom and evaluated its antidepressant effects. Six-month-old male senescence-accelerated mice prone-8 (SAMP8) were divided into positive control; negative control; and low, medium, and high-dose groups. All groups were treated with corticosterone (CORT) at 40 mg/Kg/day for 21- days to induce depression in the animals, and the effects of different test substances on animal behavior was observed. The positive control group was intraperitoneally injected with a tricyclic antidepressant (Fluoxetine, as tricyclic antidepressant), the control group was given ddH_2O, and the test substance groups were administered test samples once daily for 21 days. The open field test (OFT) and forced swimming test (FST) were applied for behavior analyses of depression animal models. The OFT results showed that the mice in the positive control and the medium-, and high-dose groups demonstrated a significantly prolonged duration in the central area and a significantly increased travel distance. In the FST, the positive control and the medium, and high-dose groups displayed significantly reduced immobility times relative to the control group. The blood analysis results showed significant decreases

in triglyceride and blood urea nitrogen levels relative to the positive control and the medium- and high-dose groups. Notably, in the positive control and the medium- and high-dose groups, brain-derived neurotrophic factor (BDNF) increase by more than in the control group. In summary, medium and high dose of extract of chlorella and lion's mane mushroom could improve depression behavior in animals and have the potential to be antidepressant health care products.

KEYWORDS

antidepressant, chlorella, lion's mane mushrooms, senescence accelerated mouse prone-8 (SAMP8), dietary supplement

Introduction

Nowadays, depression is a prevalent psychiatric disorder that seriously impairs the quality of human life. Roughly 12% of people experience depression at least once in their lifetime (1). Approximately 32% of cancer patients suffer from anxiety, depression, or adjustment disorders (2). Depression is a global emotional disorder that affects an estimated 350 million people worldwide (3). It is characterized by a psychiatric disorder that can be caused by neuroendocrine dysfunction with disabling symptoms, usually depressed mood, despair, and low curiosity, with high morbidity, disability, and mortality, seriously endangering human life and health. In preclinical and clinical studies, it has been found that exogenous stress may cause a negative feedback imbalance in the hypothalamic-pituitary-adrenal (HPA) axis, promoting the release of glucocorticoids in the body (3). The glucocorticoid, also known as corticosterone (CORT), has been described as a "stress hormone" recognized as a mediator between chronic stress and depression. Currently, the widely used CORT-induced depression-like behavior was based on the neuroendocrine model of stress theory (4). It was reported that repeated injections of CORT to mice resulted in a time-dependent rise in immobility in forced swimming and tail suspension tests. Simultaneously, this injection regularization produced time-related effects on tyrosine hydroxylase levels in the hippocampus of mice; these results are consistent with the relevance of a stress-induced depression model and indicate that repetitive corticosterone injection regularization provides a valuable and reliable mouse model (5). Even though various antidepressants have been used to treat depression, a significant proportion of patients do not respond to them, and some experience side effects.

Recently, the marine microalga chlorella (*Chlorella vulgaris*) has been available as a dietary supplement and marketed worldwide (6). Its applications include the food, pharmaceutical, and agriculture industries (7). Chlorella has been proven to have various pharmacological effects on animals and humans and has a well-established production chain and commercial product line (8). It was documented by the FDA as safe for human consumption (9). Moreover, according to a previous published study, male and female mice dosed orally with acute and repeated doses of chlorella demonstrated no toxicity or adverse effects at levels estimated at 1,000 mg/kg^{-1} body weight per day and did not die during the period of investigation (10). Available commercially, chlorella products contain nutrients essential for humans (notably, vitamin D2 and B12), high amounts of high-quality protein, dietary fiber, and polyunsaturated fatty acids (including α-linoleic and linoleic acids) (1, 11, 12). In addition, chlorella possesses valuable antioxidants such as chlorophyll, carotenoids, astaxanthin, total polyphenols, lutein, and phycobiliproteins (13–15). However, a study has shown that chlorella extract (1,800 mg/day) was well-tolerated in a human clinical trial in major depression, with no serious adverse events reported; moreover, the participants exhibited improved physical and cognitive symptoms of depression (16). It has been proposed that antioxidant nutrients and compounds are responsible for the therapeutic effect of chlorella on depression (1).

A popular saprotrophic fungus in Asia (primarily in China, Taiwan, and Japan), the lion's mane mushroom [*Hericium erinaceus* (Bull.) Pers.] is a source of health-promoting properties and nutrients, including dietary fiber, minerals, vitamins, and bioactive compounds that have beneficial effects on human health, such as β-glucan, a fungal polysaccharide with health-promoting anti-tumor and immune-stimulating properties (17–19). Specifically, the *in vivo* benefits of mushroom antioxidants include reduced lipid peroxidation (20), reduced postprandial triglyceride response (21), improved activity of antioxidant enzymes (superoxide dismutase and catalase, etc.), increased plasma antioxidant capacity (T-AOC), protection against oxidative stress, removal of non-radioactive electrophiles (e.g., hydrogen peroxide), and breakdown of superoxide anions (22). Ultimately, it would appear that antioxidants play a role in limiting or reducing cellular and neurological damage in neurodegenerative diseases such as Alzheimer's and Parkinson's disease (23). Other physiological activities contain potential therapeutic

applications in oxidative stress-related diseases such as atherosclerosis, cancer, cardiovascular disease, inflammation, and diabetes (22).

Specifically, a role of oxidative stress in the pathophysiology of depression has been identified. Thus, alternative antidepressant drugs with adequate efficacy and safety are needed. This study aimed to observe the effect of different doses of a complex extract of chlorella and lion's mane mushroom on depression behavior in SAMP8 mice.

Materials and methods

Materials

Concentrated extracted of chlorella (*Chlorella Vulgaris*) was purchased from Taiwan Chlorella Manufacturing Co. (Taipei City, Taiwan), and the total polyphenols (expressed as gallic acid equivalents), as a quality control indicator component, were 23.31–34.93 (mg GAE/g extract). Lion's mane mushroom (*Hericium erinaceus* (Bull.) Pers.) was purchased from a local market. It was washed with distilled water, wiped dry, and then frozen at −20°C for 24 h, followed by freeze-drying. The powder was dry milled in a homogenizer (through an 80-mesh sieve). Next, 3.5 L of 95% alcohol and 210 g of mushroom powder were placed in a 5 L flask. The flask was shaken every 4 h for 24 h. The obtained solution was labeled as "extract A." The alcohol was removed by rotary vacuum evaporation. The filtered mushroom powder mentioned above was then added to 3.5 L of ddH_2O for 24 h and shaken at least four times. The solution resulting from this step was labeled "extract B." The precipitate was filtered out and added to a pot containing 10.5 L of water, which was then heated to 80°C. It was kept at this temperature and stirred every 6 h for ∼36 h until the solution volume was reduced to 3.5 L. The solution was labeled as "extract C." While the decoction was cooling, the mushroom powder was filtered out and discarded/composted. The three extract solutions (designated extracts "A," "B," and "C") were combined. The final extract was obtained by rotary vacuum evaporation and concentrated to 100 mL. Acceptable quality was indicated by polysaccharide> 12% and β-glucan> 7%. The tricyclic antidepressant Fluoxetine, trade name Prozac® (each capsule contains 20 mg, Eli Lilly and Company, Indianapolis, Indiana, USA), was applied and purchased from a local hospital according to the animal experiment's apply code in accordance with the regulation.

Experimental animal

A total of 40 male, 6-month-old SAMP8 mice were purchased from the National Laboratory Animal Center (Taipei, Taiwan) and randomly distributed into positive control, negative control, and treatment groups (low, medium, and high doses of extract), for a total of five groups of eight mice each (n = 8). Additionally, a group of 6-month-old BALB/C mice served as the blank group (n= 8). The mice were housed under specific pathogen-free conditions (25°C ± 2°C, humidity of 65% ± 5%, 12 h light/dark cycle, and lights on at 7 p.m.) with diet (AIN-93M standard purified feed) and water supplied *ad libitum* during the experiment. Feed and drinking water were freshly prepared and replaced every other day in the morning. All animal procedures were conducted in accordance with the standards set forth in the guidelines for the Care and Use of Experimental Animals by the Committee for the Purpose of Control and Supervision of Experiments on Animals and the National Institutes of Health. The protocol was approved by the Committee on Animal Research, Providence University, under code 20170512-A01.

Design of animal experiments

According to a related study, the spontaneous behavior is more active when mice is in the dark period; therefore, all tests were performed during the dark period (24). All groups were subjected to an open field test (OFT) and forced swimming test (FST) before the experiments. On the first day of the experiment, all groups of mice were injected subcutaneously with corticosterone (CORT) (40 mg/ kg/day) for 21 days to induce depression. In this case, CORT was dissolved in saline (NaCl 0.9 %) containing 0.1% dimethyl sulfoxide (DMSO) and 0.1% Tween-80, followed by subcutaneous injection once daily at 0.05 mL/10 g body weight (BW) per treatment (25).

The following were given 30 min after CORT injection.

i. ddH_2O was given to both the BALB/c and the negative control group.
ii. Fluoxetine (10 mg/kg, *ig*) was given to the positive control group.
iii. In the low-dose group, extract was given at 0.25 mL/25 g BW/day via tube feeding. The complex extract ratio was 0.1 mL chlorella+ 6 mg lion's mane mushroom.
iv. The medium-dose group was given 0.5 mL/25 g BW/day via tube feeding. The complex extract ratio was 0.2 mL chlorella + 12 mg lion's mane mushroom.
v. The high-dose group was given 2.5 mL/25 g BW/day via tube feeding. The complex extract ratio was 0.4 mL chlorella+ 24 mg lion's mane mushroom.

The study duration was 21 days (Figure 1), and BW, food intake, and water intake were recorded. The degree of depression in mice was evaluated by OFT and FST on days 20 and 21, respectively. After behavioral testing was completed, animals were anesthetized with isoflurane before dissection, while their blood was used for biochemical analysis.

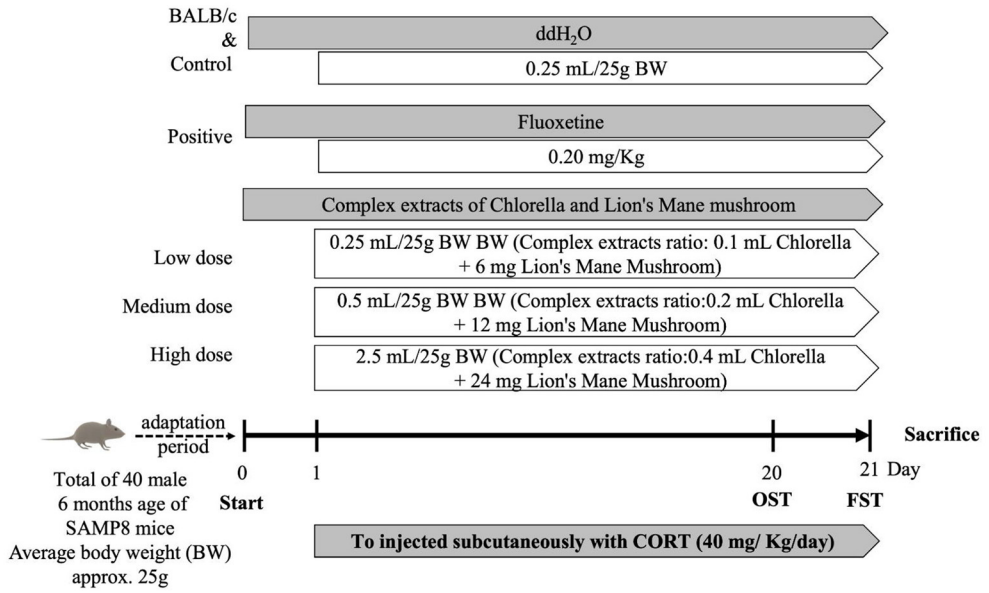

FIGURE 1
Schedule of animal experiments. Random subgroup adaptation for 7 days followed by treatment of mice with combined extracts, Fluoxetine, or water for 21 consecutive days, respectively. All mice were exposed to the CORT procedure for 21 days. Behavioral tests were performed on all mice.

Whole-brain tissue was rinsed with N_2 and stored at −80°C for further analysis of factors associated with the central nervous system.

Open field test (OFT)

The evaluation methodology was based on previous studies, with slight modifications (26–28). Rodents display characteristic of thigmotaxis to a new environment. Therefore, the central zone represents a threatening situation, while the peripheral area is relatively safe. Experiments were conducted in a location shielded from incidental noise. The space is a circular arena with a diameter of 97 and 42 cm high walls. Lighting with 850 nm far-red LEDs was used and any anxiety induced by the bright illumination was minimized. The room temperature was maintained at 25°C± 2°C during data acquisition. Each mouse was recorded for 10 min and then returned to the group housing. Mice were observed by video recording (FDR-AX700, Sony, Tokyo, Japan), and the time spent in the center, frequency of entering the center, and time spent standing were recorded for 10 min. An increase in the frequency and time spent staying in the center of the space indicated a decrease in anxiety. Video analysis was performed with TruScan software (Version 2.2; Coulbourn Instruments, Allentown, PA, USA). After each test, the space was cleaned with a 70–75% alcohol solution to avoid the effect of the odor of the previous animal on the next one.

Forced swimming test (FST)

The FST capitalizes on the fact that animals display escape behavior when exposed to adverse conditions, and when efforts to struggle fail, they present a state of abandonment. The FST, as a measure of depression, was conducted as in published studies, with modifications (29–31). The FST test was performed after 21 days of continuous gavage. The specific experimental procedure was as follows: 30 min after the last gavage, each mouse was placed individually and gently from a height of 5 cm into an open glass cylinder (20 cm diameter and 30 cm height) filled with warm water (25°C ± 2°C); under these conditions, the mice initially swam in the water to maintain their stability. Each mouse was judged to be immobile when it stopped struggling and remained floating motionless in the water, making only the movements necessary to keep its head above the water. The process was videotaped for 6 min to observe the behavior of each mouse. The time spent on activity (mobility) and inactivity (immobility) during the last 4 min of the 6 min were recorded to assess the degree of depression. The longer the duration of immobility, the higher the degree of desperation. In this case, the increase in immobility time corresponded to depression, and a decrease in immobility time was evaluated as the effectiveness of antidepressant treatment. When each mouse was finished, the test apparatus was cleaned with a 70–75% ethanol solution. To minimize experimental error, when each mice completed the test, the water was changed and the test apparatus cleaned with 70–75% ethanol.

Biochemical analysis of blood

Immediately after animal sacrifice, the blood was centrifuged at 4°C and 12,000 g for 10 min in Microfuge 22R (Beckman Coulter Inc., Brea, Calif., USA). Next, the plasma biochemical parameters, including glucose, total protein, albumin, triglycerides, total cholesterol, GOT (Glutamate Oxaloacetate Transaminase), GPT (Glutamate Pyruvate Transaminase), BUN (Blood urea nitrogen), and creatinine were analyzed in the blood using the Synchroh LX-20 system (Beckman Coulter Inc., Brea, Calif., USA), according to the manufacturer's instructions.

Analyses of factors associated with the central nervous system in the brain

Whole-brain tissues were homogenized with Tris-buffer (pH 7.4) and centrifuged at 1,200 g for 10 min at 4°C by removing unbroken tissues and debris. The tissue homogenate was obtained by centrifugation again at 13,000 g for 10 min at 4°C to prepare the cytoplasmic fraction.

Serotonin (5-HT)

Serotonin concentrations were quantified using the Serotonin Research ELISA^{TM} (Labor Diagnostika Nord GmbH & Co.KG, Nordhorn, Germany) and an ultra-sensitive enzyme immunoassay. Determination was performed according to the protocol in the reagent kit. Briefly, 100 μL of tissue homogenate and standard were added to the acylation plate, then 25 μL of acylation buffer was added at room temperature to react for 30 min. From the above-acetylated samples and standards, 100 μL were transferred to a 96-well dish, to which 25 μL of serotonin antiserum was added and then placed in a refrigerator at 4°C for 15–20 h. Then, after three washes with a Wellwash^{TM} (Thermo Fisher Scientific Co., Waltham, MA, USA), 100 μL of IgG-peroxidase conjugate (anti-rabbit) was added and allowed to react at room temperature for 30 min, and the above washing procedure was repeated. The reaction was performed by adding 100 μL of TMB at room temperature for 20 to 30 min without light and then terminated by adding 100 μL of 25 M sulphuric acid. The absorbance values of the samples and standards were determined at 450 nm (Spectrophotometer, U-2000, Hitachi High-Tech Science, Tokyo, Japan), and the serotonin concentrations were calculated by comparison with standard curves.

Dopamine (DA)

Quantification of dopamine was performed using the Dopamine Research ELISA^{TM} (Labor Diagnostika Nord) and an ultra-sensitive enzyme immunoassay as follows: 10 μL of tissue homogenate and standards were added to the extraction plate and diluted with 90 μL of deionized water. Then, 25 μL of TE buffer was added and incubated for 1 h at room temperature. After two washes, 150 μL of acylation buffer and 25 μL of acylation reagent were added and allowed to react at room temperature for 20 min. The reaction was repeated by washing twice and adding 100 μL of 0.025 M HCl to react for 10 min at room temperature. Then, 90 μL was transferred from the extraction plate to a 96-well microtiter plate, 25 μL of enzyme solution was added, and the plate was incubated at 37°C for 2 h. Then, 100 μL of the reaction solution was transferred to the dopamine ELISA plate and incubated in the refrigerator at 4°C for 15–20 h. Wellwash^{TM} was used to wash the plate three times, and 100 μL of IgG-peroxidase conjugate (anti-rabbit) was added and allowed to react for 30 min at room temperature. The washing procedure was repeated. Under sheltered conditions, 100 μL of TMB was added to the reaction at room temperature for 20–30 min, then 100 μL of 0.25 M H_2SO_4 was added to stop the reaction. The absorbance values were measured at 450 nm, and the concentration of dopamine was calculated by comparison with a standard curve.

Brain-derived neurotrophic factor (BDNF)

The *ChemiKine* BDNF Sandwich ELISA Kit (Merck KGaA, Darmstadt, Germany) was used to determine BDNF by using an enzyme immunoassay. Tissue homogenates and standards (100 μL) were added to a 96-well plate and incubated overnight in a 4°C refrigerator. Wellwash^{TM} was used to wash the plate four times. Then, 100 μL of anti-BDNF (from mouse) was added and allowed to react at room temperature for 2.5 h. Following triple washing, 100 μL of the streptavidin-enzyme conjugate was added, and the reaction was carried out at room temperature for 1 h. The plate was washed three more times and 100 μL of TMB added and allowed to react for 15 min at room temperature without light. Lastly, the reaction was terminated by adding 100 μL of HCl, and the absorbance values were measured at 450 nm, while the content of BDNF in the samples was calculated based on comparison with the standard curve.

Statistical analysis

The data obtained from this study were analyzed using IBM SPSS Statistics version 22 (IBM Corp., Armonk, N.Y., USA). The results were expressed as mean ± SEM. The data were analyzed by one-way analysis of variance (ANOVA) to test for differences between groups, and Duncan's multiple allometric tests were used to assess differences between groups for significance. When $p < 0.05$, a significant difference was indicated.

TABLE 1 Changes in body weight and records of food and water intake of SAMP8 mice supplemented with combined extracts.

Group ($n = 8$)[a,b]	Body weight (gm)		Food intake (g/day)	Water consumption (ml/day)
	Initial	Final		
Positive control	30.13 ± 0.50	29.17 ± 0.42	5.63 ± 0.08	5.60 ± 0.07
Control	29.67 ± 0.66	27.43 ± 0.43	6.08 ± 0.13	5.69 ± 0.09
Low dose	30.09 ± 0.38	28.28 ± 0.51	5.90 ± 0.10	5.51 ± 0.11
Medium dose	29.08 ± 0.55	27.69 ± 0.49	5.76 ± 0.08	5.56 ± 0.07
High dose	29.01 ± 0.40	27.62 ± 0.34	5.83 ± 0.08	5.54 ± 0.10

[a] Data are expressed as the mean ± S.E.M. (n = 8) and analyzed by one-way ANOVA. [b] Data points were not significantly different ($p > 0.05$) from each other according to ANOVA. Positive control: CORT (40 mg/kg/day) + Fluoxetine (20 mg/kg/day). Control: CORT (40 mg/kg/day). Low dose: CORT (40 mg/kg/day) + combined extracts of chlorella and lion's mane mushroom (contains 0.1 mL chlorella extract concentrate + 6 mg lion's mane mushroom extract concentrate). Medium dose: CORT (40 mg/kg/day) + combined extracts of chlorella and lion's mane mushroom (contains 0.2 mL chlorella extract concentrate + 12 mg lion's mane mushroom extract concentrate). High dose: CORT (40 mg/kg/day) + combined extracts of chlorella and lion's mane mushroom (contains 0.4 mL chlorella extract concentrate + 24 mg lion's mane mushroom extract concentrate).

Results and discussion

Changes in diet, water intake, and BW

Stress hormones such as CORT play a vital role in the development of depression (32, 33), and this relationship has been used to develop animal models of the condition (25, 34, 35). The CORT-induced depression model has a shorter test schedule, with a higher repeatability and success rate, for rapid assessment of antidepressant efficacy, enabling an expedient evaluation, and has been utilized in many studies (5, 33, 35, 36). In depressive mood disorders, continuous changes in the HPA axis are observed, usually associated with stress (32). Therefore, this study induced dysregulation of the HPA axis in male SAMP8 mice by repeated injections of CORT (40 mg/kg/day), which led to depression and anxiety. Improvements were evaluated and observed when mice were fed different doses of combined extracts of chlorella and lion's mane mushroom for 21 consecutive days. A comparison of the changes in BW, food intake, and water intake in all groups is shown (Table 1). To minimize experimental error, the mice were randomized into groups with no significant difference in initial BW. The results showed no significant differences in BW, food intake, and water intake between any of the groups from the beginning to the end of the experiment. However, each group showed a slight decrease in BW during the experimental period. In addition, the food and water intake of the control group showed an increasing trend, in comparison with the other groups. It was observed that mice injected with 40 mg/kg of CORT for 21 consecutive days showed a reduction in BW compared to the control group (37). Moreover, when CORT was added directly to the rats' drinking water, the CORT group consumed more food and water than the control group at weeks 2 and 3, while the bodyweight of the CORT group was significantly lower than that of the control group at weeks 1, 2, and 3 (38). Additionally, a previous study found that glucocorticoids act on the hypothalamus to promote appetite and increase food intake (39). The administration of glucocorticoids (such as CORT) increases catabolic processes, including lipid and muscle protein catabolism (36). Therefore, when food and water intake increase, weight loss still occurs. The above reports showed that the BW of the animals decreased with CORT administration, and the food and water intake increased. In this study, decreases in BW were observed in the positive control group, negative control group, and experimental group, but only the negative control group had a higher food and water intake.

Behavioral tests

OFT

The OFT can be used to evaluate the spontaneous activity of animals in a new environment. Animal behavior such as running away or staying in the same place may occur due to fear and stimulation when facing a new environment. The OFT allows for the study of animal performance in terms of locomotion, directed exploratory activity, and emotional state (anxiety) (27, 40). The specific evaluation approach is as follows. When mice with depression symptoms tend to move closer to the peripheral area than normal mice, they are unwilling to remain in the central zone or stay in the corner. When mice traverse the center block with increased frequency and stay there of a long time, they show a reduction in depression and increased exploration ability. The numbers of crossings, stay time, distances traveled, and speeds of movement in the central zone, of SAMP8 mice administered CORT (40 mg/kg/day) and treated with complex extract of chlorella and lion's mane mushroom for 21 consecutive days are shown in Table 2. The results showed that the number of crossings in the positive control group and the treatment groups tended to increase, yet there were no significant differences compared with the control group. Moreover, the stay time and distance traveled (as refers to the total movement distance into the central area) were significantly higher in the positive control group and the medium-, and high-dose treatment groups, compared to the control group ($p < 0.05$). The movement speed was significantly higher only in the positive control group compared with the control group ($p < 0.05$). In a study conducted on mice injected with 20 mg/kg/day of CORT for 5 weeks, a significant reduction in 5 min stays in the central zone in the CORT group compared to the control group was observed (41). Furthermore, during the 3 weeks of continuous injection of 40 mg/kg/day of CORT in mice, a trend toward an increase in the number of crossings of the central zone in 3 min in the CORT group compared to the control group was observed (37).

TABLE 2 Evaluation of the benefits of combined extracts in mice by the open field test (OFT) and the forced swimming test (FST).

	Group ($n = 8$) [a,b]	Positive control	Control	Low dose	Medium dose	High dose
Open field test	Frequency	11.38 ± 1.16	9.50 ± 1.34	10.25 ± 0.82	10.75 ± 1.08	11.25 ± 0.56
	Duration time (sec)	17.63 ± 1.13	12.13 ± 1.20	14.75 ± 1.69	16.63 ± 1.85	17.25 ± 1.45
	Distance traveled (mm)	691 ± 110.51	371.71 ± 66.74	447.05 ± 56.74	627.85 ± 72.00	663.38 ± 88.65
	Velocity (mm/s)	29.85 ± 4.15	18.18 ± 1.93	18.84 ± 1.36	19.25 ± 2.12	20.20 ± 3.14
Forced swimming test	Immobility time (sec)	207.58 ± 12.32	254.83 ± 13.81	228.35 ± 12.41	216.45 ± 8.17	210.51 ± 10.89

[a] Data are expressed as the mean ± S.E.M. (n = 8) and analyzed by one-way ANOVA. [b] Data points were not significantly different ($p > 0.05$) from each other according to ANOVA. Positive control: CORT (40 mg/kg/day) + Fluoxetine (20 mg/kg/day). Control: CORT (40 mg/kg/day). Low dose: CORT (40 mg/kg/day) + combined extracts of chlorella and lion's mane mushroom (contains 0.1 mL chlorella extract concentrate + 6 mg lion's mane mushroom extract concentrate). Medium dose: CORT (40 mg/kg/day) + combined extracts of chlorella and lion's mane mushroom (contains 0.2 mL chlorella extract concentrate + 12 mg lion's mane mushroom extract concentrate). High dose: CORT (40 mg/kg/day) + combined extracts of chlorella and lion's mane mushroom (contains 0.4 mL chlorella extract concentrate + 24 mg lion's mane mushroom extract concentrate).

TABLE 3 Investigation of biochemical analysis of blood profiles in mice treated with combined extracts.

Group ($n = 8$)[a,b]	Positive control	Control	Low dose	Medium dose	High dose
Albumin (g/dL)	3.04 ± 0.06	3.10 ± 0.08	3.01 ± 0.08	3.12 ± 0.09	3.06 ± 0.08
Glucose (mg/dL)	114.25 ± 4.20	127.38 ± 5.96	121.00 ± 7.65	116.00 ± 7.27	118.63 ± 6.91
Total Cholesterol (mg/dL)	130.88 ± 4.31	141.38 ± 4.93	136.50 ± 3.34	132.75 ± 4.66	131.38 ± 6.32
Triglyceride (mg/dL)	140.25 ± 3.12	167.50 ± 3.15	148.38 ± 4.70	144.13 ± 5.16	142.50 ± 4.81
Total Protein (g/dL)	5.26 ± 0.08	5.30 ± 0.05	5.39 ± 0.08	5.34 ± 0.06	5.33 ± 0.09
GOT (U/L)	82.25 ± 4.95	96.50 ± 2.43	89.38 ± 6.32	85.50 ± 7.12	82.88 ± 4.50
GPT (U/L)	50.63 ± 5.51	61.75 ± 3.53	53.25 ± 3.71	52.38 ± 6.22	56.88 ± 5.79
BUN (mg/dL)	32.63 ± 1.41	40.63 ± 0.94	36.88 ± 1.48	34.75 ± 1.82	35.63 ± 1.67
Creatinine (mg/dL)	0.27 ± 0.02	0.32 ± 0.01	0.30 ± 0.02	0.29 ± 0.02	0.31 ± 0.01

[a] Data are expressed as the mean ± S.E.M. (n = 8) and analyzed by one-way ANOVA. [b] Data points were not significantly different ($p > 0.05$) from each other according to ANOVA. Positive control: CORT (40 mg/kg/day) + Fluoxetine (20 mg/kg/day). Control: CORT (40 mg/kg/day). Low dose: CORT (40 mg/kg/day) + combined extracts of chlorella and lion's mane mushroom (contains 0.1 mL chlorella extract concentrate + 6 mg lion's mane mushroom extract concentrate). Medium dose: CORT (40 mg/kg/day) + combined extracts of chlorella and lion's mane mushroom (contains 0.2 mL chlorella extract concentrate + 12 mg lion's mane mushroom extract concentrate). High dose: CORT (40 mg/kg/day) + combined extracts of chlorella and lion's mane mushroom (contains 0.4 mL chlorella extract concentrate + 24 mg lion's mane mushroom extract concentrate).

In brief, according the above, continuous administration of CORT reduces the stay time and the frequency of crossings in the central region, similar to the results obtained in the current study. Hence, the positive control and the medium-, and high-dose treatment groups showed evidence of increased time spent in the central sector, which implies effective improvement in depression, greater mobility in the central zone, and improved exploratory activity in mice.

FST

The FST provides a method for evaluating the degree of depression. Depression severity was determined by observing the escape behavior of mice under adverse conditions. Normal mice would struggle in the water, but when their efforts were unsuccessful, they would behave desperately, floating in the water and giving up swimming. The experimental procedure involved video recording to observe the mice's behavior during the experiment and to measure the duration of mobility and immobility. The longer the duration of immobility, the more desperate the mice were. The FST results showed (Table 2) that the mice displayed a significant reduction in time spent immobile during the procedure in the positive control group and medium- and high-dose treatment groups, when compared to the control group ($p < 0.05$). According to previous studies, mice were significantly more immobile in the FST after 3 weeks of continuous CORT treatment (5, 42). It was reported that CORT treatment of mice significantly prolonged immobility in the FST while attenuating behavioral responses in the OFT. In contrast, the administration of catalpol (20 mg/kg for 21 days) significantly reversed CORT-induced depressive behavior in Kunming mice (25). The results of the present study showed the same phenomenon, whereby the administration of antidepressant drugs, as well as medium- and high-doses of combined extracts of chlorella and lion's mane mushroom, was able to reduce both the time that mice gave up struggling and floated on the water surface, which indicated that they were able to alleviate the behavioral manifestations of despair.

Biochemical analysis of blood

The results of blood biochemical analysis are shown in Table 3. There were significant decreases in triglycerides and

TABLE 4 Effects of combined extracts on the levels of factors correlated to the central nervous system in brain of mice.

Group ($n = 8$) [a,b]	Positive control	Control	Low dose	Medium dose	High dose
Serotonin (%)	92.50 ± 4.88	100.00 ± 8.59	96.24 ± 6.97	94.02 ± 6.70	95.64 ± 10.08
Dopamine (%)	94.45 ± 10.90	100.00 ± 6.76	98.55 ± 5.75	98.53 ± 10.34	99.42 ± 6.86
BDNF (%)	141.97 ± 8.73	100.00 ± 9.40	114.09 ± 12.68	118.84 ± 5.51	122.81 ± 8.56

[a] Data are expressed as the mean ± S.E.M. (n = 8) and analyzed by one-way ANOVA. [b] Data points were not significantly different ($p > 0.05$) from each other according to ANOVA. Positive control: CORT (40 mg/kg/day) + Fluoxetine (20 mg/kg/day). Control: CORT (40 mg/kg/day). Low dose: CORT (40 mg/kg/day) + combined extracts of chlorella and lion's mane mushroom (contains 0.1 mL chlorella extract concentrate + 6 mg lion's mane mushroom extract concentrate). Medium dose: CORT (40 mg/kg/day) + combined extracts of chlorella and lion's mane mushroom (contains 0.2 mL chlorella extract concentrate + 12 mg lion's mane mushroom extract concentrate). High dose: CORT (40 mg/kg/day) + combined extracts of chlorella and lion's mane mushroom (contains 0.4 mL chlorella extract concentrate + 24 mg lion's mane mushroom extract concentrate).

BUN in the positive control group and the group treated with a combination of chlorella and lion's mane mushroom extracts, in comparison with the control group ($p < 0.05$). In addition, the analysis showed a decreasing trend in glucose, total cholesterol, GOT, GPT, and creatinine in the positive control group and the complex-treated groups, compared with the control group. However, there were no significant differences in total protein and albumin among all groups. It has been reported that mice injected with 40 mg/kg/day of CORT for 3 consecutive weeks showed increased blood TG, TC, HDL-C, and LDL-C concentrations and a trend of increasing blood glucose concentrations (37).

According to previous studies, SD rats with high cholesterol dietary-induced hypercholesterolemia were treated with 100 mg/kg BW lion's mane mushroom extract for 4 weeks showed a significant reduction in blood total cholesterol concentration (43). According to Chovancikova and Simek (44), administration of a high-fat diet with 1% chlorella to CD1 mice for 10 weeks showed a significant reduction in TG and TC in the blood and liver. In brief, it was observed that CORT administration in mice resulted in increased lipid concentrations and elevated blood glucose levels, which were similar to the results in the literature; simultaneous administration of antidepressants and the combined extracts of chlorella and lion's mane mushroom caused a decrease in lipid and blood glucose levels. It was indicated that the combination of chlorella and lion's mane mushroom combined extracts could improve the catabolic effects of CORT.

Factors correlated with the central nervous system in the brain

Serotonin

Serotonin, otherwise known as 5-Hydroxytryptamin (5-HT), is one of the monoamine neurotransmitters in the central nervous system. Acting principally as a neurotransmitter in the synaptic gap, 5-HT is related to mood regulation, behavioral inhibition and mood stabilization, and is a transmitter of mental feelings such as happiness, peace of mind, and satisfaction. The serotonin hypothesis suggests that disorders of the 5-HT system and its components play an active role in the origin of depression (45). It has been suggested that high levels of 5-HT production regulate serotonin neuron clusters by reducing the expression of serotonin transporter and monoamine oxidase A in serotonergic cells via vitamin D (46). An imbalance in the serotonin system in the brain often leads to insomnia, which in turn leads to psychiatric disorders (such as depression and agitation) and, in severe cases, Alzheimer's disease (47). The results of a between-group comparison of brain serotonin (Table 4) revealed an upward trend in the serotonin concentration in the control group; meanwhile, the serotonin concentration in the positive control group and the treatment groups showed a decreasing trend, but it did not reach statistical difference. The results showed that 21 days of CORT administration (40 mg/kg/day) resulted in a significant increase in the 5-HT concentration in the hippocampal cortex of mice (48). Additional evidence suggests that CORT given continuously to rats for 21 days decreased the sensitivity of the prefrontal cortical serotonin receptor (5-HT1A), along with increased prefrontal cortical serotonin concentrations (49). Therefore, it was hypothesized that the increase in serotonin synthesis in the brains of animals with CORT-induced depressive behavior might be caused either by the individual's resistance to excessive stress or by the feedback regulation produced by corticosterone. The results obtained in this study were similar to the above publications concerning the use of CORT to induce depression in SAMP8 mice.

Dopamine

Dopamine is one of the neurotransmitters in the central nervous system, and its main effects are related to pleasure and desire, which can govern human actions, motivation, emotions, memory function, and adaptive behavior. It can make people feel excited, give them a desire to emerge, fill them with energy and curiosity, make them emotionally happy, and facilitate a sense of accomplishment. When the concentration of inter-synaptic neurotransmitters is unbalanced, behaviors such as depression, suppressed desire, etc. occur with ease (50). A between-group

comparison of brain dopamine concentrations is shown in Table 4. In the control group, the dopamine concentration in the brain was higher than that in the other groups, whereas in the positive control group, the dopamine concentration in the brain decreased following the administration of antidepressant drugs to the mice. In addition, the dopamine concentration in mice of the treatment group was lower than that of mice the control group, but the difference did not reach statistical significance.

According to a study, 21 days of corticosterone administration (20 mg/kg) in mice decreased the expression of glucocorticoid receptors in the cerebral cortex, resulting in dysfunction of the glucocorticoid receptor system, and increased dopamine release from the prefrontal cortex induced by high K^+ (51). Moreover, another study found that depressive animal behavior was correlated with an increased prefrontal cortical dopamine concentration (52, 53). In this study, it was observed that the dopamine concentration in the brain was similar to those reported in the publications literature.

BDNF

BDNF has several functions in the central nervous system, including regulation of nerve cell development, survival, synthesis of synapses, and the transmission of neurotransmitters, which are intracellular messages in the brain. In recent years, various studies have found that BDNF concentrations in the brain and other tissues of depressed patients and animal models were significantly lower than those in normal ones; thus, BDNF has been suggested to be related to the pathological mechanism of depression, where it could be an important therapeutic target for depression (25).

In mice of the positive control group, which were given CORT followed by antidepressant therapy, a significant increase in the BDNF concentration in the brain was observed ($p < 0.05$) (Table 4). Fascinatingly, a similar significant improvement to that in the positive control group was observed in the groups treated with chlorella and lion's mane mushroom combined extract ($p < 0.05$). Many previous studies found that exogenous corticosterone administration caused a decrease in the levels of BDNF mRNA in the hippocampus (54, 55). The continuous administration of CORT (40 mg/kg) for 21 days to rats significantly reduced the protein expression of BDNF in the hippocampal cortex of their brains, while the concurrent administration of an antidepressant (Fluoxetine, 10 mg/kg) improved the concentration of BDNF in the hippocampal cortex (56). In this study, the results were similar to those of the abovementioned studies, which showed that the BDNF concentration in the brains of mice decreased with CORT treatment, although the situation improved with treatment via Fluoxetine and combined extracts (from chlorella and lion's mane mushroom).

The goal of preventive medicine is to promote health and achieve the effect of aging and disease prevention by improving the intake of antioxidant-rich dietary substances (12). Thus, in animal models, high CORT levels contribute to the overproduction of ROS, resulting in increased lipid peroxidation and antioxidant enzyme activity in the brain (1, 25). According to the above results, it was observed that supplementation with combined extracts (from chlorella and lion's mane mushroom) improved the capability of the antioxidant defense system in the body and inhibited the production of peroxides, presumably due to the presence of carotenoids and phenolic compounds in the extracts. Overproduction of amyloid beta-protein (Aβ) causes learning memory deficits (47), and administration of the abovementioned combined extracts might have improved the amyloid deposition in the brain of SAMP8 mice. In general, to our knowledge, there is no information on the effect of chlorella on the deposition of amyloid proteins, but effectively raising antioxidant defenses and reducing the damage caused to nerve cells by oxidative stress might reduce the deposition of amyloid proteins and improve memory loss.

Conclusions

In summary, this study aimed to observe the effect of different doses of chlorella and lion's mane mushroom combined extracts on depression behavior. All groups of mice were administered CORT (40 mg/kg/day) for 21 days to induce depression *in vivo*. The OFT results showed that the positive control group, and medium- and high-dose extract groups were significantly improved in terms of prolonging the stay in the central zone ($p < 0.05$) and increasing the distance traveled ($p < 0.05$). In terms of FST, the above three groups were able to significantly reduce the immobility time as compared to the control group ($p < 0.05$). The results of blood biochemical analysis showed that the TG and BUN levels in the blood raised by CORT were reduced significantly ($p < 0.05$) in the positive control group, and medium-, and high-dose treatment groups. All three of the above treatments increase BDNF levels. To our knowledge, this is the first validation of the antidepressant-like effects of combined extracts of chlorella and lion's mane mushroom in a CORT injection-induced mouse model of depression, which may lead to the development of a new antidepressant dietary supplement. Hence, this study provides a theoretical framework for future research and application of the combined extracts of chlorella and lion's mane mushroom to prevent and treat depression.

Data availability statement

The raw data supporting the conclusions of this article will be made available by the authors, without undue reservation.

Ethics statement

The animal study was reviewed and approved by Committee on Animal Research, Providence University, under code 20170512-A01.

Author contributions

M-YC, J-HH, and M-JH: conceptualization. Y-JC, M-DY, L-HL, and W-CL: data curation. C-HC, C-HY, T-YT, and W-CL: investigation. J-KT and RJ-cH: methodology. P-HH and P-HL: writing—original draft. P-HL and M-FW: writing—review and editing.

Funding

This research was financially supported by China Grain Products Research and Development Institute, Taiwan.

Acknowledgments

The authors thank Taiwan Chlorella Manufacturing Company for providing the experimental materials.

Conflict of interest

The authors declare that the research was conducted in the absence of any commercial or financial relationships that could be construed as a potential conflict of interest.

Publisher's note

All claims expressed in this article are solely those of the authors and do not necessarily represent those of their affiliated organizations, or those of the publisher, the editors and the reviewers. Any product that may be evaluated in this article, or claim that may be made by its manufacturer, is not guaranteed or endorsed by the publisher.

References

1. Bito T, Okumura E, Fujishima M, Watanabe F. Potential of chlorella as a dietary supplement to promote human health. *Nutrients.* (2020) 12:2524. doi: 10.3390/nu12092524

2. Yeung KS, Hernandez M, Mao JJ, Haviland I, Gubili J. Herbal medicine for depression and anxiety: a systematic review with assessment of potential psycho-oncologic relevance. *Phytother Res.* (2018) 32:865–91. doi: 10.1002/ptr.6033

3. Subermaniam K, Teoh SL, Yow, Y.-Y., Tang YQ, Lim LW, et al. Marine algae as emerging therapeutic alternatives for depression: a review. *Iran J Basic Med Sci.* (2021) 24:997–1013. doi: 10.22038/ijbms.2021.54800.12291

4. Chen C, Nakagawa S, An Y, Ito K, Kitaichi Y, Kusumi I. The exercise-glucocorticoid paradox: how exercise is beneficial to cognition, mood, and the brain while increasing glucocorticoid levels. *Front Neuroendocrinol.* (2017) 44:83–102. doi: 10.1016/j.yfrne.2016.12.001

5. Zhao Y, Ma R, Shen J, Su H, Xing D, Du L. A mouse model of depression induced by repeated corticosterone injections. *Eur J Pharmacol.* (2008) 581:113–20. doi: 10.1016/j.ejphar.2007.12.005

6. Rani KP, Sandal N, Sahoo P. A comprehensive review on chlorella-its composition, health benefits, market and regulatory scenario. *Pharma Innov J.* (2018) 7:584–9.

7. Coelho DFM, Alfaia CMRPM, Assunção JMP, Costa M, Pinto RMA, de Andrade Fontes CMG, et al. Impact of dietary *Chlorella vulgaris* and carbohydrate-active enzymes incorporation on plasma metabolites and liver lipid composition of broilers. *BMC Vet Res.* (2021) 17:229. doi: 10.1186/s12917-021-02932-8

8. Yarmohammadi S, Hosseini-Ghatar R, Foshati S, Moradi M, Hemati N, Moradi S, et al. Effect of *Chlorella vulgaris* on liver function biomarkers: a systematic review and meta-analysis. *Clin Nutr Res.* (2021) 10:83–94. doi: 10.7762/cnr.2021.10.1.83

9. Latif AAE, Assar DH, Elkaw EM, Hamza HA, Alkhalifah DHM, Hozzein WN, et al. Protective role of *Chlorella vulgaris* with thiamine against paracetamol induced toxic effects on haematological, biochemical, oxidative stress parameters and histopathological changes in Wistar rats. *Sci Rep.* (2021) 11:3911. doi: 10.1038/s41598-021-83316-8

10. Yadav M, Sharma P, Kushwah H, Sandal N, Chauhan MK. Assessment of the toxicological profile of Chlorella (*C. vulgaris*) powder by performing acute and sub-acute oral toxicity studies in mice. *J Appl Phycol.* (2022) 34:363–73. doi: 10.1007/s10811-021-02632-8

11. Morgese MG, Mhillaj E, Francavilla M, Bove M, Morgano L, Tucci P, et al. Chlorella sorokiniana extract improves short-term memory in rats. *Molecules.* (2016) 21:1311. doi: 10.3390/molecules21101311

12. Sikiru AB, Arangasamy A, Alemede IC, Guvvala PR, Egena SSA, Ippala JR, et al. *Chlorella vulgaris* supplementation effects on performances, oxidative stress and antioxidant genes expression in liver and ovaries of New Zealand White rabbits. *Heliyon.* (2019) 5:e02470. doi: 10.1016/j.heliyon.2019.e02470

13. Ahmed F, Fanning K, Netzel M, Turner W, Li Y, Schenk PM. Profiling of carotenoids and antioxidant capacity of microalgae from subtropical coastal and brackish waters. *Food Chem.* (2014) 165:300–6. doi: 10.1016/j.foodchem.2014.05.107

14. Dantas DMM, Cahú TB, Oliveira CYB, Abadie-Guedes R, Roberto NA, Santana WM, et al. *Chlorella vulgaris* functional alcoholic beverage: effect on propagation of cortical spreading depression and functional properties. *PLoS ONE.* (2021) 16:e0255996. doi: 10.1371/journal.pone.0255996

15. Ru ITK, Sung YY, Jusoh M, Wahid MEA, Nagappan T. *Chlorella vulgaris*: a perspective on its potential for combining high biomass with high value bioproducts. *Appl Phycol.* (2020) 1:2–11. doi: 10.1080/26388081.2020.1715256

16. Panahi Y, Badeli R, Karami GR, Badeli Z, Sahebkar A. A randomized controlled trial of 6-week *Chlorella vulgaris* supplementation in patients with major depressive disorder. *Complement Ther Med.* (2015) 23:598–602. doi: 10.1016/j.ctim.2015.06.010

17. Hu T, Hui G, Li H, Guo Y. Selenium biofortification in Hericium erinaceus (Lion's Mane mushroom) and its *in vitro* bioaccessibility. *Food Chem.* (2020) 331:127287. doi: 10.1016/j.foodchem.2020.127287

18. Ren L, Perera C, Hemar Y. Antitumor activity of mushroom polysaccharides: a review [10.1039/C2FO10279J]. *Food Funct.* (2012) 3:1118–130. doi: 10.1039/c2fo10279j

19. Szydłowska-Tutaj M, Złotek U, Combrzyński M. Influence of addition of mushroom powder to semolina on proximate composition, physicochemical properties and some safety parameters of material for pasta production. *LWT.* (2021) 151:112235. doi: 10.1016/j.lwt.2021.112235

20. Ma Z, Cui F, Gao X, Zhang J, Zheng L, Jia L. Purification, characterization, antioxidant activity and anti-aging of exopolysaccharides by Flammulina velutipes SF-06. *Antonie Van Leeuwenhoek.* (2015) 107:73–82. doi: 10.1007/s10482-014-0305-2

21. Kozarski M, Klaus A, Jakovljevic D, Todorovic N, Vunduk J, Petrović P, et al. Antioxidants of edible mushrooms. *Molecules.* (2015) 20:19489–525. doi: 10.3390/molecules201019489

22. Sharpe E, Farragher-Gnadt AP, Igbanugo M, Huber T, Michelotti JC, Milenkowic A, et al. Comparison of antioxidant activity and extraction techniques for commercially and laboratory prepared extracts from six mushroom species. *J Agric Food Res.* (2021) 4:100130. doi: 10.1016/j.jafr.2021.100130

23. Umeno A, Biju V, Yoshida Y. *In vivo* ROS production and use of oxidative stress-derived biomarkers to detect the onset of diseases such as Alzheimer's disease, Parkinson's disease, and diabetes. *Free Radic Res.* (2017) 51:413–27. doi: 10.1080/10715762.2017.1315114

24. Miyamoto M, Kiyota Y, Yamazaki N, Nagaoka A, Matsuo T, Nagawa Y, et al. Age-related changes in learning and memory in the senescence-accelerated mouse (SAM). *Physiol Behav.* (1986) 38:399–406. doi: 10.1016/0031-9384(86)90112-5

25. Song L, Wu X, Wang J, Guan Y, Zhang Y, Gong M, et al. Antidepressant effect of catalpol on corticosterone-induced depressive-like behavior involves the inhibition of HPA axis hyperactivity, central inflammation and oxidative damage probably via dual regulation of NF-κB and Nrf2. *Brain Res Bull.* (2021) 177:81–91. doi: 10.1016/j.brainresbull.2021.09.002

26. Klibaite U, Kislin M, Verpeut JL, Bergeler S, Sun X, Shaevitz JW, et al. Deep phenotyping reveals movement phenotypes in mouse neurodevelopmental models. *Mol Autism.* (2022) 13:12. doi: 10.1186/s13229-022-00492-8

27. Stratilov VA, Vetrovoy OV, Vataeva LA, Tyulkova EI. Age-associated changes in exploratory activity in the open field test in rats surviving prenatal hypoxia. *Neurosci Behav Physiol.* (2022) 52:271–6. doi: 10.1007/s11055-022-01234-2

28. Sun DC, Wang RR, Xu H, ZhuXH, Sun Y, Qiao SQ, et al. A network pharmacology-based study on antidepressant effect of *Salicornia europaea* L. extract with experimental support in chronic unpredictable mild stress model mice. *Chin J Integr Med.* (2022) 28:339–48. doi: 10.1007/s11655-022-2879-2

29. Jafari F, Goudarzvand M, Hajikhani R, Qorbani M, Solati J. Pycnogenol ameliorates motor function and gene expressions of NF-?B and Nrf2 in a 6-hydroxydopamine-induced experimental model of Parkinson's disease in male NMRI mice. *Naunyn-Schmiedeberg's Arch Pharmacol.* (2022) 395:305–13. doi: 10.1007/s00210-022-02201-x

30. Qiao Y, Ye Y, Cai T, Li S, Liu X. Anti-fatigue activity of the polysaccharides isolated from Ribes stenocarpum Maxim. *J Funct Foods.* (2022) 89:104947. doi: 10.1016/j.jff.2022.104947

31. Ráez A, Oliveras I, Río-Álamos C, Díaz-Morán S, Cañete T, Blázquez G, et al. A missing link between depression models: forced swimming test, helplessness and passive coping in genetically heterogeneous NIH-HS rats. *Behav Processes.* (2020) 177:104142. doi: 10.1016/j.beproc.2020.104142

32. Shuster AL, Rocha FE, Wayszceyk S, de Lima DD, Barauna SC, Lopes BG, et al. Protective effect of *Myrcia pubipetala* Miq. against the alterations in oxidative stress parameters in an animal model of depression induced by corticosterone. *Brain Res.* (2022) 1774:147725. doi: 10.1016/j.brainres.2021.147725

33. Xie X, Shen Q, Ma L, Chen Y, Zhao B, Fu Z. Chronic corticosterone-induced depression mediates premature aging in rats. *J Affect Disord.* (2018) 229:254–61. doi: 10.1016/j.jad.2017.12.073

34. Lin L, Herselman MF, Zhou XF, Bobrovskaya L. Effects of corticosterone on BDNF expression and mood behaviours in mice. *Physiol Behav.* (2022) 247:113721. doi: 10.1016/j.physbeh.2022.113721

35. Zhang C, Zhu L, Lu S, Li M, Bai M, Li Y, et al. The antidepressant-like effect of formononetin on chronic corticosterone-treated mice. *Brain Res.* (2022) 1783:147844. doi: 10.1016/j.brainres.2022.147844

36. Santana P, Akana SF, Hanson ES, Strack AM, Sebastian RJ, Dallman MF. Aldosterone and dexamethasone both stimulate energy acquisition whereas only the glucocorticoid alters energy storage. *Endocrinology.* (1995) 136:2214–22. doi: 10.1210/endo.136.5.7720670

37. Li YC, Liu YM, Shen JD, Chen JJ, Pei YY, Fang XY. Resveratrol ameliorates the depressive-like behaviors and metabolic abnormalities induced by chronic corticosterone injection. *Molecules.* (2016) 21:1341. doi: 10.3390/molecules21101341

38. Donner NC, Montoya CD, Lukkes JL, Lowry CA. Chronic non-invasive corticosterone administration abolishes the diurnal pattern of tph2 expression. *Psychoneuroendocrinology.* (2012) 37:645–61. doi: 10.1016/j.psyneuen.2011.08.008

39. Tempel DL, Leibowitz SF. Adrenal steroid receptors: interactions with brain neuropeptide systems in relation to nutrient intake and metabolism. *J Neuroendocrinol.* (1994) 6:479–501. doi: 10.1111/j.1365-2826.1994.tb00611.x

40. Petit-Demouliere B, Chenu F, Bourin M. Forced swimming test in mice: a review of antidepressant activity. *Psychopharmacology.* (2005) 177:245–55. doi: 10.1007/s00213-004-2048-7

41. Yang N, Ren Z, Zheng J, Feng L, Li D, Gao K, et al. 5-(4-hydroxy-3-dimethoxybenzylidene)-rhodanine (RD-1)-improved mitochondrial function prevents anxiety- and depressive-like states induced by chronic corticosterone injections in mice. *Neuropharmacology.* (2016) 105:587–93. doi: 10.1016/j.neuropharm.2016.02.031

42. Weng L, Guo X, Li Y, Yang X, Han Y. Apigenin reverses depression-like behavior induced by chronic corticosterone treatment in mice. *Eur J Pharmacol.* (2016) 774:50–54. doi: 10.1016/j.ejphar.2016.01.015

43. Choi WS, Kim YS, Park BS, Kim JE, Lee SE. Hypolipidaemic effect of *Hericium erinaceum* grown in *Artemisia capillaris* on obese rats. *Mycobiology.* (2013) 41:94–9. doi: 10.5941/MYCO.2013.41.2.94

44. Chovancikova M, Simek V. Effects of high-fat and *Chlorella vulgaris* feeding on changes in lipid metabolism in mice. *Biologia.* (2001) 56:661–6.

45. Gregorio T, Lorenzon F, Niebisch F, Stolte RCK, Rafacho A, dos Santos GJ, et al. Antidepressant-like activity of gestational administration of vitamin D is suppressed by prenatal overexposure to dexamethasone in female Wistar rats. *Physiol Behav.* (2022) 249:113765. doi: 10.1016/j.physbeh.2022.113765

46. Sabir MS, Haussler MR, Sanchita M, Ichiro K, Lucas DA, Haussler CA, et al. Optimal vitamin D spurs serotonin: 1,25-dihydroxyvitamin D represses serotonin reuptake transport (SERT) and degradation (MAO-A) gene expression in cultured rat serotonergic neuronal cell lines. *Genes Nutr.* (2018) 13:19. doi: 10.1186/s12263-018-0605-7

47. Aaldijk E, Vermeiren Y. The role of serotonin within the microbiota-gut-brain axis in the development of Alzheimer's disease: a narrative review. *Ageing Res Rev.* (2022) 75:101556. doi: 10.1016/j.arr.2021.101556

48. Wu TC, Chen HT, Chang HY, Yang CY, Hsiao MC, Cheng ML, et al. Mineralocorticoid receptor antagonist spironolactone prevents chronic corticosterone induced depression-like behavior. *Psychoneuroendocrinology.* (2013) 38:871–83. doi: 10.1016/j.psyneuen.2012.09.011

49. Leitch MM, Ingram CD, Young AH, McQuade R, Gartside SE. Flattening the corticosterone rhythm attenuates 5-HT1A autoreceptor function in the rat: relevance for depression. *Neuropsychopharmacology.* (2003) 28:119–25. doi: 10.1038/sj.npp.1300016

50. Ceyzériat K, Gloria Y, Tsartsalis S, Fossey C, Cailly T, Fabis F, et al. Alterations in dopamine system and in its connectivity with serotonin in a rat model of Alzheimer's disease. *Brain Commun.* (2021) 3:fcab029. doi: 10.1093/braincomms/fcab029

51. Ago Y, Yano K, Araki R, Hiramatsu N, Kita Y, Kawasaki T, et al. Metabotropic glutamate 2/3 receptor antagonists improve behavioral and prefrontal dopaminergic alterations in the chronic corticosterone-induced depression model in mice. *Neuropharmacology.* (2013) 65:29–38. doi: 10.1016/j.neuropharm.2012.09.008

52. Espejo EF, Miñano FJ. Prefrontocortical dopamine depletion induces antidepressant-like effects in rats and alters the profile of desipramine during Porsolt's test. *Neuroscience.* (1999) 88:609–15. doi: 10.1016/S0306-4522(98)00258-9

53. Pani L, Porcella A, Gessa GL. The role of stress in the pathophysiology of the dopaminergic system. *Mol Psychiatry.* (2000) 5:14–21. doi: 10.1038/sj.mp.4000589

54. Schaaf MJM, de Jong J, de Kloet ER, Vreugdenhil E. Downregulation of BDNF mRNA and protein in the rat hippocampus by corticosterone. *Brain Res.* (1998) 813:112–20. doi: 10.1016/S0006-8993(98)01010-5

55. Smith MA, Makino S, Kvetnansky R, Post RM. Stress and glucocorticoids affect the expression of brain-derived neurotrophic factor and neurotrophin-3 mRNAs in the hippocampus. *J Neurosci.* (1995) 15(Pt. 1):1768–77. doi: 10.1523/JNEUROSCI.15-03-01768.1995

56. Lee B, Sur B, Shim I, Lee H, Hahm DH. Angelica gigas ameliorate depression-like symptoms in rats following chronic corticosterone injection. *BMC Complement Altern Med.* (2015) 15:210. doi: 10.1186/s12906-015-0746-9

frontiers | Frontiers in Nutrition

TYPE Original Research
PUBLISHED 06 September 2022
DOI 10.3389/fnut.2022.952588

OPEN ACCESS

EDITED BY
Gengjun Chen,
Kansas State University, United States

REVIEWED BY
Zhaohuan Lou,
Zhejiang Chinese Medical University, China
Mahboobeh Hodaei,
Isfahan University of Technology, Iran

*CORRESPONDENCE
Guiju Sun
gjsun@seu.edu.cn

SPECIALTY SECTION
This article was submitted to Nutrition and Food Science Technology, a section of the journal Frontiers in Nutrition

RECEIVED 25 May 2022
ACCEPTED 29 July 2022
PUBLISHED 06 September 2022

CITATION
Sun J, Wang Z, Lin C, Xia H, Yang L, Wang S and Sun G (2022) The hypolipidemic mechanism of chrysanthemum flavonoids and its main components, luteolin and luteoloside, based on the gene expression profile.
Front. Nutr. 9:952588.
doi: 10.3389/fnut.2022.952588

The hypolipidemic mechanism of chrysanthemum flavonoids and its main components, luteolin and luteoloside, based on the gene expression profile

Jihan Sun[1], Zhaodan Wang[1,2], Chen Lin[1,2], Hui Xia[1], Ligang Yang[1], Shaokang Wang[1] and Guiju Sun[1]*

[1]Key Laboratory of Environmental Medicine and Engineering of Ministry of Education, Department of Nutrition and Food Hygiene, School of Public Health, Southeast University, Nanjing, China, [2]College of Biology and Food Engineering, Technology Research Center of Characteristic Biological Resources in Northeast of Chongqing, Chongqing Three Gorges University, Chongqing, China

In this study, the following four groups of mice with hyperlipidemia were involved: the model control group (MC), the Chrysanthemum flavonoids group (CF), the luteolin group, and the luteoloside group. The whole gene expression profile was detected in the liver tissues of each group. Differential genes significantly enriched in the biological process of gene ontology (GO) items and Kyoto Encyclopedia of Genes and Genomes (KEGG) were selected, and 4 differential genes related to lipid metabolism were selected for further real-time quantitative PCR verification. Compared with the MC, 41 differential genes such as Sqle, Gck, and Idi1 were screened in the CF intervention group; 68 differential genes such as Acsl3, Cyp7a1, and Lpin1 were screened in the luteolin intervention group (CF); and 51 differential genes such as Acaca, Cyp7a1, and Lpin1 were screened in the luteoloside group. The mechanism of CF to improve hyperlipidemia is very complex, mainly involving biological processes such as cholesterol and fatty acid metabolism and glycolysis, luteolin mainly involves the synthesis and transport of cholesterol, and luteoloside mainly involves fatty acid metabolism. The functional pathways of CF may not be completely the same as luteolin and luteoloside, and further study is needed on the mechanism of action of other components.

KEYWORDS

chrysanthemum flavonoids, luteolin, luteoloside, hyperlipidemia, mechanism

Introduction

Hyperlipidemia refers to one or more metabolic diseases with abnormal blood lipids (1). Most patients with hyperlipidemia have no obvious clinical symptoms, but it is a major risk factor for cardiovascular and cerebrovascular diseases (2). The 2015 Survey in China showed that the rate of dyslipidemia among adults was 40.4%. In view of the

limitations of clinical lipid-lowering drugs, several studies are focusing on the lipid-lowering efficacy and application of natural products. Phytochemicals can be further developed as a potential new natural, safe, and efficient lipid-lowering drugs because of their cheap, safe, and efficient characteristics. The known phytochemicals with lipid-lowering effects are phytosterols, phenols, saponins, alkaloids, organic sulfides, and lectins (3).

At present, the research on the lipid-lowering activity of flavonoids is more and more extensive and in-depth. Foodborne flavonoids can improve lipid metabolism and prevent cardiovascular disease (4–6). The lipid-lowering activity of flavonoids may be achieved by affecting a variety of lipid metabolism pathways in the intestine and the liver, such as inhibiting intestinal absorption of lipids and increasing lipid excretion (7, 8), activating adenylate-activated protein kinase (AMPK) so as to promote lipid catabolism or inhibit lipid synthesis (9), and regulating microRNAs (miRNAs) with the function of regulating lipid metabolism (10).

Chrysanthemum has been used mainly in traditional herbal teas and beverages, and various studies have shown that it has biological activities to lower blood lipids and fight obesity. Chrysanthemum extract alleviated the fatty liver in mice by the PPARα-mediated pathway (11). After enzymatic treatment, lipid accumulation and production in obese male mice induced by a high-fat diet were reduced (12). *In vitro*, it inhibited adipogenesis by inhibiting mitosis in the early differentiation of 3T3-L1 cells (13). *In vivo* and *in vitro* experiments have shown that chrysanthemum can activate the AMPK pathway to inhibit fat production (14, 15).

In our previous study, we compared the effects of Chrysanthemum flavonoids (CF), luteolin, and luteoloside, on improving blood lipid and liver steatosis, and found that the preliminary mechanism may be related to antioxidant levels and enzymes related to regulating fatty acid, cholesterol, and triglyceride metabolism in the liver (16). In this study, differential genes are screened out by a gene chip, and the molecular mechanism of their function is further discussed from the biological process and signal pathway.

Materials and methods

Materials

The animal ethics approval was 2015ZDSYLL004.0. We selected liver tissues from the pre-study animals (16) for whole gene expression profiling to explore the mechanism of lipid lowering, with three samples from each group. The Agilent SurePrint G3 Rat GE V2.0 Microarray (8*60K,Design ID:074036) was used in this experiment, provided by Shanghai Ouyi Biomedical Technology Co., Ltd., the chip contains 45,738 probes.

Extraction of total ribonucleic acid from liver tissue

Total ribonucleic acid (RNA) of liver tissue was extracted from 100 mg liver tissue using mirVana^{TM} RNA Isolation AM1561 Kit (Thermo Fisher Scientific, China). The total RNA was preserved at -80°C. NanoDrop ND-2000 (Thermo Fisher Scientific, China) was used to detect the absorbance of the extracted RNA at 260 and 280 nm, and the concentration of the total RNA was calculated. Agilent Bioanalyzer 2100 (Agilent, United States) was used to carry out the integrity test (with 2100RIN $\geq$ 7 and 28/18 s $\geq$ 0.7 as the qualified standard) before the gene chip test can be carried out. Three samples from each group were randomly selected for follow-up chip experiments.

Expression gene profile detection

An amount of 0.2 μg of total RNA was taken, and 2.5 μl of deionized water and 2.8 μl of the reaction mixture (2 μl of Spike Mix and 0.8 μl of T7 Promoter Prime) were added. After mixing using centrifugation, denaturing for 10 min at 65°C and ice bath for 5 min were performed. A volume of 2 μl of 5 × First-Strand Buffer (preheat at 80°C for 3 min) was taken, 1 μl of 0.1 m dithiothreitol (DTT), 0.5 μl of 10 mM deoxyribonucleoside triphosphate (dNTP) mix, and 1.2 μl of AffinityScript Rnase BLock Mix were added, the sample was mixed well, and then the RNA was added. Reaction PCR was performed after mixing and centrifugation (40°C for 2 h, 70°C for 15 min, and ice bath for 5 min). All reagents were obtained from Agilent Low Input Fast Amplifier Labeling kit (Agilent, United States).

Synthesis and purification of fluorescently labeled cDNA

Notably, 0.75 μl of H_2O, 3.2 μl of 5 × transcription buffer, 0.6 μl of 0.1 m DTT, 1 μl of NTP mix, 0.21 μl of Cy3-CT (to avoid light), and 0.24 μl of T7 RNA polymerase blend were added into the sample tube and allowed to react for 2 h at 40°C. Then, 84 μl of enzyme-free water, 350 μl of BufferRLT, and 250 μl of anhydrous ethanol were added and the sample was centrifuged for 30 s (4°C, 2,500 rpm) to discard the filtrate. Next, 500 μl of buffer RPE was added to wash the filtrate two times. After washing, 30 μl of non-enzyme water was added, the sample was centrifuged (4°C, 10,000 *g*) for 1 min, and then the filtrate was collected. All reagents were obtained from Agilent Low Input Fast Amplifier Labeling kit (Agilent, United States).

Determination of cRNA concentration

The concentration of purified RNA was determined by NanoDrop ND-2000 (Thermo Fisher Scientific, China). After

TABLE 1 Primer sequences of qPCR verified genes.

Gene	Upstream primer	Downstream primers	Length (bp)
Gpam	TACGCTGAGAGTGCCACATA	GTTCTAAGACAGACGCTCG	106
Acsl3	CCTCCTCCAGTTTGCTTTG	ATCACTGCTTCCCCAGTA	81
Cyp7a1	CTTAGAACAAGTTTGATGACTC	CGTGAAACCCATCATTCTGT	100
Lpin1	GAGCAGGATGGACTGTTACT	GCCGTTCCGGTGAATTATG	112
Sqle	AAGAATGATTGTTTCCACAAAT	TTTATTGGCATGTCCCAATGA	85
Gck	GCCTCACTCTGCACTATTCA	GTGGTCTCTTGGAGGGACA	97
Gpam	TACGCTGAGAGTGCCACATA	GCTCAGTTCTAAGACAGACG	111
Acaca	CGAGATTTCACTGTGGCTT	GCAATACCATTGTTGGCGATA	95
Angptl4	GAGCCCTGGATACACTCAAT	TGTTGTGAGCTGTGCCTT	85

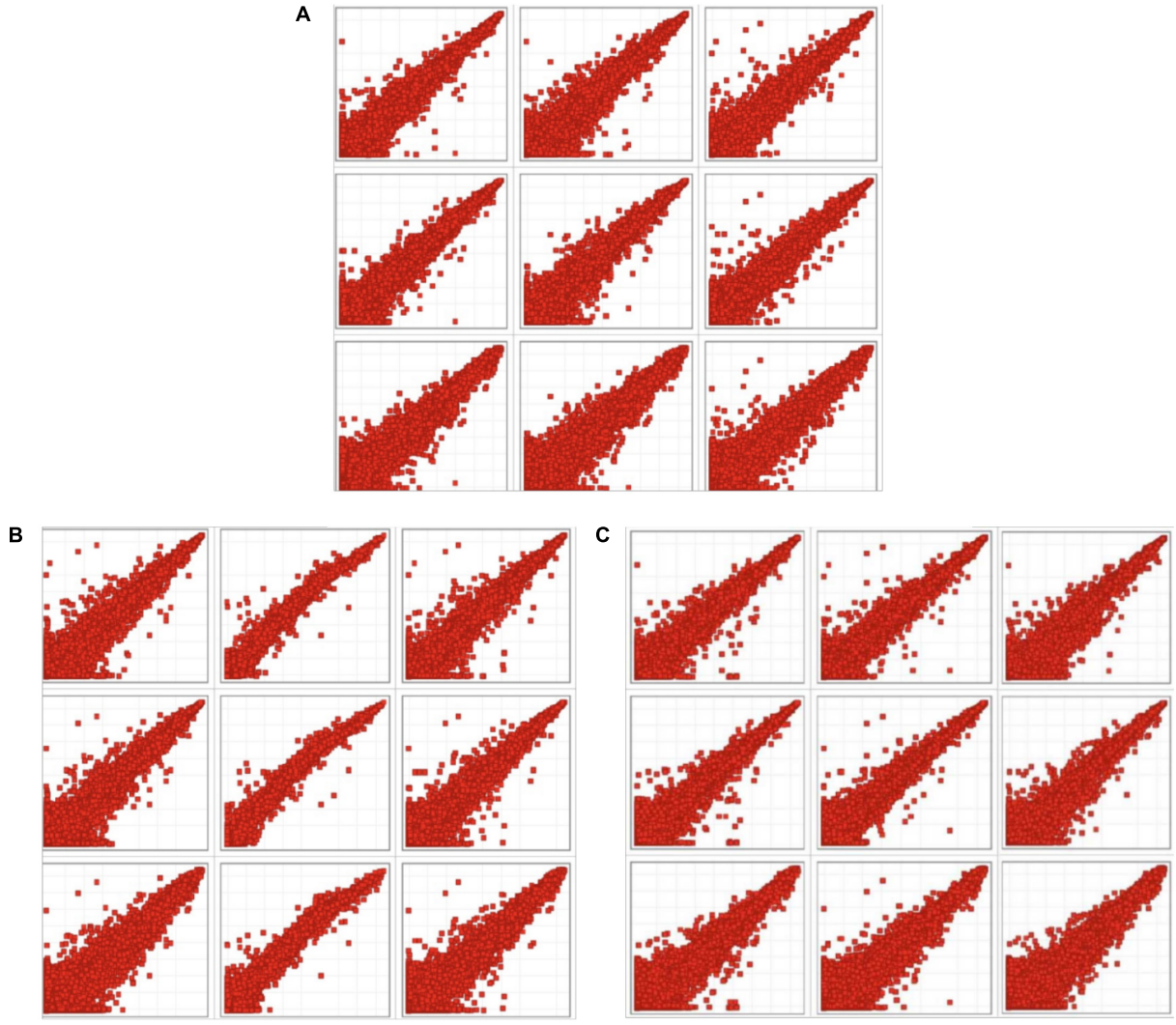

FIGURE 1
Scatter plot of intervention groups compared with the model control group. **(A)** Scatter plot of fluorescence signal values in chrysanthemum flavonoids intervention group (CF) and model control group. **(B)** Scatter plot of fluorescence signal values in luteolin intervention group and model control group. **(C)** Scatter plot of fluorescence signal values in luteoloside intervention group and model control group.

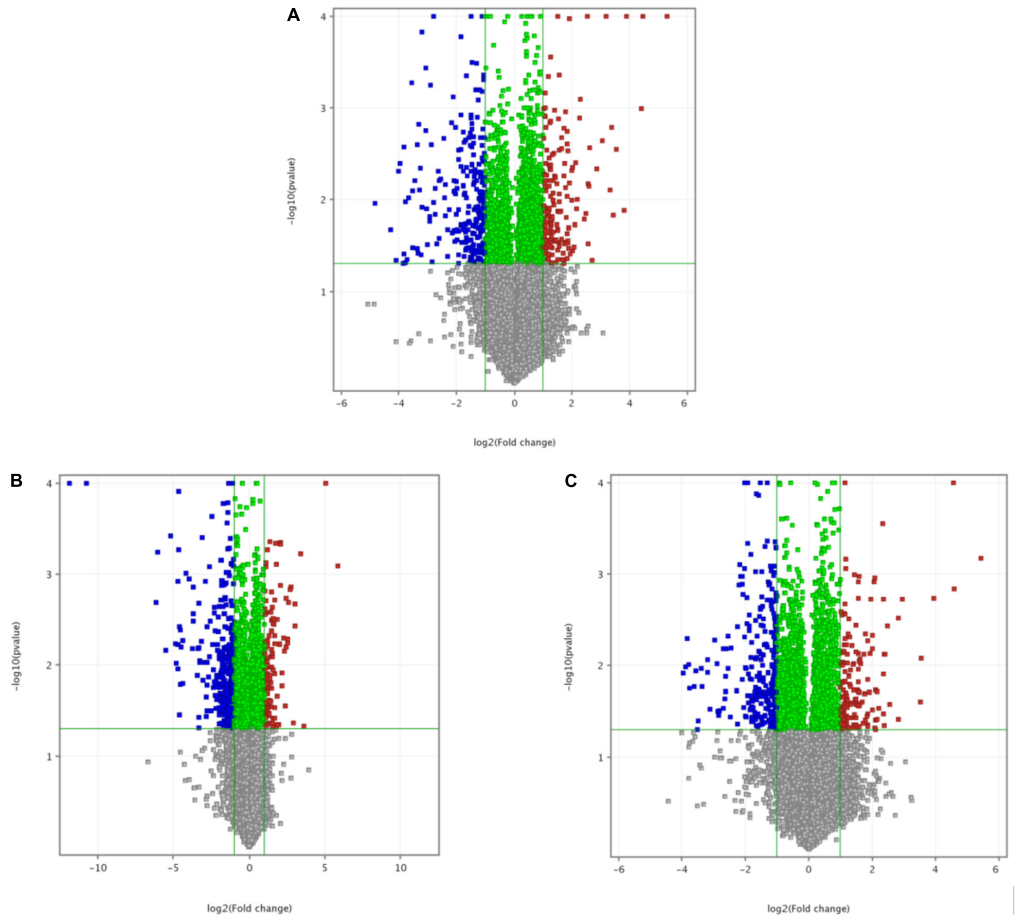

FIGURE 2
A differential gene volcano map of intervention groups compared with the model control group. **(A)** Volcano map of model control group and chrysanthemum flavonoids intervention group. **(B)** Volcano map of model control group and luteolin intervention group. **(C)** Volcano map of model control group and luteoloside intervention group.

adjusting to zero with water, 1 μl of the sample was used to determine and record the concentration of cRNA and the content of fluorescence. The specific calculation formula was given as follows: cRNA content (μg) = cRNA concentration (ng/μl) × 30 μl/1,000; Cy3-incorporation rate (pmol/μg) = Cy3-concentration/cRNA concentration (ng/μl) × 1,000.

Sample fragmentation and chip hybridization of cRNA

The hybrid furnace was preheated at 65°C, and a fragmentation mixture was added and then placed in the ice bath for 1 min. cRNA from Fragmentation Mix and 2 × GE Hyb Hi-RPM Buffer were added. The cover was removed from the hybrid rack, and samples were added to each hole of the chip. The required hybrid chip was taken out, the Agilent marker was covered face down horizontally, the hybridization device was assembled and tightened, and the chip was turned clockwise three times to fully combine the hybrid liquid with the probe. The hybrid frame was placed in a hybrid furnace for 17 h for rolling hybridization under the condition of 65°C and 10 rpm.

Chip washing and scanning

The chip was washed three times in the washing cylinder. The chip was put forward slowly to ensure that there were no residual water droplets, and the chip was carefully placed face up into the scanning rack. Agilent scanner G2505C (Agilent, United States) was used to scan the chip.

Screening of differential genes

The fluorescence signal values of the images were processed by Feature Extraction and standardized by

GeneSpring 13.1 (Agilent, United States). Taking the difference significance *P*-value and difference multiple (fold change, Fc) value as reference, the differential genes were screened according to the absolute value of Fc $\geq$ 2 and $P \leq 0.05$. The functions and pathways of annotated differential genes were analyzed.

Real-time fluorescence quantitative PCR verification

Quantification was performed with a two-step reaction process, namely, reverse transcription (RT) and PCR. Each RT reaction had two steps. The first step was to add 0.5 μg of RNA, 2 μl of 4 × gDNA wiper mix, and nuclease-free H_2O to 8 μl. The sample was allowed to react for 2 min at 42°C. The second step was to add 2 μl of 5 × HiScript II Q RT SuperMix IIa. The sample was allowed to react for 10 min at 25°C, 30 min at 50°C, and 5 min at 85°C. The 10 μl of RT reaction mix was then diluted 10 times in nuclease-free H_2O and held at -20°C. Real-time PCR was performed with a 10-μl PCR reaction mixture that included 1 μl of cDNA, 5 μl of 2 × QuantiFast® SYBR® Green PCR Master Mix (Qiagen, Germany), 0.2 μl of forward primer, 0.2 μl of reverse primer, and 3.6 μl of nuclease-free H_2O. Reactions were incubated in a 384-well optical plate (Roche, Swiss) at 95°C for 5 min, followed by 40 cycles of 95°C for 10 s and 60°C for 30 s. The primer sequences (Table 1) were designed in the laboratory and synthesized by Generay Biotech (Generay, PRC). The expression levels of mRNAs were normalized to ACTB and were calculated using the $2^{-\Delta\Delta Ct}$ method [Livak and Schmittgen, (17)].

TABLE 2 Functional classification of differentially expressed genes.

GO analyze	Biological process	Molecular function	Cellular component
CF group vs. model control group			
Annotated	1,067	304	193
Significant enrichment	121	32	9
luteolin group vs. model control group			
Annotated	1,190	323	196
Significant enrichment	159	52	23
Luteoloside group vs. model control group			
Annotated	1,133	322	212
Significant enrichment	131	37	17

Statistical analysis

The data were analyzed using SPSS16.0 (IBM, United States), which was expressed as mean ± standard deviation, and a *P*-value of < 0.05 was considered statistically significant.

Results

Chip hybrid scan image

In the scatter plot (Figure 1), each point represents a probe, the horizontal axis represents the sample fluorescence signal value of the intervention group, and the longitudinal axis represents the sample fluorescence signal value of the model control group (MC), which on the y = x line indicate that the signal values of the two samples are equal (multiple of difference Fc = 1). The point that fall above the line (y = x) represents upregulation and that fall below the line represents downregulation.

Screening of differential genes between intervention group and model control group

Figure 2 shows a differential gene volcano map of MC and intervention groups, the horizontal axis represents the logarithm of the Fc based on 2, and the vertical axis represents the negative logarithm of the *P*-value with the base of 10. Red represents significantly upregulated genes, and blue represents significantly downregulated genes. Compared with the MC, there were 427 differential genes in the CF intervention group (260 downregulated genes and 167 upregulated genes significantly), 451 differential genes in the luteolin intervention group (335 downregulated genes and 116 upregulated genes significantly), and 420 differential genes in the luteoloside intervention group (260 downregulated genes and 160 upregulated genes significantly).

GO analysis of differential genes between intervention group and model control group

The selected differential genes were functionally annotated by the GO database, which can be divided into three parts. $P \leq 0.05$ indicates that the differential genes are significantly

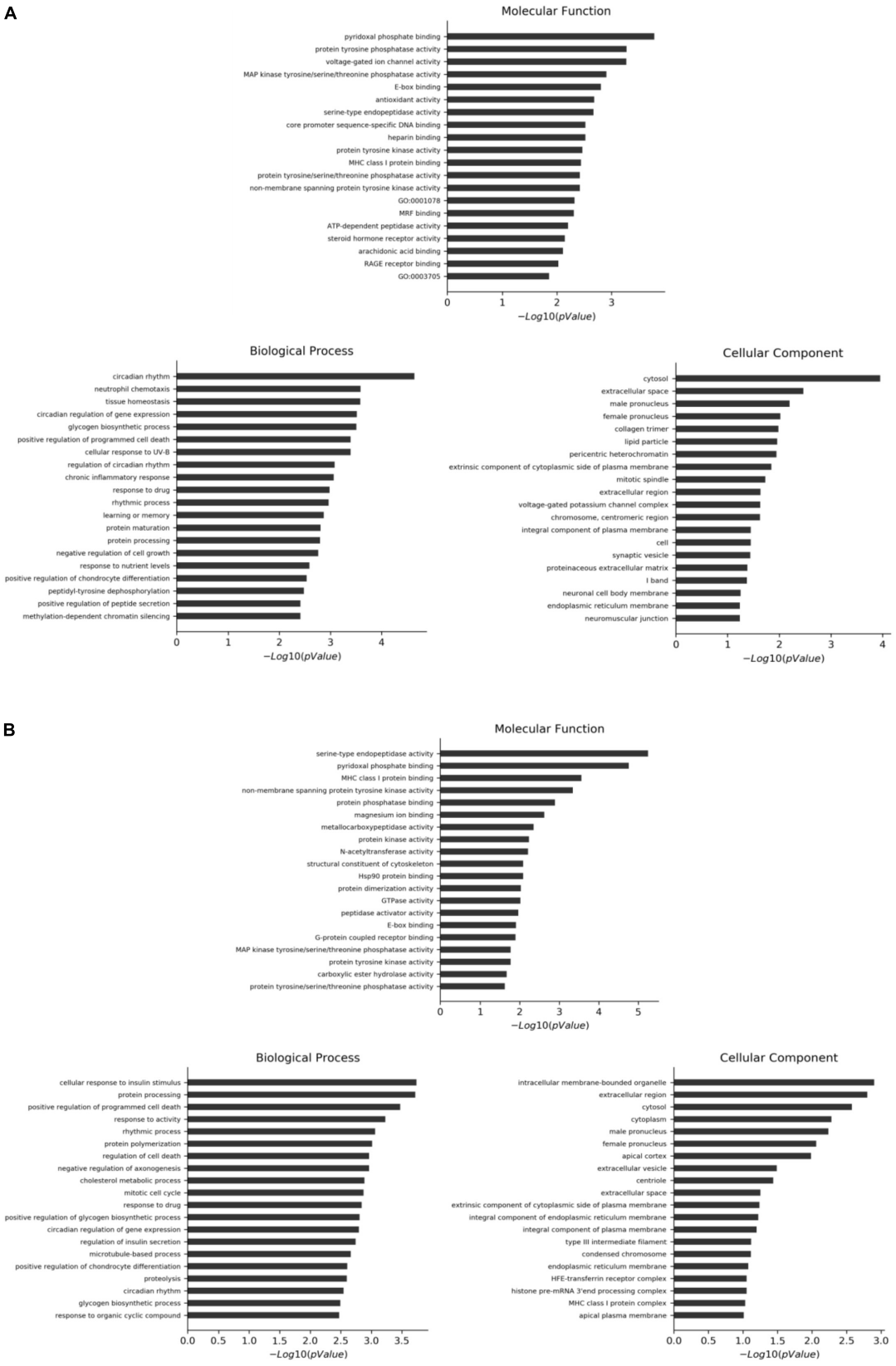

FIGURE 3
(Continued)

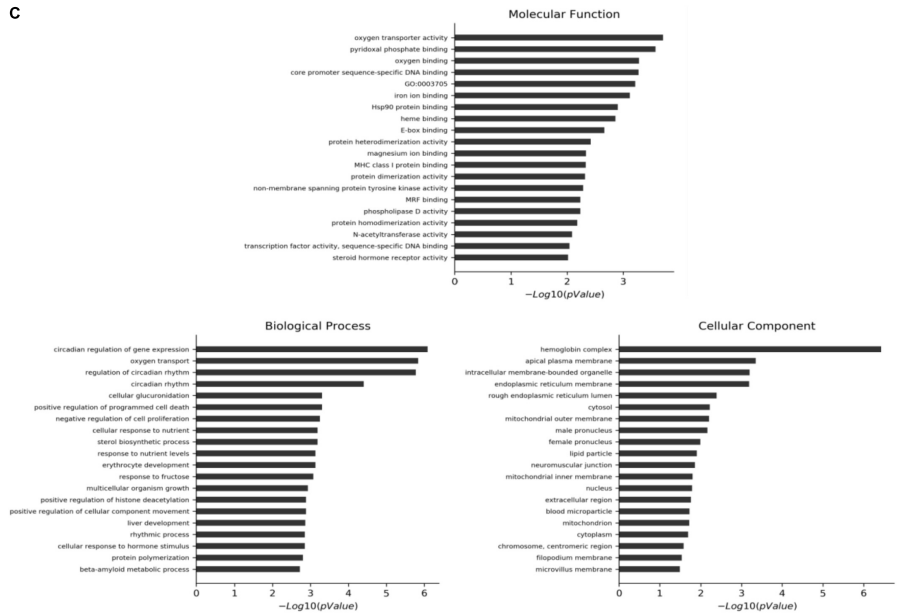

FIGURE 3
First 20 GO items with significant enrichment of differential genes in each plate. **(A)** CF group vs. model control group. **(B)** Luteolin group vs. model control group. **(C)** Luteoloside group vs. model control group.

enriched in the GO entry. Table 2 shows the number of significantly enriched items in the three GO plates in different intervention groups compared with the MC. The first 20 GO items with significant enrichment of differential genes in each plate are shown in Figure 3.

KEGG analysis of differential genes between intervention group and model control group

The differential genes were analyzed by KEGG. A *P*-value of < 0.05 indicates a significant enrichment of differential genes. The results showed that there were 186 annotable items in the CF group compared with the MC, among which 13 were significantly enriched. There were 187 annotable items in the luteolin group compared with the MC, among which 26 were significantly enriched. There were 180 annotable items in the luteoloside group compared with the MC, among which 18 were significantly enriched. The top 20 significantly enriched pathways in each group are shown in Figure 4.

Comprehensive analysis and verification gene selection

Differential genes significantly enriched in the biological process of GO items and KEGG were selected (the number of genes in each intervention group is shown in Figure 5), and 4 differential genes related to lipid metabolism were selected for further real-time quantitative PCR verification. KEGG items with a significant enrichment and GO biological process items involved in chip results are summarized in Table 3.

RT-PCR verification results of the intervention group and the model control group

The comparison between the RT-PCR and gene chip results is shown in Figure 6. The expression trend is completely the same, suggesting that the data of the gene chip are reliable. As shown in Table 4, compared with the MC, in the luteolin intervention group, the expression of Acsl3 and Cyp7a1 was significantly upregulated, and the expression of **Lpin1** was significantly downregulated, while there was no statistical difference in Gpam expression downregulation; in the CF intervention group, the expression of Sqle, Gck, and Idi1 was statistically and significantly downregulated, while there was no statistical difference in Gpam expression downregulation; in the luteoloside intervention group, the expression of Acaca and Cyp7a1 was significantly upregulated and the expression of **Lpin1** was significantly downregulated, while there was no statistical difference in Angptl4 expression downregulation.

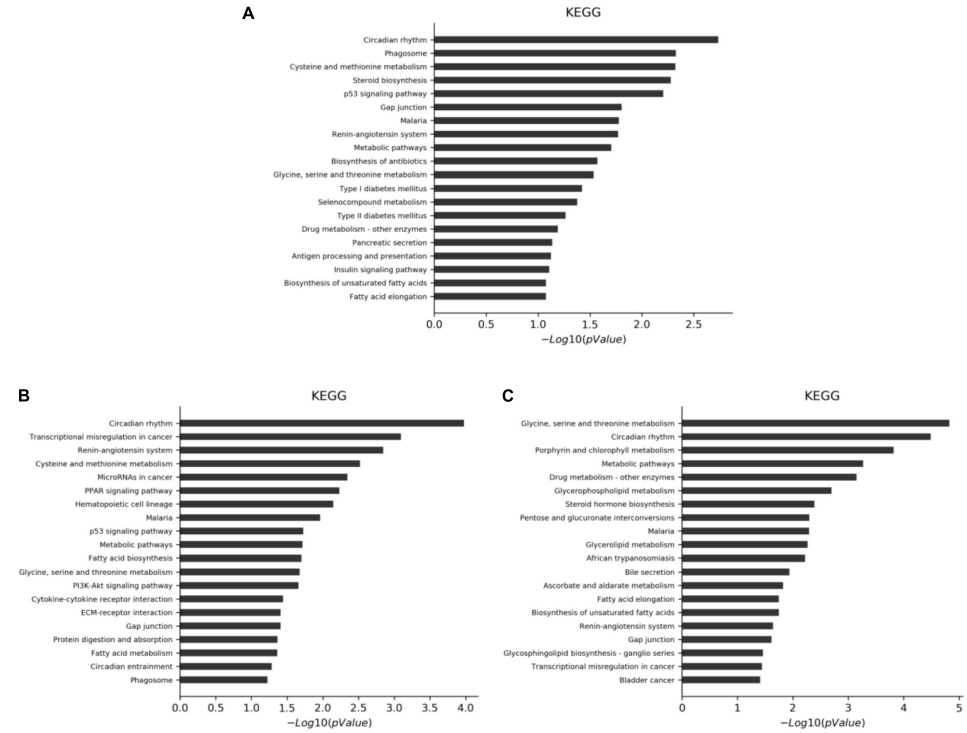

FIGURE 4
KEGG analysis of differential gene significant enrichment pathways (top 20). **(A)** CF group vs. model control group. **(B)** Luteolin group vs. model control group. **(C)** Luteoloside group vs. model control group.

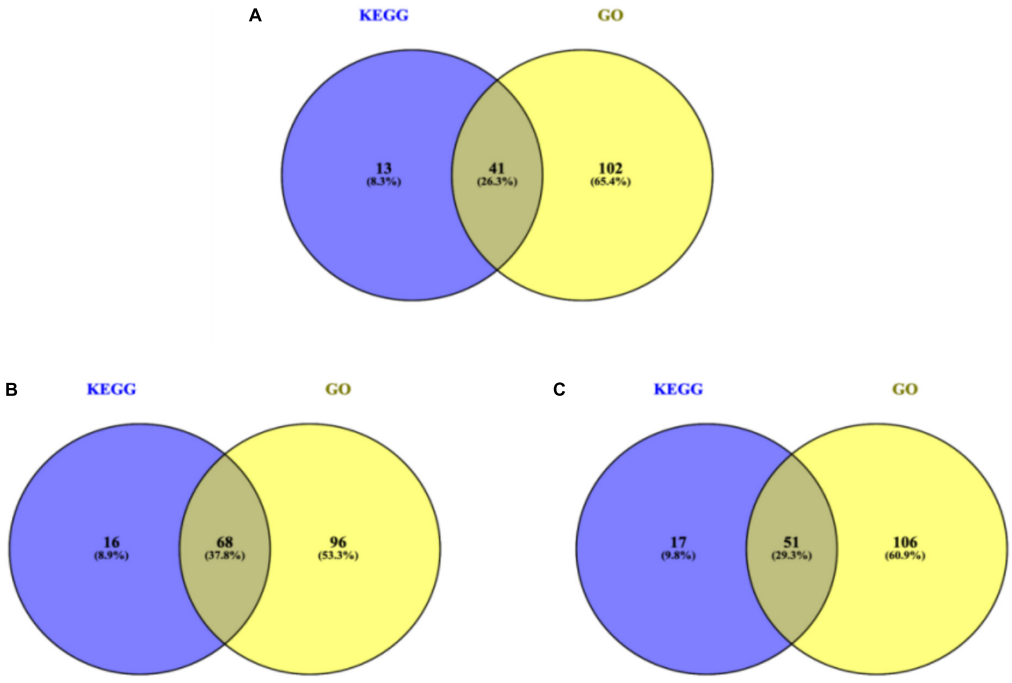

FIGURE 5
The number of genes in each intervention group. **(A)** CF group vs. model control group. **(B)** Luteolin group vs. model control group. **(C)** Luteoloside group vs. model control group.

TABLE 3 Differential genes both significantly enriched in KEGG and GO biological process items.

Group	GeneSymbol	KEGG	GO
CF group vs. model control group	Sqle	rno00100 steroid biosynthesis rno01100 metabolic pathways rno01130 biosynthesis of antibiotics	GO:0008203 metabolic pathways GO:0010033 response to organic substance
	Gck	rno01100 metabolic pathways rno01130 biosynthesis of antibiotics	GO:0032869 cellular response to insulin stimulus GO:0045725 positive regulation of glycogen biosynthetic process GO:0050796 regulation of insulin secretion GO:0005978 glycogen biosynthetic process GO:0055088 lipid homeostasis GO:0009749 response to glucose GO:0032024 positive regulation of insulin secretion
	Gpam	rno01100 metabolic pathways	GO:0032869 cellular response to insulin stimulus GO:0014823 response to activity GO:0055089 fatty acid homeostasis GO:0009749 response to glucose GO:0006641 triglyceride metabolic process GO:0010867 positive regulation of triglyceride biosynthetic process GO:0006637 acyl-CoA metabolic process GO:0006631 fatty acid metabolic process
	Idi1	rno01100 metabolic pathways rno01130 biosynthesis of antibiotics	GO:0006695 cholesterol biosynthetic process
Luteolin group vs. model control group	Acsl3	rno01100 metabolic pathways	GO:0014070 response to organic cyclic compound GO:0001676 long-chain fatty acid metabolic process
	Cyp7a1	rno01100 metabolic pathways rno00140 steroid hormone biosynthesis rno04976 bile secretion	GO:0071333 cellular response to glucose stimulus GO:0071397 cellular response to cholesterol GO:0055114 oxidation-reduction process
	Gpam	rno01100 metabolic pathways rno00564 glycerophospholipid metabolism rno00561 glycerolipid metabolism	GO:0031667 response to nutrient levels GO:0009750 response to fructose GO:0032869 cellular response to insulin stimulus GO:0006641 triglyceride metabolic process GO:0006637 acyl-CoA metabolic process GO:0014823 response to activity GO:0006631 fatty acid metabolic process GO:0055089 fatty acid homeostasis GO:0019432 triglyceride biosynthetic process GO:0046686 response to cadmium ion GO:0042104 positive regulation of activated T cell proliferation
	Lpin1	rno01100 metabolic pathways rno00564 glycerophospholipid metabolism rno00561 glycerolipid metabolism	GO:0031065 positive regulation of histone deacetylation GO:0032869 cellular response to insulin stimulus GO:0019432 triglyceride biosynthetic process GO:0006470 protein dephosphorylation GO:0000122 negative regulation of transcription from RNA polymerase II promoter
Luteoloside group vs. model control group	Acaca	rno01100 metabolic pathways rno00061 fatty acid biosynthesis rno01212 fatty acid metabolism	GO:0001894 tissue homeostasis GO:0042493 response to drug GO:0014070 response to organic cyclic compound GO:0055088 lipid homeostasis GO:0006629 lipid metabolic process
	Angptl4	rno03320 PPAR signaling pathway	GO:0019216 regulation of lipid metabolic process GO:0051260 protein homooligomerization GO:0043066 negative regulation of apoptotic process GO:0001666 response to hypoxia
	Cyp7a1	rno03320 PPAR signaling pathway rno01100 metabolic pathways	GO:0071397 cellular response to cholesterol
	Lpin1	rno01100 metabolic pathways	GO:0000122 negative regulation of transcription from RNA polymerase II promoter GO:0031065 positive regulation of histone deacetylation GO:0045598 regulation of fat cell differentiation GO:0006629 lipid metabolic process GO:0031100 organ regeneration

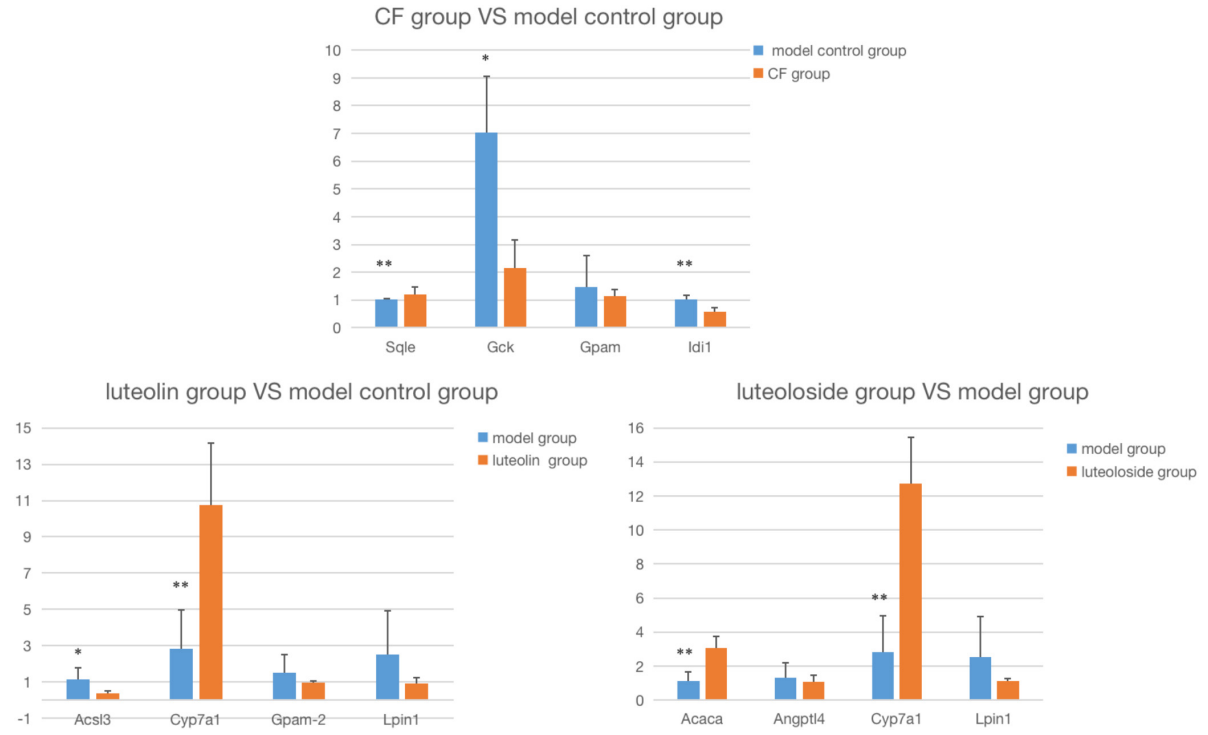

FIGURE 6
The comparison between the RT-PCR and gene chip results. Compared with the model control group: *$P < 0.05$; **$P < 0.01$.

TABLE 4 Gene expression verified by real-time PCR.

CF group vs. model control group	**Sqle**	**Gck**	**Gpam**	**Idi1**
Model control group	1.21 ± 0.27	7.04 ± 5.71	1.48 ± 0.97	1.01 ± 0.15
CF group	1.00 ± 0.04*	2.16 ± 0.87**	1.15 ± 0.21	0.57 ± 0.13*
Expression	0.83	0.31	0.78	0.56
PCR differential multiple	−1.21	−3.26	−1.28	−1.79
Gene chip differential multiple	−2.63	−5.22	−2.50	−2.91
Luteolin group vs. model control group	**Acsl3**	**Cyp7a1**	**Gpam**	**Lpin1**
Model control group	1.16 ± 0.64	2.84 ± 2.12	1.51 ± 0.99	2.52 ± 2.40
Luteolin group	0.36 ± 0.18**	10.74 ± 3.42**	0.97 ± 0.11	0.91 ± 0.32*
Expression	0.31	3.78	0.65	0.36
PCR differential multiple	−3.22	3.78	−1.55	−2.77
Gene chip differential multiple	−2.97	2.75	−3.46	−4.31
Luteoloside group vs. model control group	**Acaca**	**Angptl4**	**Cyp7a1**	**Lpin1**
Model control group	1.13 ± 0.52	1.32 ± 0.85	2.84 ± 2.12	2.52 ± 2.40
Luteoloside group	3.08 ± 0.67**	1.06 ± 0.42	12.73 ± 2.73**	1.10 ± 0.17**
Expression	2.72	0.80	4.48	0.44
PCR differential multiple	2.72	−1.24	4.48	−2.29
Gene chip differential multiple	2.06	−2.09	2.09	−3.50

Expression was $2^{-\Delta\Delta Ct}$ ratio of intervention group and model control group: Expression < 1, gene expression downregulated; Expression > 1, gene expression upregulated; Compared with model control group: *P < 0.05; **P < 0.01.

Discussion

The results suggest that compared with the normal control group, mice with hyperlipidemia have different biological processes that may involve monounsaturated fatty acid biosynthesis processes, cellular response to insulin stimulation, steroid decomposition processes, and response to fatty acids. The involved signaling pathways include the PPAR signaling pathway, biosynthesis of unsaturated fatty acids, and fatty acid metabolism.

In this experiment, differential genes in the intervention group and MC were screened and 4 genes related to lipid metabolism were selected for RT-PCR verification. Compared with the MC, 41 genes were both significantly enriched in GO and KEGG analyses in the CF intervention group. The results of gene verification are consistent with the trend of gene chip. Sqle, Gck, and Idi1 were significantly downregulated. Squalene cyclooxygenase (Sqle) is a rate-limiting and first oxygenation enzyme of cholesterol biosynthesis and is considered a proto-oncogene. Sqle induced the development of non-alcoholic fatty liver disease (NAFLD) by inducing cholesterol biosynthesis and Sqle/CA3-axis-mediated adipogenesis in Sqle overexpression transgenic mice (18). Meanwhile, SQLE silencing can limit the occurrence of liver tumors induced by NAFLD (19). The results of our previous animal experiments also support the idea that the intervention group of CF improved the hepatic steatosis of hyperlipidemic rats (16). Gluckinase (GCK) is a key enzyme regulating insulin release and the first step in catalyzing glycolysis in the liver (20). Its genetic polymorphisms are associated with susceptibility to gestational diabetes. Studies have shown that the GCK RS1799884 mutation is associated with a higher incidence of gestational diabetes mellitus (GDM) in the Chinese population (21). Its expression is also associated with hyperlipidemia, and the molecular mechanism of the regulation of hyperlipidemia by instant dark tea (IDT) has been demonstrated in rats fed with a high-fat diet and is related to the significant influence on the expression of glycoly-related genes such as GCK (22). Isoprene diphosphate isomerase (IDI) is involved in the biosynthesis of isoprene-like cholesterol, and there are two subtypes in humans, namely, IDI1 and IDI2 (23). IDI1 plays a regulatory role in atrial lipotoxic myopathy associated with atrial enlargement (24). Studies have shown that polygala tenuifolia extract (PTE) has anti-obesity activity, and its mechanism is related to the expression of genes involved in lipid and cholesterol metabolisms in the liver, such as IDI1 (25). Glycerol-3-phosphate acyltransferase mitochondrial (GPAM), also known as GPAT1, is a member of the GPAT gene family. Its protease is the first step in the biosynthesis of triglycerides and phospholipids (26). The expression of GPAM can induce the formation of at least 50% triglycerides in the liver and adipose tissue (27). GPAM can further affect the expression of mRNA of key enzymes in the second step of triglyceride synthesis to regulate lipid metabolism (28). In contrast, the expression of GPAM is consistent with the results of the gene chip, but there was no statistically significant. CF may be related to the expression of genes related to glycolysis and cholesterol metabolism in the liver, and the effect on triglyceride metabolism may not be the main way to improve hyperlipidemia.

Compared with the MC, 68 genes were both significantly enriched in GO and KEGG analyses in the luteolin intervention group. The results of gene verification are consistent with the trend of gene chip. Acsl3 and Lpin1 were significantly downregulated, and Cyp7a1 was significantly upregulated. Cholesterol 7 α-hydroxylase (CYP7A) catalyzes the synthesis of bile acid in the liver and maintains cholesterol balance in the body. Studies have shown that the upregulation of its expression can promote the conversion of cholesterol into bile acid (29, 30). This is consistent with the results of our previous study that the enzyme activity in the liver of rats in the luteolin group was significantly increased, indicating that luteolin can promote the expression of CYP7A1 and thus activate its enzyme activity to promote the conversion of bile acids and exert a hypolipidemic effect. Long-chain fatty acid (ACSL) acyl-coA synthase (FAs) plays an important role in lipid biosynthesis, in which ACSL3 activity is thought to be related to adipocyte differentiation, and ACSL3 overexpression can promote the increase of lipid drop triglyceride content (31). TNF-α increased ACSL3 expression to induce lipid droplet formation in human endothelial cells (32). The red raspberry extract (RRE) can significantly reduce the level of blood lipid in mice with hyperlipidemia, and Acsl3 is one of the regulatory genes, accelerating the conversion of triglyceride to fatty acid (33). The results of our preliminary animal experimental study showed that the metabolic enzyme activity of triglycerides was significantly higher and fatty acid synthase activity was significantly higher in the luteolin group than the intervention effect of luteoloside, which may be related to the regulatory genes for the conversion of triglycerides into fatty acids. GPAM expression was downregulated in the luteolin intervention group, but the difference was not statistically significant. The hypolipidemic effect of luteolin may be related to the expression of genes related to cholesterol biosynthesis and transformation in the liver. In addition, affecting the differentiation of adipocytes may also be a way to improve hyperlipidemia.

Compared with the MC, 51 genes were both significantly enriched in GO and KEGG analyses in the luteoloside intervention group. Lpin1 was significantly downregulated, and Acaca and Cyp7a1 were significantly upregulated. The expression of Angptl4 was downregulated but the difference was not statistically significant. Acetyl CoA carboxylase (ACACA) is a key gene for *de novo* synthesis of fatty acids, downregulation of its expression can deeply inhibit the biosynthesis of fatty acids, and its expression is significantly increased in high-

carbohydrate and high-fat diet rats (34). It plays an important role in anti-obesity and improves the pathogenesis of NAFLD by micronutrients or traditional Chinese medicine (35, 36). Studies on the anti-obesity mechanism of naringin and its glycoside showed that naringin can inhibit lipid accumulation and TG content in 3T3-L1 cells by regulating some genes related to lipid metabolism, including Acaca (37). The results of our previous animal experimental study showed significant differences in triglyceride metabolism-related enzyme activities in the luteoloside intervention group, which may be related to its regulation of gene expression including Acaca to reduce triglyceride accumulation in hepatocytes. In addition, CYP7A1 overexpression in the luteoloside intervention group was consistent with a significant increase in its enzymatic activity in the liver tissue. Angiopoietin-like protein 4 (Angptl4) is a key gene in the regulation of lipid and glucose metabolism (38), and hyperlipidemia levels were significantly reduced in Angptl4 knockout mice (39). The results of this study showed that compared with the control group, the expression of Angptl4 in liver tissues was downregulated after luteoloside intervention, but the difference was not statistically significant, indicating that Angptl4 may not be a key gene in the mechanism of luteolin lowering blood lipid.

The results of our previous *in vivo* studies showed that both CF and its main components, luteolin and luteoloside, have significant hypolipidemic and hepatic steatosis effects, but CFs seem to have stronger antioxidant and lipid metabolism-related enzyme activities, which may have better effects in the long run (16). In fact, the results of this study indicate that the hypolipidemic mechanism of CF is more complex, involving various biological processes such as cholesterol, fatty acid metabolism, and glycolysis. The hypolipidemic effect of luteolin and luteoloside is mainly through the synthesis and transport of cholesterol and the fatty acid metabolic pathway, suggesting that there may be other major components involved in the hypolipidemic mechanism of CF.

Conclusion

The mechanism of CF to improve hyperlipidemia is very complex, mainly involving biological processes such as cholesterol and fatty acid metabolism and glycolysis, including 41 differential genes such as Sqle, Gck, and Idi1. Luteolin mainly involves the synthesis and transport of cholesterol, which may include 68 differential genes such as Acsl3, Cyp7a1, and Lpin1. Luteoloside mainly involves fatty acid metabolism, which may include 51 differential genes such as Acaca, Cyp7a1, and Lpin1. The functional pathways of CF and its main components, luteolin and luteoloside, may not be completely the same, and further study is needed on the mechanism of action of other components.

Data availability statement

The original contributions presented in this study are included in the article/supplementary materials, further inquiries can be directed to the corresponding author.

Ethics statement

This animal study was reviewed and approved by the Animal Ethics Committee, Southeast University.

Author contributions

JS and ZW: experiment and thesis writing. CL: data analysis. HX and SW: scheme design. LY: quality control. GS: overall coordination. All authors contributed to the article and approved the submitted version.

Funding

This study was supported by the Jiangsu Graduate Research and Practice Innovation Program (SJCX21 0024) and General Program of Chongqing Natural Science Foundation (cstc2020jcyj-msxmX0090).

Conflict of interest

The authors declare that the research was conducted in the absence of any commercial or financial relationships that could be construed as a potential conflict of interest.

Publisher's note

References

1. Xiao C, Dash S, Morgantini C, Hegele RA, Lewis GF. Pharmacological targeting of the atherogenic dyslipidemia complex: the next frontier in CVD prevention beyond lowering LDL Cholesterol. *Diabetes.* (2016) 65:1767–78. doi: 10.2337/db16-0046

2. Karr S. Epidemiology and management of hyperlipidemia. *Am J Manag Care.* (2017) 23(9 Suppl.):S139–48.

3. Liu H, Jiao J, Zhu M, Wu X, Chen W. Cross-cultural adaptation and validation of the FRAIL-NH scale for Chinese nursing home residents: a methodological and cross-sectional study. *Int J Nurs Stud.* (2022) 128:104097.

4. Li D, Zhang Y, Liu Y, Sun R, Xia M. Purified anthocyanin supplementation reduces dyslipidemia, enhances antioxidant capacity, and prevents insulin resistance in diabetic patients. *J Nutr.* (2015) 145:742–8. doi: 10.3945/jn.114.205674

5. Hooper L, Kay C, Abdelhamid A, Kroon PA, Cohn JS, Rimm EB, et al. Effects of chocolate, cocoa, and flavan-3-ols on cardiovascular health: a systematic review and meta-analysis of randomized trials. *Am J Clin Nutr.* (2012) 95:740–51. doi: 10.3945/ajcn.111.023457

6. Curtis PJ, Sampson M, Potter J, Dhatariya K, Kroon PA, Cassidy A. Chronic ingestion of flavan-3-ols and isoflavones improves insulin sensitivity and lipoprotein status and attenuates estimated 10-year CVD risk in medicated postmenopausal women with type 2 diabetes: a 1-year, double-blind, randomized, controlled trial. *Diabetes Care.* (2012) 35:226–32. doi: 10.2337/dc11-1443

7. Liang Y, Chen J, Zuo Y, Ma KY, Jiang Y, Huang Y, et al. Blueberry anthocyanins at doses of 0.5 and 1 % lowered plasma cholesterol by increasing fecal excretion of acidic and neutral sterols in hamsters fed a cholesterol-enriched diet. *Eur J Nutr.* (2013) 52:869–75. doi: 10.1007/s00394-012-0393-6

8. Friedrich M, Petzke KJ, Raederstorff D, Wolfram S, Klaus S. Acute effects of epigallocatechin gallate from green tea on oxidation and tissue incorporation of dietary lipids in mice fed a high-fat diet. *Int J Obes.* (2012) 36:735–43. doi: 10.1038/ijo.2011.136

9. Nambiar DK, Deep G, Singh RP, Agarwal C, Agarwal R. Silibinin inhibits aberrant lipid metabolism, proliferation and emergence of androgen-independence in prostate cancer cells via primarily targeting the sterol response element binding protein 1. *Oncotarget.* (2014) 5:10017–33. doi: 10.18632/oncotarget.2488

10. Baselga-Escudero L, Pascual-Serrano A, Ribas-Latre A, Casanova E, Salvadó MJ, Arola L, et al. Long-term supplementation with a low dose of proanthocyanidins normalized liver miR-33a and miR-122 levels in high-fat diet-induced obese rats. *Nutr Res.* (2015) 35:337–45. doi: 10.1016/j.nutres.2015.02.008

11. Cui Y, Wang X, Xue J, Liu J, Xie M. *Chrysanthemum morifolium* extract attenuates high-fat milk-induced fatty liver through peroxisome proliferator-activated receptor α-mediated mechanism in mice. *Nutr Res.* (2014) 34:268–75. doi: 10.1016/j.nutres.2013.12.010

12. Lee JH, Moon JM, Kim YH, Lee B, Choi SY, Song BJ, et al. Effect of enzymatic treatment of *Chrysanthemum indicum Linné* extracts on lipid accumulation and adipogenesis in high-fat-diet-induced obese male mice. *Nutrients.* (2019) 11:269. doi: 10.3390/nu11020269

13. Kim WJ, Yu HS, Bae WY, Ko KY, Chang KH, Lee NK, et al. *Chrysanthemum indicum* suppresses adipogenesis by inhibiting mitotic clonal expansion in 3T3-L1 preadipocytes. *J Food Biochem.* (2021) 45:e13896. doi: 10.1111/jfbc.13896

14. Lee MS, Kim Y. *Chrysanthemum morifolium* flower extract inhibits adipogenesis of 3T3-L1 cells via AMPK/SIRT1 pathway activation. *Nutrients.* (2020) 12:2726. doi: 10.3390/nu12092726

15. Nepali S, Cha JY, Ki HH, Lee HY, Kim YH, Kim DK, et al. *Chrysanthemum indicum* inhibits adipogenesis and activates the AMPK pathway in high-fat-diet-induced obese mice. *Am J Chin Med.* (2018) 46:119–36. doi: 10.1142/S0192415X18500076

16. Sun J, Wang Z, Chen L, Sun G. Hypolipidemic effects and preliminary mechanism of *Chrysanthemum* flavonoids, its main components luteolin and luteoloside in hyperlipidemia rats. *Antioxidants.* (2021) 10:1309. doi: 10.3390/antiox10081309

17. Livak KJ, Schmittgen TD. Analysis of relative gene expression data using real-time quantitative PCR and the 2(-Delta Delta C(T)) Method. *Methods* (2001) 25:402–8. doi: 10.1006/meth.2001.1262

18. Liu D, Wong CC, Zhou Y, Cai Z, Huang ZP, Hu P, et al. Squalene epoxidase induces nonalcoholic steatohepatitis via binding to carbonic anhydrase III and is a therapeutic target. *Gastroenterology.* (2021) 16:2467–82.e3. doi: 10.1053/j.gastro.2021.02.051

19. Sun H, Li L, Li W, Yang F, Zhang Z, Liu Z, et al. P53 transcriptionally regulates SQLE to repress cholesterol synthesis and tumor growth. *EMBO Rep.* (2021) 22:e52537. doi: 10.15252/embr.202152537

20. Mir MM, Mir R, Alghamdi MAA, Wani JI, Elfaki I, Sabah ZU, et al. Potential impact of GCK, MIR-196A-2 and MIR-423 gene abnormalities on the development and progression of type 2 diabetes mellitus in Asir and Tabuk regions of Saudi Arabia. *Mol Med Rep.* (2022) 25:162. doi: 10.3892/mmr.2022.12675

21. She L, Li W, Guo Y, Zhou J, Liu J, Zheng W, et al. Association of glucokinase gene and glucokinase regulatory protein gene polymorphisms with gestational diabetes mellitus: a case-control study. *Gene.* (2022) 824:146378. doi: 10.1016/j.gene.2022.146378

22. Qin S, He Z, Wu Y, Zeng C, Zheng Z, Zhang H, et al. Instant dark tea alleviates hyperlipidaemia in high-fat diet-fed rat: from molecular evidence to redox balance and beyond. *Front Nutr.* (2022) 9:819980. doi: 10.3389/fnut.2022.819980.

23. Nakamura K, Mori F, Tanji K, Miki Y, Yamada M, Kakita A, et al. Isopentenyl diphosphate isomerase, a cholesterol synthesizing enzyme, is localized in Lewy bodies. *Neuropathology.* (2015) 35:432–40. doi: 10.1111/neup.12204

24. Fang CY, Chen MC, Chang TH, Wu CC, Chang JP, Huang HD, et al. Idi1 and Hmgcs2 Are Affected by Stretch in HL-1 atrial myocytes. *Int J Mol Sci.* (2018) 19:4094. doi: 10.3390/ijms19124094

25. Wang CC, Yen JH, Cheng YC, Lin CY, Hsieh CT, Gau RJ, et al. *Polygala tenuifolia* extract inhibits lipid accumulation in 3T3-L1 adipocytes and high-fat diet-induced obese mouse model and affects hepatic transcriptome and gut microbiota profiles. *Food Nutr Res.* (2017) 61:1379861. doi: 10.1080/16546628.2017.1379861

26. Brockmöller SF, Bucher E, Müller BM, Budczies J, Hilvo M, Griffin JL, et al. Integration of metabolomics and expression of glycerol-3-phosphate acyltransferase (GPAM) in breast cancer-link to patient survival, hormone receptor status, and metabolic profiling. *J Proteome Res.* (2012) 11:850–60. doi: 10.1021/pr200685r

27. Chen YQ, Kuo MS, Li S, Bui HH, Peake DA, Sanders PE, et al. AGPAT6 is a novel microsomal glycerol-3-phosphate acyltransferase. *J Biol Chem.* (2008) 283:10048–57. doi: 10.1074/jbc.M708151200

28. Yu H, Zhao Z, Yu X, Li J, Lu C, Yang R. Bovine lipid metabolism related gene GPAM: molecular characterization, function identification, and association analysis with fat deposition traits. *Gene.* (2017) 609:9–18. doi: 10.1016/j.gene.2017.01.031

29. Pizzini A, Lunger L, Demetz E, Hilbe R, Weiss G, Ebenbichler C, et al. The role of Omega-3 fatty acids in reverse cholesterol transport: a review. *Nutrients.* (2017) 9:1099. doi: 10.3390/nu9101099

30. Olkkonen VM. Role of microRNA-185 in the FoxO1-CYP7A1 mediated regulation of bile acid and cholesterol metabolism: a novel target for drug discovery? *Atherosclerosis.* (2022) 348:53–5. doi: 10.1016/j.atherosclerosis.2022.03.023

31. Lv Y, Cao Y, Gao Y, Yun J, Yu Y, Zhang L, et al. Effect of ACSL3 expression levels on preadipocyte differentiation in Chinese red steppe cattle. *DNA Cell Biol.* (2019) 38:945–54. doi: 10.1089/dna.2018.4443

32. Jung HS, Shimizu-Albergine M, Shen X, Kramer F, Shao D, Vivekanandan-Giri A, et al. TNF-α induces acyl-CoA synthetase 3 to promote lipid droplet formation in human endothelial cells. *J Lipid Res.* (2020) 61:33–44. doi: 10.1194/jlr.RA119000256

33. Tu L, Sun H, Tang M, Zhao J, Zhang Z, Sun X, et al. Red raspberry extract (*Rubus idaeus L shrub*) intake ameliorates hyperlipidemia in HFD-induced mice through PPAR signaling pathway. *Food Chem Toxicol.* (2019) 133:110796. doi: 10.1016/j.fct.2019.110796

34. Dankel SN, Bjørndal B, Lindquist C, Grinna ML, Rossmann CR, Bohov P, et al. Hepatic energy metabolism underlying differential lipidomic responses to high-carbohydrate and high-fat diets in male wistar rats. *J Nutr.* (2021) 151:2610–21. doi: 10.1093/jn/nxab178

35. Khatiwada S, Lecomte V, Fenech MF, Morris MJ, Maloney CA. Effects of micronutrient supplementation on glucose and hepatic lipid metabolism in a rat model of diet induced obesity. *Cells.* (2021) 10:1751. doi: 10.3390/cells10071751

36. Li X, Ge J, Li Y, Cai Y, Zheng Q, Huang N, et al. Integrative lipidomic and transcriptomic study unravels the therapeutic effects of saikosaponins A and D on non-alcoholic fatty liver disease. *Acta Pharm Sin B.* (2021) 11:3527–41. doi: 10.1016/j.apsb.2021.03.018

37. Dayarathne LA, Ranaweera SS, Natraj P, Rajan P, Lee YJ, Han CH. Restoration of the adipogenic gene expression by naringenin and naringin in 3T3-L1 adipocytes. *J Vet Sci.* (2021) 22:e55. doi: 10.4142/jvs.2021.22.e55

38. Xiao S, Nai-Dong W, Jin-Xiang Y, Long T, Xiu-Rong L, Hong G, et al. ANGPTL4 regulate glutamine metabolism and fatty acid oxidation in nonsmall cell lung cancer cells. *J Cell Mol Med.* (2022) 26:1876–85. doi: 10.1111/jcmm.16879

39. Li Y, Gong W, Liu J, Chen X, Suo Y, Yang H, et al. Angiopoietin-like protein 4 promotes hyperlipidemia-induced renal injury by down-regulating the expression of ACTN4. *Biochem Biophys Res Commun.* (2022) 595:69–75. doi: 10.1016/j.bbrc.2022.01.061

frontiers | Frontiers in Nutrition

TYPE Review
PUBLISHED 16 September 2022
DOI 10.3389/fnut.2022.927361

OPEN ACCESS

EDITED BY
Gengjun Chen,
Kansas State University, United States

REVIEWED BY
Syed Nasir Abbas Bukhari,
Al Jouf University, Saudi Arabia
Sutapa Biswas Majee,
NSHM Knowledge Campus, India

*CORRESPONDENCE
Sun Chao
sunchao2775@163.com
Muhammad Saeed
msaeed@cuvas.edu.pk

SPECIALTY SECTION
This article was submitted to Nutrition and Food Science Technology, a section of the journal Frontiers in Nutrition

RECEIVED 24 April 2022
ACCEPTED 25 August 2022
PUBLISHED 16 September 2022

CITATION
Saeed M, Khan MS, Amir K, Bi JB, Asif M, Madni A, Kamboh AA, Manzoor Z, Younas U and Chao S (2022) *Lagenaria siceraria* fruit: A review of its phytochemistry, pharmacology, and promising traditional uses. *Front. Nutr.* 9:927361. doi: 10.3389/fnut.2022.927361

Lagenaria siceraria fruit: A review of its phytochemistry, pharmacology, and promising traditional uses

Muhammad Saeed[1,2]*, Muhammad Sajjad Khan[2], Kinza Amir[3], Jannat Bi Bi[4], Muhammad Asif[5], Asadullah Madni[6], Asghar Ali Kamboh[7], Zahid Manzoor[2], Umair Younas[2] and Sun Chao[1]*

[1]College of Animal Science and Technology, Northwest A&F University, Yangling, China, [2]The Cholistan University of Veterinary and Animal Sciences, Bahawalpur, Pakistan, [3]Mayo Hospital Lahore, Lahore, Pakistan, [4]Department of Physical Education, Beijing Sports University, Beijing, China, [5]District Head Quarter (DHQ) Hospital, Vehari, Pakistan, [6]Department of Pharmaceutics, Faculty of Pharmacy, The Islamia University of Bahawalpur, Bahawalpur, Pakistan, [7]Department of Veterinary Microbiology, Sindh Agriculture University, Tando Jam, Pakistan

Since ancient times, the Cucurbitaceae family is used as a therapeutic option in human medicine. This family has around 130 genera and 800 species. Researchers have studied the various plants of this family including *Lagenaria siceraria* due to their medicinal potential. Various properties are beneficial for human health, that have been attributed to *L. siceraria* like antioxidant, hypolipidemic, diuretic, laxative, hepatoprotective, analgesic, antihypertensive, cardioprotective, central nervous system stimulant, anthelmintic, free radical scavenging, immunosuppressive, and adaptogenic. The fruit of this plant is commonly used as a vegetable that has a low-calorie value. The species possess a diverse set of biological compounds like flavonoids, sterols, saponins, and terpenoids. Vitamins, choline, flavonoids, minerals, proteins, terpenoids, and other phytochemicals are also found in the edible parts of this plant. Besides 17 different amino acids, many minerals are reported to be present in the seeds of *L. siceraria*. According to the USDA nutritional database per 100 g of *L. siceraria* contains 14 Kcal energy, 3.39 g carbohydrates, 0.62 g protein, 0.2 g fat, and 0.5 g fiber. *L. siceraria* performs a wide range of pharmacological and physiological actions. The literature reviewed from various sources including PubMed, Science Direct, Google scholar, etc. shows the remarkable potential to treat various human and animal illnesses due to its' potent bioactive chemicals. The key objective of this thorough analysis is to present a summary of the data about the beneficial and harmful effects of *L. siceraria* intake on human health, as well as in veterinary fields.

KEYWORDS

***Lagenaria siceraria* fruit, phytochemistry, pharmacology, nutritional potential, pharmacological effect**

Introduction

There is an emergent concern about herbal medicines across the world, which is complemented by more laboratory research into the pharmacological characteristics of bioactive substances and their capacity to cure various disorders. Through ethnopharmacology and traditional medicine, a slew of new medications has made their way onto the worldwide market (1). For centuries, herbal treatments have been used to cure and manage a variety of ailments. Herbal medications are a viable alternative to current synthetic treatments owing to their few adverse effects and are regarded as safe and useful in the treatment of human ailments. The Cucurbitaceae family includes the *Lagenaria siceraria* (Mol.) Standley fruit (Bottle gourd), utilized in a separate system of traditional medicine to cure numerous ailments (2). A significant number of medicinally beneficial plants belong to the Cucurbitaceae family. This family has around 130 genera and 800 species. Cucurbitacin, a secondary metabolite found in the seeds and fruit sections of several cucurbits, has been described to have purgative, emetic, and antihelmintic actions. This category of chemicals had been considered for its anti-inflammatory, hepatoprotective, cytotoxic, and cardiovascular properties (3). Bottle gourd (*L. siceraria*), family Cucurbitaceae is a medicinal plant whose diverse sections had been identified for their therapeutic potential. The plant's fruiting body is well-liked for its taste and extraordinary nutritional content, which includes practically all of the needed ingredients for good health. The plant might provide physiologically active polysaccharides (4). Being a domestic plant, it is for both food and medicine. Cardioprotective, antidepressant, anti-hyperglycemic, antimicrobial, cytotoxic, anti-inflammatory, antihyperlipidemic, anti-urolithiasis, antianxiety, analgesic, anticancer, diuretic, anthelmintic, antihepatotoxic, anthelmintic, antistress, immunomodulatory, antiulcer, hepatoprotective, and antioxidant activities have been studied in various parts of this plant. To emphasize the medicinal value of this plant, its phytochemical elements, and traditional, pharmacological, and medicinal applications are studied in this review. This would be beneficial in resurrecting its relevance and highlighting its many potential qualities to motivate academics to do more study on *L. siceraria* (2). The key objective of this thorough analysis is to present a summary of the data about the beneficial and harmful effects of *L. siceraria* intake on human health, as well as in veterinary fields like the poultry and livestock sector.

Botanical description

The *L. siceraria* (Molina) is a member of the Cucurbitaceae family and is also called Bottle gourd. It is a climbing perennial plant that is extensively grown as a vegetable crop in tropical nations such as Thailand, Egypt, India, Japan, and the rest of the world (1, 5). The fruits of Bottle gourd have a variety of shapes: they can be huge and rounded, small and bottle-shaped, or slim and serpentine, and they can grow to be over a meter long. Rounder varieties are typically called calabash gourds.

The fruit diversity and phytogeographical distribution of *L. siceraria* in Nigeria were studied and 24 different shapes of fruits were explored as shown in Figure 1 (6).

The bottle gourd is said to have originated in Africa and spread worldwide in pre-Columbian times, maybe *via* floating on the oceans. It moved from India to Indonesia, New Zealand, and China where it has diversified into several local kinds. It is a robust annual vine with huge leaves and a lush look that may be grown as a running or climbing vine (7) (Table 1).

Figure 2 shows different parts of *Lagenaria siceraria* (A), fresh fruit (B), ripened fruit (C).

Vernacular names

Vernacular names of *L. siceraria* in different languages across the world are given in Table 2.

Traditional uses

The fruit is extensively used as a medicinal vegetable in Asia and Africa for a variety of ailments. Alternative medicine is made from several components of this plant, including the fruit, seed, leaf, and root (9). In Ayurveda and other folk remedies, the plant's fruits had been noted to have possible therapeutic benefits. Traditional uses of the fruit include cardioprotective, antidote, aphrodisiac, cardiotonic, diuretic, and general tonic properties (5). The fruit juice had been a cure for jaundice and heal other liver ailments as it possessed good anti-oxidants (10). Various properties that are beneficial for human health have been attributed to this plant like antioxidant, hypolipidemic, diuretic, laxative, hepatoprotective, analgesic, antihypertensive, cardioprotective, central nervous system stimulant, anthelmintic, free radical scavenging, immunosuppressive, and adaptogenic (11). Anti-HIV, antipyretic, anthelmintic, anxiolytic, carminative, anti-diabetic, antibacterial, antioxidant, laxative, anti-tuberculosis, anti-diarrhoeal, and purgative are only a few of the therapeutic qualities of the Cucurbitaceae family. It's also used as a contraceptive, diuretic, and cardiotonic agent. Anti-inflammatory, antitussive, cytotoxic, and expectorant activities are also present (3). The diuretic efficacy of methanol and vacuum dried juice extract of the fruits had been studied. Albino rats had a larger urine volume when compared with the control group. Both of the extracts displayed a dose-dependent rise in electrolyte excretion (12). The plant species aids in improved digestion eliminates urinary difficulties, and aids in weight loss and blood pressure-lowering (13). For the treatment of illnesses

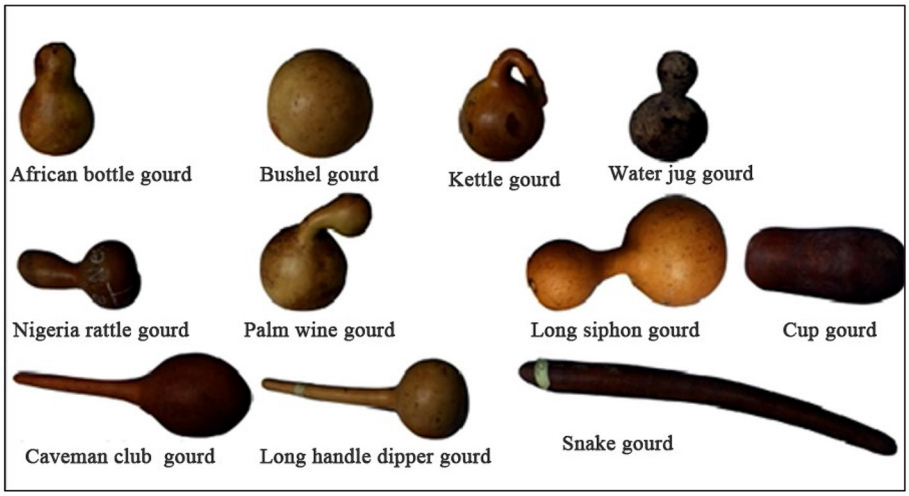

FIGURE 1
Different shapes of *Lagenaria siceraria* found across the world (6).

TABLE 1 Botanical description of various parts of *Lagenaria siceraria* (7).

Botanical description	
Vine	Branched and climbs along the stem
Leaves	15 inches wide, circular, smooth margins, broad lobes, velvety texture
Foliage	Covered with soft hairs and on crushing gives a foul musky odor
Flowers	Borne singly on the axils of the leaves, white and attractive, 4 inches in diameter, spreading petals
Seeds	Brownish, rectangular in shape, have grooved notches near the end

and disorders in humans, *L. siceraria* has been utilized in several systems of traditional medicine. This vegetable has high water content and a low-calorie count. The seeds are also utilized for headaches and constipation since they have a cooling impact on the body (8).

After drying the fruit is used as resonance boxes for the kora and balafon (xylophone). Drinking water, milk, liquor, local wine, oatmeal, food grains, animal fat, honey, tobacco, ghee, salt, perfume, medicinal herbs, and crop seeds are all stored and transported in dried bottle gourd fruits. Beehives, beer-making containers, or storing clothing and cutlery are all created from dried fruit shells. Many musical instruments and beautiful decorations are made from dried bottle gourds (14). The climber's medicinal abilities have been used to cure a variety of disorders, including jaundice, ulcers, colitis, diabetes, insanity, skin problems hypertension, piles, and congestive cardiac failure (CCF). The fruit pulp has cooling, diuretic, antibilious, and pectoral qualities, and is used as an emetic and purgative. This pulp boiled in oil is used in treating rheumatism and sleeplessness (15).

Traditional uses of various parts of *L. siceraria* are given in Table 3 (16).

Phytochemistry

Ascorbic acid, triterpenes, minerals, choline, amino acids, vitamin-B complex, triterpenoid cucurbitacins B, D, H, G, 22-deoxy cucurbitacin, β-glycosidedase-elasterase, flavonoids, sterols, and carbohydrates are all found in the edible part of the fruit (5).

Cucurbitacins B, H, G, and D, as well as the bitter principle of the Cucurbitaceae, are said to be present in the fruit along with Flavone-C glycosides (a ribosome-inactivating protein), two sterols, i.e., fucosterol and campesterol, terpene byonolic acid (an allergic compound) and Lagenin (1).

Figures 3, 4 shows the phytochemicals of *Lagenaria siceraria.*

The extract has carbohydrates, saponins, proteins, flavonoids, and glycosides as shown by the phytochemical test (17). This vegetable has high water content and a low-calorie value. Vitamins, choline, flavonoids, minerals, proteins, terpenoids, and other phytochemicals are found in the edible section. *L. siceraria* contains a variety of bioactive chemicals, including flavones, sterols, cucurbitacins, C-glycosides, triterpenoids, and -glycosides (2).

Table 4 shows phytochemicals and their functions present in different parts of *Lagenaria siceraria.*

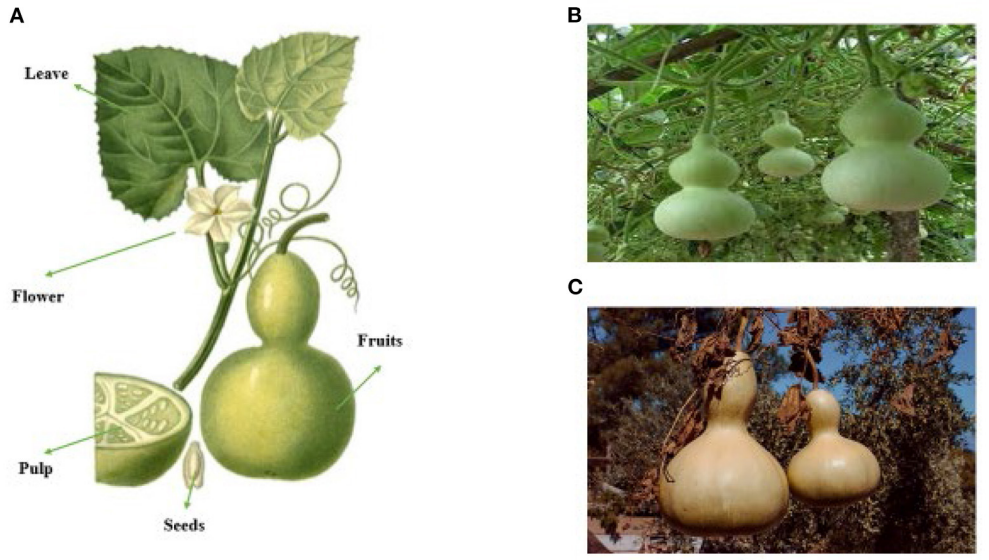

FIGURE 2
Various parts of *Lagenaria siceraria* **(A)**, fresh fruit of LS **(B)**, ripened fruit of LS **(C)**.

TABLE 2 Vernacular names of *Lagenaria siceraria* (8).

Language	Names
Sanskrit	Katutumbi, Tumbi Ishavaaku, Tiktaalaabu, Alobu, Alaabu
Bengal	Loki, Laus, tumbi
English	Bottle gourd
Malayalam	Churan, Tumburini, Choraikka, Tumburu, Piccura, Chorakka, cura
Kannada	Isugumbala, Tumbi
Hindi	Lauki, Ghiya
Gujarati	Dudi, Tumbadi
Telugu	Sorakaya, Anapakaya
Urdu	Ghiya, Lauki, Kadu
Tamil	Sorakkai, Surai, Sorakkai
Marathi	Phopla
Punjabi	Tumbi, Dani

TABLE 3 Traditional uses of different parts of *Lagenaria siceraria* (16).

Plant part	Traditional use
Fruit pulp	Emetic, purgative, cooling, antibilious, sedative, diuretic
Flowers	Poison antidote
Stem bark and rind	Diuretic
Leaf juice	Hair growth, tooth decay, heart diseases, urinary disorders, jaundice, digestive disorders, constipation, diabetes, and cooling effect.
Seed	Vermifuge
Leaves	Purgative

Nutritional profile

Seeds contained 45.0–47.8 g/100 g crude fat, 8.1–7.3 g/100 g carbohydrates, 37.2–35.0 g/100 g crude protein, and 4.0 g/100 g moisture (25).

Nutrients

The nutrient composition of *L. siceraria* (fruit and seeds) is given in Table 5.

The USDA (United States Department of Agriculture) nutritional database exhibited that each 100 g of *L. siceraria* has 14 Kcal energy, 3.39 g carbohydrates, 0.62 g protein, 0.2 g fat, and 0.5 g fiber (27).

Minerals

Calcium, Potassium, Magnesium, Lead, Iron, Sodium, Zinc, and chromium were found in the seeds of *L. siceraria* fruit (26). Furthermore, Phosphorus, Copper, Manganese, and Cobalt were also reported in this plant (28).

Table 6 shows numerous minerals present in *L. siceraria*.

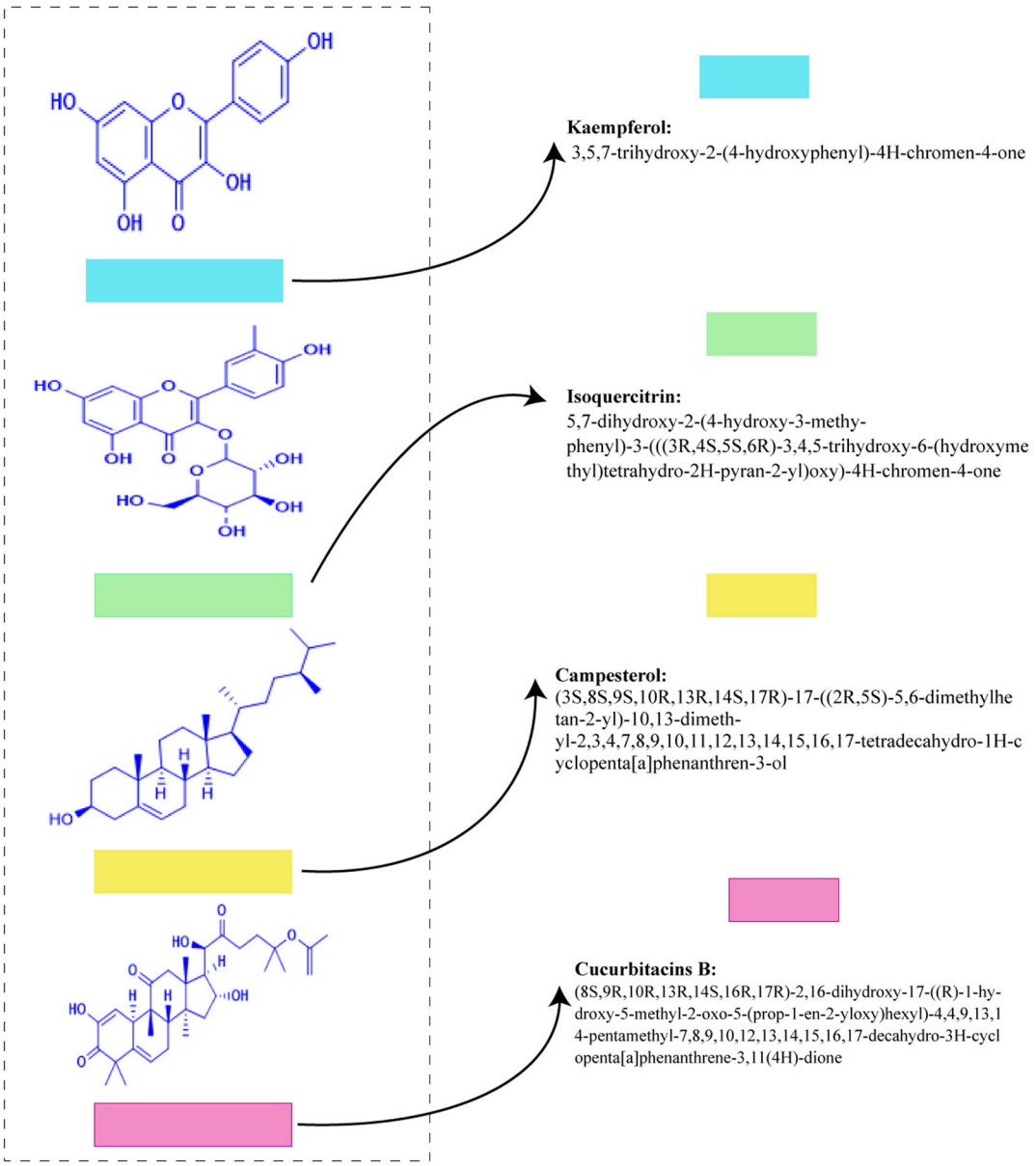

FIGURE 3
Some of the structures of different bioactive chemicals present in *Lagenaria siceraria*.

Amino acids

Seventeen amino acids lysine, methionine, threonine, proline, cysteine, glutamic acid, phenylalanine, arginine, tyrosine, histidine, valine, serine with glutamic acid, alanine, leucine, isoleucine, aspartic acid, glycine, leucine, and aspartic acid were found in seeds of *L. siceraria* (28).

Health effects of *L. siceraria*

Anti-inflammatory properties

In rats and mice, *L. siceraria*'s ethanolic extract (fruit and leaves) was tested for anti-inflammatory and analgesic properties. Carrageenan-induced edema, tail immersion pain, and acetic acid-induced writhing models were used to investigate the extract's activity. On the writhing test, the

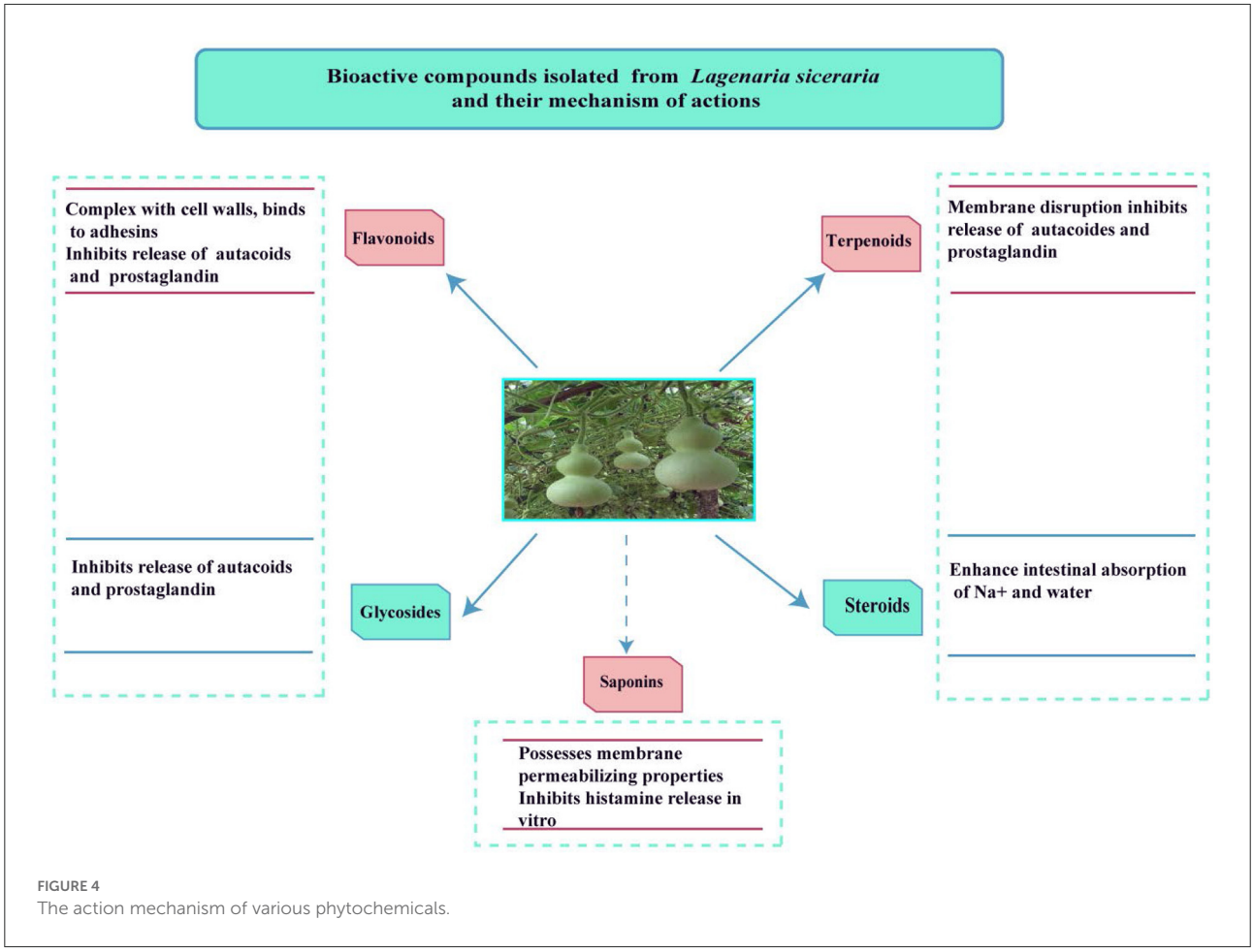

FIGURE 4
The action mechanism of various phytochemicals.

TABLE 4 Phytochemicals and their functions present in different parts of *Lagenaria siceraria*.

Phytochemical	Present in	Function	References
Cucurbitacins H, D, B, G fucosterol and campesterol (Two sterols)	Fruit	Antimicrobial	(1, 18, 19)
Flavone-C glycosides		Antidiarrhoeal	
Flavonoids, carbohydrates, proteins, glycosides, and saponins	Plant extract		(17)
Glucose and fructose and traces of sucrose	Whole fruit		(20)
Ascorbic acid, minerals, vitamin-B complex, β-carotene, choline, amino acids, 22-deoxy cucurbitacin, triterpenoid, cucurbitacins B, D, G, H, flavonoids, β-glycosidedase-elasterase, sterols, and carbohydrates, C-glycosides, triterpenes, and β-glycosides.	Fruit	Antimicrobial Antidiarrheal	(2, 5, 19)
Flavonoids, triterpenoid, sterols, β sitosterol, campesterol, isoquercitrin, and kaempferol	Methanolic extract	Antimicrobial Antidiarrhoeal Antihyperlipidemic	(19, 21, 22)
Triterpenoids (22- Deoxocucurbitacin D and 22- Deoxoisocucurbitacin D)	Fruit	Antimicrobial Antidiarrheal	(23, 24)

extract exhibited strong anti-inflammatory and analgesic potential. The extract comprises flavonoids, carbohydrates, proteins, glycosides, and saponins, according to a phytochemical analysis (17).

Anti-oxidant properties

The aqueous extract of *L. siceraria* has a strong scavenging action, and the high phenolic content of calabash fruit may help

to alleviate the oxidative stress associated with diabetes (29). Antioxidant activity is recognized for phenolics and flavonoids, which have a remarkable capacity to scavenge free radicals created in human bodies. As a result, determining the number of phenolics and flavonoids in a plant sample can help determine its antioxidant capacity. The antioxidant capacity of the pedicles of *L. siceraria* fruits was investigated *in vitro*. The ethyl acetate fraction even at low concentrations showed the most effective DPPH radical scavenger (30). *In vitro*, a methanol extract of the aerial section of *L. siceraria* was reported to scavenge DPPH, hydrogen peroxide, superoxide radical, and nitric oxide as well as prevent lipid peroxidation in a concentration-dependent way. The antioxidant action of MELS (methanol extract of *L. siceraria* aerial parts) was attributed to its high phenolic and flavonoid content (31). *In vitro* experiments such as the reducing power assay, radical scavenging assay, superoxide scavenging assay, lipid peroxidation inhibition assay, and the ethyl acetate extract of bottle gourd were shown to exhibit high antioxidant activity. The quantity of phenolic compounds found in bottle gourd extracts is proportional to their radical scavenging action (32). In an isolated rat heart model, the extract's antioxidant capacity was measured in terms of glutathione peroxidase (GPx), catalase (CAT), superoxide dismutase (SOD), vitamin C (Vit C), glutathione reductase (GR), reduced glutathione (GSH), vitamin E (Vit E), and glutathione S-transferase (GST). The activities of enzyme antioxidants such as CAT, GSH, GR, and SOD were significantly reduced in isoproterenol-induced rats. It may be determined that *L. siceraria*'s ethanolic extract has antioxidant effects (33). Extraction of seeds with ethanol resulted in a significant number of phytochemicals and antioxidant activity. All of these phytochemicals are powerful reducing agents, metal chelators, and radical scavengers, and they may be to blame for the seeds' high antioxidant activity. The methanolic extract of seeds showed good DPPH and radical scavenging capabilities in antioxidant tests (34). In human patients with dyslipidemia, the effects of *L. siceraria* fruit extract were investigated. The antioxidant potential of *L. siceraria* fruit extract was demonstrated in dyslipidemic patients by increases in Superoxide dismutase and Glutathione levels (35).

TABLE 5 Proximate analysis of fruit and seeds of *Lagenaria siceraria* (11, 26).

Nutrients	Fruit (in 100 g of edible portion)	Seeds (%)
Proximate composition		
Carbohydrate	2.5 g	45.93
Protein	0.2 g	8.93
Fat	1.0 g	38.92
Fiber	0.6 g	
Energy	12 calorie	
Mineral	0.5 g	3.5
Moisture	96.1 g	2.72

TABLE 6 Mineral composition of *Lagenaria siceraria* (USDA nutritional database).

Mineral	Value in mg
Sodium	2
Potassium	150
Magnesium	11
Copper	0.034
Phosphorus	13
Calcium	26
Manganese	0.089
Iron	0.20
Selenium	0.2
Zinc	0.70

Anti-cancer properties

The study aimed to see the effect of methanol extract of *L. siceraria* aerial parts on anti-cancer properties. In mice, Ehrlich's Ascites Carcinoma model. The effect of medication response was assessed using the research of tumor growth response, which included an increase in life duration, a study of hematological parameters, biochemical estimates, and a liver tissue antioxidant assay. The cytotoxicity and antioxidant capabilities of *L. siceraria*, as well as the flavonoid content of the methanol extract of *L. siceraria* aerial parts, demonstrated that *L. siceraria* has strong anticancer activity (36). The antitumor effectiveness of *L. siceraria* fruit was investigated using human cancer cell lines (MCF-7 and HT-29). With varied potency and selectivity, the bitter component of *L. siceraria* displayed substantial anticancer action against both cancer cell lines. Cucurbitacin I and other bioactive compounds in *L. siceraria* fruit bitter extracts had dose-dependent inhibitory and cytotoxic effects on tested cell lines, which can be ascribed to the presence of cucurbitacin I and other bioactive compounds in *L. siceraria* fruit bitter extracts (34). A methanolic extract of *L. siceraria* Standley Fruit was tested for anti-mutagenic properties. The anti-mutagenicity of plant extracts ranged from low to high. The Ames test was employed in this investigation to assess the antimutagenic activity of direct (Sodium azide) acting mutagens in *Salmonella typhimurium* strains TA98 and TA100. The study found that the TA98 and TA100 strains have considerable antimutagenicity against mutagen. The antimutagenicity of the extract discovered in this investigation suggests that *L. siceraria* Standley Fruit has chemopreventive pharmacological relevance, which is attributable to its anti-oxidant potential (37). In Swiss albino mice, the chemopreventive efficacy of bottle gourd juice (BGJ) against cutaneous papilloma genesis

was investigated. The chemopreventive properties of bottle gourd against skin cancer were demonstrated by a reduction in papilloma number, multiplicity, incidence, latency, volume, and papilloma size, as well as histological examinations. The presence of phytochemicals working through several pathways might be responsible for the protective benefits (38, 39). On lung cancer cell lines, the cytotoxic effects of plant fruit extract were investigated. According to the findings, the presence of cucurbitacin, polysaccharide inhibitor lagenin, and flavonoids in this plant's extract had a significant growth inhibitory influence on the lung cancer cell line (40). Immune-potentiating action is induced by the latex sap of dietary *L. siceraria* (LSL), which has high lectin activity. In both *in vitro* and *in vivo* tumor models, LSL inhibits tumor cell growth. Through changed gene expression, it suppresses tumor growth by targeting apoptosis and tumoral neovasculature. Its possible mechanism of action is given in Figure 5 (41).

Anti-obesity properties

Some fatty acid esters were found in the chloroform fraction of *L. siceraria*, including isopropyl palmitate, 9,12-octadecadienoic acid methyl ester, hexadecanoic acid methyl ester, and alpha-linolenic acid methyl ester. *L. siceraria's* ability to decrease pancreatic lipase activity, reducing lipid breakdown and hence lowering fat entrance into the body, is due to these chemicals. Regular consumption of the fruit's aqueous decoction may therefore be suggested for weight loss. Fatty acids and their esters acted as lipase inhibitors (42). In high-fat diet-generated obese mice, the synergistic impact of *Commiphora Mukul* (Gum Resin) with *L. siceraria* (fruit) extracts was examined. After the combined treatment, there was a substantial reduction in body weight, triglyceride, VLDL levels, fasting blood glucose, LDL, and serum cholesterol, as well as an increase in HDL levels. The results showed that combining *C. Mukul* and *L. siceraria* reduced obesity caused by a high-fat diet (43). The effects of *L. siceraria* fruit extract on human disease patients were investigated. There were significant decreases in body mass index (35). Obesity in Wistar albino rats was created by feeding them a high-fat diet and were treated with a diet containing *L. siceraria*, there was a significant reduction in body weight, locomotor activity, total cholesterol, food intake, triglycerides, organ weights, and an increase in low and high-density lipoprotein levels, indicating that *L. siceraria* has anti-obesity potential. The aqueous extract included numerous chemical ingredients such as saponins, pectin, and ellagic acid, which are essential for decreasing body weight and cholesterol levels, according to the preliminary phytochemical assessment of LS and TA. The LS fruits are high in saponins, cucurbitacins B, G, D, H, triterpenoid, and pectin, which showed lipid-lowering properties (44, 45). Different bottle gourd extracts were tested for their antihyperlipidemic and hypolipidemic properties in Triton-induced hyperlipidemic rats, as well as their hypolipidemic effects in normocholesterolemic rats. The extracts lowered total cholesterol, triglycerides, and low-density lipoproteins levels in a dose-dependent manner, while dramatically increasing high-density lipoproteins levels. The effects of petroleum ether extract were not significant. When compared to the others, the chloroform and alcoholic extracts had more substantial impacts on triglycerides, total cholesterol, and low-density lipoproteins, as well as an increase in HDL (46). The antihyperlipidemic activity of a methanolic extract of *L. siceraria* fruits (LSFE) was tested in high-fat-diet-induced hyperlipidemic rats. When compared to rats fed a high-fat diet, the gain in weight in rats given LSFE was smaller. Furthermore, LSFE caused a considerable increase in bile acid excretion. It may work by affecting endogenous cholesterol production in the liver and boosting cholesterol end product excretion. The LSFE included flavonoids, saponins and steroids, and polyphenolics, according to preliminary phytochemical screening. Plant saponins and steroids have been shown in several investigations to have hypolipidemic and antihyperlipidemic properties (47). The juice of *L. siceraria* (Bottle gourd) includes all of the active components that inhibit fat storage in adipose tissue. The anti-obesity activity of *L. siceraria* (Bottle gourd) juice has been tested in overweight and obese human individuals. Weight, waist circumference, and BMI all decreased significantly in those who consumed Bottle gourd juice, indicating it is a safe and effective treatment option for obese people (48).

Immunity boosting properties

The immunomodulatory impact of a methanolic extract of *L. siceraria* fruits in rats was investigated. The different fractions of *L. siceraria* were given orally at dosages of 100, 200, and 500 mg/kg to rats resulting in a great reduction in the delayed-type hypersensitivity reaction. Both primary and secondary antibody titers increased in a dose-dependent manner. Fractions also enhanced the number of white blood cells and lymphocytes. The findings show that test fractions have immunomodulatory potential (49).

Anti-diabetes properties

In vitro, the aqueous fraction of *L. siceraria* fruit pedicles has significant alpha-amylase inhibitory activity. This exercise is employed as a blood glucose management method. The conversion of starch to glucose is slowed when pancreatic alpha-amylase is blocked in the small intestine. As a result, less glucose is generated and enters the bloodstream, allowing it to be employed as an anti-diabetic drug (30). Supplementing

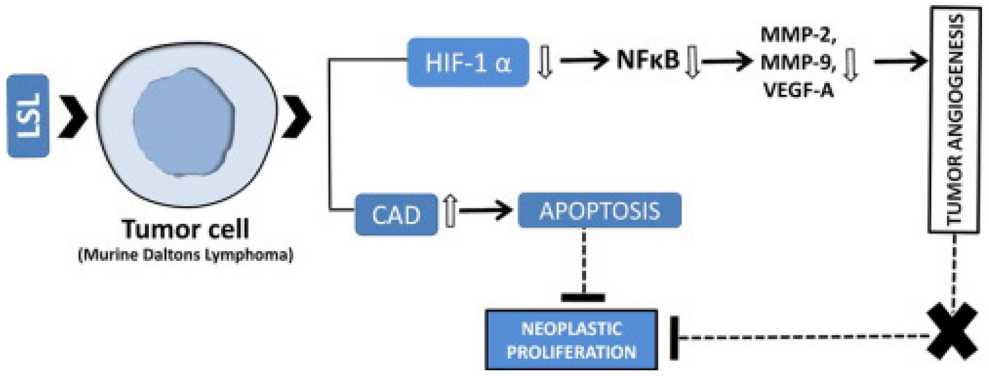

FIGURE 5
Anti-cancerous mechanism of action of *Lagenaria siceraria* (41).

MELS enhanced lipid metabolism and functions as a preventive mechanism against the formation of atherosclerosis in diabetic rats, as well as reducing diabetic sequelae from lipid peroxidation by boosting antioxidant status. As a consequence, the aerial sections of *L. siceraria* methanol extract can be considered a rich source of anti-diabetic medicines, possibly due to the extract's flavonoid and polyphenolic content (50). The pulp and seed extracts of *L. siceraria* induced alterations in the functional status of pancreatic cells. In rats with alloxan-induced diabetes, the capacity of the organism to generate and release insulin rose at the same time as the glucose level in the blood declined. The pulp and seed extract of *L. siceraria* were shown to have considerable anti-diabetic action (51). The oral glucose tolerance test was used to assess the hypoglycemic qualities of different globulins extracted from male Wistar rats, and it revealed that *L. siceraria* seeds contained globulins with high anti-hyperglycemic activity. In the profile, there was a prominent protein band with a molecular weight of 24.61 kDa that had considerable anti-hyperglycemic action. This specific protein, if present, is most likely the active peptide responsible for the observed activity (52). In human patients with dyslipidemia, the effects of *L. siceraria* fruit extract were investigated. Fasting blood glucose levels were found to be significantly lower (35). Various *in-vitro* approaches, such as amylolysis kinetics, and glucose adsorption diffusion capacity, were used to assess the hypoglycemic efficacy of the phyto-material extracts. The suppression of an enzyme (alpha-amylase) by *L. siceraria*, which restricts starch to glucose conversion, was blamed for the slowing of glucose diffusion. The extracts of *L. siceraria* have been shown to have hypoglycemic action in several *in-vitro* tests and might be employed as therapeutic agents in the treatment of diabetes (53). The presence of bioactive molecules and amylase and glucosidase inhibitors, and cholinergic esterase enzymes in ethanol and methanol seed extracts of *L. siceraria* might explain the excellent antidiabetic action found (34).

Cardio-protective properties

Ethanolic extract has a cardioprotective effect. The antioxidant function of *L. siceraria* (Mol) fruits is most likely due to its capacity to combat free radicals, or its ability to maintain the near-normal activity of free radical enzymes, which protect the cardiac membrane from oxidative damage by lowering lipid peroxidation (33).

Modern pharmacological research has revealed that the fruit of *L. siceraria* has a variety of cardioprotective characteristics. In rats with triton-induced hyperlipidemia, chloroform, and alcoholic extracts of *L. siceraria* revealed antihyperlipidemic potential. In Doxorubicin and Isoproterenol-induced cardiotoxicity in rats, the fruit demonstrated strong cardioprotective benefits (5). The goal of the study was to see if *L. siceraria* (LS) fruit powder might protect rats against the cardiotoxicity of the drug doxorubicin (Dox). The LS-treated group was shown to be protected from doxorubicin-induced cardiac damage in histopathological analysis. It was discovered that *L. siceraria* had a cardioprotective effect in rats when they were exposed to doxorubicin-induced cardiotoxicity (54). The lack of cardiac necrosis and inflammation in the *L. siceraria*-treated group showed that the plant had cardioprotective properties. The antioxidants orientin and isoorentin found in *L. siceraria* fruit powder appear to help prevent cardiac necrosis and inflammation. As a result, it may be inferred that LS fruit has cardioprotective properties (55). By preserving endogenous antioxidants and reducing lipid peroxidation in the rat heart, *L. siceraria* (Cucurbitaceous) Fruit Juice reduced Doxorubicin-induced cardiotoxicity and lowered myocardial damage (56). In isoproterenol-induced myocardial infarction, the cardioprotective benefits of *L. siceraria* fruit juice were investigated. The results show that *L. siceraria* fruit juice has a cardioprotective effect in rats with isoproterenol-induced myocardial infarction. The presence

of polyphenolic components in LS fruit may be responsible for these effects (57). Isoprenaline-induced tachycardia was decreased when *L. siceraria* fruit powder was given. Isoprenaline cardiotoxic impact was reduced in LS-pretreated mice. The cardioprotective effect of LS in isoprenaline-induced cardiotoxicity appears to be aided by its antioxidant and anti-inflammatory properties (58).

Gastro-protective properties

The anti-ulcer efficacy of a methanolic extract of *L. siceraria* fruits was examined in Wistar rats using pylorus ligation, Asprin, cold-restraint stress, and ethanol ulcer models. MELS reduced stomach volume, free acidity, ulcer index, and total acidity significantly, indicating that *L. siceraria* fruit extract may have anti-ulcer action (59). *L. siceraria* showed an increase in Gastric juice pH, whereas decreased in Total acidity, Gastric content, and Gastric juice volume. As a result of histological assessment investigations, it was shown that *L. siceraria* is both safe and effective in the treatment of stomach ulcers (60).

Hepato-protective properties

Based on improvements in serum marker enzyme levels, antioxidant parameters, and histological investigations, ethanolic extract of *L. siceraria* fruit is said to have a high hepatoprotective and antioxidant effect in antitubercular drugs induced hepatotoxicity (61).

L. siceraria has been shown to prevent the elevation of hepatic enzymes caused by long-term carbamazepine administration in rabbits, as well as liver tissue histology showing no necrosis or cholestasis. Thus, it is concluded that *L. siceraria* has a hepatoprotective effect and reduces the hepatotoxicity caused by carbamazepine (62). On rats, the hepatoprotective efficacy of *L. siceraria* fruit extracts was evaluated against carbon tetrachloride (CCl_4)-induced hepatotoxicity. The toxic effect of CCl_4 was dramatically reduced in *L. siceraria* ethanol extract-treated rats by restoring serum bilirubin, protein, and enzyme levels. The existence of normal hepatic cords, lack of necrosis, and fatty infiltration in the liver sections of the animals treated with the extracts further demonstrated the hepatoprotective potential (63). In paracetamol-induced hepatotoxicity in rats, the presence of phenolic components in ethanol extract of *L. siceraria* fruit protected against oxidative damage and liver necrosis (10).

Other pharmacological effects

L. siceraria (Molina) Standl. is a traditional medicinal as well as a portion of vegetable food. Immunomodulatory, antioxidant, hepatoprotective, anti-stress, cardioprotective, adaptogenic, anti-inflammatory, antihyperlipidemic, and analgesic activities have all been described. Lagenin (20 kDa), a new protein isolated from seeds, has been shown to have anticancer, antiviral, antiproliferative, and anti-HIV properties (64). Antioxidant, antihypertensive, hepatoprotective, cardioprotective, laxative, diuretic, central nervous system stimulant, adaptogenic, immunosuppressive, hypolipidemic, analgesic, anthelmintic, and free radical scavenging properties have also been proposed for the plant. This pulp boiled in oil is used in treating rheumatism and sleeplessness (16). Polysaccharides extracted from various portions of the plant have been found to have immune-modulating, anti-inflammatory, anti-tumor, cardioprotective, antioxidant, hepatoprotective, anti-diabetic, anti-hyperlipidemic, and analgesic activities in the last three decades. Several polysaccharides isolated from diverse sections of *L. siceraria* have been proposed with a variety of structures. Apart from its various bioactive qualities, this plant has the capacity to detoxify soil from heavy metals through the process of bioremediation (4). Antianxiety, antihyperlipidemic, diuretic, cytotoxic, cardioprotective, anti-inflammatory, antiulcer, analgesic, anticancer, antimicrobial, antidepressant, anti-hyperglycemic, anthelmintic, anti-urolithiatic, hepatoprotective, anthelmintic, immunomodulatory, antistress, and antioxidant activities have been studied in various parts of this plant (fruit, leaves, flowers, and roots) (2). Antimicrobial activity of *L. siceraria* extracts against *Enterococcus faecalis*, *Salmonella typhi*, *Staphylococcus aureus, Klebsiella pneumonia, E. coli,* and antifungal strains (*Aspergillus flavus, Trichoderma harzianum*, and *Aspergillus oryzae*) was moderate to strong (65). Fruits of *L. siceraria* have the ability to promote bile salt excretion, and their supplementation lowered fat levels in rats over time (47). Avinash et al. (66) described the antiulcer effect of *L. siceraria*. Long-term administration of *L. siceraria* fruit powder was done in dexamethasone-induced rats. According to the findings, hypertension activity in rats has decreased (58). *L. siceraria* crude methanol extract has antihelmintic efficacy against the Indian earthworm *Pheretima posthuma*. As a result, the leaves of *L. siceraria* are thought to have significant anthelmintic action (32). Adedapo et al. (67) explored the effects of the leaf extract on carrageenan- and histamine-induced paw edema in rats with swollen paws. In addition, the authors used mice to conduct acetic acid writhing and formalin tests. In rats, the scientists found a substantial reduction in paw edema, licking duration, and frequency. It has antihyperlipidemic, cardioprotective, hepatoprotective, diuretic, antidiabetic, and antihyperlipidemic effects (8). Antioxidant, antimicrobial, central nervous system activity, bronchospasm protective, antihyperglycemic, antidiarrheal activity, hepatoprotective activity, analgesic, antihelmintic activity, anti-inflammatory activity, cardioprotective effects, cytotoxic, antidiabetic, anticancer, antihyperlipidemic activity, immunomodulatory effect, and diuretic activity were discovered in the plant (68).

The analgesic efficacy of methanolic and aqueous extracts of the fruit was investigated using the tail immersion method in rats to provide scientific validity to the folkloric medicinal usage of *L. siceraria*. The methanolic extract has a moderate activity, whereas the aqueous extract has a high activity, according to the pain threshold test. This backs up the plant's historic usage in painful and inflammatory illnesses (69). Zinc oxide nanoparticles made from *L. siceraria* extract were reported for antimicrobial, anti-dandruff, and anti-arthritic properties (70).

Various extracts from the leaves and stems of *L. siceraria* were tested for their ability to repel the *Culex pipiens* L. mosquito, and it was concluded that these extracts could be developed as commercial products as an effective protection measure against mosquito bites, and thus control infections transmitted by a mosquito (71). The activity of *L. siceraria* leaves aqueous extract and silver nanoparticles (AgNPs) produced by *L. siceraria* against immature stages of *C. pipiens* and *A. phronesis* was examined. For 24 h, immature stages of both mosquito species were exposed to 400, 300, 200, 100, and 50 ppm aqueous extract of *L. siceraria* leaves and 5, 10, 20, 30, and 40 ppm *L. siceraria* generated AgNPs. The results exhibited that, AgNPs generated by *L. siceraria* were more harmful to mosquito species examined than the aqueous extract of *L. siceraria* leaves (72). The effect of manufactured zinc oxide nanoparticles (ZnO NPs) made from zinc nitrate and aqueous peel extract of *L. siceraria* on malaria prevention was investigated. The extract of *L. siceraria* and its mediated ZnO NPs were tested on *An. stephensi* III instar larvae. The influence of the ZnO NPs-based therapy on the histology and morphology of mosquito larvae was also studied. *Poecilia reticulata* (*P. reticulata*) had a 44% predation efficiency against *An. Stephensi* larvae in a normal laboratory environment, but 45.8 and 61.13% predation efficiency against *An. Stephensi* larvae in aqueous *L. siceraria* extract and its mediated ZnO NPs contaminated environment, respectively. ZnO NPs produced by *L. siceraria* were tested against *Plasmodium falciparum* CQ-sensitive strains. With an IC50 value of 62.5 g/mL, the *L. siceraria* extract and its induced ZnO NPs displayed cytotoxic effects against HeLa cell lines. According to the findings, *L. siceraria* peel extract and *L. siceraria*-produced ZnO NPs are viable green choices for fighting malarial vectors and parasites (73). Figure 6 shows the mechanism of ZnO NPs on *Plasmodium falciparum*.

Using a forced swim (behavior despair) paradigm, the antidepressant effect of methanolic extract of *L. siceraria* fruits in rats was assessed. The extract was given orally at dosages of 50, 100, and 200 mg/kg. The extract has antidepressant properties that are dosage dependent. The occurrence of triterpenoids, flavonoids, sterols, and saponins may be responsible for the action (23).

L. siceraria (LS) fruit juice has been used to treat jaundice and certain liver problems (10). The fruit is used to treat pain, ulcers, and fevers, as well as chest cough, asthma, and other bronchial problems, particularly in the form of a syrup made from sensitive fruits (1). Antioxidant, cardioprotective, hypolipidemic, diuretic, antihypertensive, hepatoprotective, analgesic, anthelmintic, free radical scavenging, immunosuppressive, central nervous system stimulant, laxative, and adaptogenic properties have also been proposed for the plant (11). Anti-inflammatory, antitussive, cytotoxic, and expectorant activities are also present in the plant (3). The plant species aids in improved digestion eliminates urinary difficulties, and aids in weight loss and blood pressure lowering (13). The seeds are used to treat headaches and constipation because they have a cooling impact on the body (8). The plant has long been renowned for its medicinal virtues, and it has been used to cure a variety of disorders, including diabetes, hypertension, ulcers, insanity, piles, jaundice, colitis, and skin infections. Its fruit pulp has cooling, diuretic, antibilious, and pectoral qualities, and is used as an emetic and purgative. This pulp is boiled in oil and used to treat rheumatism and sleeplessness (15).

The effect of *L. siceraria* on multiple systems of the human body is shown in Figure 7.

Uses in poultry and veterinary

Medicinal plants are very popular to improve the health and productivity of farm animals (67–69). The *in vitro* anthelmintic activity of crude aqueous methanolic extract (CAME) of *L. siceraria* against *Haemonchus* (H.) *contortus* and their eggs was evaluated using an adult motility assay and an egg hatch test. The *in vivo* anthelmintic activity of various dosages of crude powder (CP) and CAME in sheep naturally infected with gastrointestinal helminths was investigated using the fecal egg count reduction assay. CAME has significant antihelmintic action *in vitro* and inhibited the hatching of *H. contortus* eggs (71). In sheep infected with Moniezia and Avitellina species, the anticestodal action of *L. siceraria* seeds was examined. The powdered seeds, as well as their extracts in water and methanol, were administered orally at various doses. On the 15th day following administration, the medication powder induced a decrease in egg per gram counts (23). The purpose of the study was to develop low-salt, high-fiber, and low-fat functional chicken nuggets by substituting bottle gourd for sodium chloride and observing the effects on physicochemical parameters textural, color values, lipid, and sensory properties of pre-standardized low-fat chicken nuggets. The results of this investigation revealed that substituting bottle gourd for sodium chloride has a substantial impact on a variety of product quality parameters. Salt substitution, on the other hand, did not affect sensory qualities. Excluding the taste and quality ratings, which were impacted at greater levels, the sensory qualities of low-salt, low-fat chicken nuggets with bottle gourd were equivalent to the Control. With the addition of bottle gourd, the dietary

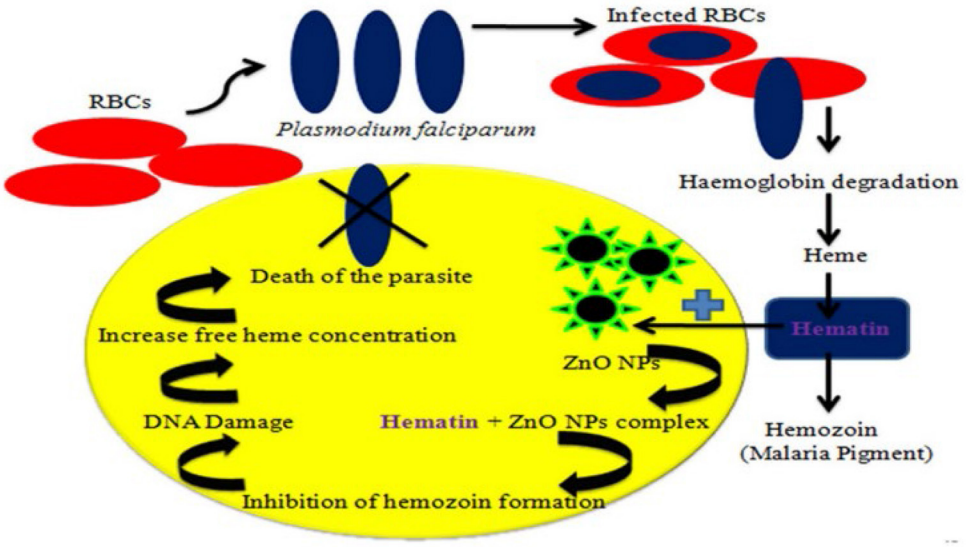

FIGURE 6
Schematic representation of the mechanism of ZnO NPs (nano-particles from LS) on *Plasmodium falciparum* (73).

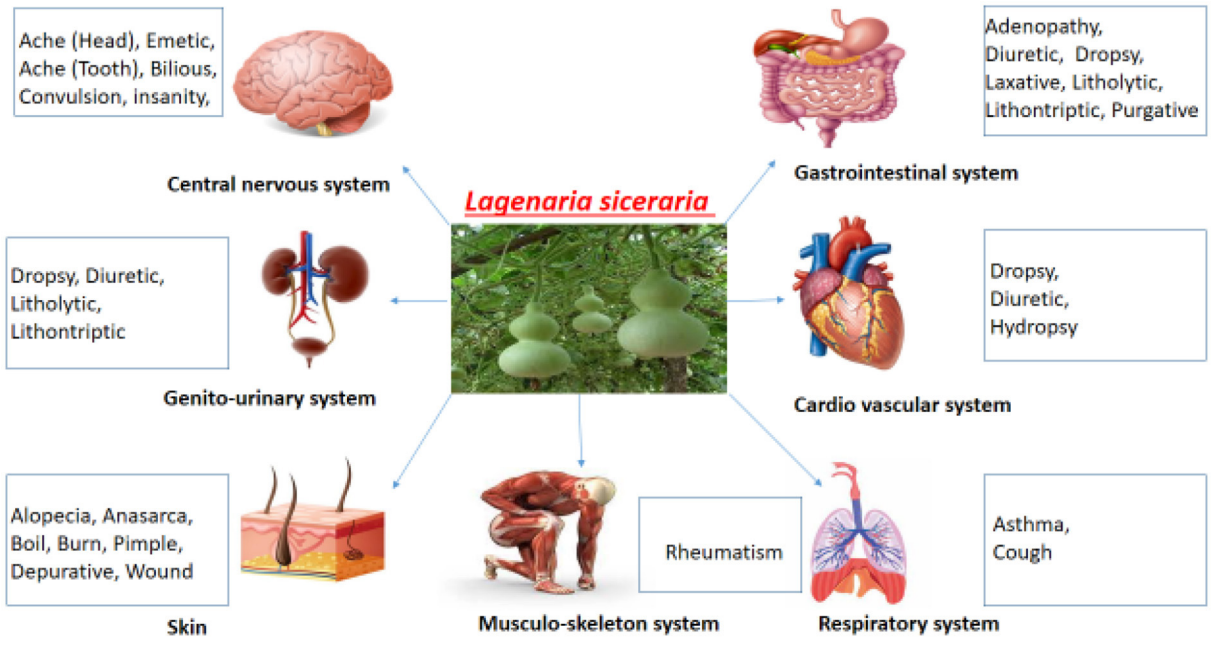

FIGURE 7
Systemic effects of *Lagenaria siceraria*.

fiber content of the goods may be increased, while the total cholesterol level can be reduced. As a result, using this technique, extremely palatable low-fat, low-salt, and high-fiber functional chicken nuggets may be developed without sacrificing their acceptability (74).

Toxicity assessment

L. siceraria is found to cause problems in the upper gastrointestinal system. The consumption of *L. siceraria* causes nausea, vomiting, gastrointestinal bleeding, abdominal pain,

and hematemesis (20). It is also said to cause gastrointestinal toxicity along with gastric erosion (first stage of ulcer) and ulcers (21, 22). This toxicity may be attributed to the presence of triterpenoid cucurbitacins (24). This data is based on clinical data but no dose of toxicity has been mentioned. Recently, it has come to light that drinking bottle gourd juice with a bitter flavor, can have extremely hazardous responses and result in symptoms like abdominal discomfort, vomiting, diarrhea, shock, and death (75).

A little number of cucurbitacins, specifically the types including B, D, G, and H, are present in bottle gourd fruit. Cucurbitacin concentrations often don't go above 130 ppm (76). The binding of cortisol to glucosteroid receptor is inhibited by Cucurbitacins in He La cells at 37°C which depicts a strong correlation with cytotoxic activity (77). The capillary permeability is enhanced by Cucurbitacin D (78) which is associated with a persistent fall in blood pressure and accumulation of fluid in thoracic and abdominal cavities in mice.

Conclusion and future perspective

The present review gives a thorough insight into *L. siceraria* phytochemistry along with pharmacology, beneficial effects, medicinal uses, and limitations that suggest its' therapeutic potential. The *L. siceraria* has various critical health-promoting benefits such as neurological, physiological, and blood biochemical changes. Though the mechanism of action for phytochemicals may differ among various species and is not fully understood, therefore, need to be exploited. Further research is also warranted to uncover and record relevant markers (bio and molecular) that are responsible for a wide range of *L. siceraria* health benefits in humans, animals, and poultry.

Author contributions

MS and MK drafted the article. JB, KA, AM, and MA downloaded the articles. UY, AK, and ZM edited the article, while SC gave the main idea. All authors contributed to the article and approved the submitted version.

Acknowledgments

The authors thankful to 2021YFF1000602/National Key Research and Development Program of China 2021NY-020/Key Research and Development Projects in Shaanxi Province, U1804106/Joint Funds of the National Natural Science Foundation of China, 2015CB943102/Major National Scientific Research Projects, funding.

Conflict of interest

The authors declare that the research was conducted in the absence of any commercial or financial relationships that could be construed as a potential conflict of interest.

Publisher's note

All claims expressed in this article are solely those of the authors and do not necessarily represent those of their affiliated organizations, or those of the publisher, the editors and the reviewers. Any product that may be evaluated in this article, or claim that may be made by its manufacturer, is not guaranteed or endorsed by the publisher.

References

1. Hussein MMA, Arisha AH, Tayel EM, Abdo SA. Effect of long-term oral exposure to carmoisine or sunset yellow on different hematological parameters and hepatic apoptotic pathways in mice. *J Anim Health Prod.* (2021) 9:80–6. doi: 10.17582/journal.jahp/2021/9.s1.80.86

2. Zahoor M, Ikram M, Nazir N, Naz S, Batiha GE-S, Kamran AW, et al. A comprehensive review on the medicinal importance; biological and therapeutic efficacy of *Lagenaria siceraria* (Mol.) (bottle gourd) Standley fruit. *Curr Top Med Chem.* (2021) 21:1788–803. doi: 10.2174/1568026621666210701124628

3. Saboo SS, Thorat PK, Tapadiya GG, Khadabadi SS. Ancient and recent medicinal uses of cucurbitaceae family. *Int J Ther Appl.* (2013) 9:11–9. Available online at: https://npaa.in/journal-ijta/admin/ufile/1373007067IJTA_9_11-19.pdf

4. Chakraborty I, Ghosh K. Nutritional potential, health effects and structural diversity of bioactive polysaccharides from *Lagenaria siceraria*: a review. *J Adv Sci Res.* (2020) 11:34–42. Available online at: https://www.sciensage.info/index.php/JASR/article/view/504

5. Upaganlawar A. *Lagenaria siceraria* (Bottle Gourd) in various cardiovascular complications. *Cardiovasc Dis.* (2017) 1:44–56. doi: 10.2174/9781681084893117010004

6. Awala FO, Ndukwu BC, Agbagwa IO. Phytogeographical distribution and fruit diversity of *Lagenaria siceraria* species in Nigeria. *Am J Plant Sci.* (2019) 10:958–75. doi: 10.4236/ajps.2019.106069

7. Stephens JM. *Gourd, Bottle– Lagenaria siceraria (Mol.) Standl.* University of Florida Cooperative Extension Service, Institute of Food and Agriculture Sciences (EDIS) (1994). Available online at: http://edis.ifas.ufl.edu/pdffiles/mv/mv06900.pdf

8. Kumar D, Sharma C, Singh B, Singh D. Pharmacognostical, phytochemical and pharmacological profile of natural remedy *Lagenaria siceraria* (Mol.) Standly: a review. *Brit J Pharm Res.* (2015) 7:340–52. doi: 10.9734/BJPR/2015/17641

9. Kumari N, Tajmul M, Yadav S. Proteomic analysis of mature *Lagenaria siceraria* seed. *Appl Biochem Biotechnol.* (2015) 175:3643–56. doi: 10.1007/s12010-015-1532-3

10. Panchal CV, Sawale JA, Poul BN, Khandelwal KR. Hepatoprotective activity of *Lagenaria siceraria* (Molina) Standley fruits against paracetamol induced hapatotoxicity in mice. *Int J Pharm Sci Res.* (2013) 4:371–7. doi: 10.13040/IJPSR.0975-8232.4(1).371-77

11. Yash P, Gill NS, Amber P. An updated review on medicinal properties of *Lagenaria siceraria*. *Inter J Univ Pharm Biol Sci.* (2014) 3:362–76. Available online at: http://www.ijupbs.com/Uploads/30.%20RPA1415114115.pdf

12. Ghule BV, Ghante MH, Yeole PG, Saoji AN. Diuretic activity of *Lagenaria siceraria* fruit extracts in rats. *Indian J Pharm Sci.* (2007) 69:817–9. doi: 10.4103/0250-474X.39441

13. Roopan SM, Devi Rajeswari V, Kalpana VN, Elango G. Biotechnology and pharmacological evaluation of Indian vegetable crop *Lagenaria siceraria*: an overview. *Appl Microbiol Biotechnol.* (2016) 100:1153–62. doi: 10.1007/s00253-015-7190-0

14. Lim TK. *Lagenaria siceraria*. In: *Edible Medicinal and Non-medicinal Plants*, Vol. 1. Dordrecht; New York, NY: Springer (2012). p. 298–313.

15. Prajapati RP, Kalariya M, Parmar SK, Sheth NR. Phytochemical and pharmacological review of *Lagenaria siceraria*. *J Ayurveda Integr Med.* (2010) 1:266–72. doi: 10.4103/0975-9476.74431

16. Tyagi NTN, Sharma GNSGN, Shrivastava BSB. Medicinal value of *Lagenaria siceraria*: an overview. *Int J Indig Herbs Drugs.* (2017) 2:36–43. Available online at: https://www.saap.org.in/journals/index.php/herbsanddrugs/article/view/50

17. Deshmukh DB, Sherkar MR. Evaluation of *in vivo* analgesic and anti-inflammatory activity of ethanolic extract of medicinal plant- *Lagenaria siceraria*. *Asian J Pharm Technol.* (2019) 9:75–8. doi: 10.5958/2231-5713.2019.00013.8

18. Akhtar MS, Riffat S. Evaluation of anticestodal activity of *Lagenaria siceraria* (Kaddoo) seeds in sheep. *Pakistan Vet J.* (1987) 7:139–41.

19. Verma AK, Sharma BD, Banerjee R. Quality characteristics of low-fat chicken nuggets: effect of common salt replacement and added bottle gourd (*Lagenaria siceraria* L.). *J Sci Food Agric.* (2012) 92:1848–54. doi: 10.1002/jsfa.5691

20. Sharma SK, Puri R, Jain A, Sharma MP, Sharma A, Bohra S, et al. Assessment of effects on health due to consumption of bitter bottle gourd (*Lagenaria siceraria*) juice. *Indian J Med Res.* (2012) 135:49–55. doi: 10.4103/0971-5916.93424

21. Puri R, Sud R, Khaliq A, Kumar M, Jain S. Gastrointestinal toxicity due to bitter bottle gourd (*Lagenaria siceraria*)– a report of 15 cases. *Indian J Gastroenterol.* (2011) 30:233–6. doi: 10.1007/s12664-011-0110-z

22. Ho CH, Ho MG, Ho S-P, Ho HH. Bitter bottle gourd (*Lagenaria siceraria*) toxicity. *J Emerg Med.* (2014) 46:772–5. doi: 10.1016/j.jemermed.2013.08.106

23. Prajapati R, Umbarkar R, Parmar S, Sheth N. Antidepressant like activity of *Lagenaria siceraria* (Molina) Standley fruits by evaluation of the forced swim behavior in rats. *Int J Nutr Pharmacol Neurol Dis.* (2011) 1:152–6. doi: 10.4103/2231-0738.84206

24. Shah BN, Seth AK, Desai RV. Phytopharmacological profile of *Lagenaria siceraria*: a review. *Asian J Plant Sci.* (2010) 9:152–7. doi: 10.3923/ajps.2010.152.157

25. Ogunbusola EM. Nutritional and antinutritional composition of calabash and bottle gourd seed flours (var *Lagenaria siceraria*). *J Culin Sci Technol.* (2018) 16:326–35. doi: 10.1080/15428052.2017.1390518

26. Ojiako OA, Igwe CU. Nutritional and anti-nutritional compositions of *Cleome rutidosperma*, *Lagenaria siceraria*, and *Cucurbita maxima* seeds from Nigeria. *J Med Food.* (2007) 10:735–8. doi: 10.1089/jmf.2007.625

27. United States Department of Agriculture (USDA) 2003 Agriculture Research Services (ARS), Nutrient Data Laboratory, National Nutrient Database for Standard Reference, Release # 15. Available online at: http://www.nal.usda.gov/fnic/foodcomp (accessed April 25, 2003).

28. Hassan LG, Sani NA, Dangoggo SM, Ladan MJ. Nutritional value of bottle gourd (*Lagenaria siceraria*) seeds. *Glob J Pure Appl Sci.* (2008) 14:301–6. doi: 10.4314/gjpas.v14i3.16812

29. Juee LYM, Naqishbandi AM. Calabash (*Lagenaria siceraria*) potency to ameliorate hyperglycemia and oxidative stress in diabetes. *J Funct Foods.* (2020) 66:103821. doi: 10.1016/j.jff.2020.103821

30. Ahmed D, Ashiq N. *In vitro* analysis of anti-diabetic and anti-oxidative potential of pedicles of fruit-vegetable bottle gourd. *Pak J Pharm Sci.* (2018) 31:2497–501.

31. Saha P, Mazumder UK, Haldar PK, Gupta M, Sen SK, Islam A. Antioxidant and hepatoprotective activity of *Lagenaria siceraria* aerial parts. *Pharmacogn J.* (2011) 3:67–74. doi: 10.5530/pj.2011.23.10

32. Mohan R, Birari R, Karmase A, Jagtap S, Bhutani KK. Antioxidant activity of a new phenolic glycoside from *Lagenaria siceraria* Stand. fruits. *Food Chem.* (2012) 132:244–51. doi: 10.1016/j.foodchem.2011.10.063

33. Vijayakumar M, Selvi M, Krishnakumari S. Cardioprotective effect of *Lagenaria siceraria* (Mol) on antioxidant tissue defense system against isoproterenol-induced myocardial infarction in rats. *Inven Impact Ethnopharmacol.* (2010) 1:207–10. Available online at: https://d1wqtxts1xzle7.cloudfront.net/30376730/Paper_6-libre.pdf?1390885928=&response-content-disposition=inline%3B+filename%3DCardioprotective_Effect_of_Lagenaria_sic.pdf&Expires=1661937652&Signature=LVl-MHDZj-lCg MTUo5iJfE-evx4trfuhd0t0NijzzPhrfKjeMFrSE0O6XNN4B IGXkPqVZQP0M2PV3pvZ 5B1U n8PdNBW9Skwirs3VT0uGMMN Uc9rL ridI3XGQ8W2PXZWw0oRFUBskdXhCKVXonxpvZ 5B1U n8PdNBW9Skx Uc9rL ridI3XGQ8W2PXZWw0oRFUBskdXhCKVXonxpvZ 5B1U n8PdNBW9Skw irs3VT0uGMMNUc9rL ridI3XGQ8W2PXZWw0oRFUBsk dXhCKVXon X3HjchJ b-LQ_&Key-Pair-Id=APKAJLOHF5GGSLRBV4ZA

34. Attar UA, Ghane SG. *In vitro* antioxidant, antidiabetic, antiacetylcholine esterase, anticancer activities and RP-HPLC analysis of phenolics from the wild bottle gourd (*Lagenaria siceraria* (Molina) Standl.). *South Afr J Bot.* (2019) 125:360–70. doi: 10.1016/j.sajb.2019.08.004

35. Singh PSB, Prasad G. Lipid-lowering and antioxidant functions of bottle gourd (*Lagenaria siceraria*) extract in human dyslipidemia. *J Evid Based Compl Alt Medi.* (2014) 19:112–8. doi: 10.1177/2156587214524229

36. Saha P, Sen SK, Bala A, Mazumder UK, Haldar PK. Evaluation of anticancer activity of *Lagenaria siceraria* aerial. *Int J Cancer Res.* (2011) 7:244–53. doi: 10.3923/ijcr.2011.244.253

37. Thakkar JH. Evaluation of *in vitro* antimutagenic potential of *Lagenaria siceraria* using Ame's test. *Am J Cancer Biol.* (2013) 1:57–61. Available online at: https://www.semanticscholar.org/paper/Evaluation-of-invitro-Antimutagenic-Potential-of-Thakkar-PatelChirag/483a97f237ca0414c184333c03a8a45a3043f9f6

38. Kumar N, Kale RK, Tiku AB. Chemopreventive effect of *Lagenaria siceraria* in two stages DMBA plus croton oil induced skin papillomagenesis. *Nutr Cancer.* (2013) 65:991–1001. doi: 10.1080/01635581.2013.814800

39. Agrawal RC, Mishra S. Identification and estimation of phytochemicals and evaluation of anticancer activity of *Lagenaria siceraria* leaves and fruit extract. *Int J Curren Key words.* (2016) 8:38899–904. Available online at: https://www.journalcra.com/sites/default/files/issue-pdf/17373.pdf

40. Shaneh M. Changes in lung cancer cell line affected by cytotoxicity of *Lagenaria siceraria* plant extract. *Pakistan J Med Health Sci.* (2021) 15:1282–4. doi: 10.53350/pjmhs211551282

41. Vigneshwaran V, Thirusangu P, Madhusudana S, Krishna V, Pramod SN, Prabhakar BT. The latex sap of the 'Old World Plant' *Lagenaria siceraria* with potent lectin activity mitigates neoplastic malignancy targeting neovasculature and cell death. *Int Immunopharmacol.* (2016) 39:158–71. doi: 10.1016/j.intimp.2016.07.024

42. Maqsood M, Ahmed D, Atique I, Malik W. Lipase inhibitory activity of *Lagenaria siceraria* fruit as a strategy to treat obesity. *Asian Pac J Trop Med.* (2017) 10:305–10. doi: 10.1016/j.apjtm.2017.03.010

43. Nadeem S. Synergistic effect of *Commiphora mukul* (gum resin) and *Lagenaria siceraria* (fruit) extracts in high fat diet induced obese rats. *Asian Pacific J Trop Dis.* (2012) 2:S883–6. doi: 10.1016/S2222-1808(12)60285-0

44. Erasto P, Mbwambo ZH. Antioxidant activity and HPTLC profile of *Lagenaria siceraria* fruits. *Tanzan J Health Res.* (2009) 11:79–83. doi: 10.4314/thrb.v11i2.45206

45. Rai PD, Dambal AA, Khatri S, Khadabadi SS. Development of an anti-obesity polyherbal formulation containing *Terminalia arjuna*, *Lagenaria siceraria* and *Piper nigrum*. *Pharma Innov.* (2015) 3(11 PartA):33–7. Available online at: https://www.thepharmajournal.com/archives/?year=2015&vol=3&issue=11&ArticleId=473

46. Ghule BV, Ghante MH, Saoji AN, Yeole PG. Hypolipidemic and antihyperlipidemic effects of *Lagenaria siceraria* (Mol.) fruit extracts. *Indian J Exp Biol.* (2006) 44:905–9.

47. Ghule BV, Ghante MH, Saoji AN, Yeole PG. Antihyperlipidemic effect of the methanolic extract from *Lagenaria siceraria* Stand. fruit in hyperlipidemic rats. *J Ethnopharmacol.* (2009) 124:333–7. doi: 10.1016/j.jep.2009.04.040

48. Vaibhav A, Singh JP, Singh OP. Role of *Lagenaria siceraria* fruit juice in overweight and obesity. *Int J Res Rev.* (2016) 3:6–11. Available online at: https://www.ijrrjournal.com/IJRR_Vol.3_Issue.7_July2016/IJRR002.pdf

49. Gangwal A, Parmar SK, Gupta GL, Rana AC, Sheth NR. Immunomodulatory effects of *Lagenaria siceraria* fruits in rats. *Pharmacogn Mag.* (2008) 4:234–8. Available online at: https://eurekamag.com/research/031/822/031822521.php

50. Saha P, Mazumder UK, Haldar PK, Sen SK, Naskar S. Antihyperglycemic activity of *Lagenaria siceraria* aerial parts on streptozotocin induced diabetes in rats. *Diabetol Croat.* (2011) 40:49–60. Available online at: https://go.gale.com/ps/i.do?p=AONE&u=googlescholar&id=GALE|A272246332&v=2.1&it=r&sid=AONE&asid=742a7907

51. Bhattacharya S, Das B. Anti-diabetic activity of *Lagenaria siceraria* pulp and seed extract in normal and alloxan-induced diabetic rats. *Int J Pharm Sci Res.* (2012) 3:3362–9. Available online at: https://ijpsr.com/bft-article/anti-diabetic-activity-of-lagenaria-siceraria-pulp-and-seed-extract-in-normal-and-alloxan-induced-diabetic-rats/

52. Teugwa CM, Boudjeko T, Tchinda BT, Mejiato PC, Zofou D. Anti-hyperglycaemic globulins from selected Cucurbitaceae seeds used as antidiabetic medicinal plants in Africa. *BMC Complement Altern Med.* (2013) 13:1–8. doi: 10.1186/1472-6882-13-63

53. Randive DS, Bhutkar MA, Bhinge SD, Shejawal KP, Sanap PR, Patil PD, et al. Hypoglycemic effects of *Lagenaria siceraria*, *Cynodon dactylon* and *Stevia rebaudiana* extracts. *J Herbmed Pharmacol.* (2019) 8:51–5. doi: 10.15171/jhp.2019.09

54. Fard MH, Bodhankar SL, Dikshit M. Cardioprotective activity of fruit of *Lagenaria siceraria* (Molina) Standley on Doxorubicin induced cardiotoxicity in rats. *Int J Pharmacol.* (2008) 4:466–71. doi: 10.3923/ijp.2008.466.471

55. Mali VR, Mohan V, Bodhankar SL. Antihypertensive and cardioprotective effects of the *Lagenaria siceraria* fruit in N G-nitro-L-arginine methyl ester (L-NAME) induced hypertensive rats. *Pharm Biol.* (2012) 50:1428–35. doi: 10.3109/13880209.2012.684064

56. Fard MH, Naseh G, Bodhankar SL, Dikshit M. Cardioprotective effect of *Lagenaria siceraria* (Molina) Standley (Cucurbitaceae) fruit juice on doxorubicin induced cardiotoxicity in rats. *Am J Pharmacol Toxicol.* (2010) 5:103–8. doi: 10.3844/ajptsp.2010.103.108

57. Upaganlawar A, Balaraman R. Cardioprotective effects of *Lagenaria siceraria* fruit juice on isoproterenol-induced myocardial infarction in Wistar rats: a biochemical and histoarchitecture study. *J Young Pharm.* (2011) 3:297–303. doi: 10.4103/0975-1483.90241

58. Mali VR, Bodhankar SL. Cardioprotective effect of *Lagenaria siceraria* (LS) fruit powder in isoprenalin-induced cardiotoxicity in rats. *Eur J Integr Med.* (2010) 2:143–9. doi: 10.1016/j.eujim.2010.03.003

59. Srivastava V, Gupta P, Sharma D. Evaluation of anti-ulcer activity of methanolic extract of *Lagenaria siceraria*. *J Appl Pharm Sci Res.* (2021) 4:15–20. doi: 10.31069/japsr.v4i2.4

60. Manchala P. Evaluation of anti-ulcer activity of *Lagenaria siceraria* chloroform extracts in pylorus ligated rats. *Electron J Biol.* (2019) 15:27–37. Available online at: https://ejbio.imedpub.com/evaluation-of-antiulcer-activity-of-lagenaria-sicerariachloroform-extracts-in-pylorus-ligated-rats.php?aid=24221

61. Funde SK, Jaju JB, Dharmadhikari SC, Pawar GR. Effect of *Lagenaria siceraria* fruit extract (Bottle gourd) on hepatotoxicity induced by antitubercular drugs in albino rats. *Int J Basic Clin Pharmacol.* (2013) 2:728–34. doi: 10.5455/2319-2003.ijbcp20131211

62. Owais F, Mehjabeen. Hepatoprotective effect of *Lagenaria siceraria* (Linn) in carbamazepine induced hepatotoxicity in rabbits. *ISRA Med J.* (2019) 10:345–8. Available online at: https://www.researchgate.net/publication/336363154_Hepatoprotective_Effect_of_Lagenaria_Siceraria_Linn_in_Carbamazepine_Induced_Hepatotoxicity_in_Rabbits

63. Lakshmi BVS, Sudhakar M. Antistress activity of *Lagenaria siceraria* fruit extracts in different experimental models. *J Pharm Res.* (2011) 4:1013–5. Available online at: https://citeseerx.ist.psu.edu/viewdoc/download?doi=10.1.1.735.8343&rep=rep1&type=pdf

64. Ahmad I, Irshad M, Rizvi MMA. Nutritional and medicinal potential of *Lagenaria siceraria*. *Int J Veg Sci.* (2011) 17:157–70. doi: 10.1080/19315260.2010.526173

65. Nagaraja YP, Geetha KN, Vinay MS. Antimicrobial effect of *Lagenaria siceraria* (Mol.) Standley, against certain bacteria and fungal strains. *J Appl Nat Sci.* (2011) 3:124–7. doi: 10.31018/jans.v3i1.169

66. Avinash K, Abha D, Ganesh NS. Peptic ulcer: a review with emphasis on plants from Cucurbetaceae family with antiulcer potential. *Int J Res Ayurveda Pharma.* (2011) 2:1714–6. Available online at: https://www.cabdirect.org/globalhealth/abstract/20123038015

67. Adedapo A, Adewuyi T, Sofidiya M. Phytochemistry, anti-inflammatory and analgesic activities of the aqueous leaf extract of *Lagenaria breviflora* (Cucurbitaceae) in laboratory animals. *Rev Biol Trop.* (2013) 61:281–90. doi: 10.15517/rbt.v61i1.11127

68. Palamthodi S, Lele SS. Nutraceutical applications of gourd family vegetables: *Benincasa hispida*, *Lagenaria siceraria* and *Momordica charantia*. *Biomed Prev Nutr.* (2014) 4:15–21. doi: 10.1016/j.bionut.2013.03.004

69. Shah BN, Seth AK. Screening of *Lagenaria siceraria* fruits for their analgesic activity. *Rom J Biol Plant Biol.* (2010) 55:23–6. Available online at: https://www.ibiol.ro/plant/volume%2055/art04.pdf

70. Kalpana VN, Payel C, Rajeswari VD. *Lagenaria siceraria* aided green synthesis of ZnO NPs: anti-dandruff, anti-microbial and anti-arthritic activity. *Res J Chem Environ.* (2017) 21:14–9. Available online at: https://www.researchgate.net/publication/320878071_Lagenaria_siceraria_aided_green_synthesis_of_ZnO_NPs_Anti-dandruff_Anti-microbial_and_Anti-arthritic_activity

71. Hassan MI, Fouda MA, Hammad KM, Tanani MA, Shehata AZ. Repellent effect of *Lagenaria siceraria* extracts against *Culex pipiens*. *J Egypt Soc Parasitol.* (2014) 44:243–8. doi: 10.21608/jesp.2014.90754

72. Shehata AZI, Mahmoud AM. Efficacy of leaves aqueous extract and synthesized silver nanoparticles using *Lagenaria siceraria* against *Culex pipiens* liston and Anopheles pharoensis theobald. *J Egypt Soc Parasitol.* (2019) 49:381–7. doi: 10.21608/jesp.2019.68148

73. Kalpana VN, Alarjani KM, Rajeswari VD. Enhancing malaria control using *Lagenaria siceraria* and its mediated zinc oxide nanoparticles against the vector *Anopheles stephensi* and its parasite *Plasmodium falciparum*. *Sci Rep.* (2020) 10:1–12. doi: 10.1038/s41598-020-77854-w

74. Khan MN, Hussain A, Iqbal Z, Sajid MS. Evaluation of anthelmintic activity of *Lagenaria siceraria* (Molina) Standl and *Albizia lebbeck* L. against gastrointestinal helminths of sheep. *Egypt J Sheep Goats Sci.* (2010) 5:1–16. Available online at: https://journals.ekb.eg/article_27383.html

75. Verma A, Jaiswal S. Bottle gourd (*Lagenaria siceraria*) juice poisoning. *World J Emerg Med.* (2015) 6:308–9. doi: 10.5847/wjem.j.1920-8642.2015.04.011

76. Miro M. Cucurbitacins and their pharmacological effects. *PhytotherRes.* (1995) 9:159–68. doi: 10.1002/ptr.2650090302

77. Witkowski A, Knopa J. Binding of the cytotoxic and antitumor triterpenes, cucurbitacins, to glucocorticoid receptors of He La cells. *Biochim Biophys Acta.* (1981) 674:246–55. doi: 10.1016/0304-4165(81)90382-2

78. Edery H, Schatzberg PG, Gitter S. Pharmacodynamic activity of elatericin (cucurbitacin D). *Arch Int Pharmacodyn.* (1961) 130:315–35.

frontiers | Frontiers in Nutrition

TYPE Review
PUBLISHED 14 October 2022
DOI 10.3389/fnut.2022.1002147

OPEN ACCESS

EDITED BY
Gengjun Chen,
Kansas State University, United States

REVIEWED BY
Sonia Malik,
Université d'Orléans, France
Anand Kumar Chaudhari,
Government Girls' P. G. College,
Ghazipur, India

*CORRESPONDENCE
Xiaonan Liu
18304625304@163.com
Peng Gao
gaopeng@sdutcm.edu.cn

†These authors have contributed equally to this work and share first authorship

SPECIALTY SECTION
This article was submitted to Nutrition and Food Science Technology, a section of the journal Frontiers in Nutrition

RECEIVED 24 July 2022
ACCEPTED 13 September 2022
PUBLISHED 14 October 2022

CITATION
Xue Q, Xiang Z, Wang S, Cong Z, Gao P and Liu X (2022) Recent advances in nutritional composition, phytochemistry, bioactive, and potential applications of *Syzygium aromaticum* L. (Myrtaceae). *Front. Nutr.* 9:1002147. doi: 10.3389/fnut.2022.1002147

Recent advances in nutritional composition, phytochemistry, bioactive, and potential applications of *Syzygium aromaticum* L. (Myrtaceae)

Qing Xue[1†], Zedong Xiang[1†], Shengguang Wang[1], Zhufeng Cong[2], Peng Gao[1*] and Xiaonan Liu[3*]

[1]College of Pharmaceutical Science, Shandong University of Traditional Chinese Medicine, Jinan, Shandong, China, [2]Shandong Provincial Institute of Cancer Prevention and Treatmen, Jinan, Shandong, China, [3]Chinese Medicine Innovation Research Institute, Shandong University of Traditional Chinese Medicine, Jinan, Shandong, China

Syzygium aromaticum is an aromatic plant native to Indonesia, and introduced to tropical regions worldwide. As an ingredient in perfumes, lotions, and food preservation, it is widely used in the food and cosmetic industries. Also, it is used to treat toothache, ulcers, type 2 diabetes, etc. A variety of nutrients such as amino acids, proteins, fatty acids, and vitamins are found in *S. aromaticum*. In addition to eugenol, isoeugenol, eugenol acetate, β-caryophyllene and α-humulene are the main chemical constituents. The chemical constituents of *S. aromaticum* exhibit a wide range of bioactivities, such as antioxidant, antitumor, hypoglycemic, immunomodulatory, analgesic, neuroprotective, anti-obesity, antiulcer, etc. This review aims to comprehend the information on its taxonomy and botany, nutritional composition, chemical composition, bioactivities and their mechanisms, toxicity, and potential applications. This review will be a comprehensive scientific resource for those interested in pursuing further research to explore its value in food.

KEYWORDS

***Syzygium aromaticum*, medicinal food, nutritional composition, phytochemistry, bioactivities, applications**

Introduction

Spices are considered to be one of the earliest recorded functional foods, with international trade in spices dating back as far as 4500–1900 B.C. They are usually aromatic, dried plant parts obtained from seeds, fruits, leaves, roots, and bark (1). More than 100 species of plants are currently used worldwide as spices and flavorings that play

Abbreviations: CEO, clove essential oil; CE, clove extract; ECE, clove ethanol extract; ACE, the aqueous extract of clove; ChNPs, chitosan nanoparticles.

an important role in cooking, health care, and preserving (2). In addition, spices serve as a rich reservoir of bioactive compounds and also have antioxidant, antibacterial, anti-inflammatory, antidiabetic, and anticancer properties that help fight various diseases in the human body (3).

Syzygium aromaticum L. (Myrtaceae), is also known as *Eugenia caryophyllata Thunb.* It is an evergreen tree native to the Maluku Islands in Indonesia (4). Its dried flower buds are referred to as "clove," it is highly sought-after for medicinal and culinary purposes. In medieval Europe, it is cultivated for commercial purposes. Currently, it is produced mainly in Indonesia, West Indies, Madagascar, India, Tanzania, and Sri Lanka (5). especially Zanzibar and Pemba Island in Tanzania, which produce about 80% of the world's production (6) (**Figure 1**). Clove has been used as a spice in ancient China for more than 2000 years and was included in the first list of medicinal food items in China in 2002. Recent studies have found that fruits, seeds and leaves of *S. aromaticum* also contain bioactive compounds. The Chinese Traditional Medicine Administration has listed the fruit as one of the 39 herbal species that should be given priority for further development. Despite having commercial and medicinal value, it is not been extensively reviewed on its nutritional composition and advances in its chemistry, pharmacology, toxicology, and applications. This review is the first time for the comprehensive analysis of the nutritional components of its various parts, which has never appeared in previous papers. Secondly, in terms of chemical composition, although some articles have introduced it, this paper summarizes the chemical compositions of each part for the first time and classifies them into volatile and non-volatile components. Thirdly, in terms of biological activity, although some articles introduced the biological activity of *S. aromaticum*, there was no detailed and clear mechanism diagram. In this paper, the biological activities of *S. aromaticum* were comprehensively summarized and the mechanism diagrams were drawn for the first time. Fourthly, in terms of application, most of the existing articles only introduced the fresh-keeping effect of clove. In this paper, the applications of *S. aromaticum* in medicine and food have been comprehensively analyzed for the first time, and the relevant popular contents of nanometer preparations have been added. Overall, this review will be a comprehensive scientific resource for those interested in pursuing further research to explore its value in medicine and food.

Taxonomy and botanical description

Syzygium aromaticum belongs to the Myrtales order, Myrtaceae family, and Syzygium genus. Myrtaceae family plants are mainly grown in tropical and subtropical regions of Australia and America (7). Syzygium is an important genus in the Myrtaceae family and contains more than 500 species, mainly distributed in tropical Asia and a few species in Oceania and Africa (8). *S. aromaticum* belongs to the plant kingdom, Angiospermae, Dicotyledoneae, and Archichlamydeae.

Syzygium aromaticum is an evergreen tree growing to about 10–20 m. The bark is gray and smooth. The leaves are large and opposite. The leaf blades are leathery, ovate-long elliptic, entire, and densely covered with oil glands. The petiole is conspicuous. The leaf buds are terminal, cymes or panicles. The flowers are red or pink, and 3 flowers are together in one group. The flowers contain 4 petals. The buds are white at the beginning and turn green and then red when the buds are 1.5 to 2cm long (9). The calyx is cylindrical, receptacle long, and 4-lobed at the tip. The lobes are triangular, bright red, with numerous stamens and an inferior ovary. The berries are oblong, red or dark purple, and contain one seed, which is oval. The fruit is called female or female *S. aromaticum*. The fruiting period is from June to July, and the flowering period is from January to February. The buds are called male or male *S. aromaticum*, and dried by removing the pedicel from the bright red buds (10). The different parts of *S. aromaticum* are shown in **Figure 2**.

Nutritional composition

The flower buds, fruits, branches, leaves, and seeds of *S. aromaticum* are rich in various nutrients, proteins, fatty acids, mineral elements, amino acids, vitamin, etc. The presence of these nutrients makes *S. aromaticum* as a plant with high economic value. The nutritional composition of each part of the plant is listed in **Tables 1–4**. Only a very few studies were conducted to identify the vitamins present in it, and the vitamins present in it are listed in **Table 5**.

Conventional nutrients composition

The fruits contain the highest amount of total carbohydrate content. The buds contain the highest amount of crude fat. The leaves contain the highest protein content. The branches contain the highest amount of fiber. **Table 1** lists the conventional nutrients present in various parts of *S. aromaticum*.

Fatty acid composition

The fatty acid composition is similar in flower buds, fruits and branches. The leaves contain many fatty acids, and the number of fatty acids is 14. The contents palmitic, stearic, linoleic and linolenic acid were high in all parts. The higher proportion of polyunsaturated fatty acids in buds and seeds, is made up of α-linolenic acid and linoleic acid. α-Linolenic acid is one of the essential nutrients,

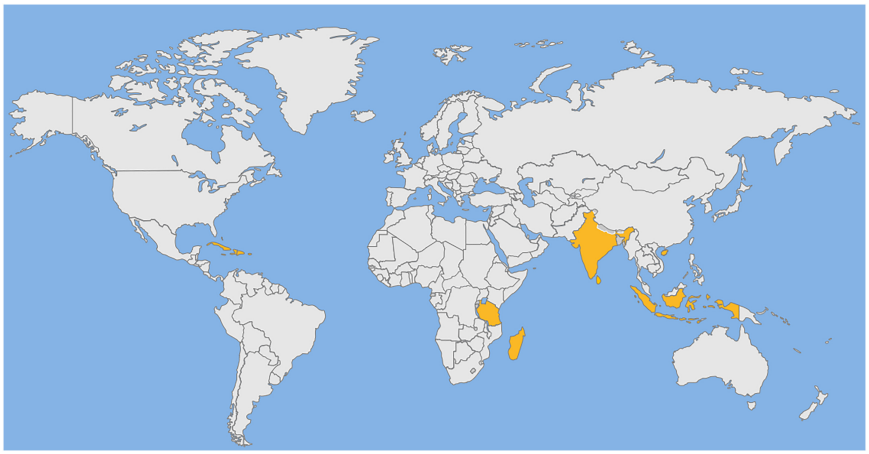

FIGURE 1
Distribution of *S. aromaticum* around the world. West Indies, Tanzania, Madagascar, India, Sri Lanka, Indonesia, Malaysia and Hainan province of China.

with anti-inflammatory, anti-thrombotic, anti-arrhythmic, anti-cancer, lower blood pressure and other effects (17). Linoleic acid can be metabolized into arachidonic acid in the body, to play a pro-inflammatory or pro-thrombotic vasoconstriction (18). The highest proportion of saturated fatty acids present in branches amounts to 73.66%. The palmitic acid content in saturated fatty acids is about 47.69%. The palmitic acid can play an antitumor role by activating Saos-2 cell apoptosis through endoplasmic reticulum stress and autophagy (19). Thus *S. aromaticum* is rich in fatty acids and has broad prospects for preparing health supplements. The fatty acid composition in each part of *S. aromaticum* is shown in **Table 2**.

Mineral elements composition

About 26 mineral elements have been detected in *S. aromaticum*. Fe is highest in the fruits, and Ca in the leaves. The total mineral element content in buds is higher than in other parts. The mineral element content of each part of *S. aromaticum* is shown in **Table 3**.

Amino acid composition

Amino acids are a combination of two organic substances, basic amino and acidic carboxyl groups, which give biochemical activity to protein molecules and are important components of proteins. The buds and fruits have similar percentages of essential amino acids, with total contents of 433.1–461.9 mg/kg and 406.2 mg/kg (32. 46%), respectively, which are higher than branches (113.9 mg/kg) and leaves (229.8 mg/kg). The details are shown in **Table 4**.

Vitamins composition

Vitamins are essential nutrients for human health. The buds contain a variety of vitamins (**Table 5**), among which Vitamin A, B_3, and Vitamin B_6 are high. These vitamins promote bone development, protect eye vision, maintain normal skin function, maintain immunity, and promote blood red blood cell metabolism (20).

Phytochemical composition

At present, it is believed that the chemical compositions of *S. aromaticum* are divided into two major parts: volatile and non-volatile components, mainly including aromatics, sesquiterpenoids, monoterpenoids, flavonoids, triterpenoids, organic acids, etc. These chemical components are mainly derived from flower buds, leaves, seeds, and other parts of *S. aromaticum*.

Volatile components

The volatile components of *S. aromaticum* have a unique and attractive fragrance. They can be used as a topical application to relieve pain and promote healing. They are also used in perfumey and flavor industries. They possess significant antioxidant and antibacterial effects. Studies have confirmed the presence of volatile components in buds, seeds and leaves, with the majority in buds. More than 110 compounds are present in the *S. aromaticum* volatile oil and are listed in **Supplementary Table 1**. The major compounds in volatile oil are eugenol, eugenyl acetate, caryophyllene and α -humulene.

FIGURE 2
Different parts of *S. aromaticum*. **(A)** Whole plant; **(B)** dried flower buds; **(C)** fruit; **(D)** leaf. Pictures are from https://baike.baidu.com/pic/%E4%B8%81%E5%AD%90%E9%A6%99/19435258.

TABLE 1 Conventional nutrients in various parts of *S. aromaticum*.

Nutrient composition	Buds			Fruits	Branches	Leaves	Seeds
	(mg/g) (11)	(%) (12)	(mg/g) (13)	(mg/g) (11)	(mg/g) (11)	(mg/g) (11)	(%) (14)
Moisture	–	9.63 ± 0.19	68.6	–	–	–	7.74 ± 0.2
Total carbohydrate	86.75 ± 5.61	8.26 ± 0.16	612.1	168.12 ± 8.92	106.47 ± 7.23	88.13 ± 6.13	51.3 ± 2.7
Crude protein	39.8 ± 3.79	6.06 ± 0.12	59.8	33.73 ± 4.26	45.1 ± 3.38	61.75 ± 5.62	6.9 ± 0.4
Crude fiber	111.72 ± 9.73	9.64 ± 0.32	342	73.38 ± 7.35	368.55 ± 23.45	253.13 ± 21.12	11.47 ± 0.5
Crude fat	123.58 ± 11.3	59.3 ± 0.15	200.7	25.78 ± 1.73	10.35 ± 0.26	41.56 ± 4.23	16.63 ± 0.3
Ash	34.17 ± 1.03	5.36 ± 0.08	58.8	23.08 ± 1.34	21.91 ± 1.53	40.59 ± 2.86	5.96 ± 0.1

"–" indicates that the value is not available.

Aromatics

Aromatic compounds (eugenol, isoeugenol and eugenyl acetate) are the main components in *S. aromaticum*. Eugenol, is a unique and widely studied volatile component of *S. aromaticum*, accounting for more than 50% of the volatile oil, with a variety of pharmacological activities (31). Eugenyl acetate, is another bioactive component of the volatile components. Forty-two aromatic compounds, including methyl eugenol,

TABLE 2 Fatty acid composition in various parts of *S. aromaticum*.

Fatty acid	Buds	Fruits	Branches	Leaves		Seeds
	(%) (11)	(%) (11)	(%) (11)	(%) (11)	(%) (15)	(%) (14)
C12:1 (n-7)	–	–	–	0.54	–	–
C14:0	3.35	2.24	3.41	2.64	0.37	1.29
C15:0	–	–	–	0.29	–	–
C16:0	32.14	38.30	47.69	43.29	7.23	6.21
C16:1 (n-7)	–	0.66	–	0.28	–	20.96
C17:0	–	–	1.42	1.10	–	–
C18:0	13.42	18.55	21.14	12.74	5.08	–
C18:1 (n-7)	–	–	–	0.44	0.44	6.20
C18:1 (n-9)	8.72	14.81	6.26	12.23	16.12	13.0
C18:1 (n-12)	–	–	1.39	–	–	–
C18:2 (n-6)	33.72	21.28	13.81	15.93	36.58	44.73
C18:3 (n-3)	8.21	4.16	4.88	9.80	30.55	2.93
C20:1 (n-9)	–	–	–	0.55	–	–
C20:0	–	–	–	–	2.82	4.68
C22:0	–	–	–	–	1.25	–
SFA	48.91	59.09	73.66	60.06	16.75	12.18
MUFA	8.72	15.47	7.65	14.04	16.12	40.16
PUFA	41.93	25.44	18.69	25.73	67.13	47.66

"–" indicates that the value is not available; SFA, saturated fatty acid; MUFA, monounsaturated fatty acid; PUFA, polyunsaturated fatty acid.

ethyl benzoate, and cinnamic aldehyde, were identified in the essential oil of clove by GC-MS.

Terpenoids

The terpenoids in *S. aromaticum* include sesquiterpenes, monoterpenes, and diterpenes, which are the material basis for the clinical efficacy and an important chemical source for further activity screening. Terpenoids are an important class of natural compounds widely used in the cosmetics and food industries and have a large market potential (32). Twenty-six sesquiterpenes and eighteen monoterpenes were reported in the volatile oil of *S. aromaticum*. Only one diterpene, menthyl chavicol, was reported from *S. aromaticum*. Caryophyllene and α-humulene account for about 7-16% of the volatile oil.

Aliphatic compounds

S. aromaticum volatile oil also contains aliphatic compounds, such as alkanes, ketones, alcohols, esters and ethers. The most abundant aliphatic compounds are tritetracontane, 2-heptanone, 2-non-anone, ethyl caproate and menthyl octanoate. The percentage of aliphatic compounds is lower than aromatic compounds in the volatile oil.

Non-volatile components

A total of 73 non-volatile components were reported from *S. aromaticum*, including 36 flavonoids, 4 chromones, 26 tannins, 3 triterpenoids, 1 coumarin and 1 phenolic ester, and 2 other components, as shown in **Table 6**.

Flavonoids

Studies have shown that flavonoids are one of the important components of *S. aromaticum* to exert strong antioxidative activity, anti-inflammatory, and immunomodulatory activities (42). Ryu et al. (33) reported the presence of luteolin, quercetin, rhamnocitrin, kumatakenin, and pachypodol in *S. aromaticum*. These flavonoids have shown anticancer activity on human ovarian cancer cells (A2780). In addition, flavonoids readily form O - and C - glycosides, with O - glycosides being more common and better absorbed. Ryu et al. (33) reported nine known flavonoid glycosides and four flavonoids from the buds.

Chromones

The chromones in *S. aromaticum* are mainly eugenin, 8-C-glucosylnoreugenin, biflorin, isobiflorin, etc. Biflorin and isobiflorin were found to be isolated from *S. aromaticum* buds by Lee et al. (38) and showed an anti-inflammatory effect on Lipopolysaccharide (LPS) induced inflammation in macrophages through STAT1 inactivation. In addition, it was demonstrated that biflorin increased the activation of protein kinase C-ζ and its downstream signaling molecules in the hippocampus. These compounds improved the cognitive dysfunction in mice and reduced the viability of melanoma cell lines through DNA interactions (43). These findings provide a

10.3389/fnut.2022.1002147

TABLE 3 Mineral elements content in various parts of *S. aromaticum*.

Mineral elements	Buds			Fruits	Branches	Leaves	Seeds	
	(mg/kg) (11)	(mg/kg)(12)	(mg/kg) (13)	(mg/kg) (11)	(mg/kg) (11)	(mg/kg) (11)	(mg/100g)(14)	(μ g/g)(16)
Potassium (K)	14 087.39	14 784.916 7	11 020	8 540.36	3 509.68	9 315.80	650.0 ± 30.0	–
Calcium (Ca)	6 888.94	6 302.166 7	6 460	2 949.98	6 294.30	9 299.14	270.0 ± 20	–
Sodium (Na)	3 995.71	4 143.166 7	2 430	2 554.04	1 660.37	3 105.66	–	–
Magnesium (Mg)	3 406.92	3 036.549 0	2 640	1 402.07	751.32	1 884.82	97.0 ± 10.0	–
Manganese (Mn)	664.88	858.033 4	300.33	411.57	430.01	870.30	43.8 ± 1.5	736.36 ± 40.42
Iron (Fe)	544.48	1 292.349 0	86.8	1 364.26	61.47	61.41	36.0 ± 0.8	4.26 ± 0.15
Aluminum (Al)	161.58	759.783 3	-	427.40	31.54	45.89	–	4.21 ± 0.34
Phosphorus (P)	-	-	1050	-	-	-	–	–
Strontium (Sr)	62.16	40.859 3	-	14.90	26.58	23.26	–	4.74 ± 0.06
Boron (B)	49.29	29.536 7		12.37	12.79	36.09		
Barium (Ba)	11.27	17.730 9	-	5.12	8.93	8.83	–	3.57 ± 0.23
Thallium (Ti)	14.61	87.541 3	-	15.14	9.99	12.02	–	–
Zinc (Zn)	13.10	10.252 5	10.9	4.04	6.84	7.60	0.7 ± 0.1	5.97 ± 4.49
Copper (Cu)	2.65	4.004 3	3.47	1.87	1.20	1.21	0.8 ± 0.1	3.55 ± 0.22
Stannum (Sn)	0.42	0.018 1	-	0.15	0.14	0.15	–	–
Vanadium (V)	0.17	5.308 7	-	0.64	0.12	0.06	–	–
Chromium (Cr)	-	0.847 500	-	-	-	-	–	0.05 ± 0.01
Nickel (Ni)	-	0.578 333	-	-	-	-	–	4.25 ± 0.39
Arsenic (As)	-	0.018 833	-	-	-	-	–	0.05 ± 0.01
Plumbum (Pb)	-	0.100 083	-	-	-	-	–	–
Hydrargyrum (Hg)	-	0.019 6250	-	-	-	-	–	–
Molybdenum (Mo)	0.05	-	-	0.07	0.03	0.08	–	–
Selenium (Se)	0.02	-	0.059	0.03	0.06	0.07	–	0.11 ± 0.01
Antimony (Sb)	0.00	-	-	0.01	0.04	0.03	–	–
Cobalt (Co)	< 1	0.1843	-	< 1	<1	<1	–	0.03 ± 0.00
Thallium (Tl)	<0.01	0.0028	-	< 0.01	<0.01	< 0.01	–	–

"–" indicates that the value is not available.

scientific basis for the neuroprotective and antitumor effects of *S. aromaticum*.

Tannins

Tannins are a group of water-soluble polyphenolic compounds with complex structures present in plants. Based on the chemical structures, these can be classified into two major groups, hydrolyzable and condensed tannins. The tannins exhibit various pharmacological effects such as antibacterial, antioxidant, antitumor, antiviral, and hypoglycemic (44). Kim et al. (39) isolated four tannins from *S. aromaticum*, eugeniin, casuarictin, 1,3-di-O-galloyl-4,6-(S)-hexahydroxydiphenoyl-β-D-glucopyranose, and tellimagrandin I. The tellimagrandin was found to have significant inhibitory activity on syncytium formation. Ali et al. (35) analyzed the polyphenol and tannin content in 12 spices (allspice, black cardamom, black cumin, black pepper, cardamom, cinnamon, clove, cumin, fennel, nutmeg, star-anise, and turmeric) using LC-ESI-QTOF-MS and evaluated their antioxidant activity. Cloves contain the highest total polyphenol and total tannin content. The antioxidant activity is positively correlated with the total phenolic content. *S. aromaticum* is the most active antioxidant (45).

Others

Triterpenoids (asiatic acid, arjunolic acid and oleanolic acid), coumarins (scopoletin), and phenolic acid esters (salvianolic acid C) were reported from *S. aromaticum*. Oleanolic acid, has shown significant analgesic effects. The oleanolic acid activates the bile acid receptor (TGR5), which plays a key role in treating metabolic diseases. The acetyl derivatives of oleanolic acid have shown better anti-inflammatory activity than oleanolic acid (46).

Biological and pharmacological activities

Different parts of *S. aromaticum* and its essential oil have various pharmacological activities, including antioxidant,

TABLE 4 Amino acid composition in various parts of *S. aromaticum*.

Amino acid composition	Buds		Fruits	Branches	Leaves
	(mg/kg) (11)	(mg/kg) (12)	(mg/kg) (11)	(mg/kg) (11)	(mg/kg) (11)
Aspartic acid	111.6	42.8	105.4	–	–
Serine	69.8	80.5	41.5	57.9	37.9
Glutamic acid	93.8	91.3	74.1	64.2	66.4
Glycine	61.2	–	42.3	40.5	41.4
Histidine	121.6	–	118.8	121.2	120.6
Arginine	133.1	113.7	96.1	250.1	89.9
Threonine*	38.4	264.0	40.1	–	34.8
Alanine	94.5	–	93.8	52.3	55.2
Tyrosine	77.5	40.0	69.3	64.1	66.7
Valine*	65.9	106.1	50.2	45.7	44.9
Methionine*	63.3	14.1	62.8	–	–
Lysine*	68.9	–	68.5	68.2	66.8
Isoleucine*	59.8	16.8	53.1	–	–
Leucine*	61.8	27.7	56.8	–	–
Phenylalanine *	75.0	21.1	74.8	–	83.3
Proline	154.9	–	203.7	97.6	63.7
Tryptophan*	–	12.1	–	–	–
Total amino acid (TAA)	1 351.1	830.2	1 251.2	861.8	771.6
Essential amino acid (EAA) *	433.1	461.9	406.2	113.9	229.8

"–" indicates that the value is not available. *Indicates Essential amino acid.

TABLE 5 Vitamin composition of *S. aromaticum* buds.

Vitamins	Buds	
	(mg/100g) (12)	(mg/100g) (13)
A	177.21 ± 3.25	–
B_1	0.04 ± 0.01	–
B_2	1.75 ± 0.04	–
B_3	173.26 ± 2.33	–
B_6	134.18 ± 2.49	0.59
C	7.31 ± 0.34	80.8
E	7.11 ± 0.52	8.52
K	–	141.8

"–" indicates that the value is not available.

hypoglycemic, antitumor, antibacterial antiviral, etc. The majority of the pharmacological investigations were mainly focused on the flower buds (clove). The details were discussed in each of the following paragraphs, and are recapitulative summary was presented in Table 7.

Antioxidant activity

Clove essential oil (CEO) has shown powerful antioxidant activity with an EC_{50} of 0.36 μL/mL and it is the most potent volatile oil compared to eucalyptus, fennel and lavender (63). Phenols and flavonoids were attributed to antioxidant effects. The antioxidant activity is mediated via scavenging the free radicals, ferric reducing capacity, increasing the activity of antioxidant enzymes, and antagonizing lipid peroxidation (LPO).

Baghshahi et al. (64) showed that the antioxidant activity of clove extract (CE) was more than 10 times higher than that of vitamin E in the DPPH free radical scavenging capacity test. Reactive oxygen species (ROS) are oxygen-containing intermediate metabolites that modulate the host's immune response *in vivo* and positively affect the clearance of dead cells and the inactivation of microorganisms, but excessive amounts of ROS *in vivo* can damage the organism at the cellular level. Neutrophils are the most abundant leukocytes in humans, and their hyperactivation can activate the NADPH oxidase to generate large amounts of ROS. Eugenol inhibits fMLF or PMA-induced superoxide anion production in neutrophils by inhibiting the Raf/MEK/ERK1/2/p47phox phosphorylation pathway, avoiding ROS accumulation (47). CEO can increase the activity of antioxidant enzymes by inducing the expression of SOD-3 or GST-4 to reduce ROS accumulation *in vivo*, exerting antioxidant effects (65). Eugenol also has Fe^{3+} reducing ability and electron donor properties, which can neutralize free radicals by forming stable products to exert antioxidant effects (66).

10.3389/fnut.2022.1002147

TABLE 6 Composition of non-volatile components of different parts of *S. aromaticum*.

Classes	Chemical compound	Molecular formula	Extraction solvent	Biological activity	References
Flower buds					
Flavonoid glycosides	Rhamnetin-3-O-β-D-glucuronide	$C_{22}H_{20}O_{13}$	70% Ethanol, Ethyl acetate	Antitumor	(33)
	Rhamnazin-3-O-β-D-glucuronide	$C_{23}H_{22}O_{13}$	70% Ethanol, Ethyl acetate	Antitumor	(33)
	Rhamnazin-3-O-β-D-glucuronide-6′′-methyl ester	$C_{24}H_{24}O_{13}$	70% Ethanol, Ethyl acetate	Antitumor	(33)
	Rhamnocitrin-3-O-β-D-glucuronide-6′′-methyl ester	$C_{23}H_{22}O_{12}$	70% Ethanol, Ethyl acetate	Antitumor	(33)
	Quercetin-3-O-β-D-glucuronide	$C_{21}H_{18}O_{13}$	70% Ethanol, Ethyl acetate	Antitumor	(33)
	Isorham-netin-3-O-β-D-glucuronide	$C_{22}H_{20}O_{13}$	70% Ethanol, Ethyl acetate	Antitumor	(33)
	Kaempferol-3-O-β-D-glucuronide-6′′-methyl ester	$C_{22}H_{20}O_{12}$	70% Ethanol, Ethyl acetate	Antitumor	(33)
	Quercetin-3-O-β-D-glucuronide-6′′- methyl ester	$C_{22}H_{20}O_{13}$	70% Ethanol, Ethyl acetate	Antitumor	(33)
	Isorhamnetin-3-O-β-D-glucuronide-6′′-methyl ester	$C_{23}H_{22}O_{13}$	70% Ethanol, Ethyl acetate	Antitumor	(33)
	Kaempferol-3-O-β-D-glucoside	$C_{21}H_{20}O_{11}$	70% Ethanol, Ethyl acetate	Antitumor	(33)
	Quercetin3-O-β-D-glucoside	$C_{21}H_{20}O_{12}$	70% Ethanol, Ethyl acetate	Antitumor	(33)
	Isorhamnetin-3-O-β-D-glucoside	$C_{21}H_{22}O_{12}$	70% Ethanol, Ethyl acetate	Antitumor	(33)
	Rhamnazin-3-O-β-D-glucoside	$C_{23}H_{24}O_{11}$	70% Ethanol, Ethyl acetate	Antitumor	(33)
	Quercetin-7-O-β-D-glucoside	$C_{21}H_{20}O_{12}$	70% Ethanol, Ethyl acetate	Antitumor	(33)
	5,7-Dihydroxy-2-methylchromone 8-C-β-D-glucopyranoside	–	Methanol	Antibacterial	(34)
	4′-*O*-Methyl—epigallocatechin 7-*O*-glucuronide	$C_{22}H_{24}O_{13}$	70% Ethanol in Milli-Q water with 0.1% formic acid	Antioxidant	(35)
	3′-*O*-Methyl-(-)-epicatechin 7-*O*-glucuronide	$C_{22}H_{24}O_{12}$	70% Ethanol in Milli-Q water with 0.1% formic acid	Antioxidant	(35)
	Hesperetin 3′-*O*-glucuronide	$C_{22}H_{22}O_{12}$	70% Ethanol in Milli-Q water with 0.1% formic acid	Antioxidant	(35)
Flavonoids	Luteolin	$C_{15}H_{10}O_6$	70% Ethanol, Ethyl acetate	Antitumor, Neuroprotective	(33)
	Quercetin	$C_{15}H_{10}O_7$	70% Ethanol, Ethyl acetate	Antitumor, Antioxidant	(33)
	Rhamnocitrin	$C_{16}H_{12}O_6$	70% Ethanol, Ethyl acetate, Methanol	Antitumor, Antibacterial	(33, 34)
	Kumatakenin	$C_{17}H_{14}O_6$	70% Ethanol, Ethyl acetate	Antitumor	(33)
	Pachypodol	$C_{18}H_{16}O_7$	70% Ethanol, Ethyl acetate	Antitumor, Antibacterial	(33)

(*Continued*)

TABLE 6 (Continued)

Classes	Chemical compound	Molecular formula	Extraction solvent	Biological activity	References
	Kaempferol	$C_{15}H_{10}O_6$	Methanol	Antibacterial, Antitumor, Anti-inflammatory	(34)
	Myricetin	$C_{15}H_{10}O_8$	Methanol	Antibacterial, Antitumor, Antiviral	(34)
	Isorhamnetin	$C_{16}H_{12}O_7$	70% Ethanol in Milli-Q water with 0.1% formic acid	Antioxidant, Antitumor, Anti-inflammatory	(35)
	3′-Hydroxygenistein	$C_{15}H_{10}O_6$	70% Ethanol in Milli-Q water with 0.1% formic acid	Antioxidant	(35)
	4′-Methoxy-2′,3,7-trihydroxyisoflavanone	$C_{16}H_{14}O_6$	70% Ethanol in Milli-Q water with 0.1% formic acid	Antioxidant	(35)
	3′,4′,7-Trihydroxyisoflavanone	$C_{15}H_{12}O_5$	70% Ethanol in Milli-Q water with 0.1% formic acid	Antioxidant	(35)
	3′-Hydroxymelanettin	$C_{16}H_{12}O_6$	70% Ethanol in Milli-Q water with 0.1% formic acid	Antioxidant	(35)
	Violanone	$C_{17}H_{16}O_6$	70% Ethanol in Milli-Q water with 0.1% formic acid	Antioxidant	(35)
	2-Dehydro-*O*-desmethylangolensin	$C_{15}H_{12}O_4$	70% Ethanol in Milli-Q water with 0.1% formic acid	Antioxidant	(35)
	5-Hydroxy-4′-methoxy-6,7-methylenedioxy Isoflavone	$C_{17}H_{12}O_6$	Petroleum ether–Ethyl acetate	–	(36)
	5,4′-Dimethoxy-6,7-methylenedioxy Isoflavone	$C_{18}H_{14}O_6$	petroleum ether-Ethyl acetate	–	(36)
Chromones	Eugenin	$C_{11}H_{10}O_4$	Ethyl acetate soluble fraction of the Methanol	Anticholinesterase	(37)
Chromone glycosides	8-C-glucosylnoreugenin	$C_{16}H_{18}O_9$	Ethyl acetate soluble fraction of the Methanol	Anticholinesterase	(37)
	Biflorin	$C_{16}H_{18}O_9$	Methanol, Ethyl acetate	Anti-inflammatory, Antiviral, Antitumor	(38, 39)
	Isobiflorin	$C_{16}H_{18}O_9$	Methanol, Ethyl acetate	Anti-inflammatory, Antiviral, Antitumor	(38, 39)
Tannins	Gallic acid	$C_7H_6O_5$	Methanol, Ethyl acetate soluble fraction of the Methanol	Antibacterial, Anticholinesterase	(34, 37, 40)
	Ellagic acid	$C_{14}H_6O_8$	Methanol	Antibacterial, Antioxidant	(34)
	Gallic acid 4-*O*-glucoside	$C_{13}H_{16}O_{10}$	70% Ethanol in Milli-Q water with 0.1% formic acid	Antioxidant	(35)
	Paeoniflorin	$C_{23}H_{28}O_{11}$	70% Ethanol in Milli-Q water with 0.1% formic acid	Antioxidant, Anti-inflammatory, Immunoregulatory, Neuroprotective	(35)
	3-*p*-Coumaroylquinic acid	$C_{16}H_{18}O_8$	70% Ethanol in Milli-Q water with 0.1% formic acid	Antioxidant	(35)
	Eugeniin	$C_{41}H_{30}O_{26}$	Methanol, Ethyl acetate	Antiviral	(39)
	Casuarictin	$C_{41}H_{28}O_{26}$	Methanol, Ethyl acetate, 70% Acetone	Antiviral, Antifungal	(39, 40)

(*Continued*)

TABLE 6 (Continued)

Classes	Chemical compound	Molecular formula	Extraction solvent	Biological activity	References
	1,3-Di-O-galloyl-4,6-(S)-hexahydroxy-diphenoyl-β-D-glucopyranose	$C_{33}H_{23}O_{22}$	Methanol, Ethyl acetate	Antiviral	(39)
	Tellimagrandin I	$C_{33}H_{23}O_{22}$	Methanol, Ethyl acetate	antiviral	(39)
	1,2-Di-O-galloyl-3-O-digalloyl-4,6-O-(S)-hexahydroxydiphenoy-β-D-glucose	$C_{34}H_{20}O_{22}$	Methanol, Ethanol, 70% Acetone	Antifungal	(40)
	Tellimagrandin II	$C_{41}H_{30}O_{26}$	Methanol, Ethanol, 70% Acetone	Antifungal	(40)
	Aromatinin A	$C_{48}H_{32}O_{30}$	Methanol, Ethanol, 70% Acetone	Antifungal	(40)
	Syzyginin A	$C_{48}H_{34}O_{31}$	Methanol, Ethanol, 70% Acetone	Antifungal	(40)
	Bicornin	$C_{48}H_{32}O_{30}$	Methanol, Ethanol, 70% Acetone	Antifungal	(40)
	Platycaryanin A	$C_{48}H_{32}O_{31}$	Methanol, Ethanol, 70% Acetone	Antifungal, Anti-inflammatory	(40)
	Alunusnin A	$C_{47}H_{25}O_{30}$	Methanol, Ethanol, 70% Acetone	Antifungal	(40)
	Rugosin C	$C_{47}H_{32}O_{30}$	Methanol, Ethanol, 70% Acetone	Antifungal	(40)
	1,2,3-Tri-O-galloyl-β-D-glucose	$C_{24}H_{37}O_{24}$	Methanol, Ethanol, 70% Acetone	Antifungal	(40)
	1,2,3,6-Tetra-O-galloyl-β-D-glucose	$C_{30}H_{47}O_{12}$	Methanol, Ethanol, 70% Acetone	Antifungal	(40)
	Heterophylliin D	$C_{82}H_{54}O_{52}$	Methanol, Ethanol, 70% Acetone	Antifungal	(40)
	Rugosin D	$C_{82}H_{58}O_{52}$	Methanol, Ethanol, 70% Acetone	Antifungal	(40)
	Rugosin F	$C_{82}H_{56}O_{5}$	Methanol, Ethanol, 70% Acetone	Antifungal	(40)
	Euprostin A	$C_{54}H_{29}O_{34}$	Methanol, Ethanol, 70% Acetone	Antifungal	(40)
	Alienanin B	$C_{72}H_{52}O_{51}$	Methanol, Ethanol, 70% Acetone	Antifungal	(40)
	Squarrosanin A	$C_{55}H_{32}O_{33}$	Methanol, Ethanol, 70% Acetone	Antifungal	(40)
	Casuarinin	$C_{41}H_{28}O_{26}$	Methanol, Ethanol, 70% Acetone	Antioxidant, Antifungal, Antitumor	(40)

(*Continued*)

TABLE 6 (Continued)

Classes	Chemical compound	Molecular formula	Extraction solvent	Biological activity	References
Triterpenoids	Oleanolic acid	$C_{30}H_{48}O_3$	Methanol	Antibacterial	(34)
	Asiatic Acid	$C_{30}H_{48}O_5$	Dichloromethane–Methanol	Antioxidant, Antitumor	(36)
	Arjunolic Acid	$C_{30}H_{48}O_5$	Dichloromethane–Methanol	Antioxidant, Antifungal, Antibacterial, Anticholinesterase, Antitumor	(36)
Coumarins	Scopoletin	$C_{10}H_8O_4$	70% Ethanol in Milli-Q water with 0.1% formic acid	Antioxidant, Antitumor	(35)
Phenolic acid esters	Salvianolic acid C	$C_{26}H_{20}O_{10}$	70% Ethanol in Milli-Q water with 0.1% formic acid	Antioxidant, Anti-inflammatory, Antitumor	(35)
Others	2,6-Dihydroxy-4-methoxyacetophenone 3-C-β-D-glucoside	$C_{15}H_{19}O_9$	Ethyl acetate soluble fraction of the Methanol	Anticholinesterase	(37)
	2,6-Dihydroxy-4-methoxyacetophenone 3-C-β-D-(6′-O-galloyl) glucoside	$C_{22}H_{23}O_{13}$	Ethyl acetate soluble fraction of the Methanol	Anticholinesterase	(37)
Seeds					
Flavonoid glycosides	Apigenin 6-C-[β-D-xylopyranosyl-(1→2″)-β-D-galactopyranoside]-7-O-β-D-glucopyranoside	$C_{32}H_{38}O_{19}$	Ethanol	–	(41)
	Apigenin 6-C-[β-D-xylopyranosyl-(1→2″)-β-D-galactopyranoside]-7-O-β-D-(6‴-O-p-coumarylglucopyranoside)	$C_{41}H_{44}O_{21}$	Ethanol	–	(41)

"–" indicates that the item is not retrieved.

One of the common oxidative reactions, LPO, is associated with many diseases. DNA damage caused by ROS is a key factor in tumorigenesis and development. Eugenol can effectively block hydroxyl radical-induced DNA oxidation and LPO and has a significantly higher inhibitory effect on hydrogen peroxide than other reactive oxygen species (67). CEO also inhibits LPO in erythrocyte membranes, thereby increasing membrane resistance to spontaneous hemolysis, reducing membrane microviscosity, maintaining its structural integrity and functional activity, and significantly decreasing the intensity of LPO in mouse liver and brain, scavenging excess ROS and other free radicals from lipid chains, increasing the antioxidant capacity of liver and brain lipids and the activity of antioxidant enzymes in the liver (68). CE also significantly prevented oxidation-induced protein damage by reducing the formation of protein carbonyl groups and preventing the loss of protein sulfhydryl groups (48).

In conclusion, *S. aromaticum* can reduce free radical accumulation *in vivo*, decrease oxidative cellular damage, and increase antioxidant capacity (**Figure 3**). Thus, it has very high potential to be used as a natural antioxidant and anti-aging supplement.

Hypoglycemic activity

Abnormal glucose metabolism leads to complications of various metabolic diseases, especially the prevalence of diabetes is increasing worldwide, but commonly used oral hypoglycemic drugs often cause serious side effects. So herbs and spices have been used in folk medicine for centuries to control the complications of diabetes. *S. aromaticum* has been widely studied for its beneficial and toxic effects. CE has shown comparable hypoglycemic effects to that of insulin in animal models and did not show toxic effects (69).

Abdulrazak et al. (51) found a significant increase in insulin and leptin levels in type 2 diabetic rabbits treated with 12.5% clove for 6 weeks suggesting its potential to use for patients with diabetes. Some studies have shown that CE and its compound nigricin enhance proximal insulin signaling by decreasing serine phosphorylation of insulin receptor substrate-1 (IRS-1),

TABLE 7 The biological effects of *S. aromaticum*.

Biological effects	Part	Extract/ Compound	Assay	Model and effective concentrations	Reference
Antioxidant activity	Buds, Flower, Seeds, Leaves	Eugenol	ABTS, DPPH, SDS-PAGE and Western blotting analysis	Neutrophils (IC_{50}: 5 μg/mL)	(47)
	Buds	Aqueous extract	DPPH, TEAC, FRAP, ORAC, HRSA, SRSA	IC_{50}: 0.29 ± 0.01 mg/ml	(48)
	Leaves	70% Ethanol extract	Spot assay, Mitochondrial, ROS Levels	Yeast Schizosaccharomyces pombe cell (100 ppm)	(49)
Hypoglycemic activity	Buds	50% Aqueous EtOH extract	Blood glucose, HbA1c levels	db/db Mouse (IC_{50}: 4.7 μM)	(50)
	Buds	-	Blood glucose, Serum insulin, Insulin receptor and Leptin levels	Male rabbits [12.5% (w/w)]	(51)
Antitumor activity	Buds	Ethyl acetate extract	Western blot and (qRT)-PCR analysis	HT-29 tumor xenograft model (IC_{50}: 66 ± 8 μg/ml)	(52)
	Buds	Methanolic extract	Sulforhodamine-B assay	Uterine cervix (GI_{50}: 36 μg/ml), Breast (GI_{50}: 50 μg/ml), Lung NCI (GI_{50}: 68 μg/ml)	(53)
Antibacterial activity	Leaves	Steam distillation method	Time-kill curve assay, Scanning electron microscopy assay	Porphyromonas gingiva (MIC: 6.25 μM)	(54)
	Seeds	Aqueous extract	Dilution method (agar), Time-kill assay	Escherichia coli, Pseudomonas aeruginosa and Staphylococcus aureus (MIC: 0.06 mg/mL, MBC:0.10 mg/mL)	(55)
	Buds	Steam distillation method	Disk diffusion method, Broth microdilution method, Scanning electron microscopy	Escherichia coli and Klebsiella pneumoniae [MIC: 0.078% (v/v)]	(56)
Immunomodulatory, anti-inflammatory, and analgesic activities	Buds	Steam distillation method	Enzyme-linked immunosorbent assay, Sulforhodamine B	Human dermal fibroblast system HDF3CGF [0.011% (v/v)]	(57)
	Buds	Alcoholic extraction and distilled water	MTT, Enzyme-linked immunosorbent assay	Female inbred Balb/c mice (100 μg mL and 1000 μg/mL)	(58)
Neuroprotective activity	Buds, Flower, Seeds, Leaves	Eugenol	Y maze alternation, Novel Object Recognition, Morris Water Maze, FD Rapid Golgi StainingTM, Hematoxylin-Eosin staining	Male Deutchland Denken Yonken mice (100 mg/kg bw)	(59)
Antiviral activity	Buds, Flower, Seeds, Leaves	Eugenol	Medium and high-throughput screens, Hoechst stains, MTT	Ebola virus (EC_{50}: 1.3 μM)	(60)
	Buds	95% Ethanol	Plaque reduction assay	Herpes simplex virus type 1 (ED_{50}: 72.8 μg/mL), Herpes simplex virus type 2 (ED_{50}: 74.4 μg/mL)	(61)
Antiobesity activity	Buds	70% Ethanol	Body weight, Hematoxylin and eosin stain, Western blotting	Male C57BL/6J mice [0.5% (w/w)]	(62)

increasing tyrosine phosphorylation, modifying distal insulin signaling by enhancing protein kinase B (PKB) and glycogen synthase kinase-3-β (GSK-3β) phosphorylation in muscle cells signaling. Thus, they decrease free fatty acid-mediated insulin resistance in mouse myogenic cells, increase glucose uptake, and promote insulin secretion in muscle cells (70).

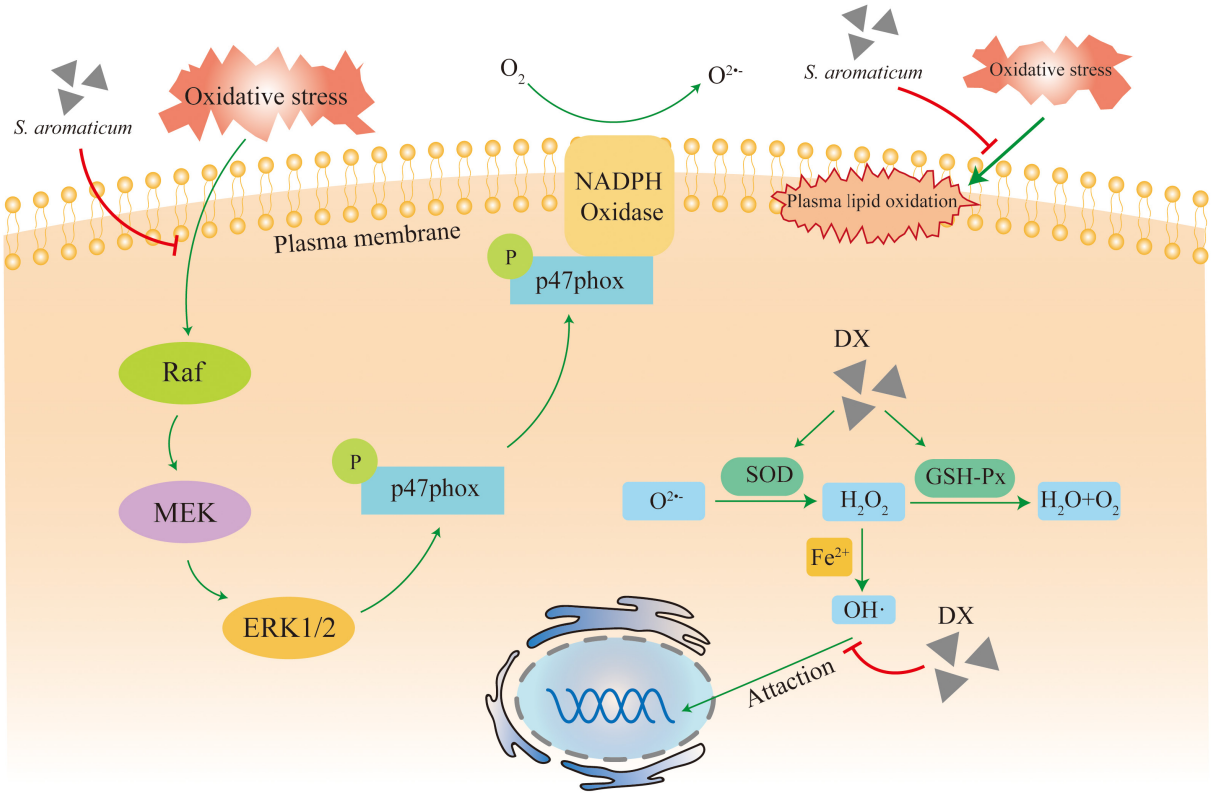

FIGURE 3
Mechanism of action for the antioxidant activity.

Glycogen metabolism has been one of the main causes of elevated blood glucose levels. Glycogen phosphorylase b (PYGB), a key enzyme in glycogen degradation, catalyzes the breakdown of glycogen to glucose-1-phosphate in the liver and skeletal muscle. Therefore, inhibition of hepatic glycogen phosphorylase is an effective therapeutic strategy to reduce hyperglycemia in type 2 diabetes. The clove's 50% aqueous ethanol extract showed strong dose-dependent inhibitory activity on glycogen phosphorylase b and glucagon-stimulated gluconeogenesis in primary rat hepatocytes, significantly suppressed blood glucose and glycated hemoglobin (HbA1c) levels in db/db mice. Thus, it caused a significant reduction in plasma triglyceride and non-esterified fatty acid levels, and improved glucose and lipid metabolism (50). In addition, the dehydrodienol and dehydrodienol B compounds of clove ethanol extracts (ECE) have potent human peroxisome proliferator-activated receptor (PPAR)-γ ligand binding activity, which can stimulate 3T3-L1 preadipocyte differentiation through PPAR-γ activation and significantly inhibit the increase in blood glucose levels in type 2 diabetic KK-Ay mice (71). Studies on the effects of C2C12 cardiomyocyte metabolism revealed that CE increased the phosphorylation of AMP-activated protein kinase (AMPK) and its substrate acetyl coenzyme A carboxylase (ACC), and also transcriptionally regulated genes involved in metabolism, including sirtuin1 (SIRT1) and PPARγ coactivator 1α (PGC1α), as a way to increase muscle glycolysis and mitochondrial function (69).

Overall, *S. aromaticum* has the potential to exert type 2 diabetes through phosphorylation pathways that modify insulin signaling, activation of receptor PPAR-γ ligand binding activity, and activation of AMPK and SIRT1 pathways (**Figure 4**).

Antitumor activity

Tumor pathogenesis is complex, and impaired apoptosis mechanism is a major cause. So selective induction of apoptosis in tumor cells is one of the effective ways to treat tumors. *S. aromaticum* has anticancer and antitumor activity on the human colon, breast, liver, cervical, and gastric cancers. Its inhibitory effects are time- and dose-dependent. Arung et al. (72) found that CEO inhibited melanin in B16 melanoma cells up to 50% and 80% at 100 and 200 μg/mL, respectively. Ethyl acetate extract of clove and its active ingredient oleanolic acid both selectively increased the protein expression of p21(WAF1/Cip1) and γ-H2AX and downregulated the expression of cell cycle regulatory proteins, promoted G_0/G_1 cell cycle arrest and induced apoptosis in a dose-dependent

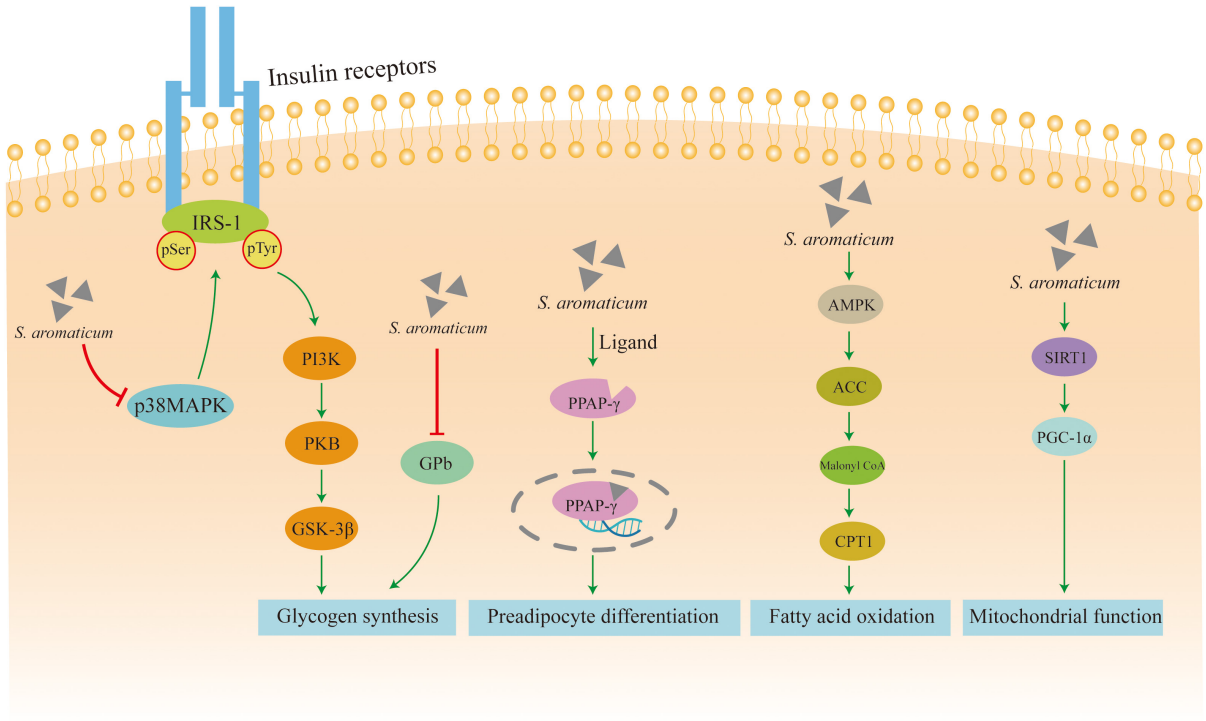

FIGURE 4
Mechanism of action for the hypoglycemic activity.

manner. Its activity on colon tumor xenografts is superior to the chemotherapeutic drug 5-fluorouracil (52). PI3K/Akt/mTOR signaling pathway is an important pathway that regulates apoptosis and can be aberrantly activated by malignant tumor cells to exert apoptosis-inhibiting and proliferation-promoting effects in tumor cells. The active ingredients of clove inhibit PI3K/Akt/mTOR signaling pathway and activate the caspase-mediated cascade response to induce apoptosis of HCT116 cells in a dose-dependent manner (73).

Bcl-2 family proteins play a key role in apoptosis and play an important role in mitochondrial-mediated apoptosis by regulating mitochondrial outer membrane permeability. The study has shown that CE can induce endogenous caspase-dependent cell death by increasing oxidative stress mediated via oxygen and nitrogen radicals. It can mediate the release of Bcl-2 family protein pro-apoptotic factors, signaling oxidative stress-mediated DNA damage by modulating the cellular antioxidant SOD system and the activity of the Akt, p38mitogen-activated protein kinases (p38MAPK), c-Jun N-terminal kinase (JNK) and extracellular signal-regulated kinases (Erk1/2) pathways to induce apoptosis in human breast cancer MCF-7 cells (74). The aqueous extract of clove (ACE) upregulated the expression of pro-apoptotic proteins p53 and Bax in benzo[a]pyrene (BP)-induced lung carcinogenesis in mice. It downregulated the expression of anti-apoptotic protein Bcl-2 in the pre-cancerous stage. In the early stage of carcinogenesis (week 8), clove significantly activated the expression of caspase-3. In addition, clove downregulated the expression of COX-2, cMyc, HRA and other growth-promoting proteins expression. All these together promote a significant decrease in proliferating cells and an increase in apoptotic cells, exerting a chemopreventive potential (75). In addition, eugenol can also exert its chemotherapeutic potential by blocking the nuclear translocation of β-catenin, thus promoting its cytoplasmic degradation through N-terminal phosphorylation of Ser37. Thus, it effectively reduces cancer complications and prolongs and improves patient life (76).

In conclusion, the main pathway of *S. aromaticum* to induce apoptosis in cancer cells by upregulating the expression of intracellular pro-apoptotic proteins such as Bax, Caspase-3, p53, etc., downregulating the expression of intracellular anti-apoptotic proteins such as Bcl-2, and downregulating the expression of pro-growth proteins such as COX-2, cMyc, and HRA (**Figure 5**).

Antibacterial activity

In recent years, the irrational application of broad-spectrum antibacterial drugs, immunosuppressive drugs, antitumor drugs and the widespread use of other surgical interventions such as organ transplantation have led to an increasingly serious crisis of bacterial and fungal drug resistance, which threatens the life

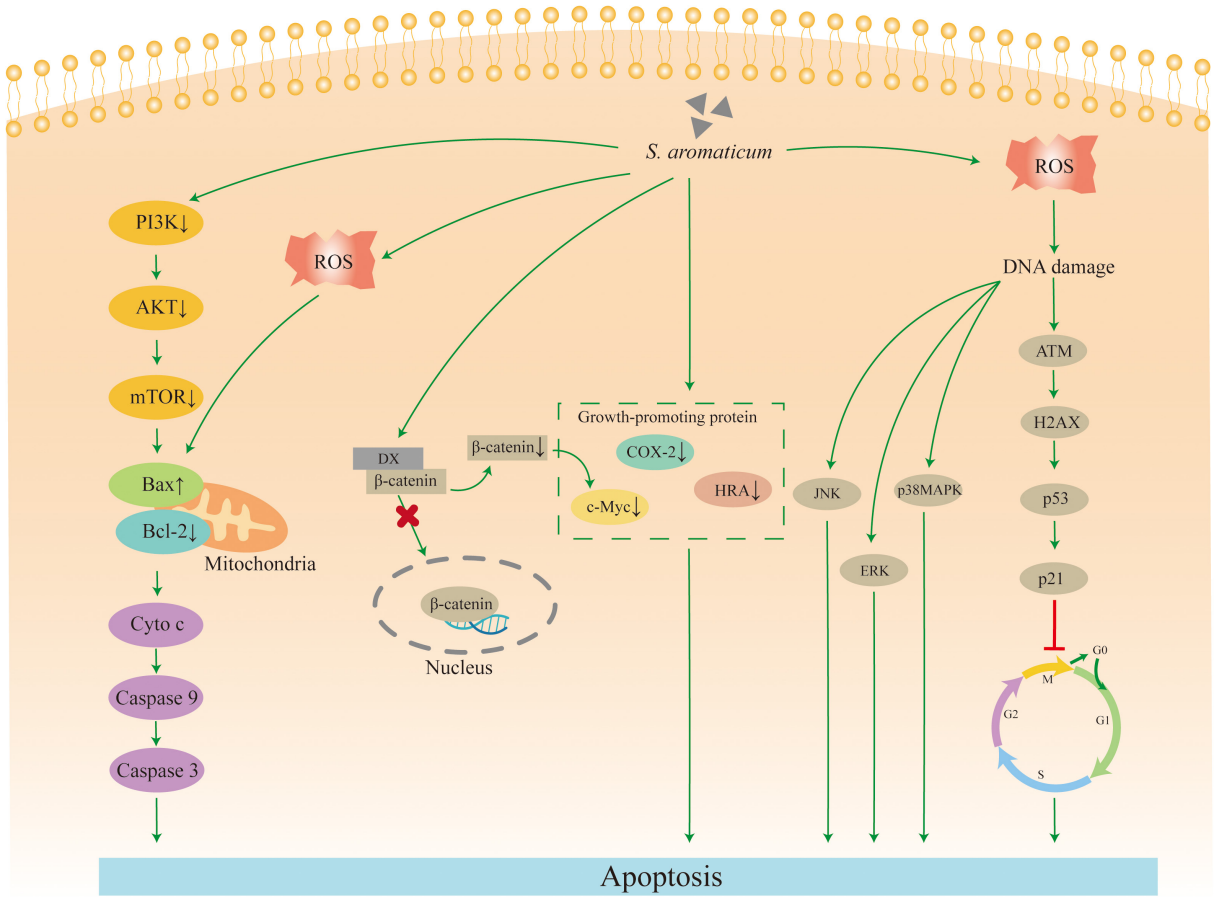

FIGURE 5
Mechanism of action for the antitumor activity.

and health of humans. Clove has strong antibacterial effects on *Staphylococcus aureus*, *Candida albicans*, *Escherichia coli* and *Listeria monocytogenes*.

It was found that ACE and ECE showed inhibitory activity against three foodborne pathogens, gram + ve *Staphylococcus aureus*, gram -ve *Escherichia coli* and *Pseudomonas aeruginosa*. *S. aureus* is the most sensitive to ACE (inhibition zone, 30.5 mm), *P. aeruginosa* is the most sensitive to ECE (inhibition zone, 38 mm). ACE inhibited the growth of *S. aureus* and *E. coli* at ≥500 μg/ml, *P. aeruginosa* at ≥700 μg/ml, respectively. ECE inhibited the growth of all three bacteria at ≥500 μg/ml (77). Similarly, Ajiboye et al. (55) found that aqueous extracts of clove seeds could enhance the membrane permeability of *Escherichia coli*, *Pseudomonas aeruginosa*, and *Staphylococcus aureus*, exerting antibacterial effects. In addition, four different CE (methanol, ethyl acetate, n-hexane and ether) showed inhibitory activity against *Candida albicans, Candida glabrata* and *Candida tropicalis*, with the ethyl acetate extract being the most active. CEO also antagonized *Candida biofilm* formation and effectively prevented the growth of *Candida* on abiotic surfaces (24). In addition, Zhang et al. (54) found that the eugenol in *S. aromaticum* leaf essential oil exhibited good antibacterial activity against *Porphyromonas gingivalis* at a concentration of 31.25 μ m.

Xu et al. (78) showed that the antibacterial activity of *S. aromaticum* is via disrupting the cell wall and membrane, inhibiting the normal synthesis of bacterial DNA and proteins, eugenol is the main component in the antibacterial activity. Quorum sensing (QS) is a communication system associated with the virulence of pathogenic bacteria such as *Pseudomonas aeruginosa*. The molecular modeling studies have shown that eugenol binds to the QS receptor overcoming the antibiotic resistance through hydrophobic interactions and hydrogen bonding to Arg61 and Tyr41 of the LasR receptor (79). Elastase A, elastase B, proteinase IV and alkaline proteases activate host matrix metalloproteinases (MMPs) to establish infection by converting pre-MMP-2 to active MMP-2. *S. aromaticum* leads to a significant reduction of signaling molecules (Acyl-homoserine lactones) involved in population-sensing regulation, which can inhibit the activity of four proteases from establishing anti-infective effects, in addition to inducing a dose-dependent production of neutrophil extracellular traps (NETs) to destroy

bacterial pathogens (80). CEO interferes with the expression of virulence-related genes involved in the flagellum, PEB1, PEB4, LPS and serine protease, with significant antibacterial and potentially virulence-modulating effects on *Campylobacter jejuni* (81). eEF1A protein interacted with several viral proteins, leading to enhanced viral replication, reduced apoptosis and increased cellular transformation; therefore, Wang et al. (82) suggested that downregulation of eEF1A protein expression may be another important mechanism for exerting its antifungal activity.

In conclusion, the permeability of phenolic substances such as eugenol to cell membranes and the irreversible disruption of plasma membrane integrity make *S. aromaticum* a potential source of natural antibacterial drugs with broad-spectrum antibacterial effects (**Figure 6**).

Immunomodulatory, anti-inflammatory, and analgesic activities

Clove essential oil (CEO) regulates the immune response and reduces inflammatory symptoms by enhancing humoral immunity and reducing the release of lymphokines to reduce cellular immunity. As a major component of *S. aromaticum*, eugenol is thought to regulate cellular inflammatory cascades in LPS induced inflammation in macrophages *via* (1) nuclear factor-κB (NF-κB) and ERK/MAPK pathways, (2) nitric oxide (NO) production, (3) pro-inflammatory interleukin release and (4) endogenous antioxidant defenses mechanisms (83). Secondly, CEO significantly inhibited the levels of several pro-inflammatory biomarkers such as (1) vascular cell adhesion molecule-1 (VCAM-1), (2) interferon γ-induced protein 10 (IP-10), (3) interferon-inducible T-cell α chemoattractant (I-TAC), and (4) monokine induced by γ interferon (MIG)-induced monokines (**Figure 7**). It also significantly inhibited (1) tissue remodeling protein molecules (collagen-I, collagen-III), (2) macrophage colony-stimulating factor (M-CSF), and (3) tissue inhibitor of metalloproteinase 2 (TIMP-2). It regulated the global gene expression and altered key signaling pathways of inflammation, tissue remodeling and cancer signaling processes (57). The water-soluble fraction of the hydroalcoholic extract of clove inhibited the production of pro-inflammatory cytokines (IL-1β and IL-6) by macrophages in BALB/c mice, thus exerting an anti-inflammatory effect (84). In addition, in an immunosuppressed mouse model, CEO (400 mg/kg) administration for one week significantly increased the total white blood cell (WBC) count. It and enhanced the delayed type hypersensitivity (DTH) in mice, restoring the cellular and humoral immune responses in a dose-dependent manner in cyclophosphamide immunosuppressed mice (85).

Ferland, Beaudry, and Vachon (86) showed eugenol (40 mg/kg) reduced substance P and CGRP, and increased the dynorphin level in a rat model of osteoarthritis. These results confirmed the therapeutic potential of eugenol in osteoarthritis. CEO also reduced the torsional movements in mice with acetic acid-induced abdominal contractions and significantly increased the latency of response to pain after 60 min by 82.3%. The CEO also inhibited the foot swelling in mice caused by carrageenan by 50.6%. It has significantly attenuated yeast-induced t hyperthermia by 2.7°C at ΔT-max (87).

Neuroprotective activity

Alzheimer's disease (AD) is a common neurodegenerative disease characterized by progressive cognitive dysfunction and memory loss, which has been increasing in recent years, seriously affecting patients' lives and quality of life. Oxidative stress plays a key role in AD, and CEO can reverse scopolamine-induced short- and long-term memory deficits by reducing oxidative stress (88). By administering CEO to intracerebroventricular (icv)-colchicine-induced cognitive dysfunction in rats, it was found that in addition to reducing oxidative stress damage, CEO exerted neuroprotective effects and improved cognitive dysfunction by improving mitochondrial dysfunction and inhibiting microglial activation (89). There are many links between SIRT1 and diseases such as AD. Studies have shown that ECE activates and increases SIRT1 level, inhibits NF-kB signaling in microglia, attenuates Aβ25-35-induced neuronal cell neurotoxicity, and also downregulates γ-secretase level, scavenges ROS and increases the percentage of antioxidant enzymes, which together delay the progression of neurodegenerative diseases and exert neuroprotective effects (90).

Glutamate is considered an excitatory neurotransmitter, but it causes oxidative stress at high concentrations and promotes apoptotic signaling cascades, leading to neurodegeneration. CE fermented with Trametes Versicolor (LTV), contains a higher content of dehydroeugenol. It inhibits apoptotic signaling such as Ca^{2+} inward flow, the excessive production of intracellular reactive oxygen species and LPO. It also has good protective properties against glutamate-induced toxicity in HT22 cells (91).

Rai et al. (92) reported that Sestrin2 (Sesn2) is a potential serum marker in Parkinson's disease (PD). The Sesn2 concentrations were significantly elevated in the serum of PD patients. ECE caused a dose-dependent downregulation of p53, Sesn2 and phosphorylated AMPK in cells, accompanied by the increased phosphorylated p70S6K, alleviating SH-SY5Y cell damage and exhibiting neuroprotective effects in PD. In addition, cloves exhibit anticholinesterase activity and are protective against brain damage induced by $CeCl_3$ and other substances (93).

In conclusion, *S. aromaticum* and its extracts exert neuroprotective effects by reducing acetylcholinesterase activity,

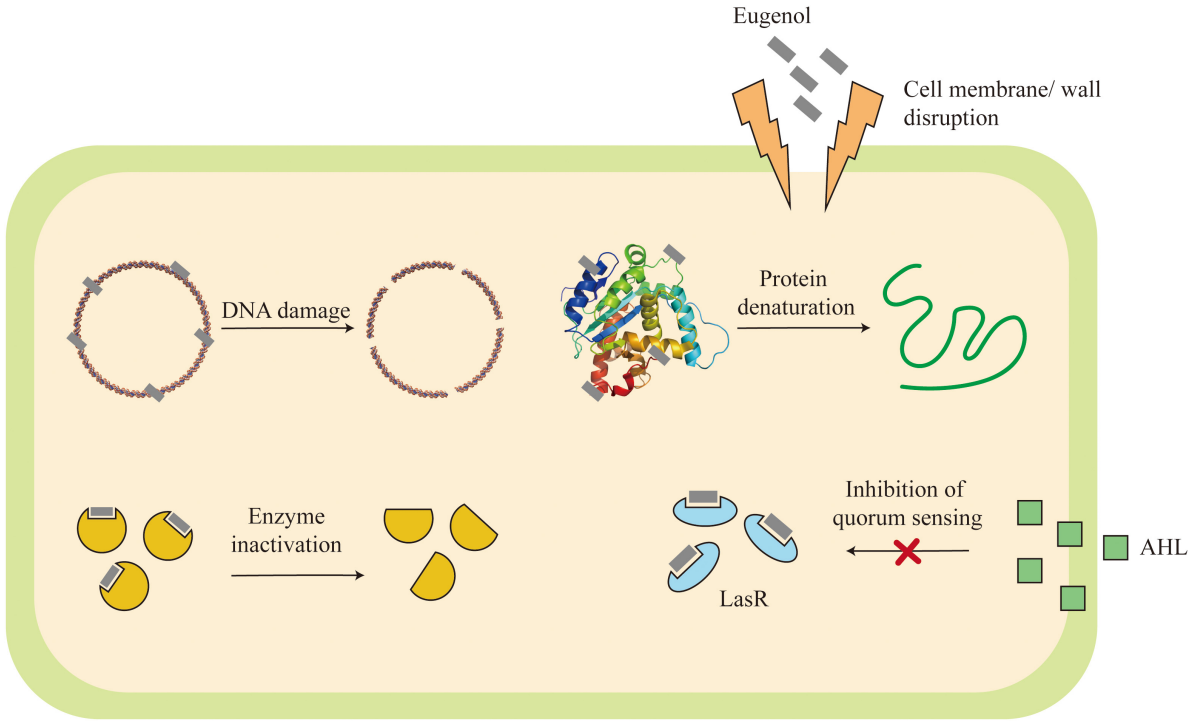

FIGURE 6
Mechanism of action for antibacterial activity.

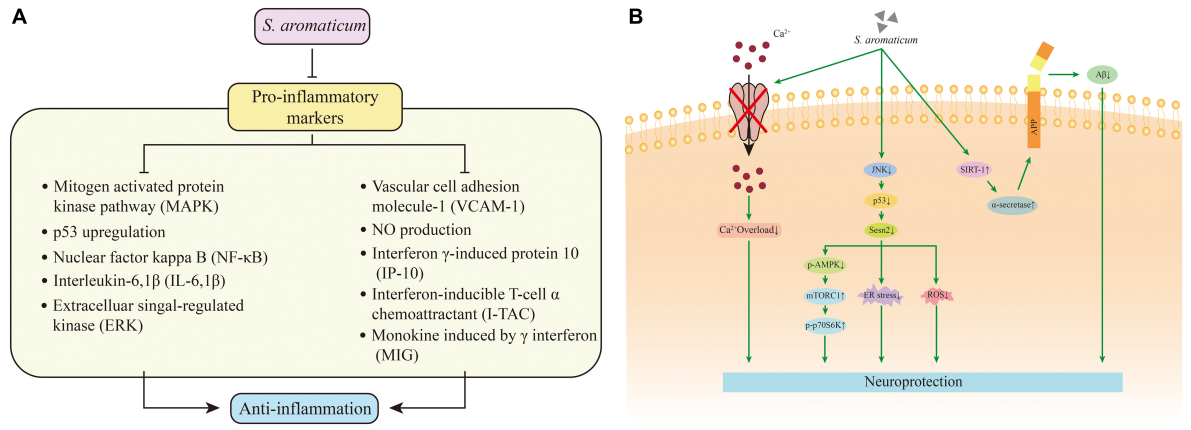

FIGURE 7
Mechanism of action for the immunomodulatory **(A)** and neuroprotective **(B)** activity.

restoring oxidative status, inhibiting microglia signaling and preventing histopathological changes (Figure 7).

Antiviral activity

Studies have shown that ACE exhibits antiviral activity similar to pure eugenol on feline calicivirus (94). The plaque reduction assay demonstrated that ECE has anti-herpes simplex virus (HSV) properties, showing direct inactivation of standard HSV particles, as well as significant inhibition of HSV-1, HSV-2, and a decrease in total HSV virus yield 30 h after treatment with the extract (61). The methanol and aqueous extracts of clove also showed inhibition of HCV protease. Eugenol inhibited influenza A virus (IAV), presumably by a mechanism attributed to the inhibition of oxidative stress and activation of ERK1/2, p38MAPK, and IKK/NF-κB pathways. Eugenol inhibits Beclin1-Bcl_2 heterodimer dissociation and autophagy,

ultimately impairing IAV replication (95). In addition, eugenol showed significant inhibitory of the West African Ebola virus (EBOV) (60). It is also used for the prevention and control of SARS-CoV-2-associated diseases. Flavonoids of *S. aromaticum* can inhibit SARS-CoV-2 virus expression, while bicornin and biflorin in clove have a high affinity for M^{pro} and exhibit potential viral inhibitory activity (96).

In summary, *S. aromaticum* exerts antiviral effects, mainly by improving oxidative stress, reducing viral replication, and inhibiting autophagic gene expression.

Anti-obesity activity

Fatty acid synthase (FAS), a key enzyme in adipogenesis, has been considered a potential therapeutic target for cancer and obesity. ECE as a FASN inhibitor can inhibit S-phase DNA replication in HepG2 cells. Adipocyte differentiation in OP9 cells, regulates the content of total triglyceride and low-density lipoprotein cholesterol, limits the development of high-fat diet-induced obesity, reduces body weight and abdominal adipose tissue weight, and reduces lipid accumulation in liver and epididymal adipose tissue, making it a potential therapeutic agent for obesity (97, 98). In addition, ECE also inhibited lipid accumulation in mice by downregulating the mRNA levels of transcription factors such as Srebp and Pparg and suppressing the expression of lipid metabolism-related proteins such as SREBP-1, FAS, CD36 and PPARγ in liver and white adipose tissue (62).

Others activities

In addition to the above effects, *S. aromaticum* also affects reproductive function, promoting transdermal absorption, and alleviating gastric injury. CE has a bidirectional effect on reproductive function in mice, with lower doses (15 mg/kg·BW) of clove increasing serum testosterone levels and testicular hydroxysteroid dehydrogenase activity, and improving sperm motility, sperm morphology, epididymal and seminal vesicle secretory activity, and the number of litters per female, but higher doses (30 and 60 mg/kg·BW) inhibiting testicular activity (99). Choi D et al. (100) hypothesized that the mechanism affects the reproductive endocrine system by acting on GnRH neuronal cells. ACE can treat ethanol-induced gastric mucosal injury in rats. The mechanism may involve antioxidant activity, promoting PGE2 production, and inhibiting gastric mucosal inflammatory cell infiltration and epithelial cell loss (101). CEO also has significant permeation-enhancing effects, and studies on the effects of CEO on the *in vivo* and *in vitro* transdermal administration of ibuprofen in rabbits revealed that clove significantly enhanced ibuprofen absorption *in vitro* and permeation *in vivo* (102). CEO can also be used for fish anesthesia, speculating that it may act through glutamate receptors.

Toxicity studies

The U.S. Food and Drug Administration (FDA) has confirmed the safety of clove buds, CEO, eugenol, and oleoresins as food additives. The World Health Organization (WHO) has established an acceptable daily intake of 2.5 mg/kg of CEO (6).

Some literature has reported cytotoxicity of eugenol, but it can rapidly reach peak plasma concentrations upon oral administration in rats and humans, with mean half-lives of 14.0 and 18.3 h, respectively, and is excreted in the urine in bound form within 24 h. Its genotoxicity and carcinogenicity are low (103). Acute toxicity studies in mice showed that LD_{50} of CEO is 4500 mg/kg upon oral administration for 24 h, which is a much higher dose than the doses usually used for infusions by humans (3 g/60 kg person in clinical therapy, equal to 9.35 mg/kg CEO). The long-term repeated toxicity studies (100, 200, and 400 mg/kg, orally) showed that only 400 mg/kg resulted in a significant decrease in body weight and no significant changes in relative organ weights and histopathological analysis were observed at all doses of CEO (104). Toxicity studies with clove buds polyphenol extract (Clovinol) in Wistar rats revealed no significant toxicity under acute (5 g/kg b.wt. for 14 days) and subchronic (0.25, 0.5 and 1 g/kg b.wt. for 90 days) conditions. The mutagenicity studies using *Salmonella typhimurium* strains revealed that Clovinol did not cause genetic mutations or shifts in the genome and showed significant mutagenic resistance against known mutagens, sodium azide, NPD, tobacco and 2-acetamidoflourene (105). In 2015, a panel of experts from the Association of Flavor and Extract Manufacturers initiated a re-evaluation of the safety of more than 250 natural flavor compounds (NFCs) and reported concluded that NFCs of clove was recognized as "Generally Recognized as Safe (GRAS)" under the conditions of their intended use as flavor ingredients (106). An acute oral toxicity study was conducted in normal rats according to the Organization for Economic Cooperation and Development (OECD) guidelines to assess the potential toxicity of *S. aromaticum* extracts after oral administration. Three animals per group were used in each step. Standard doses were given gradually, from 500 mg/kg b.w. continued up to 2500 mg/kg b.w. Mortality was recorded after 24 h. According to various acute and chronic toxicity studies of *S. aromaticum*, the oral LD_{50} of CEO in the food industry was 3597.5 mg/kg, with no adverse effects in subchronic toxicity tests and NAOEL levels of 900-2000 mg/kg/day. Oral LD_{50} of eugenol was reported as 2650–3000 mg/kg b.w. (105), all of which demonstrated the safety of *S. aromaticum* for human use at low doses.

Development and applications of *Syzygium aromaticum*

Folk medicine

As one of the traditional spices and herbs, clove has long been used to treat stomach disorders, abdominal pain, vomiting, etc. Many scientific studies have confirmed that clove possesses significant free radical scavenging and anti-inflammatory activities and has potential roles in alleviating and preventing diseases like cancer, type II diabetes and epilepsy. CEO also has a stomachic effect and can significantly improve the symptoms of loss of appetite (107). In addition, clove has long been used as a respiratory adjuvant in treating respiratory diseases such as cough, asthma, and bronchitis. It also plays an important role in preventing and early treatment of COVID-19 (108).

Because of its analgesic, anesthetic and anti-inflammatory properties, CEO is often used to treat dental diseases. The traditional treatment of toothache with CEO was first documented in 1640 in the French "practice of medicine." Modern studies have shown that brushing with herbal toothpaste containing clove resulted in a significant reduction in salivary lactate dehydrogenase (LDH), improved cellular integrity, and reduced plaque and gingivitis (109). That hexane extract of *S. aromaticum* seeds exhibits preferential growth inhibitory activity against cariogenic pathogens in dental caries and may be used to treat dental caries (110). In addition, CE may also present new natural therapeutic potential by inhibiting dentin erosion (111).

Nano technologies

In recent years, nanotechnology has rapidly evolved. A wide range of lipid nanostructures such as liposomes and solid lipid nanoparticles, metals, nanocrystals and polymeric particles have been tested in several drug delivery systems in different animal models. In addition, many nano-drug delivery systems containing *S. aromaticum* are being developed.

Metallic nanoparticles (NPs) have been widely used in cosmetics and medicine due to their unique antibacterial and antitumor properties. CE can be used as a reducing and stabilizing agent. CE-silver nanoparticles, synthesized by biosynthesis, showed good inhibitory activity against marine bacterial communities and *Nitzschia closterium* diatoms activity (112). Carboxymethyl cellulose structured silver-based nanocomposite (CMC-AgNPs) containing CE has shown antibacterial, *in vivo* anti-inflammatory, antileishmanial and antioxidant activities with low cytotoxicity (113). In addition, the synthesis of Au/Ag bimetallic nanoparticles by a single-step green route with CE significantly enhanced antioxidant and catalytic activity compared to individual monometallic nanoparticles (114).

Nano-encapsulation technology has been widely used in recent years. A study by Radün et al. (115) showed that the nano-encapsulated CEO had a strong antibacterial inhibitory capacity. CEO nanofibers formed by encapsulation in chitosan and polyethylene oxide polymers showed good antibacterial activity against *Staphylococcus aureus* and *Escherichia coli*, no cytotoxicity against humans fibroblast cell lines, and exhibited good wound healing potential (116). The retention of CEO in chitosan nanoparticles (ChNPs) was as high as 55.8-73.4%, and its antioxidant activity was significantly higher. Ashjazadeh et al. (117) also demonstrated that CE nanofibers showed the best granulation tissue by producing collagen and outperformed nanofibers such as nano zinc oxide in promoting wound healing in rats. Shetty et al. (118) found that ethosomal gel of the CEO was more effective in the treatment of cutaneous candidiasis than the pure CEO. In the croton oil-induced skin inflammation model in mice, it was found that nanofibers and nanoemulsions were more effective in the topical treatment of inflammation, and the efficacy of nanofibers was relatively higher than that of medicinal nanoemulsions (119). Plant essential oil is lipophilic, can easily cross cell membranes, and has greater anticancer efficacy potential. The CEO-based nanoemulsion system can increase drug retention time and improve bioavailability, making it a good candidate for cancer drug delivery systems. In addition, CEO nanoemulsions have greater potential in the food and agriculture industries. CEO-based nanoemulsions prepared by ultrasound using Tween 80 can be used as a natural delivery system to extend the shelf life of food products (120). The use of CEO-based nanoemulsions as green nanocarriers can significantly improve the solubility, bioavailability, and release of the pesticide Atrazine (ATZ). ATZ nanoemulsions also exhibited excellent herbicidal activity at low concentrations compared to commercial ATZ analogs (121).

Food storage

Syzygium aromaticum showed beneficial advantages in antibacterial and antifungal activity, aromaticity and safety, especially against a wide range of food-borne microorganisms, making it a potential and valuable preservative in the food industry. The antifungal activity of clove is superior to that of lemongrass and thyme essential oils to prevent the natural preservation growth of fungi on dried apricots (122). Ju et al. (123) confirmed by accelerated storage tests that the CEO can extend the shelf life of food bakery products by 2–4 days under normal packaging. Hasheminejad et al. (124) found that encapsulation of CEO by ChNPs was more effective in extending the shelf life of food than CEO alone, and in a pomegranate shelf life and quality study, CEO-ChNPs improved the antifungal

effect of CEO, effectively extending the shelf life by 54 days. Both CEO and CEO-based nanoemulsions inoculated into Talaga cheese were found to have significant inhibitory activity against foodborne pathogens such as *Listeria monocytogenes* and *Shigella flexneri*. Compared to CEO, CEO-based nanoemulsions significantly reduced the counts of inoculated pathogens from 8.2 to 1.5 $\log_{10}$cfu/g, showing greater antimicrobial effect (125). In addition, the addition of CEO to the structure of electrospun zein can better inhibit the growth of *Listeria monocytogenes* and *Escherichia coli*, effectively extending the shelf life of Iranian white cheese (126). The addition of clove powder to kimchi paste inhibited the growth of total aerobic and lactic acid bacteria, delayed the changes in O_2 and CO_2 concentrations and sugar and organic acid contents, and slowed down the decrease in pH, thus extending its shelf life (127). In addition, Eugenol-lean clove extracts can be used as a substitute for mustard flavoring in mayonnaise. They can improve its associated physical properties, giving it higher antioxidant activity and reducing capacity (128). Mixing the active ingredients in *S. aromaticum* into feeds has potential uses for improving meat quality, for example, adding *S. aromaticum* seeds to broiler chicken diets can significantly improve water retention, cooking loss percentage and tenderness of meat (129).

Insecticidal efficacy

Plant-based biopesticides have been proposed to be the best pest control tools compared to conventional synthetic molecules. Many plants' essential oils exhibit broad-spectrum insecticidal and repellent properties, are relatively non-toxic to mammals and fish and have gradually developed become potential alternatives to synthetic insecticides. *S. aromaticum* has been widely studied for its excellent insecticidal biological potential and higher safety for the environment and humans (130). The insecticidal potential of clove seed powder was evaluated by red palm weevil. It was found that *S. aromaticum* seeds powder at a dosage of 7 mg resulted in 100% mortality within three days (30). Terpenoids in *S. aromaticum* can reduce the respiratory rate of *Sitophilus granarius L.* exhibit a tropism effect, and prevent or delay the development of insecticide resistance (131). Viteri et al. (132) found that CEO had similar insecticidal activity to the synthetic pyrethroid insecticide deltamethrin, significantly affecting the oviposition of sublethally exposed *Callosobruchus maculatus* females and affecting their population growth. In addition, *S. aromaticum* showed high levels of repellency against fleas, aphids, nymphal instars, mites, mosquito species (Aedes aegypti, Anopheles gambiae, Culex quinquefasciatus etc.), termite and red imported fire ants etc. (133, 134). Toxicity assessment of clove powder, eugenol, eugenol acetate, and β-caryophyllene against red imported fire ants Solenopsis invicta Buren revealed that application of clove powder at 3 and 12 mg/cm^2 provided 100% ant mortality within 6 h and repelled 99% within 3 h. Compared to eugenol acetate, β-caryophyllene and CEO, eugenol was the compound with the fastest action against red imported fire ants. And with increasing application rates, the LT_{50} values of the chemical compounds inclined exponentially (135). The findings suggest that *S. aromaticum* has potential as a natural source of insecticides.

Other applications

While acetaldehyde is the main cytotoxin formed by alcohol metabolism and causes liver damage, extracellular matrix changes, inflammation, and hangover in heavy drinkers, clove polyphenol extract can accelerate the elimination of acetaldehyde from human blood, reduces hangover, and alleviates alcohol-related side effects (136). Clove has also been used worldwide as an anesthetic for various fish species, including several Amazon fish, Far Eastern catfish, small-sized tropical fish, and Pacific hagfish. Due to its better antioxidant effects, clove has also been used in recent years in studies on the role of skin barrier repair, where it activates the nuclear erythroid 2-related factor/antioxidant response element (Nrf2/ARE) signaling pathway to increase antioxidant activity. It significantly increases type I procollagen and elastin levels through TGF/Smad signaling and effectively ameliorates UVB-induced photoaging (137).

Conclusion and prospect

This paper review the nutritional composition, phytochemistry, pharmacological effects and application prospects of *S. aromaticum* by combining traditional literature with modern evidence. Eugenol is the main phytoconstituent of *S. aromaticum*, which is involved in almost all the pharmacological activities of *S. aromaticum* and has been extensively studied in recent years. *S. aromaticum* also has a variety of nutritional and other phytoconstituents, such as β-Caryophyllene, α-Humulene, sesquiterpene, flavonoids, etc. These compounds are responsible for the powerful antioxidant and antibacterial properties of *S. aromaticum*. Respectively, no in-depth studies were carried out on individual substances to explore their pharmacological effects and mechanisms.

The current research on *S. aromaticum* mainly focuses on the active ingredients of flower buds (clove). A large amount of literature has proved that the CE has various pharmacological activities, such as antioxidant, antibacterial, anti-inflammatory, antiviral, analgesic, neuroprotective, hypoglycemic, anticancer, etc. Clove has been widely used in food, medicine, and cosmetics. The other parts of *S. aromaticum* (seeds, leaves, etc.) also have similar active ingredients as those in flower buds.

However, no extensive studies were carried out on other parts of *S. aromaticum*. Thus, more research on other parts of the *S. aromaticum* and the compounds present is worth it.

In addition, although there is a large amount of pharmacological evidence in the literature that can lay the foundation for clinical studies on *S. aromaticum*, a search through the ClinicalTrials.gov and Chinese Clinical Trials Registry shows that there are still less than 30 registered clinical studies on *S. aromaticum*. These studies mainly focus on the effects of clove oil on pain and dental caries, as well as the clinical efficacy observation of Chinese medicine such as Dingxiang Shidi Decoction, Dingxiang Kaiwei Paste combined with other therapies. The results of the only clinical studies on *S. aromaticum* have proved that its biological activity is consistent with the results of preclinical studies. However, due to the small number and scope of clinical studies, it still cannot fully reflect the real clinical situation, and the clinical value of *S. aromaticum* has not been fully explored. Therefore, it is recommended that controlled clinical studies be conducted to understand more about the pharmacology, molecular mechanisms, and safety of *S. aromaticum*. In-depth studies on the bioactivity of the constituents, their structure-activity relationships and potential interactions (either synergistic or antagonistic) should be carried out.

In conclusion, *S. aromaticum* is an edible plant with various bioactive components and biological activities. It has a lot of opportunities for further development to improve its value and use in the food and pharmaceutical industries.

Author contributions

XL coordinated technical support and funding. PG performed data collection and coordinated technical support. QX and ZX performed the study and drafted the manuscript. SW and ZC revised the manuscript. All authors read and approved the final manuscript.

Funding

This work was financially supported by Department of Science & Technology of Shandong Province (China) (Nos. YDZX2021083 and 2019JZZY020906), and Shandong University of Traditional Chinese Medicine (China) (No. 2021-0033).

Conflict of interest

The authors declare that the research was conducted in the absence of any commercial or financial relationships that could be construed as a potential conflict of interest.

Publisher's note

Supplementary material

The Supplementary Material for this article can be found online at: https://www.frontiersin.org/articles/10.3389/fnut.2022.1002147/full#supplementary-material

References

1. Gooderham NJ, Cohen SM, Eisenbrand G, Fukushima S, Guengerich FP, Hecht SS, et al. The safety evaluation of food flavoring substances: the role of genotoxicity studies. *Crit Rev Toxicol.* (2020) 50:1–27. doi: 10.1080/10408444.2020.1712589

2. Mathot AG, Postollec F, Leguerinel I. Bacterial spores in spices and dried herbs: the risks for processed food. *Comprehens Rev Food Sci Food Safe.* (2020) 20:840–62. doi: 10.1111/1541-4337.12690

3. Guldiken B, Ozkan G, Catalkaya G, Ceylan FD, Ekin Yalcinkaya I, Capanoglu E. Phytochemicals of herbs and spices: health versus toxicological effects. *Food Chem Toxicol.* (2018) 119:37–49. doi: 10.1016/j.fct.2018.05.050

4. Batiha GES, Beshbishy AM, Tayebwa DS, Shaheen HM, Yokoyama N, Igarashi I. Inhibitory effects of *Syzygium aromaticum* and *Camellia* sinensis methanolic extracts on the growth of *Babesia* and *Theileria parasites*. *Ticks Tick-Borne Dis.* (2019) 10:949–58. doi: 10.1016/j.ttbdis.2019.04.016

5. Kamatou GP, Vermaak I, Viljoen AM. Eugenol—from the remote maluku islands to the international market place: a review of a remarkable and versatile molecule. *Molecules.* (2012) 17:6953–81. doi: 10.3390/molecules17066953

6. Cortés-Rojas DF, de Souza CRF, Oliveira WP. Clove (*Syzygium aromaticum*): a precious spice. *Asian Pacific J Trop Biomed.* (2014) 4:90–6. doi: 10.1016/s2221-1691(14)60215-x

7. Golmakani MT, Zare M, Razzaghi S. Eugenol enrichment of clove bud essential oil using different microwave-assisted distillation methods. *Food Sci Technol Res.* (2017) 23:385–94. doi: 10.3136/fstr.23.385

8. Tunç MT, Koca L. Ohmic heating assisted hydrodistillation of clove essential oil. *Indus Crops Prod.* (2019) 141:111763. doi: 10.1016/j.indcrop.2019.111763

9. Alfikri FN, Pujiarti R, Wibisono MG, Hardiyanto EB. Yield, quality, and antioxidant activity of clove (*Syzygium aromaticum*L.) bud oil at the different phenological stages in young and mature trees. *Scientifica.* (2020) 2020:9701701. doi: 10.1155/2020/9701701

10. Wei MC, Xiao J, Yang YC. Extraction of α-humulene-enriched oil from clove using ultrasound-assisted supercritical carbon dioxide extraction and studies of its fictitious solubility. *Food Chem.* (2016) 210:172–81. doi: 10.1016/j.foodchem.2016.04.076

11. Liu JG, Liu HP. Total nutrient analysis of various parts of *Eugenia caryophyllata*. *Biotic Res.* (2021) 43:357–62. doi: 10.14188/j.ajsh.2021.04.005

12. Ma SS. *Food safety standards and development of health food of clove*. Ph.D.thesis. China: Hainan University (2018).

13. Milind P, Deepa K. Clove: a champion spice. *Int J Res Ayurv Pharm.* (2011) 2:47–54.

14. Al-Jasass FM, Al-Jasser MS. Chemical composition and fatty acid content of some spices and herbs under Saudi Arabia conditions. *Sci World J.* (2012) 2012:859892. doi: 10.1100/2012/859892

15. Li YL, Liu ZS. Optimal extraction and fatty acid analysis of oil from syringa linn leaves. *Food Indus.* (2020) 41:80–2.

16. Brima EI, Siddeeg SM. Pilot study of trace elements in the infusion of medicinal plants used for diabetes treatment. *Int J Anal Chem.* (2022) 2022:3021396. doi: 10.1155/2022/3021396

17. Stark AH, Reifen R, Crawford MA. Past and present insights on alpha-linolenic acid and the omega-3 fatty acid family. *Crit Rev Food Sci Nutr.* (2016) 56:2261–7. doi: 10.1080/10408398.2013.828678

18. Marangoni F, Agostoni C, Borghi C, Catapano AL, Cena H, Ghiselli A, et al. Dietary linoleic acid and human health: focus on cardiovascular and cardiometabolic effects. *Atherosclerosis.* (2020) 292:90–8. doi: 10.1016/j.atherosclerosis.2019.11.018

19. Yang L, Guan G, Lei L, Lv Q, Liu S, Zhan X, et al. Palmitic acid induces human osteoblast-like Saos-2 cell apoptosis via endoplasmic reticulum stress and autophagy. *Cell Stress Chaperones.* (2018) 23:1283–94. doi: 10.1007/s12192-018-0936-8

20. Diyya ASM, Thomas NV. Multiple micronutrient supplementation: as a supportive therapy in the treatment of covid-19. *Biomed Res Int.* (2022) 2022:3323825. doi: 10.1155/2022/3323825

21. Chaieb K, Hajlaoui H, Zmantar T, Kahla-Nakbi AB, Rouabhia M, Mahdouani K, et al. The chemical composition and biological activity of clove essential oil,*Eugenia caryophyllata* (*Syzigium aromaticum* L. *Myrtaceae*): a short review. *Phytother Res.* (2007) 21:501–6. doi: 10.1002/ptr.2124

22. Al-Hashimi AG, Ammar AB, G L, Cacciola F, Lakhssassi N. Development of a millet starch edible film containing clove essential oil. *Foods.* (2020) 9:184. doi: 10.3390/foods9020184

23. Achar PN, Quyen P, Adukwu EC, Sharma A, Msimanga HZ, Nagaraja H, et al. Investigation of the antifungal and anti-aflatoxigenic potential of plant-based essential oils against aspergillus flavus in peanuts. *J Fungi.* (2020) 6:383. doi: 10.3390/jof6040383

24. Yassin MT, Mostafa AAF, Al-Askar AA. In vitro anticandidal potency of *Syzygium aromaticum* (clove) extracts against vaginal candidiasis. *BMC Complement Med Ther.* (2020) 20:25. doi: 10.1186/s12906-020-2818-8

25. Hemalatha R, Nivetha P, Mohanapriya C, Sharmila G, Muthukumaran C, Gopinath M. Phytochemical composition, GC-MS analysis, in vitro antioxidant and antibacterial potential of clove flower bud (*Eugenia caryophyllus*) methanolic extract. *J Food Sci Technol.* (2015) 53:1189–98. doi: 10.1007/s13197-015-2108-5

26. Muñoz Castellanos L, Amaya Olivas N, Ayala-Soto J, de la O Contreras CM, Zermeño Ortega M, Sandoval Salas F, et al. In vitro and in vivo antifungal activity of clove (*Eugenia caryophyllata*) and pepper (*Piper nigrum* L.) essential oils and functional extracts against *Fusarium oxysporum* and *Aspergillus niger* in tomato (*Solanum lycopersicum* L.). *Int J Microbiol.* (2020) 2020:1702037. doi: 10.1155/2020/1702037

27. El-Garawani IM, El-Nabi SH, Dawoud GT, Esmail SM, Abdel Moneim AE. Triggering of apoptosis and cell cycle arrest by fennel and clove oils in Caco-2 cells: the role of combination. *Toxicol Mechan Methods.* (2019) 29:710–22. doi: 10.1080/15376516.2019.1650149

28. Oboh G, Akinbola IA, Ademosun AO, Sanni DM, Odubanjo OV, Olasehinde TA, et al. Essential oil from clove bud (*Eugenia aromatica* Kuntze) inhibit key enzymes relevant to the management of type-2 diabetes and some pro-oxidant induced lipid peroxidation in rats pancreas in vitro. *J Oleo Sci.* (2015) 64:775–82. doi: 10.5650/jos.ess14274

29. Jirovetz L, Buchbauer G, Stoilova I, Stoyanova A, Krastanov A, Schmidt E. Chemical composition and antioxidant properties of clove leaf essential oil. *J Agric Food Chem.* (2006) 54:6303–7. doi: 10.1021/jf060608c

30. Al Dawsari Mona M. Insecticidal potential of cardamom and clove extracts on adult red palm weevil *Rhynchophorus ferrugineus*. *Saudi J Biol Sci.* (2020) 27:195–201. doi: 10.1016/j.sjbs.2019.07.009

31. Barboza JN, da Silva Maia Bezerra Filho C, Silva RO, Medeiros JVR, de Sousa DP. An overview on the anti-inflammatory potential and antioxidant profile of eugenol. *Oxid Med Cell Longev.* (2018) 2018:3957262. doi: 10.1155/2018/3957262

32. Tholl D. Biosynthesis and biological functions of terpenoids in plants. *Biotechnol Isopre.* (2015) 148:63–106. doi: 10.1007/10_2014_295

33. Ryu B, Kim HM, Lee JS, Lee CK, Sezirahiga J, Woo JH, et al. New flavonol glucuronides from the flower buds of *Syzygium aromaticum* (Clove). *J Agric Food Chem.* (2016) 64:3048–53. doi: 10.1021/acs.jafc.6b00337

34. Cai L, Wu CD. Compounds from *Syzygium aromaticum* possessing growth inhibitory activity against oral pathogens. *J Nat Prod.* (1996) 59:987–90. doi: 10.1021/np960451q

35. Ali A, Wu H, Ponnampalam EN, Cottrell JJ, Dunshea FR, Suleria HAR. Comprehensive profiling of most widely used spices for their phenolic compounds through LC-ESI-QTOF-MS2 and their antioxidant potential. *Antioxidants.* (2021) 10:721. doi: 10.3390/antiox10050721

36. Sara, Ali SN, Begum S, Siddiqui BS. Chemical constituents of *Syzygium aromaticum*. *Chem Nat Comp.* (2018) 54:1192–3. doi: 10.1007/s10600-018-2593-7

37. Han AR. Identification and PEP inhibitory activity of acetophenone glucosides from the clove buds (Syzygium aromaticum). *J Korean Soc Appl Biol Chem.* (2010) 53:847–51. doi: 10.3839/jksabc.2010.129

38. Lee HH, Shin JS, Lee WS, Ryu B, Jang DS, Lee KT. Biflorin, isolated from the flower buds of *Syzygium aromaticum* L., suppresses LPS-induced inflammatory mediators via STAT1 inactivation in macrophages and protects mice from endotoxin shock. *J Nat Prod.* (2016) 79:711–20. doi: 10.1021/acs.jnatprod.5b00609

39. Kim HJ, Lee JS, Woo ER, Kim MK, Yang BS, Yu YG, et al. Isolation of virus-cell fusion inhibitory components from *Eugenia caryophyllata*. *Planta Med.* (2001) 67:277–9. doi: 10.1055/s-2001-11993

40. Hatano T, Eerdunbayaer, Nozaki A, Takahashi E, Okamoto K, Ito H, et al. Hydrolysable tannins isolated from *Syzygium aromaticum*: structure of a new c-glucosidic ellagitannin and spectral features of tannins with a tergalloyl group. *Heterocycles.* (2012) 85:365. doi: 10.3987/com-11-12392

41. Nassar MI. Flavonoid triglycosides from the seeds of *Syzygium aromaticum*. *Carbohyd Res.* (2006) 341:160–3. doi: 10.1016/j.carres.2005.10.012

42. Zakaryan H, Arabyan E, Oo A, Zandi K. Flavonoids: promising natural compounds against viral infections. *Arch Virol.* (2017) 162:2539–51. doi: 10.1007/s00705-017-3417-y

43. Jeon SJ, Kim B, Ryu B, Kim E, Lee S, Jang DS, et al. Biflorin ameliorates memory impairments induced by cholinergic blockade in mice. *Biomol Ther.* (2017) 25:249–58. doi: 10.4062/biomolther.2016.058

44. Javed A, Hussain MB, Tahir A, Waheed M, Anwar A, Shariati MA, et al. Pharmacological applications of phlorotannins: a comprehensive review. *Curr Drug Disc Technol.* (2021) 18:282–92. doi: 10.2174/1570163817666200206110243

45. Jiang TA. Health benefits of culinary herbs and spices. *J AOAC Int.* (2019) 102:395–411. doi: 10.5740/jaoacint.18-0418

46. Ladurner A, Zehl M, Grienke U, Hofstadler C, Faur N, Pereira FC, et al. Allspice and clove as source of triterpene acids activating the G protein-coupled bile acid receptor TGR5. *Front Pharmacol.* (2017) 8:468. doi: 10.3389/fphar.2017.00468

47. Chniguir A, Pintard C, Liu D, Dang PMC, El-Benna J, Bachoual R. Eugenol prevents fMLF-induced superoxide anion production in human neutrophils by inhibiting ERK1/2 signaling pathway and p47phox phosphorylation. *Sci Rep.* (2019) 9:18540. doi: 10.1038/s41598-019-55043-8

48. Suantawee T, Wesarachanon K, Anantsuphasak K, Daenphetploy T, Thien-Ngern S, Thilavech T, et al. Protein glycation inhibitory activity and antioxidant capacity of clove extract. *J Food Sci Technol.* (2015) 52:3843–50. doi: 10.1007/s13197-014-1452-1

49. Fauzya AF, Astuti RI, Mubarik NR. Effect of ethanol-derived clove leaf extract on the oxidative stress response in yeast *Schizosaccharomyces pombe*. *Int J Microbiol.* (2019) 2019:2145378. doi: 10.1155/2019/2145378

50. Sanae F, Kamiyama O, Ikeda-Obatake K, Higashi Y, Asano N, Adachi I, et al. Effects of eugenol-reduced clove extract on glycogen phosphorylase b and the development of diabetes in db/db mice. *Food Funct.* (2014) 5:214–9. doi: 10.1039/c3fo60514k

51. Abdulrazak A, Tanko Y, Mohammed A, Mohammed KA, Sada NM, Dikko AA. Effects of clove and fermented ginger on blood glucose, leptin, insulin and insulin receptor levels in high fat dietinduced type 2 diabetic rabbits. *Nigerian J Physiol Sci.* (2018) 33:89–93.

52. Liu H, Schmitz JC, Wei J, Cao S, Beumer JH, Strychor S, et al. Clove extract inhibits tumor growth and promotes cell cycle arrest and apoptosis. *Oncol Res Featur Preclin Clin Cancer Ther.* (2014) 21:247–59. doi: 10.3727/096504014x13946388748910

53. Sara, Begum S, Ali SN, Farooq AD, Siddiqui F, Siddiqui BS, et al. Volatile constituents and in vitro activity of *Syzygium aromaticum* flower buds (clove) against human cancer cell lines. *Pak J Pharm Sci.* (2020) 33:2659–65.

54. Zhang Y, Wang Y, Zhu X, Cao P, Wei S, Lu Y. Antibacterial and antibiofilm activities of eugenol from essential oil of *Syzygium aromaticum* (L.)

Merr. & L. M. Perry (clove) leaf against periodontal pathogen Porphyromonas gingivalis. *Microb Pathog.* (2017) 113:396–402. doi: 10.1016/j.micpath.2017.10.054

55. Ajiboye TO, Mohammed AO, Bello SA, Yusuf II, Ibitoye OB, Muritala HF, et al. Antibacterial activity of *Syzygium aromaticum* seed: studies on oxidative stress biomarkers and membrane permeability. *Microb Pathog.* (2016) 95:208–15. doi: 10.1016/j.micpath.2016.03.011

56. Ginting EV, Retnaningrum E, Widiasih DA. Antibacterial activity of clove (*Syzygium aromaticum*) and cinnamon (*Cinnamomum burmannii*) essential oil against extended-spectrum β-lactamase-producing bacteria. *Vet World.* (2021) 14:2206–11. doi: 10.14202/vetworld.2021.2206-2211

57. Han X, Parker TL. Anti-inflammatory activity of clove (*Eugenia caryophyllata*) essential oil in human dermal fibroblasts. *Pharmac Biol.* (2017) 55:1619–22. doi: 10.1080/13880209.2017.1314513

58. Dibazar SP, Fateh S, Daneshmandi S. Clove (*Syzygium aromaticum*) ingredients affect lymphocyte subtypes expansion and cytokine profile responses: an in vitro evaluation. *J Food Drug Anal.* (2014) 22:448–54. doi: 10.1016/j.jfda.2014.04.005

59. Akbar L, Juliandi B, Boediono A, Batubara I, Subangkit M. Effects of eugenol on memory performance, neurogenesis, and dendritic complexity of neurons in mice analyzed by behavioral tests and golgi staining of brain tissue. *J Stem Cells Regen Med.* (2021) 17:35–41. doi: 10.46582/jsrm.1701005

60. Lane T, Anantpadma M, Freundlich JS, Davey RA, Madrid PB, Ekins S. The natural product eugenol is an inhibitor of the ebola virus in vitro. *Pharmac Res.* (2019) 36:104. doi: 10.1007/s11095-019-2629-0

61. Tragoolpua Y, Jatisatienr A. Anti-herpes simplex virus activities of *Eugenia* caryophyllus (Spreng.) Bullock & S. G. Harrison and essential oil, eugenol. *Phytother Res.* (2007) 21:1153–8. doi: 10.1002/ptr.2226

62. Jung CH, Ahn J, Jeon TI, Kim TW, Ha TY. Syzygium aromaticum ethanol extract reduces high-fat diet-induced obesity in mice through downregulation of adipogenic and lipogenic gene expression. *Exp Ther Med.* (2012) 4:409–14. doi: 10.3892/etm.2012.609

63. Vella FM, Calandrelli R, Cautela D, Fiume I, Pocsfalvi G, Laratta B. Chemometric screening of fourteen essential oils for their composition and biological properties. *Molecules.* (2020) 25:5126. doi: 10.3390/molecules25215126

64. Baghshahi H, Riasi A, Mahdavi A, Shirazi A. Antioxidant effects of clove bud (*Syzygium aromaticum*) extract used with different extenders on ram spermatozoa during cryopreservation. *Cryobiology.* (2014) 69:482–7. doi: 10.1016/j.cryobiol.2014.10.009

65. Zhang L, Gu B, Wang Y. Clove essential oil confers antioxidant activity and lifespan extension in C. Elegans via the DAF-16/FOXO transcription factor. *Comparat Biochem Physiol Part C.* (2021) 242:108938. doi: 10.1016/j.cbpc.2020.108938

66. Gülçin L. Antioxidant activity of eugenol: a structure–activity relationship study. *J Med Food.* (2011) 14:975–85. doi: 10.1089/jmf.2010.0197

67. Nam H, Kim MM. Eugenol with antioxidant activity inhibits MMP-9 related to metastasis in human fibrosarcoma cells. *Food Chem Toxicol.* (2013) 55:106–12. doi: 10.1016/j.fct.2012.12.050

68. Misharina TA, Fatkullina LD, Alinkina ES, Kozachenko AI, Nagler LG, Medvedeva IB, et al. Effects of low doses of essential oil on the antioxidant state of the erythrocytes, liver, and the brains of mice. *Прикладная Биохимия и Микробиология* (2014) 50:101–7. doi: 10.7868/s0555109914010097

69. Tu Z, Moss-Pierce T, Ford P, Jiang TA. *Syzygium aromaticum*L. (Clove) extract regulates energy metabolism in myocytes. *J Med Food.* (2014) 17:1003–10. doi: 10.1089/jmf.2013.0175

70. Ghaffar S, Afridi SK, Aftab MF, Murtaza M, Hafizur RM, Sara S, et al. Clove and its active compound attenuate free fatty acid-mediated insulin resistance in skeletal muscle cells and in mice. *J Med Food.* (2017) 20:335–44. doi: 10.1089/jmf.2016.3835

71. Kuroda M, Mimaki Y, Ohtomo T, Yamada J, Nishiyama T, Mae T, et al. Hypoglycemic effects of clove (*Syzygium aromaticum* flower buds) on genetically diabetic KK-Ay mice and identification of the active ingredients. *J Nat Med.* (2012) 66:394–9. doi: 10.1007/s11418-011-0593-z

72. Arung ET, Matsubara E, Kusuma IW, Sukaton E, Shimizu K, Kondo R. Inhibitory components from the buds of clove (*Syzygium aromaticum*) on melanin formation in B16 melanoma cells. *Fitoterapia.* (2011) 82:198–202. doi: 10.1016/j.fitote.2010.09.008

73. Zhao G, Zhang D, Yang XH, Li XF, Liu MH. [Inhibition effect of active fraction from clove on PI3K/Akt/mTOR signaling pathway to induce apoptosis of human colon cancer HCT116 cells]. *Zhongguo Zhong Yao Za Zhi.* (2021) 46:1197–204. doi: 10.19540/j.cnki.cjcmm.20201027.401

74. Kello M, Takac P, Kubatka P, Kuruc T, Petrova K, Mojzis J. Oxidative stress-induced DNA damage and apoptosis in clove buds-treated MCF-7 cells. *Biomolecules.* (2020) 10:139. doi: 10.3390/biom10010139

75. Banerjee S. Clove (*Syzygium aromaticum* L.), a potential chemopreventive agent for lung cancer. *Carcinogenesis.* (2006) 27:1645–54. doi: 10.1093/carcin/bgi372

76. Choudhury P, Barua A, Roy A, Pattanayak R, Bhattacharyya M, Saha P. Eugenol restricts Cancer stem cell population by degradation of β-catenin via N-terminal Ser37 phosphorylation-an in vivo and in vitro experimental evaluation. *Chemico-Biol Interact.* (2020) 316:108938. doi: 10.1016/j.cbi.2020.108938

77. Mostaqim S, Saha SK, Hani U, Paul SK, Sharmin M, Basak S, et al. Antibacterial activities of clove (*Syzygium aromaticum*) extracts against three food borne pathogens: *Staphylococcus aureus*, *Escherichia coli* and *Pseudomonas aeruginosa*. *Mymens Med J.* (2019) 28:779–91.

78. Xu JG, Liu T, Hu QP, Cao XM. Chemical composition, antibacterial properties and mechanism of action of essential oil from clove buds against *Staphylococcus aureus*. *Molecules.* (2016) 21:1194. doi: 10.3390/molecules21091194

79. H J, Omanakuttan A, Pandurangan N, Vargis SV, Maneesh M, Nair GB, et al. Clove bud oil reduces kynurenine and inhibits pqs A gene expression in P. aeruginosa. *Appl Microbiol Biotechnol.* (2016) 100:3681–92. doi: 10.1007/s00253-016-7313-2

80. Haripriyan J, Omanakuttan A, Menon ND, Vanuopadath M, Nair SS, Corriden R, et al. Clove bud oil modulates pathogenicity phenotypes of the opportunistic human pathogen *Pseudomonas aeruginosa*. *Sci Rep.* (2018) 8:3437. doi: 10.1038/s41598-018-19771-7

81. Kovács JK, Felsõ P, Makszin L, Pápai Z, Horváth G, Ábrahám H, et al. Antimicrobial and virulence-modulating effects of clove essential oil on the foodborne pathogen campylobacter jejuni. *Appl Environ Microbiol.* (2016) 82:6158–66. doi: 10.1128/aem.01221-16

82. Wang Y, Ding Y, Wang S, Chen H, Zhang H, Chen W, et al. Extract of *Syzygium aromaticum* suppress eEF1A protein expression and fungal growth. *J Appl Microbiol.* (2017) 123:80–91. doi: 10.1111/jam.13478

83. Bahramsoltani R, Rahimi R. An evaluation of traditional persian medicine for the management of SARS-CoV-2. *Front Pharmacol.* (2020) 11:571434. doi: 10.3389/fphar.2020.571434

84. Rodrigues T, Fernandes A, Sousa J, Bastos J, Sforcin J. In vitro and in vivo effects of clove on pro-inflammatory cytokines production by macrophages. *Nat Prod Res.* (2009) 23:319–26. doi: 10.1080/14786410802242679

85. Carrasco FR, Schmidt G, Romero AL, Sartoretto JL, Caparroz-Assef SM, Bersani-Amado CA, et al. Immunomodulatory activity of *Zingiber officinale* Roscoe, *Salvia officinalis* L. and *Syzygium aromaticum* L. essential oils: evidence for humor- and cell-mediated responses. *J Pharm Pharmacol.* (2009) 61:961–7. doi: 10.1211/jpp/61.07.0017

86. Ferland CE, Beaudry F, Vachon P. Antinociceptive effects of eugenol evaluated in a monoiodoacetate-induced osteoarthritis rat model. *Phytother Res.* (2012) 26:1278–85. doi: 10.1002/ptr.3725

87. Taher YA, Samud AM, El-Taher FE, ben-Hussin G, Elmezogi JS, Al-Mehdawi BF, et al. Experimental evaluation of anti-inflammatory, antinociceptive and antipyretic activities of clove oil in mice. *Libyan J Med.* (2015) 10:28685. doi: 10.3402/ljm.v10.28685

88. Halder S, Mehta A, Kar R, Mustafa M, Mediratta P, Sharma K. Clove oil reverses learning and memory deficits in scopolamine-treated mice. *Planta Med.* (2011) 77:830–4. doi: 10.1055/s-0030-1250605

89. Kumar A, Aggrawal A, Pottabathini R, Singh A. Possible neuroprotective mechanisms of clove oil against icv-colchicine induced cognitive dysfunction. *Pharmacol Rep.* (2016) 68:764–72. doi: 10.1016/j.pharep.2016.03.005

90. Shekhar S, Yadav Y, Singh AP, Pradhan R, Desai GR, Dey A, et al. Neuroprotection by ethanolic extract of *Syzygium aromaticum* in Alzheimer's disease like pathology via maintaining oxidative balance through SIRT1 pathway. *Exp Gerontol.* (2018) 110:277–83. doi: 10.1016/j.exger.2018.06.026

91. Lee HS, Yang EJ, Lee T, Song KS. Laccase fermentation of clove extract increases content of dehydrodieugenol, which has neuroprotective activity against glutamate toxicity in HT22 cells. *J Microbiol Biotechnol.* (2018) 28:246–54. doi: 10.4014/jmb.1709.09052

92. Rai N, Upadhyay AD, Goyal V, Dwivedi S, Dey AB, Dey S. Sestrin2 as serum protein marker and potential therapeutic target for Parkinson's disease. *J Gerontol A Biol Sci Med Sci.* (2020) 75:690–5. doi: 10.1093/gerona/glz234

93. Kadri Y, Nciri R, Bardaa S, Brahmi N, Saber S, Harrath AH, et al. *Syzygium Aromaticum* alleviates cerium chloride-induced neurotoxic effect in the adult mice. *Toxicol Mechan Methods.* (2019) 29:26–34. doi: 10.1080/15376516.2018.1506849

94. Aboubakr HA, Nauertz A, Luong NT, Agrawal S, El-Sohaimy SAA, Youssef MM, et al. In vitro antiviral activity of clove and ginger aqueous extracts against feline calicivirus, a surrogate for human norovirus. *J Food Protect.* (2016) 79:1001–12. doi: 10.4315/0362-028x.jfp-15-593

95. Dai JP, Zhao XF, Zeng J, Wan QY, Yang JC, Li WZ, et al. Drug screening for autophagy inhibitors based on the dissociation of Beclin1-Bcl2 complex using BiFC technique and mechanism of eugenol on anti-influenza a virus activity. *PLoS One.* (2013) 8:e61026. doi: 10.1371/journal.pone.0061026

96. Rehman MT, AlAjmi MF, Hussain A. Natural compounds as inhibitors of SARS-CoV-2 main protease (3CLpro): a molecular docking and simulation approach to combat covid-19. *Curr Pharmac Design.* (2021) 27:3577–89. doi: 10.2174/1381612826999201116195851

97. Ding Y, Gu Z, Wang Y, Wang S, Chen H, Zhang H, et al. Clove extract functions as a natural fatty acid synthesis inhibitor and prevents obesity in a mouse model. *Food Func.* (2017) 8:2847–56. doi: 10.1039/c7fo00096k

98. Pé,rez Gutiérrez RM, Arrioja MW. Rapid model to evaluate the anti-obesity potential of a combination of *Syzygium aromaticum* (Clove) and *Cuminun cyminum* (Cumin) on C57BL6/j mice fed high-fat diet. *J Visual Exp.* (2021) 173. doi: 10.3791/62087

99. Mishra RK, Singh SK. Biphasic effect of *Syzygium aromaticum* flower bud on reproductive physiology of male mice. *Andrologia.* (2016) 48:1011–20. doi: 10.1111/and.12533

100. Choi D, Roh HS, Kang DW, Lee JS. The potential regressive role of *Syzygium aromaticum* on the reproduction of male golden hamsters. *Dev Reprod.* (2014) 18:57–64. doi: 10.12717/dr.2014.18.1.057

101. Jin SE, Lee MY, Shin IS, Jeon WY, Ha H. *Syzygium aromaticum* water extract attenuates ethanol-induced gastric injury through antioxidant effects in rats. *Mol Med Rep.* (2016) 14:361–6. doi: 10.3892/mmr.2016.5269

102. Chen J, Jiang QD, Wu YM, Liu P, Yao JH, Lu Q, et al. Potential of essential oils as penetration enhancers for transdermal administration of ibuprofen to treat dysmenorrhoea. *Molecules.* (2015) 20:18219–36. doi: 10.3390/molecules201018219

103. Escobar-García M, Rodríguez-Contreras K, Ruiz-Rodríguez S, Pierdant-Pérez M, Cerda-Cristerna B, Pozos-Guillén A. Eugenol toxicity in human dental pulp fibroblasts of primary teeth. *J Clin Pediatr Dentist.* (2016) 40:312–8. doi: 10.17796/1053-4628-40.4.312

104. Liu BB, Luo L, Liu XL, Geng D, Li CF, Chen SM, et al. Essential oil of *Syzygium aromaticum* reverses the deficits of stress-induced behaviors and hippocampal p-ERK/p-CREB/brain-derived neurotrophic factor expression. *Planta Med.* (2015) 81:185–92. doi: 10.1055/s-0034-1396150

105. Vijayasteltar L, Nair GG, Maliakel B, Kuttan R, Krishnakumar IM. Safety assessment of a standardized polyphenolic extract of clove buds: subchronic toxicity and mutagenicity studies. *Toxicol Rep.* (2016) 3:439–49. doi: 10.1016/j.toxrep.2016.04.001

106. Gooderham NJ, Cohen SM, Eisenbrand G, Fukushima S, Guengerich FP, Hecht SS, et al. FEMA GRAS assessment of natural flavor complexes: clove, cinnamon leaf and West Indian bay leaf-derived flavoring ingredients. *Food Chem Toxicol.* (2020) 145:111585. doi: 10.1016/j.fct.2020.111585

107. Ogawa K, Honda M, Tanigawa A, Hatase A, Ito A, Higa Y, et al. Appetite-enhancing effects of inhaling cinnamon, clove, and fennel essential oils containing phenylpropanoid analogues. *J Nat Med.* (2020) 74:710–21. doi: 10.1007/s11418-020-01423-8

108. Vicidomini C, Roviello V, Roviello GN. Molecular basis of the therapeutical potential of clove (*Syzygium aromaticum* L.) and clues to its anti-covid-19 utility. *Molecules.* (2021) 26:1880. doi: 10.3390/molecules26071880

109. Sreenivasan PK, Kakarla VVP, Sharda S, Setty Y. The effects of a novel herbal toothpaste on salivary lactate dehydrogenase as a measure of cellular integrity. *Clin Oral Invest.* (2020) 25:3021–30. doi: 10.1007/s00784-020-03623-8

110. Uju DE, Obioma NP. Anticariogenic potentials of clove, tobacco and bitter kola. *Asian Pacific J Trop Med.* (2011) 4:814–8. doi: 10.1016/s1995-7645(11)60200-9

111. Sarialioglu Gungor A, Donmez N. Dentin erosion preventive effects of various plant extracts: an in vitro atomic force microscopy, scanning electron microscopy, and nanoindentation study. *Micro Res Techniq.* (2021) 84:1042–52. doi: 10.1002/jemt.23665

112. Lakhan MN, Chen R, Shar AH, Chand K, Shah AH, Ahmed M, et al. Eco-friendly green synthesis of clove buds extract functionalized silver nanoparticles and evaluation of antibacterial and antidiatom activity. *J Microbiol Methods.* (2020) 173:105934. doi: 10.1016/j.mimet.2020.105934

113. Asghar MA, Yousuf RI, Shoaib MH, Asghar MA, Zehravi M, Rehman AA, et al. Green synthesis and characterization of carboxymethyl cellulose fabricated silver-based nanocomposite for various therapeutic applications. *Int J Nanomed.* (2021) 16:5371–93. doi: 10.2147/ijn.s321419

114. Sharma C, Ansari S, Ansari MS, Satsangee SP, Srivastava M. Single-step green route synthesis of Au/Ag bimetallic nanoparticles using clove buds extract: enhancement in antioxidant bio-efficacy and catalytic activity. *Material Sci Eng.* (2020) 116:111153. doi: 10.1016/j.msec.2020.111153

115. Radünz M, da Trindade MLM, Camargo TM, Radünz AL, Borges CD, Gandra EA, et al. Antimicrobial and antioxidant activity of unencapsulated and encapsulated clove (*Syzygium aromaticum*, L.) essential oil. *Food Chem.* (2019) 276:180–6. doi: 10.1016/j.foodchem.2018.09.173

116. Hameed M, Rasul A, Waqas M, Saadullah M, Aslam N, Abbas G, et al. Formulation and evaluation of a clove oil-encapsulated nanofiber formulation for effective wound-healing. *Molecules.* (2021) 26:2491. doi: 10.3390/molecules26092491

117. Ashjazade MA, Jahandideh A, Abedi G, Akbarzadeh A, Hesaraki S. Histopathology and histomorphological study of wound healing using clove extract nanofibers (Eugenol) compared to zinc oxide nanofibers on the skin of rats. *Arch Razi Institute.* (2019) 74:267–77. doi: 10.22092/ari.2018.120170.1184

118. Shetty S, Jose J, Kumar L, Charyulu RN. Novel ethosomal gel of clove oil for the treatment of cutaneous candidiasis. *J Cosmetic Dermatol.* (2019) 18:862–9. doi: 10.1111/jocd.12765

119. Aman RM, Abu Hashim II, Meshali MM. Novel clove essential oil nanoemulgel tailored by taguchi's model and scaffold-based nanofibers: phytopharmaceuticals with promising potential as cyclooxygenase-2 ors in external inflammation </p&gt. *Int J Nanomed.* (2020) 15:2171–95. doi: 10.2147/ijn.s246601

120. Singh, P, Kaur G, Singh A. Physical, morphological and storage stability of clove oil nanoemulsion based delivery system. *Food Sci Technol Int.* (2021) 108201322110694. doi: 10.1177/10820132211069470 [Epub ahead of print].

121. Kumar A, Kanwar R, Mehta SK. Development of phosphatidylcholine/tween 80 based biocompatible clove oil-in-water nanoemulsion as a green nanocarrier for controlled herbicide delivery. *Environ Pollut.* (2022) 293:118558. doi: 10.1016/j.envpol.2021.118558

122. Debonne E, Yilmaz MS, Sakiyan O, Eeckhout M. Comparison of antifungal activity of essential oils of clove, lemongrass and thyme for natural preservation of dried apricots. *Food Sci Technol Int.* (2021) 108201322110496. [Epub ahead of print]. doi: 10.1177/10820132211049603

123. Ju J, Xu X, Xie Y, Guo Y, Cheng Y, Qian H, et al. Inhibitory effects of cinnamon and clove essential oils on mold growth on baked foods. *Food Chem.* (2018) 240:850–5. doi: 10.1016/j.foodchem.2017.07.120

124. Hasheminejad N, Khodaiyan F. The effect of clove essential oil loaded chitosan nanoparticles on the shelf life and quality of pomegranate arils. *Food Chem.* (2020) 309:125520. doi: 10.1016/j.foodchem.2019.125520

125. Elsherif WM, Talaat Al Shrief LM. Effects of three essential oils and their nano-emulsions on *Listeria monocytogenes* and *Shigella* flexneri in Egyptian talaga cheese. *Int J Food Microbiol.* (2021) 355:109334. doi: 10.1016/j.ijfoodmicro.2021.109334

126. Tayebi-Moghaddam S, Khatibi R, Taklavi S, Hosseini-Isfahani M, Rezaeinia H. Sustained-release modeling of clove essential oil in brine to improve the shelf life of Iranian white cheese by bioactive electrospun zein. *Int J Food Microbiol.* (2021) 355:109337. doi: 10.1016/j.ijfoodmicro.2021.109337

127. Kang M, Park J, Yoo S. Effect of clove powder on quality characteristics and shelf life of kimchi paste. *Food Sci Nutr.* (2019) 7:537–46. doi: 10.1002/fsn3.833

128. Chatterjee D, Bhattacharjee P. Use of eugenol-lean clove extract as a flavoring agent and natural antioxidant in mayonnaise: product characterization and storage study. *J Food Sci Technol.* (2015) 52:4945–54. doi: 10.1007/s13197-014-1573-6

129. Suliman GM, Alowaimer AN, Al-Mufarrej SI, Hussein EO, Fazea EH, Naiel MA, et al. The effects of clove seed (*Syzygium aromaticum*) dietary administration on carcass characteristics, meat quality, and sensory attributes of broiler chickens. *Poul Sci.* (2021) 100:100904. doi: 10.1016/j.psj.2020.12.009

130. Toledo PF, Viteri Jumbo LO, Rezende SM, Haddi K, Silva BA, Mello TS, et al. Disentangling the ecotoxicological selectivity of clove essential oil against aphids and non-target ladybeetles. *Sci Total Environ.* (2020) 718:137328. doi: 10.1016/j.scitotenv.2020.137328

131. Plata-Rueda A, Campos JM, da Silva Rolim G, Martínez LC, dos Santos MH, Fernandes FL, et al. Terpenoid constituents of cinnamon and clove essential oils cause toxic effects and behavior repellency response on granary weevil, *Sitophilus*

granarius. *Ecotoxicol Environ Safe*. (2018) 156:263–70. doi: 10.1016/j.ecoenv.2018.03.033

132. Viteri Jumbo LO, Haddi K, Faroni LRD, Heleno FF, Pinto FG, Oliveira EE. Toxicity to, oviposition and population growth impairments of *Callosobruchus maculatus* exposed to clove and cinnamon essential oils. *PLoS One*. (2018) 13:e0207618. doi: 10.1371/journal.pone.0207618

133. Wahed TB, Mondal M, Rahman MA, Hossen MS, Bhoumik NC, Saha S, et al. Protective role of syzygium cymosum leaf extract against carbofuran-induced hematological and hepatic toxicities. *Chem Res Toxicol*. (2019) 32:1619–29. doi: 10.1021/acs.chemrestox.9b00164

134. Nentwig G, Frohberger S, Sonneck R. Evaluation of clove oil, icaridin, and transfluthrin for spatial repellent effects in three tests systems against the aedes aegypti (*Diptera*: *Culicidae*). *J Med Entomol*. (2017) 54:150–8. doi: 10.1093/jme/tjw129

135. Kafle L, Shih CJ. Toxicity and repellency of compounds from clove (*Syzygium aromaticum*) to red imported fire ants *Solenopsis invicta* (*Hymenoptera*: *Formicidae*). *J Econ Entomol*. (2013) 106:131–5. doi: 10.1603/ec12230

136. Mammen RR, Natinga Mulakal J, Mohanan R, Maliakel B, Illathu Madhavamenon K. Clove bud polyphenols alleviate alterations in inflammation and oxidative stress markers associated with binge drinking: a randomized double-blinded placebo-controlled crossover Study. *J Med Food*. (2018) 21:1188–96. doi: 10.1089/jmf.2017.4177

137. Hwang E, Lin P, Ngo HTT, Yi TH. Clove attenuates UVB-induced photodamage and repairs skin barrier function in hairless mice. *Food Func*. (2018) 9:4936–47. doi: 10.1039/c8fo00843d

frontiers | Frontiers in Nutrition

TYPE Original Research
PUBLISHED 28 October 2022
DOI 10.3389/fnut.2022.1014414

OPEN ACCESS

EDITED BY
Gengjun Chen,
Kansas State University, United States

REVIEWED BY
Xiaolong Ji,
Zhengzhou University of Light Industry, China
Jinyao Li,
Xinjiang University, China

*CORRESPONDENCE
Bisheng Huang
hbsh1963@163.com
Hongzhi Du
dhz3163@hbtcm.edu.cn

†These authors have contributed equally to this work and share first authorship

SPECIALTY SECTION
This article was submitted to Nutrition and Food Science Technology, a section of the journal Frontiers in Nutrition

RECEIVED 08 August 2022
ACCEPTED 29 September 2022
PUBLISHED 28 October 2022

CITATION
Wang Z, Hou X, Li M, Ji R, Li Z, Wang Y, Guo Y, Liu D, Huang B and Du H (2022) Active fractions of golden-flowered tea (*Camellia nitidissima Chi*) inhibit epidermal growth factor receptor mutated non-small cell lung cancer *via* multiple pathways and targets *in vitro* and *in vivo*. *Front. Nutr.* 9:1014414. doi: 10.3389/fnut.2022.1014414

Active fractions of golden-flowered tea (*Camellia nitidissima Chi*) inhibit epidermal growth factor receptor mutated non-small cell lung cancer *via* multiple pathways and targets *in vitro* and *in vivo*

Ziling Wang[1†], Xiaoying Hou[2†], Min Li[3], Rongsheng Ji[1], Zhouyuan Li[1], Yuqiao Wang[1], Yujie Guo[1], Dahui Liu[1], Bisheng Huang[1*] and Hongzhi Du[1*]

[1]Key Laboratory of Traditional Chinese Medicine Resources and Chemistry of Hubei Province, School of Pharmacy, Hubei University of Chinese Medicine, Wuhan, China, [2]School of Medicine, Wuhan Institutes of Biomedical Sciences, Jianghan University, Wuhan, China, [3]Shenzhen Luohu Hospital Group Luohu People's Hospital, The Third Affiliated Hospital of Shenzhen University, Shenzhen, China

As a medicine-food homology (MFH) plant, golden-flowered tea (*Camellia nitidissima Chi*, CNC) has many different pharmacologic activities and is known as "the queen of the tea family" and "the Panda of the Plant world". Several studies have revealed the pharmacologic effects of CNC crude extract, including anti-tumor, anti-oxidative and hepatoprotective activity. However, there are few studies on the anti-tumor active fractions and components of CNC, yet the underlying mechanism has not been investigated. Thus, we sought to verify the anti-non-small cell lung cancer (NSCLC) effects of four active fractions of CNC. Firstly, we determined the pharmacodynamic material basis of the four active fractions of CNC (*Camellia. leave. saponins*, *Camellia. leave. polyphenols*, *Camellia. flower. saponins*, *Camellia. flower. polyphenols*) by UPLC-Q-TOF-MS/MS and confirmed the differences in their specific compound contents. Then, MTT, colony formation assay and EdU incorporation assay confirmed that all fractions of CNC exhibit significant inhibitory on NSCLC, especially the *Camellia. leave. saponins* (CLS) fraction on EGFR mutated NSCLC cell lines. Moreover, transcriptome analysis revealed that the inhibition of NSCLC cell growth by CLS may be *via* three pathways, including "Cytokine-cytokine receptor interaction," "PI3K-Akt signaling pathway" and "MAPK signaling pathway." Subsequently, quantitative real-time PCR (RT-qPCR) and Western blot (WB) revealed TGFB2, INHBB, PIK3R3, ITGB8, TrkB and CACNA1D as the critical targets for the anti-tumor effects of CLS *in vitro*. Finally, the xenograft models confirmed that CLS treatment effectively suppressed tumor growth, and the key targets were also

verified *in vivo*. These observations suggest that golden-flowered tea could be developed as a functional tea drink with anti-cancer ability, providing an essential molecular mechanism foundation for MFH medicine treating NSCLC.

KEYWORDS

golden-flowered tea, *Camellia nitidissima Chi* (CNC), non-small cell lung cancer (NSCLC), natural product, epidermal growth factor receptor (EGFR)

Introduction

Golden-flowered tea (*Camellia nitidissima Chi*—CNC) as an edible and medicinal plant (EMP) is an evergreen shrub belonging to the family Camellia (1). Golden-flowered tea has been known as "the panda of the plant world" and "the queen of the tea family" for its great ornamental and medicinal value. According to the "Guangxi Zhuang Autonomous Region Zhuang Medicine Quality Standard" (2), CNC has been used to treat various diseases such as pharyngitis, dysentery, liver cirrhosis and cancer for a long time. Most recently, CNC has been introduced and cultivated in Australia, Japan, the United States, and other countries (3). Moreover, a plethora of researchers are interested in the anti-cancer effects of CNC as a functional food.

Previous studies of CNC pharmacological effects had emphasized anti-tumor, anti-obesity and hypolipidemic effects (4, 5). In the last two decades, much of the research about CNC has explored the pharmacological effects of flower fractions, while the studies of leaf fractions are extremely rare. In fact, the leaves of CNC have been used as tea for a long time (6). Although, several studies have revealed the anti-cancer effects of CNC leaves crude extract, there are few reports on the anti-tumor active fractions and components of CNC (7). Thus, it is necessary to explore the differences in the pharmacological effects of different active fractions of CNC.

Previously, our research for the first time confirmed that the four active fractions of CNC (*Camellia. leave. saponins, Camellia. leave. polyphenols, Camellia. flower. saponins, Camellia. flower. polyphenols*) effectively inhibited the proliferation, metastasis and invasion of anti-NSCLC *in vitro* (8), while the anti-cancer mechanism remains to be revealed. Lung cancer is the leading type of cancer death worldwide, with NSCLC being the most common sub-type (9–12), accounting for approximately 85% (13). Among the emerging oncology therapies, molecular targeted drugs have become the first choice for treating NSCLC (14). Approximately 10–40% of NSCLC patients worldwide have tumor cells carrying epidermal growth factor receptor (EGFR) activating mutations (15). The epidermal growth factor receptor-tyrosine kinase inhibits (EGFR-TKI) targeted therapy is a milestone in tumor treatment with remarkable effects (16). However, NSCLC frequently develops acquired resistance when treated with NSCLC owing to factors such as tumor mutational burden (17), immune evasion and tumor microenvironment (TME) (18, 19). Therefore, the search for new therapeutic agents for drug-resistant NSCLC and the analysis of medicinal treatment mechanisms are frontier issues in oncology science, which have scientific value and clinical guidance significance for the treatment of NSCLC. Thus, we attempt to explore the molecular mechanism to provide more scientific evidence for the application of golden-flowered tea in the treatment of NSCLC.

In brief, the component difference between the four fractions of CNC was first reported in this study. Then, we evaluated the anti-tumor activity of four fractions of CNC on three different NSCLC cell lines. To determine the programmed cell death effect on non-small cell lung cancer cells, we investigated whether CLS treatment induces the apoptosis of NCI-H1975 cells by TdT-mediated dUTP Nick-End Labeling (TUNEL) assay, Annexin V and propidine iodide (PI) staining, reactive oxygen species (ROS) measurement, superoxide dismutase (SOD) measurement, SEM examination and lactate dehydrogenase (LDH) release. Transcriptomics analysis was employed to probe the genetic changes after treatment of NSCLC cells with CLS. Subsequently, RT-qPCR and WB confirmation were performed for the candidate pathways. Finally, Xenograft models assay also proved the inhibitory effect of CLS *in vivo*. Taken together, our study investigated the inhibitory effect of different fractions of CNC on NSCLC (**Figure 1**). Importantly, our work will facilitate the study of the anti-tumor effect and mechanism of CNC as a functional tea.

Material and methods

Extraction of chemical constituents

The leaves and flowers of CNC were collected from Fangchenggang, Guangxi Province, China. The extraction method was based on the previous research of our team (7, 20). The leaves and flowers were air-dried and grinded into powder. The powder of leaves (6.3 kg) and flowers (6.0 kg) were separately refluxed with 95% ethanol for 3 times (3, 2 and

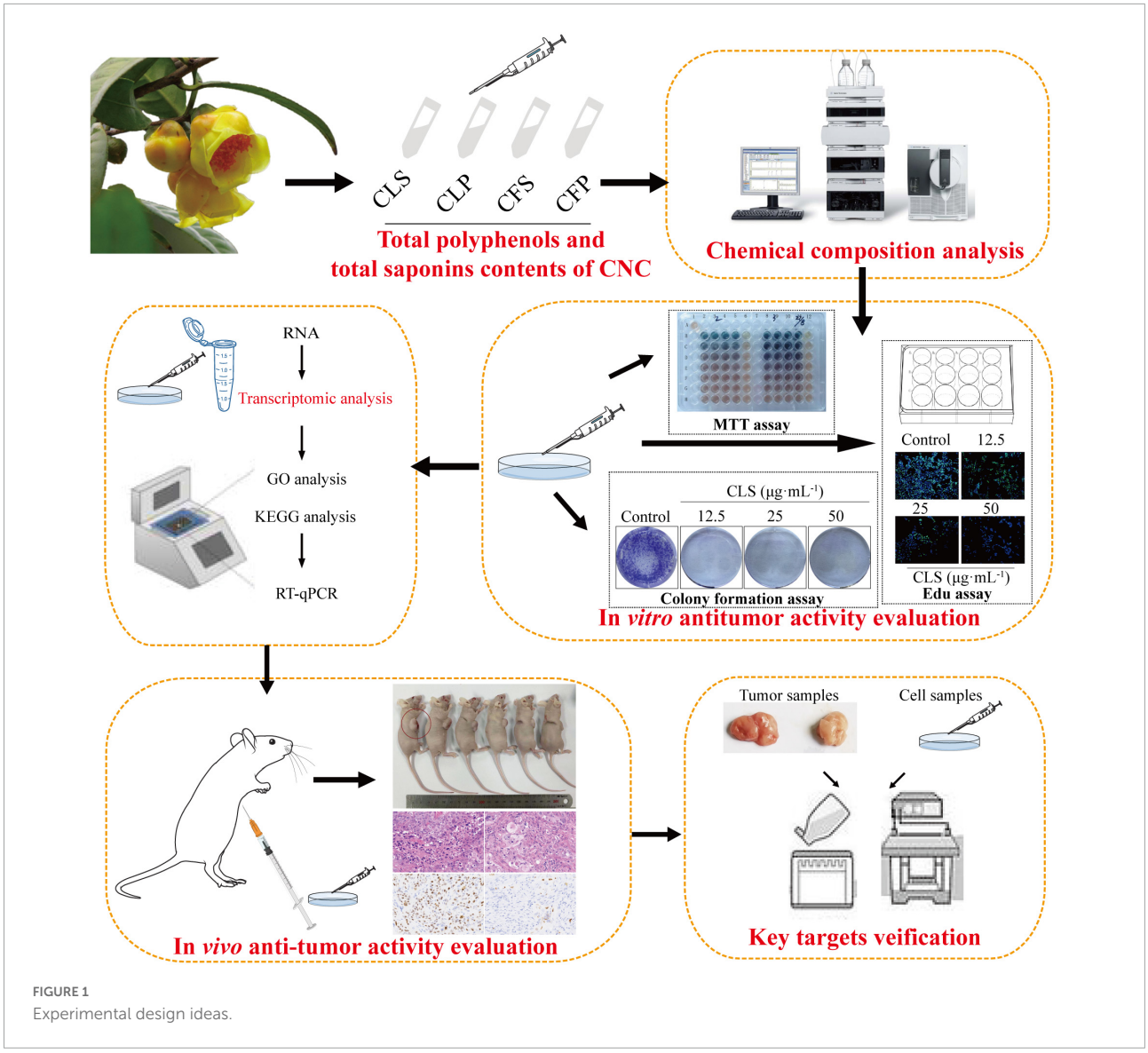

FIGURE 1
Experimental design ideas.

1 h). The extracts were combined and evaporated in a rotary evaporator to obtain ethanol extracts. Finally, four different active fractions of CNC (*Camellia. leave. polyphenols, Camellia. flower. polyphenols, Camellia. leave. saponins, Camellia. flower. saponins*) were obtained by macroporous resin purification process (21, 22).

Chemical characterization of active fractions of *Camellia nitidissima Chi*

Determination of total polyphenols

Total polyphenols were determined by Follin-Ciocalteu (FC) assay. The FC reagent (diluted 1:10 in water) and aqueous Na2CO3 (10%) were added to the two fractions of CNC (*Camellia. leave. polyphenols, Camellia. flower. polyphenols*) in sequence. Gallic acid control solution was prepared to draw the calibration curve. The absorbance value was measured at 765 nm after constant shaking at 37°C for 30 min.

Determination of total saponins

Total saponins were determined by Vanillin-acetate method. Firstly, 5.0 g of vanillin was weighed to configure a 5% solution of vanillin acetate. Ginsenoside Re control solution was prepared to draw the calibration curve. Prepared 1 mL of 1 mg/mL of the solution (*Camellia. leave. saponins, Camellia. flower. saponins*) to be measured in the test tube in a water bath to evaporate. The 5% vanillin-acetate solution and Perchloric acid were added to the two fractions of CNC in sequence. After heating the test tubes at 60 degrees for 10 min, the test tubes were cooled with ice water and 5 mL of glacial acetic acid was added. The absorbance value was measured at 560 nm.

Qualitative and quantitative analysis of active fractions of *Camellia nitidissima Chi*

The four active fractions of CNC were identified by the UPLC-Q-TOF-MS/MS. After being dissolved in methanol, the sample was filtered through a 0.22 μm microfiltration membrane for analysis. The UPLC-Q-TOF-MS/MS has equipped with an Agilent SB-C18 (1.8 μm, 2.1 mm × 100 mm) column. The mobile phase is composed of solvent A, 0.1% formic acid in water and solvent B, 0.1% formic acid of acetonitrile. The elation gradient procedure was performed: 0–9 min, 5–95% B; 9–10 min 95% B; 10–11.10 min 95–5% B; 11.10–14 min 5% B. The flow rate was 0.35 mL/min and the sample injection volume was 4 μL. The effluent was alternatively connected to an ESI-triple quadrupole-linear ion trap (QTRAP)-MS. The ESI source operation parameters were as follows: an ion source, turbo spray; source temperature 550°C; ion spray voltage (IS) 5,500 V (positive ion mode)/-4,500 V (negative ion mode); ion source gas I (GSI), gas II (GSII), curtain gas (CUR) was set at 50, 60, and 25.0 psi, respectively; the collision-activated dissociation (CAD) was high (23).

Cell culture

NCI-H1975 cells, A549 cells and HCC827 cells were grown in RPMI Medium 1,640 basic (1×) supplemented with 10% fetal bovine serum(GEMINI BIO-Products)in a humidified chamber with 5% CO_2 and 37°C. The cell culture method is the same as the previous culture method of our team (24).

Cell viability assay

NCI-H1975 cells, A549 cells and HCC827 cells were seeded at 3,000, 5,000, and 3,000 cells per well of 96-well plates in triplicate. Cell viability was measured at 72 h by using a 3-(4, 5-dimethylthiazol-2-yl)-2, 5-diphenyl tetrazolium bromide (MTT) assay.

Colony formation assay

NCI-H1975 and HCC827 cells were seeded at 500 cells per well of 6-well plates in a medium containing Penicillin-Streptomycin-Gentamicin Solution (Solarbio, P1410). After 24 h of incubation, the cells were treated with different concentrations of CNC every 5 days until colonies formed in 10 days. The remaining colonies were stained with crystal violet.

EdU incorporation assay

After NCI-H1975 and HCC827 cells were treated by different fractions of CNC in 12-well plates for 24 h, the cells were cultured with 10 μM EdU (KevGEN BioTECH, KGA331-500) for 2 h, followed by incubation with 4% polychloraldehyde for 15 min. Washed by 3% BSA in PBS twice, the cells were incubated with 0.5% Triton X-100 (Solarbio, 9002-39-1) in PBS for 20 min. The cell plates were washed twice with 3% BSA in PBS and incubated with a 1 × Click-iT reactant mixture for 30 min. The cells treated with 1 × Click-iT reactant mixture were incubated with 1 × Hochest 33342 for 30 min under dark conditions. The proliferating cells (green) and the nuclei of all cells were observed under a laser confocal microscope under dark conditions. Different visual fields were randomly taken for image collection and synthesis analysis. Finally, the proliferation rate was calculated.

TdT-mediated dUTP Nick-End Labeling staining

After NCI-H1975 were cultured in 12-well plates for 24 h, the cells were treated with different concentration of CLS for 24 h. Cells were subsequently incubation with 4% polychloraldehyde for 30 min. Washed by PBS twice, the cells were incubated with 0.3% Triton X-100 (Solarbio, 9002-39-1) in PBS for 10 min. The cell plates were washed twice with PBS and incubated with a TUNEL reactant mixture for 60 min at 37°C (Beyotime, C1086). Different visual fields were randomly taken for image collection and synthesis analysis. And the TUNEL positive rate was calculated and normalized to that of the control group.

Annexin V and propidine iodide staining

The apoptosis rate of NCI-H1975 cells using Annexinv-fluorescein isothiocyanate (FITC) and PI double staining technique (KevGEN BioTECH, KGA107). NCI-H1975 cells were processed at different concentrations of CLS for 48 h. The cells were collected by digestion with EDTA-free trypsin and washed twice with PBS. After processing according to the steps in the instructions, all groups were measured by flow cytometer.

Reactive oxygen species measurement

The effect of different concentrations on CLS-mediated ROS production in NCI-H1975 cells was determined using the cell-permeable fluorescent probe 2',7'-dihydrofluorescein-diacetate ($DCFH_2$-DA). NCI-H1975 cells were incubated in different

concentration of CLS for 24 h, the cells were cultured with 1 μM $DCFH_2$-DA (Solarbio, D6470) for 30 min at 37°C. And the ROS positive rate was calculated and normalized to that of the control group.

Superoxide dismutase measurement

The effect of different concentrations on CLS-mediated SOD production in NCI-H1975 cells was determined using the SOD reagent kit (Njjcbio, A001-3-2). After being processed at different concentrations of CLS for 48 h, the proteins of NCI-H1975 cells were extracted. The relative content of SOD was determined by the reagent kit. The SOD positive rate was calculated and normalized to the control group.

Scanning electron microscope examination

After NCI-H1975 cells were treated in accordance with the above-described experimental design, SEM was used to observe the difference between the treated and control groups. After cell crawling was washed with PBS, electron microscope fixative (Servicebio, G1102) was added and placed in a four-degree refrigerator for 1 h. Ethanol gradients were used to remove water from the samples, with dehydrating agent concentrations of 30, 50, 70, 80, 90, and 100% (twice) in order, with each dehydration time of 5 min. Finally, the samples were dried in the desiccator for 1.5 h and then sprayed with gold and photographed.

Lactate dehydrogenase release

The release of IL-1β and LDH can be detected during the onset of pyroptosis (25). After NCI-H1975 cells were treated in accordance with the above-described experimental design, LDH release was measured by LDH assay kit (Njjcbio, A020-2) to observe the difference between the treated and control groups. The absorbance was measured at a wavelength 450 nm using microplate reader.

Ribonucleic acid sequencing analysis and differential expression analysis

RNA degradation and contamination were monitored on 1% agarose gels. The preparation of each RNA sample requires 3 μg of RNA as input material (26). Sequencing libraries were generated using the NEBNext® Ultra™® RNA Library Preparation Kit (NEB, USA), and index codes were added to the attribute sequences of each sample. After the library inspection is qualified, the different libraries are pooled according to the requirements of effective concentration and target data volume. And illumine sequencing is performed, and the generated 150 bp paired-end reads. Differential expression analysis was performed for two conditions/groups (two biological replicates per condition) using the DESeq2 R package (1.16.1). Genes identified by DESeq2 with adjusted p-values < 0.05 were designated as differentially expressed genes. Gene Ontology (GO) enrichment analysis and Kyoto Encyclopedia of Genes and Genomes (KEGG) analysis of differentially expressed genes was implemented by the cluster profile R package (27, 28).

Reverse transcription and real time-quantitative polymerase chain reaction

Total RNA was extracted from cell culture samples using the TRNzol Universal Reagent (Tiangen, W9712) according to the manufacturer's instructions. The cDNA was synthesized from total RNA (1 μg) using reverse transcription (Vazyme, R323-01). Primer sequences were as follows in **Table 1**. PCR amplification was executed by the SYBR Green PCR master mix (LightCycler 480, 30408), and the PCR-amplified gene products were analyzed.

Western blot analysis

After the cells were treated with CLS for the indicated time, cell lysates were lysed by RIPA buffer supplemented with a complete protease and phosphatase inhibitor mixture (Beyotime, 45482). Samples of mouse tumor tissues were stored in a −80°C refrigerator and homogenized with RIPA (Solarbio, 676). Proteins were separated on a 6–10% SDS-PAGE system and transferred to a polyvinylidene fluoride (PVDF) membrane. WB was performed according standard protocol with following primary antibodies: Anti-ACTB (Abclonal, AC004; 1:10,000), Anti-INHBB (Abclonal, A8553;1:1,000), Anti-TGFB2 (Abclonal, A3640; 1:1,000), Anti-ITGB8 (Abclonal, A8433; 1:1,000), Anti-PIK3R3 (Abclonal, A17112; 1:1,000), Anti-TrkB (Abclonal, A2099; 1:1,000), Anti-CACNA1D (Abclonal, A16785; 1:1,000), HPR Goat Anti-Mouse (Abclonal, AS003; 1:2,000) or HPR Goat Anti-Rabbit (Abclonal, AS014; 1:2,000) secondary antibodies were used. Protein bands were visualized by chemiluminescence reagents (Meilunbio, MA0186-1) and were performed using a luminescent image analyzer (Proteinsimple, 601577). Raw data were analyzed by using Fuji film v3.0.

TABLE 1 Primer sequences.

Gene	Forward sequence	Reverse sequence
18S	AGGTCTGTGATGCCCTTAGATG	TCCTCGTTCATGGGGAATAATTG
INHBB	GAAATCATCAGCTTCGCCGAGAC	GGCAGGAGTTTCAGGTAAAGCC
TGFB2	AAGAAGCGTGCTTTGGATGCGG	ATGCTCCAGCACAGAAGTTGGC
PIK3R3	CCACCTAAGCCAATGACTTCAGC	GTTGAGGCATCTCGGACCAAGA
ITGB8	CTGTTTGCAGTGGTCGAGGAGT	TGCCTGCTTCACACTCTCCATG
TNFRSF10C	GGTGTGGATTACACCAACGCTTC	CTGACACACTGTGTCTCTGGTC
MEF2C	TCCACCAGGCAGCAAGAATACG	GGAGTTGCTACGGAAACCACTG
EIF4E1B	GACAAGATCGCTGTGTGGACGA	GTTGCTCTTGGTGGCTGTGTCT
TrkB	ACAGTCAGCTCAAGCCAGACAC	GTCCTGCTCAGGACAGAGGTTA
CACNA1D	CTTCGACAACGTCCTCTCTGCT	GCCGATGTTCTCTCCATTCGAG
IL-1β	TGCTCAAGTGTCTGAAGCAG	TGGTGGTCGGAGATTCGTAG

Xenograft models

Thirty 5-week-old BALB/c-nude mice were obtained from the Biont (Jiangsu, No.320727210100432325). All mice were housed in a temperature-controlled environment (24 ± 2°C) with a 12/12 h dark/light cycle at the Animal Center of Hubei university of Chinese medicine. The standard rat chow and water used for animal feeding and all animal experiments were conducted by the animal ethics-related regulations of Hubei University of Traditional Chinese Medicine, permission number: SYXK2017-0067-ZYZYZX2022-2. BALB/c-nude mice were injected subcutaneously in the armpit with NCI-H1975 (5×10^6 cells/mice) in 150 μL PBS. After the mean tumor volume reached 50 mm^3, BALB/c-nude mice were randomly divided into model control group (n = 6), tax group (n = 6), low-dose group (n = 6), medium-dose group (n = 6), high-dose group (n = 6). Low-dose orally took 100 mg/kg CLS every day, medium-dose orally took 200 mg/kg CLS every day, and high-dose orally took 400 mg/kg CLS every day. And taxol (anhydrous ethanol: castor oil = 1:1) was injected at 20 mg/kg every 2 days in the tail vein. Tumor volume was monitored by vernier calipers throughout the experiment. All mice were executed and tumors were removed on day 13.

$RTV = \frac{Vt}{V0}$, where V0 represents the tumor volume of day 1 (the day of CLS first administration), Vt represents the tumor volume of day 13 (29).

Immunohistochemistry

Samples from the tumor xenografts and liver were dissected, formalin-fixed and paraffin-embedded. Paraffin blocks were placed on the pre-cooling table and adjusted the knees to 4-Mm thickness. Sections were incubated with citric acid (pH 6.0) antigen retrieval buffer (Beyotime, P0085) for antigen retrieval in a microwave oven. After blocking endogenous peroxidase with 3% hydrogen peroxide, and serum sealing by 3% BSA (Beyotime, P0007), sections were then incubated by Ki67 antibody (Abcam, Ab16667) and further processed with secondary antibody (Abcam, Ab6721). The chromogenic reaction was performed by DAB (Solarbio, DA1010). Sections were counterstained with hematoxylin (Solarbio, H8070) and observed under a microscope. The nucleus of hematoxylin stained is blue, and the positive expression of DAB is brownish yellow.

TABLE 2 Total polyphenols and saponins in different fractions of CNC (n = 6).

Bio active substance	Fraction of CNC	mg/g dry mass
Total polyphenol content	CLP	136.89 ±3.18
	CFP	327.03 ±4.03
Total saponin content	CLS	38.83 ±0.57
	CFS	56.53 ±0.83

Data presentation and statistical analysis

All graphs were generated using GraphPad Prism 8.0 (SanDiego, CA, USA). One-way ANOVA with Bonferroni correction was used for statistical analyses. Statistical significance was set at $^*p < 0.05$, and $^{**}p < 0.01$ compared to control unless stated differently.

Results

Total polyphenols and total saponins contents of *Camellia nitidissima Chi*

As is known, total polyphenols and total saponins are important active ingredients in tea beverages. Therefore, we first

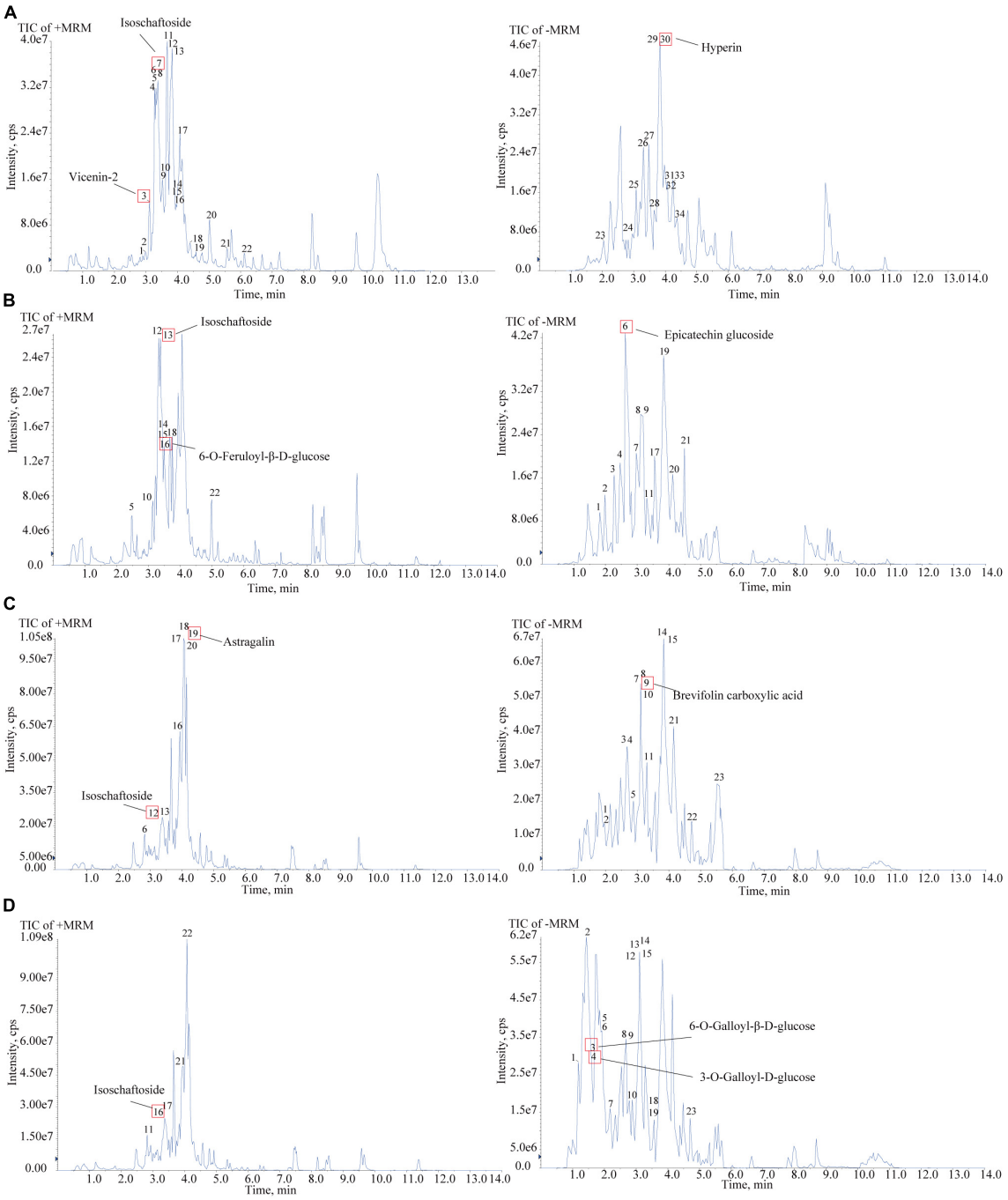

FIGURE 2
Chemical composition analysis of CLS, CLP, CFS, and CFP by using UPLC-QTOF-MS. **(A)** Total Ion Chromatography (TIC) in the positive and negative ion mode of CLS by UPLC-QTOF-MS. **(B)** Total Ion Chromatography (TIC) in the positive and negative ion mode of CLP by UPLC-QTOF-MS. **(C)** Total Ion Chromatography (TIC) in the positive and negative ion mode of CFS by UPLC-QTOF-MS. **(D)** Total Ion Chromatography (TIC) in the positive and negative ion mode of CFP by UPLC-QTOF-MS/MS.

determined the contents of total polyphenols and total saponins in each of the four active fractions of CNC. The polyphenols contents of *Camellia. leave. polyphenols* (CLP) and *Camellia. flower. Polyphenols* (CFP) in terms of gallic acid equivalent (standard curve equation: y = 4.2285x+0.0597, r^2 = 0.999) were from 20 to 100 μg/mL and listed in Table 2. The polyphenols contents in CLP were 136.89 ± 3.18 mg/g and the phenolic contents in CFP were 327.03 ± 4.03 mg/g. Table 2 also

showed the content of total saponins reported as Ginsenoside Re equivalent (standard curve equation: y = 1.4807x+0.0223, r^2 = 0.99), which were from 0.02 to 0.14 mg/mL. Saponin contents were 38.83 ± 0.57 mg/g in CLS and 56.53 ± 0.83 mg/g in CFS as shown in **Table 2**. The results indicated that total saponins and total polyphenols might be important active components in goldenrod tea.

Active compounds analysis in *Camellia nitidissima Chi* by UPLC-QTOF-MS/MS

To confirm the material basis of CNC, the active chemical components of the four active fractions of CNC were detected separately by UPLC-QTOF-MS/MS. As is shown in **Figure 2A** and **Table 3**, the three components with the highest content in CLS are isoschaftoside, hyperin and vicenin-2. In CLP, the three main effective compounds are 6-O-Feruloyl-β-D-glucose, epicatechin glucoside and isoschaftoside (**Figure 2B** and **Table 3**). However, astragalin, isoschaftoside and brevifolin carboxylic acid are the most abundant substances in CFS (**Figure 2C** and **Table 4**). And in CFP, 6-O-Galloyl-β-D-glucose, 3-O-Galloyl-D-glucose and isoschaftoside demonstrated extremely high content (**Figure 2D** and **Table 4**). In conclusion, we initially revealed the specific chemical composition of different fractions of CNC, which laid the foundation for the subsequent activity study.

Camellia nitidissima Chi inhibited the proliferation of multifarious non-small cell lung cancer cell lines

To determine the anti-cancer effect on different non-small cell lung cancer cells, we firstly investigated whether CNC treatment inhibits the proliferation of NSCLC by MTT assay. Treating with CNC significantly suppressed the proliferation of NCI-H1975, A549 and HCC827 cells (**Figures 3A,B**). After 72 h of treatment, the results confirmed that CLS, CLP, CFS and CFP could significantly inhibit the proliferation of NCI-H1975, A549, and HCC827 cells. It was worth noting that the active fractions of CNC exhibited high inhibitory effect on 3 NSCLC cell lines, especially on EGFR mutant cells NCI-H1975.

Combining the information from the previous MTT assay, we selected NCI-H1975 and HCC827 cells as the main research object. Thus, we performed a colony formation assay by giving CNC every 5 days for 10 days into NCI-H1975 and HCC827 cells. The results demonstrated that CNC treatment significantly restrained anchorage-dependent colony formation of NCI-H1975 and HCC827 cells (**Figure 3C** and **Supplementary Figure 1**). At low doses, the NCI-H1975 cells eventually all died as well, demonstrating the remarkable anti-tumor activity of CNC.

Furthermore, the EdU assay is one of the most accurate and direct methods for detecting cell proliferation. Observed by laser confocal microscope, the proportion of proliferating NCI-H1975 and HCC827 cells (green) was significantly lower than the control group after 24 h of different concentrations of CNC treatment (**Figure 4** and **Supplementary Figure 1**). Expectedly, CNC treatment led to the significantly decreasing proliferation of NCI-H1975 cells. Simultaneously, we found that CLS had a higher proliferating inhibitory effect on NCI-H1975 cells. These collective data indicated that CNC inhibited the proliferation of NSCLC, supporting that CNC is a new anti-cancer EMP with promising research prospects.

Camellia. leave. saponins induced programmed non-small cell lung cancer death through pyroptosis

To determine the programmed cell death effect on non-small cell lung cancer cells, we investigated whether CLS treatment induces the apoptosis of NCI-H1975 cells by TUNEL assay. Treating with CLS significantly induced the apoptosis of NCI-H1975 cells (**Figure 5A**). Subsequently, we found that CLS inhibited ROS production, suggesting that NCI-H1975 may not induce programmed cell death through ferroptosis (**Figure 5B**). These results might originate from the antioxidant effect of CNC related (6). Annexin V-FITC/PI assay results showed that CLS treatment significantly unregulated the appearance of labeled cells in Q3 (from 1.98 ± 0.51 to 5.27 ± 2.87) suggesting that there was an increased early apoptosis in NCI-H1975 cells (**Figure 5C**). Moreover, scanning electron microscope (SEM) showed that the cell in the control group were normal and cell membranes were intact. By contrast, the cell in CLS group showed the damaged cell membranes and evidently increased number of scorched corpuscle (**Figure 5D**). To further confirm whether the cells underwent pyroptosis, we examined the levels of LDH in the cell supernatant and the relative mRNA expression of IL-1β. These results showed LDH content and IL-1β expression increased with increasing concentrations of CLS administration, which gave the best agreement with CLS induced programmed cell death through pyroptosis (**Figure 5E**).

Transcriptome analysis of *Camellia. leave. saponins* -treated NCI-H1975 cells

The above studies confirmed the anti-tumor activity of CLS, yet the mechanism of CLS treatment is unknown. Therefore, we applied transcriptome analysis to initially study the mechanism of CLS treatment. The global gene expression changes induced by CLS treatment were determined by comparing the gene profiled NCI-H1975 cells based on microarray data. We

TABLE 3 Compounds of CLS and CLP.

Fractions of CNC	Compound	Rt(min)	Molecular formula	Ion	Tentative identification	Measured m/z	MS/MS	Relative content (%)
CLS	1	2.94	$C_{33}H_{40}O_{21}$	$[M+H]^+$	Quercetin-3-O-rutinoside-7-O-glucoside	773.21	303.05	0.003
	2	2.97	$C_{15}H_{14}O_6$	$[M+H]^+$	Catechin	291.09	139.04	0.09
	3	3.11	$C_{27}H_{30}O_{15}$	$[M+H]^+$	Apigenin-6,8-di-C-glucoside (vicenin-2)*	595.17	457.20	2.36
	4	3.28	$C_{15}H_{14}O_6$	$[M+H]^+$	Epicatechin	291.09	139.04	0.83
	5	3.32	$C_{17}H_{24}O_{10}$	$[M+H]^+$	Geniposide	389.14	209.08	1.89
	6	3.34	$C_{26}H_{28}O_{14}$	$[M+H]^+$	Schaftoside	565.16	529.13	0.02
	7	3.35	$C_{26}H_{28}O_{14}$	$[M+H]^+$	Isoschaftoside*	565.16	409	4.39
	8	3.38	$C_{16}H_{22}O_9$	$[M+H]^+$	Swerosideit	359.13	197	2.1
	9	3.51	$C_{22}H_{18}O_{11}$	$[M+H]^+$	Gallocatechin gallate	459.09	139.04	0.006
	10	3.52	$C_{21}H_{20}O_{13}$	$[M+H]^+$	Myricetin-3-O-glucoside	481.10	319.04	0.008
	11	3.66	$C_{27}H_{30}O_{16}$	$[M+H]^+$	Quercetin-3-O-glucoside-7-O-rhamnoside	611.16	303.05	1.01
	12	3.77	$C_{33}H_{40}O_{20}$	$[M+H]^+$	Kaempferol-3-O-(6”-Rhamnosyl-2”-Glucosyl) Glucoside (camelliaside A)	757.22	287.06	1.36
	13	3.77	$C_{21}H_{20}O_{10}$	$[M+H]^+$	Apigenin-8-C-Glucoside (vitexin)	433.11	313.07	0.46
	14	3.83	$C_{21}H_{20}O_{12}$	$[M+H]^+$	Quercetin-5-O-β-D-glucoside	465.10	303	2.08
	15	3.90	$C_{27}H_{30}O_{15}$	$[M+H]^+$	Kaempferol-3-O-glucorhamnoside	595.17	287.06	0.29
	16	4.00	$C_{20}H_{18}O_{11}$	$[M+H]^+$	Quercetin-3-O-xyloside (reynoutrin)	435.09	303.06	0.35
	17	4.04	$C_{30}H_{26}O_{12}$	$[M+H]^+$	Apigenin-7-O-(6”-p-Coumaryl) glucoside	579.15	271	0.89
	18	4.16	$C_{21}H_{20}O_{10}$	$[M+H]^+$	Apigenin-7-O-glucoside (cosmosiin)*	433.11	271	0.34
	19	4.34	$C_{21}H_{20}O_{11}$	$[M+H]^+$	Quercetin-3-O-rhamnoside (quercitrin)	449.11	303.05	0.02
	20	5.02	$C_{15}H_{10}O_7$	$[M+H]^+$	Quercetin	303.05	137	1.82
	21	5.67	$C_{15}H_{10}O_6$	$[M+H]^+$	Kaempferol	287.06	153.02	0.14
	22	6.12	$C_{11}H_{12}O_3$	$[M+H]^+$	p-Coumaric acid ethyl ester	193.09	147	0.68
	23	1.74	$C_7H_6O_5$	$[M-H]^-$	Gallic acid	169.01	125	0.68
	24	3.05	$C_7H_6O_3$	$[M-H]^-$	Salicylic acid	137.03	108	0.26
	25	3.08	$C_7H_6O_3$	$[M-H]^-$	Protocatechualdehyde	137.02	93	0.45
	26	3.40	$C_9H_{10}O_2$	$[M-H]^-$	p-Coumaryl alcohol	149.06	131	0.002

(Continued)

TABLE 3 (Continued)

Fractions of CNC	Compound	Rt(min)	Molecular formula	Ion	Tentative identification	Measured m/z	MS/MS	Relative content (%)
	27	3.75	$C_{21}H_{20}O_{10}$	$[M-H]^-$	Apigenin-6-C-glucoside (isovitexin)	431.10	311	1.2
	28	3.76	$C_{36}H_{36}O_{18}$	$[M-H]^-$	Kaempferol-3-p-coumaroyldiglucoside	755.19	285	0.1
	29	3.81	$C_{21}H_{20}O_{12}$	$[M-H]^-$	Quercetin-3-O-glucoside (isoquercitrin)	463.09	300	2.08
	30	3.81	$C_{21}H_{20}O_{12}$	$[M-H]^-$	Quercetin-3-O-galactoside (hyperin)*	463.09	300	2.45
	31	3.84	$C_{22}H_{18}O_{10}$	$[M-H]^-$	Epicatechin gallate*	441.08	169	0.03
	32	3.84	$C_{22}H_{18}O_{10}$	$[M-H]^-$	Catechin gallate*	441.08	169.02	0.03
	33	4.21	$C_{15}H_{10}O_7$	$[M-H]^-$	Morin	301.04	151	1.9
	34	5.87	$C_{30}H_{46}O_4$	$[M-H]^-$	Camaldulenic acid	469.33	425	1.92
CLP	1	1.86	$C_{13}H_{18}O_8$	$[M-H]^-$	4-O-Glucosyl-3,4-dihydroxybenzyl alcohol	301.09	139.05	1.36
	2	1.94	$C_{13}H_{16}O_9$	$[M-H]^-$	Protocatechuic acid-4-O-glucoside	315.07	153.02	1.35
	3	2.29	$C_{14}H_{20}O_9$	$[M-H]^-$	2-(3,4-dihydroxyphenyl) ethanediol 1-O-β-D-glucopyranoside	333.1	153.02	2.21
	4	2.44	$C_{21}H_{24}O_{11}$	$[M-H]^-$	Epicatechin-4'-O-β-D-glucopyranoside	451.13	289.0	0.96
	5	2.47	$C_{11}H_{12}N_2O_2$	$[M+H]^+$	1-Methoxy-indole-3-acetamide	205.1	146.06	1.01
	6	2.63	$C_{21}H_{24}O_{11}$	$[M-H]^-$	Epicatechin glucoside*	451.12	289.07	3.43
	7	2.97	$C_{15}H_{18}O_8$	$[M-H]^-$	p-Coumaric acid-4-O-glucosidep-Coumaric acid-4-O-glucoside	325.09	163.04	2.36
	8	3.1	$C_7H_6O_3$	$[M-H]^-$	Protocatechualdehyde	137.02	93.04	0.99
	9	3.11	$C_7H_6O_3$	$[M-H]^-$	4-Hydroxybenzoic acid	137.02	93	1.52
	10	3.14	$C_{27}H_{30}O_{15}$	$[M+H]^+$	Apigenin-6,8-di-C-glucoside (vicenin-2)	595.17	457.2	1.01
	11	3.18	$C_{16}H_{20}O_9$	$[M-H]^-$	1-O-Feruloyl-β-D-glucose	355.1	193.05	2.42
	12	3.32	$C_{17}H_{24}O_{10}$	$[M+H]^+$	Geniposide	389.14	209.08	1.68
	13	3.35	$C_{26}H_{28}O_{14}$	$[M+H]^+$	Isoschaftoside*	565.16	409.09	2.89
	14	3.38	$C_{16}H_{22}O_9$	$[M+H]^+$	Sweroside	359.13	197	1.36
	15	3.38	$C_{26}H_{28}O_{14}$	$[M+H]^+$	Apigenin-6-C-(2"-glucosyl) arabinoside	565.16	427.1	1.83
	16	3.44	$C_{29}H_{39}N_3O_8$	$[M+H]^+$	N1, N8-Bis (sinapoyl) spermidine	558.28	207.07	1.95
	17	3.57	$C_{16}H_{20}O_9$	$[M-H]^-$	6-O-Feruloyl-β-D-glucose*	355.1	193.05	3.85
	18	3.67	$C_{27}H_{30}O_{14}$	$[M+H]^+$	Isovitexin-2'-O-rhamnoside	579.17	313.07	1.00

(Continued)

TABLE 3 (Continued)

Fractions of CNC	Compound	Rt(min)	Molecular formula	Ion	Tentative identification	Measured m/z	MS/MS	Relative content (%)
	19	3.88	$C_9H_{10}O_5$	$[M-H]^-$	Gallic acid ethyl ester	197.05	124.02	1.63
	20	3.89	$C_{27}H_{30}O1_5$	$[M-H]^-$	Kaempferol-3-O-robinobioside (biorobin)	593.15	285	1.08
	21	4.5	$C_{15}H_8O_8$	$[M-H]^-$	3-O-Methylellagic acid	315.01	299.99	0.99
	22	4.98	$C_{15}H_{10}O_7$	$[M+H]^+$	Quercetin	303.05	137.02	1.09

*Indicates the top three compounds from different fractions of CNC with the highest relative content.

found that 1,008 were significantly down-regulated after CLS treatment, while 1,077 genes were significantly up-regulated (Figure 6A), suggesting the global transcriptome changes after CLS treatment.

The pathway-enrichment analysis was annotated based on different databases (GO and KEGG) for homologous alignment to classify the function of differentially expressed genes (DEGs) between control and CLS-treated groups. String-based GO pathway analysis revealed several enriched pathways, including leukocyte migration, chemotaxis, taxis, proteinaceous extracellular matrix, and cytokine activity (Figure 6B). Moreover, "cytokine activity" was the most abundant term for DEGs in the metabolic process which indicated cytokine-mediated signaling pathway could be in-depth investigate (30).

Based on the KEGG, we attempted to perform a standard pathway enrichment analysis to identify the major active pathways for the inhibitory effect of CLS on NCI-H1975 cells. According to the pathway-enrichment analyses of these DEGs (Q-value<0.05), the most significantly enriched pathways are "Cytokine-cytokine receptor interaction" and "PI3K-Akt signaling pathway" (Figure 6C). Specifically, 22 DEGs were relevant to "Cytokine-cytokine receptor interaction," and 23 DEGs of the PI3K-Akt signaling pathway were involved in the anti-tumor process (Figures 6D,E). Transform growth factors (TGF), as an important class of cytokines, have been identified as mediators of a large number of diseases and can regulate the TME (31). TGF can also activate TGFB receptors on the MAPK signaling pathway, thereby affecting the MAPK signaling pathway. Besides, a large number of papers confirmed the existence of multi-level crosstalk between Ras/MAPK and PI3K/Akt signaling pathways (Figure 6H) (32, 33). Moreover, CLS treatment regulated 16 DEGs in the "MAPK signaling pathway" while suppressing NCI-H1975 cells growth (Figure 6F). These results indicated that CLS inhibited NSCLC cells growth *via* multiple targets and pathways, especially by inhibiting signal transduction of "Cytokine-cytokine receptor interaction," "PI3K-Akt signaling pathway" and "MAPK signaling pathway," while the involvement of the above pathways needs further experimental verifications (Figures 6H,I).

Camellia. leave. saponins inhibited non-small cell lung cancer *via* multiple pathways and targets

To verify the results of transcriptome analysis, we used RT-qPCR to validate the key genes of these three pathways separately. As shown in Figure 7A, the results showed that CLS could concentration-dependently inhibit the mRNA levels of TGFB2, INHBB (Cytokine-cytokine receptor interaction), PIK3R3, ITGB8 (PI3K-Akt signaling pathway), NTRK and CACNA1D (MAPK signaling pathway) were relatively significant and concentration-dependent ($p < 0.05$) compared to the control group. The transcriptomic data and RT-qPCR validation unveiled that TGFB2, INHBB, PIK3R3, ITGB8, NTRK (TrkB) and CACNA1D might be a critical targeted gene for NSCLC inhibition by CLS.

To further verify the changes in NSCLC protein expression after CLS treatment, we measured the expression of proteins encoded by crucial genes in NSCLC using the Western Blot assay (Figure 7B). Compared to the control group, the expression of these six key genes was observably decreased. These results were consistent with the result of RT-qPCR, indicating that CLS inhibited Cytokine-cytokine receptor interaction, PIK-Akt and MAPK signaling pathways.

Camellia. leave. saponins suppressed tumor development in nude mice

To further explore the effect of CLS treatment on tumor development *in vivo*, tumor-bearing mice were treated with different CLS concentrations. NCI-H1975 cells were inoculated subcutaneously into an underarm flank of athymic mice. Intriguingly, the body weight of low-dose, medium-dose and high-dose treated mice were slightly lower than the untreated animals (Figure 8B), but all vital signs such as activity status were normal. In addition, H&E results and physiological and biochemical results of the liver and kidney showed no significant hepatic or renal toxicity with CLS treatment (Supplementary Figure 2). This result might be based on the ability of CNC

TABLE 4 Compounds of CFS and CFP.

Fractions of CNC	Compound	Rt(min)	Molecular formula	Ion	Tentative identification	Measured m/z	MS/MS	Relative content (%)
CFS	1	1.94	$C_{14}H_{20}O_9$	$[M-H]^-$	Vanilloloside	315.11	153.02	1.33
	2	1.94	$C_{13}H_{16}O_9$	$[M-H]^-$	Protocatechuic acid-4-O-glucoside	315.07	153.02	1.55
	3	2.68	$C_{15}H_8O_9$	$[M-H]^-$	Vanillic Acid-4-O-Glucuronide	341.09	161.02	1.38
	4	2.68	$C_{15}H_8O_9$	$[M-H]^-$	1-O-Caffeoyl-β-D-glucose	341.09	161.02	1.32
	5	2.75	$C_{20}H_{20}O_{14}$	$[M-H]^-$	1,4-Di-O-Galloyl-D-glucose	483.08	169.01	1.73
	6	2.83	$C_{27}H_{30}O_{17}$	$[M+H]^+$	Quercetin-3,7-Di-O-glucoside	627.14	303.05	1.23
	7	3.10	$C_7H_6O_3$	$[M-H]^-$	Protocatechualdehyde	137.02	93.04	1.13
	8	3.10	$C_{30}H_{26}O_{12}$	$[M-H]^-$	Procyanidin B2	577.14	407.08	1.02
	9	3.11	$C_{13}H_8O_8$	$[M-H]^-$	Brevifolin carboxylic acid*	291.01	247	2.15
	10	3.11	$C_7H_6O_3$	$[M-H]^-$	4-Hydroxybenzoic acid	137.02	93	1.60
	11	3.29	$C_{14}H_{10}O_7$	$[M-H]^-$	4-(3,4,5-Trihydroxybenzoxy) benzoic acid	289.04	137.02	1.21
	12	3.35	$C_{26}H_{28}O_{14}$	$[M+H]^+$	Isoschaftoside*	565.16	409.09	2.55
	13	3.35	$C_{26}H_{28}O_{14}$	$[M+H]^+$	Apigenin-8-C-(2"-glucosyl) arabinoside	565.16	457.11	1.53
	14	3.79	$C_{22}H_{24}O_{11}$	$[M-H]^-$	Hesperetin-5-O-glucoside	463.12	301	1.13
	15	3.89	$C_{27}H_{30}O_{15}$	$[M-H]^-$	Kaempferol-3-O-robinobioside (Biorobin)	593.15	285	1.43
	16	3.97	$C_{24}H_{22}O_{15}$	$[M+H]^+$	Quercetin-7-O-(6"-malonyl) glucoside	551.1	303.05	1.06
	17	4.03	$C_{27}H_{30}O_{14}$	$[M+H]^+$	Apigenin-7-O-neohesperidoside (Rhoifolin)	579.17	271.07	1.48
	18	4.04	$C_{27}H_{30}O_{14}$	$[M+H]^+$	Apigenin-7-O-rutinoside (Isorhoifolin)	579.17	271.01	1.33
	19	4.06	$C_{21}H_{20}O_{11}$	$[M+H]^+$	Kaempferol-3-O-glucoside (Astragalin)*	449.11	287.06	2.68
	20	4.07	$C_{21}H_{20}O_{11}$	$[M+H]^+$	Kaempferol-4'-O-glucoside	449.11	287.06	1.26
	21	4.17	$C_{21}H_{20}O_{12}$	$[M-H]^-$	Quercetin-7-O-glucoside*	463.09	301.03	1.14
	22	4.72	$C_9H_{10}O_4$	$[M-H]^-$	3,4-Dihydroxybenzoic acid Ethyl Ester (Protocatechuic acid ethyl ester)	181.05	108	1.61
	23	5.51	$C_9H_{10}O_4$	$[M-H]^-$	Ethylparaben	165.06	92.03	1.11
CFP	1	1.19	$C_{20}H_{18}O_{14}$	$[M-H]^-$	4,6-(S)-Hexahydroxydiphenoyl-β-D-glucose	481.06	301	1.62

(Continued)

TABLE 4 (Continued)

Fractions of CNC	Compound	Rt(min)	Molecular formula	Ion	Tentative identification	Measured m/z	MS/MS	Relative content (%)
	2	1.39	$C_{20}H_{18}O_{14}$	$[M-H]^-$	4,6-(S)-Hexahydroxydiphenoyl-D-glucose	481.06	275	2.85
	3	1.51	$C_{13}H_{16}O_{10}$	$[M-H]^-$	6-O-Galloyl-β-D-glucose*	311.07	169.01	3.88
	4	1.51	$C_{13}H_{16}O_{10}$	$[M-H]^-$	3-O-Galloyl-D-glucose*	311.07	169.01	3.13
	5	1.94	$C_{14}H_{20}O_8$	$[M-H]^-$	Vanilloloside	315.11	153.02	1.61
	6	1.95	$C_{13}H_{16}O_9$	$[M-H]^-$	1-O-Gentisoyl-β-D-glucoside	315.07	153	2.07
	7	2.18	$C_{20}H_{20}O_{14}$	$[M-H]^-$	2,3-Di-O-Galloyl-β-D-Glucose	483.08	169.01	1.03
	8	2.68	$C_{15}H_{18}O_9$	$[M-H]^-$	1-O-Caffeoyl-β-D-glucose	341.09	161.02	1.22
	9	2.68	$C_{15}H_{18}O_9$	$[M-H]^-$	Vanillic acid-4-O-Glucuronide	341.09	161.02	1.10
	10	2.75	$C_{20}H_{20}O_{14}$	$[M-H]^-$	1,4-Di-O-Galloyl-D-glucose	483.08	169.01	1.43
	11	2.83	$C_{27}H_{30}O_{17}$	$[M+H]^+$	Quercetin-3,7-Di-O-glucoside	627.14	303.05	1.18
	12	3.10	$C_7H_6O_3$	$[M-H]^-$	Protocatechualdehyde	137.02	93.04	1.23
	13	3.10	$C_{30}H_{26}O_{12}$	$[M-H]^-$	Procyanidin B2	577.14	407.08	0.98
	14	3.11	$C_7H_6O_3$	$[M-H]^-$	4-Hydroxybenzoic acid	137.02	93	1.71
	15	3.11	$C_{13}H_8O_8$	$[M-H]^-$	Brevifolin carboxylic acid	291.01	247	1.67
	16	3.35	$C_{26}H_{28}O_{14}$	$[M+H]^+$	Isoschaftoside*	565.16	409.09	3.05
	17	3.38	$C_{26}H_{28}O_{14}$	$[M+H]^+$	Apigenin-6-C-(2"-glucosyl)arabinoside	565.16	427.1	1.51
	18	3.79	$C_{22}H_{24}O_{11}$	$[M-H]^-$	Hesperetin-5-O-glucoside	463.12	301	1.05
	19	3.89	$C_{27}H_{30}O_{15}$	$[M-H]^-$	Kaempferol-3-O-robinobioside (Biorobin)	593.15	285	1.23
	20	3.97	$C_{24}H_{22}O_{15}$	$[M+H]^+$	Quercetin-7-O-(6"-malonyl) glucoside	551.1	303.05	0.98
	21	4.04	$C_{27}H_{30}O_{14}$	$[M+H]^+$	Apigenin-7-O-rutinoside (Isorhoifolin)	579.17	271.01	1.42
	22	4.06	$C_{21}H_{20}O_{11}$	$[M+H]^+$	Kaempferol-3-O-glucoside (Astragalin)	449.11	287.06	2.15
	23	4.72	$C_9H_{10}O_4$	$[M-H]^-$	3,4-Dihydroxybenzoic acid Ethyl Ester	181.05	108	1.41

*Indicates the top three compounds from different fractions of CNC with the highest relative content.

to inhibit lipase activity (34, 35). Compared with untreated mice in the control group, the CLS 100 mg/kg showed a tumor inhibition effect since day 9 (Figure 8C) while CLS 200 mg/kg and 400 mg/kg treated group significantly suppressed tumor growth starting at day 5 (Figures 8C,D). In addition, the tumor weights of the mice were significantly different in all the administered groups after execution compared to the control group (Figure 8E). Suppression of Ki67 by CLS was also confirmed *in vivo* by IHC analysis in CLS-treated BALB/c-nude mice tumors (Figures 8F,G). Based on the *in vitro* transcriptome analysis and validation of "cytokine-cytokine receptor interaction," "PI3K-Akt signaling pathway" and "MAPK signaling pathway," we measured the relative protein expression of TGFB2, INHBB, PIK3R3, ITGB8, NTRK, and CACNA1D in tumor tissue. Interestingly, we found that the paramount targets previously validated by cell samples in Western blot experiments were also corroborated in tumor samples (Figures 8H,I). Taken together, these results proved that CLS treatment could effectively inhibit the growth of NCI-H1975 tumor xenografts in a dose-dependent

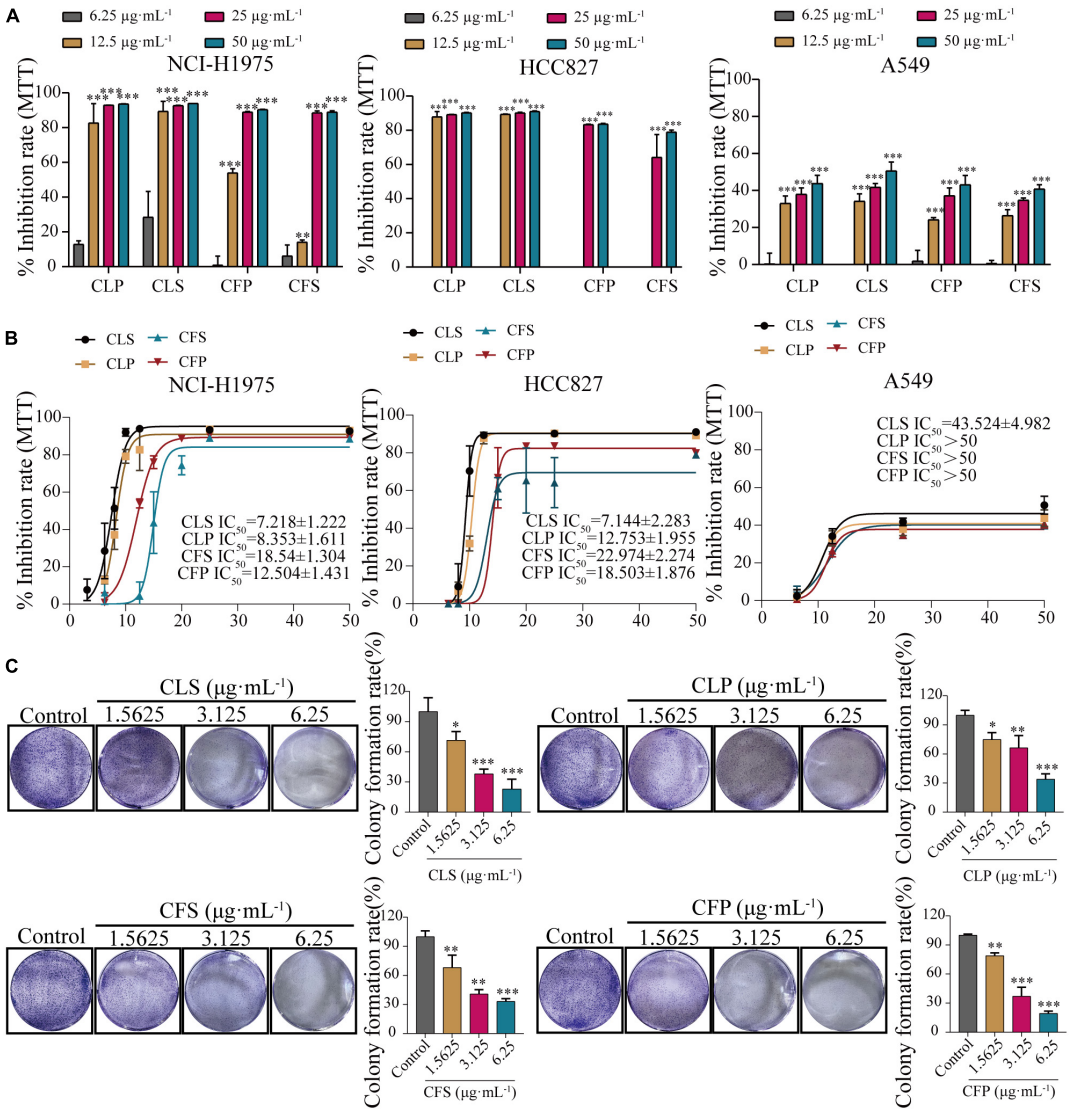

FIGURE 3
Inhibition of proliferation and clonogenic ability of NSCLC cell lines by four active fractions of CNC. **(A)** Inhibitory effects of different concentrations of CLP, CLS, CFP, and CFS (6.25, 12.5, 25, 50 μg·mL^{-1}) on NCI-H1975, HCC827 and A549 cells, respectively. **(B)** IC50 of different concentrations of CLP, CLS, CFP, and CFS (6.25, 8, 10, 12.5, 15, 20, 25, and 50 μg·mL^{-1}) on NCI-H1975, HCC827, and A549 cells, respectively. **(C)** Inhibitory effects of different concentrations of CLS, CLP, CFS, and CFP (1.5625, 3.125, 6.25 μg·mL^{-1}) on colony formation of NCI-H1975 cells, respectively. *Indicates $p < 0.05$, **indicates $p < 0.01$ and *** indicates $p < 0.001$ relative to the control by ANOVA. The data are presented as the mean ± standard deviation ($n = 3$).

manner through cytokine-cytokine receptor interaction, PIK-Akt, MAPK signaling pathways.

Discussion

Although EGFR-TKI have become a first-line inhibitor of EGFR mutation-positive NSCLC, nearly half of NSCLC patients are resistant to EGFR-TKI-based chemotherapies. Thus, it is an urgent need for development of drugs that could inhibit NSCLC with EGFR mutations. In this study, we identified inhibitory effects of different active fractions of CNC on NSCLC cell lines. Four fractions of CNC demonstrated remarkable anti-NSCLC effect. Intriguingly, upon treatment with CLS on NCI-H1975 cells, CLS suppressed the cytokine-cytokine receptor interaction, PIK-Akt and MAPK signaling pathways, leading to growth inhibition of the tumor *in vitro* and *in vivo*. Briefly, this study suggested that CNC, as a functional food, could provide a more efficient treatment in EGFR mutated NSCLC.

As a plant with both medicinal and ornamental value, the pharmacological effects of its flower fractions have been thoroughly studied (34, 36, 37), while the research on leave

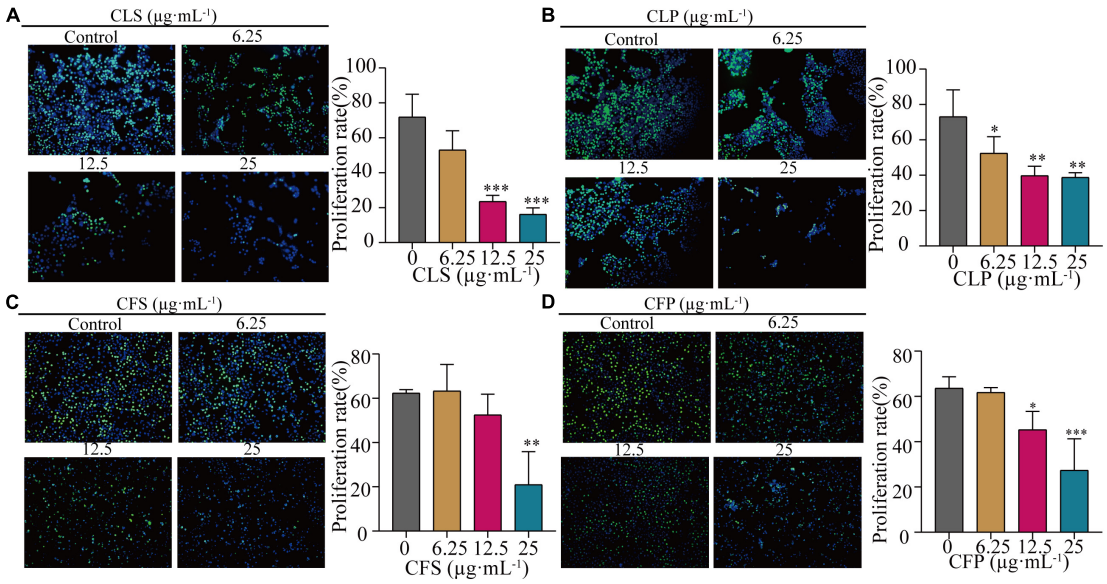

FIGURE 4
Inhibition of proliferation rate of NCI-H1975 cells by four active fractions of CNC. **(A–D)** Representative field of view of immunofluorescence assay with anti-EdU antibody is shown, where in NCI-H1975 cells, the signal of incorporating with EdU was green and the nucleus was stained blue by Hoechst. Histograms showed the mean values of cell proliferation rates after administration of different concentrations of CLS, CLP, CFS, and CFP (6.25, 12.5, 25 μg·mL^{-1}). *Indicates $p < 0.05$, **indicates $p < 0.01$ and ***indicates $p < 0.001$ relative to the control by ANOVA. The data are presented as the mean ± standard deviation ($n = 3$).

fractions was rare. Furthermore, few studies have systematically investigated the differences in the chemical composition of the four active fractions of CNC. In this study, we firstly identified the three main components of CLS are isoschaftoside, vicenin-2 and hyperin (Table 3). And recently reported, Vicenin-2 and Hyperin were identified as two novel nature medicine against NSCLC, indicating that CLS possess anti-NSCLC properties and play a crucial role in patients' defense against tumor (38, 39). However, the pharmacology effects of isoschaftoside have been rarely reported. Hence, further investigation is needed to evaluate the effects of isoschaftoside on NSCLC cells. Besides, the chemical composition of the four active fractions of CNC was found to be various by UPLC-QTOF-MS/MS (Table 4). In the two extracted fractions of the leaves of CNC, the content of geniposide (CLS 1.89 %, CLP 1.68 %) was high, while the content of the two extracted fractions of the flowers was almost absent. Extensive experiments and analysis demonstrate that geniposide possesses relatively strong anti-tumor activity (40, 41) and pulmonary protective effect (42). This suggests that the variation in geniposide content could contribute to the difference in anti-tumor activity between CNC leaf fractions and flower fractions. It is reasonable to make assumptions that the anti-tumor activity of different fractions of CNC also differed based on the composition differences.

Nowadays, few studies have investigated the effect of different active fractions of CNC on NSCLC. In this study, we examined the inhibitory of four active CNC fractions on three cell lines of NSCLC (NCI-H1975, HCC827, A549). These results showed that the four active fractions of CNC possessed remarkable inhibitory on NSCLC cell lines, especially on EGFR-T790-mutated NCI-H1975 cells (Figure 3A). To further confirm the inhibitory effect on EGFR-T790-mutated NCI-H1975 cells, colony formation assay and EdU incorporation assay were performed (Figures 3B, 4). Combining the above results, we concluded that the active fractions of CNC could effectively inhibit the proliferation of NSCLC, among which CLS had the better inhibitory effect on NCI-H1975 (Supplementary Figure 1). In addition, we found that CLS could induced programmed NSCLC death through pyroptosis (Figure 5).

Altered levels of NSCLC-related genes have been inspected by transcriptome analysis after CLS treatment. Interestingly, CLS appears to suppress tumor cell growth *via* "Cytokine-cytokine receptor interaction," "PI3K-Akt signaling pathway" and "MAPK signaling pathway"(Figure 6). According to transcriptomic results, the expression of TNFRSF10C, INHBB, TGFB1, TGFB2, and TGFB3 were down-regulated after CLS stimulation (Figure 6D). Studies of cytokines suggested that chemokines as a cytokine can promote anti-tumor immunity to NSCLC (43). At present, anti-cytokine antibodies and cytokine blockers have been extensively studied in tumor therapy (44). Transform growth factors (TGF), as an important class of cytokines, have been identified as mediators of a large number of diseases and can regulate the TME (31). Consequently, we choose TGF-β, Activin and TRAIL as the key cytokines

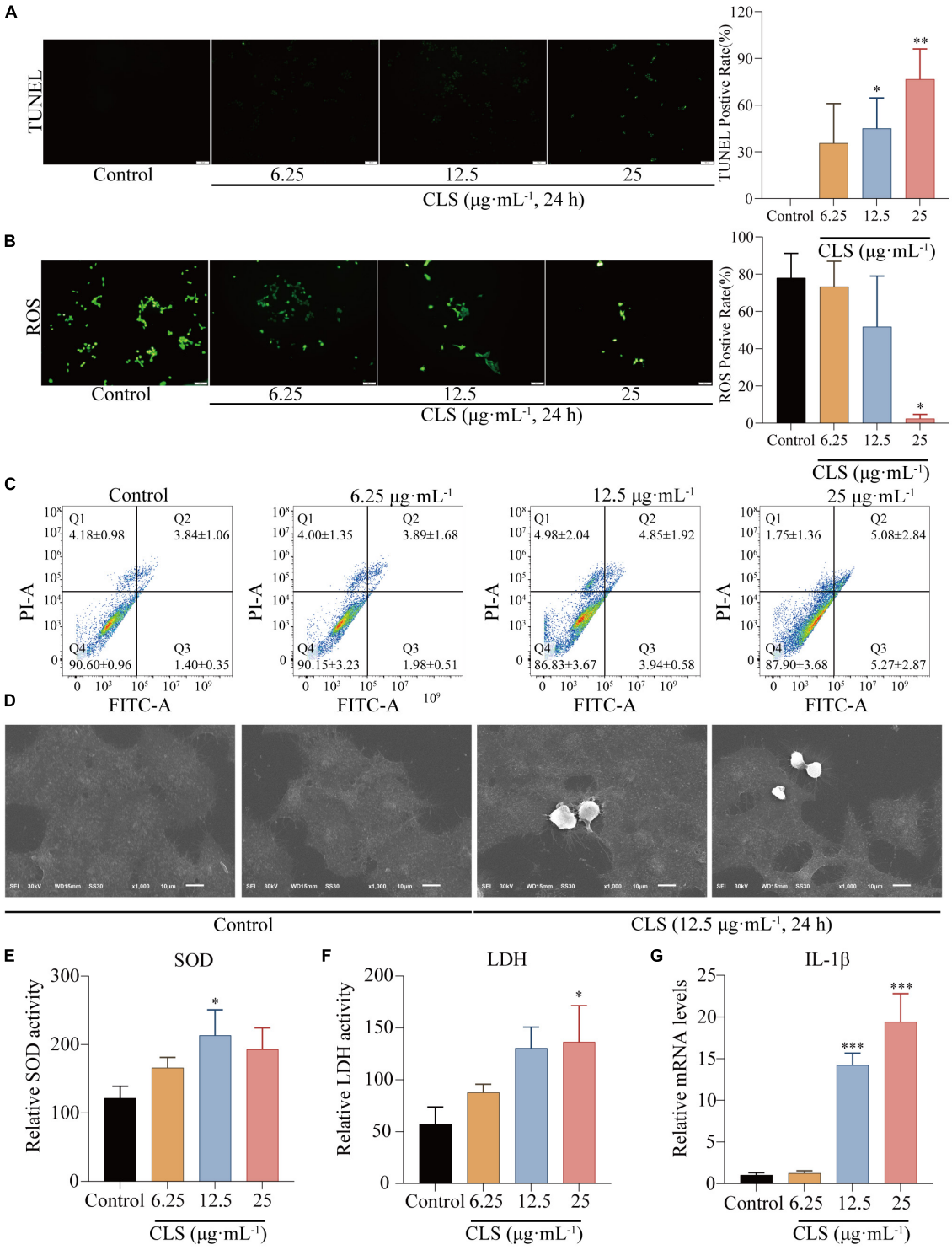

FIGURE 5
CLS induced programmed NSCLC death through pyroptosis. **(A)** TdT-mediated dUTP Nick-End Labeling (TUNEL) positive rate of NCI-H1975 cells after administration of different concentrations of CLS (6.25, 12.5, 25 $\mu g \cdot mL^{-1}$). **(B)** Reactive oxygen species (ROS) positive rate of NCI-H1975 cells after administration of different concentrations of CLS (6.25, 12.5, 25 $\mu g \cdot mL^{-1}$). **(C)** Annexin V-FITC/propidine iodide (PI) staining of NCI-H1975 cells after 48 h was performed to identify early/late apoptosis, and the data were analyzed *via* flow cytometry. **(D)** SEM was used to detect the morphological changes of NCI-H1975 cells. **(E,F)** Relative uperoxide dismutase (SOD) activity and relative lactate dehydrogenase (LDH) activity of NCI-H1975 cells after administration of different concentrations of CLS (6.25, 12.5, 25 $\mu g \cdot mL^{-1}$). **(G)** Relative IL-1β activity and relative LDH activity of NCI-H1975 cells after administration of different concentrations of CLS (6.25, 12.5, 25 $\mu g \cdot mL^{-1}$). *Indicates $p < 0.05$, **indicates $p < 0.01$ and ***indicates $p < 0.001$ relative to the control by ANOVA. The data are presented as the mean ± standard deviation ($n = 3$).

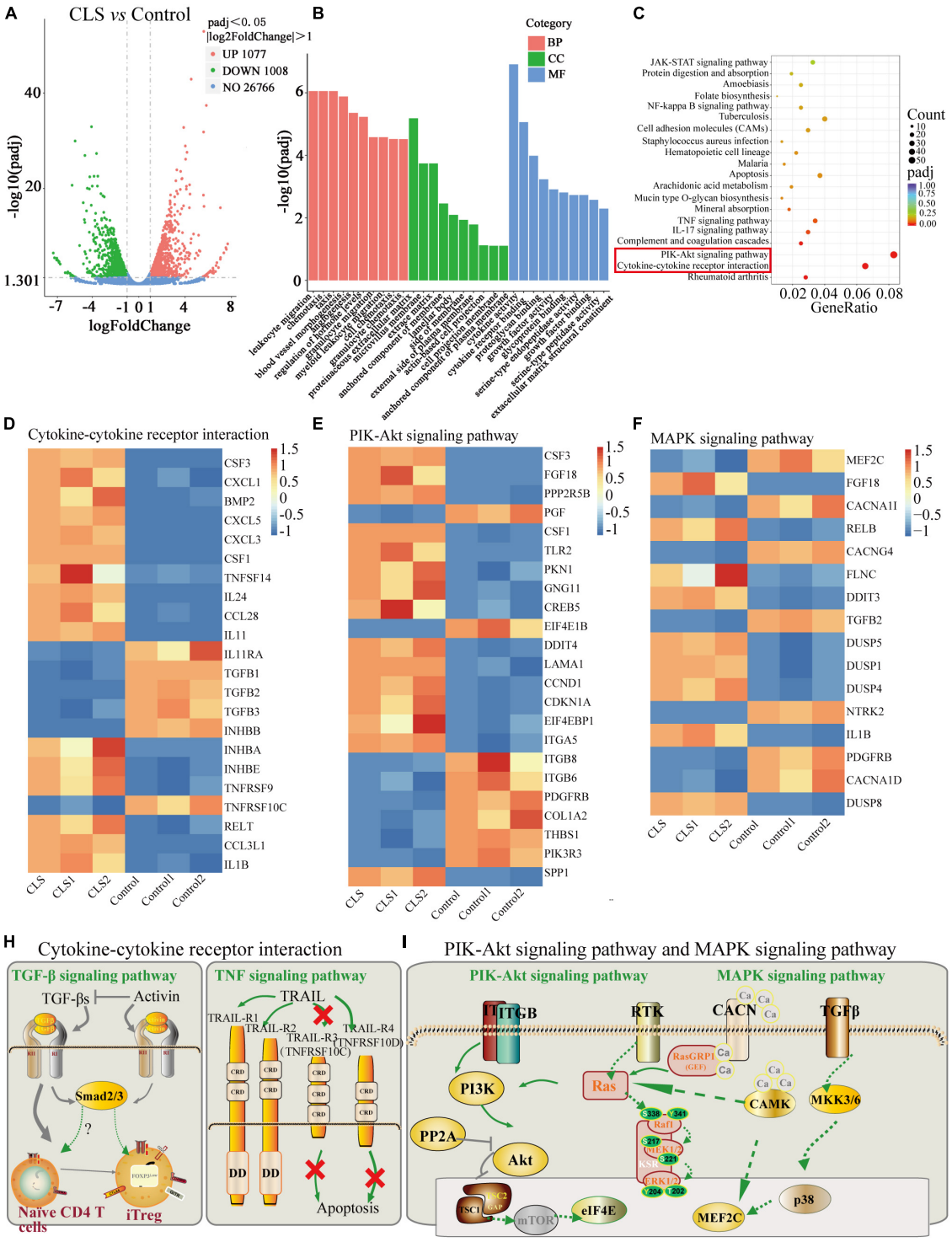

FIGURE 6
Transcriptome analysis of NCI-H1975 cells between the control group and CLS-treated group. **(A)** Volcano plot with 1,077 DEGs up-regulated and 1,008 DEGs down-regulated. **(B)** GO enrichment analysis of up-regulated and down-regulated DEGs. **(C)** KEGG enrichment analysis of up-regulated and down-regulated DEGs. **(D)** The expression heatmap of 22 DEGs related to Cytokine-cytokine receptor interaction and Rheumatoid arthritis signaling pathway in each sequencing sample. **(E)** The expression heatmap of 23 DEGs related to PIK-Akt signaling pathway in each sequencing sample. **(F)** The expression heatmap of 16 DEGs related to MAPK signaling pathway in each sequencing sample. **(H,I)** Interaction relationships of DEGs on four signaling pathways, including TGF-β signaling pathway, TNF signaling pathway, PIK-Akt signaling pathway and MAPK signaling pathway.

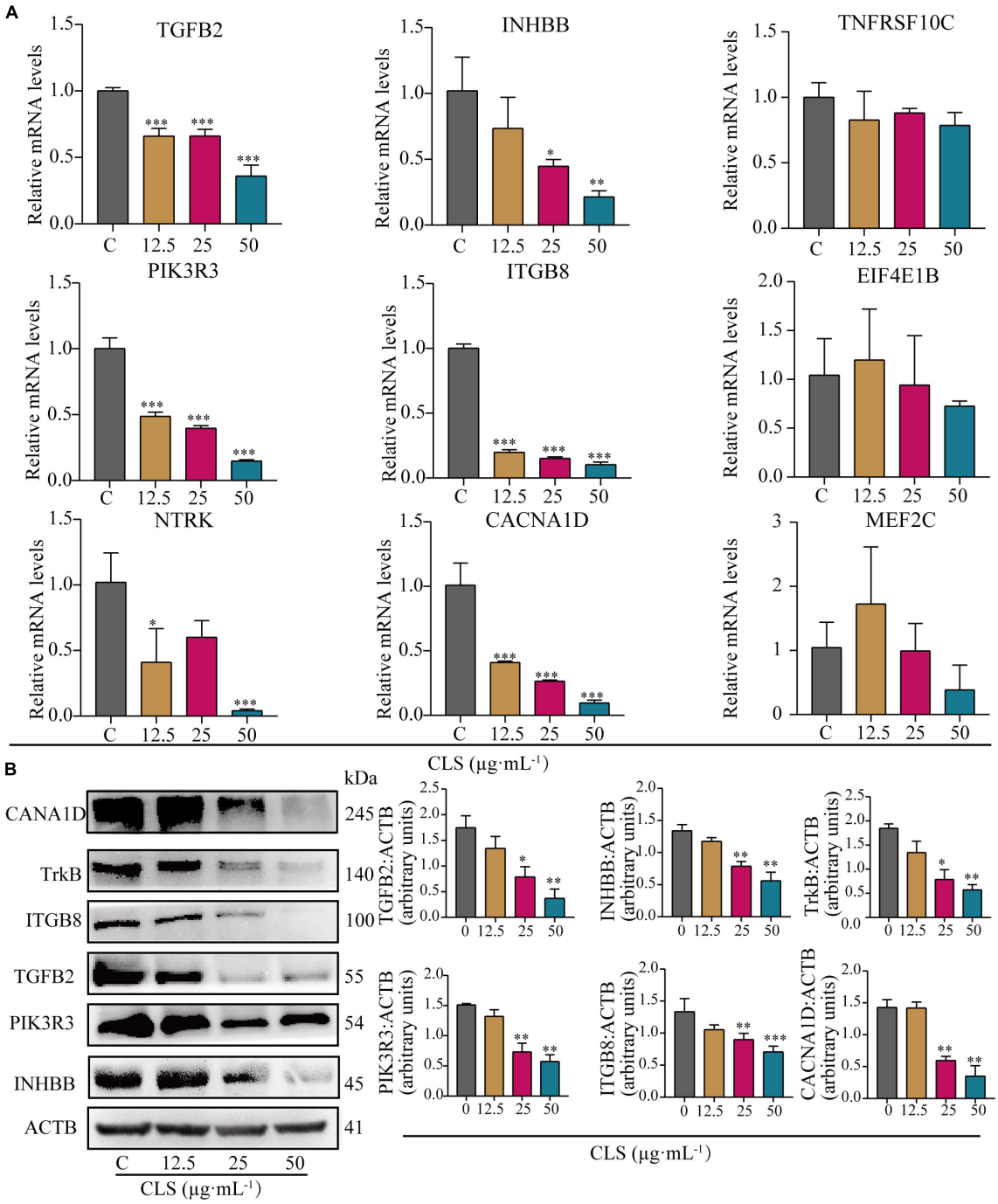

FIGURE 7
Comparative analysis of quantitative real-time PCR (RT-qPCR) data and Western Blot (WB) data. **(A)** Relative mRNA levels of nine genes including TGFB2, INHBB, TNFRSF10C, PIK3R3, ITGB8, EIF4E1B, NTRK, CACN1D, MEF2C. **(B)** Protein levels of INHBB, PIK3R3, TGFB2, ITGB8, TrkB, CACNA1D detected in CLS-treated NCI-H1975 cells were detected by Western blot with quantification of each protein, $n = 3$ biologically independent embryos. *Indicates $p < 0.05$, **indicates $p < 0.01$ and ***indicates $p < 0.001$ relative to the control by ANOVA. The data are presented as the mean ± standard deviation ($n = 3$).

and cytokine receptors. In this research, CLS treatment might promote T cell differentiation and tumor immune response by inhibiting the expression of three TGF phenotypes (TGF-β1, TGF-β2, and TGF-β3), thereby inhibiting tumor angiogenesis and invasion. At the same time, by inhibiting TNFRSF10C competitively binding with tumor necrosis factor-associated

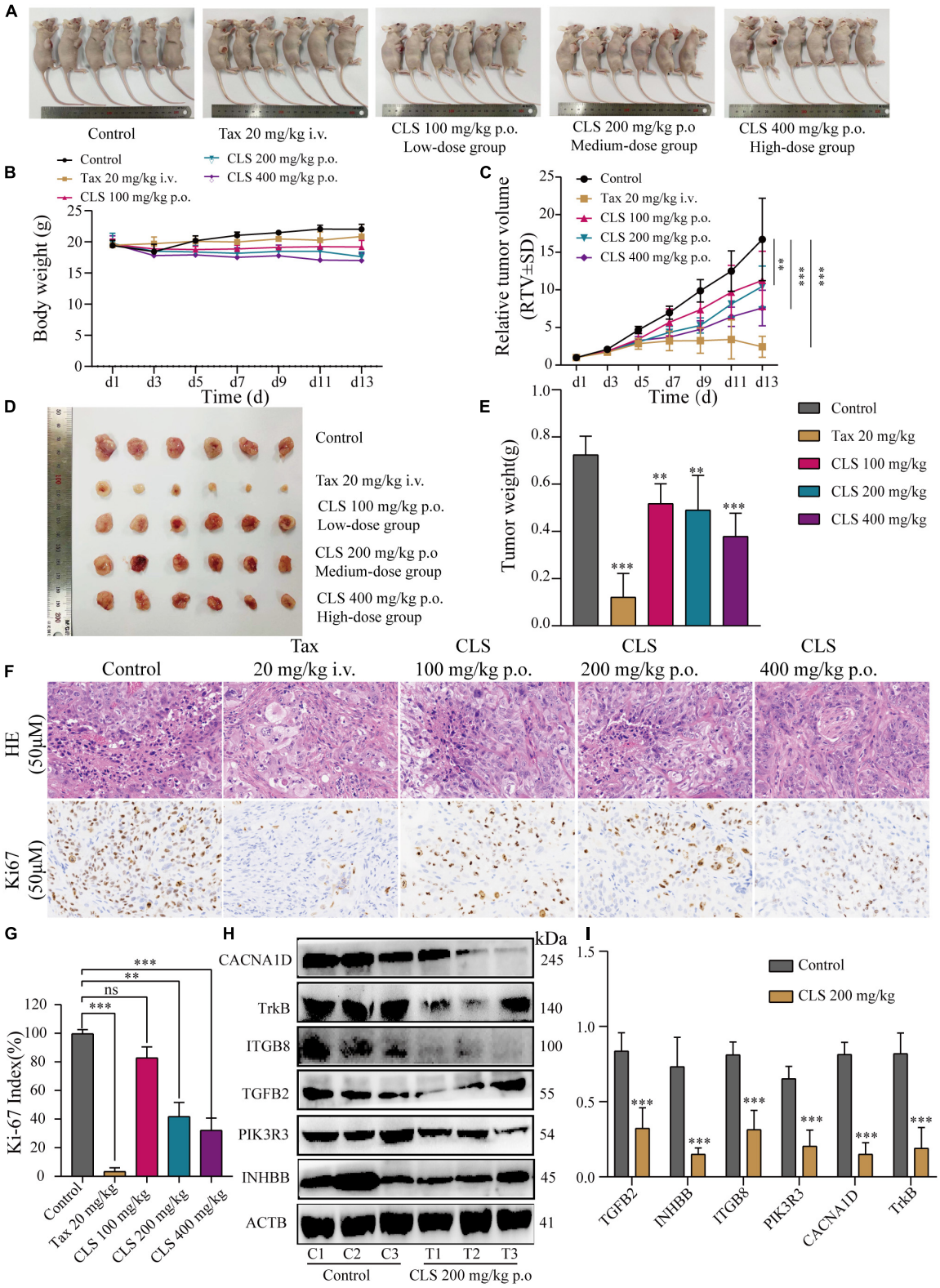

FIGURE 8
CLS suppressed tumor growth in nude mice. **(A,B)** Signs and weight changes in nude mice, $n = 6$ biologically independent embryos. **(C,D)** Variations in relative tumor volume (RTV) and tumor size in nude mice, $n = 6$ biologically independent embryos. **(E)** Tumor weight in nude mice, $n = 6$ biologically independent embryos. **(F,G)** Morphological observation of tumor by H&E staining and Ki67 detected by DAB yellow staining. **(H,I)** Protein levels of INHBB, PIK3R3, TGFB2, ITGB8, TrkB, CACNA1D detected in CLS-treated tumors were detected by Western blot with quantification of each protein, $n = 3$ biologically independent embryos. $^{*}p < 0.05$, $^{**}p < 0.01$, and $^{***}p < 0.001$ relative to the control by ANOVA.

apoptosis-inducing ligand (TRAIL), TRAIL-induced tumor cell apoptosis can be promoted, thus possibly inhibiting the proliferation and metastasis of tumor cells (**Figures 6D,H**). Alternatively, tumor cells promote the expression of cytokines to escape the immune response. Overall, the inhibitory of CLS on tumor growth might be exerted by affecting the interaction of cytokines-cytokines receptors. Among them, TGF-β and TNFRSF10C might be the two most critical targets for suppressing NSCLC growth. Therefore, remodeling the immune microenvironment of NSCLC through inhibiting Cytokine-cytokine receptor interaction provides new perspectives for the treatment of NSCLC. Besides, our RT-qPCR and WB results also suggested that the down-regulation of the levels of TGFB2 and INHBB genes might be important targets that suppress the proliferation of NCI-H1975 cells (**Figures 7A,B**).

TGF-β induces EMT in tumor cells through Smad and non-Smad signaling pathways, whereas non-Smad includes signaling pathways such as PI3K, MAPK (45). Based on transcriptomic data, we found that ITGB8 down-regulation cascades its downstream signal PIK3R3 expression to be suppressed (**Figures 6E,I**). We hypothesized that the up-regulation of PPP2R5B combined with the down-regulation of PIK3R3 resulted in the inhibition of the Akt-mTOR signaling pathway (**Figures 6E,I**). As a result, eukaryotic initiation factor 4E (elF4E) was down-regulated. Furthermore, numerous studies have shown that ITGB8 and EIL4E proteins are associated with cancer migration, invasion and metastasis and autophagy (46, 47). We speculate that CLS may induce autophagy-mediated cell death by inhibiting the PIK3R3-Akt-mTOR axis through ITGB8 down-regulation. Mitogen-activated protein kinase (MAPK) signaling pathway, as one of the key pathways to induce tumor production, is involved in a series of cell physiological activities such as cell growth, differentiation and apoptosis (48). According to the transcriptomic analysis, CLS inhibited both CACN receptors (CACNA1D, CACNG4, CACNA1I) and RTK receptors (NTRK2, PDGFRB) and cascade RAS was inhibited (**Figures 6F,I**). The loss of Ca^{2+} caused by CACN receptors repression also resulted in the down-regulation of RAS and MEF2C expression. It is worth mentioning that intracellular Ca^{2+} can be considered a major regulator of autophagy. Therefore, we selected six genes related to PIK-Akt and MAPK signaling pathways for RT-qPCR validation (PIK3R3, ITGB8, EIF4E1B, TrkB, CACNA1D, and MEF2C), and the results indicated that PIK3R3, ITGB8, NTRK, and CACNA1D could be used as new targets for NCI-H1975 (**Figures 7A,B**). This observation supports the hypothesis that CLS could induce cell autophagy and inhibit tumor growth *via* PI3K and MAPK signaling pathways. However, the mechanism by which PIK3R3, ITGB8, TrkB, and CACNA1D induce cell autophagy and inhibit tumor growth remains to be elucidated. We speculate that suppression of TGFB2, CACNA1D, TrkB, and ITGB8 could result in reduced PI3K expression, which ultimately would inhibit the metastatic and invasive ability of NCI-H1975 (**Figure 6I**). In this regard, it has been reported that Vicenin-2 (the content in CLS is 2.36%) inhibited the expression of key proteins of PI3K/Akt and TGF-β/Smad signaling pathway in A549 and NCI-H1299 cells, resulting in reduced EMT (39). These observations suggesting TGFB2, INHBB, PIK3R3, ITGB8, NTRK, and CACNA1D as major mediators in CLS-induced NCI-H1975 cell death. Importantly, these results indicated that CNC as a functional food has the advantage of being multi-channel and multi-target against NSCLC.

Based on the observed effects of CLS on NSCLC, we also constructed the xenograft models assay in nude mice to verify whether CLS is effective *in vivo* NSCLC models. In this work, we found that CLS significantly inhibited the growth of transplanted tumors in nude mice in a concentration-dependent manner (**Figure 8A**). Interestingly, the slight change in body weight of nude mice with increasing drug doses. However, physiological and biochemical results and H&E sections of the liver and kidney confirmed the absence of significant drug toxicity, suggesting CLS may play a role in lipid-lowering (**Figure 8B** and **Supplementary Figure 2**) (35). Also, we performed WB validation in tissue samples of the proteins screened in the previous experiments, with results generally consistent with cell samples (**Figures 8H,I**). Also, we verified the pathological patterns of tumors and the expression level of Ki67 in tumors by H&E and IHC, which indicating tumor proliferation rate was significantly suppressed (**Figures 8F,G**). Collectively, our findings identified CLS as a new EMP for NSCLC, providing an essential molecular foundation for enhanced understanding of CNC treatment for NSCLC.

In this work, we preliminarily elucidated the anti-tumor effect by which the four active fractions of CNC against NSCLC and the anti-tumor mechanism of CLS. However, this investigation has several limitations. As an essential method to evaluate pharmacological effects of Chinese medicine, Serum Pharmacology is an important auxiliary analysis method (49, 50). Despite the compositions of different fractions of CNC having been identified, the compounds in serum after oral administration of CLS in mice still require in-depth research. In addition, the specific compounds that affect these signaling pathways and targets still require further corroboration. Although the details of effective compounds and their mechanism in CNC remain unknown, our findings revealed a basic mechanism for the anti-NSCLC effect of CLS, providing scientific support for the application of CNC as a functional food with anti-cancer activity.

Data availability statement

The original contributions presented in the study are publicly available. This data can be found here: https://www.ncbi.nlm.nih.gov/bioproject/PRJNA891478/.

Ethics statement

The animal study was reviewed and approved by Hubei University of Chinese Medicine.

Author contributions

ZW: methodology, data curation, formal analysis, study design, investigation, writing, and validation. XH: study design and writing – original draft. ML: writing – original draft. RJ: software, methodology, and supervision. ZL: software, data curation, and supervision. YW: validation, investigation, and methodology. YG: data curation. DL: formal analysis, software, and supervision. BH: resources, supervision, and writing – original draft. HD: resources, supervision, investigation, writing – original draft and editing, and project administration. All authors contributed to the article and approved the submitted version.

Funding

This work was financially supported by the National Natural Science Foundation of China (Grant no. 81903845) and the Young Elite Scientists Sponsorship Program by CAST (2021-QNRC2-B16).

Acknowledgments

We thank to the Hubei University of Traditional Chinese Medicine for nurturing me. We are grateful to Shengtao Yuan of China Pharmaceutical University and Aiqun Jia of Hainan University for providing samples and guidance.

Conflict of interest

The authors declare that the research was conducted in the absence of any commercial or financial relationships that could be construed as a potential conflict of interest.

Publisher's note

Supplementary material

The Supplementary Material for this article can be found online at: https://www.frontiersin.org/articles/10.3389/fnut.2022.1014414/full#supplementary-material

SUPPLEMENTARY FIGURE 1
Inhibition of proliferation and clonogenic ability of HCC827 cells by four active fractions of CNC. **(A,B)** Inhibitory effects of different concentrations of CLS, CLP, CFS, and CFP (6.25 $\mu g \cdot mL^{-1}$) on colony formation and EdU assay of HCCC827 cells. **(C,D)** Inhibitory effects of different concentrations of CLS (1.5625, 3.125, 6.25 $\mu g \cdot mL^{-1}$) on colony formation and EdU assay of HCCC827 cells, respectively. *Indicates $p < 0.05$, **indicates $p < 0.01$ and ***indicates $p < 0.001$ relative to the control by ANOVA. The data are presented as the mean ± standard deviation ($n = 3$).

SUPPLEMENTARY FIGURE 2
CLS treatment without significant hepatic or renal toxicity. **(A)** H&E pathological sections of liver and kidney tissues. **(B)** Aspartate aminotransferase (AST/GOT) and Alanine aminotransferase (ALT/GTP) of livers in nude mice, $n = 6$ biologically independent embryos. **(C)** Urea nitrogen (BUN) and Sreatinine (Scr) of livers in nude mice, $n = 6$ biologically independent embryos.

References

1. Sun SG, Huang ZH, Chen ZB, Huang SQ. Nectar properties and the role of sunbirds as pollinators of the golden-flowered tea (*Camellia petelotii*). *Am J Bot.* (2017). 104:468–76. doi: 10.3732/ajb.1600428

2. Huang XC, Wei JF, Lu MY. *Guangxi herbal medicine standard*. (Vol. 2). Guangxi: Zhuang Autonomous Region Health Department (1990).

3. Chen QR, Liu FYQ, Lin SC, Sin SQ. Key points on the introduction and cultivation techniques of Golden Flower Tea. *South Agric.* (2018) 12:48–9.

4. Wang Z, Guan Y, Yang R, Li J, Wang J, Jia AQ. Anti-inflammatory activity of 3-cinnamoyltribuloside and its metabolomic analysis in LPS-activated RAW 264.7 cells. *BMC Complement Med Ther.* (2020) 20:329. doi: 10.1186/s12906-020-03115-y

5. Yang R, Guan Y, Wang WX, Chen HJ, He ZC, Jia AQ. Antioxidant capacity of phenolics in *Camellia nitidissima* Chi flowers and their identification by HPLC Triple TOF MS/MS. *PLoS One.* (2018) 13:e0195508. doi: 10.1371/journal.pone.0195508

6. An L, Zhang W, Ma G, Wang K, Ji Y, Ren H, et al. Neuroprotective effects of *Camellia nitidissima* Chi leaf extract in hydrogen peroxide-treated human neuroblastoma cells and its molecule mechanisms. *Food Sci Nutr.* (2020) 8:4782–93. doi: 10.1002/fsn3.1742

7. Hou XY, Du HZ, Yang R, Qi J, Huang Y, Feng SY, et al. The antitumor activity screening of chemical constituents from *Camellia nitidissima* Chi. *Int J Mol Med.* (2018) 41:2793–801. doi: 10.3892/ijmm.2018.3502

8. Wang ZL, Guo YJ, Zhu YY, Le L, Wu T, Liu DH, et al. Active fractions of *Camellia nitidissima* inhibit non-small cell lung cancer via suppressing epidermal growth factor receptor. *Chin J Tradit Chin Med.* (2021) 46:5362–71. doi: 10.19540/j.cnki.cjcmm.20210628.701

9. Siegel RL, Miller KD, Jemal A. Cancer statistics, 2020. *CA Cancer J Clin.* (2020) 70:7–30.

10. Li Y, Yu X, Wang Y, Zheng X, Chu Q. Kaempferol-3-O-rutinoside, a flavone derived from *Tetrastigma hemsleyanum*, suppresses lung adenocarcinoma via the calcium signaling pathway. *Food Funct.* (2021) 12:8351–65. doi: 10.1039/d1fo00581b

11. Zhu H, Liu H, Zhu JH, Wang SY, Zhou SS, Kong M, et al. Efficacy of ginseng and its ingredients as adjuvants to chemotherapy in non-small cell lung cancer. *Food Funct.* (2021) 12:2225–41.

12. Siegel RL, Miller KD, Fuchs HE, Jemal A. Cancer Statistics, 2021. *CA Cancer J Clin.* (2021) 71:7–33.

13. Stevens D, Ingels J, Van Lint S, Vandekerckhove B, Vermaelen K. Dendritic cell-based immunotherapy in lung cancer. *Front Immunol.* (2020) 11:620374. doi: 10.3389/fimmu.2020.620374

14. Imyanitov EN, Iyevleva AG, Levchenko EV. Molecular testing and targeted therapy for non-small cell lung cancer: Current status and perspectives. *Crit Rev Oncol Hematol.* (2021) 157:103194.

15. Zeng H, Castillo-Cabrera J, Manser M, Lu B, Yang Z, Strande V, et al. Genome-wide CRISPR screening reveals genetic modifiers of mutant EGFR dependence in human NSCLC. *Elife.* (2019) 8:e50223. doi: 10.7554/eLife.50223

16. Niu M, Xu J, Liu Y, Li Y, He T, Ding L, et al. FBXL2 counteracts Grp94 to destabilize EGFR and inhibit EGFR-driven NSCLC growth. *Nat Commun.* (2021) 12:5919. doi: 10.1038/s41467-021-26222-x

17. Wang Z, Duan J, Cai S, Han M, Dong H, Zhao J, et al. of Blood tumor mutational burden as a potential biomarker for immunotherapy in patients with non-small cell lung cancer with use of a next-generation sequencing cancer gene panel. *JAMA Oncol.* (2019) 5:696–702.

18. Marzio A, Kurz E, Sahni JM, Di Feo G, Puccini J, Jiang SW, et al. EMSY inhibits homologous recombination repair and the interferon response, promoting lung cancer immune evasion. *Cell.* (2022) 185:169–83. doi: 10.1016/j.cell.2021.12.005

19. Herbst RS, Morgensztern D, Boshoff C. The biology and management of non-small cell lung cancer. *Nature.* (2018) 553:446–54.

20. Yang R, Guan Y, Zhou J, Sun B, Wang Z, Chen H, et al. Phytochemicals from *Camellia nitidissima* Chi flowers reduce the pyocyanin production and motility of *Pseudomonas aeruginosa* PAO1. *Front Microbiol.* (2017) 8:2640. doi: 10.3389/fmicb.2017.02640

21. Hou M, Hu W, Xiu Z, Shi Y, Hao K, Cao D, et al. Efficient enrichment of total flavonoids from *Pteris ensiformis* Burm. extracts by macroporous adsorption resins and in vitro evaluation of antioxidant and antiproliferative activities. *J Chromatogr B Analyt Technol Biomed Life Sci.* (2020) 1138:121960. doi: 10.1016/j.jchromb.2019.121960

22. Zhou YF, Wang LL, Chen LC, Liu TB, Sha RY, Mao JW. Enrichment and separation of steroidal saponins from the fibrous roots of Ophiopogon japonicus using macroporous adsorption resins. *RSC Adv.* (2019) 9:6689–98. doi: 10.1039/c8ra09319a

23. Fraga CG, Clowers BH, Moore RJ, Zink EM. Signature-discovery approach for sample matching of a nerve-agent precursor using liquid chromatography-mass spectrometry, XCMS, and chemometrics. *Anal Chem.* (2010) 82:4165–73. doi: 10.1021/ac1003568

24. Wang ZQ, Zhang ZB, Li Y, Sun L, Peng DZ, Du DY, et al. Preclinical efficacy against acute myeloid leukaemia of SH1573, a novel mutant IDH2 inhibitor approved for clinical trials in China. *Acta Pharm Sin B.* (2021) 11:1526–40. doi: 10.1016/j.apsb.2021.03.005

25. Kayagaki N, Kornfeld OS, Lee BL, Stowe IB, O'Rourke K, Li Q, et al. NINJ1 mediates plasma membrane rupture during lytic cell death. *Nature.* (2021) 591:131–6.

26. Parkhomchuk D, Borodina T, Amstislavskiy V, Banaru M, Hallen L, Krobitsch S, et al. Transcriptome analysis by strand-specific sequencing of complementary DNA. *Nucleic Acids Res.* (2009) 37:e123.

27. Chen L, Li JX, Zhu YY, Zhao TT, Guo LJ, Kang LP, et al. Weed suppression and molecular mechanisms of isochlorogenic acid a isolated from *Artemisia argyi* extract via an activity-guided method. *J Agr Food Chem.* (2022) 70:1494–506. doi: 10.1021/acs.jafc.1c06417

28. Ji X, Hou C, Gao Y, Xue Y, Yan Y, Guo X. Metagenomic analysis of gut microbiota modulatory effects of jujube (*Ziziphus jujuba* Mill.) polysaccharides in a colorectal cancer mouse model. *Food Funct* (2020) 11:163–73. doi: 10.1039/c9fo02171j

29. Hou XY, Zhang P, Du HZ, Chu WH, Sun RQ, Qin SY, et al. *Akkermansia muciniphila* potentiates the antitumor efficacy of FOLFOX in colon cancer. *Front Pharmacol.* (2021) 12:725583. doi: 10.3389/fphar.2021.725583

30. Mohsenzadegan M, Peng RW, Roudi R. Dendritic cell/cytokine-induced killer cell-based immunotherapy in lung cancer: What we know and future landscape. *J Cell Physiol.* (2020) 235:74–86. doi: 10.1002/jcp.28977

31. Colak S, Ten Dijke P. Targeting TGF-beta Signaling in Cancer. *Trends Cancer.* (2017) 3:56–71.

32. Aksamitiene E, Kiyatkin A, Kholodenko BN. Cross-talk between mitogenic Ras/MAPK and survival PI3K/Akt pathways: a fine balance. *Biochem Soc Trans.* (2012) 40:139–46. doi: 10.1042/BST20110609

33. Steelman LS, Pohnert SC, Shelton JG, Franklin RA, Bertrand FE, McCubrey JA. JAK/STAT, Raf/MEK/ERK, PI3K/Akt and BCR-ABL in cell cycle progression and leukemogenesis. *Leukemia.* (2004) 18:189–218. doi: 10.1038/sj.leu.2403241

34. Zhang HL, Wu QX, Qin XM. *Camellia nitidissima* Chi flower extract alleviates obesity and related complications and modulates gut microbiota composition in rats with high-fat-diet-induced obesity. *J Sci Food Agric.* (2020) 100:4378–89. doi: 10.1002/jsfa.10471

35. Chen J, Wu X, Zhou Y, He J. *Camellia nitidissima* Chi leaf as pancreatic lipase inhibitors: Inhibition potentials and mechanism. *J Food Biochem.* (2021) 45:e13837. doi: 10.1111/jfbc.13837

36. He X, Li H, Zhan M, Li H, Jia A, Lin S, et al. *Camellia nitidissima* chi extract potentiates the sensitivity of gastric cancer cells to paclitaxel via the induction of autophagy and apoptosis. *Onco Targets Ther.* (2019) 12:10811–25. doi: 10.2147/OTT.S220453

37. Lin JN, Lin HY, Yang NS, Li YH, Lee MR, Chuang CH, et al. Chemical constituents and anticancer activity of yellow camellias against MDA-MB-231 human breast cancer cells. *J Agric Food Chem.* (2013) 61:9638–44. doi: 10.1021/jf4029877

38. Chen D, Wu YX, Qiu YB, Wan BB, Liu G, Chen JL, et al. Hyperoside suppresses hypoxia-induced A549 survival and proliferation through ferrous accumulation via AMPK/HO-1 axis. *Phytomedicine.* (2020) 67:153138. doi: 10.1016/j.phymed.2019.153138

39. Luo Y, Ren Z, Du B, Xing S, Huang S, Li Y, et al. Structure Identification of ViceninII Extracted from Dendrobium officinale and the Reversal of TGF-beta1-Induced Epithelial(-)Mesenchymal Transition in Lung Adenocarcinoma Cells through TGF-beta/Smad and PI3K/Akt/mTOR Signaling Pathways. *Molecules.* (2019) 24:144. doi: 10.3390/molecules24010144

40. Lv K, Zhu J, Zheng S, Jiao Z, Nie Y, Song F, et al. Evaluation of inhibitory effects of geniposide on a tumor model of human breast cancer based on 3D printed Cs/Gel hybrid scaffold. *Mater Sci Eng C Mater Biol Appl.* (2021) 119:111509. doi: 10.1016/j.msec.2020.111509

41. Zhang C, Wang N, Tan HY, Guo W, Chen F, Zhong Z, et al. Direct inhibition of the TLR4/MyD88 pathway by geniposide suppresses HIF-1alpha-independent VEGF expression and angiogenesis in hepatocellular carcinoma. *Br J Pharmacol.* (2020) 177:3240–57. doi: 10.1111/bph.15046

42. Xiaofeng Y, Qinren C, Jingping H, Xiao C, Miaomiao W, Xiangru F, et al. Geniposide, an iridoid glucoside derived from Gardenia jasminoides, protects against lipopolysaccharide-induced acute lung injury in mice. *Planta Med.* (2012) 78:557–64. doi: 10.1055/s-0031-1298212

43. Zhang M, Yang W, Wang P, Deng Y, Dong YT, Liu FF, et al. CCL7 recruits cDC1 to promote antitumor immunity and facilitate checkpoint immunotherapy to non-small cell lung cancer. *Nat Commun.* (2020) 11:6119. doi: 10.1038/s41467-020-19973-6

44. Sandler A, Gray R, Perry MC, Brahmer J, Schiller JH, Dowlati A, et al. Paclitaxel-carboplatin alone or with bevacizumab for non-small-cell lung cancer. *N Engl J Med.* (2006) 24:2542–50.

45. Hasan M, Neumann B, Haupeltshofer S, Stahlke S, Fantini MC, Angstwurm K, et al. Activation of TGF-beta-induced non-Smad signaling pathways during Th17 differentiation. *Immunol Cell Biol.* (2015) 93:662–72. doi: 10.1038/icb.2015.21

46. Devis-Jauregui L, Eritja N, Davis ML, Matias-Guiu X, Llobet-Navas D. Autophagy in the physiological endometrium and cancer. *Autophagy.* (2021) 17:1077–95.

47. Wu P, Wang Y, Wu Y, Jia Z, Song Y, Liang N. Expression and prognostic analyses of ITGA11. ITGB4 and ITGB8 in human non-small cell lung cancer. *PeerJ*. (2019) 7:e8299. doi: 10.7717/peerj.8299

48. Lee S, Rauch J, Kolch W. Targeting MAPK signaling in cancer: mechanisms of drug resistance and sensitivity. *Int J Mol Sci*. (2020) 21:1102.

49. Bochu W, Liancai Z, Qi C. Primary study on the application of serum pharmacology in chinese traditional medicine. *Colloids Surf B Biointerfaces*. (2005) 43:194–7. doi: 10.1016/j.colsurfb.2005.04.013

50. Chang Z, Jian P, Zhang Q, Liang W, Zhou K, Hu Q, et al. Tannins in *Terminalia bellirica* inhibit hepatocellular carcinoma growth by regulating EGFR-signaling and tumor immunity. *Food Funct*. (2021) 12:3720–39. doi: 10.1039/d1fo00203a

frontiers | Frontiers in Nutrition

TYPE Review
PUBLISHED 28 October 2022
DOI 10.3389/fnut.2022.929554

OPEN ACCESS

EDITED BY
Gengjun Chen,
Kansas State University, United States

REVIEWED BY
Martin C. H. Gruhlke,
RWTH Aachen University, Germany
Chunpeng (Craig) Wan,
Jiangxi Agricultural University, China

*CORRESPONDENCE
Jarosław Proćków
jaroslaw.prockow@upwr.edu.pl
José M. Pérez de la Lastra
jm.perezdelalastra@csic.es
Abhijit Dey
abhijit.dbs@presiuniv.ac.in

†PRESENT ADDRESS
Tusheema Dutta,
School of Biology, Indian Institute of Science Education and Research, Thiruvananthapuram, India

SPECIALTY SECTION
This article was submitted to Nutrition and Food Science Technology, a section of the journal Frontiers in Nutrition

RECEIVED 27 April 2022
ACCEPTED 05 September 2022
PUBLISHED 28 October 2022

CITATION
Tudu CK, Dutta T, Ghorai M, Biswas P, Samanta D, Oleksak P, Jha NK, Kumar M, Radha, Proćków J, Pérez de la Lastra JM and Dey A (2022) Traditional uses, phytochemistry, pharmacology and toxicology of garlic (*Allium sativum*), a storehouse of diverse phytochemicals: A review of research from the last decade focusing on health and nutritional implications.
Front. Nutr. 9:949554.
doi: 10.3389/fnut.2022.929554

Traditional uses, phytochemistry, pharmacology and toxicology of garlic (*Allium sativum*), a storehouse of diverse phytochemicals: A review of research from the last decade focusing on health and nutritional implications

Champa Keeya Tudu[1], Tusheema Dutta[1†], Mimosa Ghorai[1], Protha Biswas[1], Dipu Samanta[2], Patrik Oleksak[3], Niraj Kumar Jha[4,5,6], Manoj Kumar[7], Radha[8], Jarosław Proćków[9]*, José M. Pérez de la Lastra[10]* and Abhijit Dey[1]*

[1]Department of Life Sciences, Presidency University, Kolkata, India, [2]Department of Botany, Dr. Kanailal Bhattacharyya College, Howrah, India, [3]Department of Chemistry, Faculty of Science, University of Hradec Kralove, Hradec Kralove, Czechia, [4]Department of Biotechnology, School of Engineering and Technology, Sharda University, Greater Noida, Uttar Pradesh, India, [5]Department of Biotechnology, School of Applied and Life Sciences, Uttaranchal University, Dehradun, India, [6]Department of Biotechnology Engineering and Food Technology, Chandigarh University, Mohali, India, [7]Chemical and Biochemical Processing Division, ICAR-Central Institute for Research on Cotton Technology, Mumbai, India, [8]School of Biological and Environmental Sciences, Shoolini University of Biotechnology and Management Sciences, Solan, India, [9]Department of Plant Biology, Institute of Environmental Biology, Wrocław University of Environmental and Life Sciences, Kożuchowska, Poland, [10]Biotechnology of Macromolecules, Instituto de Productos Naturales y Agrobiología, IPNA (CSIC). Avda, Astrofísico Francisco Sánchez, San Cristóbal de la Laguna, Spain

Allium sativum L. (Garlic) is a fragrant herb and tuber-derived spice that is one of the most sought-after botanicals, used as a culinary and ethnomedicine for a variety of diseases around the world. An array of pharmacological attributes such as antioxidant, hypoglycemic, anti-inflammatory, antihyperlipidemic, anticancer, antimicrobial, and hepatoprotective activities of this species have been established by previous studies. *A. sativum* houses many sulfur-containing phytochemical compounds such as allicin, diallyl disulfide (DADS), vinyldithiins, ajoenes (*E*-ajoene, *Z*-ajoene), diallyl trisulfide (DATS), micronutrient selenium (Se) etc. Organosulfur compounds are correlated with modulations in its antioxidant properties. The garlic compounds have also been recorded as promising immune-boosters or act as potent immunostimulants. *A. sativum* helps to treat cardiovascular ailments, neoplastic growth, rheumatism, diabetes, intestinal worms, flatulence, colic, dysentery, liver diseases, facial paralysis, tuberculosis, bronchitis, high blood

10.3389/fnut.2022.929554

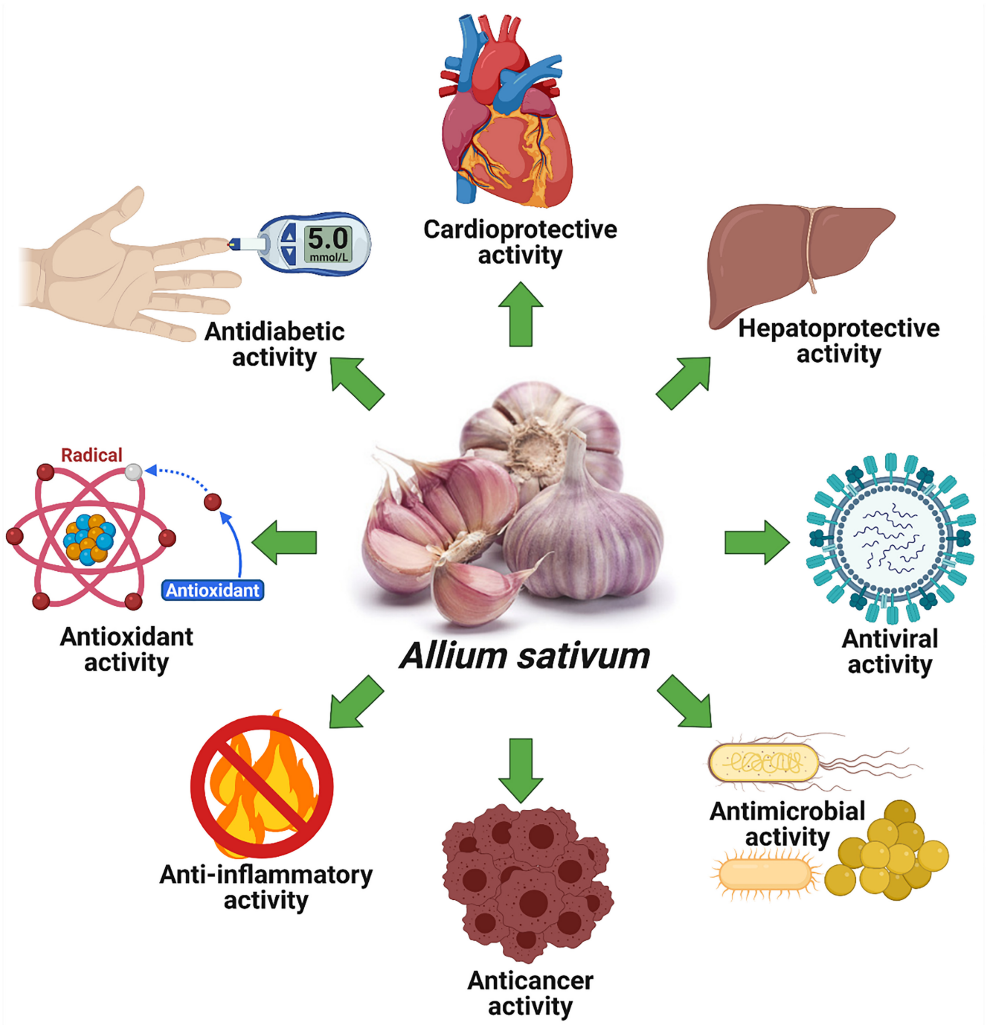

GRAPHICAL ABSTRACT

Some of the pharmacological attributes of Garlic (*Allium sativum*).

pressure, and several other diseases. The present review aims to comprehensively enumerate the ethnobotanical and pharmacological aspects of *A. sativum* with notes on its phytochemistry, ethnopharmacology, toxicological aspects, and clinical studies from the retrieved literature from the last decade with notes on recent breakthroughs and bottlenecks. Future directions related to garlic research is also discussed.

KEYWORDS

allium sativum, traditional uses, ethnobotany, phytochemistry, pharmacology, toxicology

Highlights

- Due to the numerous health benefits of *Allium sativum*, there is a growing interest in its use in various industries.
- Phytochemistry, ethnobotanical, and various pharmacological activities of *A. sativum* are extensively reviewed.
- *Allium sativum* contains various phytochemical compounds such as allicin, E-ajoene, and Z-ajoene that are of various therapeutic importance.
- Some of the sulfur-containing compounds extracted from *A. sativum* are reviewed along with their structures.
- Toxicological and clinical studies of *A. sativum* are summarized.

Introduction

Allium sativum L. (Garlic) belongs to the family Amaryllidaceae, has been originated in Asia, and is also widely cultivated in Egypt, Mexico, China, and Europe (1). This plant is highly consumed in Iran, where its foliage, flowers, and cloves are employed in local medicine (1). All parts of *A. sativum*, bulbs, leaves, cloves, and flowers are utilized to prepare mixtures and decoctions to deal with various ailments. It is also a common spice and food additive. Studies on its phytochemistry indicate that sulfur-containing compounds, such as allicin, are the essential components. Allicin (diallyl-dithiosulfinate) is the most important alkaloid responsible for its beneficial effects. Other sulfur-containing phytochemicals found in *A. sativum* include diallyl disulphide (DDS), diallyl trisulfide (DTS), and S-allyl cysteine (SAC), which have a variety of pharmacological properties (1). In India, *A. sativum* is used to treat fever, coughs and is administered topically against scabies, graying of hair, and eczema, as well as against inflammation of the tetanus and lungs (2). In Pakistan, the plant extract is consumed orally against stomach ailments, respiratory problems, and fever. In Nepal, the Middle East and East Asia, the plant is applied against fevers, rheumatism, liver disorders, diabetes, colic, intestinal worms, dysentery, flatulence, tuberculosis, high blood pressure, facial paralysis, and bronchitis. In Africa, the plant has been reported to be an antibiotic, antiviral, hypolipidemic, hypoglycemic, and antithrombotic (2–4). In this review, the phytotherapeutic properties of garlic have been comprehensively investigated to provide an updated overall view of one of the most used (and best-selling) medicinal and food plants in the world with notes on ethnobotanical information validated by preclinical bioactivities (i.e., *in vitro* and *in vivo*), emphasizing the mechanisms and signaling pathways involved. We have also discussed the recent breakthroughs and bottlenecks of relevant research on garlic with notes on future perspectives on garlic research.

Botany and geographical distribution of *Allium sativum*

A. sativum L. (**Figure 1**), commonly known as garlic, belongs to the family Amaryllidaceae (5). The bulb is mostly used to treat ailments and the perennial herbaceous plant is large, with upright flowering stems that extend up to 1 m (6). The leaf blades are linear, flattened, robust, and approximately 0.5–1.0 inch (1.25–2.5 cm) long, with a pointed apex and violet to fuchsia flowers that bloom in the Northern Hemisphere during monsoons. Slender leaves on the exterior of the odoriferous bulb surround an internal sheath containing the cloves, and each bulb contains 10–20 cloves.[1] Its medical benefits have been documented in Sanskrit texts dating back about 5,000 years and it first appeared in traditional Chinese medicine (TCM) at least 3,000 years ago (5). Today, garlic is grown almost everywhere and is known to have more than 300 varieties (7). At present, *A. sativum* is cultivated around the world. It was first discovered in Central Asia, then spread throughout China, the Near East, and the Mediterranean before making its way to the southern and middle parts of Europe, Mexico, and northern Africa, especially Egypt (5). Garlic is a perennial herb that thrives in mild regions and can be grown all year. Sowing each clove in the ground is a method to propagate the plant in cultivation asexually. Cloves are usually sown 6 weeks before the land freezes in the cold season. The bulbs only produce roots and have no stems above the surface.

Phytochemistry of *Allium sativum*

A. sativum bulbs are reported to have many bioactive compounds, many of which are sulfur-containing, *viz.* thiosulfinates (allicin), sulfides [diallyl disulfide (DADS)], vinyldithiins (2-vinyl-(4H)-1,3-dithiin, 3-vinyl-(4H)-1,2-dithiin), ajoenes (*E*-ajoene and *Z*-ajoene) diallyl trisulfide (DATS), and so on constituting up to 82% of the total sulfur content in garlic. Allicin, S-methyl cysteine sulfoxide (MCSO), and S-propylcysteine sulfoxide (PCSO) are the main noxious compounds, with allicin being the predominant cysteine sulfoxide. Allicin, MCSO and PCSO, upon acted on by various enzymes, further produce molecules that include allyl methane thiosulfinates, methyl methanethiosulfonate and other thiosulfinates (8–10). **Table 1** depicts a list of phytochemicals present in *A. sativum* with their molecular formula and

1 https://www.drugs.com/npp/garlic.html

FIGURE 1
Different parts of garlic **(A,B)** habit; **(C,D)** flowers; **(E–G)** bulb (obtained from Wikimedia commons).

IUPAC names. Figure 2 represents the chemical structures of phytochemicals (obtained from ChemSpider and PubChem).

Ethnobotanical uses of *Allium sativum*

Garlic is a well-known culinary ingredient and seasoning due to its strong aroma, which is attributed to organosulfur compounds such as allicin and DADS. Garlic's promising therapeutic advantages in ethnomedicine include its application against hypertension, pneumonia, hair loss, snakebite, diabetes, wounds, cough, paralysis, scabies, malaria, hemorrhoids, carbuncles, heart diseases, asthma, pain, respiratory disorders, influenza, female infertility, etc., which are mainly attributed to its antidiabetic, anti-atherosclerotic, antimicrobial, antihypertensive, anticancer, cardioprotective, diuretic, aphrodisiac, sedative, carminative, and antipyretic properties evidenced by various studies. Supplementary Table 1 shows the ethnobotanical and

TABLE 1 Phytochemistry of *A. sativum*.

Compounds	Molecular formula	IUPAC name	References
Allicin	$C_6H_{10}OS_2$	3-prop-2-enylsulfinylsulfanylprop-1-ene	(7, 10, 65–67)
Alliin	$C_6H_{11}NO_3S$	(2*R*)-2-amino-3-prop-2-enylsulfinylpropanoic acid	(7, 10, 65, 67, 68)
E-ajoene	$C_9H_{14}OS_3$	(1E)-1-(Allyldisulfanyl)-3-(allylsulfinyl)-1-propene	(7, 10, 69)
Z-ajoene	$C_9H_{14}OS_3$	(1Z)-1-(Allyldisulfanyl)-3-(allylsulfinyl)-1-propene	(7, 10, 65)
Diallyl disulfide (DADS)	$C_6H_{10}S_2$	3-(prop-2-enyldisulfanyl) prop-1-ene	(7, 10, 68, 70, 71)
Diallyl sulfide (DAS)	$C_6H_{10}S$	3-prop-2-enylsulfanylprop-1-ene	(7, 10, 67, 68)
3-Vinyl-1,2-dithiin	$C_6H_6S_2$	3-Vinyl-1,2-dithiine	(5, 7, 65)
Diallyl trisulfide (DATS)	$C_6H_{10}S_3$	3-(prop-2-enyltrisulfanyl) prop-1-ene	(7, 10, 67, 68, 71)
S-allyl-cysteine (SAC)	$C_6H_{11}NO_2S$	(2R)-2-amino-3-prop-2-enylsulfanylpropanoic acid	(5, 67, 68, 72, 73)
S-allylmercaptocysteine (SAMC)	$C_6H_{11}NO_2S_2$	(2R)-2-amino-3-(prop-2-enyldisulfanyl) propanoic acid	(67, 68)
Caffeic acid	$C_9H_8O_4$	(2E)-3-(3,4-Dihydroxyphenyl) prop-2-enoic acid	(66)
Diallyl tetrasulfide	$C_6H_{10}S_4$	3-(prop-2-enyltetrasulfanyl) prop-1-ene	(31, 70)
Allyl methyl trisulfide	$C_4H_8S_3$	3-(methyltrisulfanyl) prop-1-ene	(70, 71)

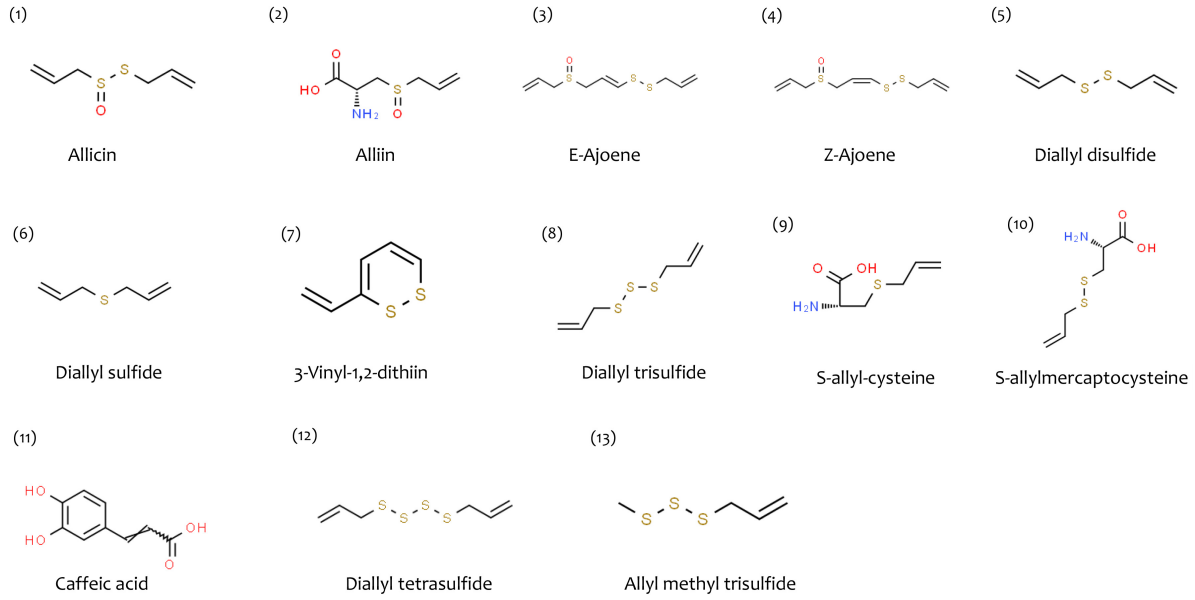

FIGURE 2
Structures of some of the phytochemicals reported from *A. sativum* (obtained from ChemSpider and PubChem).

ethnotherapeutic uses of *A. sativum* with information on the place of the report, local names, using ethnic groups, modes of administration, preparatory techniques and applied dosages.

Pharmacology of *Allium sativum*

The ethno-medicinal applications of *A. sativum* have been studied in a number of pharmaceutical studies and clinical investigations. The next section will gather the results of *in vitro*, *in vivo*, and *ex vivo* therapeutic studies using the plant to investigate pharmacological functions. The pharmacokinetic characteristics of *A. sativum* are shown in Table 2.

Biological activity of plant extracts

Antioxidant activity

According to research, *A. sativum* possesses high antioxidant properties. A study compared the antioxidant qualities of raw and cooked cloves, finding that uncooked garlic has an intense antioxidant potential, while prepared ones have extensive antioxidant effects due to -carotene decolorization (11). Oxygen radical absorption capacity (ORAC) and DPPH

TABLE 2 Pharmacological investigations of *A. sativum*.

Pharmacological activity	Extract/fractions/plant parts	*In vitro*/*in vivo*/*ex vivo* assays/models	Underlying mechanism	References
Antioxidant activity	Raw garlic samples	DPPH radical scavenging assay, ABTS radical scavenging assay, FRAP assay	Inhibitory activity of the pro-oxidant enzyme, the ability to break radical chain propagation reactions, and β-carotene bleaching	(11)
	Ethanolic extract	DPPH assay, oxygen radical absorption capacity (ORAC) assays, HT22 mouse hippocampal neuronal cell line	Prevent Aβ- or glutamate-induced cell death, early stage of sprouting	(12)
	Ethanolic extract, distilled water extract	DPPH, ABTS, FRAP, H_2O_2 scavenging, and Fe^{2+} chelating assays	Flavonoids and phenolic compounds, fenton reaction	(13)
	Ethanolic clove extract	DPPH and superoxide radical assay	Scavenge H_2O_2, inhibition of lipid peroxidation	(14)
	Bulb extract of aged garlic	Human endothelial cells	Inducing the expression of several antioxidant enzymes, the ho-1 and GCLM subunit, through nrf2- are the pathway	(143)
	Saponin based methanolic extract	Mouse-derived c2c12 myoblasts	Scavenging intracellular reactive oxygen species	(144)
Hepatoprotective activity	Ethanolic clove extract	CCl_4 induced male rabbits	Orally received 3 ml/kg of CCl_4 in olive oil (1: 1) as 1/4 LD50, serum ALT, AST, ALP, TB, and TSP were determined	(14)
	Lactic acid-fermented garlic extract	Acetaminophen (AAP)-induced acute liver injury in rats	Suppressing MAPK phosphorylation, downregulating p53	(15)
	Lactic acid-fermented garlic extract	Alcohol-induced fatty liver damage in C57BL/6J mice	Decreased TBIL and DBIL values, low serum enzymes such as ALT, AST, and ALP	(145)
	Aqueous bulb extract	Wistar rats	Improving plasma biochemical factors of liver function, such as urea, creatinine, and aspartate transaminase and alanine transaminase	(17)
Anti-inflammatory activity	Aged garlic extract	Apolipoprotein E-knockout mice	Reducing the level of TNF-α and interleukin IL-1 receptor-associated kinase 4, increasing AMPK activity in the liver	(20)
	Hexane clove extract	Lipopolysaccharide-induced macrophage cell line RAW264.7	Down-regulating the expression of iNOS and COX2	(21)
	Bulb extract or Allicin	BALB/c mice with schistosomiasis (*S. mansoni* infection)	Expression of IL13, tTG, IL-1β, IL-6, and TNF-α, immunohistochemical expression of fibronectin, and α-SMA, mRNA expression	(22)
	Aqueous bulb extract	LPS induced J774A.1 macrophages	Inhibition of NF-kB transcription factor signaling pathway	(19)
Cardioprotective activity	Aged garlic extract	Isolated rat aortic rings	Stimulation of nitric oxide production, leading to endothelial-dependent vasodilation	(23)
	Fermented garlic extract by *Bacillus subtilis*	Spontaneous hypertension rats	Modulation of the sGC-cGMP-PKG pathway	(146)
	Fermented garlic extract	Monocrotaline-induced pulmonary hypertension rats	Decreasing the expression of vascular endothelial cell adhesion molecule-1 and MMP-9, increasing the expression of PKG and eNOS	(25)

(Continued)

10.3389/fnut.2022.929554

TABLE 2 (Continued)

Pharmacological activity	Extract/fractions/plant parts	*In vitro*/*in vivo*/*ex vivo* assays/models	Underlying mechanism	References
	Black garlic extract (1.5%)	High-fat diet-fed male Sprague–Dawley rats	Reducing the mRNA expression of sterol regulatory element-binding protein-1c	(147)
	Aqueous garlic homogenate	Male Sprague–Dawley rats	Increasing Na^+/K^+-ATPase protein level	(148)
	Raw garlic	Streptozotocin-induced diabetic rats	Deacetylation of manganese superoxide dismutase, SIRT3 modulation	(149)
	Garlic extract powder capsule	Insulin-resistant obese rats	Cardiac mitochondrial ROS production, cardiac mitochondrial swelling	(150)
	Garlic extract	Rat model of gentamicin-induced chronic renal failure	Reducing oxidative stress, controlling Na^+/K^+-ATPase activity and Ca_2 + levels	(151)
Anticancer activity	Ethanolic clove extract	DLD-1 human colon cancer cells	Down-regulating the expression of cyclin B1 and CDK1, inhibiting of activation of NF-kB	(26)
	Clove extract	Human prostate cancer (PC-3), colon cancer (Caco-2), breast cancer (MCF-7), liver cancer (Hep-G2), mouse macrophage cell line (TIB-71)	Inhibiting cell proliferation, inducing cell cycle arrest inducing apoptosis	(27)
	Aged garlic extract	Human gastric carcinoma cell line (SGC-7901)	Accumulating Bax, p53, and cytochrome C and decreasing the expression of Bcl-2, MAPK pathway	(28)
	Crude garlic extract	Human breast cancer cells (MDA-MB-231), human esophageal cancer cells (WHCO1)	Targeting the folding of proteins in the endoplasmic the reticulum of cancer cells	(152)
	Ethanolic bulb extract	Human colorectal carcinoma cell line (SW620)	Regulate the JNK and p38 MAPK pathways, reducing cell viability	(153)
	Aqueous extract	Gastric adenocarcinoma (AGS) cells and normal intestinal cells (INT-407)	Reducing the potential of the mitochondrial membrane Bax/Bcl-2, Up-regulating cytochrome C	(154)
	Ethanolic extract	Mouse xenograft model of hepatoma Huh-7 cells	Interaction with the Wnt pathway co-receptor LRP6 on the cell membrane	(155)
	Aqueous garlic extract with lemon extract	BALB/c mice xenograft model of breast cancer EMT6/P cells	Inhibition of the expression of vascular endothelial growth factor, increasing interferon-γ, IL-2, and IL-4 levels	(156)
Antimicrobial activity	Ethanolic bulb extract	*Staphylococcus aureus, Escherichia coli, Pseudomonas aeruginosa, Bacillus cereus, Aspergillus versicolor*, and *Penicillium citrinum, P. expansum*	Increase bacterial growth inhibition	(157)
	Aged garlic bulb extract	*Burkholderia cepacia*	Increase bacterial growth inhibition	(158)
	Ethanolic bulb extract	*Bacillus subtilis, B. megaterium, B. polymyxa, B. sphaericus, Staphylococcus aureus, Escherichia coli, Penicillium oxalicum, Aspergillus flavus, A. luchuensis, Rhizopus stolonifer, Scopulariopsis* sp. and *Mucor* sp.	Increase bacterial growth inhibition	(159)
	Ethanolic bulb extract	*Staphylococcus aureus, Pseudomonas aeruginosa, Escherichia coli*	Increase bacterial growth inhibition	(31)

(Continued)

10.3389/fnut.2022.929554

TABLE 2 (Continued)

Pharmacological activity	Extract/fractions/plant parts	*In vitro/in vivo/ex vivo* assays/models	Underlying mechanism	References
	Aqueous bulb extract	*Bacillus subtilis, Staphylococcus aureus, Escherichia coli, Klebsiella pneumoniae, Candida albicans*	Increase bacterial growth inhibition	(6)
	Garlic oil	*Penicillium funiculosum*	Destroying the cell structure, leading to the leakage of cytoplasm and macromolecules, inhibiting the bacterial growth	(32)
	Methanolic and water extracts of clove	*Bacillus cereus, Listeria monocytogenes, Staphylococcus aureus, Pseudomonas aeruginosa, Escherichia coli, Candida albicans, Rhodotorula mucilaginosa*	Inhibiting the bacterial growth	(33)
	Garlic clove oil	*Staphylococcus aureus, Escherichia coli, Pseudomonas aeruginosa, Salmonella typhi, Candida albicans*	Inhibiting the bacterial growth	(160)
Antidiabetic activity	Ethanolic extract	Streptozotocin and alloxan-induced diabetic mice and rabbits	Increased plasma insulin level, decreased plasma glucose levels, glucose-induced insulin secretion on the pancreas	(34)
	Aged garlic extract	Streptozotocin (STZ)-induced diabetic rats	Decreased blood glucose, increased serum insulin, accumulate insulin-glucose pathway	(35)
	Garlic pill	Prediabetic pregnant women	Reduced fasting blood sugar (FBS) level, prediabetic symptoms, and diastolic blood pressure	(36)

experiments with HT22 rodent hippocampus cell culture revealed that the ethanolic infusion of garlic seedlings had antioxidant properties by DPPH scavenging activity and suppression of ROS (12). AG or aged garlic, as well as NG or non-aged garlic by-products that were extracted with distilled water, ethyl alcohol, or dichloromethane, showed distinct antioxidant effects as measured by radical scavenging tests ABTS, DPHH and H_2O_2, total Fe^{3+} reducing antioxidant power (FRAP) assay and Fe^{2+} chelating experiment (13). Unlike MCG or multi clove garlic isolates, SCG or single clove garlic ones exhibited a substantial increase in scavenging activity in the DPPH test and superoxide radicals. SCG is more resistant to CCl4-induced hepatotoxicity than MCG, and it may be an effective substitute drug for severe oxidative hepatotoxicity (14).

Hepatoprotective activity

The liver-protecting potential of fermented garlic extracts produced by lactic acid bacteria toward acetaminophen (AAP) resulted in acute liver damage in rodents was discovered in a study. Bacteria suppress AAP-induced cell death in hepatocytes by inhibiting the MAPK phosphorylation route and down-regulating p53, which is involved in liver autophagy, and by cytoplasmic redox command, as evidenced by reduction of oxidative stress, glutathione and ATP exhaustion, and antioxidant enzyme actions (15). Further analysis revealed that alcohol administration increased ROS/RNS generation in various animals. It depleted liver antioxidant status, decreased liver glutathione (GSH) concentrations, and decreased superoxide dismutase activity (SOD). Only garlic compounds can shield the liver from ethanol-induced peroxidation, as evidenced by a decrease in the marker of oxidative damage (malondialdehyde, MDA) and recovery of hepatoprotective action (16). The consequences of aqueous Garlic bulb isolate on alloxan-induced plasma advancements in liver enzymes and urinary metabolic indicators in Wistar rats were examined. The liver enzymes alanine transaminase, aspartate transaminase, and alkaline phosphatase have been associated with the leakage of cytoplasm from hepatocytes into the circulation as a condition of hepatotoxicity. The result showed that when compared to control, the plasma levels of all the parameters evaluated in the rats given garlic [urea, creatinine, albumin, aspartate transaminase (AST), alanine transaminase (ALT), and alkaline phosphate (ALP)] were unaltered (17). In the livers of albino rodents, Kaur and Sharma (18) found that ethanol extracts of garlic and ascorbic acid mixtures have hepatoprotective action toward Cd damage. Cadmium administered mice had a substantial increase in the amount of malignant growth, such as multinucleated nuclei and gigantic cells, which was reversed by administering ascorbic acid and ethanolic extract, which provided protection against the toxicity. Garlic also show hepatoprotective properties due to its organosulfur compounds like diallyldisulfide (DDS) and diallyltrisulfides (DTS), which have antioxidant and detoxifying properties. These compounds

can reduce Cd-induced oxidative stress below the threshold level, produce preconditioning effects by activating survival signals, and activate DNA repair systems by reducing the binding of Cd with DNA (18).

Anti-inflammatory activity

In lipopolysaccharide treated J774A.1 macrophages (19) probed the anti-inflammatory attributes of *Allium* 14-kDa protein, something that impeded inflammatory agents such as nitric oxide (NO), prostaglandin E (PGE), TNF-, and interleukin (IL)-1 by impairing the nuclear factor-kappa B (NF-kB) signaling route (19). Morihara et al. (20) discovered that AG extract has a significant anti-inflammatory action and can assist to inhibit inflammatory responses in mouse models with apolipoprotein E knockout (ApoE-KO). In hepatocytes, AG treatment decreased TNF constructions, a prominent stimulus resulting in CRP synthesis, by 35%, downregulated interleukin-1 receptor-associated kinase 4 (IRAK4) by 60%, and increased adenosine monophosphate-activated protein kinase (AMPK) production (20). Ethyl linoleate (ELA), an essential fatty acid separated from garlic cloves, was demonstrated to suppress inducible nitric oxide synthase (iNOS) formed as a result of LPS treatment, transcription of cyclooxygenase-2 (COX-2) and the generation of pro-inflammatory cytokines. The inactivation of NF-B as well as the MAPKs and phosphorylation of the Akt circuits were responsible for this action. In RAW 264.7 cells, ELA-triggered heme oxygenase-1 (HO-1) regulates the reduction of LPS-induced NO and pro-inflammatory cytokine synthesis. In this study, the anti-inflammatory effects of ELA were established and ELA could be employed as a medical therapy to treat inflammation-related disorders (21). In BALB/c mice experiencing schistosomiasis, Metwally et al. (22) evaluated the possible anti-inflammatory effect of garlic extract and allicin against liver inflammatory indicators (*S. mansoni* infection). Both preventive and therapeutic injection of garlic extract or allicin into affected mice showed considerable immunomodulatory and anti-inflammatory benefits in this investigation. The immunohistochemical production of fibronectin and -SMA, as well as the transcription of inflammatory cytokines mRNA as indicators of liver fibrosis, indicate these consequences. Garlic significantly inhibited inflammatory cytokine expression, suggesting that the altered Th1/Th2 cytokine balance was the cause of the serum concentrations of liver fibrosis markers and proinflammatory cytokines. These markers were maintained by decreasing serum ALT and AST levels, granuloma size as well as the number of inflammatory cells, collagen fibers, and eggs in the granuloma (22).

Cardioprotective activity

Takashima et al. (23) found that the vasorelaxant impact of AG on the rat aorta had a substantial cardioprotective action in lowering arterial pressure. Endothelium-dependent vasorelaxation of the aorta is caused by AGE, which promotes vasodilation by increasing the synthesis of NO controlled by eNOS. L-arginine, a NOS precursor, was found to be one of the key elements of the AGE's vasorelaxant action. Additionally, the source of AGE's action to reduce arterial pressure in drug testing and *in vivo* testing remains unknown (23). On 22 total cholesterol tests (TC), 17 LDL cholesterol experiments (LDL-C), 18 HDL cholesterol tests (HDL-C), four fasting blood glucose tests (FBG), nine tribulations of systolic blood pressure (SBP) and 10 tests of diastolic blood pressure (DBP), *A. sativum* particle isolate was found to have cardioprotective activity. Garlic flour formulations were found to be a universal cardiac and circulatory tonic, lowering blood TC, LDL-C, HDL-C, FBG, SBP, and DBP (24). Another study looked at the effects of fermented garlic extract (FGE) on pulmonary arterial hypertension in rats given monocrotaline (MCT). In the right ventricular, MCT treatment increased weight, arterial stiffness, and atrial natriuretic peptide levels, although not in the left ventricle. FGE decreased these impacts, as well as pulmonary arteriole endothelial dysfunction and medial hypertrophy, pulmonary fibrosis produced by translations of PKG, MCT, and eNOS proteins in the lung, and increased translations of the VCAM-1 and MMP-9 proteins in the lung. FGE also inhibited an available guanylyl cyclase (sGC) inhibitor. The impact of FGE on MCT-induced heart attack in rats has been found to have cardioprotective effects, according to this research (25).

Anticancer activity

In rodents with 1,2-dimethylhydrazine (DMH)-induced tumorigenesis and multiplication of human colon tumor cells, Jikihara et al. (26) studied the anticancer effects of alcohol extracts of *A. sativum*. Pathological study shows that *A. sativum* extract can decrease adenocarcinoma and adenoma. Jikihara et al. (26) investigated the cytotoxic activity of *A. sativum* aqueous preparations in rodents with 1,2-dimethylhydrazine (DMH)-induced carcinogenesis and human colorectal tumor cell proliferation. Adenocarcinoma and adenoma can be reduced by isolate of *A. sativum*, according to histopathological research. Apoptosis was not induced by AGE, but it did slow down cell cycle progression by decreasing the expression of cyclin B1 and cdk1 in human colorectal cancer cells (26). The impacts of garlic extract on the growth of human breast cancer cell lines (MCF-7), prostate (PC-3), liver (Hep-G2), and colon (Caco-2), as well as mice macrophage cells, were investigated in a study (TIB-71). Exposure of Hep-G2, MCF-7, TIB-71, and PC-3 cells with crude garlic excerpt decreased cell proliferation by 80–90%, but only 40–55% in Caco-2 cells. It also caused growth arrest and a four-fold increase in caspase activation (apoptosis) in PC-3 cells. According to this research, crude garlic powder contains reactive fatty components and could be employed as a chemoprevention (27). A study examined the antitumor properties of diallyl trisulfide

(DATS). *In vitro* and *in vivo* treatment of patient gastric cancer cell SGC-7901 using a flavonoid molecule produced from *A. sativum* isolate. Treatment with DATS hindered SGC-7901 cell growth by inducing apoptosis and amplifying the MAPK route by phosphorylating JNK, ERK, and p38. It also inhibited invasiveness by attenuating the utterances of the MMP9 and E cadherin proteins, induce cell death and amplifies the MAPK route by initiating JNK, ERK, and p38. Furthermore, DATS therapy increased cytokine release, such as TNF- and IFN-, which promoted the inflammatory system of the host in cancer care (28).

Gastric cancer chemoprevention by allicin

Allicin, a component of *A. sativum*, was found to be effective against stomach cancer, the fifth most common cancer in the world. For a long time, the mode of action was unknown. Allicin functions by halting the cell cycle during the G2/M phase and apoptosis in gastric tumor cells, while normal stomach cells remain unaffected, according to numerous investigations. Furthermore, even in the scientific results, allicin-mediated inhibition of stomach tumorigenesis can be seen. TGF-alpha (TGF-) and its receptor epidermal growth factor receptor (EGFR) are both inhibited by allicin (EGFR). This causes cyclin E and cyclin D1 to be down-regulated, which can cause cells in the G2 phase to enter the M phase. Allicin can cause DNA damage by causing reactive oxygen species (ROS), resulting in phosphorylated P53 and P21 proteins. P21 then inhibits the cyclin-dependent kinase 4/6 (CDK4/6)-cyclin D complex, causing the cell to enter G2/M arrest.

Furthermore, the P21 polypeptide can block the P21-CDK2 and P21-proliferating cell nuclear antigen (PCNA) assemblages, causing the CDK1-cyclin B1 complex to diminish and the G2/M cell stage to be arrested. The particle's lipid-soluble nature enables it to simply transfer across cellular barriers. Allicin significantly lowers the potential of the exterior mitochondrial membrane. Elevation in the proportion of pro-apoptotic polypeptide associated with BCL2 (BAX) to anti-apoptotic protein of B cell lymphoma 2 (BCL2) caused by allicin may promote cell death *via* the mitochondrial route. A greater BAX/BCL2 ratio causes cytochrome c to be released into the cytoplasm, accompanied by caspase-9 involvement. First, caspase-3 is triggered which results in poly ADP-ribose polymerase (PARP) and apoptosis-inducing polymerase (AIP) activation. Intrinsic stimulation of p38 mitogen-activated kinase or p38 MAPK activity was greater in allicin-induced gastric tumor cells. The synthesis of the Fas membrane-spanning peptide and P53 may be increased if p38 MAPK is increased. The Fas protein is part of the tumor necrosis factor or TNF receptor superfamily and contains 3 domains (extracellular, cytoplasmic, and transmembrane). The association of Fas' cysteine-rich signal peptide with the Fas ligand (FasL) is a critical regulator of tumor growth (29). Caspase-8 is activated as a result of the interaction and can stimulate two separate apoptosis mechanisms. Caspases-8 trigger caspase-3 and caspase-7 in the mitochondrial independent route to trigger apoptosis. Caspase-8 is responsible for the liberation of Cyt c from mitochondria in the mitochondrial-dependent route (30). Allicin can also result in cell death through a process devoid of caspases. In this route, mitochondria generate apoptosis effectors such as apoptosis-inducing factor (AIF) and endonuclease G. (EndoG) which is the coactivator of AIF. EndoG and AIF are then teleported to the nuclei, where they lead to cell death through breaks in the nuclear material strands. Furthermore, allicin can cause apoptotic cell death by boosting unbound Ca^{2+} cation concentrations and inducing endoplasmic reticulum (ER) strain (**Figure 3**) (29).

Antimicrobial activity

The antibacterial activities of *Allium sativum* are extensive. Garlic essential oil [rich in diallyl monosulfide, diallyl disulfide (DADS), diallyl trisulfide, and diallyl tetrasulfide] extracted from raw bulbs had a good antibacterial action against *Pseudomonas aeruginosa, Staphylococcus aureus*, and *Escherichia coli*. The results suggest that the presence of the allyl group is essential for the antimicrobial property of such sulfide derivatives found in *Allium* (31). Additional studies have demonstrated that watery bulb infusion has high antibacterial efficacy against *Bacillus subtilis, Staphylococcus aureus, Klebsiella pneumoniae, Escherichia coli*, and *Candida albicans* due to disfunction in phospholipid bilayer synthesis by the activity of allicin (6). Garlic essential oil suppresses the fungal pathogen *Penicillium funiculosum*, presumably by infiltrating membranes and compartments, disrupting the cytoskeleton, and causing cytoplasmic and biomolecules leaks. In addition, proteomic analysis revealed the ability of garlic oil to increase or decrease the expression of few major proteins in relation to physiological metabolism (32). The antimicrobial effect of Australian garlic methanol and aqueous clove formulations was also described on *Candida albicans*, *Bacillus cereus, Escherichia coli, Staphylococcus aureus, Listeria monocytogenes, Pseudomonas aeruginosa*, and *Rhodotorula mucilaginosa*. The identification and quantification of pharmacologically potent compounds was done using ultra-high performance liquid chromatography with mass spectrometry and photodiode array detection (UHPLC-PDA-MS) and a correlation assessment was performed between the compounds and antioxidant and antimicrobial properties (33).

Antidiabetic activity

According to a research article, due to enhanced insulin-like efficacy, the antidiabetic behavior of *A. sativum* ethyl ether extract (at 0.0025 g/kg) was investigated in alloxan-induced diabetic rodents. The parietal cells of the pancreas are stimulated by ingestion of ethanol excerpt, pulp, and oil. Allicin boosted liver metabolism and pancreatic β cell insulin response (34). Another investigation found that 3 progressive doses of aged

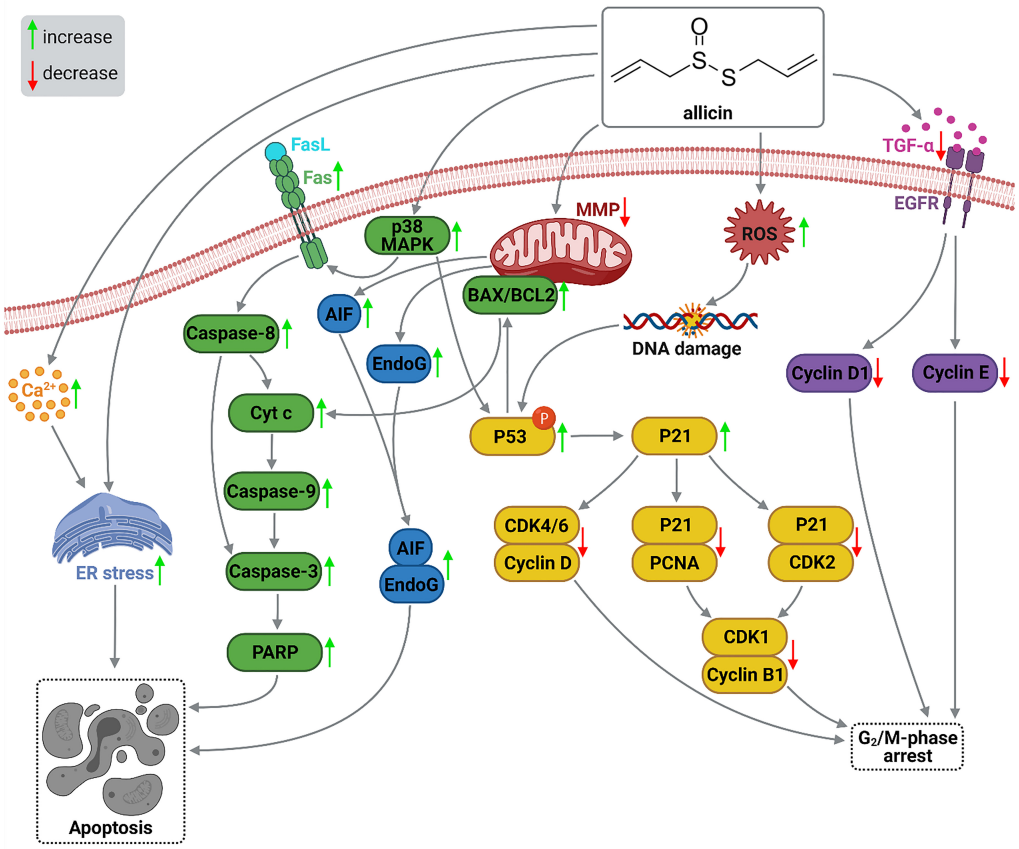

FIGURE 3
Allicin-mediated apoptosis signaling pathways in gastric cancer cells. AIF, apoptosis induce factor; BAX, BCL2-associated X protein; BCL2, B-cell lymphoma 2 protein; CDK, cyclin-dependent kinase; Cyt c, cytochrome c; EGFR, epidermal growth factor receptor; EndoG, endonuclease G; ER, endoplasmic reticulum; Fas, apoptosis antigen 1 protein; FasL, Fas receptor ligand; MAPK, mitogen-activated protein kinase; MMP, mitochondrial membrane potential; PARP, poly ADP-ribose polymerase; PCNA, proliferating cell nuclear antigen; ROS, reactive oxygen species; TGF-α, transforming growth factor alpha (29). This figure was prepared with BioRender.com.

AE extracts have hypoglycemic activities in rats treated with streptozotocin. Diabetic rats were divided into two groups: control diabetics (CD), which served as negative control, and AGE-treated diabetics (AGE-D). AGE-Ds were classified into 3 groups and given AGE at 600, 300, and 100 mg/kg every day for a period of 2 months, as well as a normal control group (CN) which was the positive control for comparison. CD rodents had higher sugar levels (almost four times), twice the amount of serum cholesterol, triglycerides, and erythrocyte glycosylated hemoglobin, and thrice the amount of kidney and liver fatty acid oxidation, compared to the CN cohort. In the streptozotocin-treated diabetic group, the findings revealed that AGE had a dosage-dependent mitigative effect on hyperglycemia markers (35). In prediabetic expectant mothers, Faroughi et al. (36) evaluated the effects of the *A. sativum* tablet on the primary outcomes of fasting blood sugar or FBS and the recurrence of signs of prediabetes, as well as secondary outcomes such as hypertension, infant anthropometric parameters, and delivery method. Throughout 2015–2016, 49 mothers with prediabetes at 24–28 weeks of gestation were included in the triple-blind, randomly selected controlled study in Tabriz, Iran. The average concentration of FBS in the garlic-treated cohort reduced from 106.6 (11.1) mg/dL before therapy to 83.6 (6.3) mg/dL after 4 weeks and 79.4 (6.1) mg/dL 8 weeks later, according to the findings. The garlic drug also resulted in a substantial reduction in pre-diabetic signs at 4 weeks after therapy and diastolic arterial tension at 4 and 8 weeks. There was no substantial difference in systolic pressure between the cohorts at 4 and 8 weeks after treatment. As a result, the *A. sativum* tablet reduced FBS levels, prediabetes indicators, and diastolic BP in this study (36).

Antiviral activity

A. sativum has long been traditionally used to cure a variety of viral illnesses. Garlic isolates or compounds have been shown to have antiviral action in several investigations (**Figure 4**). Extracts or isolates include chemical constituents that can attack different stages of the viral life cycle. Prevention of viral infection

can be as simple as inhibiting the virus's admission stage. Both encapsulated and non-enveloped pathogens are destroyed by this technique. *A. sativum* and its potent organosulfur components have been shown to promote antiviral activity by interacting with components on the exterior of the virion. This results in partial inhibition or complete blocking of the virus entry step (3). The aqueous extract of *A. sativum* expressed an effective inhibition of viral infection of influenza A subtype H1N1 with EC_{50} = 0.01 mg/ml in the Madin-Darby canine kidney (MDCK) cell line (37). The exact value of EC_{50} (0.01 mg/ml) was observed against Measles morbillivirus in Vero cells treated with gold nanoparticles containing aqueous extracts of *A. sativum* because it causes an obstruction of the viral receptors, stopping cell adsorption and the start of viral infection in the host cell (38). Furthermore, garlic extracts inhibited the binding of Newcastle disease virus (NDV) to chick embryo cell receptors (39). Quercetin, a flavonoid commonly present in fruits and vegetables, including *A. sativum*, possesses antiviral properties against influenza virus and enterovirus by affecting viral attachment to the surface of the host cell. Furthermore, organosulfur compounds in garlic such as allicin, ajoene, and diallyl trisulfide play an important role in the antiviral properties of garlic. These substances can prevent a virus from attaching to a host cell, change how the viral genome is translated in the host cell, and affect viral RNA polymerase, which is required for viral replication. They can also prevent the viral process that changes the host cell's signaling pathway, and prevent viral multiplication (40). Even if the virus enters the host cell, there are still various steps suitable for its inhibition. One of these represents inhibition in the viral replication step. Replication may occur in the cytoplasm or in the nucleus of the host cell. In the current history, numerous investigations have proven the ability of *A. sativum* to prevent viral proliferation. The methanolic and ethanolic garlic extracts revealed inhibition of viral RNA polymerase and nucleoprotein synthesis activity against the influenza A (H1N1) pdm09 virus. This property may be attributed to their ability to block viral attachment and to suppress viral hemagglutinin (HA) (41). Furthermore, the study evaluating the influence of aqueous garlic extracts on avian infectious bronchitis virus (IBV), a coronavirus that infects birds of the Coronaviridae family, suggested the potential of *A. sativum* to inhibit the viral replication step (42). The members of the retrovirus family utilize reverse transcriptase (RT) to convert viral RNA into DNA. As a result, RT suppression is a major clinical strategy in the treatment of retrovirus transmission (3). The hexane extracts of *A. sativum* expressed a powerful activity against the RT of human immunodeficiency virus 1 (HIV-1) with an IC_{50} of approximately 64.08 ± 1.09 μg/mL (43). Furthermore, allicin was evaluated in the study to relieve immune dysfunction caused by the reticuloendotheliosis virus (REV). The study suggests that allicin downregulated the ERK/MAPK signaling pathway resulting in inactivation of REV replication (3, 44).

The World Health Organization (WHO) proclaimed a worldwide pandemic of COVID-19 on March 11th, 2020, triggered by SARS-CoV-2. Although various studies have been reported for the treatment of COVID-19, an effective remedy is still missing. However, several herbal or pharmaceutical drugs have been reported with possible beneficial effects on COVID-19. One of them is *A. sativum*. As mentioned above, aqueous garlic extracts possess an inhibitory effect against IBV of the Coronaviridae family. Therefore, it is assumed that it may also be beneficial against other members of the virus family, including SARS-CoV-2. Furthermore, some constituents of *A. sativum* seem to be helpful in reducing viral replication. Quercetin, a flavonoid present in garlic, bears the potential to inhibit the main protease of SARS-CoV-2 (M^{pro}), a crucial antiviral target (45). As reported before, quercetin-3-β-galactoside was a suppressor of SARS-CoV-1 M^{pro} with IC_{50} = 42.79 ± 4.97 μM (46). Furthermore, there is a high structural similarity of M^{pro} between SARS-CoV-1 and 2 (∼96%). *In silico* molecular docking of organosulfur compounds in *A. sativum* revealed an inhibitory potential of alliin against M^{pro} SARS-CoV-2. The results suggested that alliin has potential antiviral activity against COVID-19 by binding to M^{pro} of SARS-CoV-2 (47). On the other hand, after the coronavirus outbreak, various hoaxes have been posted on the Internet about preventing COVID-19. Some of them argued that: "eating garlic prevents from COVID-19" (48). However, the WHO subsequently declared that there is no indication that garlic consumption has safeguarded patients from the novel coronavirus in the recent outbreak. Indeed, to date, no studies have been reported to confirm the prevention of *A. sativum* against COVID-19. However, there are no doubts about the beneficial effects of garlic on human health. In addition, studies recently reported confirming that despite garlic's inability to prevent COVID-19, its antiviral activity can play a crucial role in alleviating patients suffering from COVID-19.

Toxicological studies

Many investigations have been conducted on the toxicity assessment of *A. sativum* in laboratory animals. According to OECD standards 423, research explained the acute toxicity of A. sativum ethyl acetate concentrates and then determined the LD50 to demonstrate the acceptability of the extract in rodents (49). To test cytotoxic activity, all 3 animals in each set received ethanolic extract of *A. sativum* in a solitary administration of 3, 20, and 50 g/kg of lean mass. For each treatment, effects on body mass, skin tone, salivation, cornea, mucous system, drowsiness, tremor, unconsciousness, spasm, malaise, diarrhea, and death were observed after 30 min, 4 h, 24 h, 48 h, 1 week, and 2 weeks (49). Sections of the lungs, spleen, heart, kidneys, liver, and intestines were viewed during gross postmortem and microscopy using standard forensic methods.

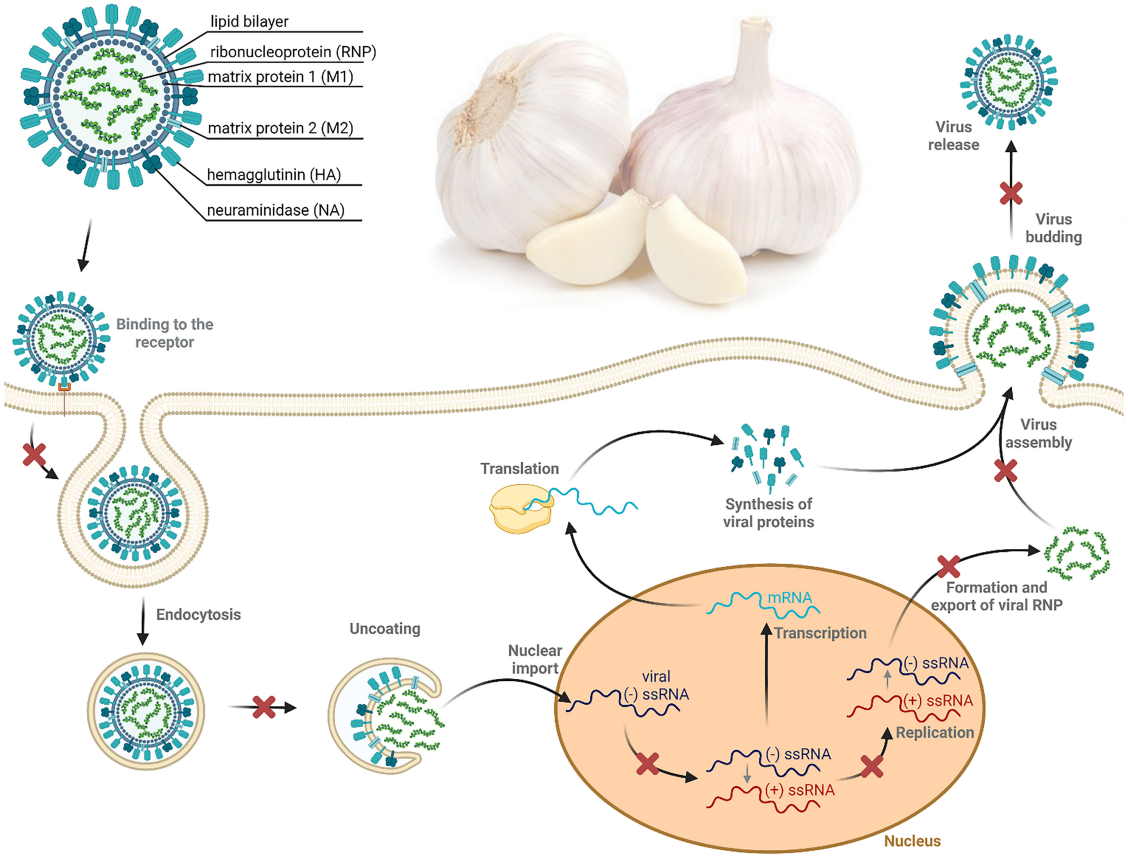

FIGURE 4
Proposed antiviral effects of *A. sativum* against (−) ssRNA viruses. This figure depicts the life cycle steps of influenza A with possible inhibition (shown as a red X-shaped symbol) mediated by garlic extracts or its organosulfur constituents. As shown in the figure, *A. sativum* bears potential for the prevention of viral penetration into the host membrane, virus uncoating associated with the release of viral genetic material into the cytoplasm, conversion of viral (−) ssRNA to viral (+) ssRNA, replication of the viral RNA, virus assembly and release (3). Figure made using BioRender.com.

The rodents did not die as a consequence of the dose increase and there was no significant change in any of the criteria used for general post mortem and histopathological alteration. As a result, the extract is fine for humans to consume (49). Another investigation looked at whether *A. sativum* preparations had a suppressive effect on lead nitrate poisoning. Their potential to eliminate free radicals and avoid GSH deficiency could describe the function of garlic organosulfur compounds in reducing $Pb(NO_3)_2$ poisoning (50). Total erythrocyte count, hemoglobin concentration, total leukocyte count, lymphocyte and monocyte percentage all decreased significantly after chronic consumption of lead nitrate. In the renal and central nervous system, the intake of lead nitrate resulted in an increase in the levels of reactive components of thiobarbituric acid, as well as a reduction in glutathione peroxidase levels and antioxidant molecules such as superoxide dismutase and catalase. Nitrate aids lower peptide levels, whereas cholesterol and lead burden increase exponentially in lead-exposed mice, resulting in decreased plaque count, immunoglobulin level, phagocytic index, and macrophage viability (50). Orally ingested extracts of *A. sativum* by exposed groups to $Pb(NO_3)_2$, on the other hand, may be a preventive strategy against heavy metal toxicity (50). In cultivated Vero cells, Abid-Essefi et al. (51) explored the role of an aqueous extract of *A. sativum* (AEA) vs. zearalenone (ZEN) mediated lethality, reactive oxygen species (ROS), and genomic instability. The findings revealed that ZEN caused several harmful consequences and major changes in the body, which were regulated through the oxidative stress system. Administration with the smallest amount of AEA (250 g/ml) in combination with ZEN resulted in a considerable decrease in ZEN-induced impairments for each marker evaluated, as well as a notable fall in DNA disintegration. As a result, AEA can assist guards against ZEN risks. The great potential of AEA to compensate for the inflammatory process generated by ZEN is probably responsible for its preventive action (51). Many research has suggested that garlic could be used as a food additive for people who are not protected from ecological toxins. Irkin et al. (52) studied the effects of dietary garlic granules on

young European sea bass (*Dicentrarchus labrax*). For 2 months, the fish received enhanced meals with *A. sativum* powder at concentrations of 0 (control), 2 percent, 4 percent, or 6 percent. The RBC count, hemoglobin level, amount of hemoglobin and mean corpuscular hemoglobin in treated fish at dietary incorporation stages of 4 and 6% were considerably less than baseline data after this study. In contrast to the reference cohort, serum sugar levels in fish supplemented with garlic powder were considerably lower, and cholesterol values in the treatment groups of 6 and 2% were smaller than those of the control group. As a consequence, it is recommended that garlic powder fortification in the diets of juvenile fish not surpass 2%. As a result, this experiment concluded that nutritional garlic powder is critical to improving the physiological and hematological state of immune improvements in young sea bass (52).

Clinical studies

A. sativum preparations are used in drug testing to alleviate a variety of human disorders. The bulbs have been used successfully as nutrition and treatment in human societies since antiquity. The possible hypoglycemic benefits of *A. sativum* in patients with type 2 diabetes were examined by Ashraf et al. (53). The purpose of this study was to compare the impact of garlic pills exposure to routine anti-diabetic analyzes on glucose levels in 60 confirmed type 2 diabetic patients with fasting blood glucose levels above 126 mg/dl. Participants were placed into two categories. Serum triglycerides and fasting blood glucose were measured at weeks 0, 12, and 24. Compared to group 2, group 1 reported a substantial reduction in fasting blood glucose at week 24. A mixture of *A. sativum* with traditional anti-diabetic medication improved glucose control and hypocholesterolemic action, according to this research. Garlic's antilipidemic effects are thought to be caused by allicin's ability to inhibit hydroxymethylglutaryl-CoA reductase, which lowers LDL-C levels as well as total cholesterol (53). Sukandar et al. (54) investigated the efficacy and tolerability of combining curcumin and *A. sativum* powder as an antidiabetic and hypocholesterolemic treatment for type 2 diabetes-dyslipidemia. 3 replicates were calculated which were 1.2, 1.6, and 2.4 g, respectively. The garlic-curcuma mixture was observed to lower glucose concentration and HbA1C while also improving dyslipidemia. The 2.4 g dose was found to reduce fasting glucose, glucose levels two hours after lunch, lipid profile, HbA1C, LDLs, cholesterol, and body mass index and increased HDLs greater than the other two prescriptions (54). The benefits of *A. sativum* supplementation on serum concentrations of certain markers of inflammation, somatic manifestations, and exhaustion in females with chronic rheumatoid arthritis or RA were studied by Moosavian et al. (55). In this investigation, a double-blind, placebo-controlled, randomized experiment was used. A group of 70 women with RA were randomly classified into two parts for 8 weeks, where the treatment group received 1,000 mg of *A. sativum* and the control team received a placebo (55). After therapy, the bioavailability of the C-reactive peptide (CRP) and TNF (TNF-a) was found to be considerably lower in the garlic cohort compared to the placebo category. Additionally, relative to the placebo group, pain severity, sensitive joint tally, disease activity score, and exhaustion were considerably lower, and the number of enlarged joints was markedly smaller in the garlic unit, but nothing of this type was demonstrated in the placebo. The result showed that garlic improved the inflammatory mediators like serum level of CRP and TNF-a, though there was no change in erythrocyte sedimentation rate (ESR) (55).

Discussion

A. sativum was found to have a spectrum of therapeutic benefits in this investigation, including antibacterial, cardioprotective, anti-inflammatory, antitumor, and antispasmodic activities, among others. The most essential components of *A. sativum* are organosulfur molecules, which are responsible for most of their medicinal uses. allyl methyl sulfide, Allicin, ajoene, and DTS are the primary physiologically active chemicals responsible for the antibacterial, antifungal, antiviral, and antiprotozoal effects of *A. sativum*, respectively (1). The main ingredient of garlic, allicin, can cause stomach disturbances, particularly when taken in large doses. Most cardiac investigations have focused on triglycerides, LDL, cholesterol level, HDL, and arteriosclerosis (56). According to suggestions, *A. sativum* lowers LDL and triglyceride concentrations in people with dyslipidemia (56). Consumption of *A. sativum* reduces triglyceride levels, which may help slow the progression of hypertension. In addition to considerable studies, its antidiabetic, antibacterial, anti-inflammatory, and antioxidant effects have been linked in various models. Several investigations have looked into the antitumor and anticarcinogenic properties of *A. sativum* and its components *in vitro* and in animal experiments. According to the findings, *A. sativum* encompasses a set of crucially significant compounds with anticancer and chemopreventive activities. Garlic includes various physiologically and pharmacologically important components, according to clinical and scientific research. For cardiac, hyperglycemia, rheumatism, gastrointestinal disorders, colitis, liver disorders, bloating, diarrhea, bronchitis, sensory loss, hypertension, asthma, and other ailments, these are vital for health. Several investigations are underway throughout the world to make efficient and unscented garlic formulations and identify bioactive constituents that may have medicinal value (57–59). However, the extraction, production, molecular, physicochemical and structural properties and structure–activity relationships of garlic compounds (60–64) are beyond the scope of the present review. The metabolic processes of

ingested garlic constituents (as food or supplements), their mechanisms of action in healthy humans have not been detailed well. Besides structure-bioactivity relationships remain unclear in many pharmacological attributes.

Conclusion

For centuries, *A. sativum* has been widely consumed as a culinary and therapeutic herb as protective and curative agents. It contains essential minerals, vitamins, and protein and is widely used as a spice or condiment in continental cooking. In addition, this plant has various potential pharmacological activities against various diseases and disorders owing to its potent antioxidative, anti-inflammatory and immunomodulatory properties. Based on preclinical studies, *A. sativum* compounds especially the sulfur-containing compounds, some flavonoids and polyphenols may help treat certain human conditions, particularly those related to cancer and cardiovascular disease. The roles of *A. sativum* and the preparations of *A. sativum* in human health will help to benefit from additional well-designed human studies and various human diseases that carefully characterize the garlic interferences used and examine possible differential effects in several human populations. This research also looked at the key ingredients of the plant, such as sulfur-containing chemicals. Many significant advances have been found in the phytochemistry and related medicinal properties of *A. sativum*; data regarding clinical aspects and impact on human health-related properties are acceptable. Therefore, it is inferred that *A. sativum* is a fantastic seasoning that needs to be handled with prudence to fully benefit from its immense medicinal benefits, taking into account that misapplication may result in unintended consequences.

Author contributions

CT, TD, MG, PB, DS, PO, NJ, MK, Radha, JP, JMP, and AD contributed to the concept, literature mining, writing, and methodology of the review, provided critical feedback, and critically revised the manuscript. CT came up with the study idea, planned and designed the review structure, wrote the first draft of the manuscript, prepared the table and figures, and had the right to list his name first in his CV, any other scientific documents, and scientific profile. TD, MG, PB, and DS contributed to writing review and editing, arranged references, and revised the table and figures. PO contributed to study idea, writing-review and editing, prepared the table and figures, arranged the references, and acquired funding. NJ, MK, and Radha participated in review structure, writing-review and editing, completed the critical revision of the entire manuscript, response, data validation, and suggestions. JP completed the critical revision of the entire manuscript, formal interpretation, and supervised the drafting process of the review, response, final draft, and resources. JMP contributed to manuscript revision, formal interpretation, supervision, response, resources, project administration, and funding acquisition. AD came up with the study idea, revised the review structure, suggestions, completed the critical revision of the entire manuscript, formal interpretation, and supervised the drafting process of the review, resources, and final draft. All authors have read and approved the final version of the manuscript for submission to this journal and contributed to the writing or revision of the final manuscript.

Funding

This work was supported by the UHK (Project No. VT2019-2021), APOGEO (Cooperation Program INTERREG-MAC 2014–2020), with European Funds for Regional Development-FEDER, the "Agencia Canaria de Investigación, Innovación y Sociedad de la Información (ACIISI) Gobierno de Canarias" (Project No. ProID2020010134), and Caja Canarias (Project No. 2019SP43).

Acknowledgments

We are grateful to our respective departments/institutes for providing the space and other necessary facilities that helped draft this manuscript.

Conflict of interest

The authors declare that the research was conducted in the absence of any commercial or financial relationships that could be construed as a potential conflict of interest.

Publisher's note

Supplementary material

The Supplementary Material for this article can be found online at: https://www.frontiersin.org/articles/10.3389/fnut.2022.929554/full#supplementary-material

References

1. Subroto E, Cahyana Y, Tensiska M, Lembong F, Filianty E, Kurniati E, et al. Bioactive compounds in garlic (*Allium sativum* L.) as a source of antioxidants and its potential to improve the immune system: a review. *Food Res.* (2021) 5:1. doi: 10.26656/fr.2017.5(6).042

2. Qiu Z, Qiao Y, Zhang B, Sun-Waterhouse D, Zheng Z. Bioactive polysaccharides and oligosaccharides from garlic (*Allium sativum* L.): production, physicochemical and biological properties, and structure–function relationships. *Comprehens Rev Food Sci Food Saf.* (2022) 21:3033–95. doi: 10.1111/1541-4337.12972

3. Rouf R, Uddin SJ, Sarker DK, Islam MT, Ali ES, Shilpi JA, et al. Antiviral potential of garlic (*Allium sativum*) and its organosulfur compounds: a systematic update of pre-clinical and clinical data. *Trends Food Sci Technol.* (2020) 104:219–34. doi: 10.1016/j.tifs.2020.08.006

4. Bhatwalkar SB, Mondal R, Krishna SB, Adam JK, Govender P, Anupam R. Antibacterial properties of organosulfur compounds of garlic (*Allium sativum*). *Front Microbiol.* (2021) 12:613077. doi: 10.3389/fmicb.2021.613077

5. Londhe VP. Role of garlic (*Allium sativum*) in various diseases: an overview. *Angiogenesis.* (2011) 12:13.

6. Meriga B, Mopuri R, MuraliKrishna T. Insecticidal, antimicrobial and antioxidant activities of bulb extracts of *Allium sativum*. *Asian Pacific J Trop Med.* (2012) 5:391–5. doi: 10.1016/S1995-7645(12)60065-0

7. Majewski M. *Allium sativum*: facts and myths regarding human health. *Roczniki Państwowego Zakładu Higieny.* (2014) 65:1–8.

8. Al-Snafi A. Pharmacological effects of *Allium* species grown in Iraq. An overview. *Int J Pharmaceutical Healthcare Res.* (2013) 1:132–47.

9. Zeng Y, Li Y, Yang J, Pu X, Du J, Yang X, et al. Therapeutic role of functional components in alliums for preventive chronic disease in human being. *Evid Based Complement Alternat Med.* (2017) 2017:9402849. doi: 10.1155/2017/9402849

10. El-Saber Batiha G, Magdy Beshbishy A, Wasef L, Elewa YH, Al-Sagan A, El-Hack A, et al. Chemical constituents and pharmacological activities of garlic (*Allium sativum* L.): a review. *Nutrients.* (2020) 12:872. doi: 10.3390/nu12030872

11. Locatelli DA, Nazareno MA, Fusari CM, Camargo AB. Cooked garlic and antioxidant activity: correlation with organosulfur compound composition. *Food Chem.* (2017) 220:219–24. doi: 10.1016/j.foodchem.2016.10.001

12. Zakarova A, Seo JY, Kim HY, Kim JH, Shin JH, Cho KM, et al. Garlic sprouting is associated with increased antioxidant activity and concomitant changes in the metabolite profile. *J Agric Food Chem.* (2014) 62:1875–80. doi: 10.1021/jf500603v

13. Jang HJ, Lee HJ, Yoon DK, Ji DS, Kim JH, Lee CH. Antioxidant and antimicrobial activities of fresh garlic and aged garlic by-products extracted with different solvents. *Food Sci Biotechnol.* (2018) 27:219–25. doi: 10.1007/s10068-017-0246-4

14. Naji KM, Al-Shaibani ES, Alhadi FA, D'souza MR. Hepatoprotective and antioxidant effects of single clove garlic against CCl 4-induced hepatic damage in rabbits. *BMC Complement Alternat Med.* (2017) 17:411. doi: 10.1186/s12906-017-1916-8

15. Lee HS, Lim WC, Lee SJ, Lee SH, Yu HJ, Lee JH, et al. Hepatoprotective effects of lactic acid-fermented garlic extract against acetaminophen-induced acute liver injury in rats. *Food Sci Biotechnol.* (2016) 25:867–73. doi: 10.1007/s10068-016-0143-2

16. Guan MJ, Zhao N, Xie KQ, Zeng T. Hepatoprotective effects of garlic against ethanol-induced liver injury: a mini-review. *Food Chem Toxicol.* (2018) 111:467–73. doi: 10.1016/j.fct.2017.11.059

17. Aprioku JS, Amah-Tariah FS. Garlic (*Allium sativum* L.) protects hepatic and renal toxicity of alloxan in rats. *J Pharmaceutical Res Int.* (2017) 17:1–7. doi: 10.9734/JPRI/2017/34909

18. Kaur, S, Sharma S. A histometric study to assess preventive action of ascorbic acid and garlic on cadmium induced hepatotoxicity in albino mice. *Int J Pharmaceutical Phytopharmacol Res.* (2015) 5:8–14.

19. Rabe SZT, Ghazanfari T, Siadat Z, Rastin M, Zamani Taghizadeh Rabe S, Mahmoudi M. Anti-inflammatory effect of garlic 14-kDa protein on LPS-stimulated-J774A. 1 macrophages. *Immunopharmacol Immunotoxicol.* (2015) 37:158–64. doi: 10.3109/08923973.2015.1005229

20. Morihara N, Hino A, Miki S, Takashima M, Suzuki JI. Aged garlic extract suppresses inflammation in apolipoprotein E-knockout mice. *Mol Nutr Food Res.* (2017) 61:1700308. doi: 10.1002/mnfr.201700308

21. Park SY, Seetharaman R, Ko MJ, Kim TH, Yoon MK, Kwak JH, et al. Ethyl linoleate from garlic attenuates lipopolysaccharide-induced pro-inflammatory cytokine production by inducing heme oxygenase-1 in RAW264. 7 cells. *Int Immunopharmacol.* (2014) 19:253–61. doi: 10.1016/j.intimp.2014.01.017

22. Metwally DM, Al-Olayan EM, Alanazi M, Alzahrany SB, Semlali A. Antischistosomal and anti-inflammatory activity of garlic and allicin compared with that of praziquantel in vivo. *BMC Complement Alternat Med.* (2018) 18:135. doi: 10.1186/s12906-018-2191-z

23. Takashima M, Kanamori Y, Kodera Y, Morihara N, Tamura K. Aged garlic extract exerts endothelium-dependent vasorelaxant effect on rat aorta by increasing nitric oxide production. *Phytomedicine.* (2017) 24:56–61. doi: 10.1016/j.phymed.2016.11.016

24. Kwak JS, Kim JY, Paek JE, Lee YJ, Kim HR, Park DS, et al. Garlic powder intake and cardiovascular risk factors: a meta-analysis of randomized controlled clinical trials. *Nutr Res Pract.* (2014) 8:644–54. doi: 10.4162/nrp.2014.8.6.644

25. Park BM, Chun H, Chae SW, Kim SH. Fermented garlic extract ameliorates monocrotaline-induced pulmonary hypertension in rats. *J Funct Foods.* (2017) 30:247–53. doi: 10.1016/j.jff.2017.01.024

26. Jikihara H, Qi G, Nozoe K, Hirokawa M, Sato H, Sugihara Y, et al. Aged garlic extract inhibits 1, 2-dimethylhydrazine-induced colon tumor development by suppressing cell proliferation. *Oncol Rep*. (2015) 33:1131–40. doi: 10.3892/or.2014.3705

27. Bagul M, Kakumanu S, Wilson TA. Crude garlic extract inhibits cell proliferation and induces cell cycle arrest and apoptosis of cancer cells in vitro. *J Med Food.* (2015) 18:731–7. doi: 10.1089/jmf.2014.0064

28. Jiang X, Zhu X, Huang W, Xu H, Zhao Z, Li S, et al. Garlic-derived organosulfur compound exerts antitumor efficacy via activation of MAPK pathway and modulation of cytokines in SGC-7901 tumor-bearing mice. *Int Immunopharmacol.* (2017) 48:135–45. doi: 10.1016/j.intimp.2017.05.004

29. Luo R, Fang D, Hang H, Tang Z. The mechanism in gastric cancer chemoprevention by allicin. *Anti Cancer Agents Med Chem.* (2016) 16:802–9. doi: 10.2174/1871520616666151111115443

30. Burz C, Berindan-Neagoe I, Balacescu O, Irimie A. Apoptosis in cancer: key molecular signaling pathways and therapy targets. *Acta Oncol.* (2009) 48:811–21. doi: 10.1080/02841860902974175

31. Casella S, Leonardi M, Melai B, Fratini F, Pistelli L. The role of diallyl sulfides and dipropyl sulfides in the in vitro antimicrobial activity of the essential oil of garlic, *Allium sativum* L., and leek, *Allium porrum* L. *Phytother Res.* (2013) 27:380–3. doi: 10.1002/ptr.4725

32. Li WR, Shi QS, Liang Q, Huang XM, Chen YB. Antifungal effect and mechanism of garlic oil on *Penicillium funiculosum*. *Appl Microbiol Biotechnol.* (2014) 98:8337–46. doi: 10.1007/s00253-014-5919-9

33. Phan ADT, Netzel G, Chhim P, Netzel ME, Sultanbawa Y. Phytochemical characteristics and antimicrobial activity of australian grown garlic (*Allium sativum* L.) cultivars. *Foods.* (2019) 8:358. doi: 10.3390/foods8090358

34. Patel DK, Prasad SK, Kumar R, Hemalatha S. An overview on antidiabetic medicinal plants having insulin mimetic property. *Asian Pacific J Trop Biomed.* (2012) 2:320–30. doi: 10.1016/S2221-1691(12)60032-X

35. Thomson M, Al-Qattan KK, Divya JS, Ali M. Anti-diabetic and anti-oxidant potential of aged garlic extract (AGE) in streptozotocin-induced diabetic rats. *BMC Complement Alternat Med.* (2015) 16:17. doi: 10.1186/s12906-016-0992-5

36. Faroughi F, Charandabi SMA, Javadzadeh Y, Mirghafourvand M. Effects of garlic pill on blood glucose level in borderline gestational diabetes mellitus: a triple blind, randomized clinical trial. *Iran Red Crescent Med J.* (2018) 20. doi: 10.5812/ircmj.60675

37. Mehrbod P, Amini E, Tavassoti-Kheiri M. Antiviral activity of garlic extract on influenza virus. *Iran J Virol.* (2009) 3:19–23. doi: 10.21859/isv.3.1.19

38. Meléndez-Villanueva MA, Morán-Santibañez K, Martínez-Sanmiguel JJ, Rangel-López R, Garza-Navarro MA, Rodríguez-Padilla C, et al. Virucidal activity of gold nanoparticles synthesized by green chemistry using garlic extract. *Viruses.* (2019) 11:1111. doi: 10.3390/v11121111

39. Harazem R, Rahman S, Kenawy A. Evaluation of antiviral activity of *Allium cepa* and *Allium sativum* extracts against newcastle disease virus. *AJVS.* (2019) 61:108. doi: 10.5455/ajvs.29663

40. Sharma N. Efficacy of garlic and onion against viru. *Int J Res Pharmaceutical Sci.* (2019) 10:3578–86. doi: 10.26452/ijrps.v10i4.1738

41. Chavan RD, Shinde P, Girkar K, Madage R, Chowdhary A. Assessment of Anti-Influenza activity and hemagglutination inhibition of *Plumbago indica* and *Allium sativum* extracts. *Pharmacogn Res.* (2016) 8:105. doi: 10.4103/0974-8490.172562

42. Mohajer Shojai T, Ghalyanchi Langeroudi A, Karimi V, Barin A, Sadri N. The effect of *Allium sativum* (Garlic) extract on infectious bronchitis virus in specific pathogen free embryonic egg. *Avicenna J Phytomed.* (2016) 6:458–267.

43. Silprasit K, Seetaha S, Pongsanarakul P, Hannongbua S, Choowongkomon K. Anti-HIV-1 reverse transcriptase activities of hexane extracts from some Asian medicinal plants. *JMPR* (2011) 5:4899–906.

44. Wang L, Jiao H, Zhao J, Wang X, Sun S, Lin H. Allicin alleviates reticuloendotheliosis virus-induced immunosuppression via ERK/Mitogen-activated protein kinase pathway in specific pathogen-free chickens. *Front Immunol.* (2017) 8:1856. doi: 10.3389/fimmu.2017.01856

45. Khubber S, Hashemifesharaki R, Mohammadi M, Gharibzahedi SMT. Garlic (*Allium sativum* L.): a potential unique therapeutic food rich in organosulfur and flavonoid compounds to fight with COVID-19. *Nutr J.* (2020) 19:124. doi: 10.1186/s12937-020-00643-8

46. Chen L, Li J, Luo C, Liu H, Xu W, Chen G, et al. Binding interaction of quercetin-3-β-galactoside and its synthetic derivatives with SARS-CoV 3CLpro: structure–activity relationship studies reveal salient pharmacophore features. *Bioorg Med Chem.* (2006) 14:8295–306. doi: 10.1016/j.bmc.2006.09.014

47. Pandey P, Khan F, Kumar A, Srivastava A, Jha NK. Screening of potent inhibitors against 2019 novel coronavirus (Covid-19) from *Allium sativum* and *Allium cepa*: an in silico approach. *Biointerface Res Appl Chem.* (2021) 11:7981–93. doi: 10.33263/BRIAC111.79817993

48. Hernández-García I, Giménez-Júlvez T. Characteristics of YouTube videos in spanish on how to prevent COVID-19. *Int J Environ Res Public Health.* (2020) 17:4671. doi: 10.3390/ijerph17134671

49. Njue LG, Ombui JN, Kanja LW, Gathumbi JK, Nduhiu JG. Evaluation of oral toxicity level of ethyl acetate extract, from garlic (*Allium sativum*) in onorrh dawleys rats as per oecd guidelines 423. *J Food Sci Technol.* (2015) 2:56–64.

50. Sharma V, Sharma A, Kansal L. The effect of oral administration of *Allium sativum* extracts on lead nitrate induced toxicity in male mice. *Food Chem Toxicol.* (2010) 48:928–36. doi: 10.1016/j.fct.2010.01.002

51. Abid-Essefi S, Zaied C, Bouaziz C, Salem IB, Kaderi R, Bacha H. Protective effect of aqueous extract of *Allium sativum* against zearalenone toxicity mediated by oxidative stress. *Exp Toxicol Pathol.* (2012) 64:689–95. doi: 10.1016/j.etp.2010.12.012

52. Irkin LC, Yigit M, Yilmaz S, Maita M. Toxicological evaluation of dietary garlic (*Allium sativum*) powder in european sea bass *Dicentrarchuslabrax juveniles*. *Food Nutr Sci.* (2014) 5:1–8.

53. Ashraf R, Khan RA, Ashraf I. Garlic (*Allium sativum*) supplementation with standard antidiabetic agent provides better diabetic control in type 2 diabetes patients. *Pakistan J Pharmaceutical Sci.* (2011) 24:565–70.

54. Sukandar EY, Permana H, Adnyana IK, Sigit JI, Ilyas RA, Hasimun P, et al. Clinical study of turmeric (*Curcuma longa* L.) and garlic (*Allium sativum* L.) extracts as antihyperglycemic and antihyperlipidemic agent in type-2 diabetes-dyslipidemia patients. *Int J Pharmacol.* (2010) 6:456–63. doi: 10.3923/ijp.2010.456.463

55. Moosavian SP, Paknahad Z, Habibagahi Z, Maracy M. The effects of garlic (*Allium sativum*) supplementation on inflammatory biomarkers, fatigue, and clinical symptoms in patients with active rheumatoid arthritis: a randomized, double-blind, placebo-controlled trial. *Phytother Res.* (2020) 34:2953–62. doi: 10.1002/ptr.6723

56. Bhandari PR. Garlic (*Allium sativum* L.): a review of potential therapeutic applications. *Int J Green Pharm.* (2012) 6:118. doi: 10.4103/0973-8258.102826

57. Drugs.com. *Garlic*. (2018). Available online at: https://www.drugs.com/npp/garlic.html (accessed October 31, 2018).

58. Bakht J, Muhammad T, Ali H, Islam A, Shafi M. Effect of different solvent extracted sample of *Allium sativum* (Linn) on bacteria and fungi. *Afr J Biotechnol.* (2011) 10:5910–5. doi: 10.5897/AJB11.232

59. Charron CS, Milner JA, Novotny JA. *Garlic*. (2016). p. 184–90. doi: 10.1016/B978-0-12-384947-2.00346-9

60. Goldy R. *October is Garlic Planting Time, Michigan State University Extension, 2011*. East Lansin, MI: Michigan State University (2019).

61. Hosseini A, Hosseinzadeh H. A review on the effects of *Allium sativum* (Garlic) in metabolic syndrome. *J Endocrinol Investigat.* (2015) 38:1147–57. doi: 10.1007/s40618-015-0313-8

62. Karuppiah P, Rajaram S. Antibacterial effect of *Allium sativum* cloves and *Zingiber officinale* rhizomes against multiple-drug resistant clinical pathogens. *Asian Pacific J Trop Biomed.* (2012) 2:597–601. doi: 10.1016/S2221-1691(12)60104-X

63. Rahman AHMM, Kabir EZMF, Sima SN, Sultana RS, Nasiruddin M, Naderuzzaman ATM. Study of an ethnobotany at the village Dohanagar, Naogaon. *J Appl Sci Res.* (2010) 6:1466–73.

64. Rahman MM, Fazlic V, Saad NW. Antioxidant properties of raw garlic (*Allium sativum*) extract. *Int Food Res J.* (2012) 19:589–91.

65. Martins N, Petropoulos S, Ferreira IC. Chemical composition and bioactive compounds of garlic (*Allium sativum* L.) as affected by pre-and post-harvest conditions: a review. *Food Chem.* (2016) 211:41–50. doi: 10.1016/j.foodchem.2016.05.029

66. Kallel F, Driss D, Chaari F, Belghith L, Bouaziz F, Ghorbel R, et al. Garlic (*Allium sativum* L.) husk waste as a potential source of phenolic compounds: influence of extracting solvents on its antimicrobial and antioxidant properties. *Industrial Crops Prod.* (2014) 62:34–41. doi: 10.1016/j.indcrop.2014.07.047

67. Suleria HAR, Butt MS, Khalid N, Sultan S, Raza A, Aleem M, et al. Garlic (*Allium sativum*): diet based therapy of 21st century–a review. *Asian Pacific J Trop Dis.* (2015) 5:271–8. doi: 10.1016/S2222-1808(14)60782-9

68. Chekki RZ, Snoussi A, Hamrouni I, Bouzouita N. Chemical composition, antibacterial and antioxidant activities of Tunisian garlic (*Allium sativum*) essential oil and ethanol extract. *Mediterranean J Chem.* (2014) 3:947–56. doi: 10.13171/mjc.3.4.2014.09.07.11

69. Capasso A. Antioxidant action and therapeutic efficacy of *Allium sativum* L. *Molecules.* (2013) 18:690–700. doi: 10.3390/molecules18010690

70. Zhao NN, Zhang H, Zhang XC, Luan XB, Zhou C, Liu QZ, et al. Evaluation of acute toxicity of essential oil of garlic (*Allium sativum*) and its selected major constituent compounds against overwintering *Cacopsylla chinensis* (Hemiptera: psyllidae). *J Econ Entomol.* (2013) 106:1349–54. doi: 10.1603/EC12191

71. Dziri S, Casabianca H, Hanchi B, Hosni K. Composition of garlic essential oil (*Allium sativum* L.) as influenced by drying method. *J Essential Oil Res.* (2014) 26:91–6. doi: 10.1080/10412905.2013.868329

72. Mikaili P, Maadirad S, Moloudizargari M, Aghajanshakeri S, Sarahroodi S. Therapeutic uses and pharmacological properties of garlic, shallot, and their biologically active compounds. *Iran J Basic Med Sci.* (2013) 16:1031.

73. Quintero-Fabián S, Ortuño-Sahagún D, Vázquez-Carrera M, López-Roa RI. Alliin, a garlic (*Allium sativum*) compound, prevents LPS-induced inflammation in 3T3-L1 adipocytes. *Mediators Inflamm.* (2013) 2013:1–11. doi: 10.1155/2013/381815

74. Devi A, Rakshit K, Sarania B. Ethnobotanical notes on *Allium* species of Arunachal Pradesh, India. *Ind J Trad Knowledge.* (2014) 13:606–12.

75. Jariæ S, Maèukanoviæ-Jociæ M, Djurdjeviæ L, Mitroviæ M, Kostiæ O, Karadžiæ B, et al. An ethnobotanical survey of traditionally used plants on Suva planina mountain (south-eastern Serbia). *J. Ethnopharmacol.* (2015) 175:93–108. doi: 10.1016/j.jep.2015.09.002

76. Gbolade A. Ethnobotanical study of plants used in treating hypertension in Edo State of Nigeria. *J Ethnopharmacol.* (2012) 144:1–10. doi: 10.1016/j.jep.2012.07.018

77. Ugulu I. Traditional ethnobotanical knowledge about medicinal plants used for external therapies in Alasehir, Turkey. *Int J Med Aromatic Plants.* (2011) 1:101–6.

78. Soladoye MO, Adetayo MO, Chukwuma EC, Adetunji AN. Ethnobotanical survey of plants used in the treatment of haemorrhoids in South-Western Nigeria. *Ann Biol Res.* (2010) 1:1–15.

79. Ogbole OO, Gbolade AA, Ajaiyeoba EO. Ethnobotanical survey of plants used in treatment of inflammatory diseases in Ogun State of Nigeria. *Eur J Sci Res.* (2010) 43:183–91.

80. Soladoye MO, Amusa NA, Raji-Esan SO, Chukwuma EC, Taiwo AA. Ethnobotanical survey of anti-cancer plants in Ogun State, Nigeria. *Ann Biol Res.* (2010) 1:261–73.

81. Keter LK, Mutiso PC. Ethnobotanical studies of medicinal plants used by Traditional Health Practitioners in the management of diabetes in Lower Eastern Province, Kenya. *J Ethnopharmacol.* (2012) 139:74–80. doi: 10.1016/j.jep.2011.10.014

82. Barkaoui M, Katiri A, Boubaker H, Msanda F. Ethnobotanical survey of medicinal plants used in the traditional treatment of diabetes in Chtouka Ait Baha and Tiznit (Western Anti-Atlas), Morocco. *J Ethnopharmacol.* (2017) 198:338–50. doi: 10.1016/j.jep.2017.01.023

83. Phondani PC, Maikhuri RK, Rawat LS, Farooquee NA, Kala CP, Vishvakarma SR, et al. Ethnobotanical uses of plants among the Bhotiya tribal communities of Niti Valley in Central Himalaya, India. *Ethnobot Res Appl.* (2010) 8:233–44. doi: 10.17348/era.8.0.233-244

84. Teklay A, Abera B, Giday M. An ethnobotanical study of medicinal plants used in Kilte Awulaelo District, Tigray Region of Ethiopia. *J Ethnobiol Ethnomed.* (2013) 9:65. doi: 10.1186/1746-4269-9-65

85. Lagnika L, Adjileye RAA, Yedomonhan H, Amadou BSK, Sanni A. Ethnobotanical survey on antihypertensive medicinal plants in municipality of Ouémé, Southern Benin. *Adv Herb Med.* (2016) 2:20–32.

86. Karou SD, Tchacondo T, Djikpo Tchibozo MA, Abdoul-Rahaman S, Anani K, Koudouvo K, et al. Ethnobotanical study of medicinal plants used in the management of diabetes mellitus and hypertension in the Central Region of Togo. *Pharmaceutical Biol.* (2011) 49:1286–97. doi: 10.3109/13880209.2011.621959

87. Sher Z, Khan Z, Hussain F. Ethnobotanical studies of some plants of Chagharzai valley, district Buner, Pakistan. *Pakistan J Bot.* (2011) 43:1445–52.

88. Shende JJ, Rajurkar BM, Mhaiskar MN, Dalal LP. Ethnobotanical studies of Samudrapur Tahsil of Wardha district. *Int Organ Sci Res.* (2014) 9:16–23.

89. Getaneh S, Girma Z. An ethnobotanical study of medicinal plants in Debre Libanos Wereda, Central Ethiopia. *Afr J Plant Sci.* (2014) 8:366–79. doi: 10.5897/AJPS2013.1041

90. Kayani S, Ahmad M, Zafar M, Sultana S, Khan MPZ, Ashraf MA, et al. Ethnobotanical uses of medicinal plants for respiratory disorders among the inhabitants of Gallies–Abbottabad, Northern Pakistan. *J Ethnopharmacol.* (2014) 156:47–60. doi: 10.1016/j.jep.2014.08.005

91. Calvo MI, Akerreta S, Cavero RY. Pharmaceutical ethnobotany in the riverside of Navarra (Iberian Peninsula). *J Ethnopharmacol.* (2011) 135:22–33. doi: 10.1016/j.jep.2011.02.016

92. Mesfin F, Seta T, Assefa A. An ethnobotanical study of medicinal plants in Amaro Woreda, Ethiopia. *Ethnobotany Res Appl.* (2014) 12:341–54. doi: 10.17348/era.12.0.341-354

93. Soladoye MO, Chukwuma EC, Sulaiman OM, Feyisola RT. Ethnobotanical survey of plants used in the traditional treatment of female infertility in Southwestern Nigeria. *Ethnobotany Res Appl.* (2014) 12:81–90.

94. Bekele G, Reddy PR. Ethnobotanical study of medicinal plants used to treat human ailments by Guji Oromo tribes in Abaya District, Borana, Oromia, Ethiopia. *Univ J Plant Sci.* (2015) 3:4. doi: 10.13189/ujps.2015.030101

95. Sen S, Chakraborty R, De B, Devanna N. An ethnobotanical survey of medicinal plants used by ethnic people in West and South district of Tripura, India. *J Forestry Res.* (2011) 22:417. doi: 10.1007/s11676-011-0184-6

96. Birhanu T, Abera D, Ejeta E, Nekemte E. Ethnobotanical study of medicinal plants in selected Horro Gudurru Woredas, Western Ethiopia. *J Biol Agric Healthcare.* (2015) 5:83–93.

97. Šavikin K, Zduniæ G, Menkoviæ N, Živkoviæ J, Æujiæ N, Tereščenko M, et al. Ethnobotanical study on traditional use of medicinal plants in South-Western Serbia, Zlatibor district. *J Ethnopharmacol.* (2013) 146:803–10. doi: 10.1016/j.jep.2013.02.006

98. Thapa S. Medico-ethnobotany of Magar community in Salija VDC of Parbat district, central Nepal. *Our Nat.* (2012) 10:176–90. doi: 10.3126/on.v10i1.7780

99. Šariæ-Kundaliæ B, Dobeš C, Klatte-Asselmeyer V, Saukel J. Ethnobotanical study on medicinal use of wild and cultivated plants in middle, south and west Bosnia and Herzegovina. *J Ethnopharmacol.* (2010) 131:33–55. doi: 10.1016/j.jep.2010.05.061

100. Megersa M, Asfaw Z, Kelbessa E, Beyene A, Woldeab B. An ethnobotanical study of medicinal plants in Wayu Tuka district, east Welega zone of oromia regional state, West Ethiopia. *J Ethnobiol Ethnomed.* (2013) 9:68. doi: 10.1186/1746-4269-9-68

101. Olanipekun MK, Arowosegbe S, Kayode JO, Oluwole TR. Ethnobotanical survey of medicinal plants used in the treatment of women related diseases in Akoko Region of Ondo-State, Nigeria. *J Med Plants Res.* (2016) 10:270–7.

102. González JA, García-Barriuso M, Amich F. Ethnobotanical study of medicinal plants traditionally used in the Arribes del Duero, western Spain. *J Ethnopharmacol.* (2010) 131:343–55. doi: 10.1016/j.jep.2010.07.022

103. Asase A, Yohonu DT. Ethnobotanical study of herbal medicines for management of diabetes mellitus in Dangme West District of southern Ghana. *J Herb Med.* (2016) 6:204–9. doi: 10.1016/j.hermed.2016.07.002

104. Polat R, Satıl F. An ethnobotanical survey of medicinal plants in Edremit Gulf (Balıkesir–Turkey). *J Ethnopharmacol.* (2012) 139:626–41. doi: 10.1016/j.jep.2011.12.004

105. Mustafa B, Hajdari A, Pajazita Q, Syla B, Quave CL, Pieroni A. An ethnobotanical survey of the Gollak region, Kosovo. *Genet Resour Crop Evol.* (2012) 59:739–54. doi: 10.1007/s10722-011-9715-4

106. Regassa R, Bekele T, Megersa M. Ethnobotanical study of traditional medicinal plants used to treat human ailments by Halaba people, southern Ethiopia. *J Med Plants Stud.* (2017) 5:36–47.

107. Fred-Jaiyesimi A, Ajibesin KK, Tolulope O, Gbemisola O. Ethnobotanical studies of folklore phytocosmetics of South West Nigeria. *Pharmaceutical Biol.* (2015) 53:313–8. doi: 10.3109/13880209.2014.918155

108. Agize M, Demissew S, Asfaw Z. Ethnobotany of medicinal plants in Loma and Gena bosa districts (woredas) of dawro zone, southern Ethiopia. *Topclass J Herb Med.* (2013) 2:194–212.

109. Mustafa B, Hajdari A, Krasniqi F, Hoxha E, Ademi H, Quave CL, et al. Medical ethnobotany of the Albanian Alps in Kosovo. *J Ethnobiol Ethnomed.* (2012) 8:6. doi: 10.1186/1746-4269-8-6

110. Karunamoorthi K, Hailu T. Insect repellent plants traditional usage practices in the Ethiopian malaria epidemic-prone setting: an ethnobotanical survey. *J Ethnobiol Ethnomed.* (2014) 10:22. doi: 10.1186/1746-4269-10-22

111. Alemayehu G, Asfaw Z, Kelbessa E. Ethnobotanical study of medicinal plants used by local communities of Minjar-Shenkora District, North Shewa Zone of Amhara Region, Ethiopia. *J Med Plants Stud.* (2015) 3:1–11.

112. Olorunnisola OS, Adetutu A, Balogun EA, Afolayan AJ. Ethnobotanical survey of medicinal plants used in the treatment of malarial in Ogbomoso, Southwest Nigeria. *J Ethnopharmacol.* (2013) 150:71–8. doi: 10.1016/j.jep.2013.07.038

113. Sarkhel S. Ethnobotanical survey of folklore plants used in treatment of snakebite in Paschim Medinipur district, West Bengal. *Asian Pacific J Trop Biomed.* (2014) 4:416–20. doi: 10.12980/APJTB.4.2014C1120

114. Cavero RY, Akerreta S, Calvo MI. Pharmaceutical ethnobotany in the Middle Navarra (Iberian Peninsula). *J Ethnopharmacol.* (2011) 137:844–55. doi: 10.1016/j.jep.2011.07.001

115. Abouri M, El Mousadik A, Msanda F, Boubaker H, Saadi B, Cherifi K. An ethnobotanical survey of medicinal plants used in the Tata Province, Morocco. *Int J Med Plants Res.* (2012) 1:99–123.

116. Kichu M, Malewska T, Akter K, Imchen I, Harrington D, Kohen J, et al. An ethnobotanical study of medicinal plants of Chungtia village, Nagaland, India. *J Ethnopharmacol.* (2015) 166:5–17. doi: 10.1016/j.jep.2015.02.053

117. Pieroni A, Giusti ME, Quave CL. Cross-cultural ethnobiology in the Western Balkans: medical ethnobotany and ethnozoology among Albanians and Serbs in the Pešter Plateau, Sandžak, South-Western Serbia. *Hum Ecol.* (2011) 39:333. doi: 10.1007/s10745-011-9401-3

118. Rigat M, Vallès J, Gras A, Iglésias J, Garnatje T. Plants with topical uses in the Ripollès district (Pyrenees, Catalonia, Iberian Peninsula): ethnobotanical survey and pharmacological validation in the literature. *J Ethnopharmacol.* (2015) 164:162–79. doi: 10.1016/j.jep.2015.01.055

119. Ohemu TL, Agunu A, Olotu PN, Ajima U, Dafam DG, Azila JJ. Ethnobotanical survey of medical plants used in the traditional treatment of viral infections in Jos, plateau state, Nigeria. *Int J Med Aromatic Plants.* (2014) 4:74–81.

120. Maryo M, Nemomissa S, Bekele T. An ethnobotanical study of medicinal plants of the Kembatta ethnic group in Enset-based agricultural landscape of Kembatta Tembaro (KT) Zone, Southern Ethiopia. *Asian J Plant Sci Res.* (2015) 5:42–61.

121. Purbashree S, Rajamohan MR, Kumar PA. Ethnobotany of Chothe tribe of Bishnupur district (Manipur). *Ind J Nat Prod Resour.* (2012) 3:414–25.

122. Abbasi AM, Khan MA, Ahmed M, Zafar M. Herbal medicines used to cure various ailments by the inhabitants of Abbottabad district, North West Frontier Province, Pakistan. *Ind J Trad Knowledge.* (2010) 9:175–83.

123. Nath M, Choudhury MD. Ethno-medico-botanical aspects of Hmar tribe of Cachar district, Assam (Part I). *Ind J Trad Knowledge.* (2010) 9:760–4.

124. Singh VN, Chanu LI, Baruah MK. An ethnobotanical study of Chirus-A less known tribe of Assam. *Ind J Trad Knowledge.* (2011) 10:572–4.

125. Gaur RD, Sharma J, Painuli RM. Plants used in traditional healthcare of livestock by Gujjar community of Sub-Himalayan tracts, Uttarakhand, India. *Ind J Nat Prod Resour.* (2010) 1:243–8.

126. Saha MR, Sarker DD, Sen A. Ethnoveterinary practices among the tribal community of Malda district of West Bengal, India. *Ind J Trad Knowledge.* (2014) 13:359–67.

127. Shaheen H, Nazir J, Firdous SS, Khalid AUR. Cosmetic ethnobotany practiced by tribal women of Kashmir Himalayas. *Avicenna J Phytomed.* (2014) 4:239.

128. Murthy SM, Vidyasagar GM. Traditional knowledge on medicinal plants used in the treatment of respiratory disorders in Bellary district, Karnataka, India. *Ind J Natural Prod Resour.* (2013) 4:189–93. doi: 10.5958/j.0975-4261.4.4.029

129. Namsa ND, Mandal M, Tangjang S, Mandal SC. Ethnobotany of the Monpa ethnic group at Arunachal Pradesh, India. *J Ethnobiol Ethnomed.* (2011) 7:31. doi: 10.1186/1746-4269-7-31

130. Thirumalai T, Beverly CD, Sathiyaraj K, Senthilkumar B, David E. Ethnobotanical Study of Anti-diabetic medicinal plants used by the local people in Javadhu hills Tamilnadu, India. *Asian Pacific J Trop Biomed.* (2012) 2:910–3. doi: 10.1016/S2221-1691(12)60335-9

131. Sargın SA, Akçicek E, Selvi S. An ethnobotanical study of medicinal plants used by the local people of Alaşehir (Manisa) in Turkey. *J Ethnopharmacol.* (2013) 150:860–74. doi: 10.1016/j.jep.2013.09.040

132. Abe R, Ohtani K. An ethnobotanical study of medicinal plants and traditional therapies on Batan Island, the Philippines. *J Ethnopharmacol.* (2013) 145:554–65. doi: 10.1016/j.jep.2012.11.029

133. Sonibare NA, Abegunde RB. Ethnobotanical study of medicinal plants used by the Laniba village people in South Western Nigeria. *Afr J Pharm Pharmacol.* (2012) 6:1726–32. doi: 10.5897/AJPP11.680

134. Gupta R, Vairale MG, Deshmukh RR, Chaudhary PR, Wate SR. Ethnomedicinal uses of some plants used by Gond tribe of Bhandara district, Maharashtra. *Ind J Trad Knowledge.* (2010) 9:713–7.

135. Jain SP, Srivastava S, Singh J, Singh SC. Traditional phytotherapy of Balaghat district, Madhya Pradesh, India. *Ind J Trad Knowledge.* (2011) 10:334–8.

136. Baharvand-Ahmadi B, Asadi-Samani M. A mini-review on the most important effective medicinal plants to treat hypertension in ethnobotanical evidence of Iran. *J Nephropharmacol.* (2017) 6:3. doi: 10.15171/jnp.2017.20

137. Kefalew A, Asfaw Z, Kelbessa E. Ethnobotany of medicinal plants in Ada'a District, East Shewa Zone of Oromia regional state, Ethiopia. *J Ethnobiol Ethnomed.* (2015) 11:25. doi: 10.1186/s13002-015-0014-6

138. Otang WM, Grierson DS, Ndip RN. Ethnobotanical survey of medicinal plants used in the management of opportunistic fungal infections in HIV/AIDS patients in the Amathole District of the Eastern Cape Province, South Africa. *J Med Plants Res.* (2012) 6:2071–80. doi: 10.5897/JMPR11.069

139. Zenebe G, Zerihun M, Solomon Z. An ethnobotanical study of medicinal plants in Asgede Tsimbila district, Northwestern Tigray, northern Ethiopia. *Ethnobot Res Appl.* (2012) 10:305–20. doi: 10.17348/era.10.0.305-320

140. Mekonnen N, Abebe E. Ethnobotanical knowledge and practices of traditional healers in Harar, Haramaya, Bati and Garamuleta, Eastern Ethiopia. *Ethiopian Veter J.* (2017) 21:40–61. doi: 10.4314/evj.v21i2.4

141. Nigam G, Sharma NK. Ethnoveterinary plants of Jhansi district, Uttar Pradesh. *Ind J Trad Knowledge.* (2010) 9:664–7.

142. Akgül G, Yılmaz N, Celep A, Celep F, Çakılcıoğlu U. Ethnobotanical purposes of plants sold by herbalists and folk bazaars in the center of *Cappadocica* (Nevşehir, Turkey). *Ind J Trad Knowledge.* (2016) 15:103–8.

143. Liu J, Guo W, Yang M, Liu L, Huang S, Tao L, et al. Investigation of the dynamic changes in the chemical constituents of Chinese "Laba" garlic during traditional processing. *RSC Adv.* (2018) 8:41872–83. doi: 10.1039/C8RA09657K

144. Kang JS, Kim SO, Kim GY, Hwang HJ, Kim BW, Chang YC, et al. An exploration of the antioxidant effects of garlic saponins in mouse-derived C2C12 myoblasts. *Int J Mol Med.* (2016) 37:149–56. doi: 10.3892/ijmm.2015.2398

145. Choi JH, Kim MS, Yu HJ, Kim KH, Lee HS, Cho HY, et al. Hepatoprotective effects of lactic acid-fermented garlic extracts on fatty liver-induced mouse by alcohol. *J Korean Soc Food Sci Nutr.* (2014) 43:1642–7. doi: 10.3746/jkfn.2014.43.11.1642

146. Park BM, Cha SA, Kim HY, Kang DK, Yuan K, Chun H, et al. Fermented garlic extract decreases blood pressure through nitrite and sGC-cGMP-PKG pathway in spontaneously hypertensive rats. *J Funct Foods.* (2016) 22:156–65. doi: 10.1016/j.jff.2016.01.034

147. Ha AW, Ying T, Kim WK. The effects of black garlic (*Allium satvium*) extracts on lipid metabolism in rats fed a high fat diet. *Nutr Res Pract.* (2015) 9:30–6. doi: 10.4162/nrp.2015.9.1.30

148. Khatua TN, Borkar RM, Mohammed SA, Dinda AK, Srinivas R, Banerjee SK. Novel sulfur metabolites of garlic attenuate cardiac hypertrophy and remodeling through induction of Na+/K+-ATPase expression. *Front Pharmacol.* (2017) 8:18. doi: 10.3389/fphar.2017.00018

149. Sultana MR, Bagul PK, Katare PB, Mohammed SA, Padiya R, Banerjee SK. Garlic activates SIRT-3 to prevent cardiac oxidative stress and mitochondrial dysfunction in diabetes. *Life Sci.* (2016) 164:42–51. doi: 10.1016/j.lfs.2016.08.030

150. Supakul L, Pintana H, Apaijai N, Chattipakorn S, Shinlapawittayatorn K, Chattipakorn N. Protective effects of garlic extract on cardiac function, heart rate variability, and cardiac mitochondria in obese insulin-resistant rats. *Eur J Nutr.* (2014) 53:919–28. doi: 10.1007/s00394-013-0595-6

151. Gomaa AM, Abdelhafez AT, Aamer HA. Garlic (*Allium sativum*) exhibits a cardioprotective effect in experimental chronic renal failure rat model by reducing oxidative stress and controlling cardiac Na+/K+-ATPase activity and Ca 2+ levels. *Cell Stress Chaperones.* (2018) 23:913–20. doi: 10.1007/s12192-018-0898-x

152. Kaschula CH, Hunter R, Cotton J, Tuveri R, Ngarande E, Dzobo K, et al. The garlic compound ajoene targets protein folding in the endoplasmic reticulum of cancer cells. *Mol Carcinogenesis.* (2016) 55:1213–28. doi: 10.1002/mc.22364

153. Zhang Y, Li HY, Zhang ZH, Bian HL, Lin G. Garlic-derived compound S-allylmercaptocysteine inhibits cell growth and induces apoptosis via the JNK and p38 pathways in human colorectal carcinoma cells. *Oncol Lett.* (2014) 8:2591–6. doi: 10.3892/ol.2014.2579

154. Mansingh DP, Dalpati N, Sali VK, Vasanthi AHR. Alliin the precursor of allicin in garlic extract mitigates proliferation of gastric adenocarcinoma cells by modulating apoptosis. *Pharmacogn Magazine.* (2018) 14:84. doi: 10.4103/pm.pm_342_17

155. Xiao J, Xing F, Liu Y, Lv Y, Wang X, Ling MT, et al. Garlic-derived compound S-allylmercaptocysteine inhibits hepatocarcinogenesis through targeting LRP6/Wnt pathway. *Acta Pharmaceutica Sin B.* (2018) 8:575–86. doi: 10.1016/j.apsb.2017.10.003

156. Talib WH. Consumption of garlic and lemon aqueous extracts combination reduces tumor burden by angiogenesis inhibition, apoptosis induction, and immune system modulation. *Nutrition.* (2017) 43:89–97. doi: 10.1016/j.nut.2017.06.015

157. Fratianni F, Riccardi R, Spigno P, Ombra MN, Cozzolino A, Tremonte P, et al. Biochemical characterization and antimicrobial and antifungal activity of two endemic varieties of garlic (*Allium sativum* L.) of the campania region, southern Italy. *J Med Food.* (2016) 19:686–91. doi: 10.1089/jmf.2016.0027

158. Wallock-Richards D, Doherty CJ, Doherty L, Clarke DJ, Place M, Govan JR, et al. Garlic revisited: antimicrobial activity of allicin-containing garlic extracts against Burkholderia cepacia complex. *PLoS One.* (2014) 9:e112726. doi: 10.1371/journal.pone.0112726

159. Pundir RK, Jain P, Sharma C. Antimicrobial activity of ethanolic extracts of *Syzygium aromaticum* and *Allium sativum* against food associated bacteria and fungi. *Ethnobotanical Leaflets.* (2010) 2010:11.

160. Johnson OO, Ayoola GA, Adenipekun T. Antimicrobial activity and the chemical composition of the volatile oil blend from *Allium sativum* (garlic clove) and Citrus reticulate (tangerine fruit). *Int J Pharmaceutical Sci Drug Res.* (2013) 5:187–93.

frontiers | Frontiers in Nutrition

TYPE Original Research
PUBLISHED 23 December 2022
DOI 10.3389/fnut.2022.1062616

OPEN ACCESS

EDITED BY
Gengjun Chen,
Kansas State University, United States

REVIEWED BY
Emmanuel Oladeji Alamu,
International Institute of Tropical Agriculture, Zambia
Thuan Chew Tan,
Universiti Sains Malaysia (USM), Malaysia

*CORRESPONDENCE
Muhammad Sameem Javed
✉ sameemjaved@gmail.com

SPECIALTY SECTION
This article was submitted to Nutrition and Food Science Technology, a section of the journal Frontiers in Nutrition

RECEIVED 06 October 2022
ACCEPTED 30 November 2022
PUBLISHED 23 December 2022

CITATION
Shah F-u-H, Sharif MK, Ahmad Z, Amjad A, Javed MS, Suleman R, Sattar D-e-S, Amir M and Anwar MJ (2022) Nutritional characterization of the extrusion-processed micronutrient-fortified corn snacks enriched with protein and dietary fiber. *Front. Nutr.* 9:1062616. doi: 10.3389/fnut.2022.1062616

Nutritional characterization of the extrusion-processed micronutrient-fortified corn snacks enriched with protein and dietary fiber

Faiz-ul-Hassan Shah[1], Mian Kamran Sharif[2], Zulfiqar Ahmad[1], Adnan Amjad[3], Muhammad Sameem Javed[4]*, Raheel Suleman[5], Dur-e-Shahwar Sattar[5], Muhammad Amir[5] and Muhammad Junaid Anwar[5]

[1]Department of Food Science and Technology, Faculty of Agriculture and Environment, The Islamia University of Bahawalpur, Bahawalpur, Punjab, Pakistan, [2]National Institute of Food Science and Technology, University of Agriculture Faisalabad, Faisalabad, Punjab, Pakistan, [3]Department of Human Nutrition and Dietetics, Bahauddin Zakariya University Multan, Multan, Punjab, Pakistan, [4]Department of Food Safety and Quality Management, Bahauddin Zakariya University Multan, Multan, Punjab, Pakistan, [5]Department of Food Science and Technology, Bahauddin Zakariya University Multan, Multan, Punjab, Pakistan

The current study focused on developing protein- and dietary fiber-enriched, micronutrient-fortified corn snacks using extrusion technology. Corn, soybean, and chickpea flour were used to develop micronutrient-fortified (Fe, Zn, I, and vitamin A, and C) extruded snacks, followed by an exploration of their nutritional traits. Soybean and chickpea were supplemented discretely (20–40/100 g) or in a combination of both (10:10, 15:15, and 20:20/100 g). According to the results, the relative proportion of the raw material composition was reflected in corn snacks' proximate composition and mineral and vitamin levels. Corn snacks with 40/100 g soy flour showed the best nutrient profile, with a maximum percent increase in protein (171.9%) and fiber (106%), as compared to the snacks developed using chickpea and/or mixed supplementation with soy and chickpea. Total dietary fiber (18.44 ± 0.34%), soluble dietary fiber (10.65 ± 0.13%), and insoluble dietary fiber (7.76 ± 0.38%) were also found to be highest in the soy-supplemented snacks (40/100 g). It was discovered that 100 g of corn snacks could provide 115–127% of the RDA for iron, 77–82% of the RDA for zinc, 90–100% of the RDA for vitamin A, and 45–50% of the RDA for vitamin C. The results for the effect of extrusion processing on amino acids showed a 2.55–45.1% reduction in essential amino acids, with cysteine and valine showing the greatest decrease and leucine and tryptophan remaining relatively stable during extrusion.

KEYWORDS

extrusion, snacks, fortification, protein, dietary fiber

1. Introduction

South Asian countries are facing serious health issues because of malnutrition. The situation is worse in India, Pakistan, and Bangladesh, where half of the world's malnourished children and women reside (1). Factors such as growth and development are mainly dependent on the status of human beings. Micronutrients are required for the normal functioning of the body, including for nerve impulse conduction, for normal physical and mental function, for maintaining electrolyte balance, for regulating blood pressure, and as part of most enzymes and hormones (2). Therefore, awareness of eradicating micronutrient malnutrition has improved over the last few years (3).

Nutrition-related problems could be best addressed by food-based approaches. The use of food fortification to improve micronutrient status in a population (4, 5) without requiring any radical changes in food habits and reaching almost all sections of society (6) is one of the most effective and long-term approaches. The most important considerations are to calibrate the nutrient profile during fortification to avoid any toxicological effects, the use of multiple micronutrients, and the cost-effective addition of nutrients to foods (7).

The Composite Flour Program has been initiated by FAO, especially for the development of healthy bakery items for the masses. This initiative has paved the way to introduce an array of products with commercial significance, nutritional benefits, and additional advantages in functional and textural parameters. During the development of composite flours, factors such as consumer acceptability, nutritional quality, and functional and prophylactic benefits are considered (8). Composite flours are developed by supplementing cereal flours (rice, maize, sorghum, and pearl millet) with legume flours to alleviate prevailing malnutrition in South Asia without disturbing the quality of finished products. Despite many advancements, there are still many hurdles in preparing cereal, tuber, and legume-based formulations to replace the gluten in cereal-based products. Rice and maize as composite flours provide a better option to mimic gluten properties. Corn is an underutilized crop in Pakistan. The escalating prices of dietary staples such as wheat flour and rice in Pakistan have created an opportunity to utilize composite flour technology to produce diverse food products and to improve the economic access of the masses to food availability and security (9). In food processing, extrusion technology has been used commercially to develop shelf-stable food products. Extrusion has several advantages, including the development of the desired shape of products, the reduction of anti-nutritional factors, and improved digestibility and palatability of nutrients. During extrusion processing, the digestibility of the starch also increases due to its gelatinization (10). Corn (*Zea mays L.*) is an ideal ingredient for producing snacks through extrusion due to its starch content (11). Corn is one of the chief cash crops of Pakistan and is ranked third in importance after wheat and rice. Corn is used in various forms in the food processing industry. In developing countries, its utilization is limited to forage forms for livestock and poultry. Therefore, the production of value-added food products from corn is required.

Soybean (*Glycine max*) contains high levels of good-quality protein, making it an ideal option to increase the protein content of different food products. Soybeans contain nearly all the nutrients required for good health, including nine essential amino acids. Similarly, chickpea (*Cicer arietinum*), a good source of protein, especially after defatting, provides 25.3–28.9% protein and is a substantial source of essential fatty acids, essential amino acids, and minerals (12). Guar gum is one of the excellent sources of dietary fiber, with a high concentration of soluble dietary fiber (75%) and insoluble dietary fiber (7.6%). Physiological, structural, chemical, and technological traits of soluble and insoluble dietary fiber are different. The addition of soluble dietary fiber, which forms a gel, results in increased satiety and gastric emptying time.

The consumption of snack foods has increased with the changing lifestyle of the 21st century. Snacks are foods that are typically smaller than a regular meal and consumed between meals. In the United States, children take snacks on average six times a day. Keeping in view the increased consumption of snacks in the diet, public departments in various countries, such as Health Canada, are recommending people replace conventional snacks with healthier snacks in their diet (13).

The current study was designed to formulate corn-based micronutrient-fortified extruded snacks enriched with protein by supplementing corn with soybean, chickpea, and dietary fiber from guar gum. These snacks not only fulfill the dietary requirements of the community but also help mitigate certain micronutrient and macronutrient deficiencies in children in developing countries. Therefore, it can serve as a miracle to alleviate the malnutrition burden.

2. Materials and methods

2.1. Procurement and preparation of raw materials

For this study, corn (*Zea mays*), soybeans (*Glycine max*), chickpeas (*Cicer arietinum*), and guar gum were procured from the local market in Faisalabad, Pakistan. Micronutrient premix (Fe, Zn, I, and vitamins A and C) was provided by Fortitech Inc. A vitamin/mineral pre-mix comprising five micronutrients used for fortification (Fe as NaFeEDTA, Zn as zinc oxide, I as sodium iodide, vitamin A as retinyl palmitate, and vitamin C as ascorbic acid) was provided by Fortitech in Schenectady, New York, USA. Megazyme total dietary fiber (TDF) test kits were procured from Novozymes, Karachi, Pakistan. All reagents and standards used in the study were procured from Sigma-Aldrich (Merck KGaA, Darmstadt, Germany). Physical impurities were

removed with manual cleaning. Dehulling and milling of both soybeans and chickpeas were carried out to get flour, followed by defatting with the solvent method. Defatted soy and chickpea flours were stored in separate polythene bags with the corn flour at 25°C for further use.

2.2. Analysis of the raw materials

2.1.1. Proximate composition

Corn, soybean, and chickpea flours were analyzed for crude fat (AACC Method No. 30-25), crude protein (AACC method no. 46-10), moisture (AACC Method No. 46-30), crude fiber (AACC method no. 32-10), and total ash (AACC method no. 08-01) by the respective methods described by AACC (14).

2.2.2. Mineral content

Raw materials (corn, soybean, and chickpea flours) were analyzed for a mineral profile by wet digestion according to the method given in AOAC (15). The sample (0.5) was first digested at low temperature (60–70°C) with 10 mL of HNO_3 for 20 min in a 100-mL conical flask on a hot plate. Then, it was digested at a high temperature (190°C) with 5 mL of concentrated $HClO_4$ until the contents of the flask became clear. The mineral contents of the samples were determined using the respective standard curves prepared for each element. Aliquots were used to estimate Na and K by a flame photometer (Sherwood Flame Photometer, Cambridge, UK). Sodium and potassium contents were determined by using the flame photometer 410 (Sherwood Scientific Ltd., Cambridge, UK), whereas magnesium, calcium, iodine, iron, and zinc contents were determined through an atomic absorption spectrophotometer (Varian AA240, Varian Medical Systems Australasia Ltd., Belrose, Australia). The samples were quantified against standard solutions of known concentrations that were analyzed concurrently.

2.2.3. Analysis of vitamins

AOAC, method no. 2012.09, was used for the determination of the vitamin A content of flour samples (15). In contrast, Hernández et al. (16) method was used for vitamin C determination.

2.2.3.1. Vitamin A

Stock solutions (100 μg/mL) of retinyl palmitate were separately prepared in 100 mL of absolute ethanol. The working standard (5 μg of retinyl palmitate/mL) was prepared by diluting 5 mL of retinyl palmitate stock solution to 100 mL with ethanol. The concentration of the working standard was determined by measuring absorbance at 328 nm and dividing it by the specific absorption coefficient E (1%/1 cm) of 975 for retinyl palmitate. Calibration was performed using a concentration range of 0.09–2.0 μg/mL.

Samples were diluted with hexane (1:10), and 200 mL of the sample was transferred to a screw-capped tube, followed by the addition of 600 mL of methanol. The solution was vortex mixed, followed by centrifugation (3,000 g, 5 min) and filtration through a 0.45 mm pore-size filter, and the aliquot was injected into the HPLC (17).

The HPLC system (Perkin Elmer-200 Series, PerkinElmer Life, and Analytical Sciences, USA) was used in this study. HPLC was assisted with a degasser, an auto-sampler, a binary pump, and a UV/Vis detector. A reversed-phase C_{18} column (150 × 4.6 mm, 3.5 μm particle sizes) was used. Total Chrome Software was used to evaluate and quantify. Acetonitrile/methanol (75:25%) was used as the mobile phase, which was delivered at a 1.0 mL/min flow rate and held at 40°C.

The sample volume to be injected into HPLC was 20 μL with the (96:4) mobile phase consisting of methanol and water; elution was performed at a flow rate of 2 mL/min. The temperature of the analytical column was 45°C. Vitamin A was detected at 265 and 325 nm for 15 min. The quantification was performed using the retention times and peak areas of the standards and samples.

2.2.3.2. Vitamin C

Then, 0.25 g of DCIP was dissolved in 500 mL of distilled water to prepare the 2,6-dichloroindophenol (DCIP) solution, followed by the addition of sodium bicarbonate (0.21 g). The final volume of the solution was made up to 1 L with the help of distilled water. The concentration of the DCIP was almost 250 mg of DCIP/L. The next step was the standardization of the DCIP solution. Subsequently, 5 mL of an ascorbic acid solution was carefully pipetted into a 250-mL Erlenmeyer flask. The concentration of standard ascorbic acid was recorded. Afterward, 2 mL of the sulfuric acid mixture was added, and about 25 mL of distilled water was added to the flask. The flask was swirled to mix the solution. Then, 50 mL of the DCIP solution was added to the burette. DCIP was used to titrate the ascorbic acid until a permanent light red or pink color appeared, which lasted more than 30 s. After standardization, a standard DCIP solution was used to titrate the sample until a permanent light red or pink appeared, which lasted for more than 30 s. Vitamin C was calculated by the oxidation balance (16).

2.3. Extrusion formulations

As shown in Table 1, different levels of soybean and chickpea flour were used for the preparation of extrusion formulations. All formulations contained 7 g of guar gum per 100 g, except Control 1 treatment. In all treatments, minor ingredients (table salt, distilled mono-glycerides, and lecithin) were added, along

TABLE 1 Extrusion formulations (g/100 g).

Treatments*	Guar gum	Corn flour	Soy flour	Chickpea flour
Control 1	–	97	–	–
Control 2	7	90	–	–
T_1	7	70	20	–
T_2	7	60	30	–
T_3	7	50	40	–
T_4	7	70	–	20
T_5	7	60	–	30
T_6	7	50	–	40
T_7	7	70	10	10
T_8	7	60	15	15
T_9	7	50	20	20

*The remaining formulation (3/100 g) was distilled mono-glycerides, table salt, and lecithin along with micronutrient premix comprising nutrients according to the percent daily value of added nutrients.

with a micronutrient premix (Fe, Zn, I, and vitamins A and C) as per 3 g of the RDA per 100 g of the treatment formulations.

2.4. Extrusion processing

A pilot-scale single screw extruder (DGP-50, Henan Manufacturer, China) with instrumental specifications, i.e., a feed rate of 30 kg/h, a barrel diameter of 50 mm, and a temperature of 120–180°C, was used. The temperature was maintained at 150°C during the processing of corn snacks with the help of water circulation and monitored with the help of a thermocouple. The die was fitted with one circular insert of 4.2 mm diameter × 18.90 mm length. The operating variable was adjusted with the help of a pre-run of the extruder so that products with desired physical and textural properties were obtained. As the product exited the extruder barrel, it was collected in the trays and cooled at room temperature, followed by the collection of samples in the zip-lock polythene bags for further analysis.

2.5. Chemical composition of micronutrient-fortified corn snacks

Proximate composition, mineral content, and vitamins A and C were determined by following the methods described earlier.

Megazyme Test Kit was used to determine the dietary fiber content of corn snacks using the AACC (Method 32-05) and AOAC (Method 985.29) methods. The details of the procedures are given as follows:

2.5.1. Total dietary fiber (TDF)

The samples were dispersed in a buffer solution and incubated with heat-stable α-amylase at a temperature of 95–100°C for 35 min. After cooling the samples to 60°C, 100 l of protease solution was added and incubated at 60°C for 30 min. Finally, these contents were incubated with amyloglucosidase at 60°C for 30 minutes. The fiber contents were precipitated by the addition of alcohol in 1:4 ratio. The contents were filtered and washed with alcohol and acetone. A blank was run through the entire procedure along with test samples to calculate any contribution from reagents to the residue.

2.5.2. Soluble dietary fiber (SDF)

The samples were dispersed in a buffer solution and incubated with heat-stable α-amylase at 95–100°C for 35 min. After cooling the samples to 60°C, 100 μL of protease solution was added, and the contents were incubated at 60°C for 30 min. Finally, the contents by adding amyloglucosidase were incubated at a temperature of 60°C for 30 min. The residue after filtration was washed and rinsed with 10 mL of water. The filtrate and water washing were weighed, and soluble dietary fiber was precipitated with four volumes of ethyl alcohol. The contents were filtered and dried, and corrected for ash and protein contents. A blank was also run simultaneously through the entire procedure along with test samples to calculate any contribution from reagents to the residue.

2.5.3. In-soluble dietary fiber (IDF)

The samples were dispersed in a buffer solution and incubated with heat-stable α-amylase at a temperature of 95–100°C for 35 min. After cooling up to 60°C, the samples were incubated by adding 100 μL protease solutions at 60°C for 30 min, and then the contents were incubated by adding amyloglucosidase at 60°C for 30 min. The residue after filtration was washed and rinsed with 10 mL of water. The resultant residue was weighed, and soluble dietary fiber was precipitated with four volumes of ethyl alcohol. The contents were filtered, dried, and corrected for ash and protein contents. A blank was also run simultaneously through the entire procedure to calculate any contribution from reagents to the residue.

2.5.4. Calorific value

The calorific value of the extruded snack was determined by using an oxygen bomb calorimeter (C2000 Basic, IKA-WERKE, Germany), as described by 9. The sample (0.5 g) was taken into the metallic decomposition vial. The vial was unscrewed and fastened by a cotton thread with a loop onto the middle of the ignition wire before loading the sample. Then, the screw cap was tightened. The decomposition vial was guided into the filler head through the open measuring cell cover until it was in place.

The start button was pushed, and the measuring cell cover was closed. An electric spark was used to burn the sample contained within the vial. The heat produced was noted by C5040 CalWin software of the computer (IKA-Werke, Germany) and displayed as calories per gram of a sample.

2.6. Amino acids profile

The amino acid profile of the raw materials was assessed to calculate the relative amino acid concentration in the extrusion formulations as per proportion in the final formulation treatments, followed by the evaluation of the fortified corn snacks for the essential and non-essential amino acids. The amino acid composition of the extrusion formulations and extruded snacks was used to estimate the impact of extrusion processing on the amino acid profile in extruded fortified corn snacks. The amino acid profile of the snacks was determined through an automatic amino acid analyzer (Hitachi L8500, Tokyo, Japan) by following the method described by Adeyeye and Afolabi (18). Then, 30 mg of defatted ground sample, 5 μm of leucine, and 5 mL of 6 M HCl were filled in a glass ampule. Evacuation of the ampule was done using liquid nitrogen, followed by ampule sealing with a burner. The hydrolyzation of the ampoules was done in an oven at 110°C for 24 h. The tip of the ampoule was broken down to cool and filter the contents in it. The contents were dried in a rotary evaporator at 40°C under a vacuum. Acetate buffer (pH 2.2) was used for the preparation of samples for different amino acids. Subsequently, 5 μL of acetate buffer was used for neutral amino acids and 10 μL for basic amino acids. The resultant sample solution was dispensed into the amino acid analyzer cartridge. A peak area comparison of the standards and samples was made for the quantification of the amino acid content.

2.7. Statistical analysis

The collected data were subjected to statistical analysis using SPSS version 25. For the quantitative variables, frequency, percentages, and means (standard deviation) were used. An analysis of variance (ANOVA) was performed to determine the significance of the treatments used in the study. Tukey's honest significance test was used for posthoc analysis. The level of significance was taken as a p-value of ≤ 0.005 (19).

3. Results and discussion

Protein- and dietary fiber-enriched, nutrient-dense extruded snacks were developed using soy, chickpea, and corn flours, along with micronutrient fortification. Soybean, chickpea, and corn flours were subjected to chemical and nutritional analyses for the estimation of nutrient potential. The extruded snacks were studied for nutritional traits such as proximate composition, vitamins, minerals, amino acids, dietary fiber, and caloric evaluation.

3.1. Chemical composition of raw materials

The results of the proximate composition of raw materials (corn, soy, and chickpea flours) showed the highest moisture content (10.61 ± 0.21%) in the corn flour and the lowest in the soy flour (7.20 ± 0.27%). Soy flour had the highest protein level (46.2 ± 0.17%), followed by chickpea flour (22.5 ± 0.11%). Soy flour was subjected to defatting before use, which is why crude fat was lowest (1.22 ± 0.13%) in defatted soy flour, followed by corn flour (3.86 ± 0.07%) and chickpea flour (6.51 ± 0.12%). The crude fiber of the chickpea flour was found to be the highest (17.5 ± 0.08%) among all raw materials. Ash content was highest (3.06 ± 0.03%) in soy flour among all the raw materials.

Mineral analysis depicted that corn and chickpeas were excellent sources of sodium, i.e., 57.3 ± 4.2 mg/100 g and 64 ± 5.4 mg/100 g, respectively. Soybean showed a relatively low sodium content (20 ± 1.5 mg/100 g). The highest levels of potassium, calcium, and magnesium (2,384 ± 48.2 mg/100 g, 241 ± 25.3 mg/100 g, and 290 ± 12.3 mg/100 g, respectively) were found to be in soybeans. Zinc and iron contents, which ranged from 1.73 ± 0.10 to 2.81 ± 0.14 mg/100 g and 2.38 ± 0.64 to 9.24 ± 0.71 mg/100 g, respectively, were far below the daily requirements, which highlighted the need for the fortification of the food products containing corn, soybean, and chickpea as chief ingredients.

Corn showed maximum vitamin A content (214 ± 5.3IU), followed by chickpea (41 ± 2.2IU) and soy (40 ± 3.1IU). It is worth mentioning that none of the raw materials contained vitamin C. It was concluded from the results that the fortification of vitamin C would be obligatory to fulfill nutrient requirements in the diet. The results for proximate composition, mineral composition, and vitamin composition were consistent with earlier findings (20–22).

3.2. Compositional and nutritional analysis of micronutrient-fortified corn snacks

Significant differences were observed for the crude protein, moisture, crude fat, crude fiber, and ash content in fortified corn snacks (Figure 1). It was noted that the lowest moisture level (3.40 ± 0.02%) was present in corn snacks developed with 40/100 g of soy flour supplementation. Corn snacks developed without supplementation had a high moisture

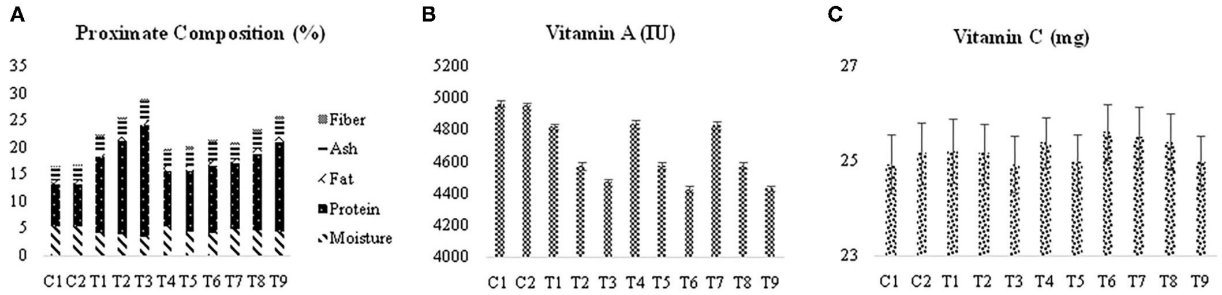

FIGURE 1
(A) Means for the effect of treatments on the proximate composition (%). **(B)** Means for the effect of treatments on the vitamin A content, **(C)** means for the effect of treatments on the vitamin C content. C1, control 1; C2, control 2; T1, corn snacks supplemented with 20/100 g of soy flour; T2, corn snacks supplemented with 30/100 g of soy flour; T3, corn snacks supplemented with 40/100 g of soy flour; T4, corn snacks supplemented with 20/100 g of chickpea flour; T5, corn snacks supplemented with 30/100 g of chickpea flour; T6, corn snacks supplemented with 40/100 g of chickpea flour; T7, corn snacks supplemented with 10:10/100 g of soy and chickpea flour; T8, corn snacks supplemented with 15:15/100 g of soy and chickpea flour; T9, corn snacks supplemented with 20:20/100 g of soy and chickpea flour.

content (5.400.01%). It can be concluded from the results that the supplementation with soy and chickpea flours resulted in decreased moisture content in the corn snacks. Varied moisture content (7.1 ± 0.17 to 9.1 ± 0.34%) in extruded snacks prepared using corn and rice was reported in another study as well (23). Means for crude protein content (7.600.10%) were lowest in corn snacks extruded without soy or chickpea flour supplementation. The maximum value (20.67 ± 0.46%) of proteins was noticed in corn snacks developed with 40/100 g of soy flour supplementation, while the lowest value (14.0 ± 0.50%) was noted in corn snacks developed with 20/100 g of soy flour supplementation. It was also concluded from the results that the protein contents of soy-supplemented corn snacks were higher than those of chickpea-supplemented snacks at each supplementation level.

A minimum amount of crude fat (0.79 ± 0.01%) was found in non-supplemented corn snacks. An increase in crude fat was observed with increasing supplementation levels, and corn snacks supplemented with chickpea flour showed higher crude fat content as compared to both the soy-supplemented and mixed-supplemented snacks.

Ash content was lowest (2.50 ± 0.03%) in the non-supplemented corn snacks, followed by corn snacks that contained only 7/100 g of guar gum (2.64 ± 0.01%). Soy flour-based snacks had the highest ash content (3.390.02%) of any supplemented snack. It was also observed that the ash of soy-supplemented corn snacks was higher than that of chickpea-supplemented corn snacks at each level of supplementation.

The proximate composition of the corn snacks revealed that the non-supplemented corn snacks contained the least amount of crude fiber (0.300.02%). Soy-supplemented corn snacks depicted the highest amount of crude fiber content as compared to others due to escalated levels of supplementation.

The results of the present research cohere with a previous study on the development of crisp from soy flour (25–40/100 g) and rice flour by supercritical fluid extrusion. Protein (334–568%) and dietary fiber (571–901%) were improved in the final products due to soy flour supplementation (24). Another study suggested that the incorporation of soy flour into cereals can assist in overcoming the deficiency of the protein (25). Similarly, in a study, a novel source of protein, i.e., spirulina, was used to increase the protein content of dry pasta, with the amount of protein ranging from 12.91/100 to 23.49/100 g in the final products (26). Another study concluded that protein-rich (40–60/100 g dry basis) extruded products prepared from a soy protein isolate-corn flour blend can be prepared with minimum moisture, ranging from 2.2 to 3.5% (11).

3.3. Mineral profile

Fortified corn snacks showed significant differences in calcium, potassium, magnesium, sodium, iron, and zinc content in comparison with the control (Table 2). The maximum value (100.70 ± 9.21 mg/100 g) of calcium was observed in corn snacks containing 40/100 g of soy flour, whereas the least value (6.62 ± 0.59 mg/100 g) was observed in corn snacks extruded without soy or chickpea flour supplementation.

Corn snacks showed potassium levels ranging from 402.82 ± 34.21 to 1,124.4 ± 55.32 mg/100 g in the snacks that contained soy and chickpeas. In contrast, non-supplemented corn snacks contained 296.88 ± 16.64 mg/100 g potassium. An analysis of treatment supplemented with soy or chickpea flour for magnesium content revealed a range of 102.98 ± 9.53 to 166.92 ± 4.98 mg/100 g among all the soy or chickpea flour-supplemented snacks. However, sodium content ranged from 7.67 ± 0.74 to 28.35 ± 1.23 mg/100 g among the soy- and chickpea-supplemented treatments. Non-supplemented corn snacks showed the lowest sodium content (4.71 ± 0.21 mg/100 g), whereas the highest sodium content (28.35 ± 1.23 mg/100 g) was noted in corn snacks containing 40/100 g of chickpea flour.

TABLE 2 Means for the effect of treatments on the mineral content (mg/100 g), dietary fiber (g/100 g), and calories (K cal/g) of extruded corn snacks.

Treatments	Ca	K	Mg	Na	Fe	Zn	Total dietary fiber	Soluble dietary fiber	Insoluble dietary fiber	Calorific value
C1	6.62 ± 0.59i	296.88 ± 16.64i	88.36 ± 5.54f	4.71 ± 0.21j	10.95 ± 0.89c	10.65 ± 0.43c	10.36 ± 0.43c	4.56 ± 0.21e	5.80 ± 0.21c	3,933 ± 4.22f
C2	6.65 ± 0.53i	297.27 ± 18.94i	89.93 ± 6.35f	4.73 ± 0.82j	10.27 ± 1.32b	10.59 ± 0.64c	15.40 ± 0.67b	8.33 ± 0.17d	6.36 ± 0.31bc	3,910 ± 3.68g
T1	53.69 ± 4.21d	710.50 ± 25.32d	129.60 ± 8.53c	7.67 ± 0.74i	15.49 ± 1.01ab	10.78 ± 0.64bc	17.12 ± 0.63ab	10.03 ± 0.32abc	7.05 ± 0.12ab	4,009 ± 6.43e
T2	76.58 ± 6.32b	913.84 ± 30.67b	148.67 ± 7.52b	9.25 ± 0.22h	15.98 ± 1.32ab	10.86 ± 0.86abc	17.78 ± 0.56ab	10.34 ± 0.22ab	7.41 ± 0.25ab	4,030 ± 4.87d
T3	100.70 ± 9.21a	1,124.4 ± 55.32a	166.92 ± 4.98a	10.69 ± 0.82g	17.03 ± 1.56a	10.92 ± 0.94abc	18.44 ± 0.34a	10.65 ± 0.13a	7.76 ± 0.38a	4,064 ± 6.31a
T4	14.41 ± 1.32h	402.82 ± 34.21h	102.98 ± 9.53e	16.57 ± 1.39d	14.47 ± 0.93ab	11.02 ± 0.91abc	15.50 ± 0.61b	8.60 ± 0.42cd	6.87 ± 0.19abc	4,043 ± 5.35c
T5	18.04g ± 1.42h	456.50 ± 29.54g	110.23 ± 10.01de	22.44 ± 1.11b	15.05 ± 0.78ab	11.23 ± 0.65ab	15.60 ± 0.52b	8.87 ± 0.34bcd	6.70 ± 0.21abc	4,049 ± 4.62bc
T6	21.93 ± 2.03g	510.88 ± 40.23f	117.56 ± 9.32d	28.35 ± 1.23a	15.31 ± 1.11ab	11.33 ± 0.34a	15.77 ± 0.53ab	9.41 ± 0.13abcd	7.04 ± 0.15ab	4,061 ± 3.53ab
T7	33.27 ± 3.12f	558.97 ± 49.32e	115.04 ± 10.65d	12.14 ± 1.76f	14.65 ± 1.12ab	10.80 ± 1.02bc	16.36 ± 0.61ab	9.45 ± 0.21abcd	6.88 ± 0.20abc	4,005 ± 6.72e
T8	47.84 ± 3.89e	688.33 ± 54.34d	128.51 ± 9.43c	15.82 ± 0.98e	15.22 ± 1.26ab	10.85 ± 0.53bc	16.64 ± 0.48ab	9.47 ± 0.18abcd	7.14 ± 0.17ab	4,015 ± 5.98e
T9	61.04 ± 5.87c	816.55 ± 38.2c	142.42 ± 12.76b	19.51 ± 0.78c	15.64 ± 1.43ab	10.95 ± 0.32abc	16.92 ± 0.58ab	9.49 ± 0.17abcd	7.40 ± 0.19ab	4,030 ± 3.47d

The means carrying the same letter in a column differed non-significantly ($p > 0.05$).
C1, control 1; C2, control 2; T1, corn snacks supplemented with 20/100 g of soy flour; T2, corn snacks supplemented with 30/100 g of soy flour; T3, corn snacks supplemented with 40/100 g of soy flour; T4, corn snacks supplemented with 20/100 g of chickpea flour; T5, corn snacks supplemented with 30/100 g of chickpea flour; T6, corn snacks supplemented with 40/100 g of chickpea flour; T7, Corn snacks supplemented with 10:10/100 g of soy and chickpea flour; T8, corn snacks supplemented with 15:15/100 g of soy and chickpea flour; T9, Corn snacks supplemented with 20:20/100 g of soy and chickpea flour.

Soy and chickpea-supplemented corn snacks showed iron content ranging from 14.47 ± 0.93 to 15.98 mg/100 g. In contrast, non-supplementation snacks contained 10.95 ± 0.89 mg/100 g of iron. It was also noted that the iron level decreased to 10.27 ± 1.32 mg/100 g with the addition of guar gum. Zinc was found to be more abundant in the snacks supplemented with chickpea flour as compared to soy flour, with the highest content of this nutrient (11.33 ± 0.34 mg/100 g) in snacks made with 40/100 g of chickpea flour. However, a minimum (10.65 ± 0.43 mg/100 g) level of zinc was noted in the non-supplemented snacks.

Existing literature suggests that the bioavailability of the minerals improves during extrusion processing owing to the inactivation of anti-nutritional factors, e.g., phytates (24, 27). Moreover, instead of harsh processing conditions, mineral content remains steady during extrusion, and nearly no mineral loss occurs. Some studies even observed an increase in iron, which is linked to the liberation of iron from complex molecules that increases its bioavailability (27). Similarly, another study that used superficial fluid extrusion to prepare micronutrient-fortified rice soy crisp found iron content ranging from 26.19 to 32.09 mg/100 g and zinc content ranging from 13.65 to 14.92 mg/100 g. The study revealed 100% retention of all added minerals, with even a 25% increase in iron level in the crisps (24). Another study revealed that 10% of the RDA of Zn can be filled by consuming spirulina-supplemented corn crisps (28).

3.4. Vitamin A and C content

Vitamin A, the content of the corn snacks, was observed at its maximum (4,962.0 ± 20.12IU) in the non-supplemented corn snacks, followed by the corn snacks (4,950.5 ± 19.32IU) containing 7 g/100 of guar gum (Figure 1). It was also noted that the lowest levels of soy, chickpeas, and mixed supplementation with soy and chickpea contain 4,820.2 ± 17.43, 4,834.5 ± 23.42, and 4,825.5 ± 23.82 IU vitamin A, respectively. Corn is the best source of vitamin A among all the raw materials, as shown by the composition of the raw materials. As a result, corn-based snacks have a higher level of vitamin A. No statistical difference was observed regarding mean vitamin C content. This indicates that supplementation with soy and chickpea has no effect on the vitamin C content of the extruded snacks. The only source of vitamin C is the fortification of snacks with ascorbic acid.

The nutritional composition of the extruded product is mainly dependent on the processing variables of extrusion (29). Some studies utilizing novel extrusion processes retain about 50% of vitamins A and C at low-shear and low-temperature conditions (24). Similarly, 64–76% retention of vitamin C and 55–58% retention of vitamin A were noted in puffed rice made using supercritical fluid extrusion (27).

3.5. Dietary fiber

Dietary fiber in the corn snacks developed with 40/100 g of soy flour showed a maximum level of 18.44 ± 0.34%, whereas a minimum level of 10.36 ± 0.43% was observed in the non-supplemented corn snacks (Table 2). The total dietary fiber of the corn snacks containing soy flour was higher at each supplementation level as compared to the other snacks. The study conducted by Alonso et al. (30) and Varo showed an insignificant variation in total dietary fiber in the product extruded at 161–180°C. Although extrusion showed insignificant changes in the total dietary fiber, the distribution of the soluble to insoluble dietary fiber changed during extrusion (31).

Overall, soluble dietary fiber ranged from 9.41 ± 0.13 to 10.65 ± 0.13%. It was observed that dietary fiber increased with increased supplementation. Soy-supplemented corn snacks have more soluble dietary fiber as compared to the other treatments. Onwulata et al. (32) revealed a 10% increase in soluble dietary fiber after the extrusion of the food product.

As depicted in Table 2, the means for the insoluble dietary fiber of corn snacks showed that insoluble dietary fiber was lowest (5.80 ± 0.21%) in the non-supplemented corn snacks, followed by corn snacks containing guar gum along with corn (6.36 ± 0.31%). The insoluble dietary fiber of the soy-supplemented corn snacks was higher than that of the remaining corn snacks at each supplementation level. Insoluble dietary fiber reduction is linked with extrusion processing, as presented in a study conducted on the extrusion of black beans and cereals (31).

3.6. Calorific value

The corn snack containing 40/100 g soy flour had the highest mean calorific value (40,646.31 kcal/g). The minimum calorific value (3,933 ± 4.22 kcal/g) was noted in non-supplemented corn snacks. Overall, soy-supplemented corn snacks showed higher calorific values as compared to chickpea-supplemented snacks (Table 2).

3.7. Effect of extrusion on the amino acid composition of fortified corn snacks

The basic aim behind supplementing soy and chickpeas with corn was to improve the quantity and quality of protein in the final extruded product. Extrusion has both positive and negative effects on different amino acids. In the current study, first, raw materials, i.e., soy, chickpea, and corn flour, were analyzed for

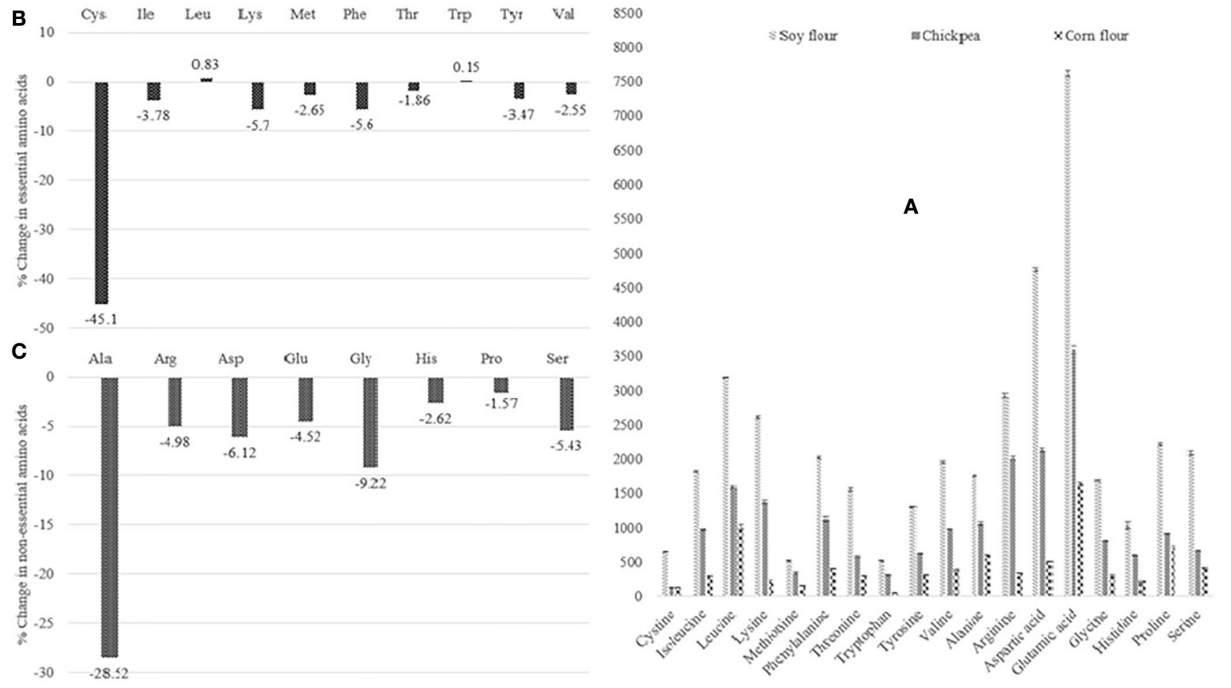

FIGURE 2
(A) Means for the amino acid profile of raw materials [x-axis, amino acids; Y-axis, concentration (mg/100 g)]; **(B)** Effect of extrusion processing on the essential amino acid of extruded corn snacks (x-axis, essential amino acids; Y-axis, % change in essential amino acid); **(C)** Effect of extrusion on the non-essential amino acid of extruded corn snacks (x-axis, non-essential amino acids; Y-axis, % change in non-essential amino acids).

TABLE 3 Amino acids composition (mg/100g) of extrusion formulation of corn snacks based on raw material composition.

Treatments	Essential amino acids								
	Cysteine	Isoleucine	Lucien	Lysine	Methionine	Phenylalanine	Threonine	Tryptophan	Tyrosine
C1	124.16 ± 8.41f	285.18 ± 3.22j	979.70 ± 9.15j	211.46 ± 5.33i	149.38 ± 3.24g	397.70 ± 3.87j	285.18 ± 2.47j	49.47 ± 2.43i	372.48 ± 5.46j
C2	115.20 ± 6.91g	264.60 ± o5.95k	909.43 ± 7.17k	196.20 ± 8.34j	138.60 ± 8.72h	369.23 ± 4.35k	264.60 ± 9.60kS	45.90 ± 1.78j	345.60 ± 6.54k
T1	220.23 ± 4.44c	569.80 ± 8.51e	1,345.67 ± 8.53d	674.60 ± 5.85d	212.45 ± 8.90d	691.43 ± 9.07e	517.87 ± 4.67d	139.96 ± 4.65f	660.83 ± 7.85e
T2	272.40 ± 2.12b	722.40 ± 8.90b	1,563.45 ± 9.35b	913.80 ± 5.13a	248.72 ± 5.63b	852.12 ± 7.25b	644.44 ± 5.83b	186.91 ± 2.46c	818.41 ± 9.35b
T3	324.80 ± 8.72a	875.33 ± 7.55a	1,781.43 ± 9.80a	115.34 ± 9.24k	285.40 ± 7.50a	1,013.45 ± 4.53a	771.34 ± 4.84a	233.92 ± 8.72a	976.23 ± 8.39a
T4	114.35 ± 3.82h	400.23 ± 6.20i	1,026.05 ± 8.20i	427.55 ± 5.42h	176.20 ± 6.17f	512.32 ± 5.35i	321.45 ± 7.10i	96.90 ± 1.57h	463.65 ± 7.54i
T5	113.95 ± 3.24h	468.34 ± 4.60h	1,084.75 ± 9.14h	543.22 ± 7.17g	195.34 ± 0.08e	583.50 ± 4.97h	349.87 ± 9.35h	122.44 ± 2.46g	522.65 ± 4.14h
T6	113.53 ± 2.40h	535.85 ± 5.67f	1,143.12 ± 7.18g	658.90 ± 3.95e	213.85 ± 2.50d	655.23 ± 6.35f	378.33 ± 8.34g	147.92 ± 3.75e	581.70 ± 5.20f
T7	167.17 ± 2.65e	485.13 ± 5.18g	1,185.52 ± 4.60f	551.07 ± 4.40f	194.13 ± 3.58	601.50 ± 8.93g	419.62 ± 2.54f	118.42 ± 1.45h	562.25 ± 4.80g
T8	193.16 ± 2.44d	595.24 ± 7.70d	1,323.78 ± 9.80e	728.51 ± 5.20c	221.85 ± 2.98c	717.75 ± 8.56d	497.13 ± 5.30e	154.65 ± 3.53d	670.53 ± 4.35d
T9	219.15 ± 5.23c	705.42 ± 2.48c	1,462.05 ± 2.40c	905.95 ± 9.15b	249.62 ± 5.72b	834.42 ± 5.20c	574.65 ± 2.69c	190.92 ± 3.24b	778.85 ± 3.53c

Treatments	Non-Essential amino acids							
	Alanine	Arginine	Aspartic acid	Glutamic acid	Glycine	Histidine	Proline	Serine
C1	583.94 ± 7.64j	323.01 ± 3.20j	496.64 ± 3.95j	1,600.5 ± 6.11h	285.18 ± 2.23i	211.46 ± 3.25i	695.49 ± 2.53j	397.70 ± 7.43j
C2	541.80 ± 7.25k	299.70 ± 2.24k	460.80 ± 2.51k	1,485.78 ± 5.32i	264.60 ± 3.76j	196.20 ± 1.41j	645.30 ± 5.83k	369.53 ± 8.75k
T1	773.46 ± 6.94e	819.10 ± 5.42f	1,310.48 ± 9.35e	2,679.64 ± 10.2d	543.80 ± 6.28d	360.68 ± 3.24d	945.92 ± 4.97d	705.34 ± 4.34d
T2	889.25 ± 3.20b	1,078.87 ± 6.17c	1,735.20 ± 8.42b	3,276.78 ± 20.2b	683.40 ± 7.21b	442.86 ± 2.99b	1,096.21 ± 8.22b	873.24 ± 3.20b
T3	1,005.55 ± 9.74a	1,338.55 ± 5.35a	2,160.56 ± 9.42a	3,873.78 ± 18.1a	823.64 ± 6.42a	525.46 ± 5.32a	1,246.52 ± 9.30a	1,041.76 ± 5.42a
T4	633.35 ± 4.54i	636.34 ± 5.42i	785.45 ± 5.21i	1,873.65 ± 10.2g	367.35 ± 2.18h	273.22 ± 2.87h	685.05 ± 6.32i	420.20 ± 6.11i
T5	679.13 ± 4.23h	804.63 ± 5.20g	947.17 ± 8.01h	2,067.98 ± 9.81f	418.73 ± 5.32g	311.74 ± 3.64g	704.93 ± 7.17h	445.83 ± 5.23h
T6	724.95 ± 7.62f	972.95 ± 8.56d	1,109.27 ± 9.98f	2,262.30 ± 10.4e	470.10 ± 4.37e	350.22 ± 2.34e	724.80 ± 4.22g	471.42 ± 8.37g
T7	703.38 ± 5.51g	727.77 ± 8.93h	1,047.74 ± 8.29g	2,276.33 ± 9.81e	455.58 ± 4.99f	316.94 ± 5.10f	815.48 ± 7.32f	562.61 ± 7.42f
T8	784.16 ± ± 8.23d	941.78 ± 6.35e	1,341.15 ± 9.13d	2,671.99 ± 10.9d	551.06 ± 6.98d	377.25 ± 4.26c	900.56 ± 6.91e	659.42 ± 5.45e
T9	864.95 ± 4.12c	1,155.70 ± 4.97b	1,634.63 ± 7.99c	3,067.65 ± 12.2c	646.55 ± 5.62c	437.64 ± 3.53b	985.65 ± 7.77c	756.20 ± 6.98c

The means carrying the same letter in a column differed non-significantly ($p > 0.05$).

C1, control 1; C2, control 2; T1, corn snacks supplemented with 20/100 g of soy flour; T2, corn snacks supplemented with 30/100 g of soy flour; T3, corn snacks supplemented with 40/100 g of soy flour; T4, corn snacks supplemented with 20/100 g of chickpea flour; T5, corn snacks supplemented with 30/100 g of chickpea flour; T6, corn snacks supplemented with 40/100 g of chickpea flour; T7, corn snacks supplemented with 10:10/100 g of soy and chickpea flour; T8, corn snacks supplemented with 15:15/100 g of soy and chickpea flour; T9, corn snacks supplemented with 20:20/100 g of soy and chickpea flour.

10.3389/fnut.2022.1062616

TABLE 4 Means for the effect of treatments on essential and non-essential amino acids (mg/100g) of extruded corn snacks.

Treatments	Cysteine	Isoleucine	Lucien	Lysine	Methionine	Phenylalanine	Threonine	Tryptophan	Tyrosine	Valine
C1	68.160 ± 3.23g	145.79 ± 4.22e	987.54 ± 3.35j	199.41 ± 5.07j	149.38 ± 6.42f	376.62 ± 4.34j	280.33 ± 6.53j	49.770 ± 3.92j	287.37 ± 4.41h	363.91 ± 5.25i
C2	63.480 ± 4.14i	135.41 ± 6.41f	918.09 ± 5.06k	185.61 ± 3.01k	138.60 ± 7.51f	346.86 ± 6.41k	260.37 ± 4.41	46.310 ± 4.63k	267.18 ± 6.31i	336.61 ± 3.22j
T1	121.66 ± 5.02c	207.34 ± 2.29d	1,361.1 ± 21.7d	640.20 ± 10.03e	212.00 ± 4.32c	651.61 ± 3.14e	508.48 ± 3.33d	140.32 ± 8.95f	457.33 ± 3.53d	642.30 ± 5.04d
T2	151.18 ± 3.12b	243.48 ± 5.5b	1,584.9 ± 51.8b	869.94 ± 9.05b	248.70 ± 7.32b	805.99 ± 7.05b	636.67 ± 5.66b	187.27 ± 6.37c	551.81 ± 6.62b	793.85 ± 3.75b
T3	180.91 ± 6.33a	276.84 ± 2.35a	1,809.5 ± 62.2a	1,101.1 ± 41.9a	285.40 ± 3.53a	961.34 ± 51.4a	762.52 ± 8.37a	235.77 ± 7.58a	650.60 ± 2.77a	955.50 ± 6.57a
T4	63.920 ± 4.51h	171.09 ± 2.54e	1,044.5 ± 27.5i	409.59 ± 5.73i	176.20 ± 3.71e	482.30 ± 4.73i	312.77 ± 5.46i	97.380 ± 2.56i	326.89 ± 6.33g	451.60 ± 2.73h
T5	62.320 ± 3.01j	190.13 ± 6.26d	1,091.1 ± 66.9h	510.63 ± 3.64h	195.00 ± 7.41d	550.82 ± 7.63h	336.93 ± 6.43h	122.64 ± 8.54g	359.01 ± 3.72f	508.56 ± 6.44g
T6	61.860 ± 5.62k	208.24 ± 6.65c	1,147.7 ± 63.6g	617.39 ± 6.58f	213.80 ± 6.71c	616.36 ± 3.29f	371.87 ± 7.64g	148.05 ± 6.46e	389.44 ± 8.82e	567.16 ± 8.79e
T7	90.780 ± 1.42f	188.86 ± 8.74d	1,187.9 ± 30.7f	514.70 ± 3.29g	194.10 ± 5.82d	568.42 ± 7.37g	414.17 ± 3.83f	118.40 ± 1.55h	393.57 ± 9.93e	549.29 ± 5.38f
T8	104.50 ± 6.71e	215.64 ± 4.28b	1,323.8 ± 71.8e	678.25 ± 7.28d	221.85 ± 4.42c	676.84 ± 2.46d	486.20 ± 5.32e	153.88 ± 5.34d	456.29 ± 4.08d	653.77 ± 4.37d
T9	118.13 ± 8.23d	242.36 ± 3.66b	1,459.1 ± 71.9c	840.73 ± 4.43c	249.60 ± 8.31b	787.30 ± 4.57c	566.04 ± 3.51c	188.05 ± 3.43b	516.73 ± 3.01c	758.60 ± 7.05c

	Alanine	Arginine	Aspartic acid	Glutamic acid	Glycine	Histidine	Proline	Serine
C1	418.68 ± 8.31j	307.51 ± 6.31i	464.36 ± 9.32j	1,525.3 ± 13.44h	257.80 ± 7.42j	205.12 ± 2.41g	682.28 ± 4.43i	375.43 ± 6.01j
C2	389.55 ± 7.52k	285.91 ± 3.41j	432.69 ± 8.21k	1,412.2 ± 15.33i	238.93 ± 4.31k	191.49 ± 4.31g	635.62 ± 7.32k	350.18 ± 4.41k
T1	552.21 ± 5.65e	784.70 ± 6.09f	1,229.2 ± 15.17e	2,561.1 ± 20.54d	497.58 ± 6.45e	350.14 ± 2.63d	923.20 ± 5.67d	666.93 ± 6.35d
T2	634.00 ± 8.04b	1,024.9 ± 13.56c	1,625.9 ± 23.26b	3,128.6 ± 26.30b	626.68 ± 8.65b	433.50 ± 6.05b	1,091.8 ± 14.46b	823.24 ± 4.76b
T3	720.59 ± 9.35a	1,270.2 ± 15.38a	2,023.9 ± 29.28a	3,710.3 ± 31.64a	747.28 ± 4.33a	509.77 ± 6.46a	1,216.6 ± 18.06a	978.54 ± 3.47a
T4	457.28 ± 6.63i	602.58 ± 10.82h	731.62 ± 8.39i	1,780.0 ± 14.77g	331.35 ± 7.24i	267.46 ± 7.22f	672.72 ± 8.72j	398.77 ± 7.24i
T5	492.37 ± 4.74h	774.83 ± 9.05f	889.33 ± 7.59h	1,966.6 ± 12.97f	377.27 ± 5.57h	302.97 ± 4.62e	697.17 ± 9.36h	421.73 ± 8.73h
T6	508.88 ± 6.06f	933.01 ± 12.33d	1,037.1 ± 10.14f	2,162.8 ± 27.25e	426.38 ± 8.77f	339.69 ± 5.64d	711.03 ± 7.27g	444.53 ± 5.86g
T7	500.80 ± 7.68g	692.04 ± 11.52g	975.41 ± 12.08g	2,176.2 ± 18.30e	412.75 ± 4.09g	308.98 ± 9.83e	798.35 ± 5.69f	531.66 ± 9.44f
T8	555.97 ± 4.69d	898.38 ± 18.98e	1,247.3 ± 18.12d	2,562.4 ± 27.21d	500.92 ± 7.36d	369.33 ± 4.36c	896.96 ± 8.88e	625.77 ± 6.84e
T9	616.72 ± 3.88c	1,088.7 ± 12.46b	1,520.2 ± 21.20c	2,938.8 ± 14.70c	590.96 ± 9.66c	424.47 ± 5.75b	971.86 ± 7.49c	717.63 ± 7.45c

The means carrying the same letter in a column differed non-significantly ($p > 0.05$); C1, control 1; C2, control 2; T1, corn snacks supplemented with 20/100 g of soy flour; T2, corn snacks supplemented with 30/100 g of soy flour; T3, corn snacks supplemented with 40/100 g of soy flour; T4, corn snacks supplemented with 20/100 g of chickpea flour; T5, corn snacks supplemented with 30/100 g of chickpea flour; T6, corn snacks supplemented with 40/100 g of chickpea flour; T7, corn snacks supplemented with 10:10/100 g of soy and chickpea flour; T8, corn snacks supplemented with 15:15/100 g of soy and chickpea flour; T9, corn snacks supplemented with 20:20/100 g of soy and chickpea flour.

10.3389/fnut.2022.1062616

the amino acid profile. The results are summarized in Figure 2. These concentrations of the amino acids were used to compute the amino acid profile of the extrusion premixes based on their proportion in the final formulation. The amino acid profile was evaluated using the essential and non-essential amino acid composition (mg/100 g) of extruded corn snacks based on the raw material composition. The results of the analysis are shown in Table 3. The means for the essential and non-essential amino acids (mg/100 g) of extruded fortified corn snacks are shown in Table 4.

These values of the amino acid composition of the extrusion formulations were compared with the experimental results of the final extruded snacks' amino acid profile to estimate the effect of extrusion processing on amino acid retention. The percent change during extrusion for the essential and non-essential amino acids is shown in Figure 2C. The results revealed that the amino acid that is affected the most by extrusion processing is cysteine (45.1%). Essential amino acids sensitive to extrusion processing can be arranged in the following descending order, starting from most affected to least affected, i.e., lysine, phenylalanine, isoleucine, tyrosine, methionine, and valine, with reduction percentages of 5.7, 5.6, 3.78, 3.47, 2.65, and 2.55%, respectively. Leucine (0.83%) and tryptophan (0.15%) are among the essential amino acids that remained almost unaffected during extrusion processing. Among the non-essential amino acids, the most unstable is alanine (−28.52%). Similarly, as per the results of the study, non-essential amino acids could be arranged in descending order, starting from most affected to least affected, i.e., glycine, aspartic acid, serine, arginine, glutamic acid, histidine, and proline, with reduction percentages of 9.22, 6.12, 5.43, 4.98, 4.52, 2.62, and 1.57%, respectively. This increase is probably due to the inactivation of anti-nutritional compounds such as phytates and trypsin. However, heat-sensitive amino acids' levels decreased during extrusion; the operating temperature of conventional extrusion is always more than 100°C to change the moisture in the recipe to water vapors, which in turn gives extrudates their characteristic puffiness. Another reason is the Millard reaction between sugars and amino acids due to heat during extrusion. It is a leading cause of amino acid loss during extrusion. The findings of the current study were verified by the results of the previous studies. In a study, the effect of heat treatment on the retention of amino acids in infant formula was studied. The results of the study revealed that amino acid destruction during autoclaving is almost 19.5% greater than the usual preparation method that does not include heat treatment. The study reported losses in the range of 4.1–71.5%. Maximum reductions were observed in valine, glutamine, and lysine, i.e., 71.5, 60.6, and 39.2%, respectively. Overall, 28.17% of essential and 27.13% of non-essential amino acids were affected by heat treatment (18). Another study conducted on amino acid retention in canned baby foods also provided similar results on heat treatment of the amino acid profile. It was reported that there was a decrease in amino acids during heat processing; however, it also showed that isoleucine remained unaffected by the heat treatment. The percent recovery of phenylalanine, tryptophan, and tyrosine was 116, 107, and 102%, respectively, which indicates the positive effect of heat treatment on these amino acids (33, 34).

Conclusions

Supplementing corn snacks with soy and chickpeas increased the protein and dietary fiber content of the snacks. Soy-fortified snacks were nutritionally superior to chickpea-supplemented snacks. Corn snacks, developed by using 40/100 g soy flour, showed a high content of protein (20.67 ± 0.46%), dietary fiber (18.44 ± 0.34/100 g), calcium (100.70 ± 9.21 mg/100 g), magnesium (166.92 ± 4.98 mg/100 g), potassium (1,124.4 ± 55.32 mg/100 g), and iron (17.03 ± 1.56 mg/100 g) contents. The supplementation with soy and chickpea improved balance in the amino acid profile of the corn snacks. Amino acids such as lysine (5.70%), phenylalanine (5.6%), isoleucine (3.78%), tyrosine (3.47%), methionine (2.65%), and valine (2.55%) decrease when processed by extrusion technology to produce corn snacks.

Data availability statement

The original contributions presented in the study are included in the article/supplementary material, further inquiries can be directed to the corresponding author.

Author contributions

F-u-HS: writing—original draft. MS: conceptualization. ZA and RS: review and editing. AA: investigation and supervision. MJ: conducting research and performing the experiments, data analysis resources provision, and formal analysis. D-e-SS: validation and verification of data. MA: data interpretation. MJA: formal analysis. All authors contributed to the article and approved the submitted version.

Acknowledgments

This research was supported by the Higher Education Commission of Pakistan and is part of the thesis submitted to the University of Agriculture, Faisalabad, for the award of a degree.

Conflict of interest

The authors declare that the research was conducted in the absence of any commercial or financial relationships that could be construed as a potential conflict of interest.

Publisher's note

References

1. United Nations Children's Fund. *Improving Child Nutrition: The Achievable Imperative for Global Progress*. New York, NY: United Nations Children's Fund (2013). Available online at: https://data.unicef.org/resources/improving-child-nutrition-the-achievable-imperative-for-global-progress (accessed November 10, 2020).

2. Shah FUH, Sharif MK, Bashir S, Ahsan F. Role of healthy extruded snacks to mitigate malnutrition. *Food Rev. Int.* (2019) 35:299–323. doi: 10.1080/87559129.2018.1542534

3. Altaf U, Hussain SZ, Qadri T, Iftikhar F, Naseer B, Rather AH. Investigation on mild extrusion cooking for development of snacks using rice and chickpea flour blends. *J Food Sci Technol.* (2021) 58:1143–55. doi: 10.1007/s13197-020-04628-7

4. World Health Organization. *Supplementary Foods for the Management of Moderate Acute Malnutrition in Infants and Children 6–59 Months of Age*. Geneva: World Health Organization (2012). Available online at: https://www.who.int/nutrition/publications/moderate-malnutrition/9789241504423/en/ (accessed February 18, 2021).

5. Shah FUH, Sharif MK, Butt MS, Shahid M. Development of protein, dietary fiber, and micronutrient enriched extruded corn snacks. *J Text Stud.* (2017) 48:221–30. doi: 10.1111/jtxs.12231

6. Darnton-Hill I, Nalubola R. Fortification strategies to meet micronutrient needs: sucesses and failures. *Proc Nutr Soc.* (2002) 61:231–41. doi: 10.1079/PNS2002150

7. Reshi M, Shafiq F, Hussain SZ, Naseer B, Amin T. Physicochemical properties of iron-fortified, low glycemic index (GI) barley based extruded ready-to-eat snacks developed using twin-screw extruder. *J Food Process Preserv*. (2020) 44:14606. doi: 10.1111/jfpp.14606

8. Muldabekova BZ, Umirzakova GA, Assangaliyeva ZR, Maliktayeva PM, Zheldybayeva AA, Yakiyayeva MA. Nutritional evaluation of buns developed from chickpea-mung bean composite flour and sugar beet powder. *Int J Food Sci.* (2022) 2022:9998. doi: 10.1155/2022/6009998

9. Hasmadi M, Noorfarahzilah M, Noraidah H, Zainol MK, Jahurul MHA. Functional properties of composite flour: a review. *Food Res.* (2020) 4:1820–31. doi: 10.26656/fr.2017.4(6).419

10. Stojceska V, Ainsworth P, Plunkett A, Ibanoglu S. The advantage of using extrusion processing for increasing dietary fibre level in gluten-free products. *Food Chem.* (2010) 121:156–64. doi: 10.1016/j.foodchem.2009.12.024

11. Lai YC, Wang SY, Gao HY, Nguyen KM, Nguyen CH, Shih MC, et al. Physicochemical properties of starches and expression and activity of starch biosynthesis-related genes in sweet potatoes. *Food Chem.* (2016) 199:556–64. doi: 10.1016/j.foodchem.2015.12.053

12. Zia-Ul-Haq M, Iqbal S, Ahmad S, Imran M, Niaz A, Bhanger MI. Nutritional and compositional study of desi chickpea (*Cicer arietinum* L.) cultivars grown in Punjab, Pakistan. *Food Chem.* (2007) 105:1357–63. doi: 10.1016/j.foodchem.2007.05.004

13. Smart Snacking. *Canada's Food Guide*. (2012). Available online at: http://en.wikipedia.org/wiki/Snack_food (accessed October 25, 2020).

14. AACC. *Approved Methods of American Association of Cereal Chemists, 10th ed.* St. Paul, MN: The American Association of Cereal Chemists (2000).

15. AOAC. *Association of Official Analysis Chemists. Official Methods of Analysis 18th edn.* Arlington, VA: AOAC Press (2012).

16. Hernández Y, Lobo MG, González M. Determination of vitamin C in tropical fruits: a comparative evaluation of methods. *Food Chem.* (2006) 96:654–64. doi: 10.1016/j.foodchem.2005.04.012

17. Ryynänen M, Lampi AM, Salo-Väänänen P, Ollilainen V, Piironen V. A small-scale sample preparation method with HPLC analysis for determination of tocopherols and tocotrienols in cereals. *J Food Comp Anal.* (2004) 17:749–65. doi: 10.1016/j.jfca.2003.09.014

18. Adeyeye EI, Afolabi EO. Amino acid composition of three different types of land snails consumed in Nigeria. *Food Chem.* (2004) 85:535–9. doi: 10.1016/S0308-8146(03)00247-4

19. Steel RGD, Torrie JH, Dickey DA. Principles and procedures of statistics. In: *A Biometrical Approach, 3rd edn.* New York, NY: McGraw HillBook Co. Inc. (1997), p. 352–399.

20. Pérez AA, Drago SR, Carrara CR, De Greef DM, Torres RL, González RJ. Extrusion cooking of a maize/soybean mixture: factors affecting expanded product characteristics and flour dispersion viscosity. *J Food Eng.* (2008) 87:333–40. doi: 10.1016/j.jfoodeng.2007.12.008

21. Cordesse R. Value of chickpea as animal feed. In: Saxena MC, Cubero JI, Wery J, editors. *Present Status and Future Prospects of Chickpea Crop Production and Improvement in the Mediterranean Countries*. Zaragoza: International Centre for Advanced Mediterranean Agronomic Studies (1990). p. 127–31. Available online at: https://om.ciheam.org/om/pdf/a09/91605019.pdf (accessed February 18, 2021).

22. Kaisangsri N, Kowalski RJ, Wijesekara I, Kerdchoechuen O, Laohakunjit N, Ganjyal GM. Carrot pomace enhances the expansion and nutritional quality of corn starch extrudates. *LWT-Food Sci Technol.* (2016) 68:391–9. doi: 10.1016/j.lwt.2015.12.016

23. Pastor-Cavada E, Drago SR, González RJ, Juan R, Pastor JE, Alaiz M, et al. Effects of the addition of wild legumes (*Lathyrus annuus* and *Lathyrus clymenum*) on the physical and nutritional properties of extruded products based on whole corn and brown rice. *Food Chem.* (2011) 128:961–7. doi: 10.1016/j.foodchem.2011.03.126

24. Sharif MK, Rizvi SS, Paraman I. Characterization of supercritical fluid extrusion processed rice–soy crisps fortified with micronutrients and soy protein. *LWT Food Sci Technol.* (2014) 56:414–20. doi: 10.1016/j.lwt.2013.10.042

25. Nicole M, Fei HY, Claver IP. Characterization of ready-to-eat composite porridge flours made by soy-maize-sorghum-wheat extrusion cooking process. *Pak J Nutr.* (2010) 9:171–8. doi: 10.3923/pjn.2010.171.178

26. Baik OD, Marcotte M. Modeling the moisture diffusivity in a baking cake. *J Food Eng.* (2003) 56:27–36. doi: 10.1016/S0260-8774(02)00144-9

27. Paraman I, Wagner ME, Rizvi SS. Micronutrient and protein-fortified whole grain puffed rice made by supercritical fluid extrusion. *J Agric Food Chem.* (2012) 60:11188–94. doi: 10.1021/jf3034804

28. Voltarelli FA, Araujo BM, Moura LP, Garcia A, Silva CMS, Junior RCV, et al. Nutrition recovery with spirulina diet improves body growth and muscle protein of protein-restricted rats. *Int J Nutr Metab.* (2011) 3:22–30. doi: 10.5897/IJNAM.9000028

29. Riaz MN. Healthy baking with soy ingredients. *Cereal Foods World.* (1999) 44:136–9.

30. Alonso R, Rubio LA, Muzquiz M, Marzo F. The effect of extrusion cooking on mineral bioavailability in pea and kidney bean seed meals. *Anim Feed Sci Technol.* (2001) 94:1–13. doi: 10.1016/S0377-8401(01)00302-9

31. Berrios JDJ. Extrusion cooking of legumes: dry bean flours. *Encyclopedia Agric Food Boil Eng.* (2006) 1:1–8. doi: 10.1081/E-EAFE-120041506

32. Onwulata CI, Konstance RP, Smith PW, Holsinger VH. Co-extrusion of dietary fiber and milk proteins in expanded corn products. *LWT Food Sci. Technol.* (2001) 34:424–9. doi: 10.1006/fstl.2000.0742

33. American Association of Cereal Chemists and Approved Methods Committee. *Approved Methods of the American Association of Cereal Chemists, Vol. 1*. Saint Paul, MN: Amer. Assn. of Cereal Chemists (2000).

34. Saadat S, Akhtar S, Ismail T, Sharif MK, Shabbir U, Ahmad N, et al. Multilegume bar prepared from extruded legumes flour to address protein energy malnutrition. *Ital J Food Sci.* (2020) 32:1559. doi: 10.14674/IJFS-1559

Frontiers in Nutrition

Explores what and how we eat in the context of health, sustainability and 21st century food science

A multidisciplinary journal that integrates research on dietary behavior, agronomy and 21st century food science with a focus on human health.

Discover the latest Research Topics

See more →

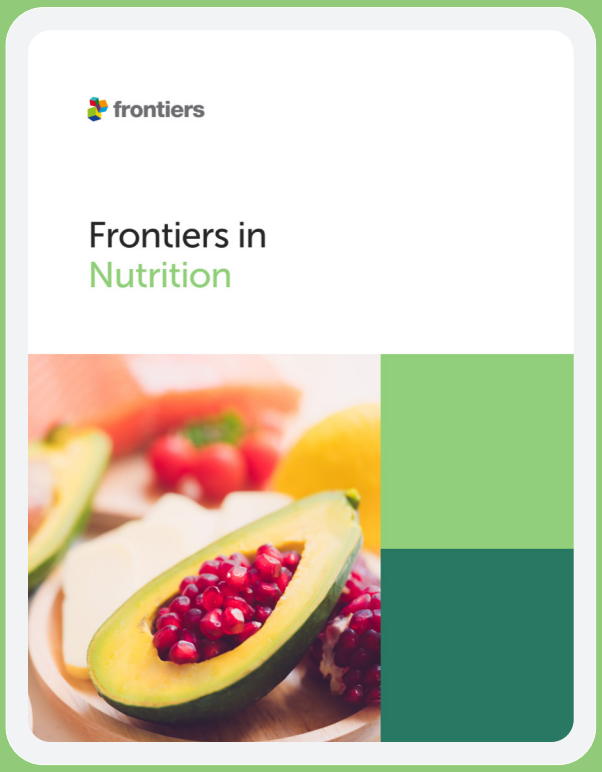

Frontiers

Avenue du Tribunal-Fédéral 34
1005 Lausanne, Switzerland
frontiersin.org

Contact us

+41 (0)21 510 17 00
frontiersin.org/about/contact